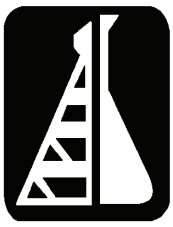

CANADIAN MINING INDUSTRY RESEARCH ORGANIZATION (CAMIRO) EXPLORATION DIVISION

Project 08E01

Multi-media Techniques for Direct Detection of Covered Unconformity Uranium Deposits in the Athabasca Basin

Phase III
Final Report on Results of Soil Geochemistry Using Selective Leaches

Graeme Bonham-Carter and Gwendy Hall

April 27, 2010

Table of Contents

Executive Summary and Recommendations

Summary of main results

Geochemical anomalies in soil occur over the surface trace of pods at both Cigar Lake and at McClean Lake. These anomalies are expressed by several ore-related elements, particularly U, Co, Ni (and the REEs) and to a lesser extent by Mo and several other elements. The second year of data collection (2009) helped to clarify the initial results of 2008, confirming that certain anomalies are repeatable and reliable. The infill line that was added in 2009 at both sites was particularly important in affirming lateral continuity.

The best and most reliable anomalies occur in the A1 humus horizon at both Cigar and McClean. The B1 and C horizons also show anomalies over the ore pod traces for some elements in some leaches, but the results are in general not as convincing and reliable as those in the A1 horizon.

Most of the best results were obtained by an ordinary aqua regia near-total decomposition on A1 samples. The pyrophoshate partial leach on A1 samples showed similar results to aqua regia, although the element content in the leach data was usually about one third of the content obtained by aqua regia. Halides determined using the Enzyme leach showed haloes around the ore traces ("rabbit ears") at some horizons. The MMI leach on the MMI horizon showed anomalies over the McClean pods for certain elements. The ammonium acetate leach in particular and the hydroxylamine hydrochloride leach on inorganic soils often suffered from inadequate detection limits and are not recommended for this particular application.

It is not clear from this study whether the added cost of sample collection other than the A1 horizon, as well as the added cost of partial leach analysis is cost effective for exploring for this type of deposit under these conditions.

The anomalies at Cigar Lake do not appear to be controlled by LOI or pH-related factors, nor by ground elevation. At McClean Lake care was taken to remove the effect of peat as far as possible for the A1 humus, and the anomalies remain after removing this effect. In order to remove the effect of element anomalies due to elevated levels in transported surficial material (till), a multivariate statistical approach was used. A major N-S divide occurs at McClean, with elements such as barium being enriched to the south relative to the north. It is uncertain whether this is related to the geological boundary in the sub-unconformity geology, but the geochemical change is coincident the geological boundary.

Variability between years was monitored and did not affect the most significant anomalies, although some elements did show substantial inter-year variability. The aqua regia digestion showed the best repeatability by far, with the pyrophosphate leach a close second. Numerous elements by the Bioleach show systematic bias between years, and to a lesser, but significant, extent the Enzyme leach. It is not clear whether this is a field-related factor (e.g. time of year, moisture conditions, soil temperature) or a laboratory-related QC problem but the former is more likely.

Analysis and display methods are critical because the anomalies for the most part are subtle, and great care must be exercised to understand where possible the presence and sources of variability, and to remove, where possible, artifacts due to known factors that can be controlled or removed. Gridding of data is useful for providing general spatial trends, whereas proportional dots reveal information about spatial variability, and variability of duplicates.

Stacked profiles and QC plots were helpful for identifying anomalies and assessing year-to-year and along-line variability.

Recommendations

Use A1 soils for geochemical exploration for buried unconformity-related uranium deposits such as Cigar and McClean Lakes. The least expensive approach would be to use aqua regia decomposition possibly in conjunction with a partial leach such as sodium pyrophosphate which selectively decomposes the organic fraction.

Spatial variability suggests the sample spacing should preferably be no more than 100 m between lines and 50 m between samples, with 5% of the samples being field duplicates. About 1 in 20 samples should also be standards inserted to evaluate accuracy and any change between sample submissions. For the Enzyme leach and Bioleach data, multi-year variability suggests that it is dangerous to combine data from different years. A grid approach is recommended because trends across lines can be identified, and it increases confidence in the robustness of anomalies.

If peat samples are included, special care must be used to look for peat-related artifacts and to correct for them by leveling or some other method. Any change in soil type, as seen here in mixing podsols and gleysols, can lead to false anomalies.

A knowledge of till composition and how it varies over the sampled area would be helpful in interpreting whether anomalies are related to spatial changes in till, or other factors. Perhaps till could be sampled and geochemically analyzed at 1 in 10 of the humus sites for this purpose.

Because the pyrophosphate partial leach data in the A1 horizon usually gave the same patterns of anomalies as the aqua regia data, it would be useful to experiment with changing the decomposition conditions (concentration, sample-to-volume ratio, duration) to optimize the response and identify the organic phase being targeted.

Boron has been reported as an ore-related element, and has been found at elevated levels in Athabasca sandstones above McClean and other deposits. We recommend that boron be included in the element suite analyzed in future surveys.

Discussion

The question arises: how do geochemical elements enriched in these deeply buried uranium deposits (~150 m at McClean, 400 m at Cigar) reach the surface, and why are they to be found best in the humus horizon, and not so reliably in the B and C horizons?

It is well known that perched mineralization occurs in Athabasca sandstones and conglomerates above many of the uranium deposits. Elevated levels of uranium and other ore-related elements form haloes above many of the deposits, even reaching the upper surface of the sandstones in some places. Reactivated faulting provides the pathway for fluids carrying these elements.

At the Cigar Lake site, a prominent uranium (and other elements such as Co, Ni, and As) anomaly in A1 humus runs SW-NE across the westerly tip of the surface trace of the pod. It is close to a mapped fault that has the same orientation. One may speculate that the origin of the anomaly is related to this fault, although there may be alternative mechanisms.

Movement of dissolved metals from the Athabasca sandstone in groundwater through the overlying Quaternary tills (that may have moved distances of many kilometres from source) may have been enhanced by roots of plants. Over time, decaying plant material may have led to an accumulation of metals in the humus. This might help to explain why we see anomalies in humus that are not clear in the B and C soil horizons.

Although the anomalies shown for spruce needle samples in this study do not necessarily coincide with the humus anomalies, other plant species with various preferences (and barriers) for different metals may be the explanation.

Despite the spatial location of anomalies over ore pods, further work, possibly with isotope methods, needs to be done to prove that the anomalies do represent guides to the buried deposits. Any changes in till geochemistry within the survey area should also be delineated.

SOME HIGHLIGHTS

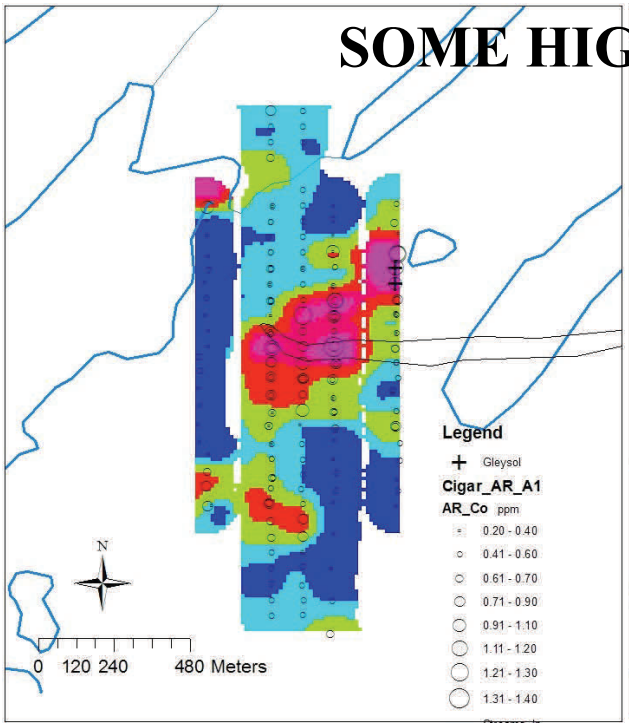

Cobalt in A1 horizon by aqua regia, showing prominent SW-NE trend, close to a mapped fault.

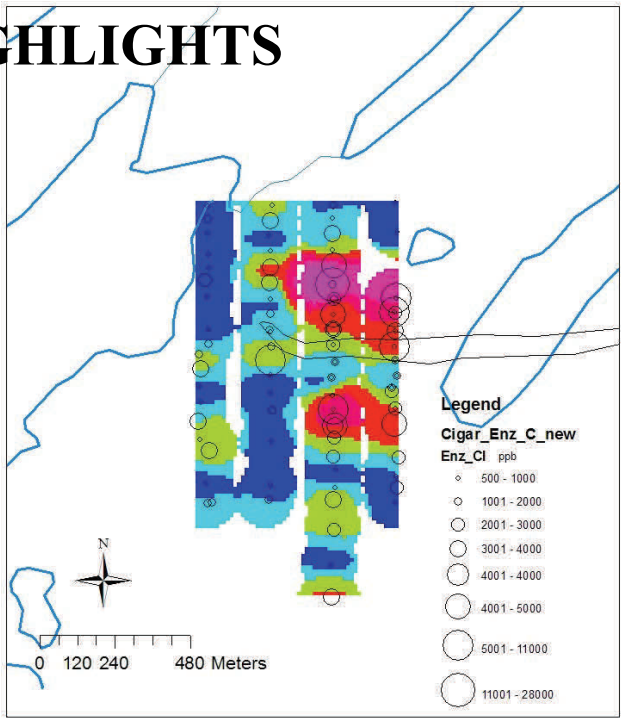

Chlorine in C horizon by enzyme leach. Notice the halo effect around the pod. A N-S profile would show "rabbit-ears" over the pod.

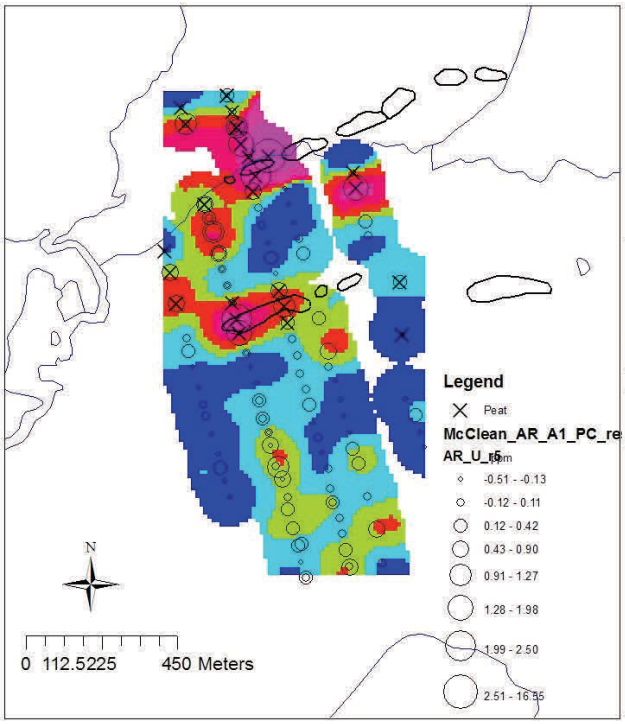

Uranium in A1 anomaly by aqua regia at McClean. This is a residual map after removing the effect of peat and a general geological factor.

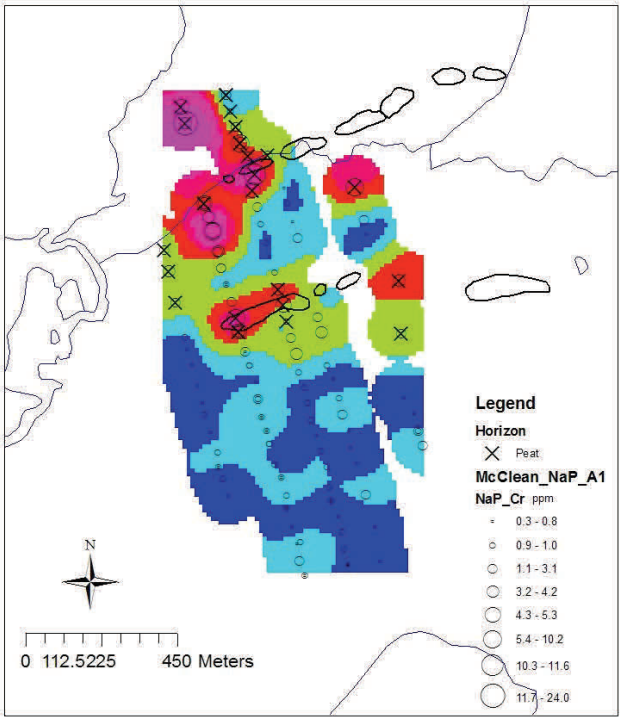

Molybdenum in A1 horizon by sodium pyrophosphate. Here the partial leach shows an anomaly over the McClean pods.

Acknowledgments

Thanks are due to all those many people who assisted in the field during both the 2008 and 2009 field seasons.

For preparing this report, we would like to thank several company people who supplied data and information, mainly for the second chapter on general description of the areas: Don Wright (Cameco), Dave Quirt, Greg Gudmundson, Greg Bell, Kelly Sikorski and Brian Derrow (Arevea Resources). Thanks to Janet Campbell (GSC) for discussions on till geochemistry, and Pouran Behnia (GSC) for help in georectifying an image. We are particularly grateful to Dave Lawie (ioGlobal) for loaning us a copy of the ioGAS software, which we found very useful for this project,

Finally, we wish to acknowledge the significant contribution made by Robert Jackson who led the project at the outset and did an extraordinarily good job of data analysis and report writing (Phase II) during what must have been a very difficult period of failing health.

PART I

1. INTRODUCTION

This report should be read in conjunction with the Phase II report by Robert Jackson, the final vegetation report by Colin Dunn and the final SGH report by Dale Sutherland.

This introduction provides some background material on using partial leaches of soils to explore for deeply buried mineral deposits. In particular, the list of leaches used in this study is summarized in Table 1.1, and indicates the various mineral phases targeted by each leach.

The report summarizes the results and interpretation of data collected in 2008 and 2009 at the Cigar Lake and McClean Lake sites. In particular, the focus is to answer the following questions:

1) Can partial leaches of soils show the presence and location of buried uranium deposits in the Athabasca Basin?
2) If the answer to question 1) is positive, which are the best soil horizons to use? And which of the various leaches applied is the most effective?
3) Can the anomalies be distinguished from artifacts caused by factors other than buried mineralization? What are the best ways to remove these confounding factors?
4) What sampling density and sampling protocol is recommended?
5) How are data best analyzed and displayed?

Indications from the 2008 data, as described in the Phase II report, were that metal anomalies could be recognized in various soil horizons. There was a concern, however, that variability from various sources might make this approach unreliable and impractical to apply. This report makes a special effort to summarize quality control results, to evaluate year-over-year variability, and to interpret where possible the anomalies seen in light of various factors that might produce false anomalies or artifacts in the data.

1.1 Background to partial extractions

Partial leaches, rather than total decompositions, are used to digest soil or sediment samples collected in mineral exploration surveys to highlight that portion of an element that is *loosely bound* to various constituents (e.g. to organic matter, oxides, hydroxides, clay minerals) of the sample. This fraction of the element would have arrived at the site dissolved in solution (hydromorphically rather than mechanically), perhaps simply from the weathering of the soil's primary minerals but more importantly, for the explorationist, from an ore body at depth or at some distance. The latter fraction is termed the *exogenic* constituent of the soil, reflecting a distant source of the element while the former is termed the *endogenic* portion, reflecting the primary composition of the soil itself as it undergoes natural soil-forming processes. As is demonstrated in Figure 1, the exogenic component, the target for exploration, gradually becomes more strongly bound with time, binding to and within crystalline structures such as oxides and silicates. Thus, the component of the soil to be dissolved and analysed is that representing the highest percentage of exogenic material (the dark sections in Fig. 1) and the most efficient way to do this, when dealing with large numbers of samples, is to use weak chemical extractions or 'partial leaches'.

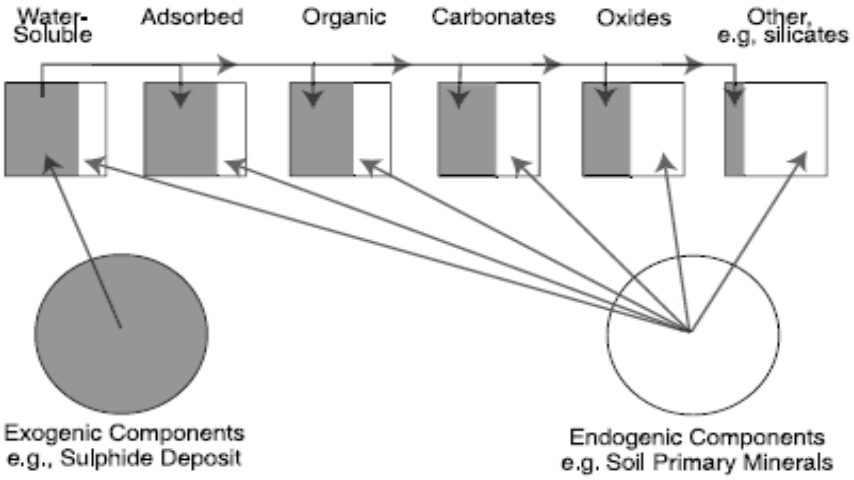

Fig. 1.1. *Conceptual model of exogenic and endogenic phases amongst soil-forming minerals. From Cameron et al. (2004).*

The principal resident sites in the secondary environment capable of capturing or fixing migrating elements include hydrous iron and manganese oxides/hydroxides, humic and fulvic components of organic matter, and clay-sized aluminosilicates. There are two approaches in designing partial leaches to define this labile fraction of the soil. One is to extract loosely bound elements from *any site* in the solid sample by adding a solution containing one or more complexing agents (ligands) which would preferentially bind with the elements of interest and maintain them in a stable state in solution. A simple water leach would fall into this category of *non-selective* leach, as would the commercial MMI and Ionic leaches. The second approach is to dissolve only that scavenging phase (e.g. iron or manganese oxides) most likely to contain the highest exogenic proportion, thereby dissolving not only elements loosely bound on the surface but also those that have been incorporated within their structure. A leach such as the commercial Enzyme leach, purported to dissolve amorphous Mn oxides and associated elements, or one

of the hydroxylamine hydrochloride-based leaches would fall into this category and is termed a *selective* (partial) leach. Phases such as manganese oxides, iron oxides and 'organics' are generally not discrete but rather exist linked together as colloids and this natural state makes designing a leach to be truly selective extremely challenging. Furthermore, binding mechanisms are not simple, comprising physical and chemical adsorption at surfaces, occlusion within structures, chelation, complexation and coprecipitation.

Whichever approach is taken, the operating conditions of the leach must be optimised; these include the concentrations of the reagents, pH, temperature, solution-to-sample ratio, duration and type of mixing. Studies of such extractions, and their application in exploration, were carried out as far back as the 1950s and were particularly prevalent in the 1960s and early '70s, especially at Geological Surveys (e.g. USGS). This early work on partial extractions and their application in exploration geochemistry was summarised in T.T. Chao's excellent paper (1984) in the Journal of Geochemical Exploration (on CD). When ICP emission spectrometry was established in the late 1970s, interest in partial extractions diminished, to be replaced by enthusiasm for the dazzling suite of elements offered by this simultaneous multi-element technique where the digestion commonly employed was aqua regia, a strong oxidising digestion of 3 parts HCl to 1 part HNO_3.

The advent of the ultra-sensitive multi-element technique of ICP mass spectrometry, first on the market in 1983 but not robust until the late 1980s, stimulated interest in partial leaches once more. At the Geological Survey of Canada (GSC), as part of the analytical component of the 'EXTECH I' program – to develop new methods of exploration for buried volcanogenic massive sulphide deposits - the Analytical Method Development Section, led by Hall, initiated research into designing a sequential leach extraction scheme composed of various selective leaches to identify elements bound to different sites and phases of soils and sediments (see papers in the CD). Several of these leaches were developed to dissolve the same phases that the Russians had found to be most useful in exploration: organic matter, manganese oxide, amorphous and crystalline iron oxides. The reagents focused on in this work at the GSC comprise sodium pyrophosphate, ammonium acetate and three variants of the hydroxylamine hydrochloride-based leach.

Concurrent with this project at the GSC, J.R. Clark of the USGS developed a method to dissolve amorphous and pseudo-crystalline Mn oxides, and associated labile elements, using low concentrations of hydrogen peroxide formed in-situ (Clark, 1992, Patent 5491078). Activation laboratories of Ancaster then marketed this method as the 'Enzyme' leach wherein >50 elements were reported. Another commercial leaching process was created about this time in Australia by Alan Mann of Wamtech Pty.: the 'MMI' or Mobile Metal Ion series of leaches. Unlike the approach taken at the GSC and at Activation Labs, the MMI strategy was not to dissolve a particular scavenging phase with its associated elements but rather to use ligands to strongly complex or chelate loosely bound elements of interest while leaving the phases, such as the oxides, in tact.

The activity in partial leaching in mineral exploration was so great by 1996, especially in North America, China, Russia and Australia, that Hall organised a dedicated special issue of the Journal of Geochemical Exploration which was subsequently published in 1998 (Hall and Bonham-Carter, 1998). By the early 2000s, the exploration industry was becoming less enthusiastic about

spending vast sums of money on partial leach surveys. The technique had been oversold by the labs themselves: it had been heralded as an easy method to find buried mineralisation, the reality being quite the opposite. An extensive, well supported project was undertaken by CAMIRO (Canadian Mining Industry Research Organization), called 'Deep Penetrating Geochemistry', and was led by Eion Cameron (ex-GSC) with a team from the GSC (Hall, McClenaghan) and from the OGS (Hamilton). In applying the partial leach approach extensively to known buried deposits in Ontario, Nevada and Chile, much greater insight was obtained into such critical issues as the various mechanisms of element migration from depth, the optimum sample type to collect in different climatic and geological settings, and the characteristics of the different leaches, both proprietary and known (Cameron *et al*., 2004, on CD). The work in Ontario, specifically at Cross Lake, was further carried on under an OMET (Ontario Mineral Exploration Technology) project, 'Three Dimensional Geochemistry in the Abitibi – Development of Geochemical Methods', led by Hall with the same teams members (see full report at http://www.mndm.gov.on.ca/mines/ogs/ims/pub/digcat/mrd_e.asp). The results of these two projects showed the folly of the notion of "one size fits all" in terms of a universal partial leach, or indeed sample type, and emphasized the complexity of this geochemical exploration method and hence the absolute requirement for a trained geochemist to interpret data. A selection of published papers is attached (on the CD) to provide more detailed information on partial leaches and their application.

The array of partial leaches available to the explorationist has changed slightly over the last decade; Table 1.1 lists today's most commonly used selective and non-selective leaches. Those used in this project comprise: 1M ammonium acetate at pH 5; 'cold' hydroxylamine hydrochloride in 0.01 M HNO_3; 0.1 M sodium pyrophosphate at pH 10; Enzyme; Bioleach; MMI; and the Ionic leach. Of these only the pyrophosphate and the Bioleach are designed to be employed on organic-rich the soils, the majority being suited to inorganic media.

Table 1.1. List of commonly available partial leaches in today's geochemical labs, those in italics were not used in this project.

Leach	Key components	Targets
Selective leach		
'Enzyme', From Actlabs	Glucose oxidaze, generating H_2O_2	Elements bound within/on amorphous Mn oxide phase, usually applied to B horizon
'Acetate', 'AA5', From most labs	NH_4OAc, pH 5	Elements bound to and within carbonate.
'Cold hydroxylamine', From most labs	0.1 M $NH_2OH.HCl$ in 0.01 M HNO_3	Elements bound to and within Mn oxide
'Hot hydroxylamine', From most labs	*0.25 M $NH_2OH.HCl$ in 0.25M HCl at 60°C*	*Elements bound to and within amorphous Fe oxide and Mn oxide*
Pyrophosphate, From most labs	0.1 M $Na_4P_2O_7$ at pH 10	Elements bound to and within humates and fulvates ('organics')
Non-selective leach		
'MMI-M', From SGS labs	Proprietary. Mixture of reagents as this replaces previous individual leaches (termed A, B, D, F, G) which solubilised certain groups of compatible elements	45 'loosely-bound' elements, no particular phase targeted
'Bioleach', From Actlabs	Proprietary	Elements bound to bacterial remnant proteins, suggested application to B-horizon on website (Actlabs)
'Terrasol', From Actlabs	*Proprietary*	*No information, suggested applied to B-horizon*
'Ionic', From ALS/Chemex	Heavily buffered weak alkaline cyanide solution.	Elements used in gold, silver, PGE, base metal and uranium exploration.
'Regoleach', From ALS/Chemex	*Proprietary*	*Elements adsorbed to clays, organics, Fe/Mn oxides. Targets gold, base metals, pathfinders*
'TL' series From Intertek/Genalysis Labs, Australia	*TL 0, 9-13 are conventional, TL 1-8 are proprietary but the targeted elements/matrix are discussed.*	*Individual packages for type of soil and elements.*
'Acetate', AA7, From most labs	*NH_4OAc, pH 7.*	*Loosely bound elements, weaker than AA5 leach*
Miscellaneous leaches on request from most labs	*Weak acid (HCl, HNO_3), EDTA*	*'Loosely bound' elements*

2. DESCRIPTION OF SAMPLING AREAS

This section describes the two field areas studied, the sampling and analysis program, and some general information to aid the interpretation of soil geochemical data. Both the Cigar Lake and the McClean Lake sites were sampled in 2008 and 2009, with sample traverses ("Lines") that cross the surface traces of known ore pods, and extend into areas that are "background". Because a main objective of the project is to determine whether deeply buried uranium deposits can be detected in one or more soil horizons, a knowledge of the surface topography, the glacial geology, the sandstones that overlie the unconformity at or above which the deposits occur, as well as the sub-unconformity geology and structure, may all be factors contributing to the distribution of elements in overlying soils.

The stratigraphic setting of the unconformity-associated uranium deposits of the Athabasca Basin is summarized in Jefferson et al. (2007) and numerous other sources, e.g. Wallis et al., 1983 for McClean). The deposits are pods, veins and replacements occurring close to an unconformity between the Athabasca sandstone and conglomerates (~400 m thick at Cigar Lake, 200 m thick at McClean Lake) overlying a crystalline basement of metamorphic rocks , including graphitic metapelite gneisses (usually associated with the deposits), pegmatoids, gneisses and other rock types. The Athabasca sandstones are extensively altered in places and elevated values of uranium (and other ore-related elements) occur in zones of perched mineralization overlying deposits. Besides uranium, Ni, As, Co (and other elements that may be used as pathfinders) occur as haloes in the sandstone over known deposits. Elements enriched in the ores at McClean and Cigar are summarized in Table 2.1. The Athabasca sandstone is intensely faulted in places, and reactivated faults are often cited as likely pathways of metal dispersion from mineralized zones. Quaternary tills overlying the sandstones vary in thickness from 0 to 10s of metres (Campbell, 2007). The tills reflect multiple ice-flow directions, and are composed mainly of detritus from the Athabasca sandstones, with varying amounts of material from the basement. Soils developed since the last glacial advance are mainly podsols (with some gleysols), with defined A, B and C horizons in most places. Peat occurs in poorly drained areas, and this is particularly a factor at the McClean Lake site.

Table 2.1. Elements enriched in ores at McClean Lake and Cigar Lake (from Phase II report)

Element	McClean Pod 8W	Cigar West	Units
U	100 - 100000	30 - 538000	ppm
As	200 - 100000	*	ppm
B	20 - 630	*	ppm
Ce	40 - 100	*	ppm
Co	100 - 2000	100 - 18000	ppm
Cu	20 - 21000	100 - 16900	ppm
Dy	1.5 - 6.0	*	ppm
Fe_2O_3	2 - 30	2 – 11	%
Mo	5 - 33500	10 - 3300	ppm
Nb	6 - 30	*	ppm
Ni	300 - 6300	200 - 74800	ppm
Pb	50 - 10000	200 - 44800	ppm
V	300 - 10000	*	ppm

2.1 Sampling and analysis 2009

The sampling and analysis of the 2008 survey were fully described by Jackson in his Phase II report. Sampling at Cigar and McClean Lakes in August 2009 was aimed mainly at repeating some of the lines taken in 2008 and taking an infill line at each survey area.

At Cigar Lake (Figs. 2.3, 2.4) on Aug 11 and 12, Lines 1 and 2 were partially resampled, a new infill line, Line 3, was taken, and Line 4 was resampled and extended at either end. Samples collected comprise:

A1 humus at all sites (~ 1 kg)
B1 at all sites (~2-3 kg)
C on Lines 1 and 2, only 12 samples per line
'MMI' at all sites (MMI interval, 10-25 cm from bottom of A1)
A1 sample at all sites for SGH and Bioleach
A few peat samples (P)
Spruce twigs (separate report by Colin Dunn)

Table 2.2. Samples taken at Cigar Lake by year, horizon and line, with leaches applied[1]

Year	2008					2009				
Line\horizon	A1	A2	B1	B2	C	A1	A2	B1	B2	C
1	ABCDEFG	ABCDEFG	ABCDEFG	ABCDEFG	ABCDEFG	ABF	-	ACEH	-	ACEH
2	ABCDEFG	ABCDEFG	ABCDEFG	ABCDEFG	ABCDEFG	ABF	-	ACEH	-	ACEH
3	-	-	-	-	-	ABF	-	ACEH	-	-
4	ABCDEFG	ABCDEFG	ABCDEFG	ABCDEFG	ABCDEFG	ABF	-	ACEH	-	-
5	ABCDEFG	ABCDEFG	ABCDEFG	ABCDEFG	ABCDEFG	-	-	-	-	-

[1]A-aqua regia; B –pyrophosphate; C-ammonium acetate; D-hydroxylamine hydrochloride; E-Enzyme; F-Bioleach; G-MMI; H-Ionic leach. MMI leach on MMI horizon at lines 1, 2, 4, 5 (2008) and 1,2,3,4 (2009).

At McClean Lake (Figs. 2.11-2.12) on Aug 14 and 15, an infill line, Line 3, was taken and Line 4 was resampled with extension north of the north pod. Unfortunately, the area to the north of the creek running between McClean and Candy Lakes was boggy throughout and soil profiles were impossible to obtain. The samples taken, according to availability, comprise:

A1
B1
'MMI' at 10-25 cm below base of A1
A1 for SGH and Bioleach
Peat
Spruce twigs (separate report by Colin Dunn)

Table 2.3. Samples taken at McClean Lake by year, horizon and line, with leaches applied[1]

Year	2008					2009				
Line\horizon	**A1**	**A2**	**B1**	**B2**	**C**	**A1**	**A2**	**B1**	**B2**	**C**
1	ABC D EFG	ABC D EFG	ABC D EFG	ABC D EFG	ABC D EFG	-	-	-	-	-
2	ABC D EFG	ABC D EFG	ABC D EFG	ABC D EFG	ABC D EFG	-	-	-	-	-
3	-	-	-	-	-	ABF	-	ACE H	-	-
4	ABC D EFG	ABC D EFG	ABC D EFG	ABC D EFG	ABC D EFG	ABF	-	ACE H	-	-
5	ABC D EFG	ABC D EFG	ABC D EFG	ABC D EFG	ABC D EFG	-	-	-	-	-

[1] MMI leach on MMI horizon at Lines 1, 2, 4, 5 (2008) and Lines 3 and 4 only (2009).

Samples were collected in the same manner as in 2008. The A1 sample for SGH and bioleach was sent without preparation to Activation Labs (Actlabs) and similarly the 'MMI' sample was sent to SGH labs in Toronto. The bulk of the samples were prepared at SRC labs in Saskatoon, exactly as they were in 2008 (low-temperature drying and sieving to < 80-mesh). Loss-on-ignition at 500 and 1000^{o}C was carried out on the organic samples by SRC. Bulk A1 and B1 standards ('STD') had been collected in the field and were prepared and inserted appropriately at a rate of 1 in 20 samples. SRC staff organized all the prepared samples into sets for shipment as follows:

All A1 and P samples, organic-rich media, to
Acme labs for pH, conductivity, aqua regia
ALS/Chemex labs for the pyrophosphate leach

All B1 and C samples, inorganic media, to
Acme labs for pH, conductivity, aqua regia, and the ammonium acetate leach
Actlabs for the Enzyme leach
ALS/Chemex for the Ionic leach (requires a large sample, ~ 50 g)

The labs were asked to report the data in the groups by which they were submitted, i.e.:
At Cigar Lake, File 1116 (A1), File 1211 (B1), File 1212 (C)
At McClean Lake, File 1117 (A1), File 1223 (B1) and File 1224 (P)

2.2 Cigar Lake Description

A satellite image (Fig. 2.1) shows the general location of sampling with respect to lakes and roads. The Lidar DEM (Fig. 2.2) shows that the ground surface ranges from about 460 to 490 m above sea level, i.e. about 30 m of relief. The topography is streamlined in a NE-SW orientation, similar to McClean. Samples (Fig. 2.3) were taken in 2008 along four N-S lines that cross the surface trace of the ore pod. The 2009 samples (red) provided an infill line and repeats as shown on Fig. 2.4. Line numbering used in the report (Fig. 2.4) follows the same convention as McClean, starting with Line 1 (green, East) to Line 5 (purple, West). The infill line (red) is Line 3, with repeats at some sites in Lines 1-4, depending on horizon. No peat occurs at the Cigar sites, but two gleysol samples occur on Line 1 (shown on the geochemical maps as plus symbols).

A grid with elevation of the unconformity in m above sea level (Fig. 2.5), made from drillhole data shows that the unconformity surface is deepest towards the W end of the ore pod. A grid of sandstone plus overburden thickness (calculated as Lidar surface elevation minus unconformity elevation, Fig 2.6) shows that the unconformity is between 370 and 480 m (400-470 m at the sample sites) below surface. No detailed Quaternary geological map was available for this small area. Some basement geology could be inferred from drillhole logs, but this was not made into a map. However, a black and white map showing some basement faults was rectified and superimposed on the satellite image (Fig. 2.7). Of particular interest is a NE-SW trending fault that intersects the pod near the west end, as will be mentioned in the report. A table of drillhole data was used to make the plot in Fig. 2.8 that shows intersections with mineralized sections of the Athabasca sandstone. The top of the perched uranium mineralization (drill hole designated with red square) occurred about 290 m below the collar at this site, whereas in the other holes (green squares) similar mineralization occurred closer to the base of the sandstone between about 410 to 430 m below collar. However, perched mineralization in the sandstone may occur at various levels, a potentially important factor in explaining the vertical migration of mineral-related elements into the overburden and soils at surface.

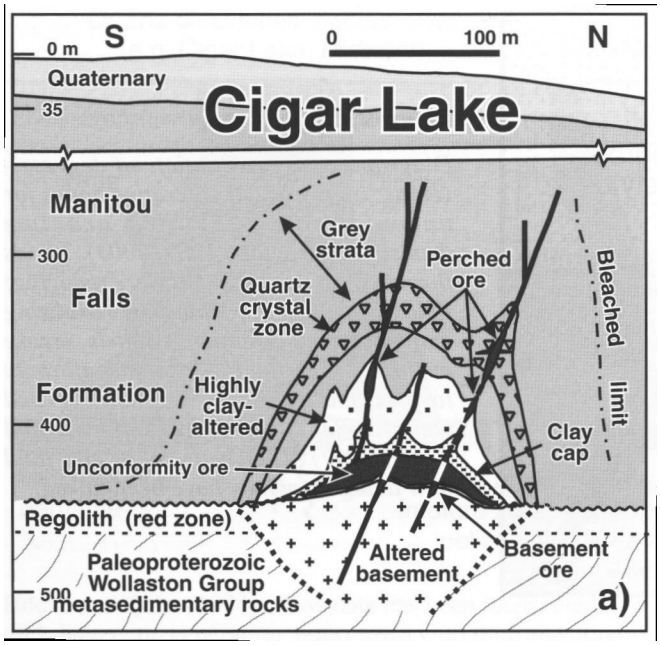

Idealized cross section of Cigar Lake deposit (from Jefferson et al., 2007)

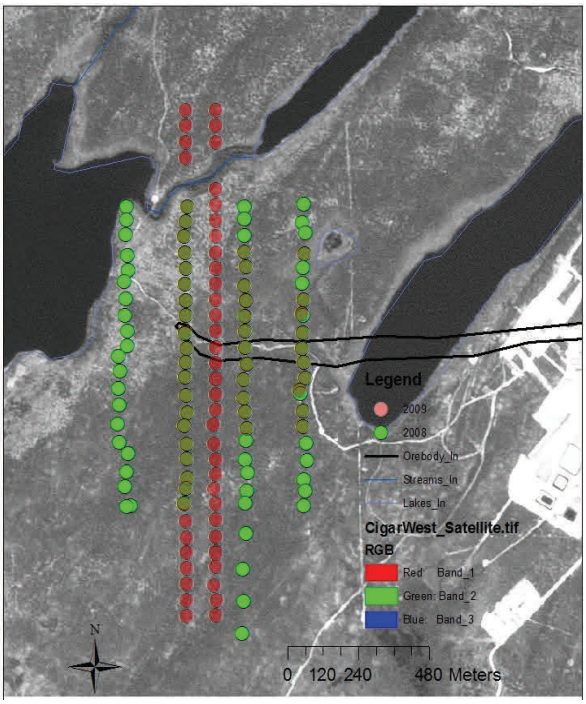

Fig 2.1 Satellite image showing sample locations and location of ore pod trace

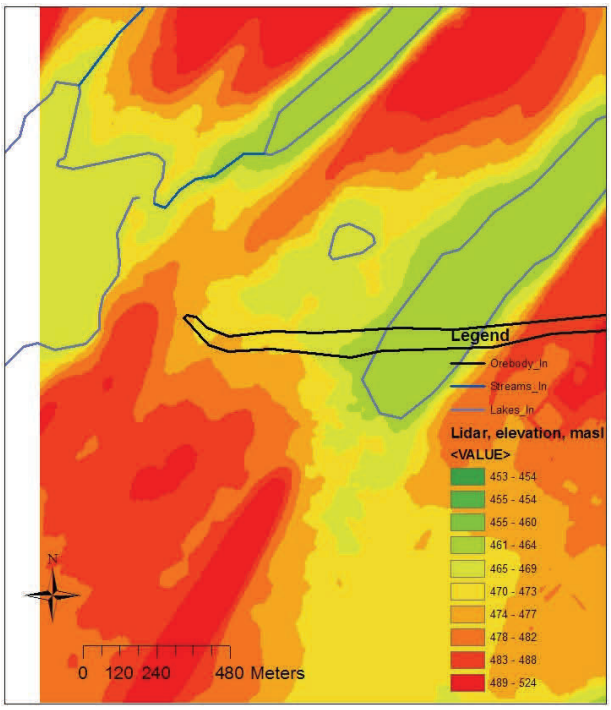

Fig 2.2 Lidar image shows elevation metres above sea level

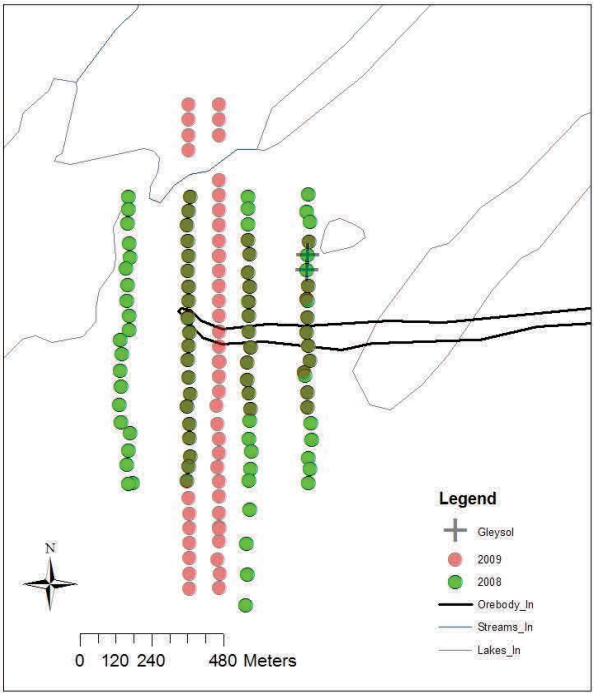

Fig 2.3 Sample locations. Showing years of collection. Darker dots are sites with samples collected both years.

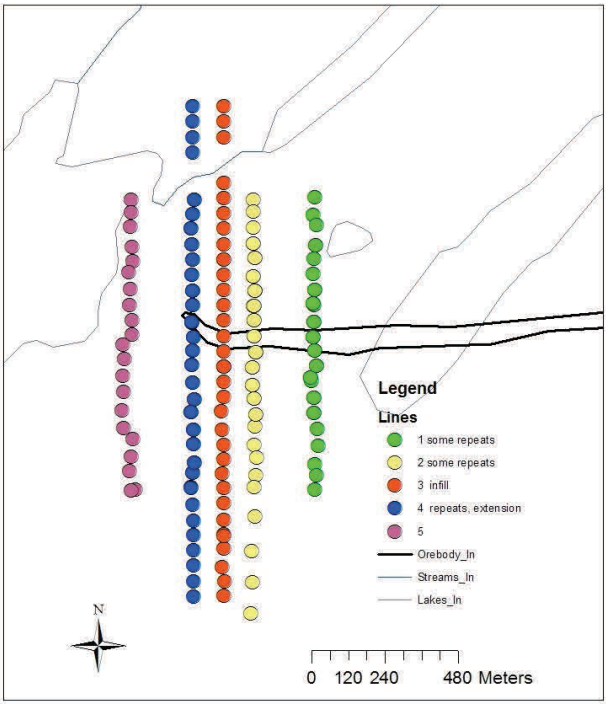

Fig 2.4 Numbering of sample traverses, with line 1 (green) being the furthest east. Line 3 (red) is an infill line. Line spacing for 2008 was 200 m, so infill line 3 is 100 m from lines 2 and 4.

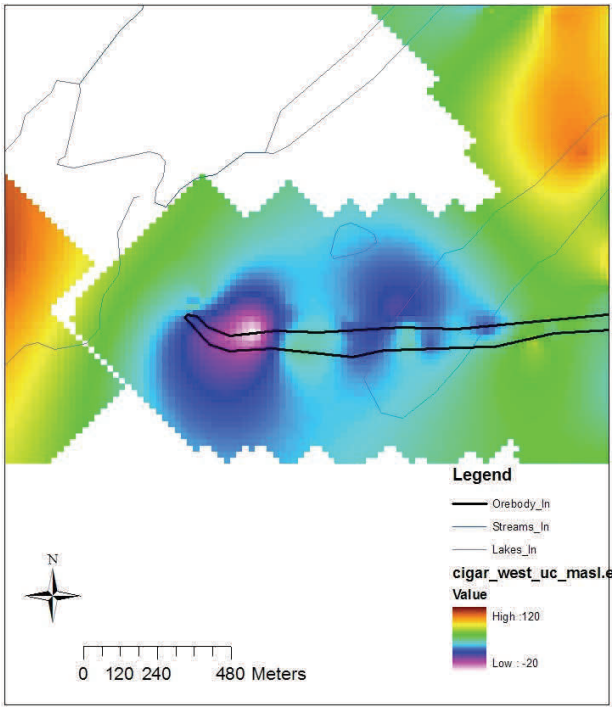

Fig 2.5 Elevation of unconformity in metres above sea level, from drillhole data

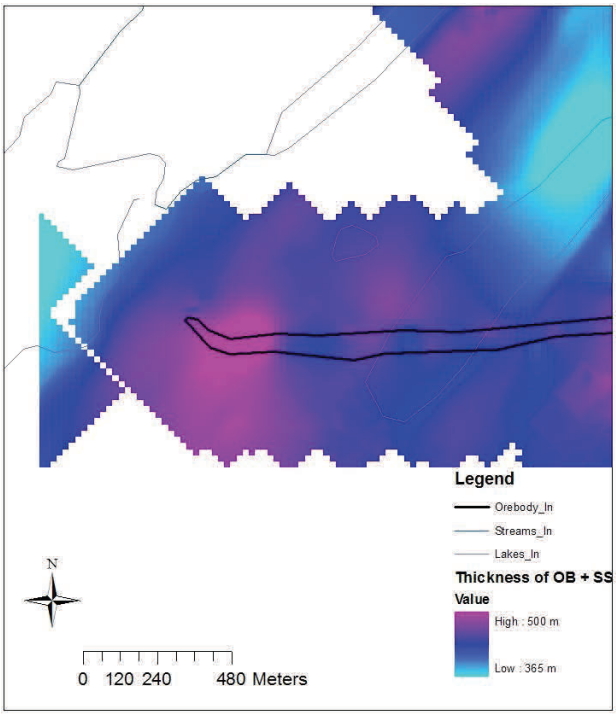

Fig 2.6 Thickness of Quaternary overburden and sandstone overlying unconformity (combined thickness)

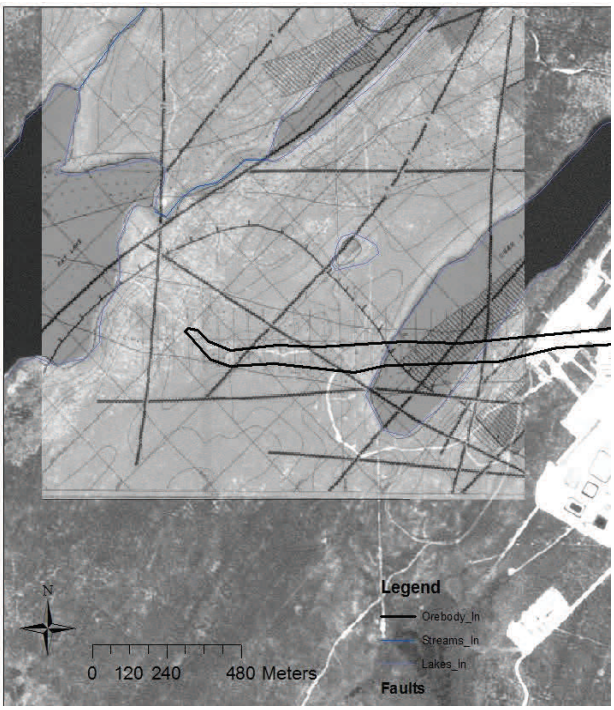

Fig 2.7 Locations of major faults superimposed on satellite image. Note fault NE-SW that intersects west of pod trace.

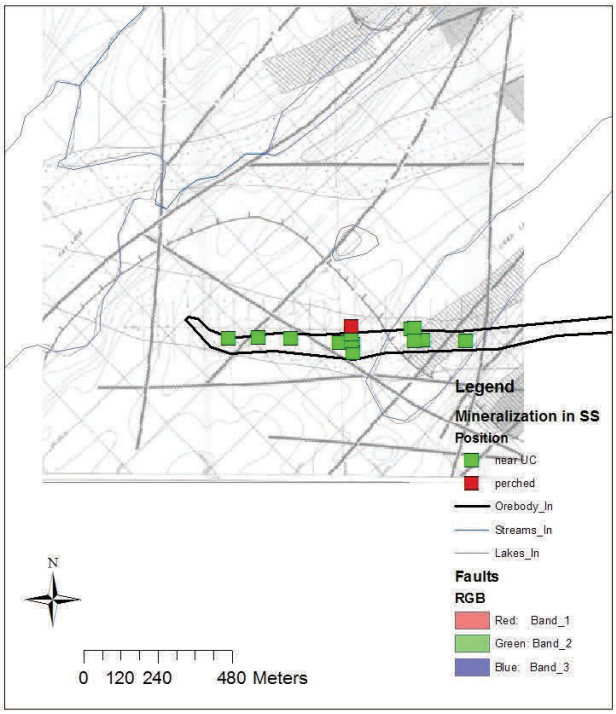

Fig 2.8 Drillholes that intersect mineralization in sandstone above unconformity. Perched mineralization (red dot), mineralization close to UC (green).

2.3 McClean Lake

The satellite image (not georeferenced) in Fig. 2.9 shows the location of the sampled site in relation to the road and lakes. The ground at the McClean Lake site reaches about 450 m above sea level at the crest of the drumlin that runs NE-SW in the south part of the sampled area, and drops to about 435 m in the NW, i.e. about 15 m of relief (Fig 2.10). Four lines of samples (Fig. 2.11) were taken in 2008 (green dots), and the 2009 samples (red dots) included an infill line, and repeats at some of the 2008 sites. The line numbering is shown in Fig. 2.12. Line spacing of the 2008 samples was nominally 200 m (so the infill Line 3 in 2009 is about 100 m from Lines 2 and 4). Along-line sample spacing was nominally 50 m, as at Cigar.

The generalized sub-unconformity geology (Fig. 2.13) shows that the samples traverse the contact between units with graphitic metapelite to ground mapped as an Archean gneiss (red on map) to the south. Basement faults are not marked explicitly on this map, but several faults that run NE-SW can be seen from the stratigraphy. Overburden (comprising Quaternary tills and overlying soil) ranges from <1 m to about 15 m thick (Fig 2.14). There were no detailed Quaternary maps available. The Athabasca sandstone overlying the unconformity here ranges from about 150 to 170 m thick (Fig 2.15).

Peat occurs in some of the low-lying areas. Samples that intersected peat are shown as crosses on the elevation map (Fig. 2.16), and are marked on the geochemical plots as large Xs.

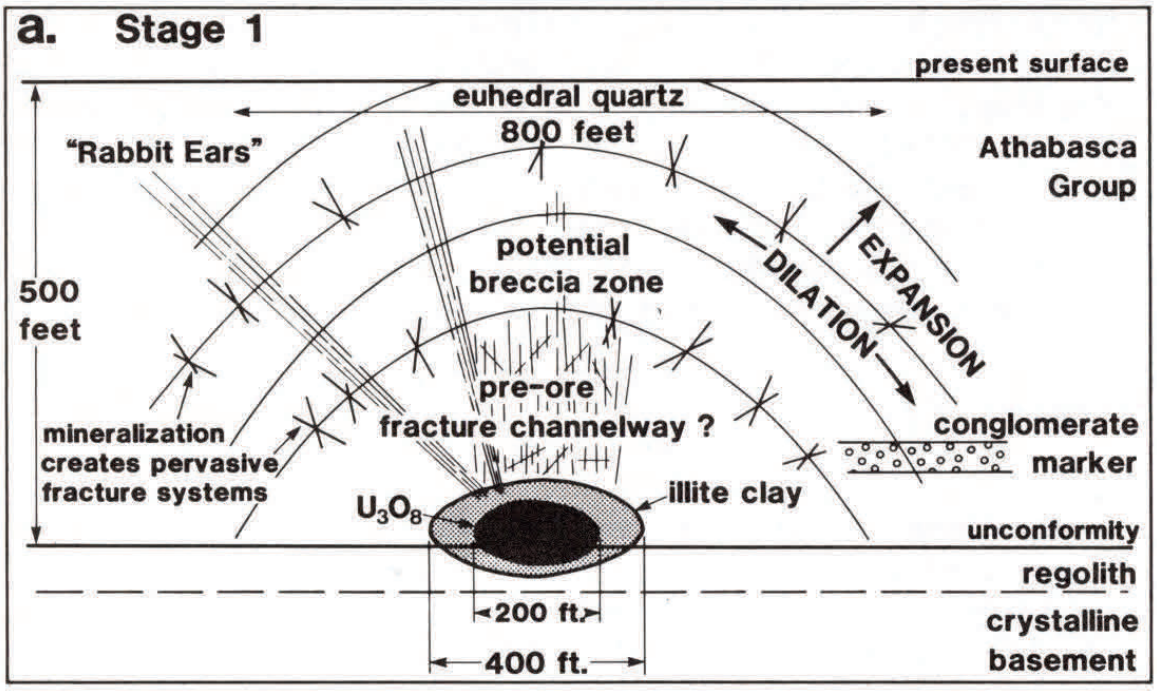

Idealized cross section of McClean deposit (From Wallis et al., 1983)
"Rabbit ears" refer to altered fractured zones above the deposit in the Athabasca sandstone. Term used here predates use by authors describing halo-type anomalies in partial leach data?

Fig 2.9 Satellite image of McClean Lake area (not georeferenced)

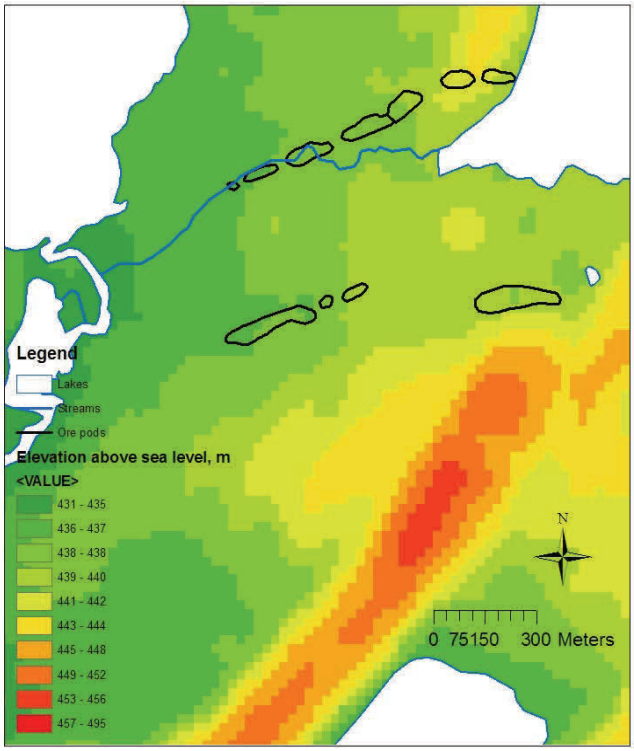

Fig 2.10 Lidar, metres above sea level, showing ore pods

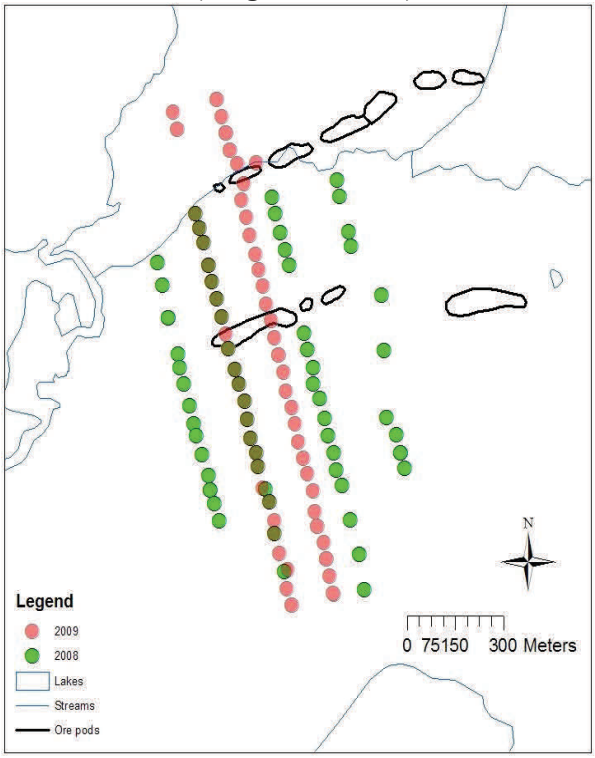

Fig 2.11 Sample sites at McClean. Green for 2008, red for 2009. Darker colour, both years

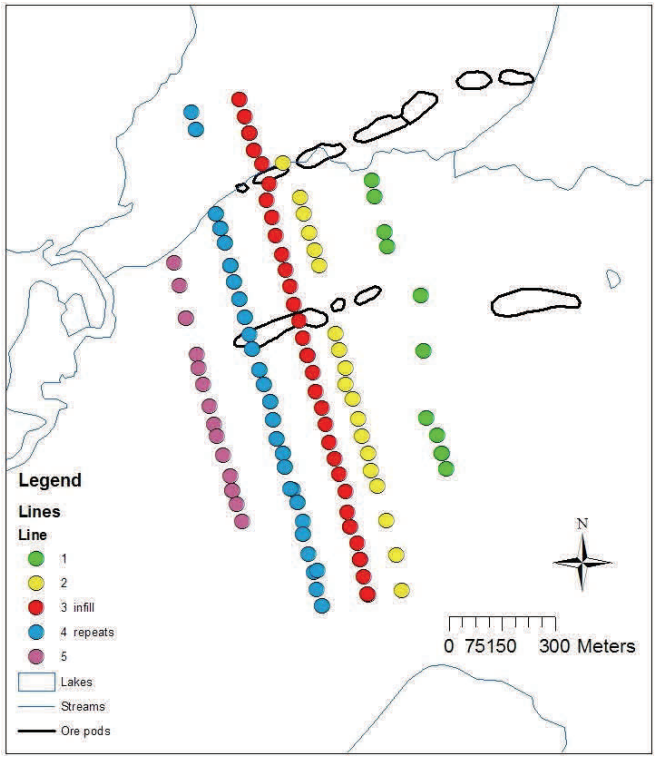

Fig 2.12 Line numbering, Line 1 (green) is furthest east. Line 3 (red) is an infill line. Line 4 (blue) is the repeat line

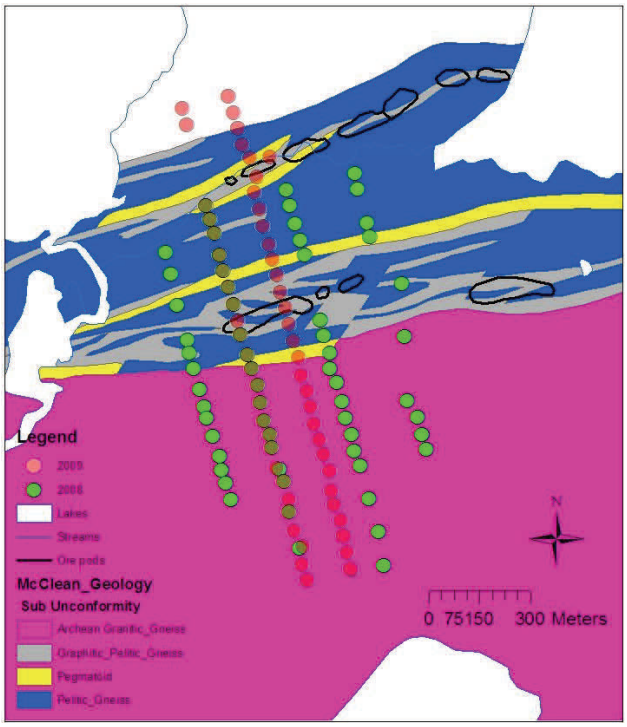

Fig 2.13 Sub-unconformity geology. Faults not marked but visible in stratigraphy.

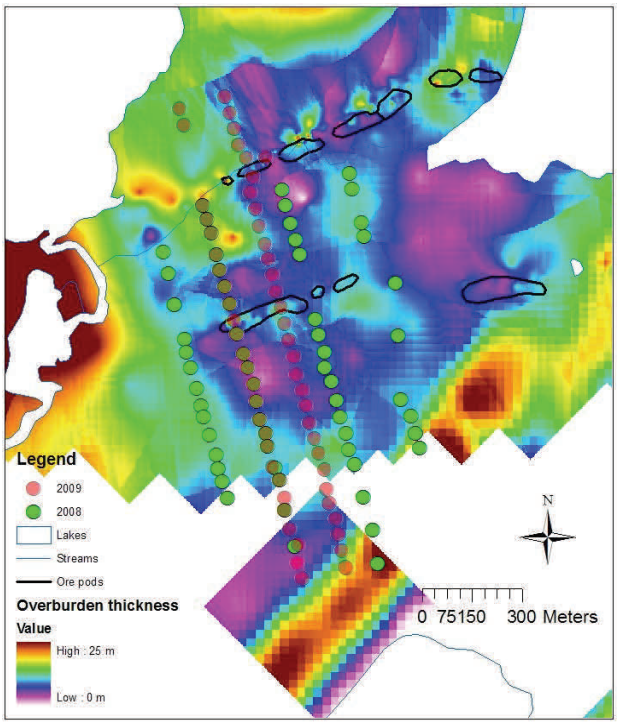

Fig 2.14 Overburden thickness in m., based on drillhole data

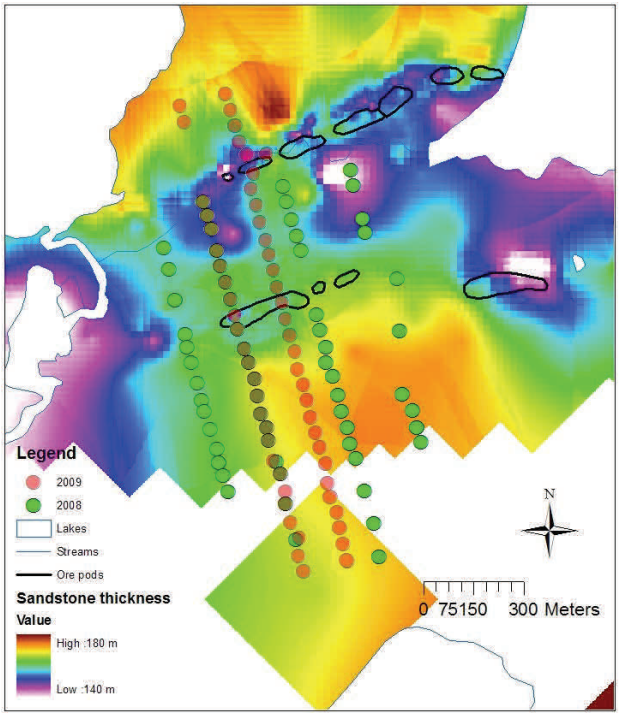

Fig 2.15 Athabasca sandstone thickness in m.

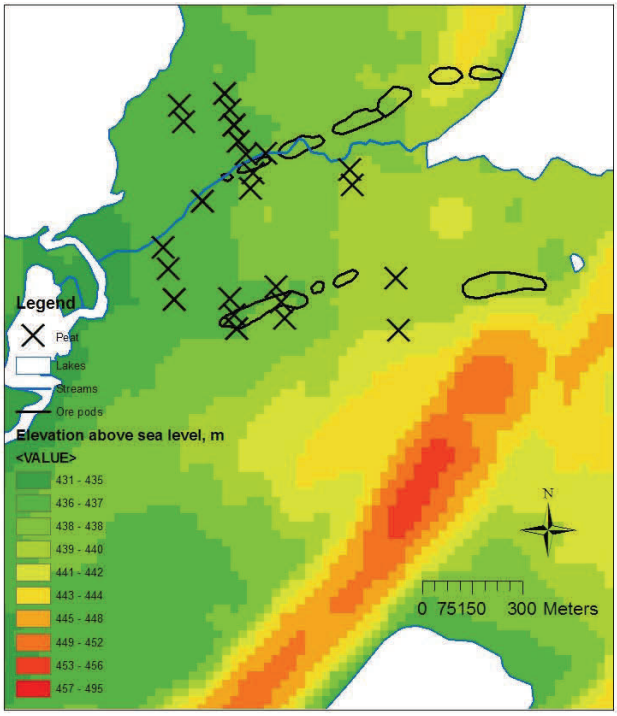

Fig 2.16 Locations of sample sites with peat. Generally in low lying areas, but not exclusively so.

3. INTERPRETATION OF RESULTS

3.1 Introduction

This section of the report provides a discussion of some key aspects of the results. A more complete description of the methods and results is in Part II of the report, which includes geochemical maps, profile graphs and grids for all five soil horizons and all the pertinent leaches.

The interpretation of regional geochemical surveys is not simply a matter of making interpolated maps on which anomalies can be seen. First, it is vital to understand how good the data are by examining sources of variation due to analysis and sampling. A later section of this chapter section discusses the QC results determined from lab and field duplicates, and results using standards. Of particular interest is to examine inter-year variability, as well as spatial variability as seen along traverses: are anomalies 'one point' phenomena, or do they represent multi-point zones where elevated geochemical values can give confidence in a real spatial pattern? The methods used to make the maps are discussed more fully in Part II, but it should be emphasized that the gridding provides general information about spatial trends, whereas proportional dots superimposed provide specific information on actual values, repeatability and spatial variation. Profile plots give an alternative view, often revealing patterns and information on repeatability not so easily seen on maps.

The problem faced here is that with half the periodic table, up to eight different leaches and up to five soil horizons from 2 sample areas, it is almost inevitable that some maps will look 'promising'. The challenge is to find robust anomalies that stand up to a critical analysis, and then attempt to see if they are artifacts that can be explained by some source other than buried mineralization. For example, well-known in stream and lake sediment surveys is the problem of scavenging by Fe and Mn hydroxides that can produce false anomalies. Here we must consider whether anomalies are the result of elevated values in till (which may have been transported 10s or even 100s of km), effects of peat or organic content, or effects of topography or proximity to roads spreading dust. These factors have been considered here where possible and practical, but the analysis is by no means exhaustive.

3.2 Key Results from Cigar Lake.

A1 horizon

The dominant result from the Cigar Lake data is that a subtle geochemical anomaly occurs in the A1 horizon in a variety of elements. This anomaly is seen reliably in the aqua regia data, but is also visible in the sodium pyrophosphate data, as well as in the data from several other leaches, including ammonium acetate. Various approaches have been used to determine whether it can be explained by a factor other than the presence of buried mineralization (over the ore pods), as discussed next.

Figures 3.1 to 3.8 show, respectively, that an anomaly in Co, U, Ni and Mo runs SW-NE, intersecting the surface trace of the ore pod. Some other elements also show this trend (see Part II). How reliable is this anomaly, and is it an artifact due to the composition of the underlying till?

Although not a definitive answer, we used robust principal components analysis (PCA) to approach this problem. PCA applied to regional geochemical datasets often shows that the first few components (PC1, PC2, etc) 'explain' a large proportion of the variation in the dataset. The elements that are strongly loaded (correlated) to PC1, for example, usually reflect a major geological factor such as the dominant lithological composition. We do not usually expect to see an element association in PC1 that is the result of a mineralizing process. It will more likely be, in this situation, to be a reflection of movement of elements from the tills into the overlying soils.

Maps of PC scores for PC1-PC4 are shown in Fig. 3.9– 3.12, with the principal elements correlated with each one at the top of the plot. The first three components (particularly the first) all show a spatial pattern similar to the single element patterns for Co, U, Ni and Mo (Fig 3.1 to Fig 3.8).

Table 3.1. Elements associated with the first 4 PCs, A1 horizon aqua regia.

PC	Elements	Variance explained %	Cumulative Variance %
1	Pb, Mo, Cd, Pb, Sb, Bi, Ni, Hg, S, K, Co	30.5	30.5
2	Ga, La, Fe, Nb, V, Y, U, Li	20.2	50.7
3	Sr, Ba, Ni, Al, Y, Co	12.6	63.2
4	Ti, Th, Mg, Zr, Nb, Li	5.3	68.6

In some situations, one of the PCs that come after 4, explaining progressively smaller amounts of the total variance, will be associated with the elements that are due to a mineralizing source. However, in this case the spatial patterns associated with later PCs were not clear, and an alternative approach was taken. The key elements under consideration were treated singly, and replaced by their residuals after regressing them against PC1. For example, the residual uranium was the uranium not accounted for by PC1. Similarly the residuals were calculated for Co, Ni and Mo. The residual plots are shown in Figs. 3.2, 3.4, 3.6 and 3.8, alongside the raw value plots for comparison. Although PC1 accounts for more than 30% of the total variation, the residual plots still show very similar trends to the raw data. This was true also for other elements. Furthermore, even if more than one PC is removed from uranium, this strong spatial trend is still present in the data. Fig 3.13 shows the effect of successively removing PC1, PC1 and PC2, PC1, PC2 and PC3, etc. up to PC6. This was carried out by a robust (downweighted outliers) multiple linear regression. Even after removing all of the first 6 components, the trend remains. Fig 3.14 shows scatterplots of uranium in A1 (aqua regia) after removing PC1 (top) and PC1-6 (bottom). Even after removing PC1-6, the correlation with raw uranium is still present.

This strongly suggests that the uranium trend is not accounted for by a general geological factor, such as might be accounted for by the chemistry of the till, but is due to something else. Fig 3.15 shows scatterplots of uranium against loss on ignition, pH and conductivity, again A1 horizon and aqua regia leach. There is no obvious association with any of these factors as can also be seen from maps shown in Figs 3.16-3.19. Note that LOI at 500C is virtually identical to LOI at 1000C. It is interesting, and maybe not surprising that dividing by LOI 1000C (Fig 3.20) still leaves the anomaly intact, although tends to centre it more over the surface trace of the ore pod.

A simple test to see if the spatial patterns of U and Co differed by year is shown in Fig 3.21. The plots for combined years are clearer than single years, but still evident.

Although the amount of various elements dissolved by partial leaches is less than dissolved by aqua regia (usually about one third in the sodium pyro A1), the spatial patterns from partial leaches of soil samples from A1 tend to be similar to aqua regia. For example, plots of U, Co, Ni and Mo for A1 by sodium pyrophosphate leach (Fig. 3.22 to Fig 3.25, respectively) show the same SW-NE trend as the aqua regia data. The PC analysis of the pyrophosphate leach data (Figs 3.26—3.29) show that the spatial patterns differ from the corresponding PCs of aqua regia data, and different element associations occur. Nevertheless, the anomalous trend in the raw data is roughly preserved in the residuals from PCs, as shown in Figs 3.30-3.33.

Gridded images of all elements, for all leaches and all soil horizons (and maps with proportional dots for some) are shown in Part II of this report and are available also on the CD. Only a few figures are included in this section to illustrate some features of the results.

The anomalous trend seen in aqua regia and sodium pyrophosphate data is reinforced by results from other leaches. The ammonium acetate leach shows the anomaly clearly for Co, Fe, Ni and U. The hydroxylamine leach is perhaps not so convincing, although Co, Fe, Ni and U all show the NE-SW anomaly. The enzyme leach shows a coincident Co anomaly in A1, whereas the bioleach has an interesting iodine anomaly in A1 over the pod trace.

A2, B1, B2 and C horizons

Maps of uranium in the A2 (Fig 3.34), B1 (Fig. 3.35), B2 (Fig. 3.36) and C (Fig. 3.38) horizons show that there is no clear anomalous pattern in these horizons, using aqua regia. It is perhaps surprising that the anomaly discussed previously for uranium in the A1 humus horizon does not also show up in the deeper horizons of the soil profile.

Cobalt by aqua regia in these horizons (Fig2. 3.38-3.41) shows some indications of enrichment a little north of the A1 anomaly in the B1 horizon. The enrichment in line 1 on the A2 horizon is accounted for by the two gleysol samples (shown with plus signs on Fig. 3.38) that are enriched in many metallic elements. The B2 and C horizons do not show a similar pattern to A1.

The following figures show some highlights of the partial leach results, concentrating on the B1 and C horizons.

In the B1 horizon, the halides by enzyme leach show a halo effect around the pod trace, as shown on the right side of Fig 3.42. There is some suggestion that the variability between years is suspect—taken up later in the QC section. In Fig 3.42, plots for each year are shown alongside the combined data. In general the combined data is strongly influenced by the data from 2009, whereas the 2008 data on its own would not be convincing.

The ionic leach was only used on 2009 data, and the MMI leach was used only on 2008 data. Nevertheless in the B1 horizon, both these leaches show interesting anomalies spatially associated with the ore pod (Figs. 3.43-3.46).

In the C horizon, there is a suggestion of an anomaly just north of the pod in aqua regia data for silver (Fig. 3.47) and molybdenum (Fig. 3.48). In the ammonium acetate data (Fig 3.49 and 3.50), there are two features of interest, but these are for two elements (P and Mn) that have not shown up as anomalies in other leaches.

The most convincing anomalies associated with the pod in C horizon are in the enzyme leach data, both the halides and other data (Fig. 3.49-3.52). Here the halides form a halo—the well-known "rabbit-ears" pattern. And copper and uranium both show an anomaly (not a halo) just N of the pod, but without the NE-SW trend we see in A1.

Its unfortunate that we only have ionic leach data for 2009 at Cigar for the C horizon, because there are anomalies for iodine and molybdenum (Figs. 3.55-3.56) over the pod. However, with so few data one cannot have confidence in these patterns.

The MMI leach applied to the "MMI horizon" (taken at a fixed depth 10-25 cm below the humus, i.e. mostly B) does not show very good anomalies. We show copper and uranium (Figs. 3.57-58) here, where there is a suggestion of the NE-SW anomaly across the pod.

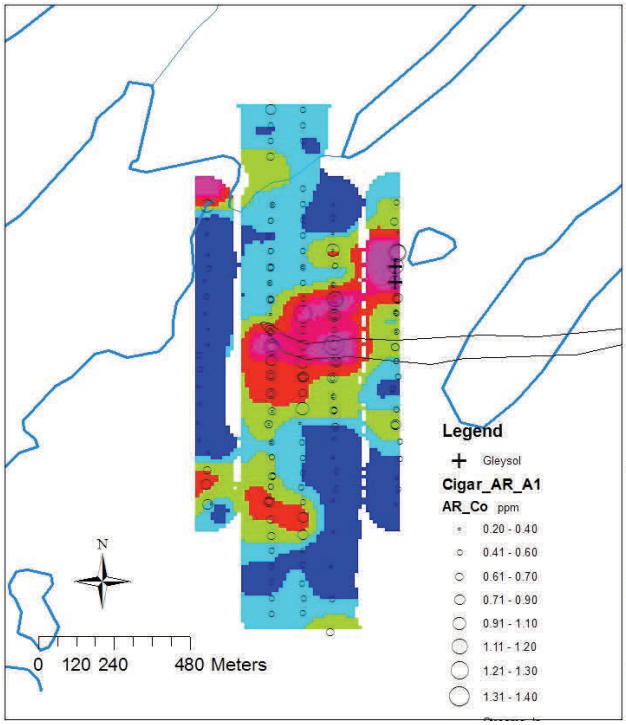

Fig. 3.1 Raw cobalt. A1. Aqua regia

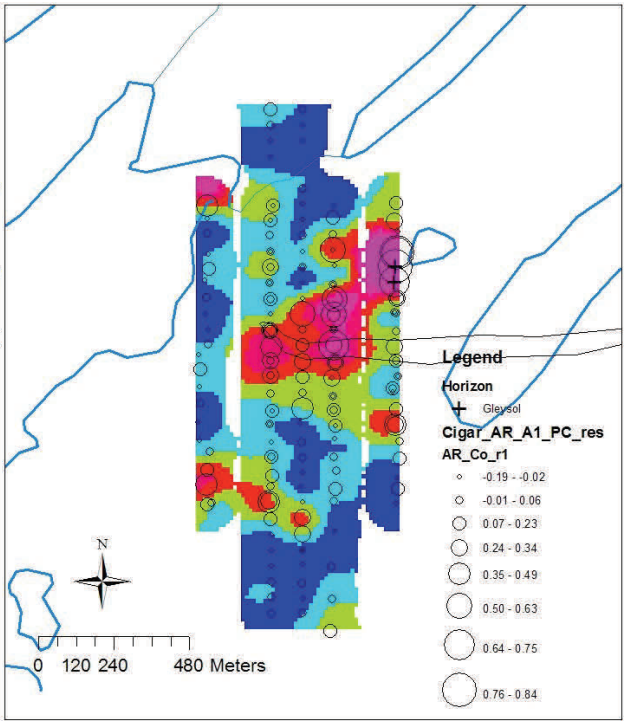

Fig 3.2 Residual cobalt, after removing PC1.

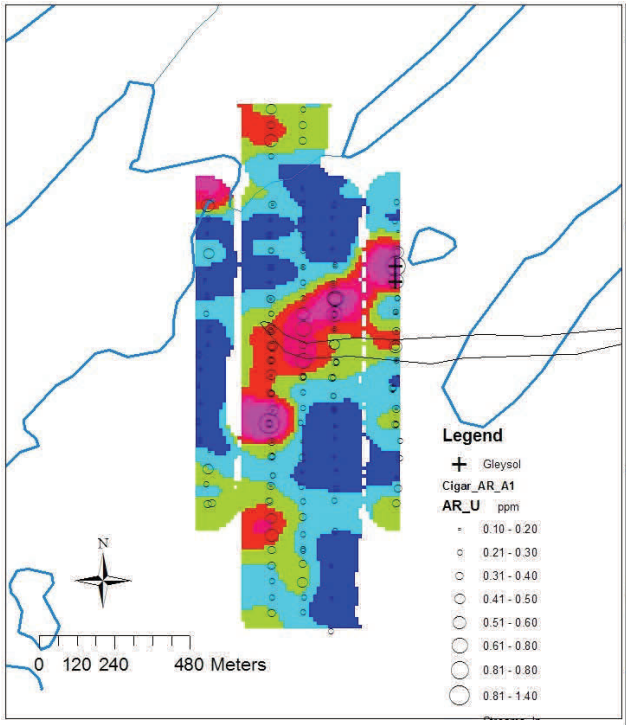

Fig 3.3 Raw uranium. A1. Aqua regia leach

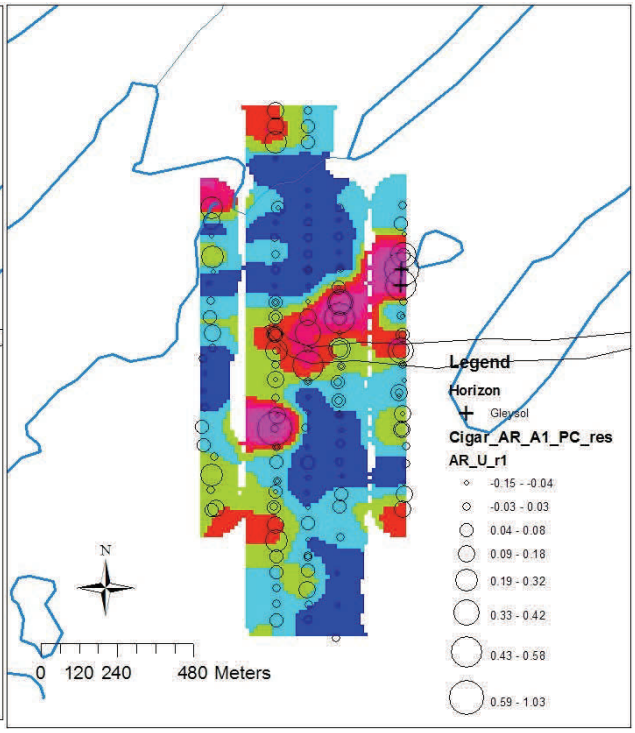

Fig 3.4 Residual uranium, after removing PC1.

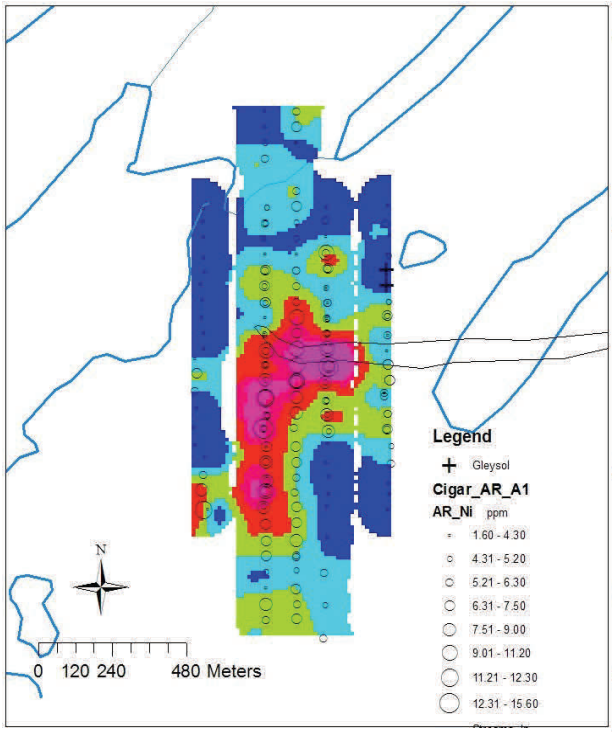

Fig 3.5 Raw nickel. A1 horizon. Aqua regia .

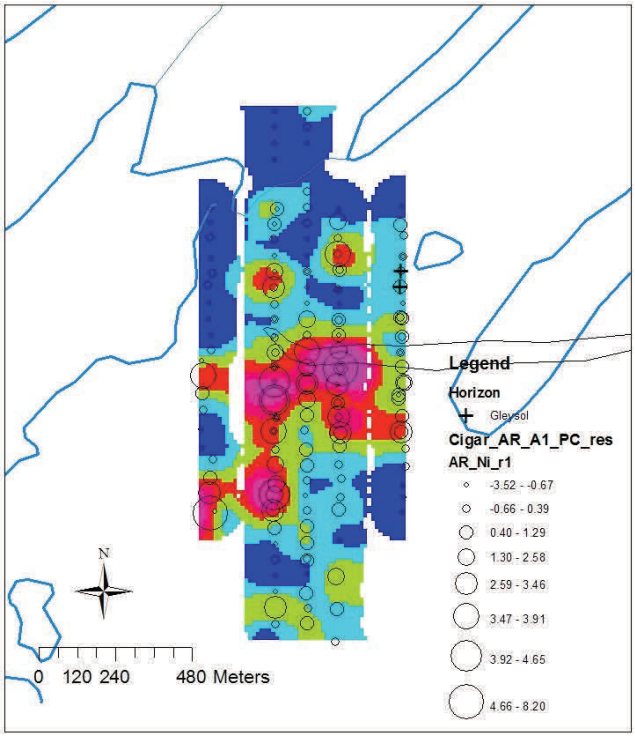

Fig 3.6 Residual nickel, after removing PC1.

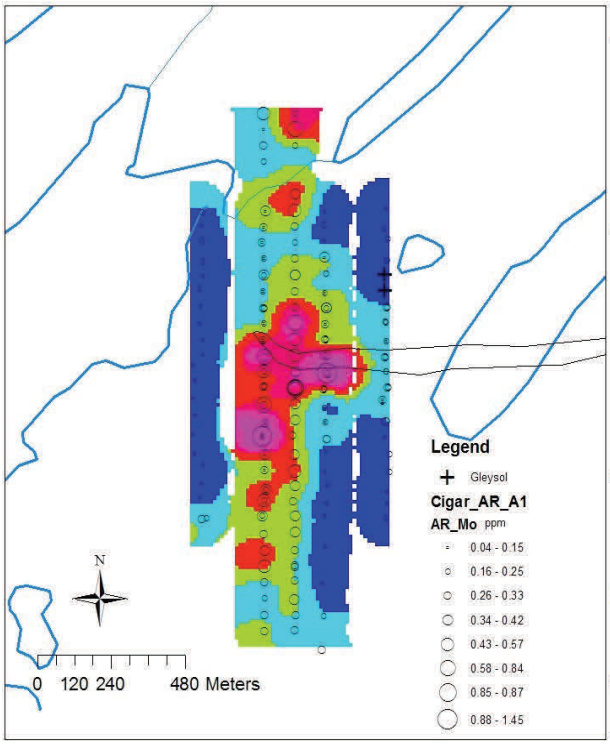

Fig 3.7 Raw molybdenum. A1 horizon. Aqua regia

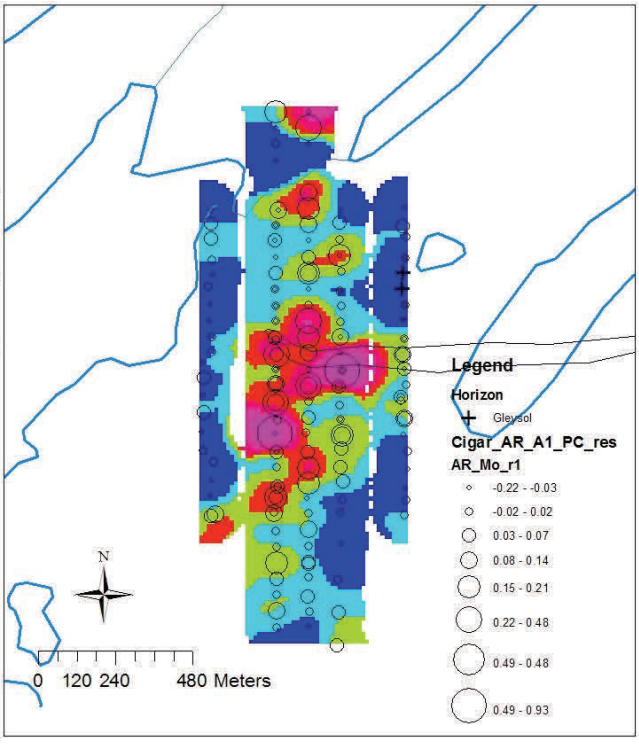

Fig 3.8 Residual molybdenum, after removing PC1.

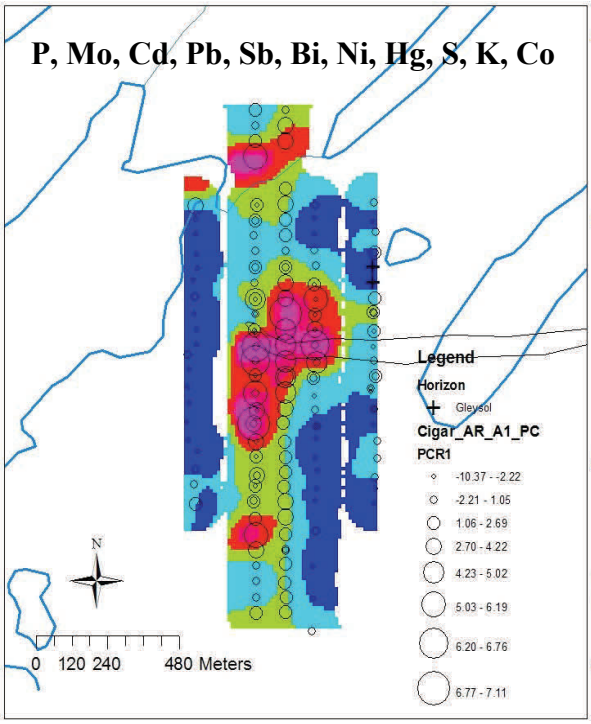

Fig. 3.9 PC 1. A1 horizon. Aqua regia

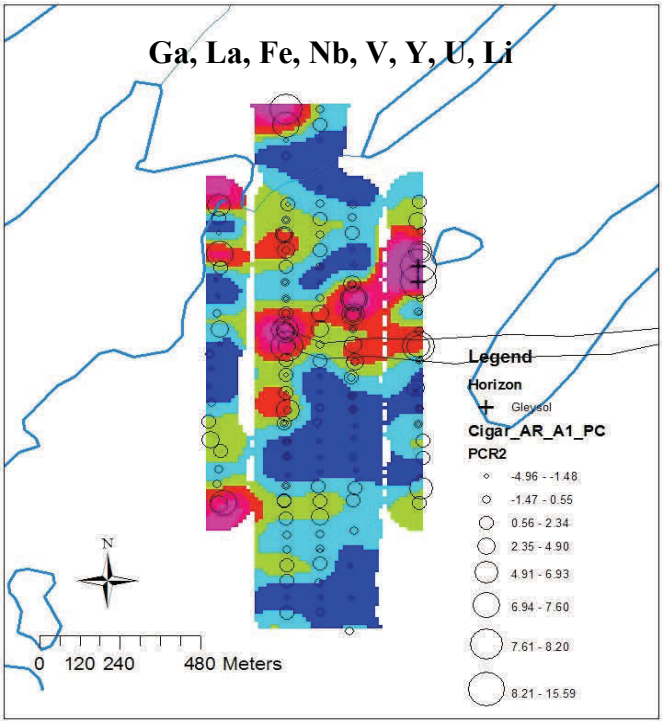

Fig 3.10 PC 2. A1 horizon. Aqua regia

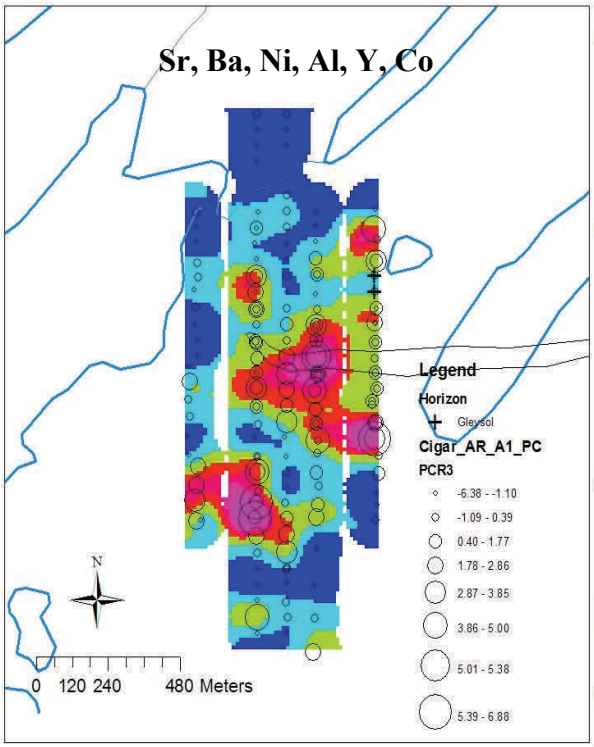

Fig 3.11 PC 3. A1 horizon. Aqua regia

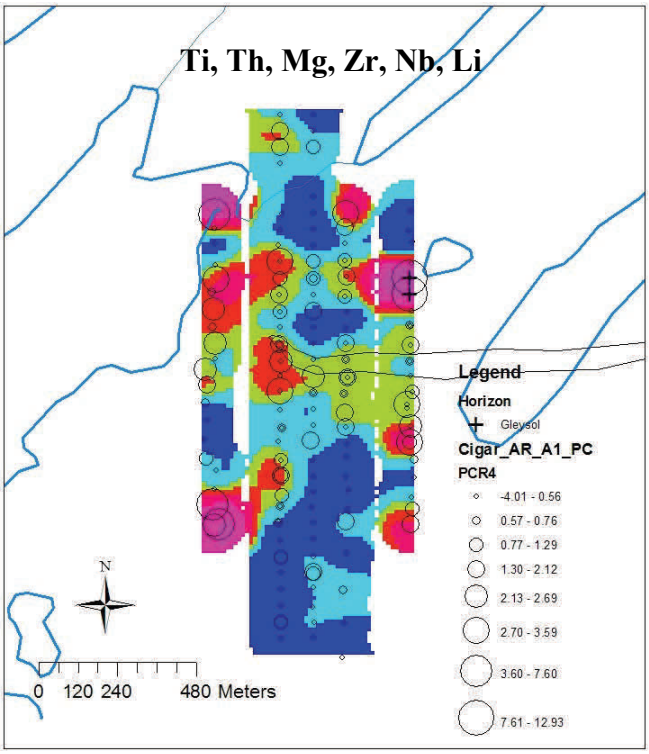

Fig 3.12 PC 4. A1 horizon. Aqua regia

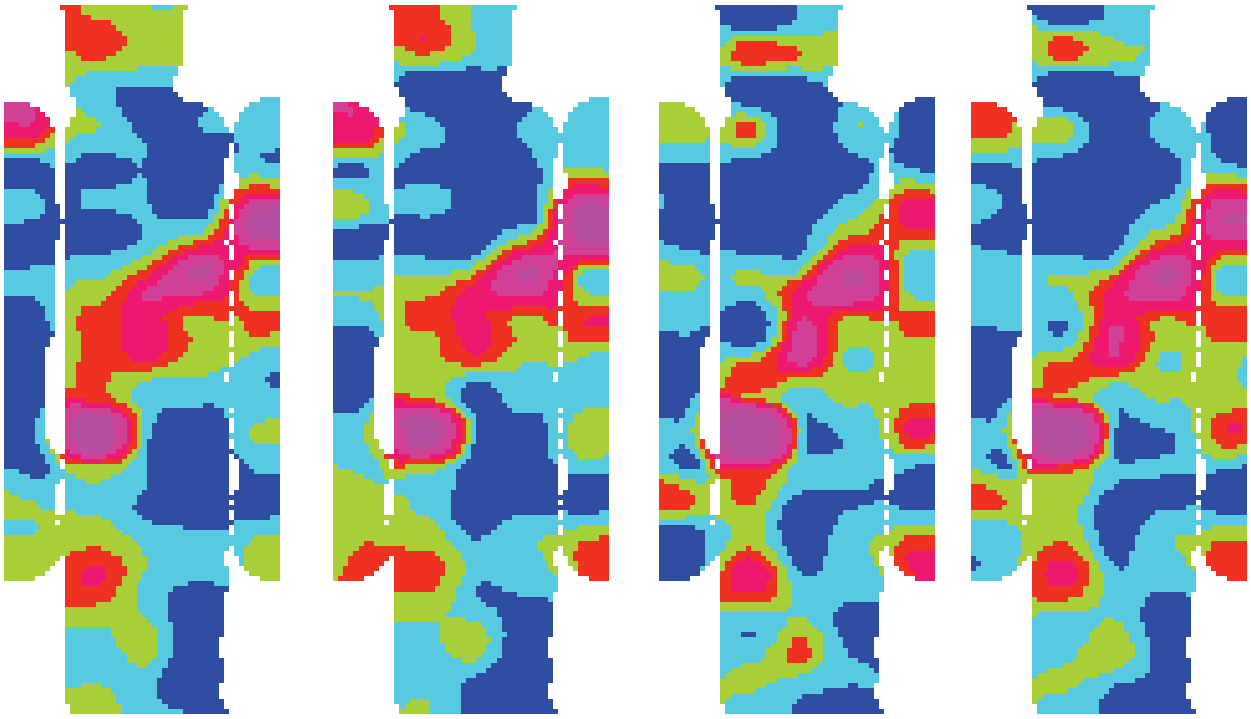

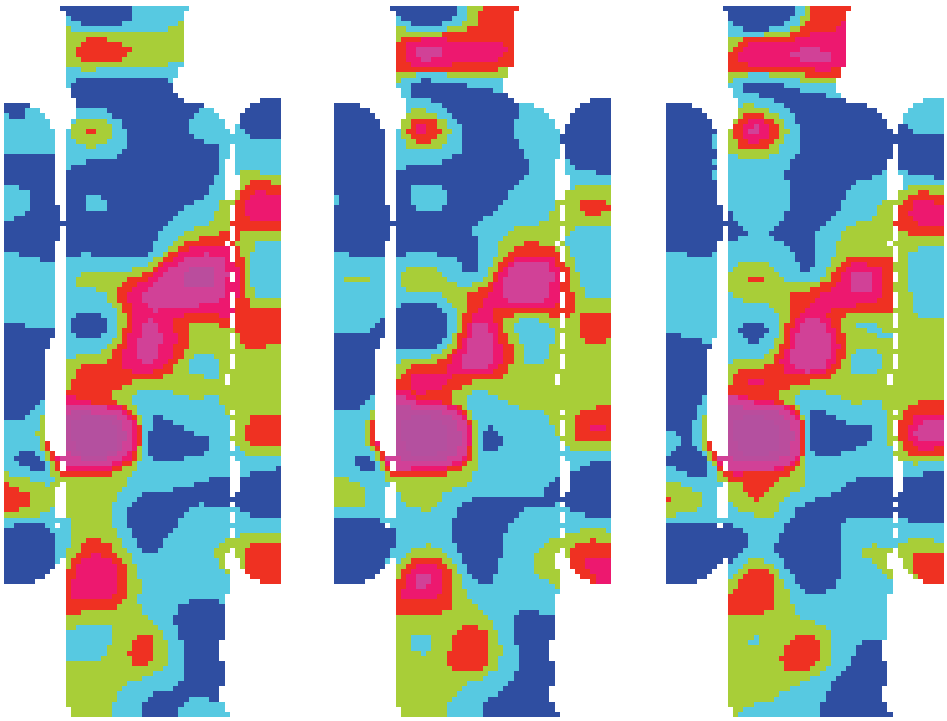

Fig. 3.13. Effect of successively removing effects of PC1 to PC6 on uranium (A1, AR)

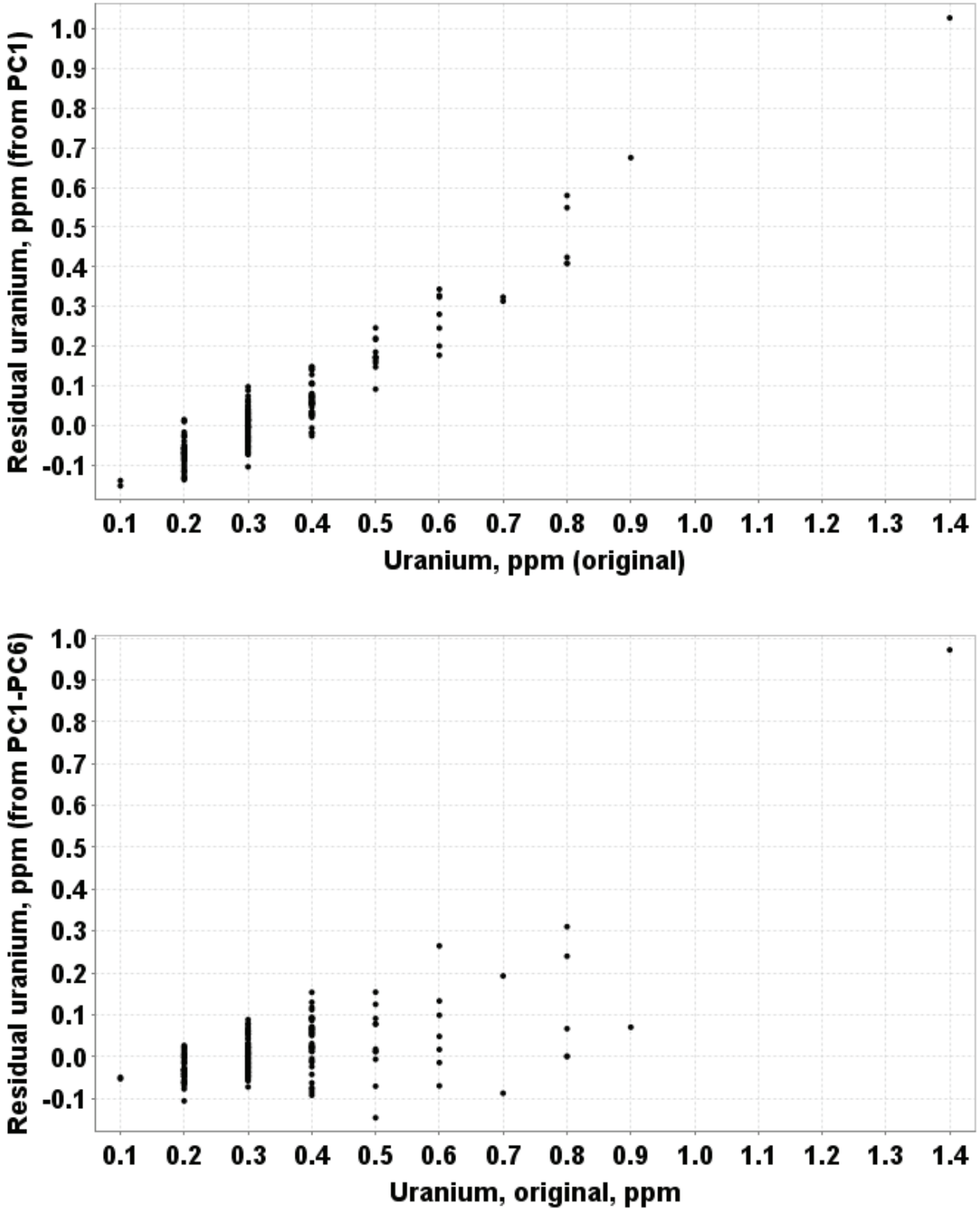

Fig 3.14. Top. Plot of raw uranium versus uranium residuals after removing the effect of PC1. Bottom. Plot of raw uranium versus uranium residuals after removing the effect of PC1 to PC6.

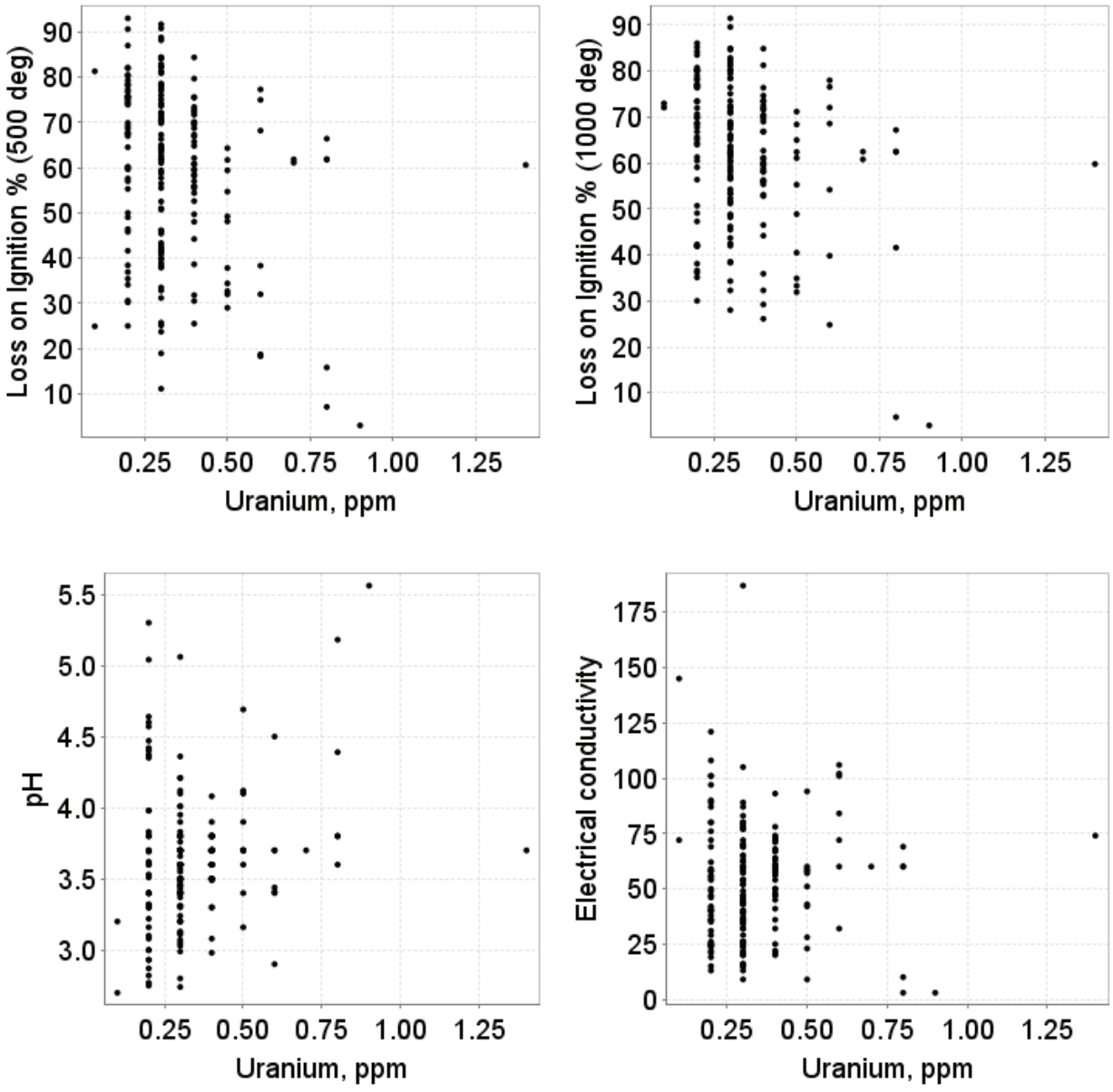

Fig 3.15 Uranium plots versus loss on ignition (LOI) at 500 and 1000 degrees, pH and electrical conductivity

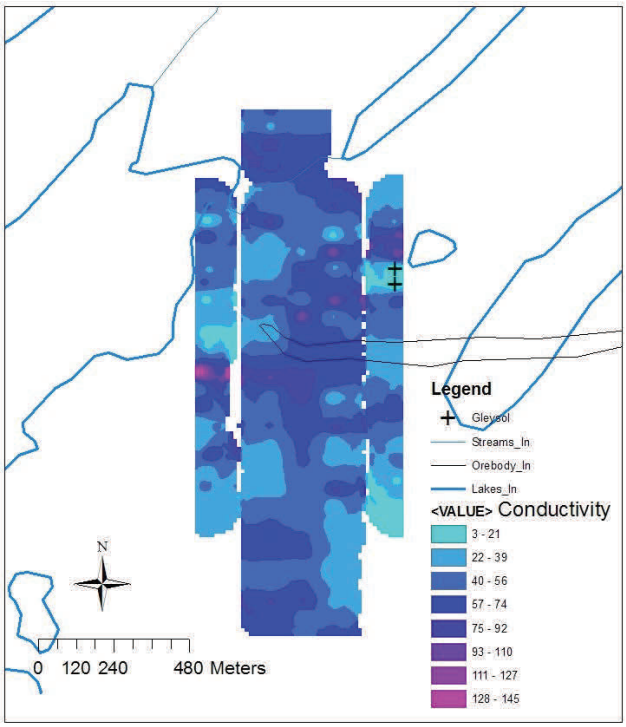

Fig 3.16 Cigar Lake. A1 Electrical conductivity

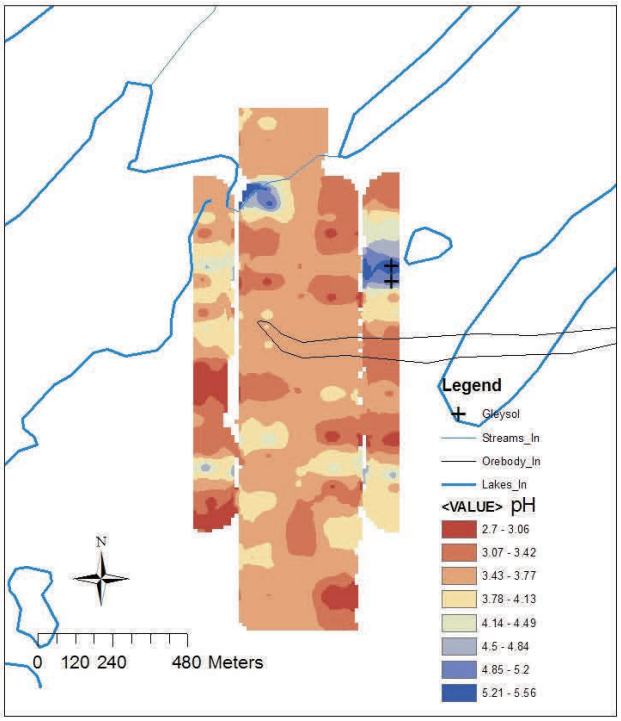

Fig 3.17 Cigar Lake. A1. pH

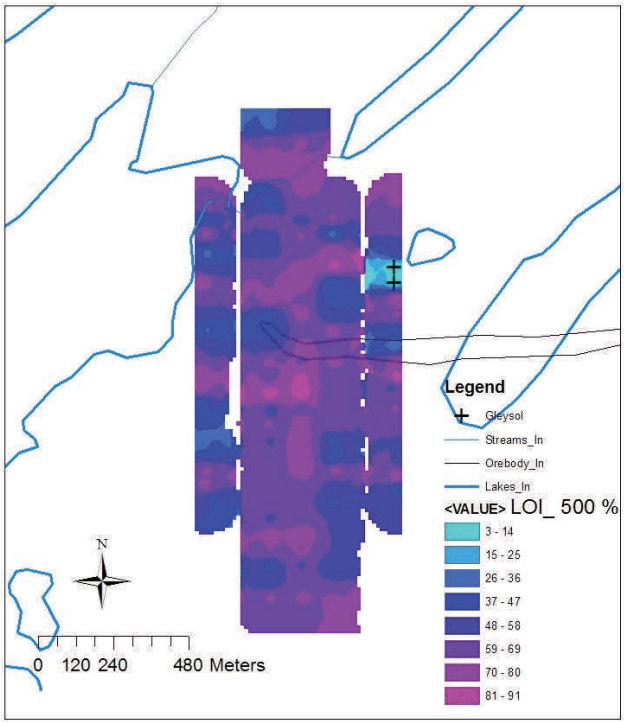

Fig 3.18 Cigar Lake. A1. LOI at 500ºC

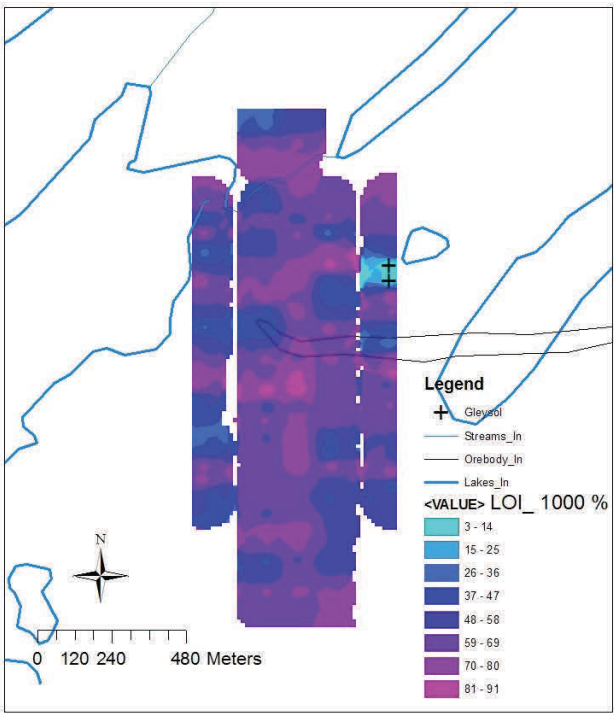

Fig 3.19 Cigar Lake. A1. LOI at 1000ºC

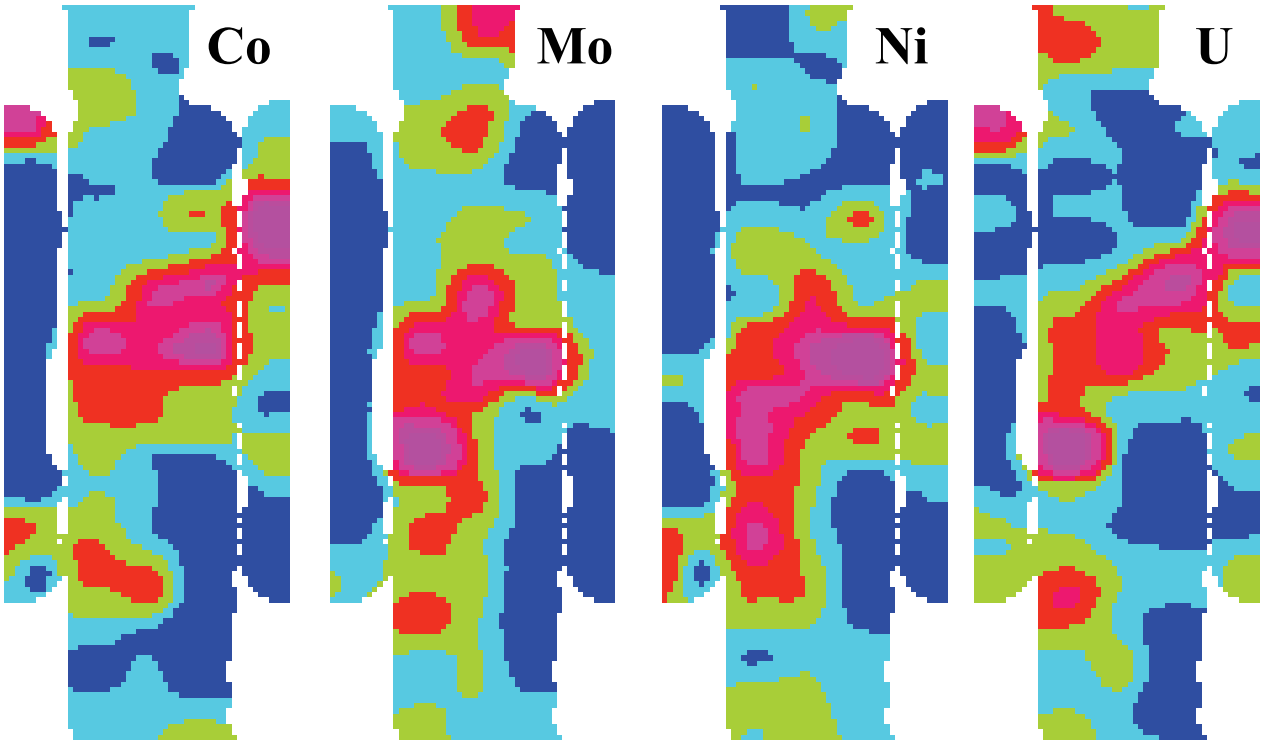

Fig 3.20 ABOVE: RAW DATA PLOTS. A1. Aqua Regia

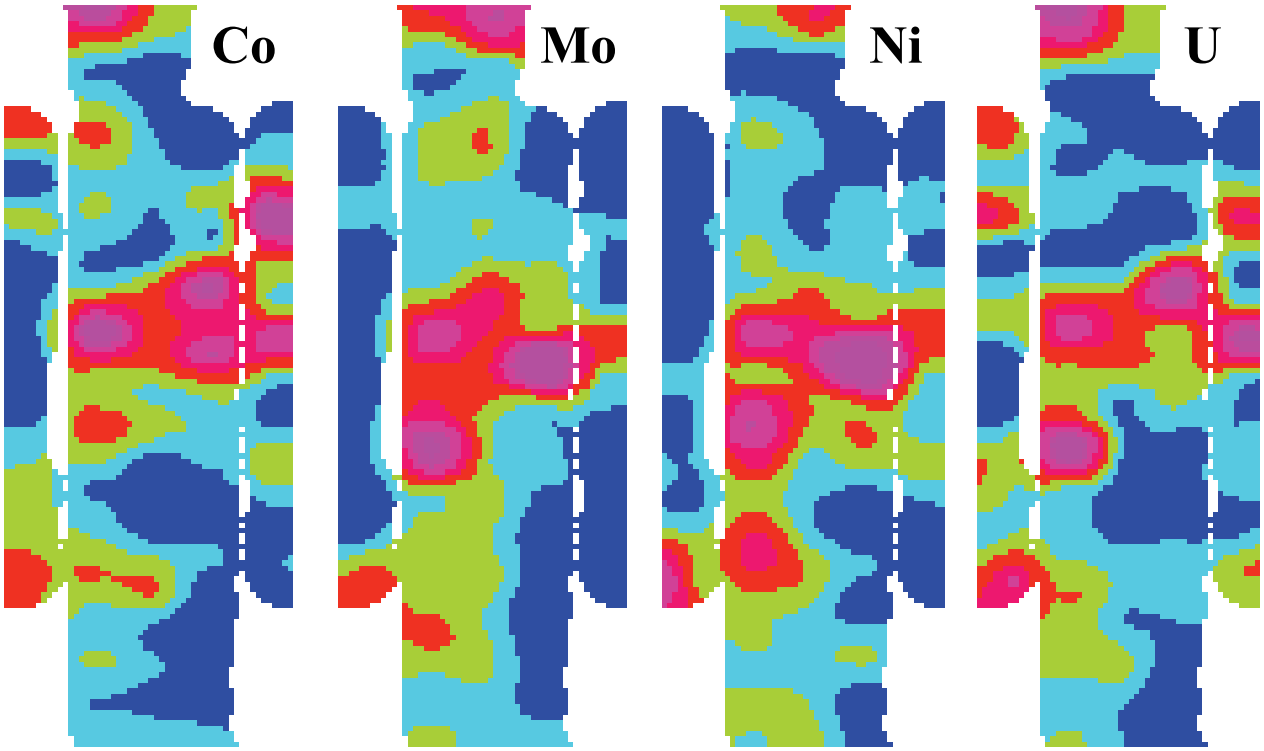

Fig 3.20 BELOW: DIVIDED BY LOI 1000. A1. Aqua Regia

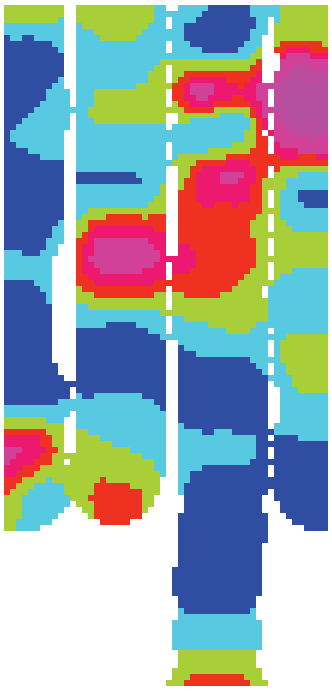

Co. AR. A1. 2008

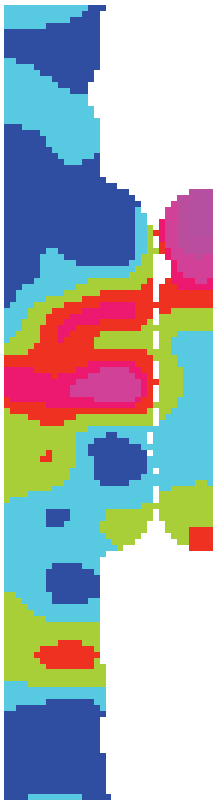

Co. AR. A1. 2009

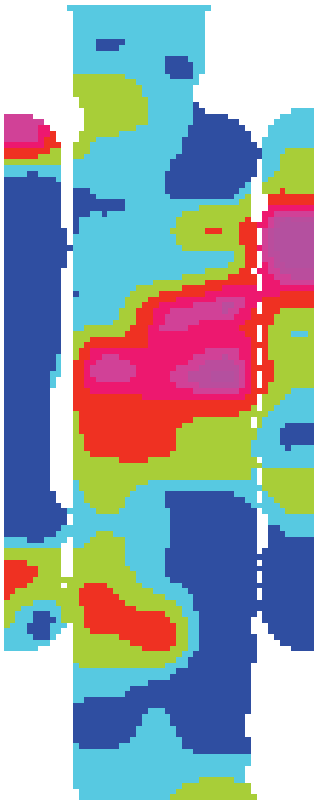

Co. 2008-2009

U. AR. A1. 2008

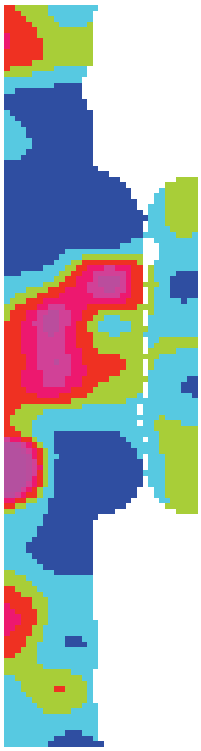

U. AR. A1. 2009

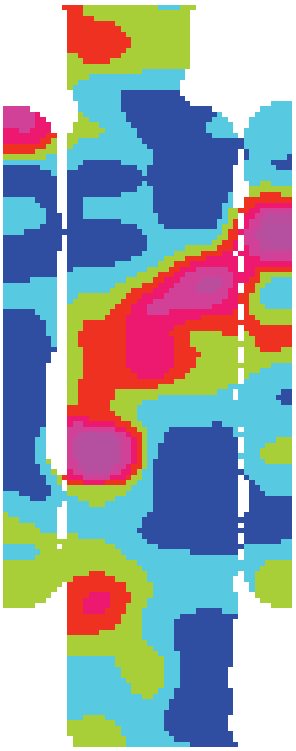

U. 2008-2009

Fig. 3.21 Co (above) and U (below) plotted by year, to test year-over- year variability

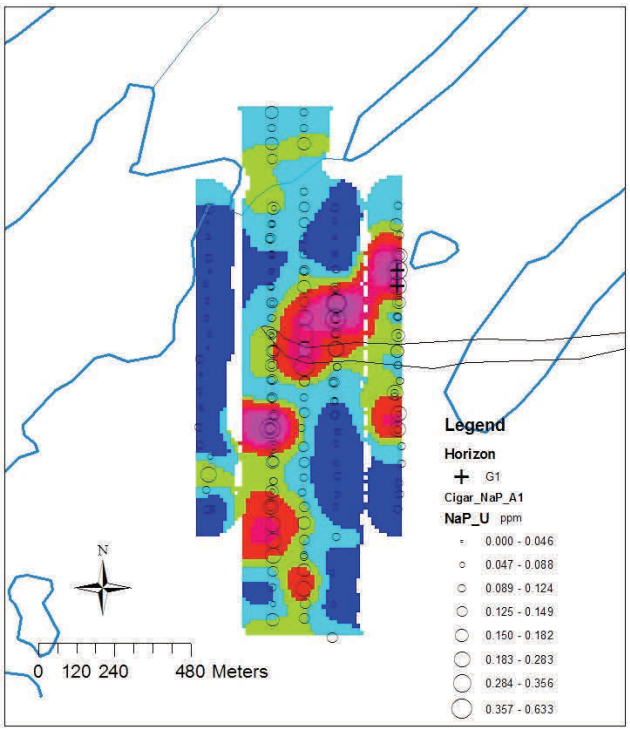

Fig 3.22 Uranium. A1 horizon. Sodium pyro leach.

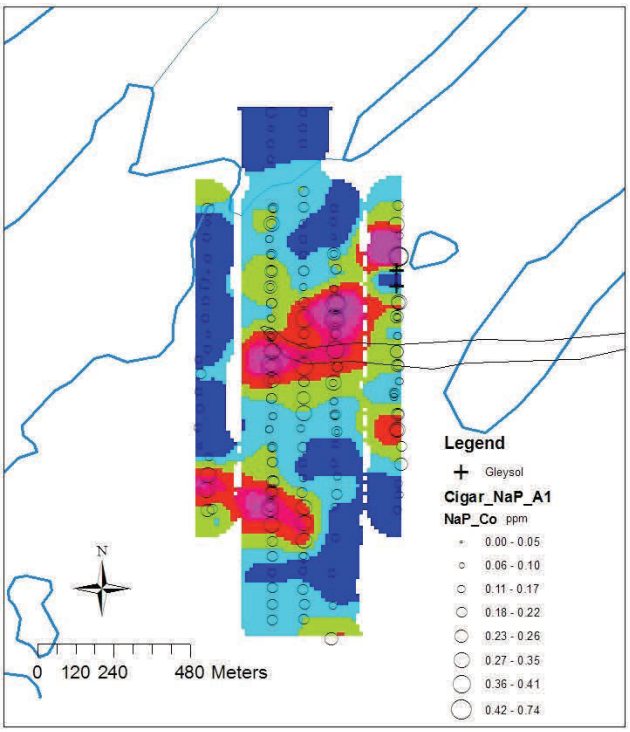

Fig 3.23 Cobalt. A1 horizon. Sodium pyro leach.

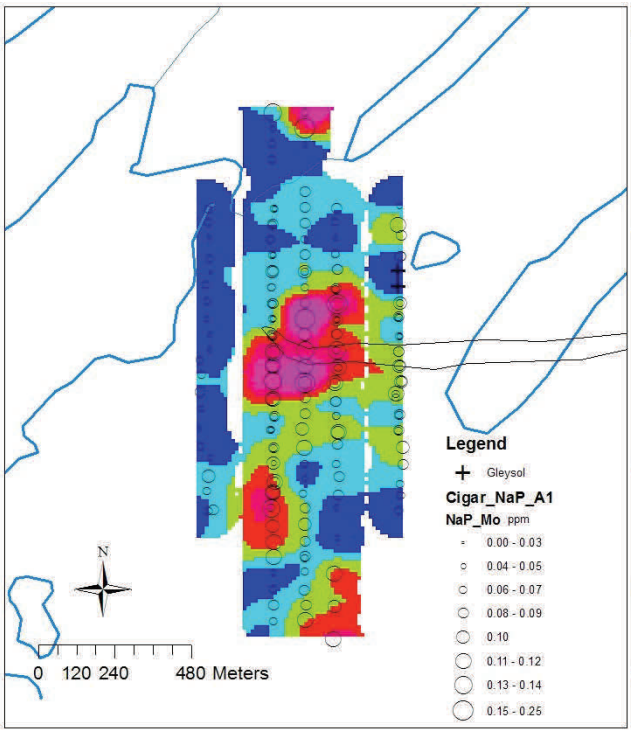

Fig 3.24 Molybdenum. A1 horizon. Sodium pyro

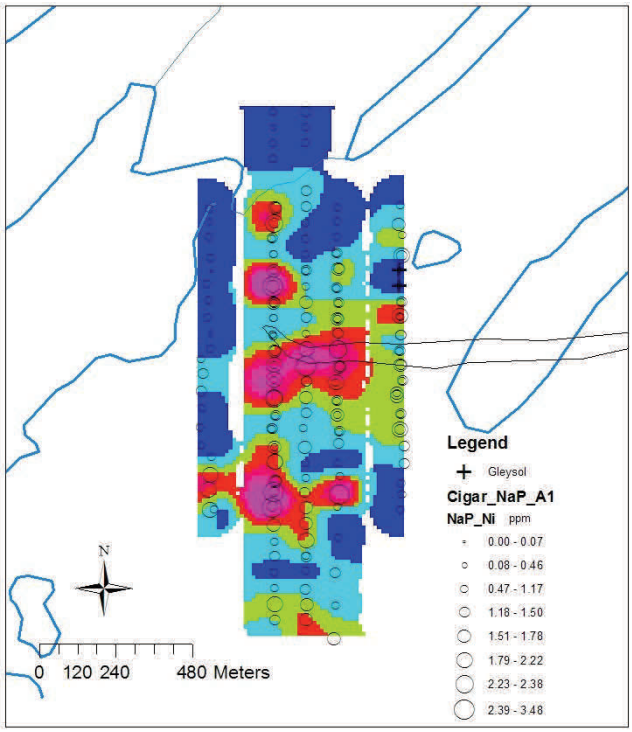

Fig 3.25 Nickel. A1 horizon. Sodium pyro leach.

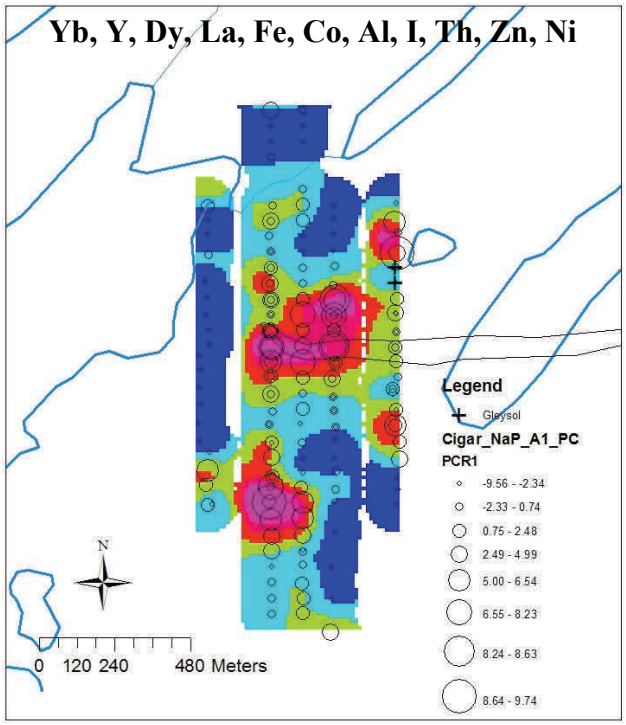

Fig 3.26 PC1 scores. A1 horizon. Sodium pyrophosphate leach.

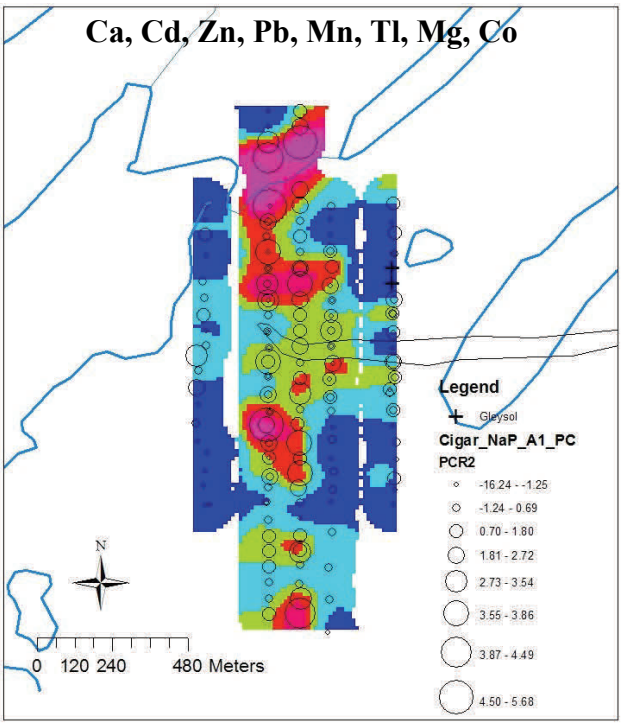

Fig 3.27 PC2 scores. A1 horizon. Sodium pyrophosphate leach

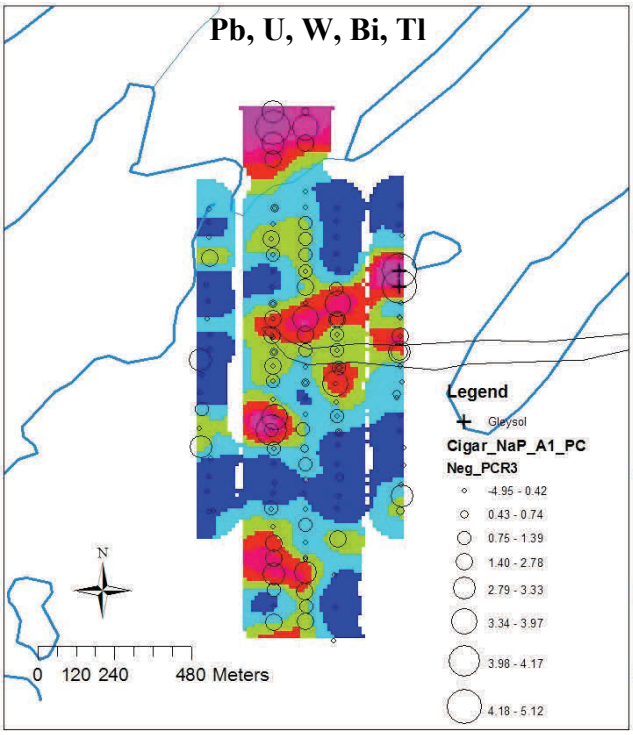

Fig 3.28 PC3 scores. A1 horizon. Sodium pyrophosphate leach.

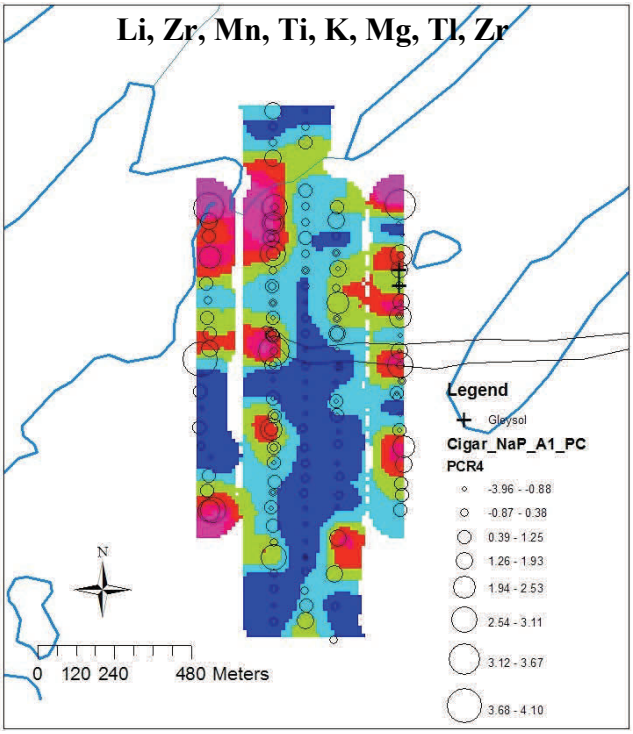

Fig 3.29 PC4 scores. A1 horizon. Sodium pyrophosphate leach.

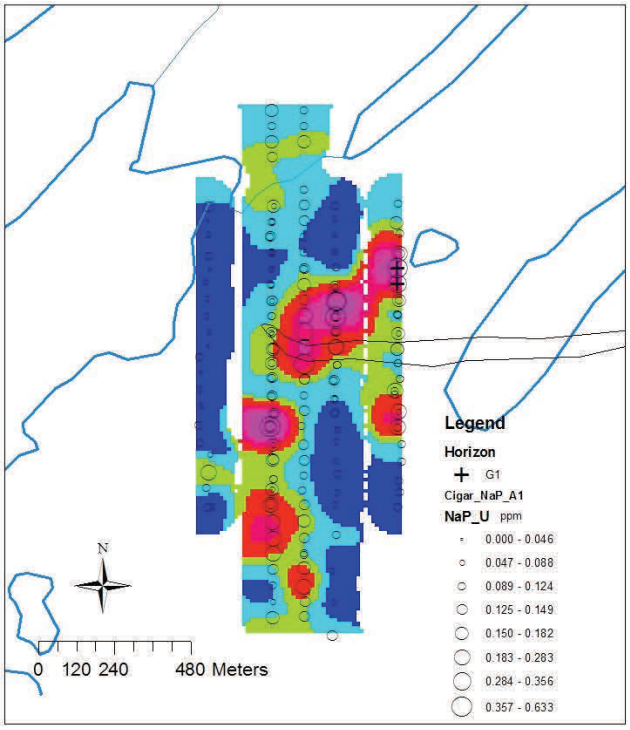

Fig 3.30 Uranium, original, A1 horizon. Pyro leach.

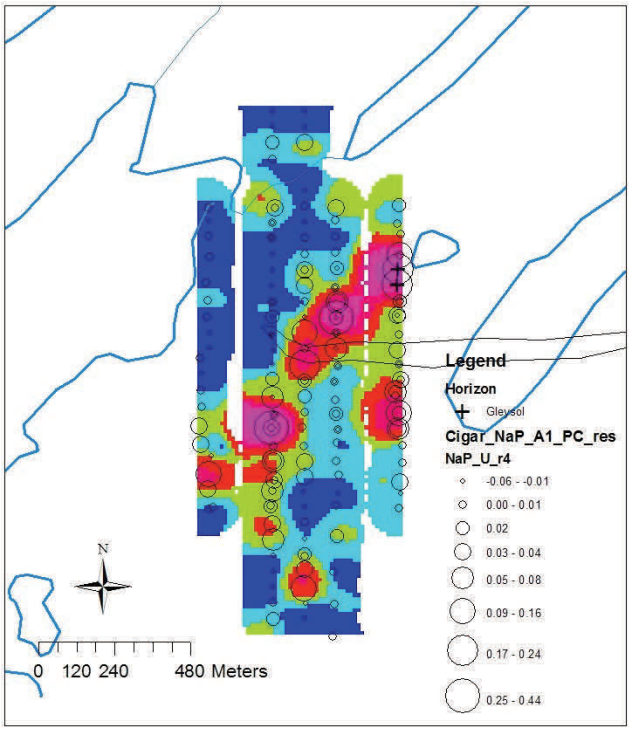

Fog 3.31 Uranium residuals after removing PC1.

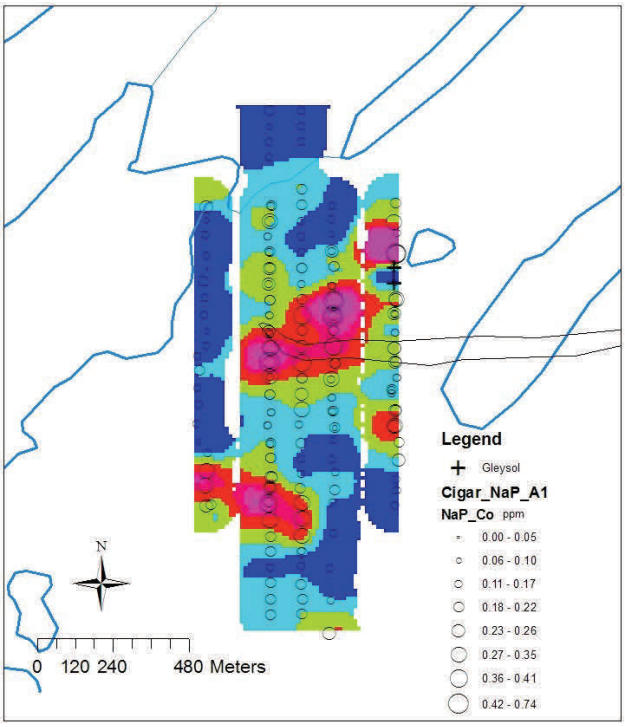

Fig 3.32 Cobalt, original, A1 horizon. Sodium pyro leach.

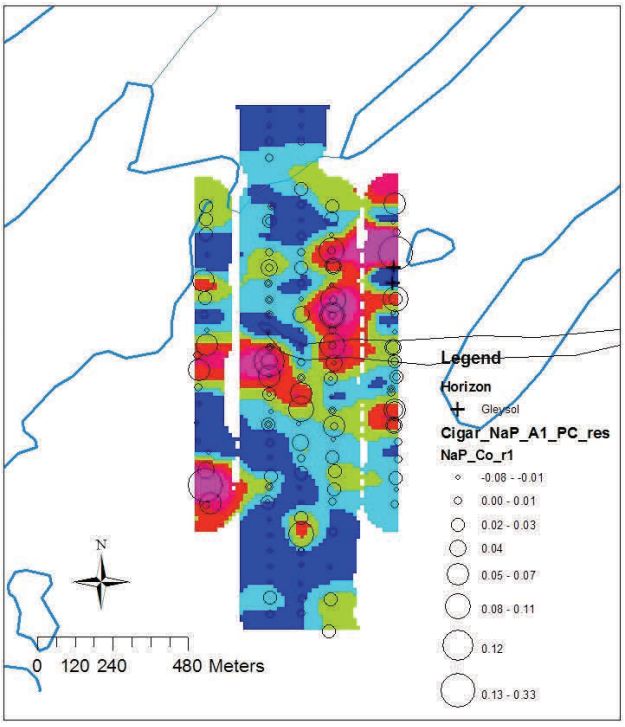

Fig 3.33 Cobalt residuals after removing PC1.

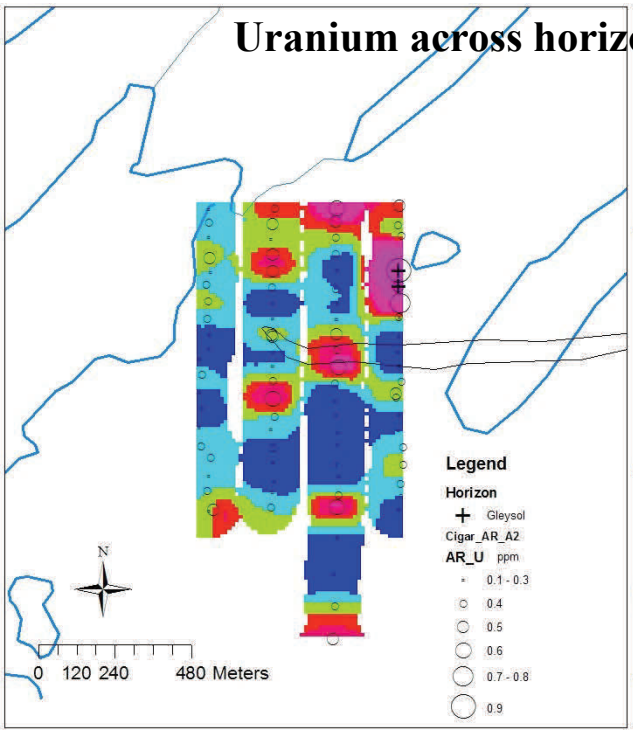

Fig. 3.34 Uranium. A2 horizon. Aqua regia leach

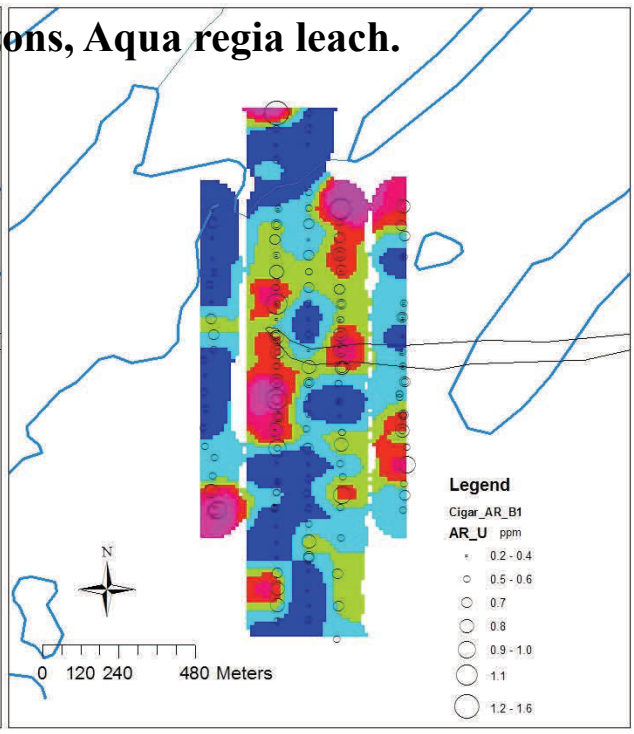

Fig. 3.35 Uranium. B1 horizon. Aqua regia leach

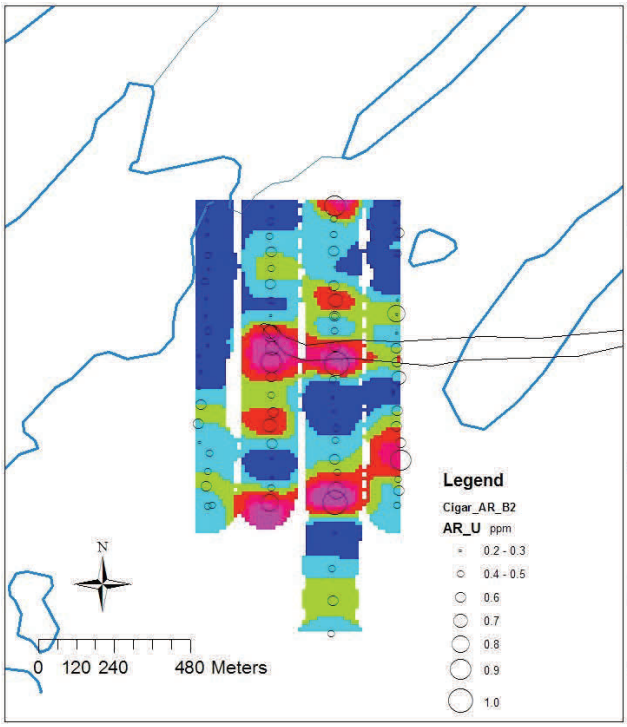

Fig. 3.36 Uranium. B2 horizon. Aqua regia leach

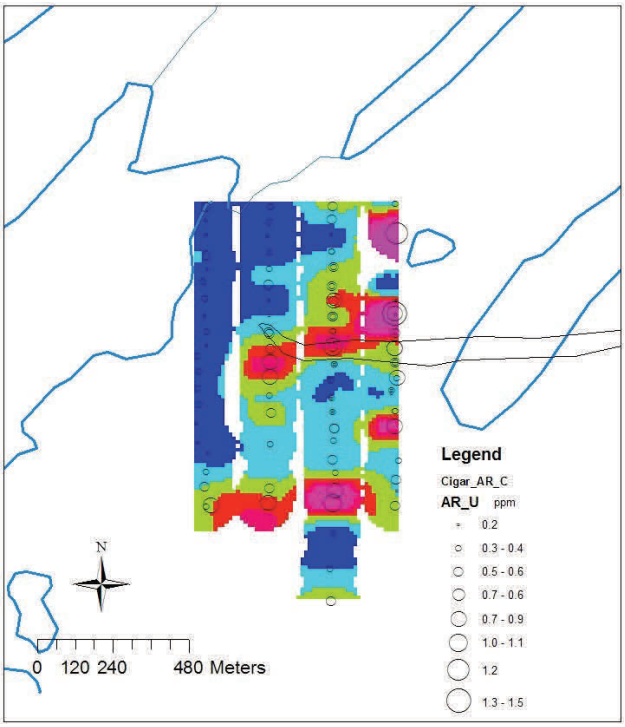

Fig 3.37 Uranium. C horizon. Aqua regia leach

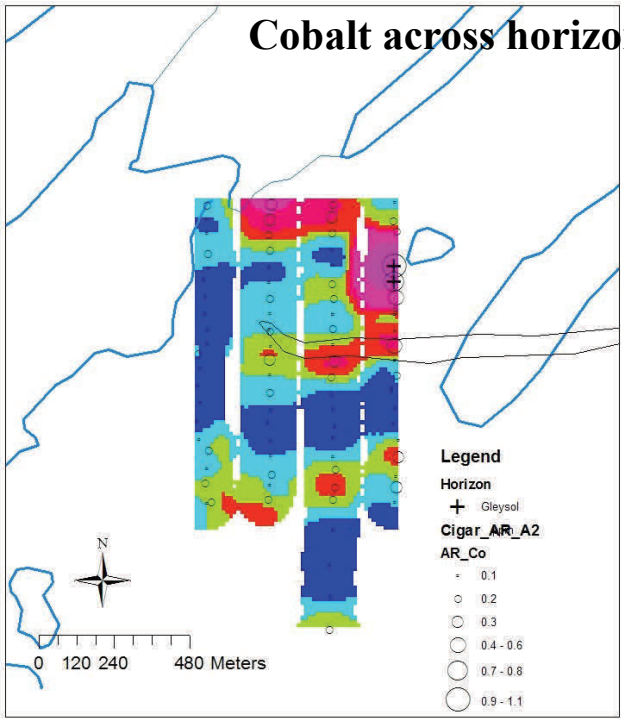

Fig. 3.38 Cobalt. A2 horizon. Aqua regia leach.

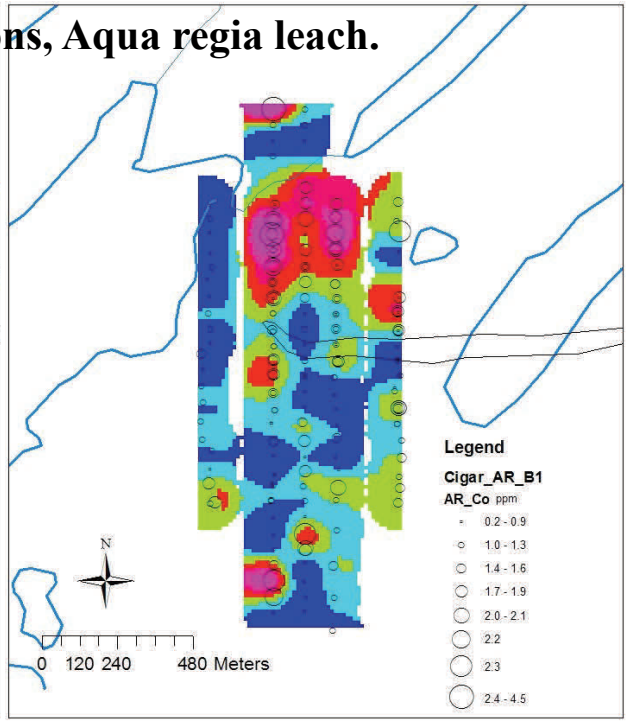

Fig. 3.39 Cobalt. B1 horizon. Aqua regia leach.

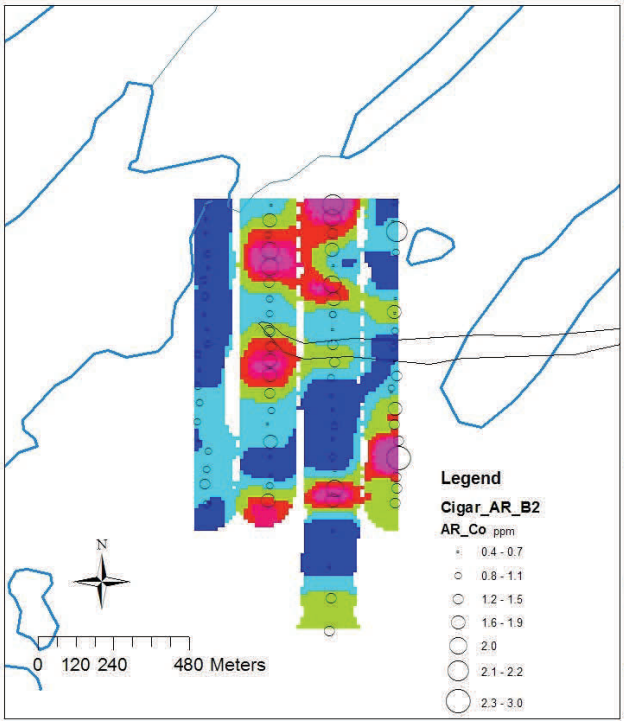

Fig 3.40 Cobalt. B2 horizon. Aqua regia leach.

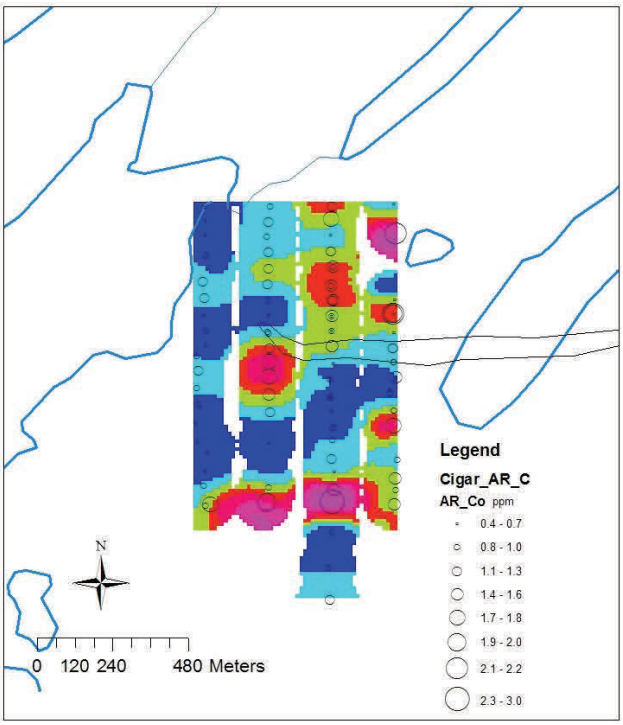

Fig 3.41 Cobalt. C horizon. Aqua regia leach.

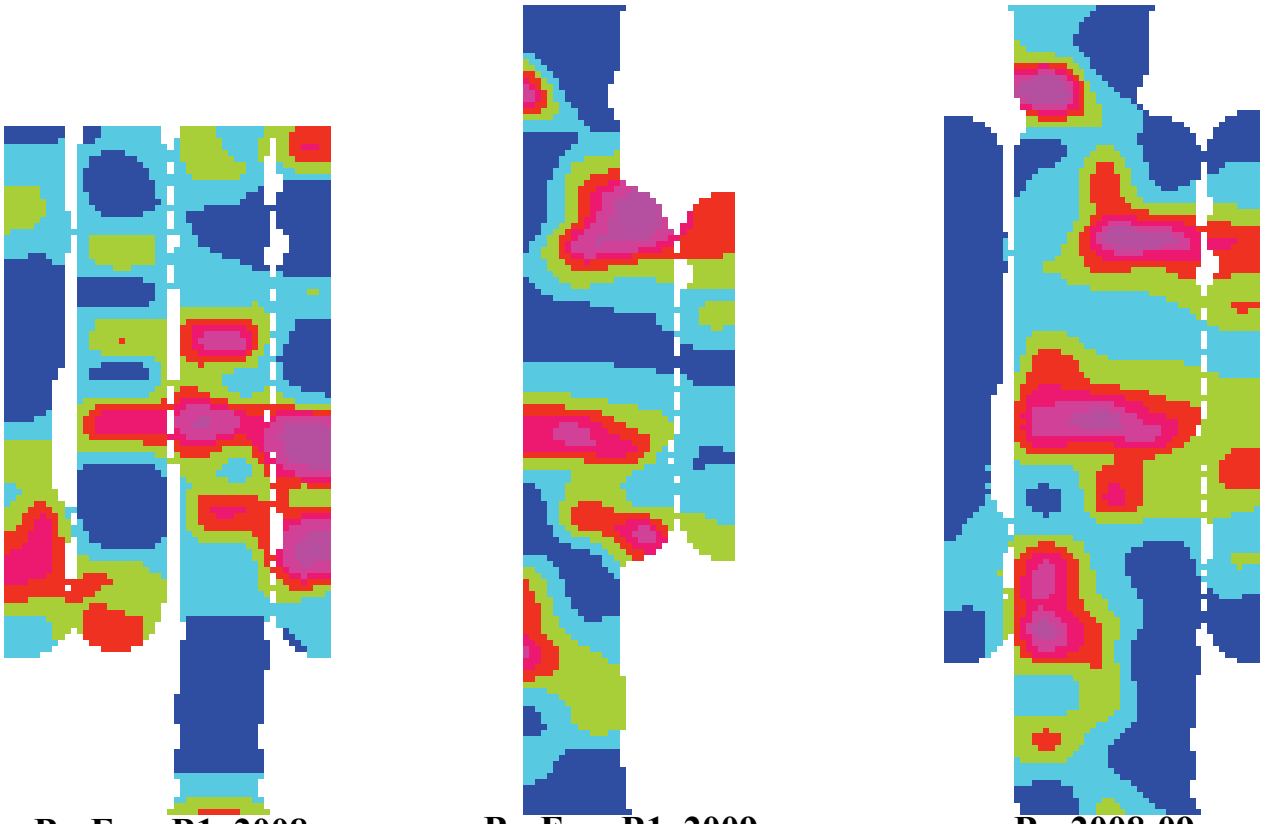

Br. Enz. B1. 2008
Median=257 ppb

Br. Enz. B1. 2009
Median=464 ppb

Br. 2008-09
Median=354 ppb

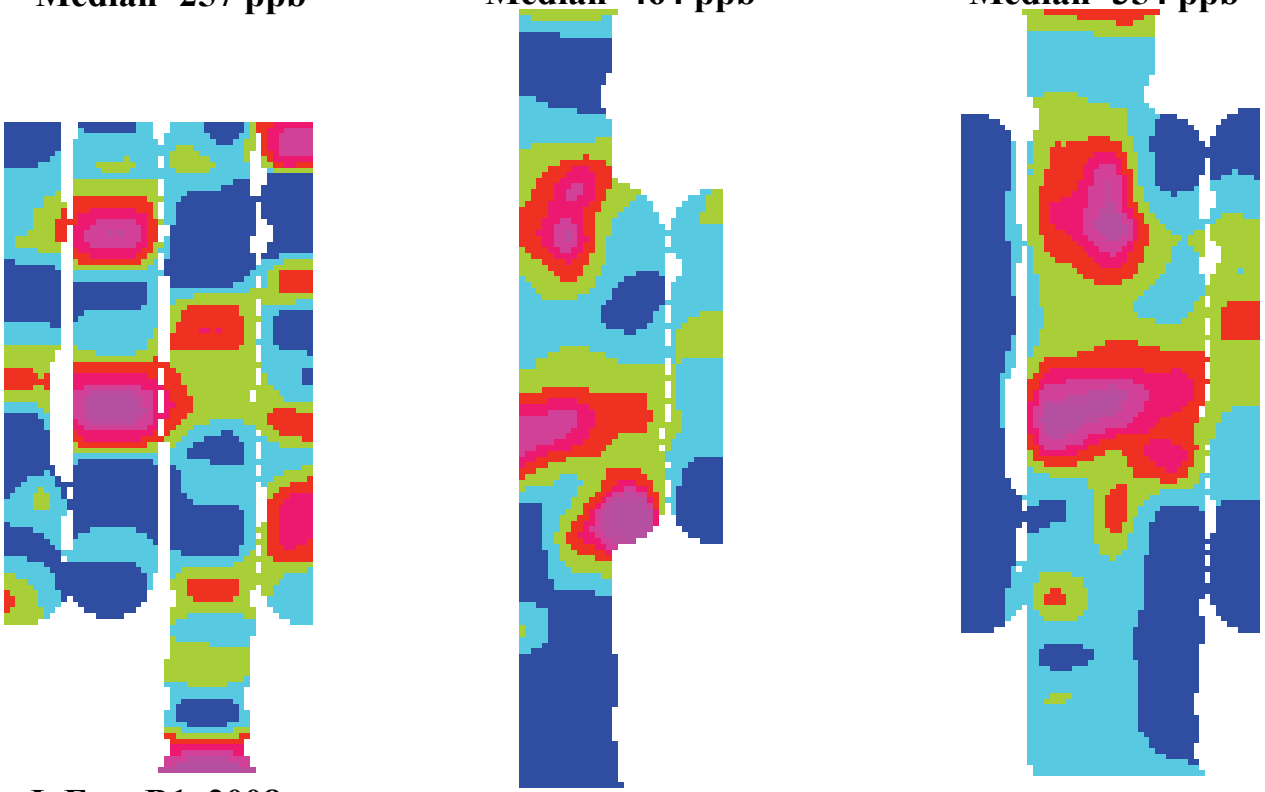

I. Enz. B1. 2008
Median=18 ppb

I. Enz. B1. 2009
Median=50 ppb

I. 2008-09
Median=27 ppb

Fig. 3.42. Halide elements in the B1 horizon by enzyme leach.

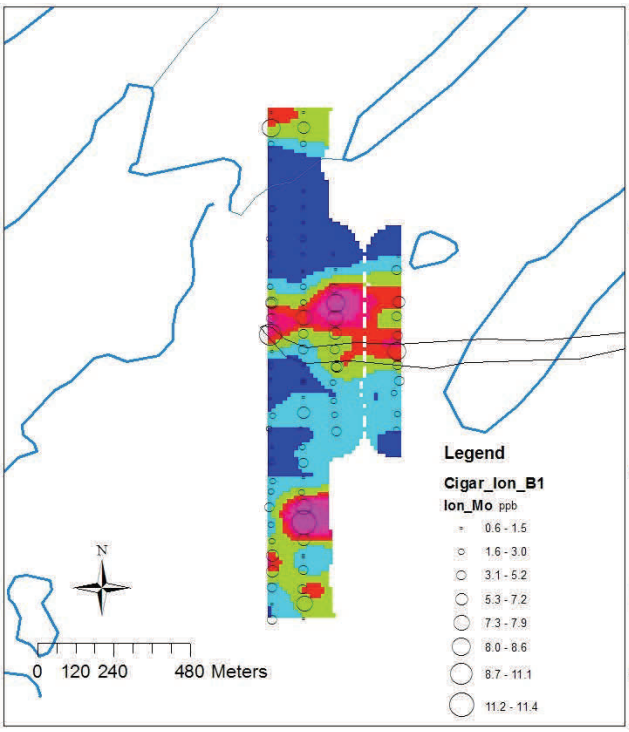

Fig. 3.43 Molybdenum. B1 horizon. Ionic

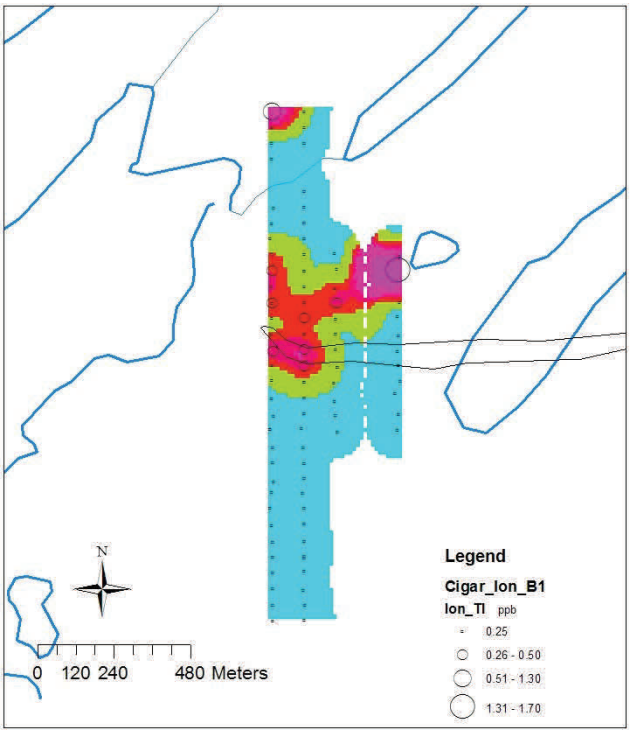

Fig. 3.44 Thallium. B1 horizon. Ionic leach.

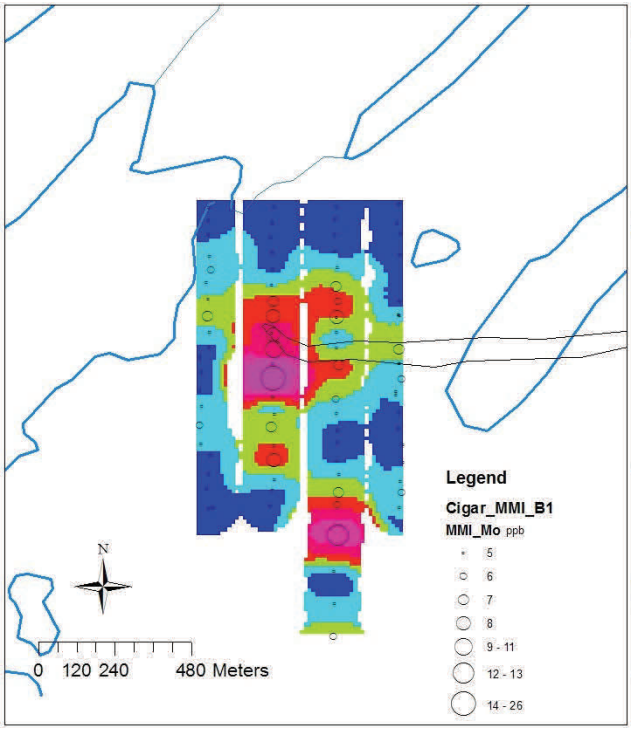

Fig. 3.45 Molybdenum. B1 horizon. MMI leach. Data from 2008 only.

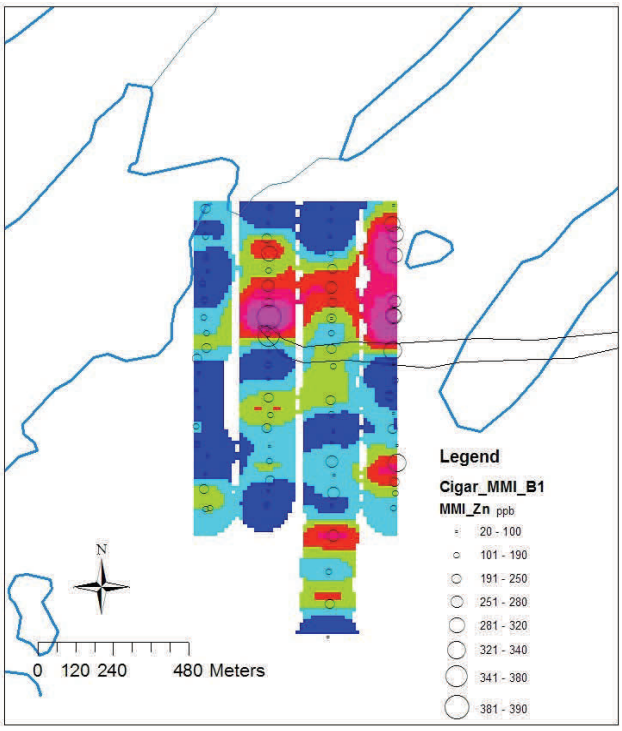

Fig. 3.46 Zinc. B1 horizon. MMI leach. Data from 2008 only.

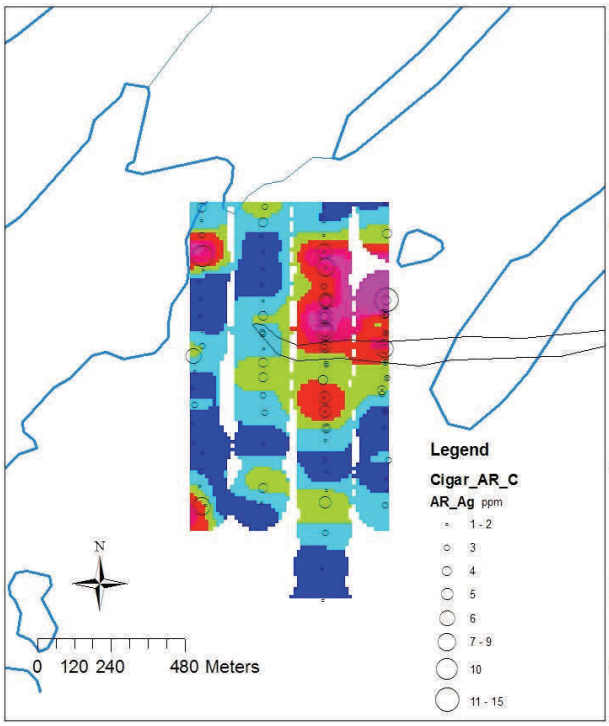

Fig 3.47 Silver, aqua regia. C horizon.

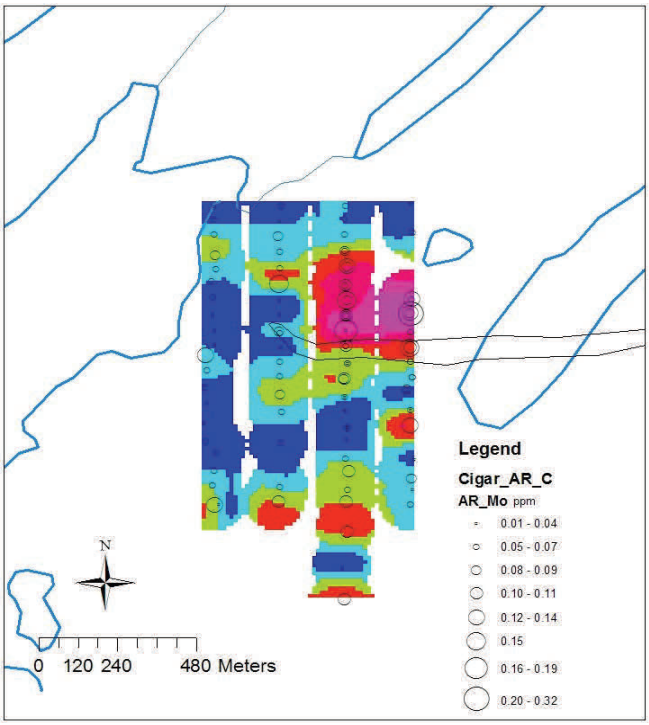

Fig 3.48 Molybdenum, aqua regia. C horizon.

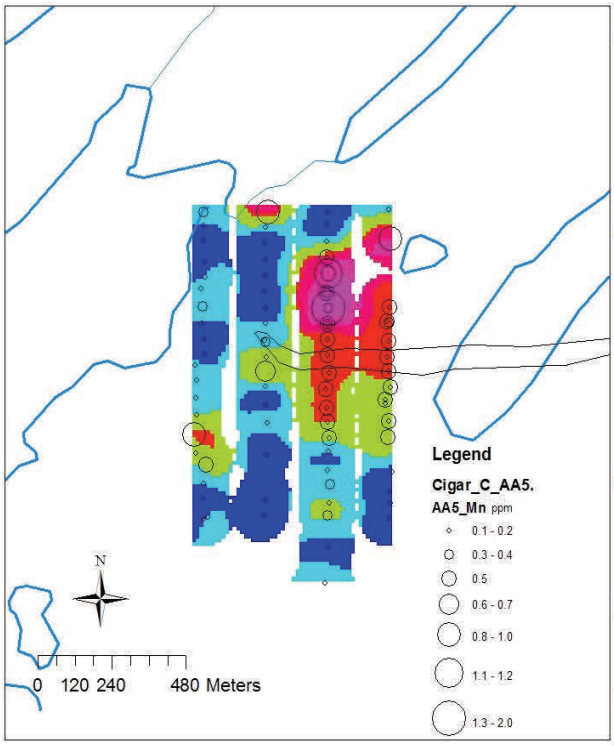

Fig 3.49 Manganese. C horizon. Ammonium acetate leach.

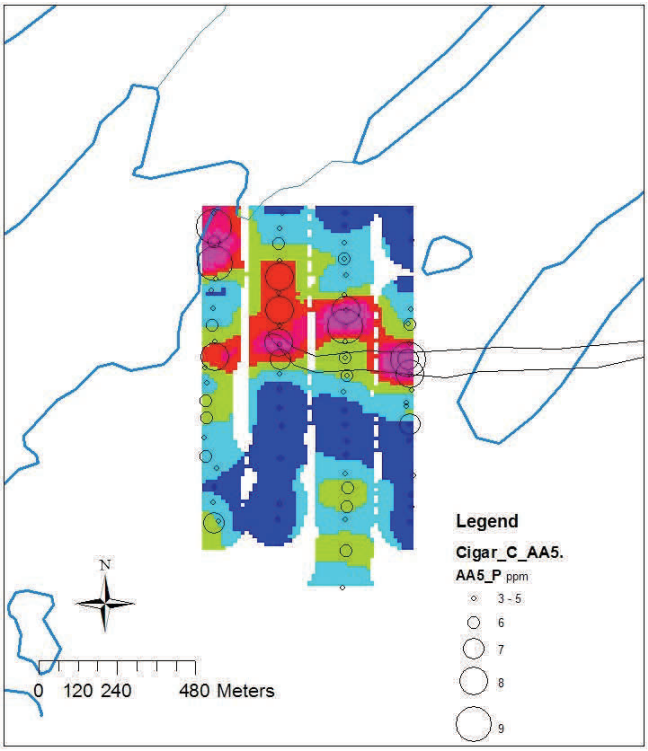

Fig 3.50 Phosphorus. C horizon. Ammonium acetate leach.

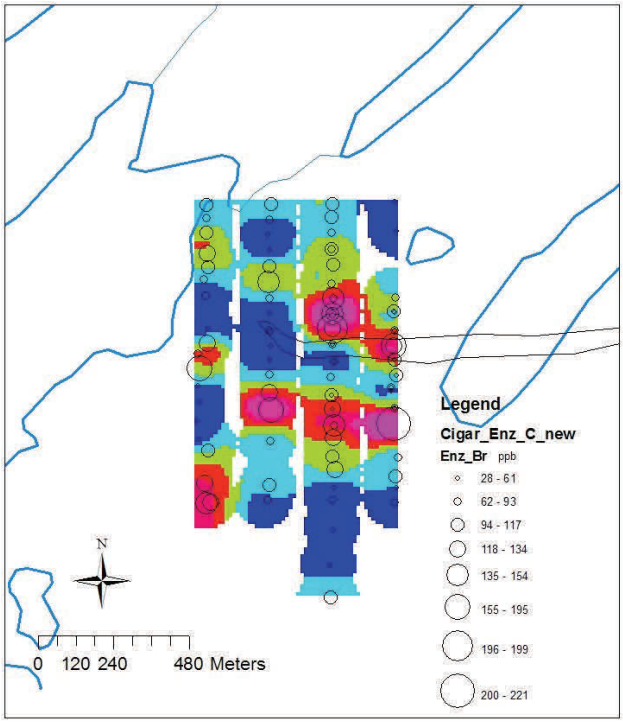

Fig 3.51 Bromine. C horizon. Enzyme leach. 2008 only

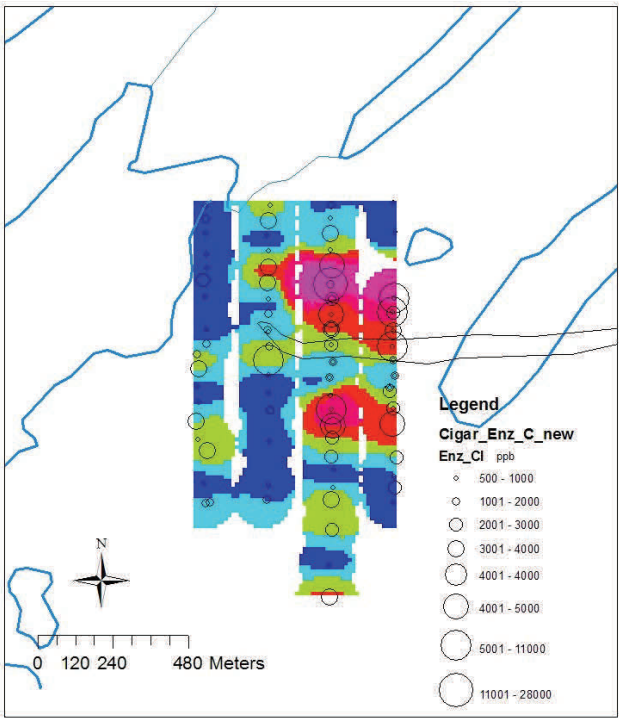

Fig 3.52 Chlorine. C horizon. Enzyme leach. 2008 only

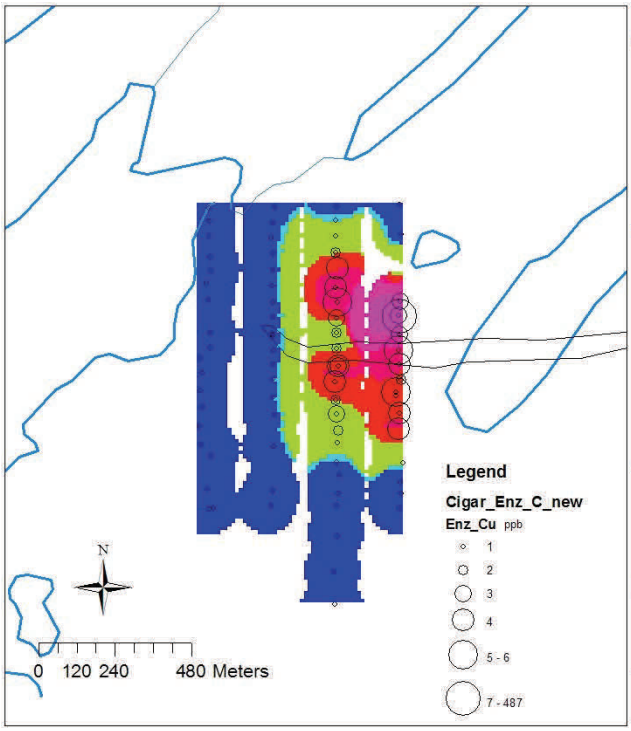

Fig 3.53 Copper. C horizon.

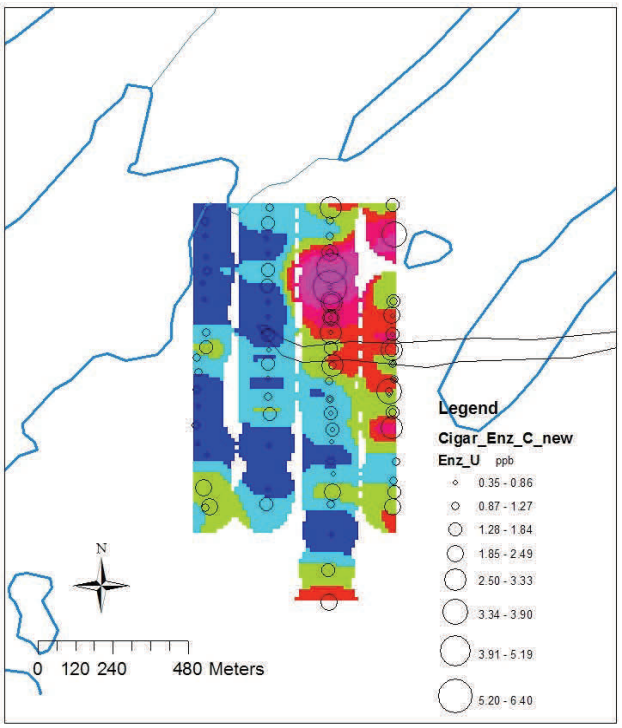

Fig 3.54 Uranium. C horizon.

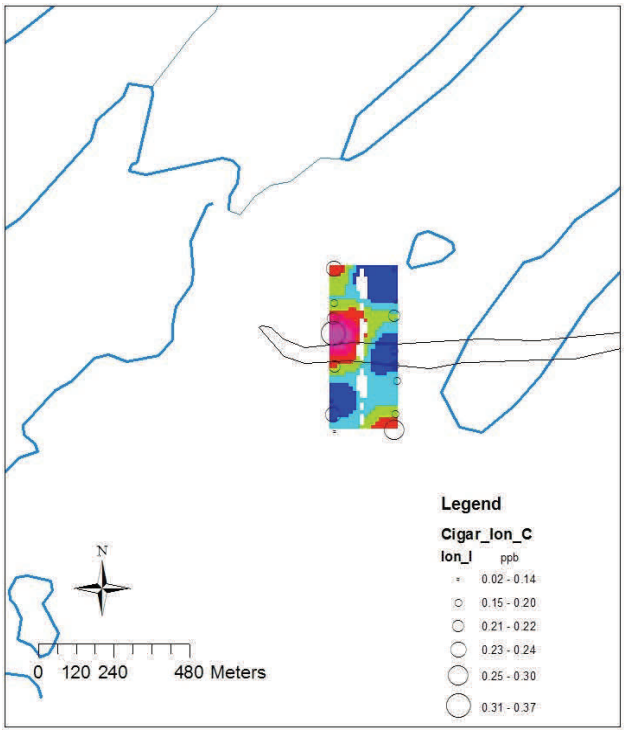

Fig. 3.55 Iodine. C horizon. Ionic leach. 2009 data only on lines 1 and 2.

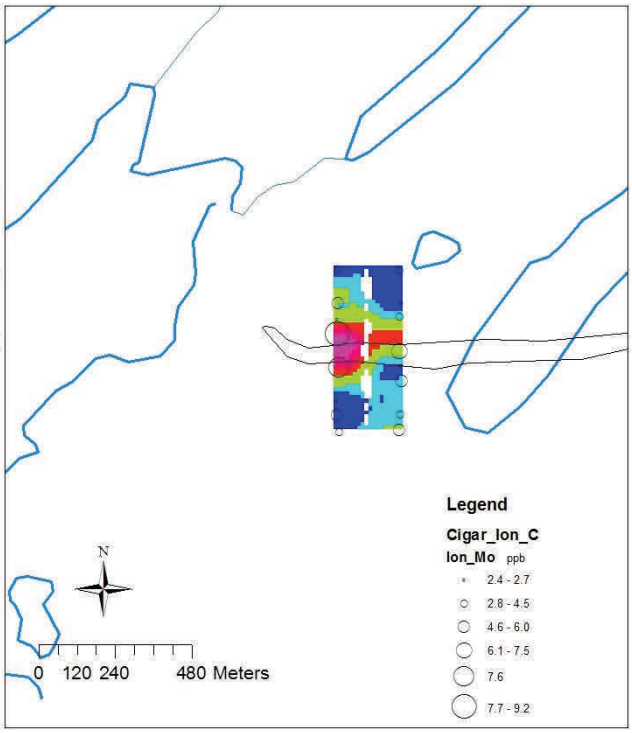

Fig. 3.56 Moly. C horizon. Ionic leach. 2009 data only on lines 1 and 2.

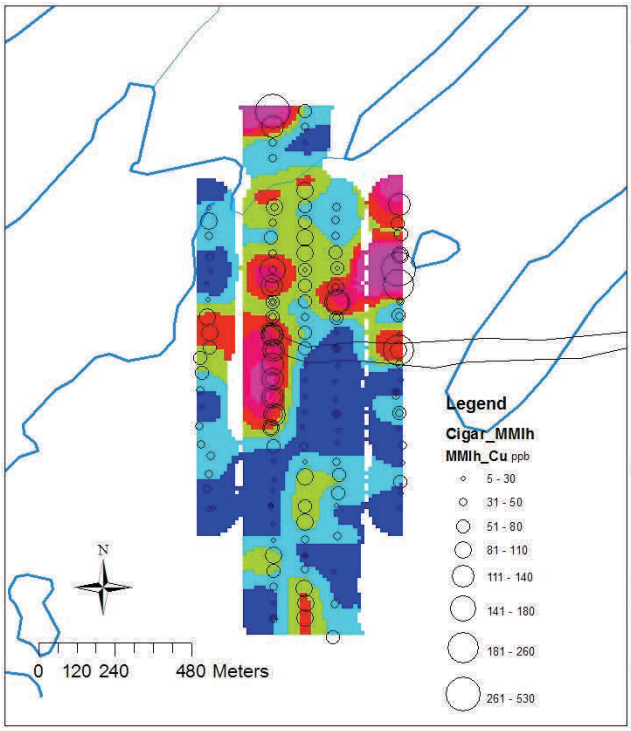

Fig 3.57 Copper. MMI leach on MMI horizon.

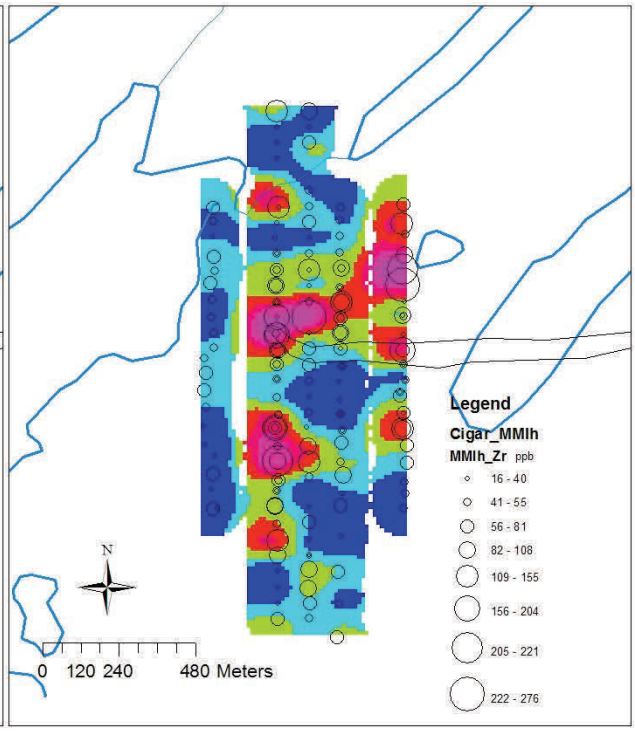

Fig 3.58 Zirconium. MMI leach on MMI horizon.

3.3 Key Results from McClean Lake.

A1 horizon

Because the McClean Lake deposit is not covered by such a great thickness of Athabasca sandstone as compared to Cigar Lake (roughly 160 m versus 400 m), one might perhaps expect a stronger response in the soil geochemistry. Although we do see a response in the A1 horizon, similar in some respects to the Cigar anomalies in A1, the interpretation is confounded by the presence of peat in the north part of the area, mostly in low-lying areas (as discussed previously in the Description of Areas section.)

Following the approach taken with the Cigar data in A1 aqua regia, a PC analysis was carried out to look at the main characteristics of data. As was noticed for the 2008 data, a number of associated elements show a marked increase in the south part of the area compared with the north. This is immediately apparent in the first PC, shown in Fig. 3.59, with a prominent anomaly in the southern and central part of the sample area. [*The loadings on PC1 are negative, but large—the sign of the scores has been changed to make interpretation easier*]. The elements associated with this component are Zn, Hg, Cd, Ba, Ni, Sb and Cu. Plots of Ba, Ni, Hg and Zn confirm the presence of this dominant feature (Figs. 3.63-3.66). Interpretation of this pattern is unclear, but one conclusion is that the difference may reflect a change in the basement, moving from strata that contain graphitic metapelites (north) to a more uniform Archean gneiss in the south (Fig. 2.13). Two other possible explanations: there could be a significant change in till composition from north to south; or the change might be related to the presence of peat to the north, whereas the south is higher in elevation and peat-free.

Box and whisker plots of -PC1, PC2, PC3 and PC8 show that the elements correlated with PC1 are generally low in value when peat is present, whereas the elements correlated with PC2 are higher in the peat samples than in normal A1 humus. PC3 and PC8 show no clear relationship with peat.

Although there is a gradation in pH across the area in the humus horizon, (Fig. 3.71) with peat samples tending to be less acid than normal A1 humus, uranium has no clear relationship with pH (Fig. 3.70), nor does normalizing uranium to pH make any change to the pattern of the uranium map (Fig. 3.72).

Maps of LOI at 500 degrees and LOI at 1000 degrees have a very similar pattern (Fig. 3.73 and 3.74), with little clear relation to peat samples (Fig. 3.75). Electrical conductivity does not show any pattern related to the chemistry in A1 (Fig. 3.76).

Using the same argument as in the case at Cigar, it was decided to remove the effect of PC1 from the most interesting elements (to account for the effect of the main variation that is likely to be in the average composition of the till). However, the effect of peat on PC1 was first removed by leveling it against peat. This involved a simple percentile transformation of values in the peat group, and a similar transformation of the non-peat group, followed by recombination of the two percentile sets. The residuals for selected elements were then calculated by regressing the element against the leveled PC. The goal was to remove both the effect of average geology and of peat.

The effect of ratioing the aqua regia and sodium pyrophosphate data by loss on ignition was also found to be helpful, particularly for the sodium pyrophosphate data. The next few figures compare the results of various data treatments. In Fig. 3.81 uranium in aqua regia is simply ratioed to LOI. This does not entirely remove the area of elevated concentration that runs N-S south of the pods. However, when uranium by sodium pyrophosphate is ratioed to loss on ignition, a clean horseshoe pattern right over the pods is produced (Fig. 3.82). The result of the more involved approach on the aqua regia uranium (i.e. residual U from the leveled PC) also shows the same horseshoe result, not quite as cleanly (Fig. 3.83). And finally, the unleveled scores of PC8 (which has a strong uranium loading) shows the same horseshoe pattern.

We conclude that uranium, after removing geological and peat effects, shows as an anomaly over both sets of McClean pods, and that this is visible in both the aqua regia data and the sodium pyrophosphate leach data in the A1 horizon.

A2, B1, B2 and C Horizons

Although there are some interesting features in the A2, B1, B2 and C horizons at McClean by some of the leaches, we do not see such a convincing and consistent response to the pods as in the A1 horizon. To illustrate a sample of results, a series of figures are presented that show the results for uranium and nickel across horizons for several leaches, starting with aqua regia.

Figs 3.85-3.89 show how uranium varies between horizons by aqua regia, and Figs 3.90-3.94 does the same for nickel. Both elements show some response over the southerly pods in A2, but in the lower horizons, both uranium and nickel highs occur south of the McClean deposits.

Uranium in the Enzyme leach shows no consistent pattern in any of the horizons, although nickel (and some other elements) definitely shows a response over the pods, which is particularly clear in the B1 horizon. Unfortunately, B1 was not sampled in 2009 on the northerly extension of lines 3 and 4 (too wet), and A2, B2 and C only had data collected in 2008, leaving some doubt about the reliability of these results.

A PC analysis done on the C horizon Enzyme leach (PC scores for PC1-PC4 shown in Figs 3.101-104) shows that PC4 (with high loadings of Mo, Pb, U) shows an anomaly just south of the northerly pods.

The hydroxylamine leach (Figs 3.105-3.108 for U and Figs 3.109-3.112 for Ni) shows similar responses to the Enzyme leach data, with uranium being somewhat scattered and nickel with more defined anomalies in the pod areas.

Ammonium acetate shows no clear response for uranium, and gives a mixed response for nickel (Figs 3.113-3.116, U; Figs 3.117-3.120, Ni).

The MMI leach on the MMI horizon did not work well on uranium (Fig. 3.121), but nickel, vanadium and zirconium show a good response over and near the pods.

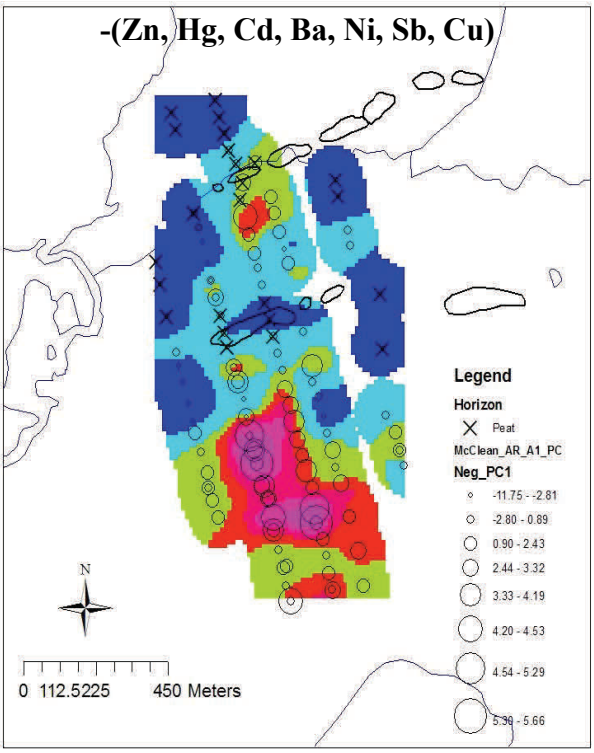

Fig 3.59 PC1 scores. A1 horizon. Aqua regia leach.

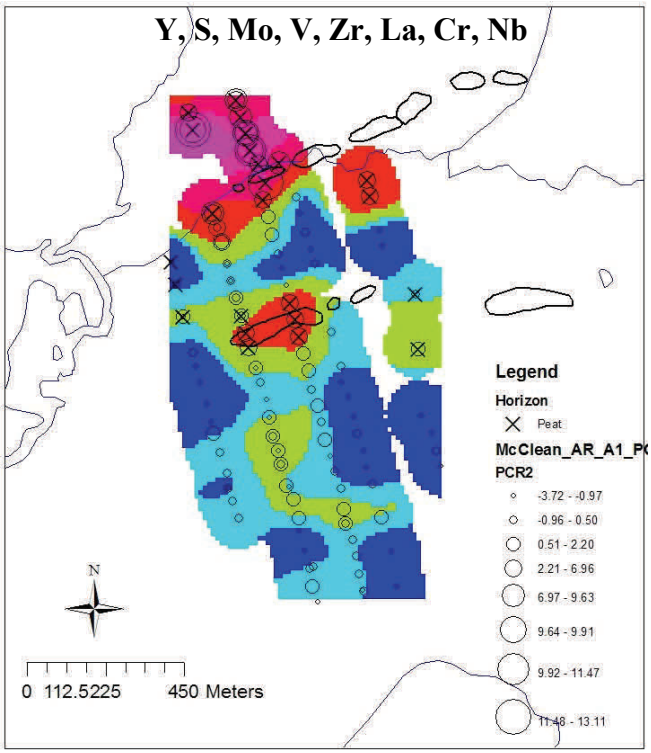

Fig 3.60 PC2 scores. A1 horizon. Aqua regia leach.

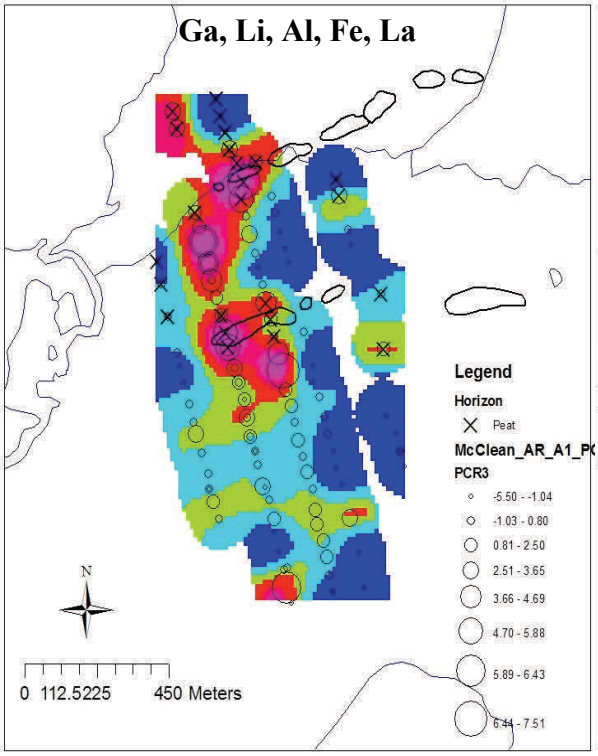

Fig. 3.61 PC3 scores. A1 horizon.

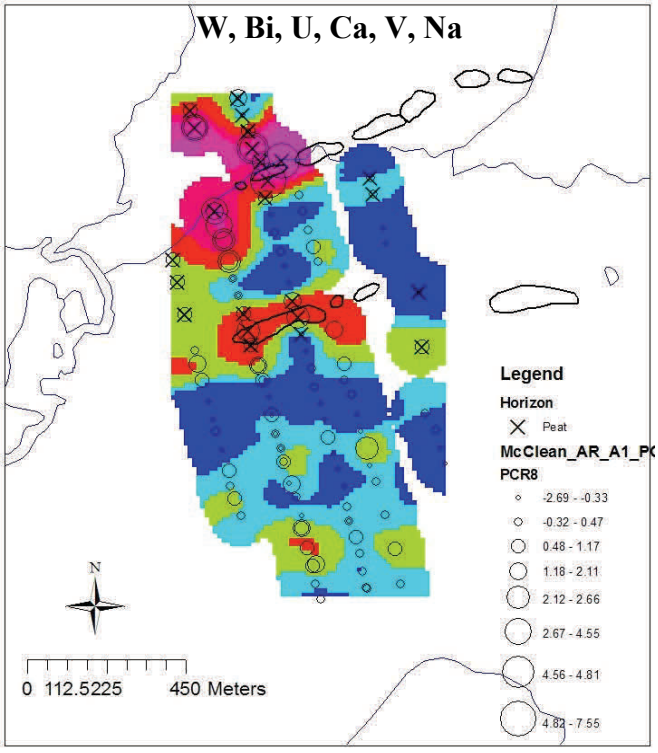

Fig. 3.62 PC8 scores. A1 horizon.

Elements strongly correlated with –PC1

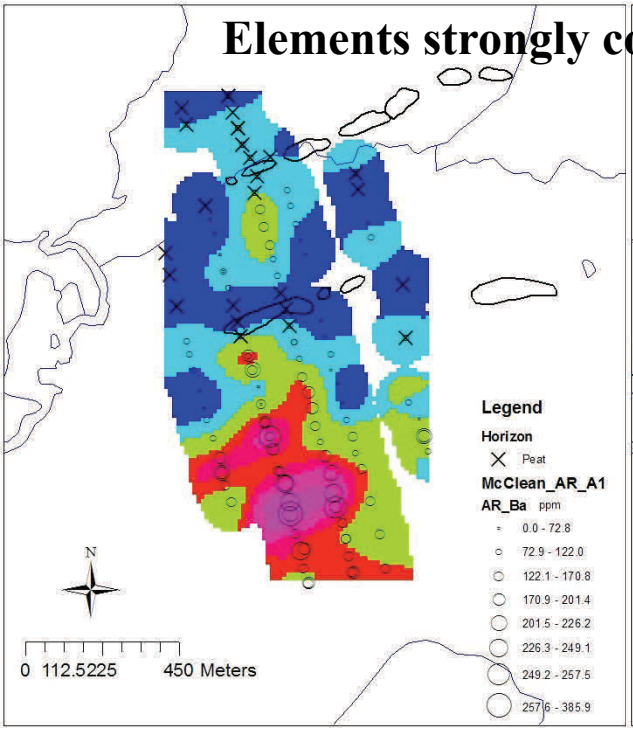

Fig. 3.63 Barium. A1 horizon. Aqua regia leach

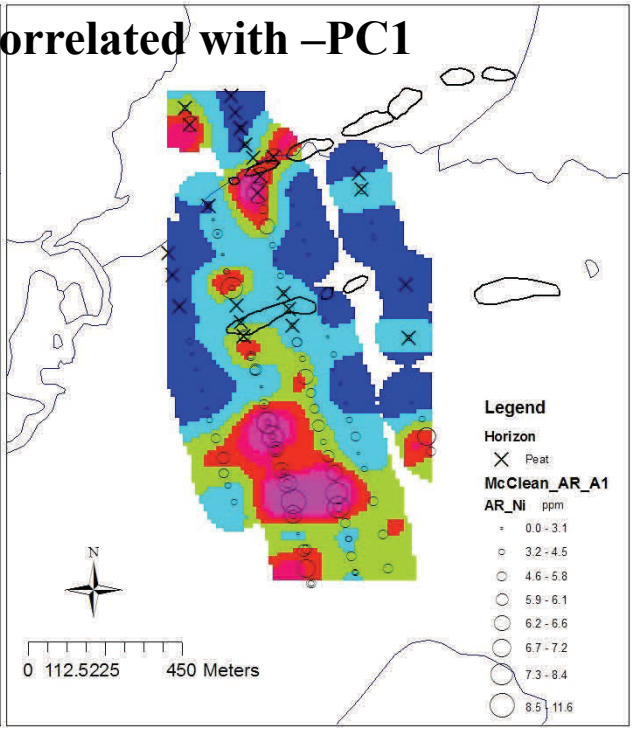

Fig. 3.64 Nickel. A1 horizon. Aqua regia leach

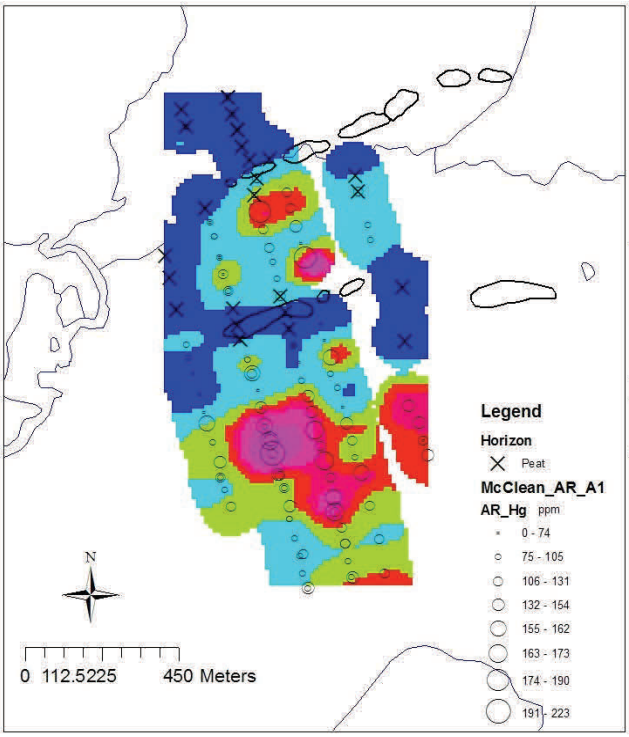

Fig. 3.65 Mercury. A1 horizon. Aqua regia leach

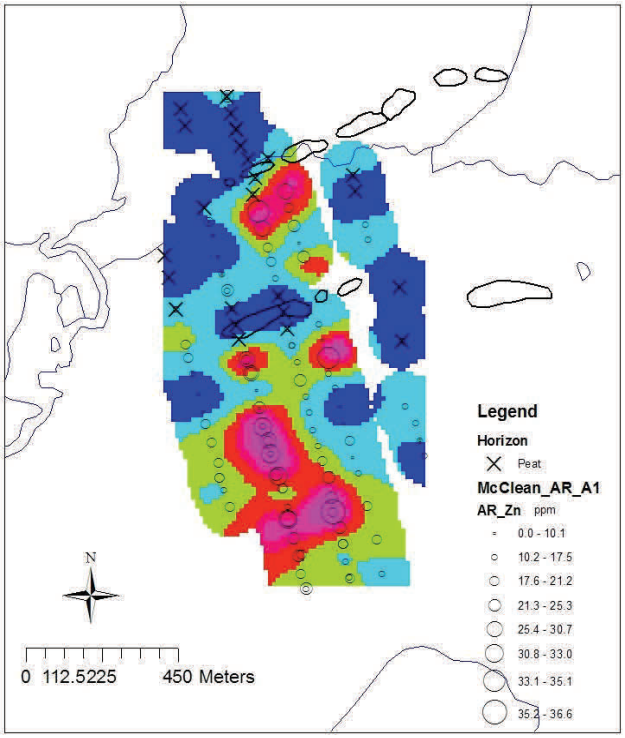

Fig. 3.66 Zinc. A1 horizon. Aqua regia leach

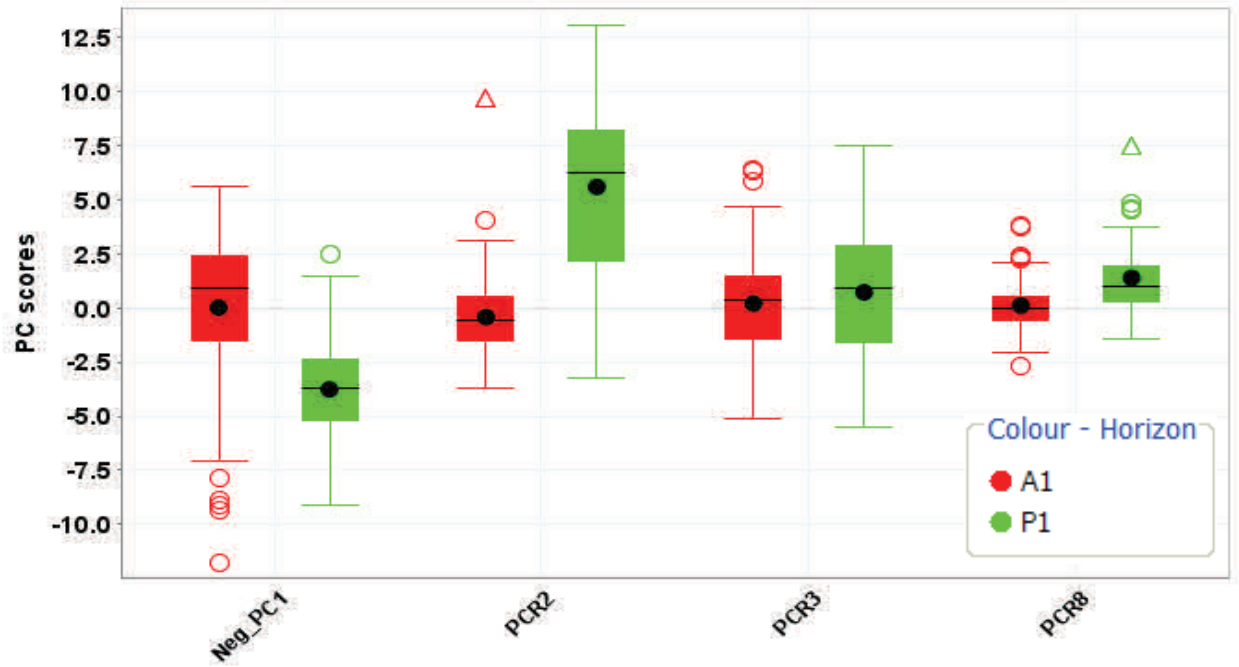

Fig 3.67. Box and whisker plots of PC1, PC2, PC3 and PC8 on A1 aqua regia data. Peat in green, normal A1 in red. Note significant relationship with peat and PC1, and PC2, but 3 and 8 not much different between peat and non-peat.

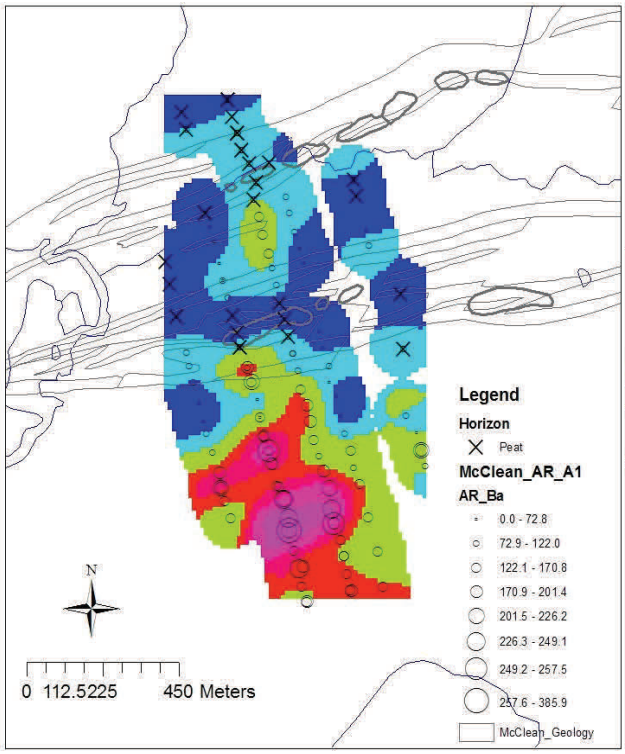

Fig. 3.68 Barium. A1 horizon, aqua regia. Geological boundaries superimposed. Note E-W boundary in middle of sample area.

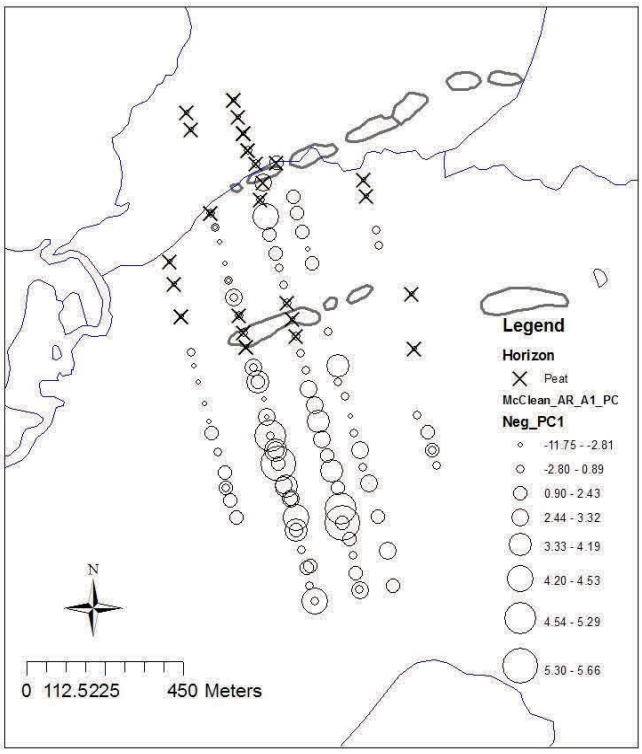

Fig. 3.69. PC1 scores showing relation to peat samples. No peat sample has a high value.

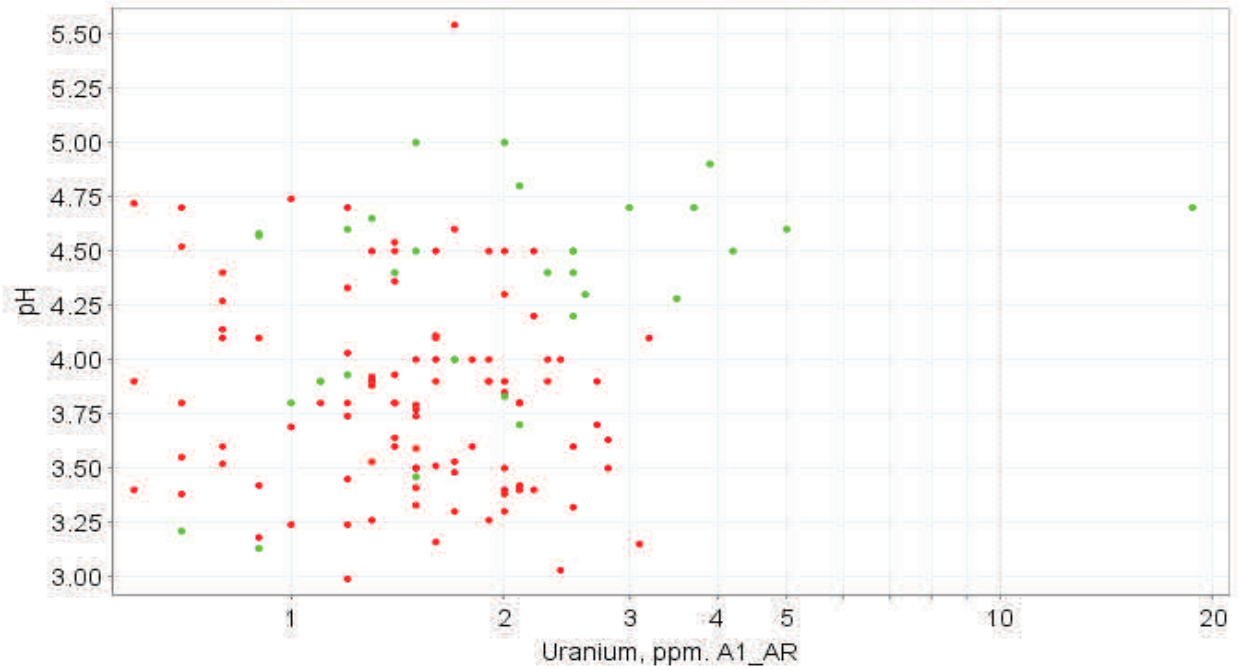

Fig. 3.70 Uranium (aqua regia) versus pH at McClean. Green dots are peat, red dots A1 horizon.

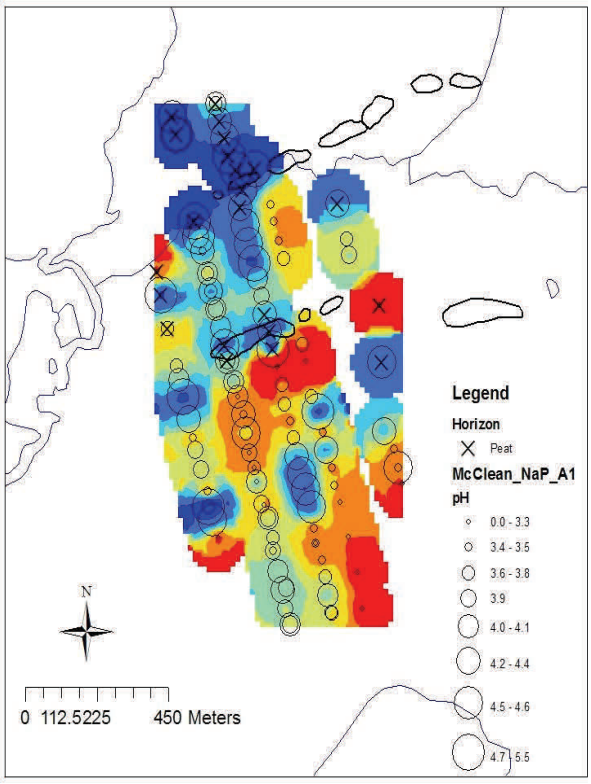

Fig 3.71 Map of pH in A1 horizon. Note that red is low pH and blue is high pH. Peat samples tend to be less acid (higher pH).

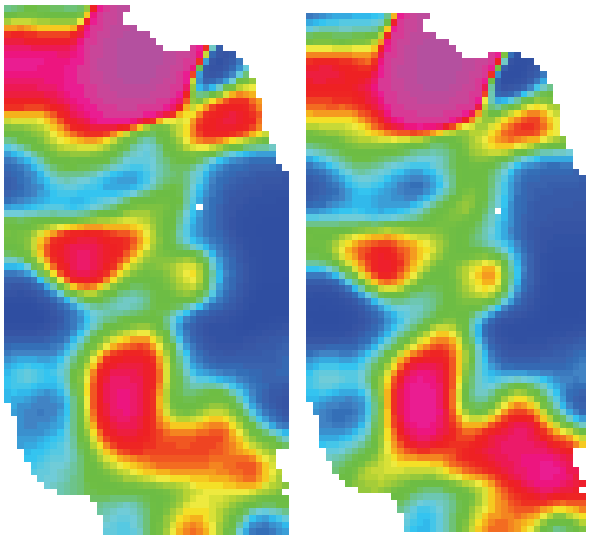

U —raw values **U-ratioed to pH**

Fig 3. 72 Normalizing to pH—no effect

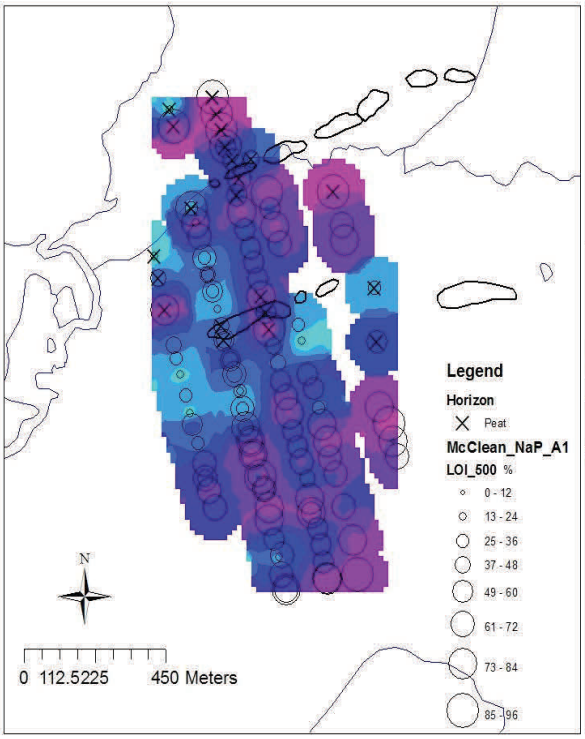

Fig 3.73 Loss on ignition at 500 deg. Peat marked with X

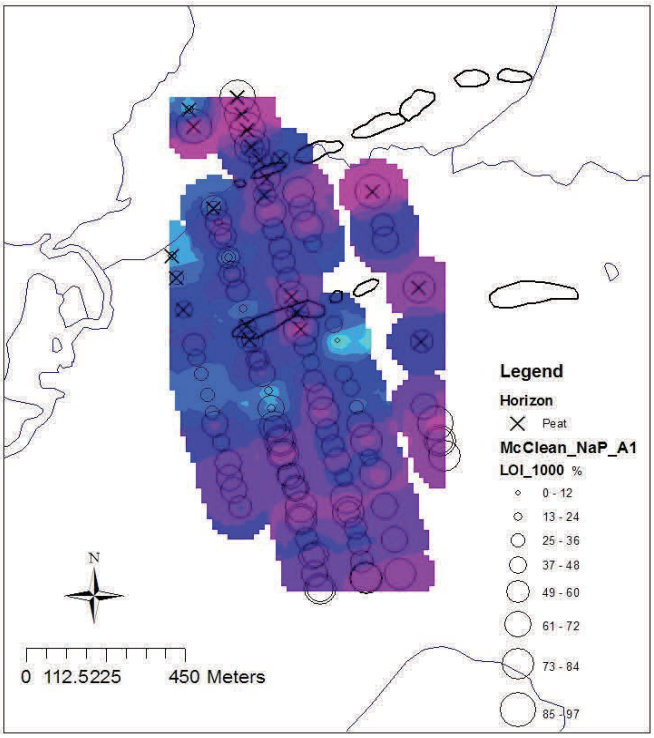

Fig 3.74 Loss on ignition at 1,000 deg. Peat marked with X

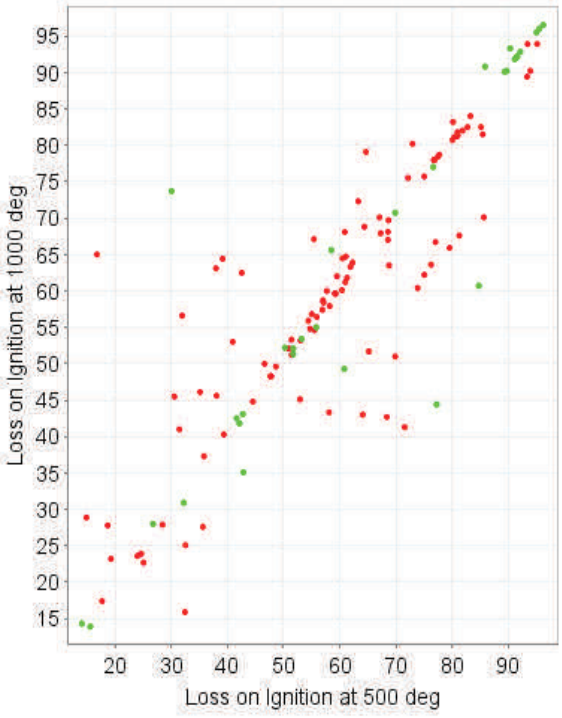

Fig 3.75 LOI 500 versus LOI 1000. Green dots are peat.

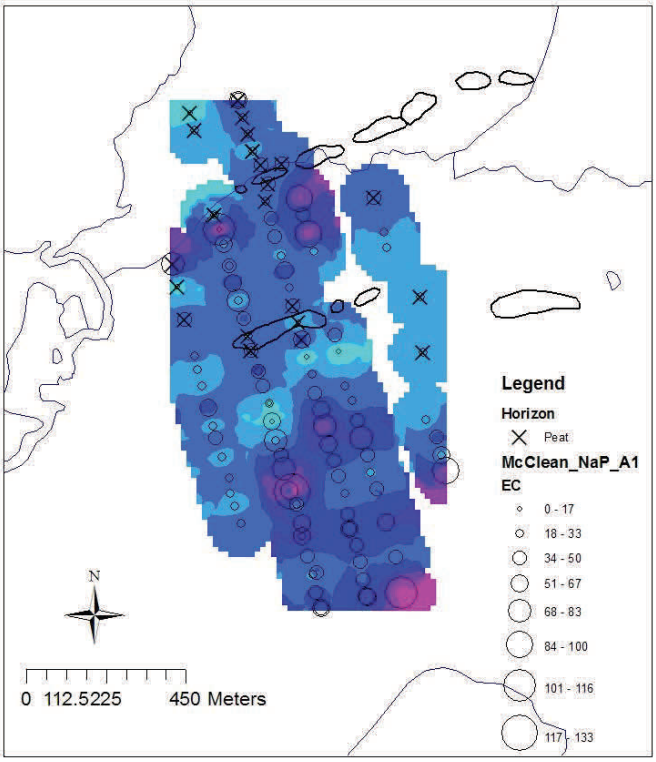

Fig 3.76 Electrical conductivity in A1. Peat marked with X.

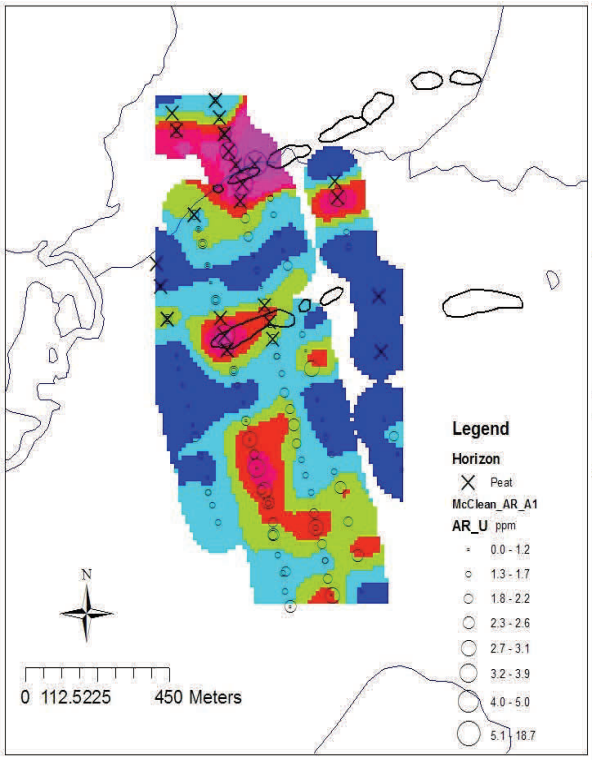

Fig 3.77 Raw uranium. A1 horizon. Aqua

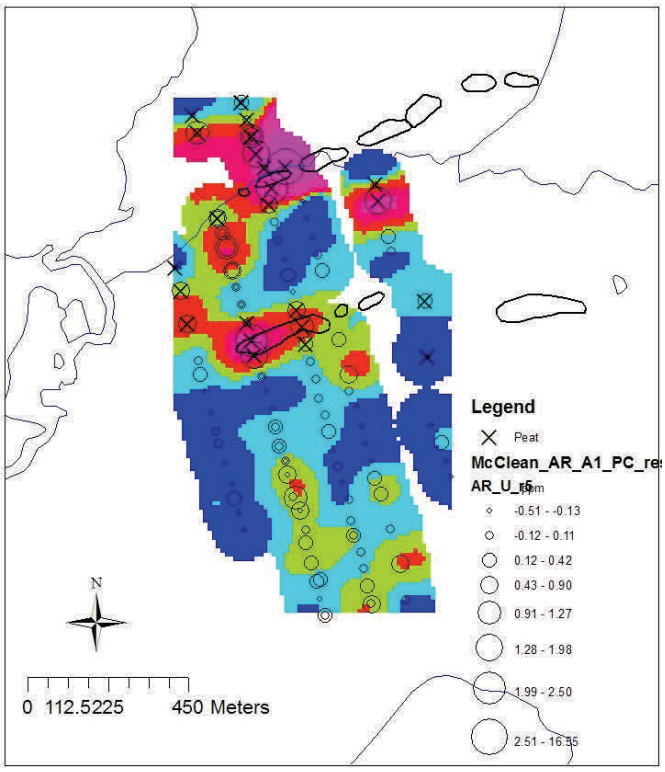

Fig 3.78 Uranium residuals from PC1

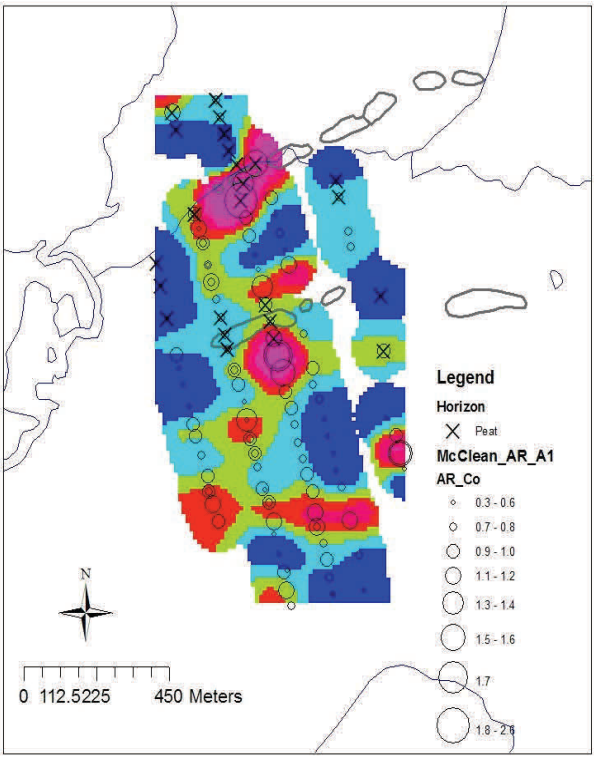

Fig 3.79 Raw cobalt. A1 horizon. Aqua

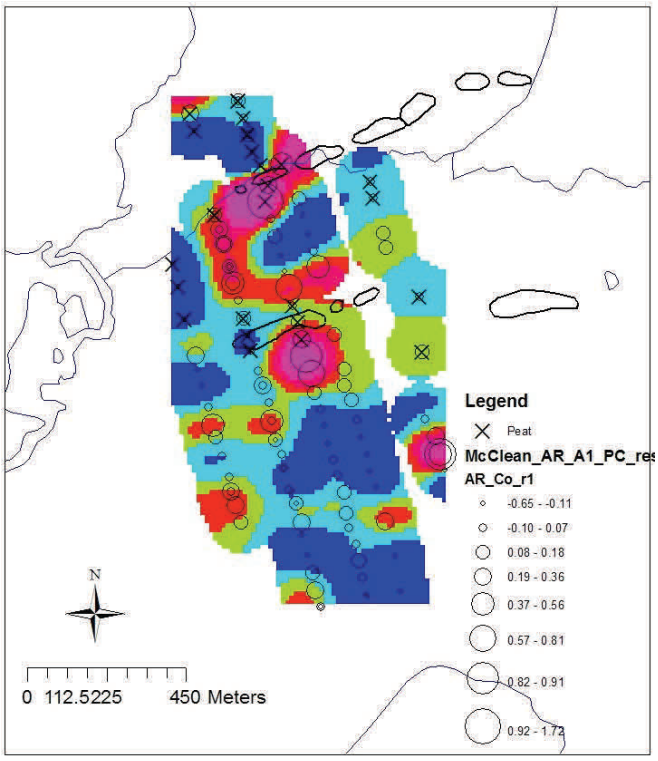

Fig 3.80 Cobalt residuals from PC1

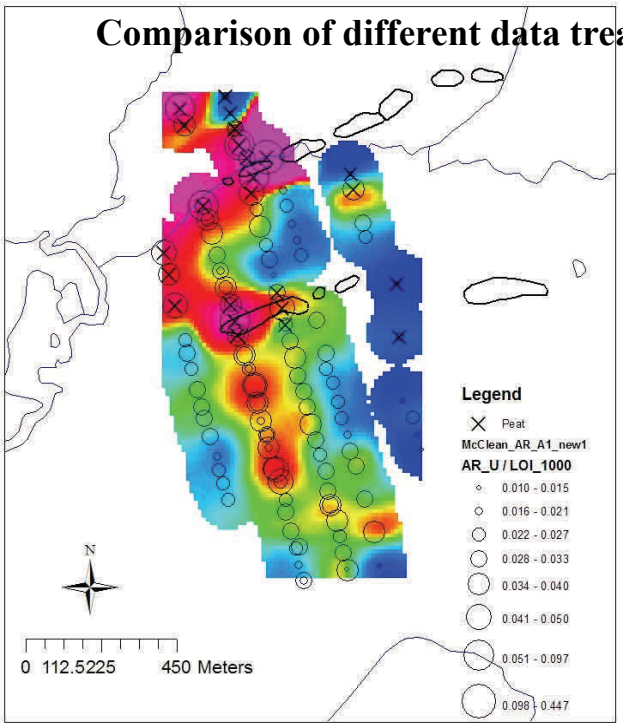

Fig 3.81 Uranium. A1/AR. Ratioed to LOI 1000

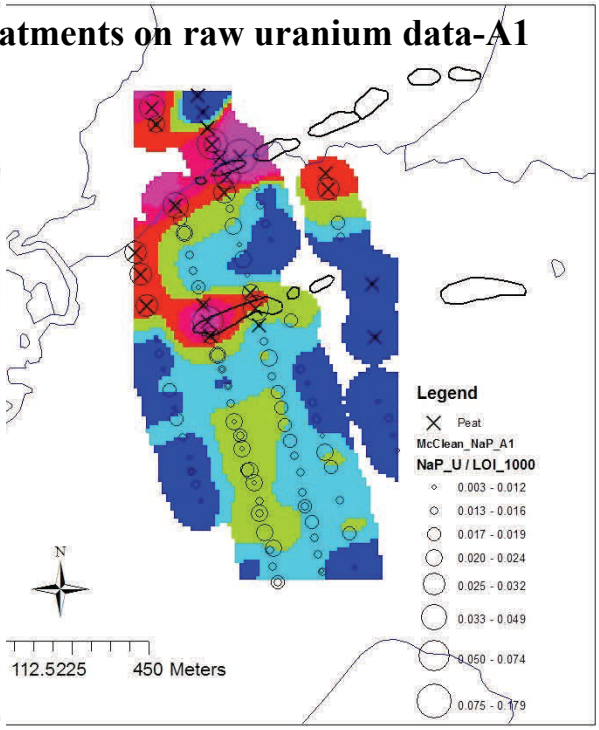

Fig 3.82. Uranium. A1/NaP. Ratioed to LOI 1000

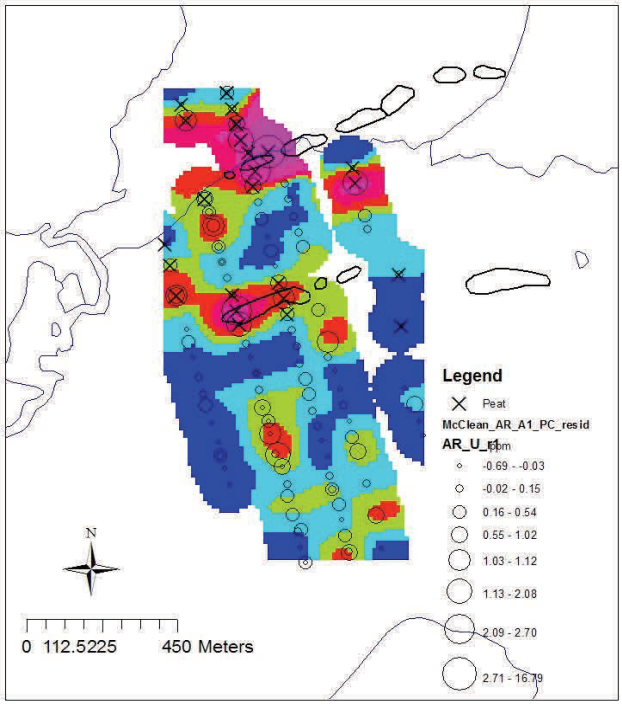

Fig 3.83 U residuals from PC1,

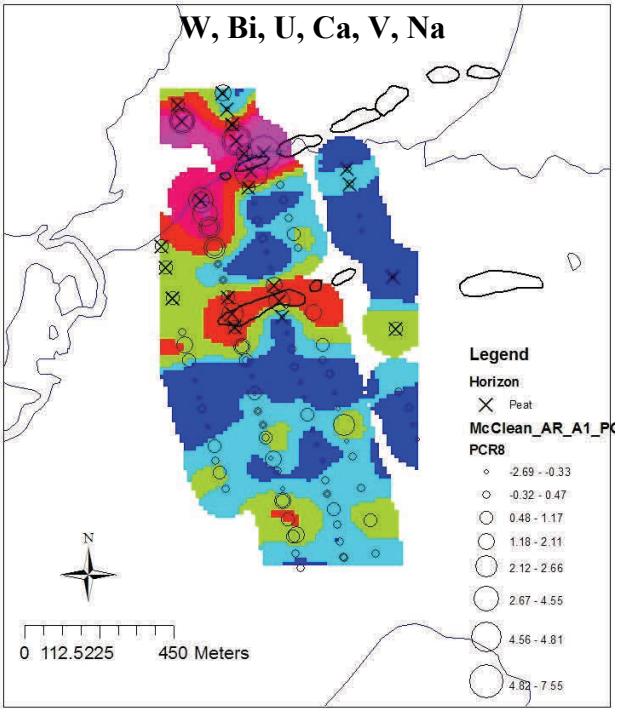

Fig 3.84 PC8 on A1 by aqua regia

Uranium across horizons by aqua regia

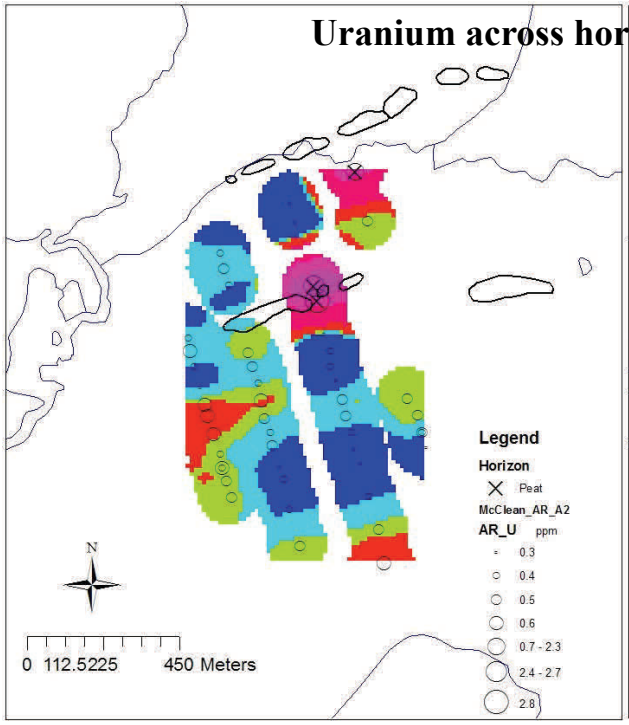

Fig 3.85 Uranium. A2 horizon. Aqua regia.

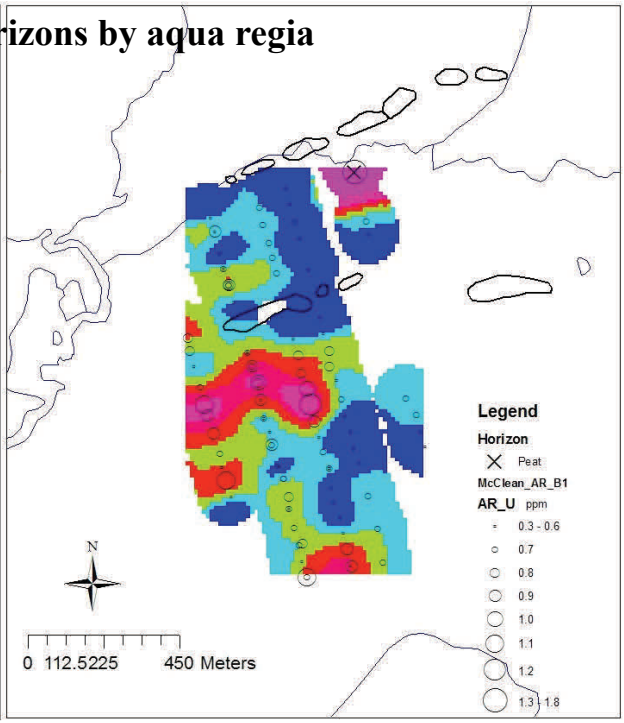

Fig 3.86 Uranium. B1 horizon. Aqua regia.

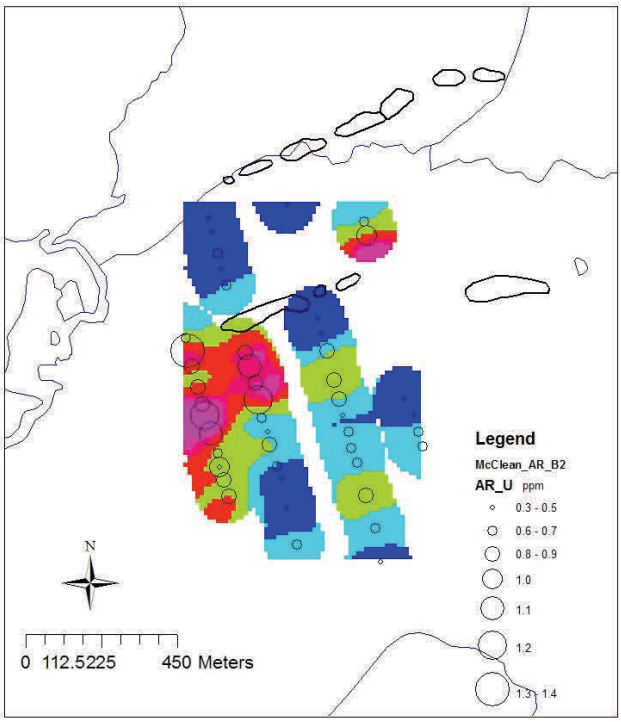

Fig 3.87 Uranium. B2 horizon. Aqua regia.

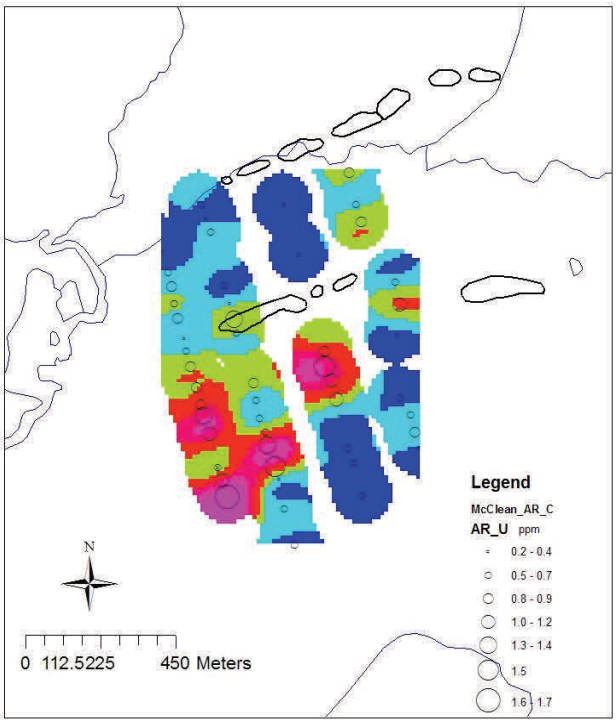

Fig 3.88 Uranium. C horizon. Aqua regia.

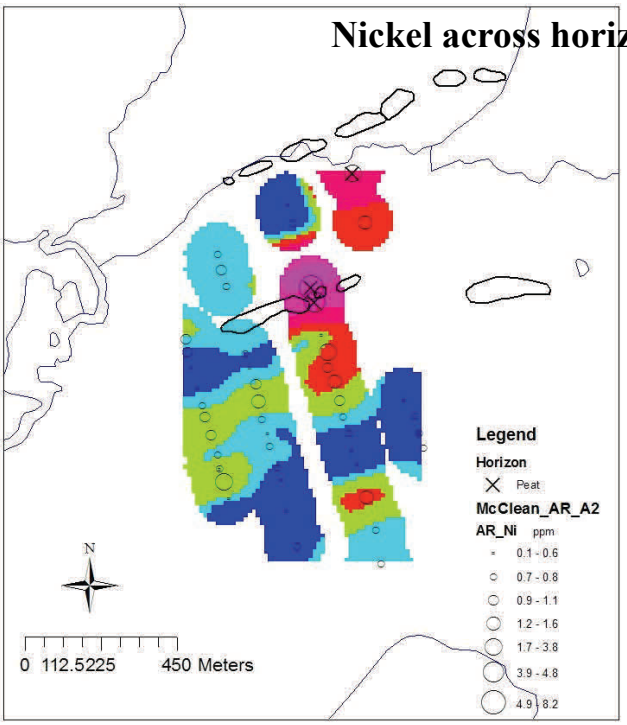

Fig. 3.89 Nickel. A2 horizon. Aqua regia.

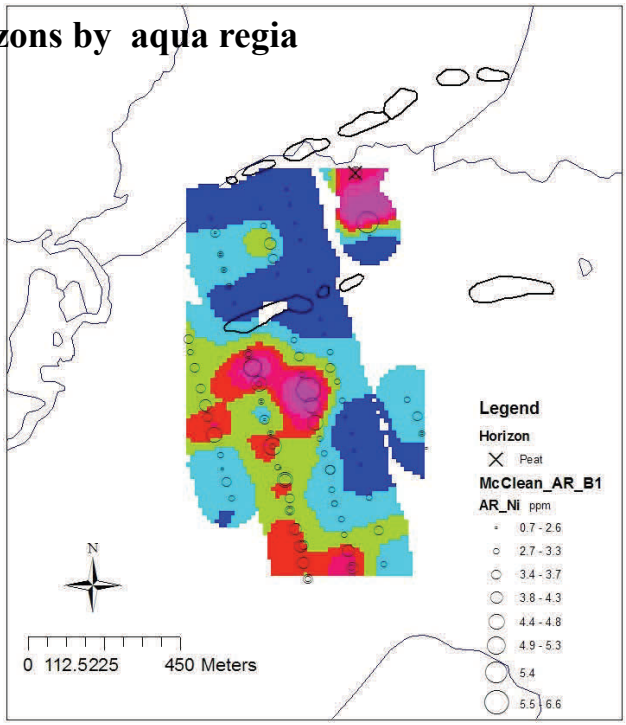

Fig 3.90 Nickel. B1 horizon. Aqua regia.

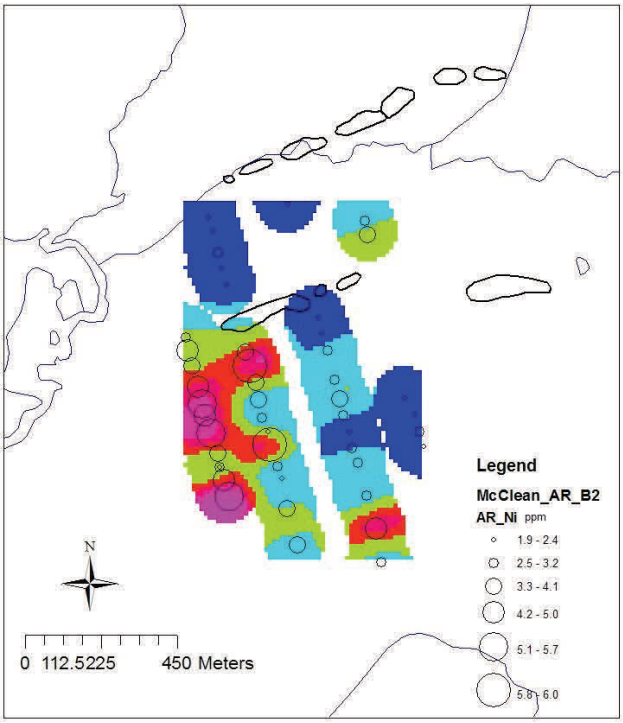

Fig 3.91 Nickel. B2 horizon. Aqua regia.

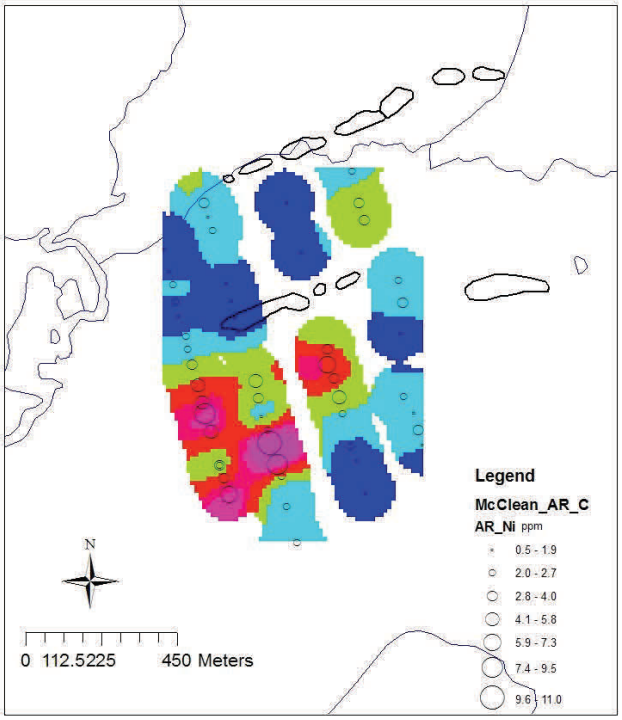

Fig 3.92 Nickel. C horizon. Aqua regia.

Uranium across horizons by enzyme leach

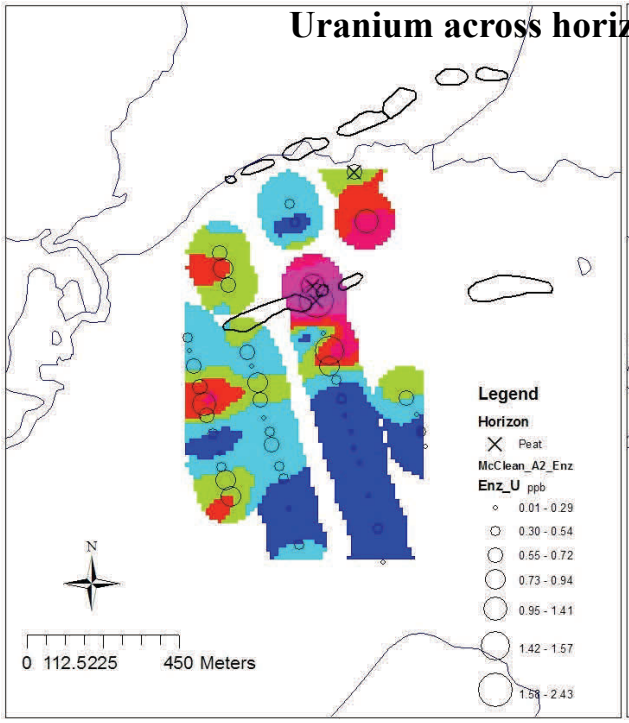

Fig 3.93 Uranium. A2 horizon. Enzyme leach.

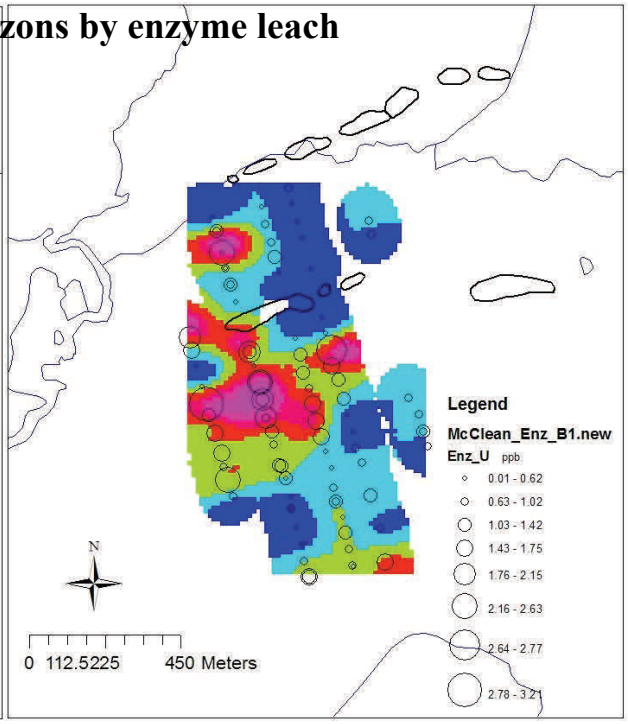

Fig 3.94 Uranium. B1 horizon. Enzyme leach.

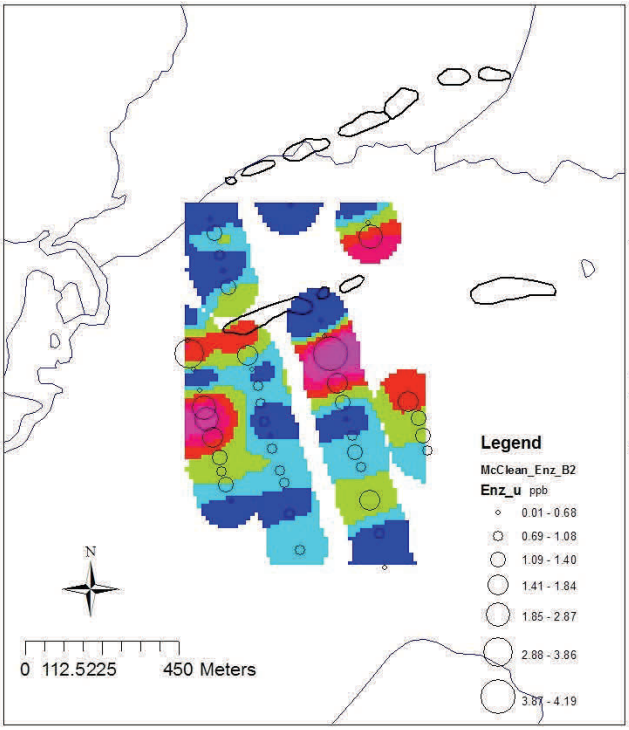

Fig 3.95 Uranium. B2 horizon. Enzyme leach.

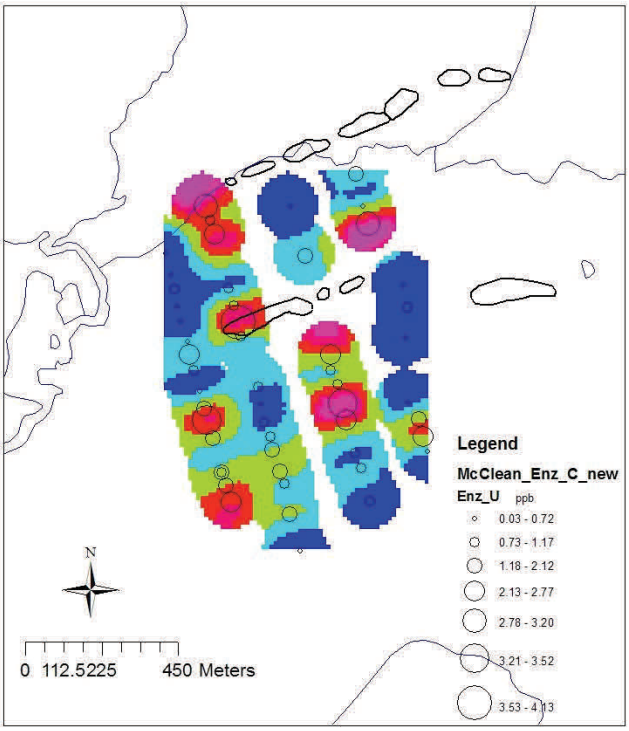

Fig 3.96 Uranium. C horizon. Enzyme leach.

Nickel across horizons by enzyme leach

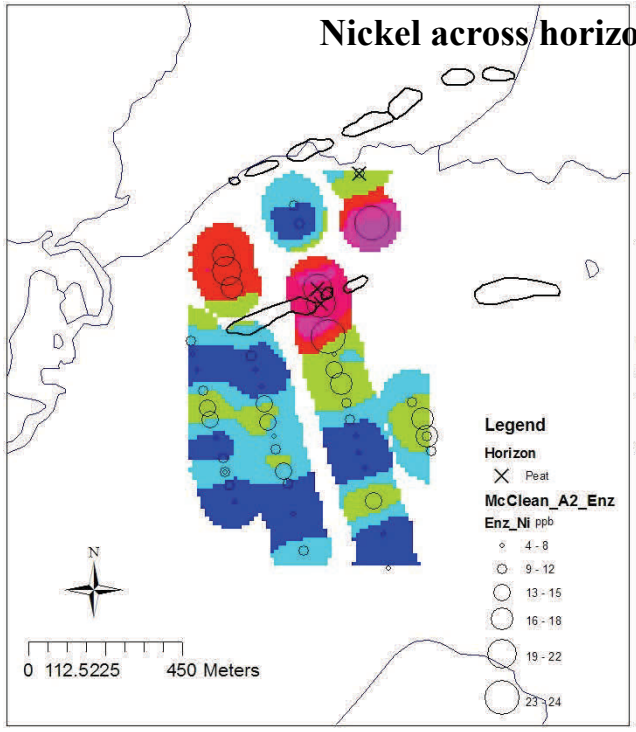

Fig 3.97 Nickel. A2 horizon. Enzyme leach

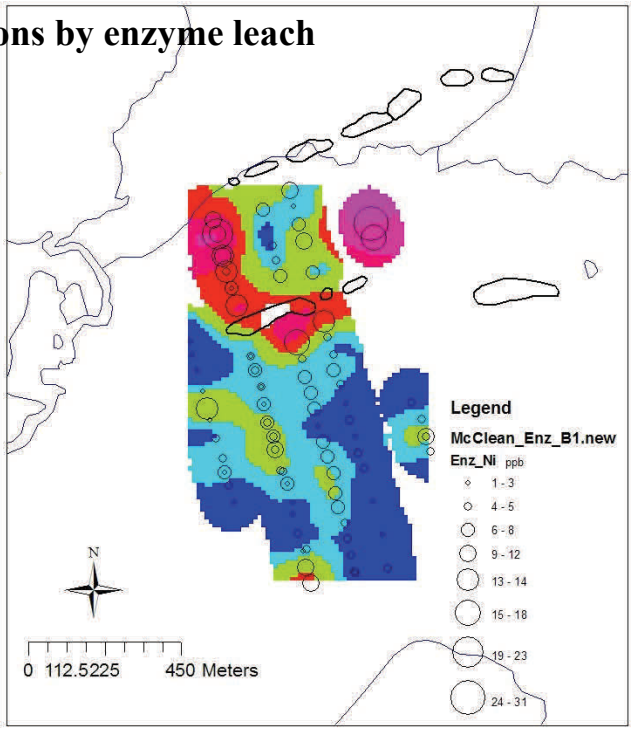

Fig 3.98 Nickel. B1 horizon. Enzyme leach

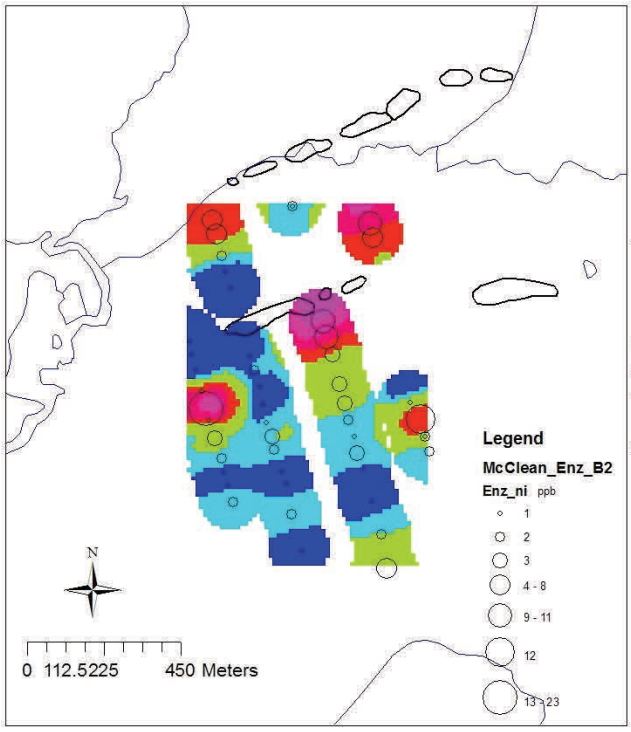

Fig 3.99 Nickel. B2 horizon. Enzyme leach
No 2009 data available

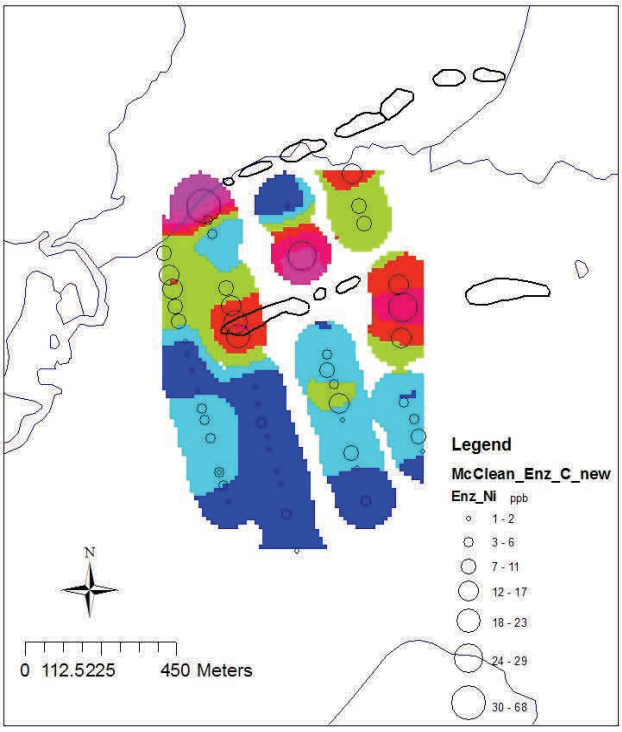

Fig 3.100 Nickel. C horizon. Enzyme leach
No 2009 data available

PC analysis on Enzyme leach data in C horizon

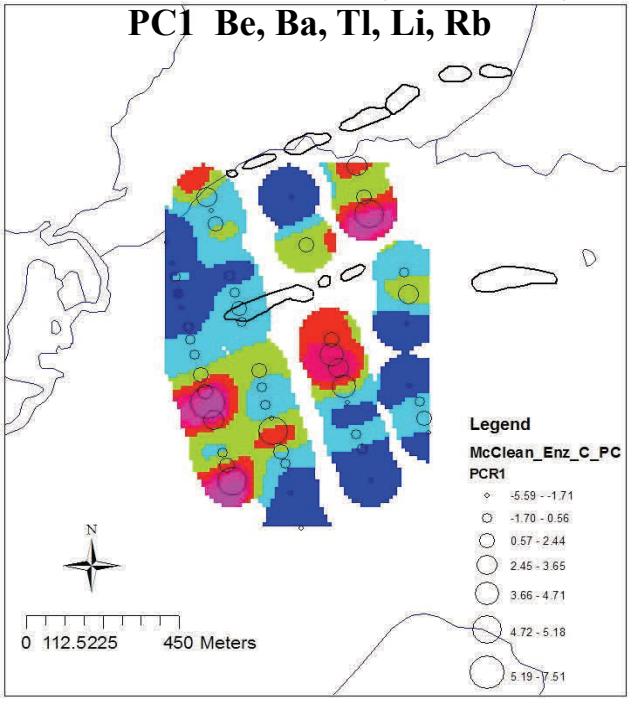

Fig 3.101 PC1 scores. C horizon Enzyme leach

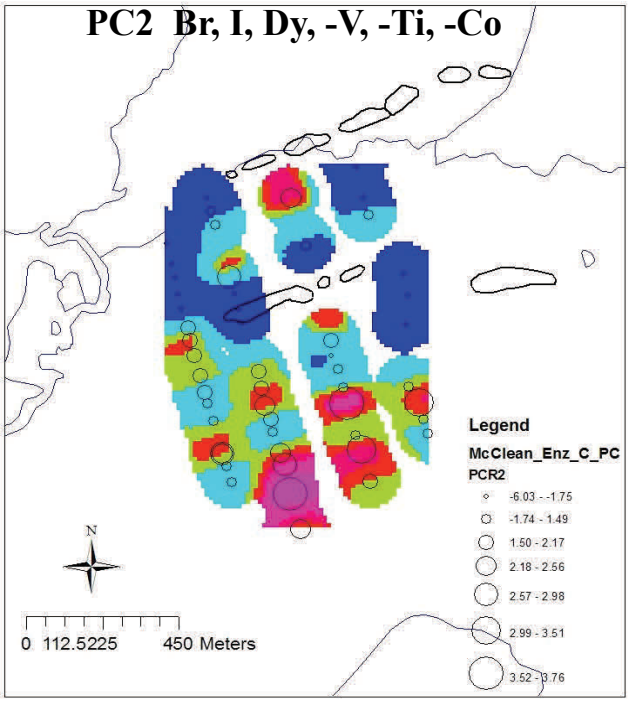

Fig 3.102 PC2 scores. C horizon Enzyme leach

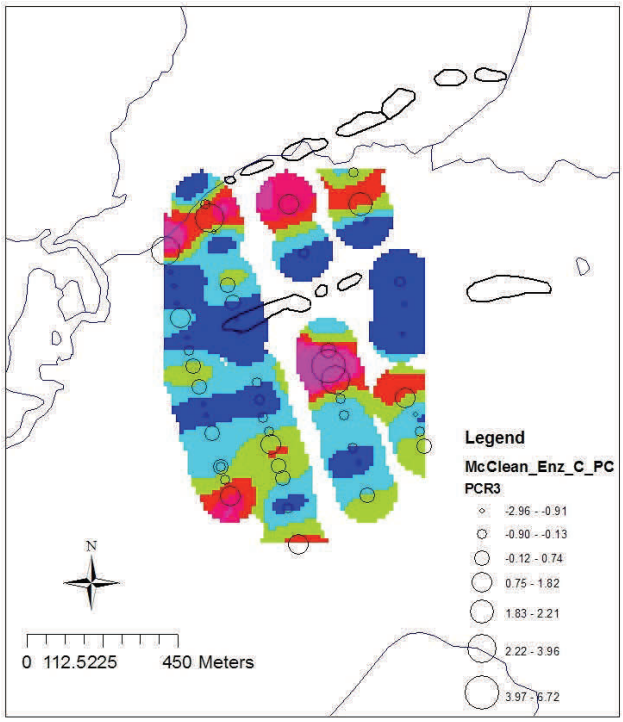

Fig 3.103 PC1 scores. C horizon Enzyme leach

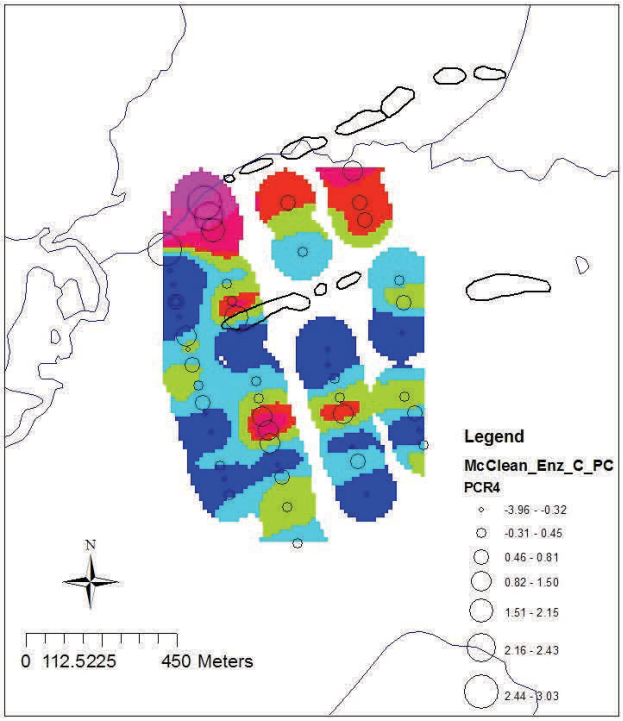

Fig 3.104 PC1 scores. C horizon Enzyme leach

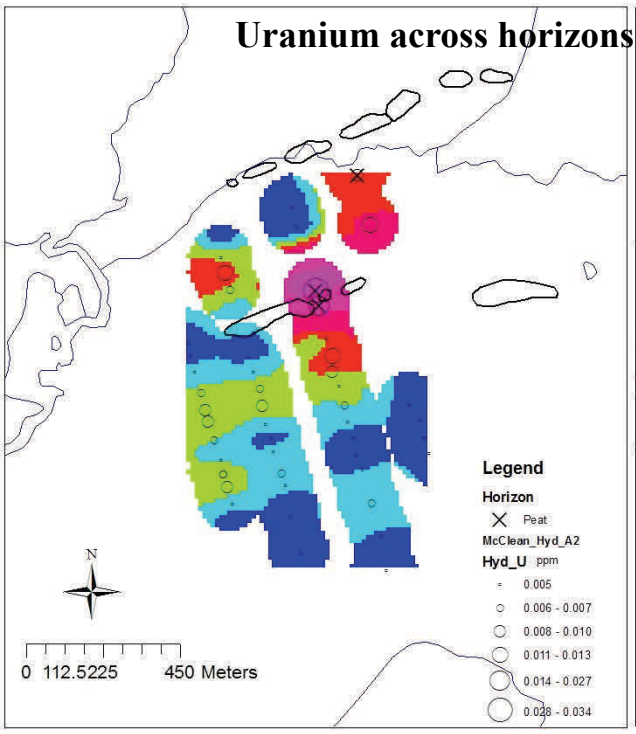

Fig 3.105 Uranium. A2 horizon. Hydroxylamine leach.

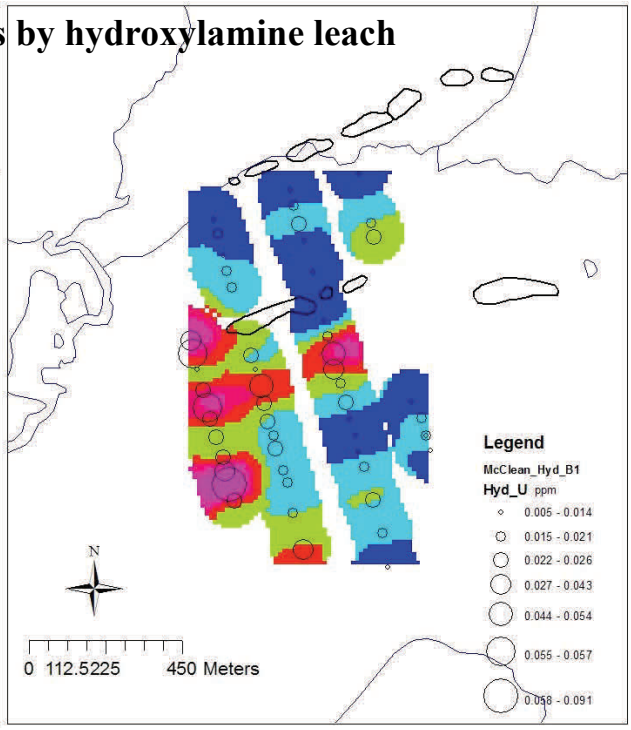

Fig 3.106 Uranium. B1 horizon. Hydroxylamine leach.

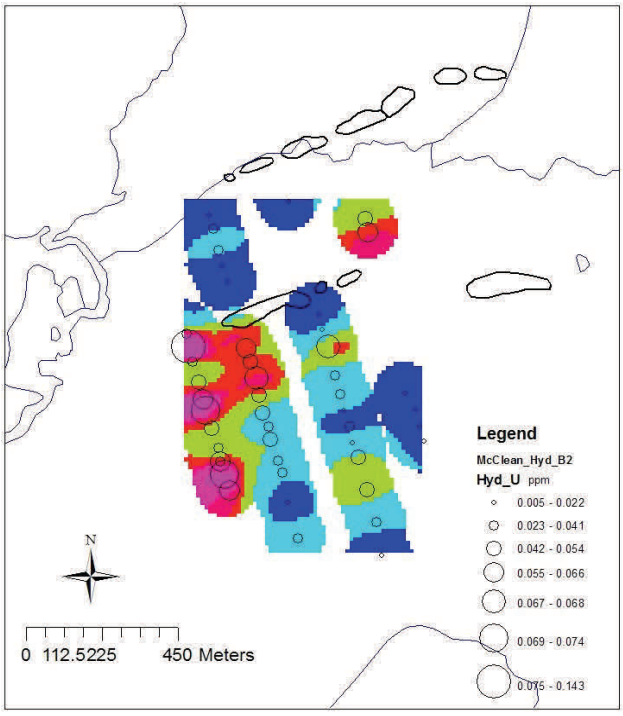

Fig 3.107 Uranium. B2 horizon. Hydroxylamine leach.

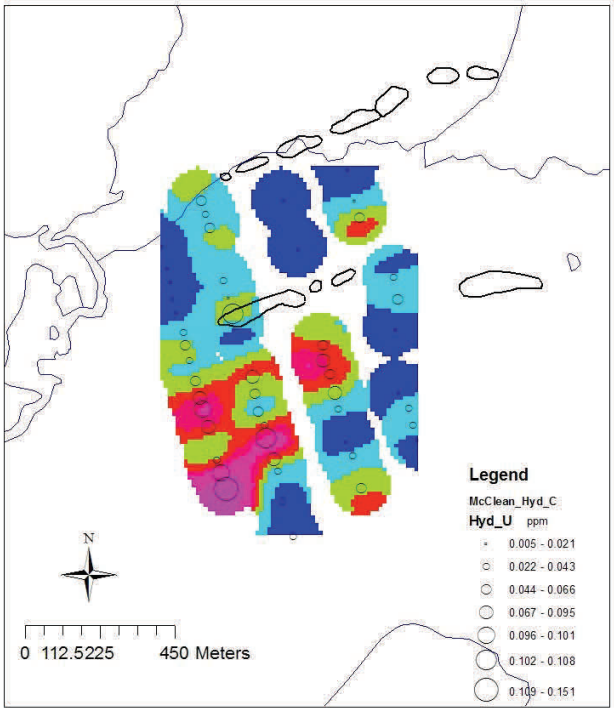

Fig 3.108 Uranium. C horizon. Hydroxylamine leach.

Nickel across horizons by hydroxylamine leach

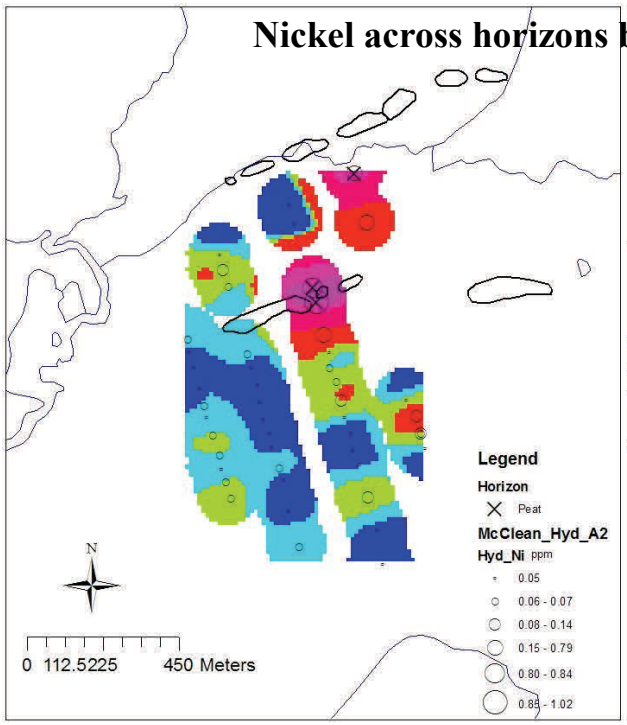

Fig 3.109 Nickel. A2 horizon. Hydroxylamine leach

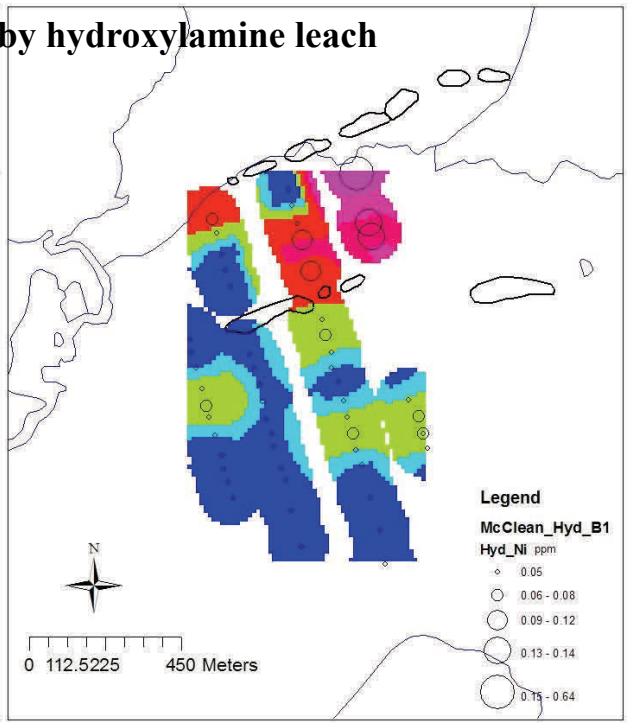

Fig 3.110 Nickel. B1 horizon. Hydroxylamine leach

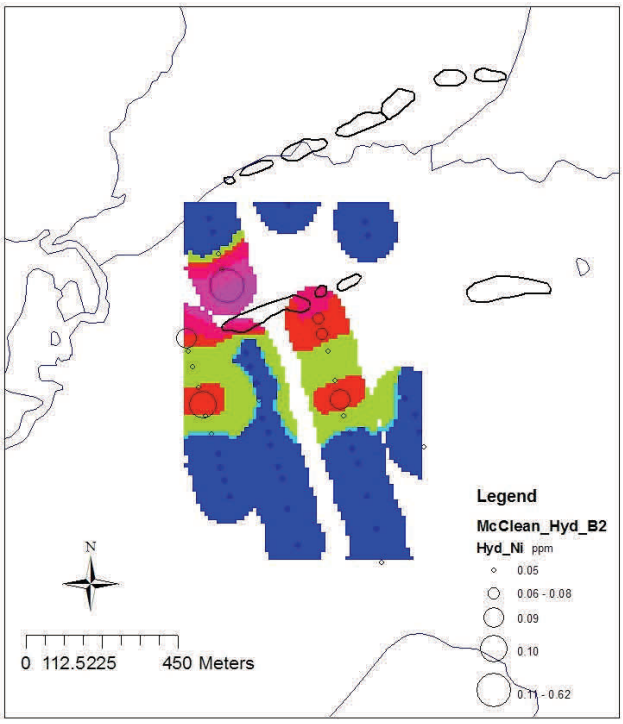

Fig 3.111 Nickel. B2 horizon. Hydroxylamine leach

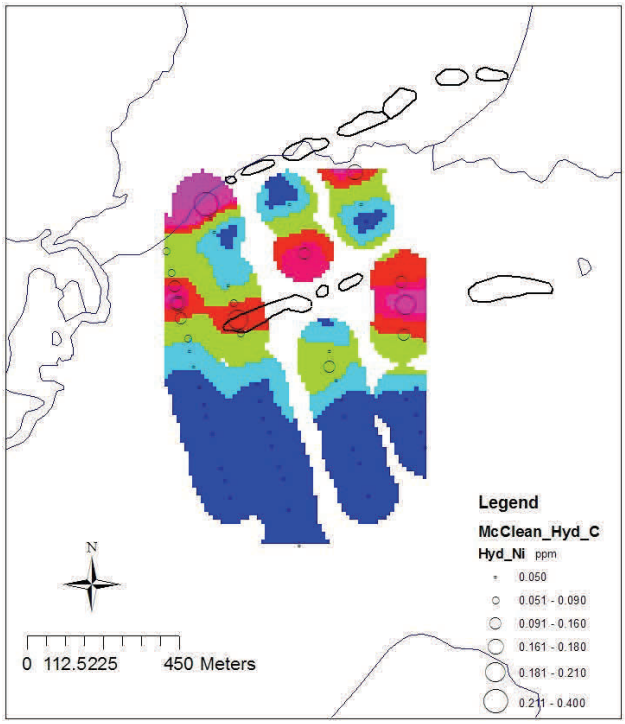

Fig 3.112 Nickel. C horizon. Hydroxylamine leach

Uranium across horizons by ammonium acetate leach

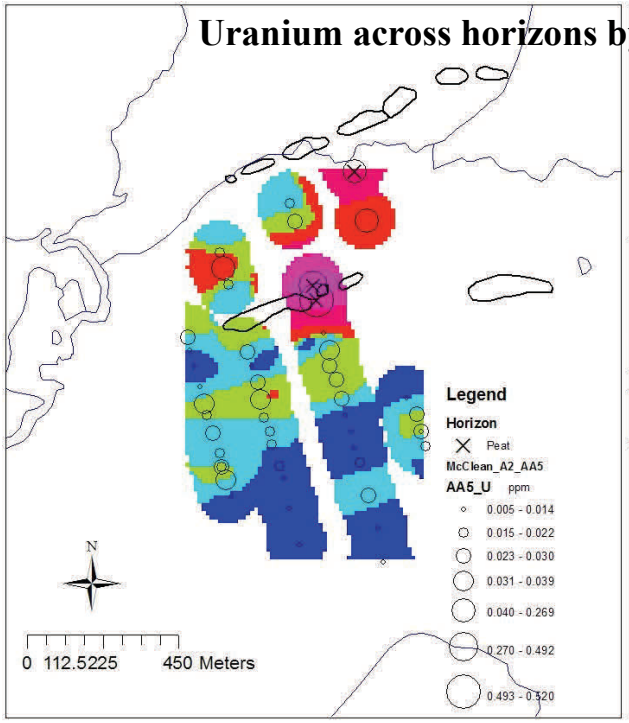

Fig 3.113 Uranium. A2 horizon Ammonium acetate leach

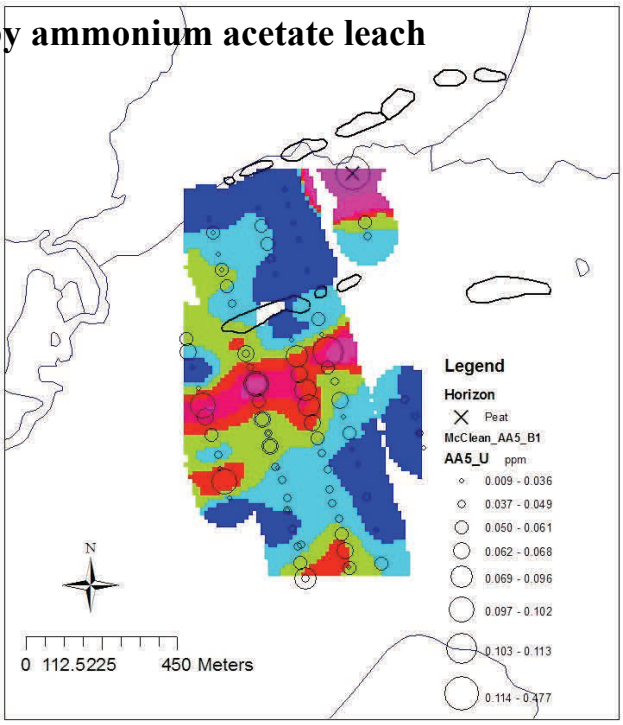

Fig 3.114 Uranium. B1 horizon Ammonium acetate leach

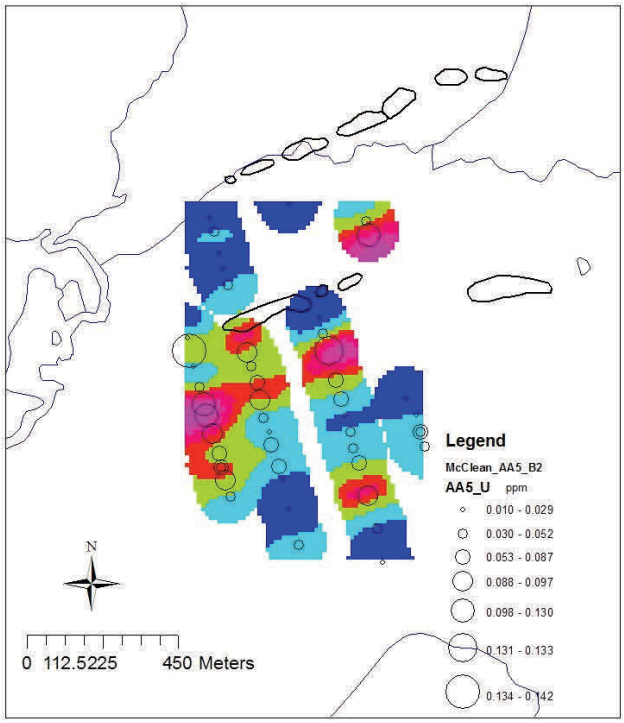

Fig 3.115 Uranium. B2 horizon Ammonium acetate leach

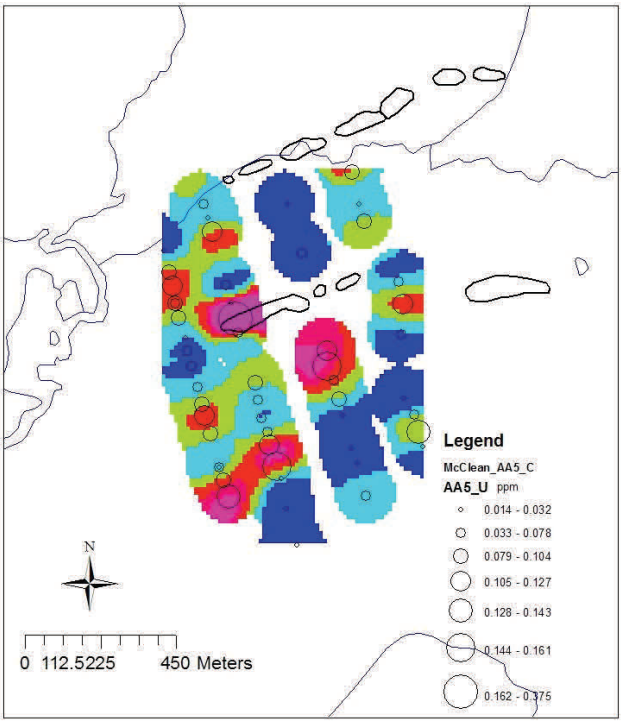

Fig 3.116 Uranium. C horizon Ammonium acetate leach

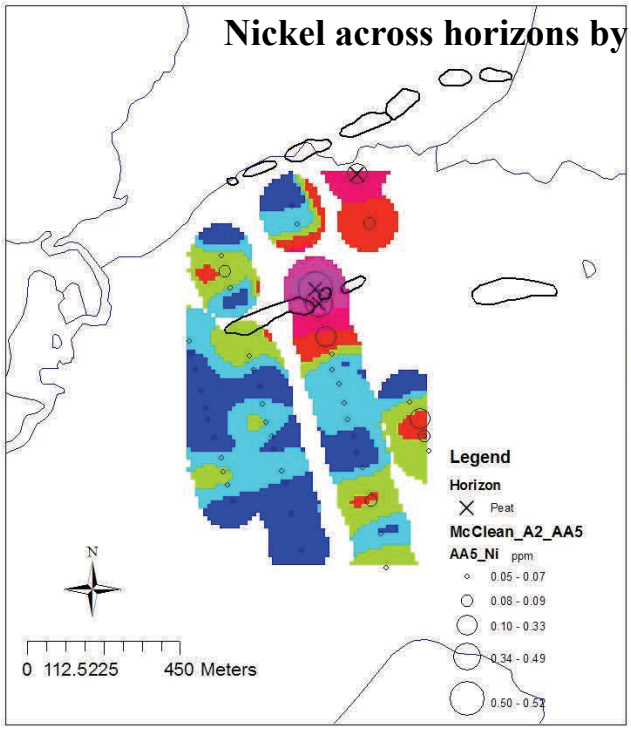

Fig 3.117 Nickel. A2 horizon Ammonium acetate leach

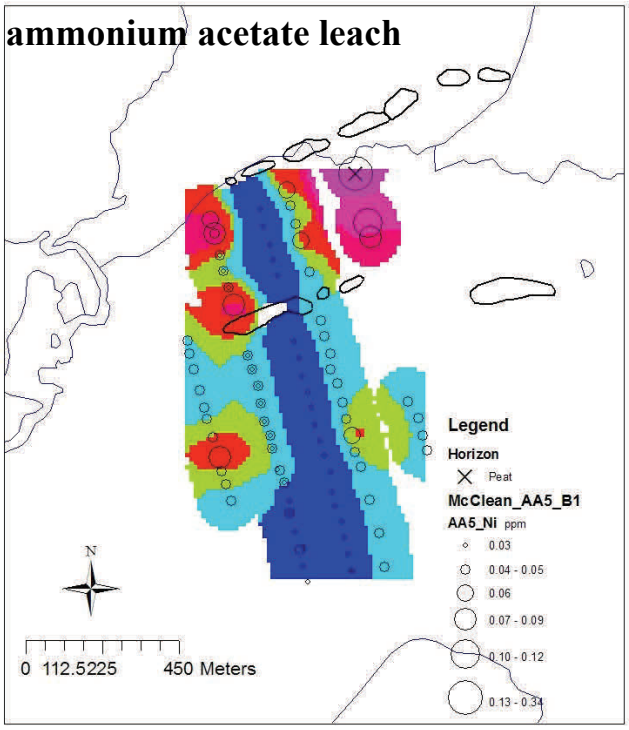

Fig 3.118 Nickel. B1 horizon Ammonium acetate leach

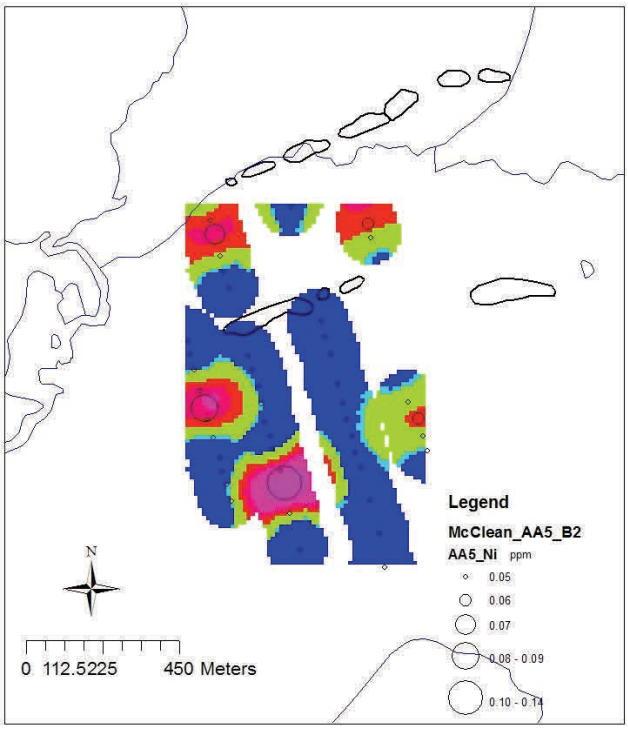

Fig 3.119 Nickel. B2 horizon Ammonium acetate leach

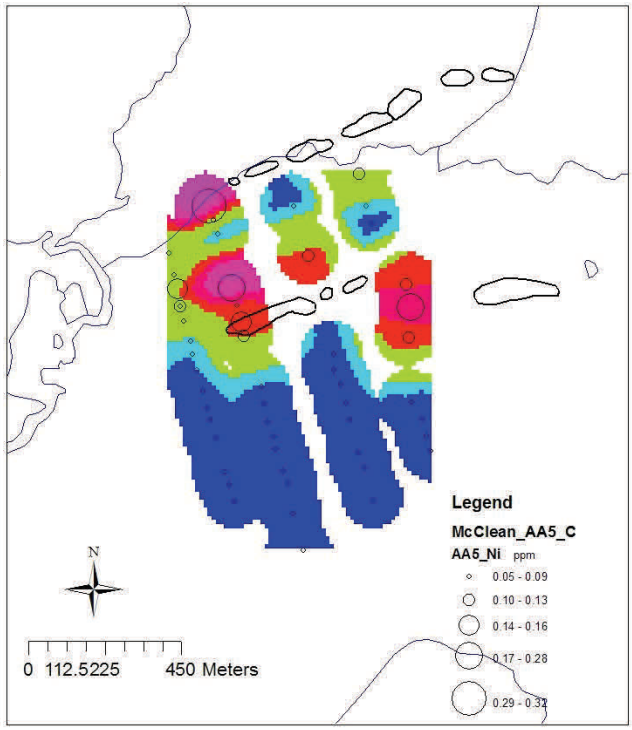

Fig 3.120 Nickel. C horizon Ammonium acetate leach

MMI leach on MMI horizon. Uranium, nickel, vanadium and zirconium

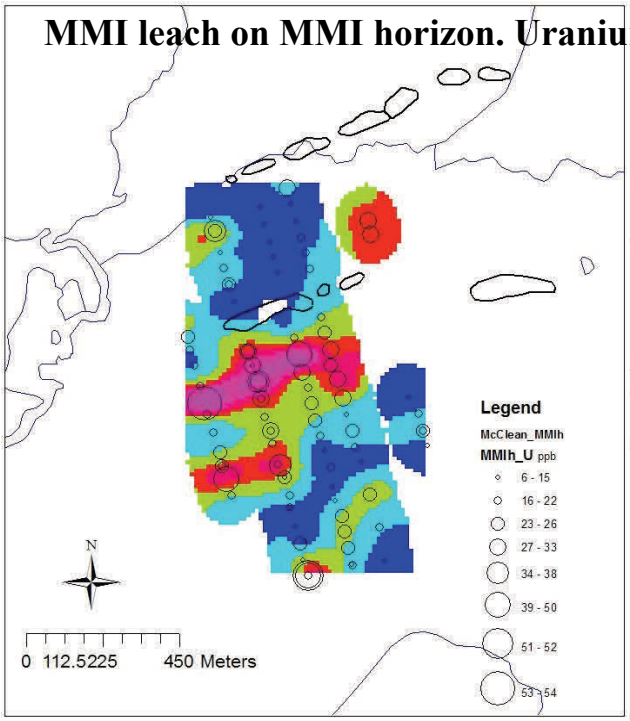

Fig 3.121 MMI Horizon. Uranium.

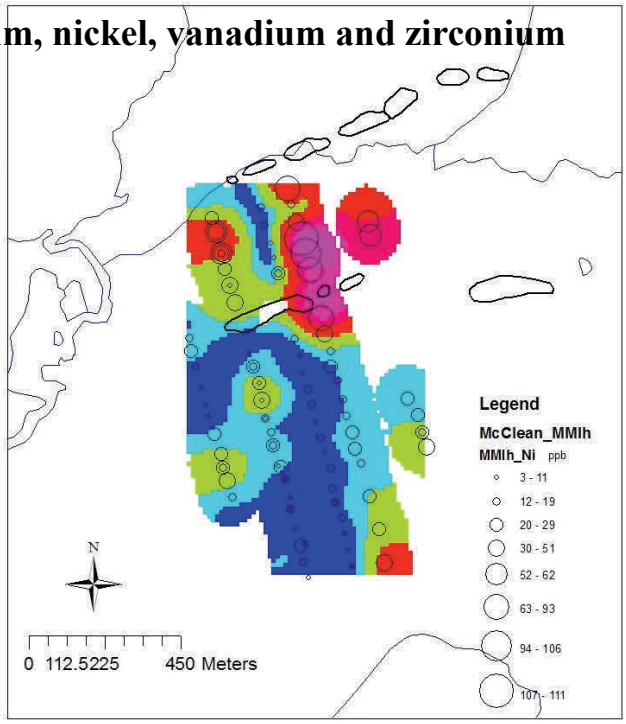

Fig 3.122 MMI Horizon. Nickel.

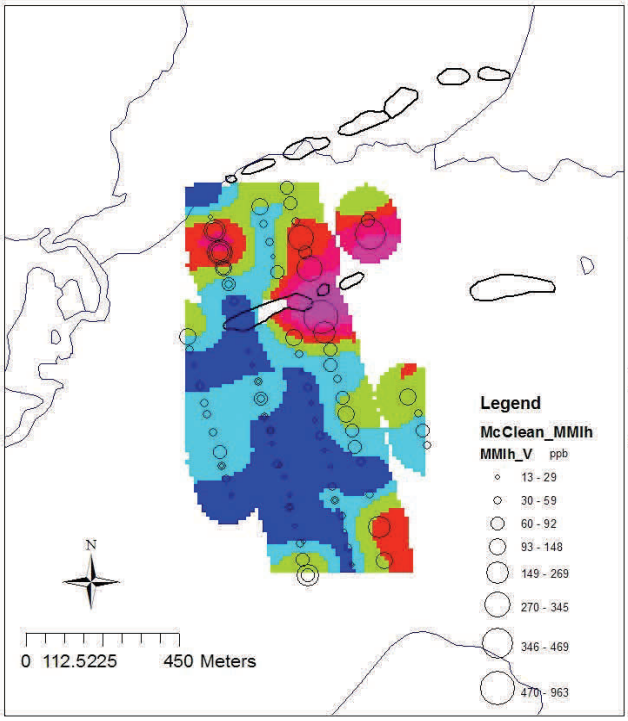

Fig 3.123 MMI Horizon. Vanadium.

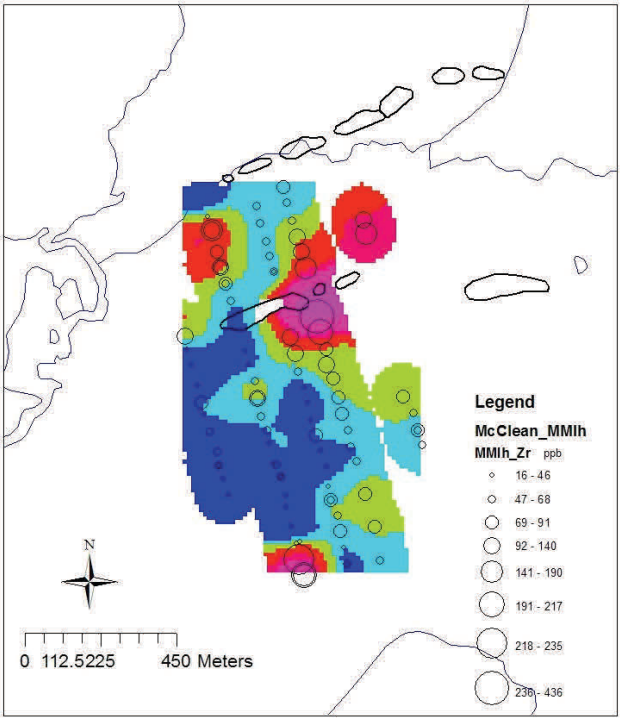

Fig 3.124 MMI Horizon. Zirconium.

4. Quality Assurance

4.1 Relative Standard Deviations of Duplicates

Field duplicate samples were taken in both years; crews were asked to take field duplicates at a rate of 1 in 20 but this rule was adhered to more in the second year of sampling. Duplicate holes were dug within a metre of the first where possible. Field duplicates were treated as separate samples and given different numbers. The various lines that were resampled in 2009 provided year-to-year field duplicates; the proximity of these samples to each other is generally less than that of the field duplicates sampled in the same year but the crews attempted to sample within ~ 2 m.

No standards were inserted in the first year but in the second a bulk sample of A1 humus and one of B1 horizon were obtained and these were prepared along with the samples at SRC. Each laboratory was asked to intersperse the standards equally amongst the samples (i.e. they were identifiable to the lab). Laboratory duplicates are splits of samples that the lab has taken through the leach and analytical procedures separately.

There are several contributions to the variance of the data for each sample site; these comprise the sampling variance and the analytical variance. These are additive and therefore the variance obtained for field duplicates is the sum of both the sampling and the analytical variances, the latter usually being much lower (smaller) than the former. In this survey, we have two sets of field duplicates: those representing differences in sample sites spaced ~ 1 m apart, and those representing differences in time (almost 14 months) and space (within ~ 2 m of the original sample). No splits were taken after sample preparation so we cannot estimate the variance of the sample processing step itself but this should be small as only sieving was employed (Au, a typically heterogeneous element, is not a critical one in this work).

Analytical reproducibility depends mostly on (1) the reproducibility of the leaching process and (2) the variation of the instrumental response (ICP-MS; less frequently ICP-ES) during the run. Reproducibility of a strong digestion such as aqua regia should not be an issue because the concentrations of elements determined will, by and large, be well above analytical detection limits. However, very weak partial leaches will inherently be associated with greater analytical variance as this increases as the element concentration decreases. The analytical variance here is based on laboratory repeats where a separate sample was leached and analysed (confirmed with lab).

The mean and RSD (relative standard deviation) of each dataset were calculated; the RSD was obtained using the formula:

$$s^2 = (\sum(x_i - x_j)^2)/2N$$

where the squares of the differences between duplicate pairs are summed, then divided by 2N, N being the number of pairs, to produce the variance s^2. The RSD in %, or Coefficient of Variation, is calculated from

RSD = 100s/X
where X is the mean of all duplicates.

Histograms of these RSD data were then created; elements where > 90% of the data was below detection limit were omitted. Values below detection limit were set to DL/2 for the 2009 data (Jackson set them to the actual DL in 2008). Examples of these histograms are shown in Figures 4.1-4.2 for aqua regia digestion of the A1 and P1 (organic) soils (all histograms are provided and discussed in detail in Part II). We see a typical steady progression to more variability as we go from lab duplicates, to the A1 STD, to field duplicates and finally to year-to-year duplicates.

Table 4.1 provides the RSD data (minimum, median and maximum) for field and year-to-year duplicates whereas Table 4.2 provides the RSD data for the standard, A1 for an organic suite and B1 for an inorganic suite, where analysed and for lab duplicates, where provided by the lab.

Table 4.1. Relative standard deviation for field duplicates and year-to-year duplicates for various leaches. 'n' refers to the number of duplicates, for example there are 15 field duplicate pairs for aqua regia on organic samples and 58 pairs of year-to-year field duplicates. Organics include A1 and P1 (peat) horizons. Inorganics are all other samples.

	Field dup RSD, %			Yr-to-Yr field, RSD, %		
Leach	**Min**	**Median**	**Max**	**Min**	**Median**	**Max**
Aqua regia, organics, n=15, 58	13, Cu	28, Sb	105, Sn	22, Ga	36, K	118, Au
Aqua regia, inorganics, n=21, 75	14, Ti	25, Li	241, Au	20, Pb	28, La	66, Ag
Enzyme leach, inorganics, n=10, 60	11, Ta	52, Re	142, Mo	33, Rb	72, La	174, Sb
Pyrophosphate, organics, n=12, 58	12, Pb	32, Bi	107, Mn	25, Ba	51, I	257, Ta
Ammonium acetate, inorganics, n=22, 73	9.6, Tl	38, La	75, Sr	28, Rb	56, Mg	105, La
MMI, n=10, 56	17, Ta	53, La	132, Sn	29, Sc	68, Ag	173, Sn
Hydroxylamine, inorganics, n=12	8.0, Co	30, U	217, Zn			
Hydroxylamine, organics, n=3	7.4, V	28, La	108, Pb			
Bioleach, organics, n=19, 51	33, Sc	62, Tl	384, Cd	61, Be	109, Sc	319, W
Bioleach, inorganics, n=12	20, Mo	32, Lu	315, Li			

From the median RSD data in Table 4.2 the performance of the Enzyme leach ('ENZ') on the B1 STD is significantly inferior to that of the ammonium acetate leach ('AA5') or aqua regia (medians of 24, 9.2, 10%, respectively) which is not surprising given the much lower concentrations leached. The same is true for the lab duplicate variability (Table 4.2). Data for the A1 STD indicates that the pyrophosphate leach ('PYRO') variability is in the same order at that of aqua regia ('AR'). The lab duplicate RSDs for the Bioleach and Enzyme leach are significantly worse than those of the other partial leach, MMI.

The median RSDs for the field duplicates fall into two groups: the best comprise aqua regia, pyrophosphate, ammonium acetate and hydroxylamine leaches ('HYD') (25-38%); and the worst include the Bioleach, Enzyme and MMI (52-62%) (Table 4.1, Fig. 4.3). Again, the major difference between these two groups is concentration levels, the first group being higher, although numerous elements are below detection limits for these partial leaches. Given these performances it is not surprising that the order of RSD, from best to worst, for year-to-year reproducibility is AR<PYRO<AA5<MMI<ENZ<BIO (Table 4.1). This is demonstrated by the scatterplots in Figs 4.4 and 4.5. A median RSD for year-to-year variability of 109% for the Bioleach, where the number of pairs is as high as 51, is cause for concern. A scan of this dataset indicates that most of the elements report significantly lower concentrations in 2009, as shown by Fig 4.4 for U and Br (W, however, has far higher concentrations in 2009). This may well be due to the gap of almost 14 months in sampling, but it would have been useful to have had a standard or two analysed in both years. Interestingly, the pyrophosphate leach, also applied to the organic soils, does not show this bias (Fig. 4.5). Bromine by the Enzyme leach on inorganic soils, shows much higher concentrations in 2009 (Fig. 4.6).

Table 4.2. Relative standard deviation for the standard ('STD', A1 for organics and B1 for inorganics, 2009 only) and laboratory duplicates. 'n' refers to the number of STD samples analysed and to the number of laboratory duplicates, for example there are 7 subsamples of the STD analysed and 4 lab duplicate pairs for aqua regia on organic samples.

	STD RSD, %			Lab dup RSD, %		
Leach	**Min**	**Median**	**Max**	**Min**	**Median**	**Max**
Aqua regia, organics, n=7, 4	6.2, S	11, Li	70, Au	1.1, Pb	4.4, Rb	37, Au
Aqua regia, inorganics, n=5, 5	4.3, Zn	10, Sr	103, W	1.8, Mn	6.1, Sc	51, Cd
Enzyme leach, inorganics, n=6, 11	6.3, Mn	24, Tb	140, Dy	2.6, I	16, Pr	53, Pb
Pyrophosphate, organics, n=6	4.6, Gd	9.5, La	59, Li			
Ammonium acetate, inorganics, n=6, 6	5.2, Rb	9.2, Ce	160, V	1.0, Zn	4.5, Gd	175, V
MMI, n=11				4.2, Dy	9.4, Fe	33, Cd
Bioleach, organics, n=11				4.9, U	20, La	293, Li
Ionic leach, n=3	1.3, Au	6.2, Ag	Eu, 21			

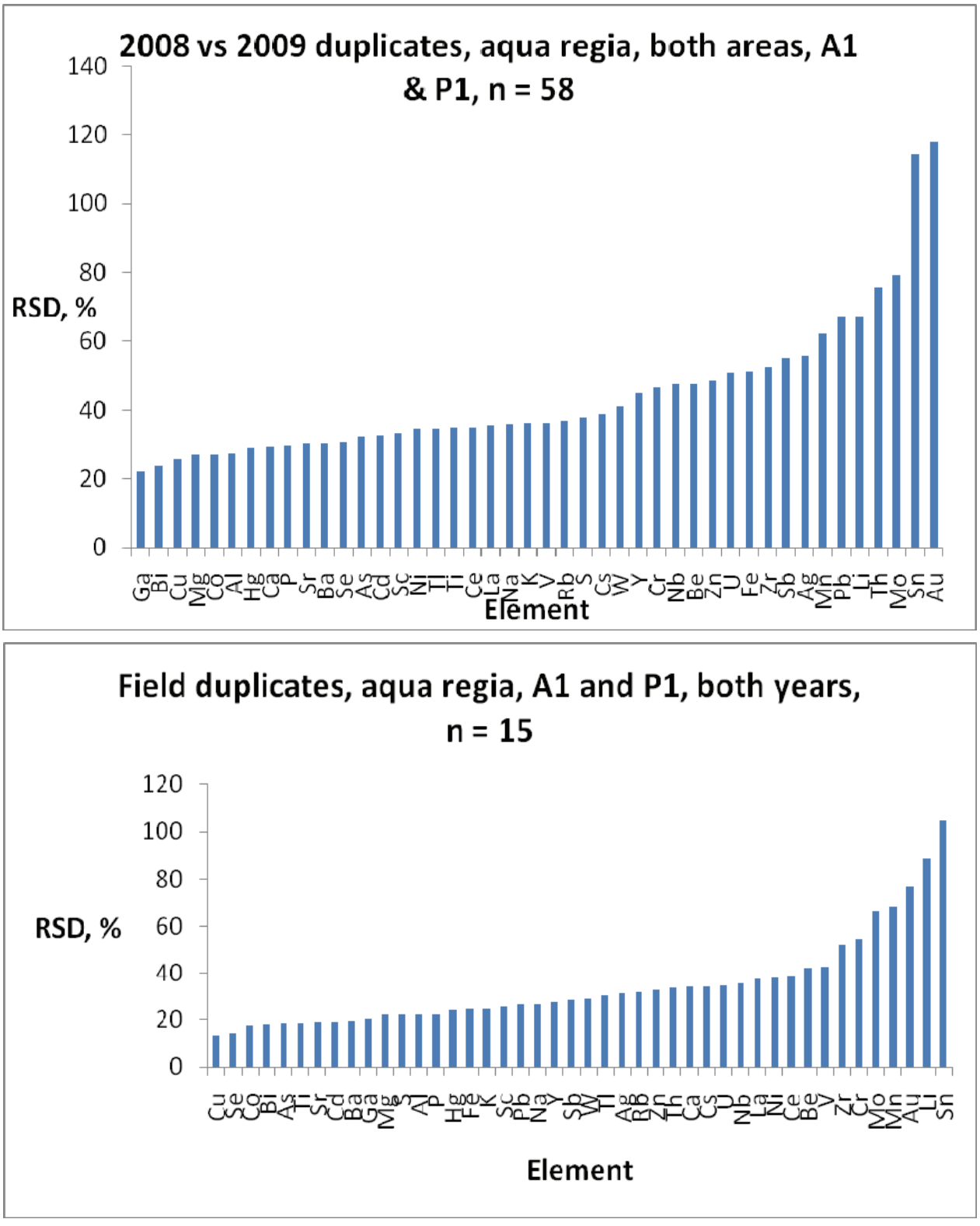

Fig 4.1 RSDs for aqua regia on organic soils (A1 and P1 horizons).

Top: year over year duplicates; bottom: field duplicates , same year

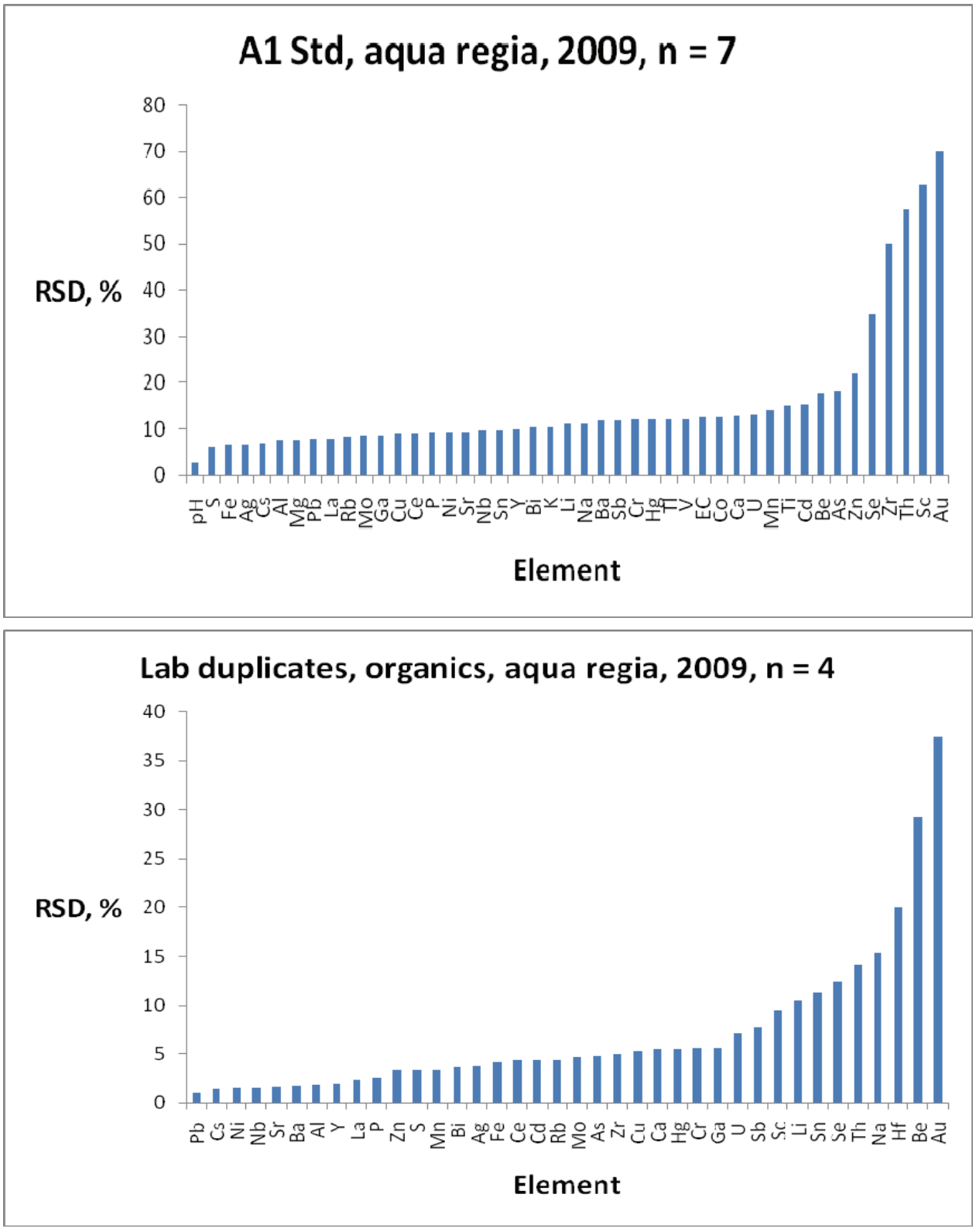

Fig 4.2 RSDs for aqua regia on organic soils
Top: for A1 STD (standard); bottom: for lab duplicates

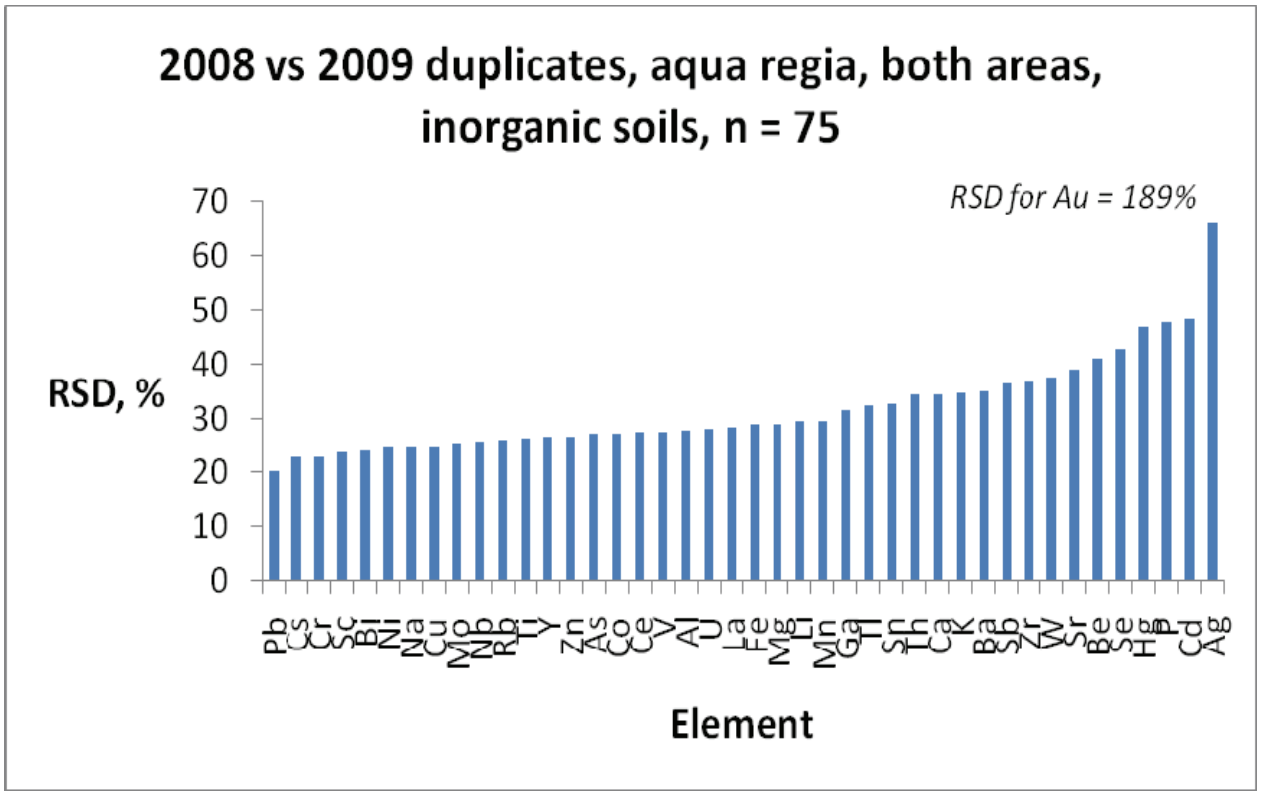

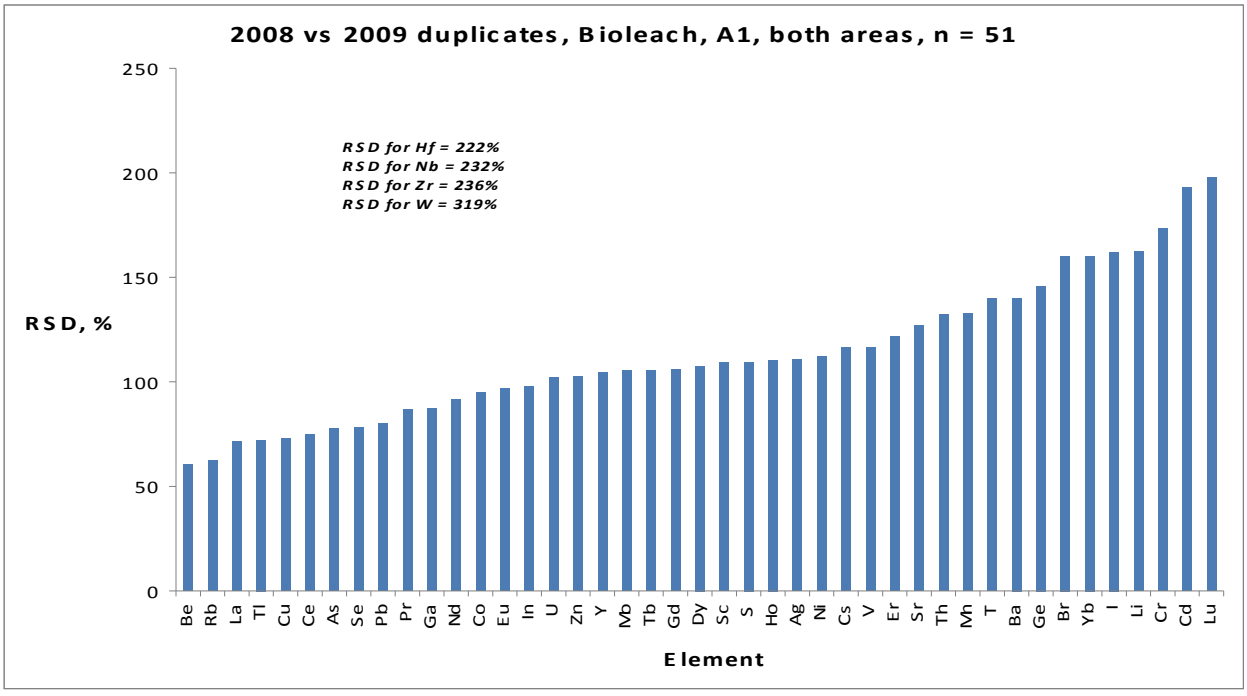

Fig 4.3 Contrasting performance of year-to-year variability.
Top: aqua regia on inorganic soils (A1, P1), Bioleach on organic soils (bottom).

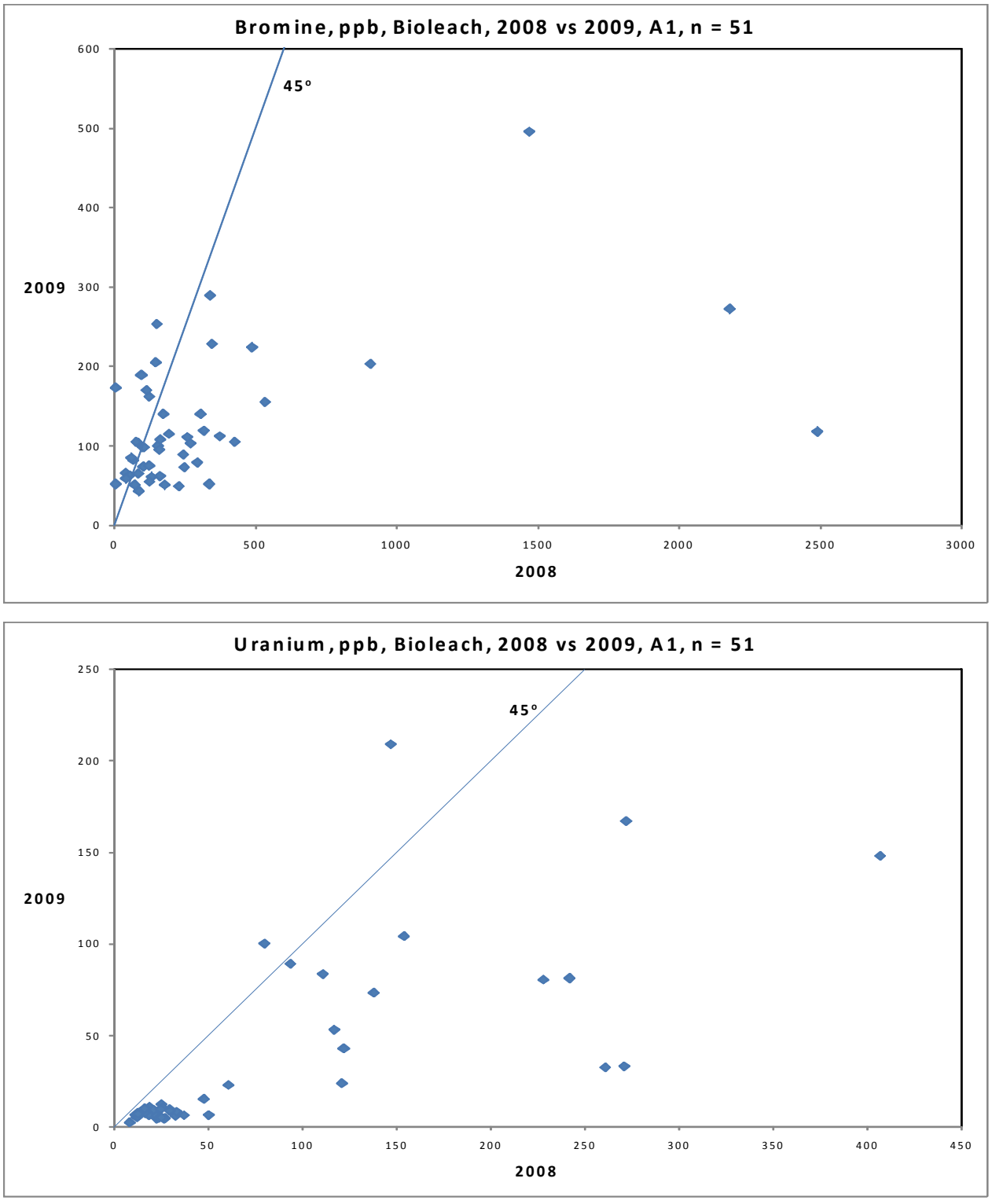

Fig 4.4. Bromine (top) and uranium (bottom) plots of samples taken at the same sites in both 2009 vs 2008, i.e. year-to-year duplicates for the Bioleach

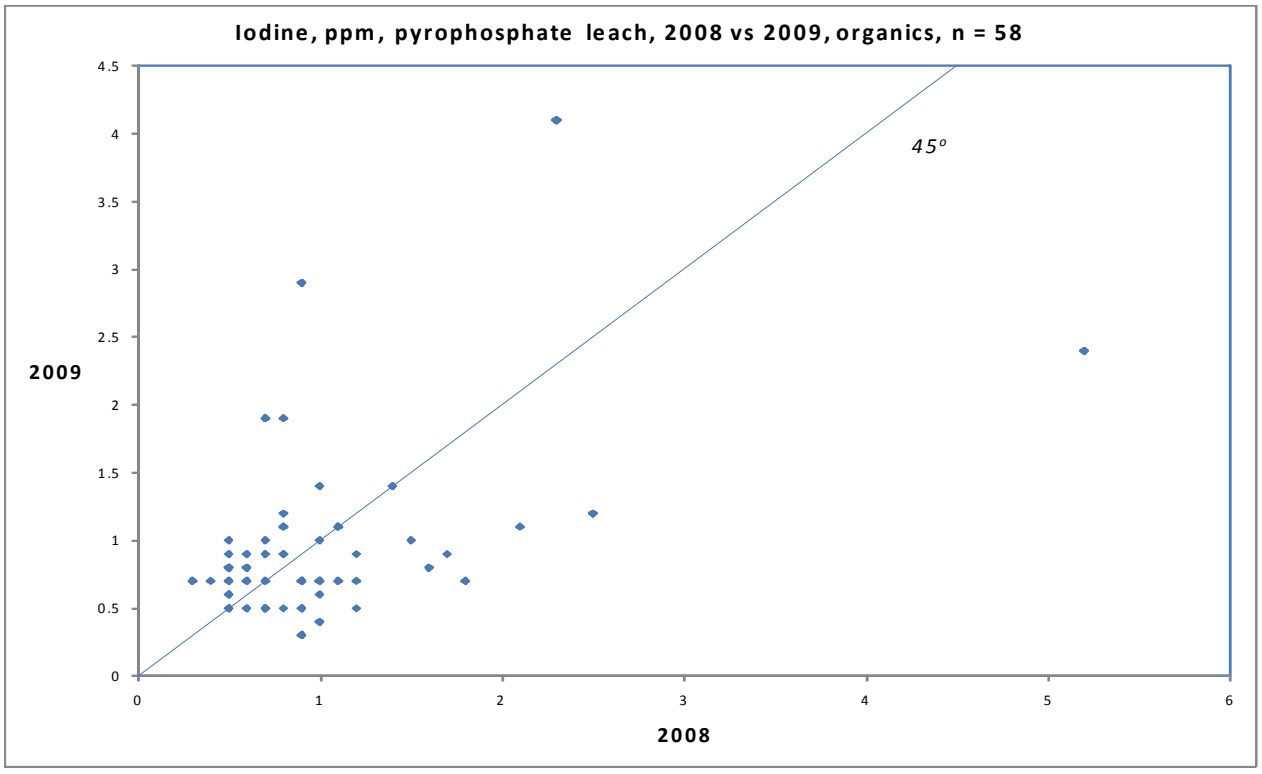

Fig. 4.5. Iodine in 2009 vs 2008; year-to-year duplicates for the pyrophosphate leach

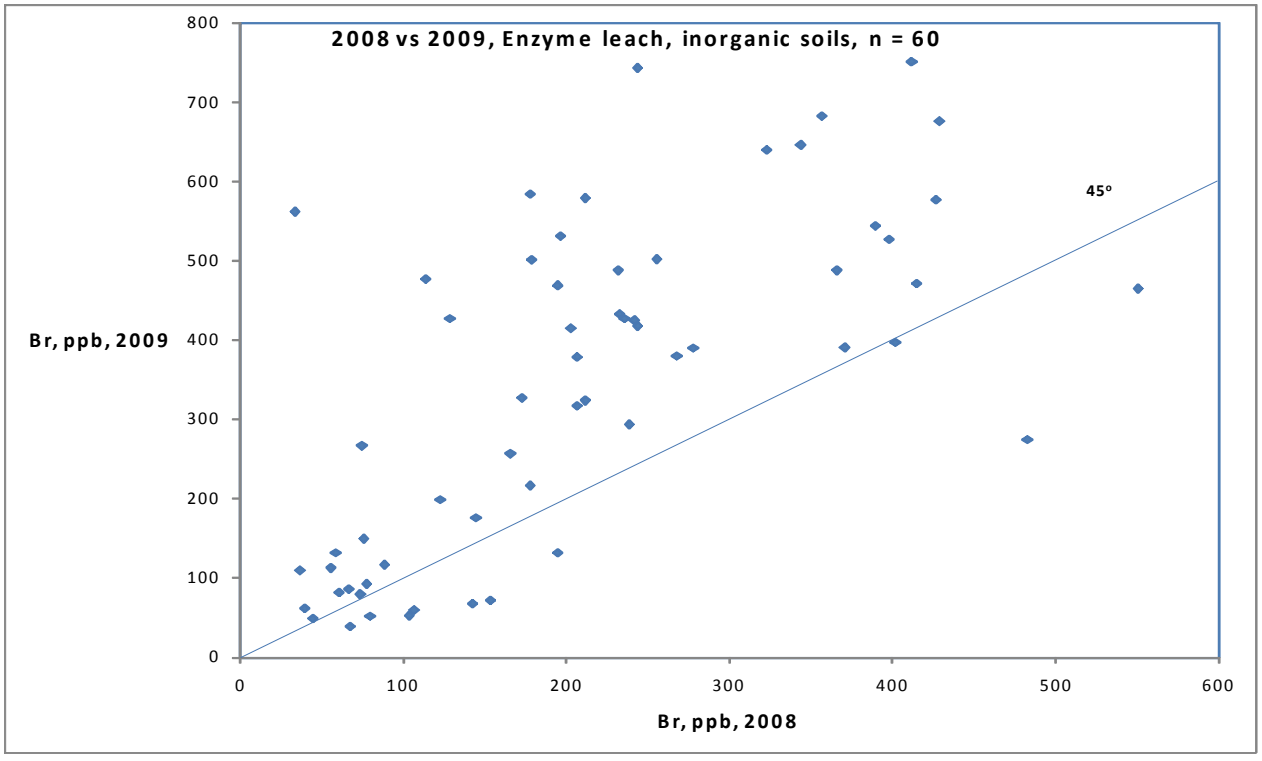

Fig 4.6 Bromine in 2009 vs 2008; year-to-year duplicates for Enzyme leach

4.2 Variability using Element Profiles

The folders of plots under review are those on the CD labelled 'jpeg' (showing Box and Whisker and X-Y plots of year-to-year duplicates, to evaluate any bias between years of sampling) and 'jpeg 1' (showing responses of A1, B1 and C horizons for all five Lines, to evaluate consistency of anomalies). There are 'jpeg' and 'jpeg1' folders for each leach in each area. Fig 4.7 illustrates two of these 'jpeg' plots for S and Sb at Cigar in the A1 horizon by aqua regia. They show that some bias in these two elements exists between years. Each 'jpeg' plot has 4 graphs: the upper left shows a scatterplot of field duplicates (from all horizons, shown as squares) 2008 vs 2009. The 45 deg line is solid, and line of best fit is dashed (only constrained to go through the origin). Bias is indicated if the dashed line deviates strongly from 45 deg. Triangles show duplicates taken at the same site and year, but are not included in the best fit calculation. The box and whisker plot (upper right) compares the data by year and also does not include the same year duplicates (triangles in first plot). The boxes are notched, with the notch being centered on the median, and width of notch being equal to a 95% confidence interval on the median. Thus the medians of the two years are different at 95% level of confidence if the notches do not overlap. The line profiles in the lower two plots show year by colour, so where both years are sampled, then two colours are present. 'jpeg1' plots are straightforward stacked profiles in three columns (A1, B1, C) looking across lines from east to west, with Line 1 at the bottom of the page, and Line 5 at the top. Colour is used to indicate year of sampling, so these are useful to check for inter-year differences also.

Only those element profiles where there is a problem are commented upon here and therefore, by inference, those not mentioned show no significant bias. Furthermore, those elements where most of the values are close to the detection limit are omitted from discussion (i.e. there may be sporadic one-point highs along some lines but these are ignored). There are year-to-year duplicates for: aqua regia (A1, P1, B1, C); pyrophosphate leach (A1, P1); Enzyme (B1, C); MMI (MMI horizon); and Bioleach (A1, P1). The complete set of QC plots and profiles are on the CD and in Part II of the report accompanied by more discussion.

Cigar Lake
In 2009 parts of Lines 1 and 2 were resampled for A1, B1 and C horizons while Line 4 was completely resampled (and extended) for A1 and B1 horizons.

Only sulphur and antimony by aqua regia show any bias between years (Fig 4.7, top, S; and bottom, Sb). Sulphur is at detection limit for most of the inorganic soil samples but is measurable, albeit at very low levels, in the A1 horizon. While the Box and Whisker (B&W) plots indicate a significant difference in medians and therefore a bias, this is probably the influence of setting values < DL to DL/2 in the second year and not in the first. However, there is clearly a bias towards higher values in 2009. The response of S in the A1 horizon on Line 3 over the deposit is interesting, a consistently elevated signal over ~ 500 m of the line. The multi-line plots for Ce, Fe, La, Nb, Th, Ti, U, V, Y and Zr by aqua regia show anomalies in A1 on Line 1 that are present in 2008 but not in 2009; these are in the gleysol area (Fig 4.8, U). This figure demonstrates that, although there are occasional one–point highs (e.g. Line 4, 2009), the *trends* remain. The non-reproducible anomalies on Line 1 and 4 also are evident in the pyrophosphate leach, indicating this is not an analytical problem.

The pyrophosphate leach shows a small bias evident between years for Bi, Cd, Mo, Pb, Tl, U and V, all showing higher concentrations in 2009 and for Nb, Sb and Ti showing higher concentrations in 2008 (Fig 4.9, top U; bottom Sb).

As mentioned previously, there is a shift in Br values by the Enzyme leach between years but

this shift is even larger for I, as indicated by the multi-line plots (Fig. 4.10, iodine). This large shift for Br and I, to much higher concentrations in 2009, is not evident in the Bioleach for these two elements (in fact most elements are higher in *2008* in the Bioleach, though Br and I are only moderately different). As both analyses are carried out at the same lab, this suggests these changes are not due to analytical error but to real changes in the field that have a profound effect on these particular methods. While the trends in the Enzyme leach on Line 4 in B1 are still evident, those on Line 2 in C-horizon are not. The anomaly for the REEs and U on Line 4 in B1 just south of the pod in 2008 has shifted to just north of the pod in 2009; furthermore, the patterns in the C-horizon on Line 2 are quite different (4.11, Ce).

In the ammonium acetate leach, only Th shows a bias between years (Fig. 4.12 Th). There are, however, numerous one-point anomalies close to the DL that do not repeat, as shown for P (Fig. 4.13, P).

As with other partial leaches, much of the data for the MMI leach are at or close to the detection limit for elements such as As, Bi, Ca, Mg, Mo and Tl. Concentrations of Rb, U, V, Zn and Zr are significantly higher in 2008 (Fig.4.14 top,Rb; bottom U). Note the high in U over the pod on Line 4 repeats in the 2009 data, though of less magnitude, but that to the south does not. In the multi-line plots, Lines 1 and 4 show two one-point anomalies for the REEs over the pod in 2009 that were not in evidence in 2008 (Fig 4.15, Ce).

Data for the Bioleach are not comparable year-to-year: Fig 4.16, U demonstrates the much higher concentrations reported in 2008 for the vast majority of elements. The multi-line profiles for Ba and I show that anomalies evident in one year are not repeated in the next (Fig. 4.17, Ba; Fig 4.18, I); this is the case for numerous elements.

McClean Lake

This dataset is much smaller as only part of Line 4 was repeated in 2009.

The only significant inconsistencies in the aqua regia dataset are for Mo and P, showing higher concentrations in 2009 and sometimes dissimilar patterns on Line 4 (Figs.4.19, Mo; Fig 4.20, P).

As with aqua regia, the year-to-year repeatability of the pyrophosphate leach is excellent for most elements (e.g. Fig. 4.21, Th). Note the clear multi-point anomalies over the pods on Line 3 which are evident for numerous elements (including Mo).

Elements that have significantly higher concentrations in the Enzyme leach in 2009 include Br, Cd, Co, Cu, Mn, Ni, I, Pb and Sr (Fig. 2.22, top: I). Note that the trend towards higher levels of I in the south is still there but is much more dramatic in 2009. Significantly greater values in 2008 are evident for Dy, Tl, W and Zn (Fig. 22, bottom: Tl). These shifts are more prevalent than at Cigar Lake. Some trends are similar, as for U south of the pod, and some are not, as for U north of the pod.

The ammonium acetate dataset shows good performance, though the number of elements with

adequately high concentrations is limited. The only bias is that for Th, as at Cigar Lake and, as it is the only element behaving this way, the cause is probably a calibration change in the analysis.

There are no instances of bias for MMI here, as there are at Cigar Lake. Both years show a general increase in Fe, Nb, Cr and V from the south pod towards the north but the site-to-site agreement is poor (Fig. 4.23, top: Fe).

As at Cigar Lake, elements such as As, Cd, Co, Pb, Th, U and the REEs by the Bioleach all show significant differences in concentrations between years, with higher values in 2008, and these responses can also differ in pattern (Fig 4.23, bottom: U).

Summary

- All leaches showed the expected trend towards higher variability when moving from lab duplicates, to field and finally to year-to-year duplicates. Repeatability of data for the A1 and B1 standards and for lab duplicates was acceptable for all leaches.
- The repeatability of the aqua regia leach (AR), applied to organic or inorganic soils, is excellent for both field and year-to-year duplicates, the precision for the latter being somewhat less good but certainly acceptable (median RSDs of 27 and 32%, respectively).
- The performance of the pyrophosphate leach (PYRO) is only slightly inferior to that of aqua regia. One area (Cigar) shows a small bias in year-to-year data for Bi, Cd, Mo, Nb, Pb, Sb, Ti, Tl, U and V but this does not indicate significant changes in response patterns.
- Dramatic shifts in concentration between years are evident for Br and I in the Enzyme leach (ENZ), resulting in instances of different patterns. At McClean Lake significant changes in concentration (both up and down) between years are also evident for Br, Cd, Co, Cu, Dy, Mn, Ni, I, Pb, Sr, Tl, W and Zn. Such lack of agreement leads to a median RSD of 72% for year-to-year variability.
- The ammonium acetate leach (AA5), though severely compromised by inadequate detection limits, shows bias between years only for Th. Generally trends are maintained but one-point anomalies often do not repeat.
- There are shifts in concentration in the MMI leach for Rb, U, V, Zn and Zr at Cigar Lake; the year-to-year variability is high, with a median RSD of 68%.. Numerous one-point anomalies do not repeat.
- The Bioleach (BIO) performs very badly for most elements between years, leading to a very high median RSD of 109%. These shifts in concentration levels between years, shown for most elements by this leach and by the Enzyme leach for Br and I and several other elements, suggest that changes in the field during such a period profoundly affect the results of these very weak partial extractions.
- Given these performances it is not surprising that the order of RSD, from best to worst, for year-to-year reproducibility is AR<PYRO<AA5<MMI<ENZ<BIO. Repeatability of field duplicates is much better and in general, is acceptable. The median RSDs for the field duplicates fall into two groups: the best comprise aqua regia, pyrophosphate, ammonium acetate and hydroxylamine leaches (‘HYD’) (25-38%); and the worst include

the Bioleach, Enzyme and MMI (52-62%). It is interesting that the MMI field variability is not better than that of the Enzyme leach and yet a much larger sample is taken.

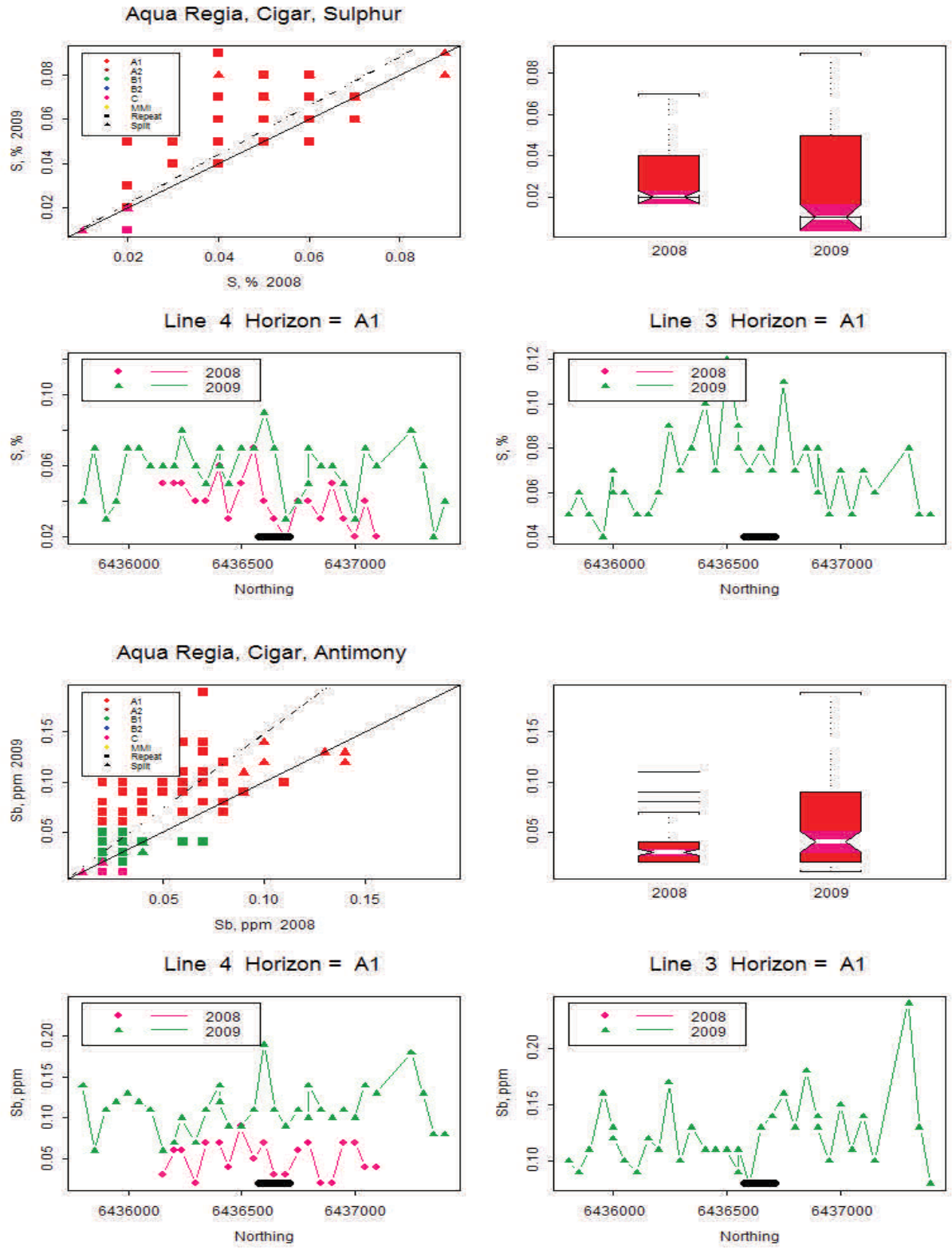

Fig 4. 7. Sulphur (top) and Antimony (bottom) from Cigar. 2009 data higher than 2008 showing in duplicates scatterplot of 2008 vs 2009, and line 4 profiles with both years

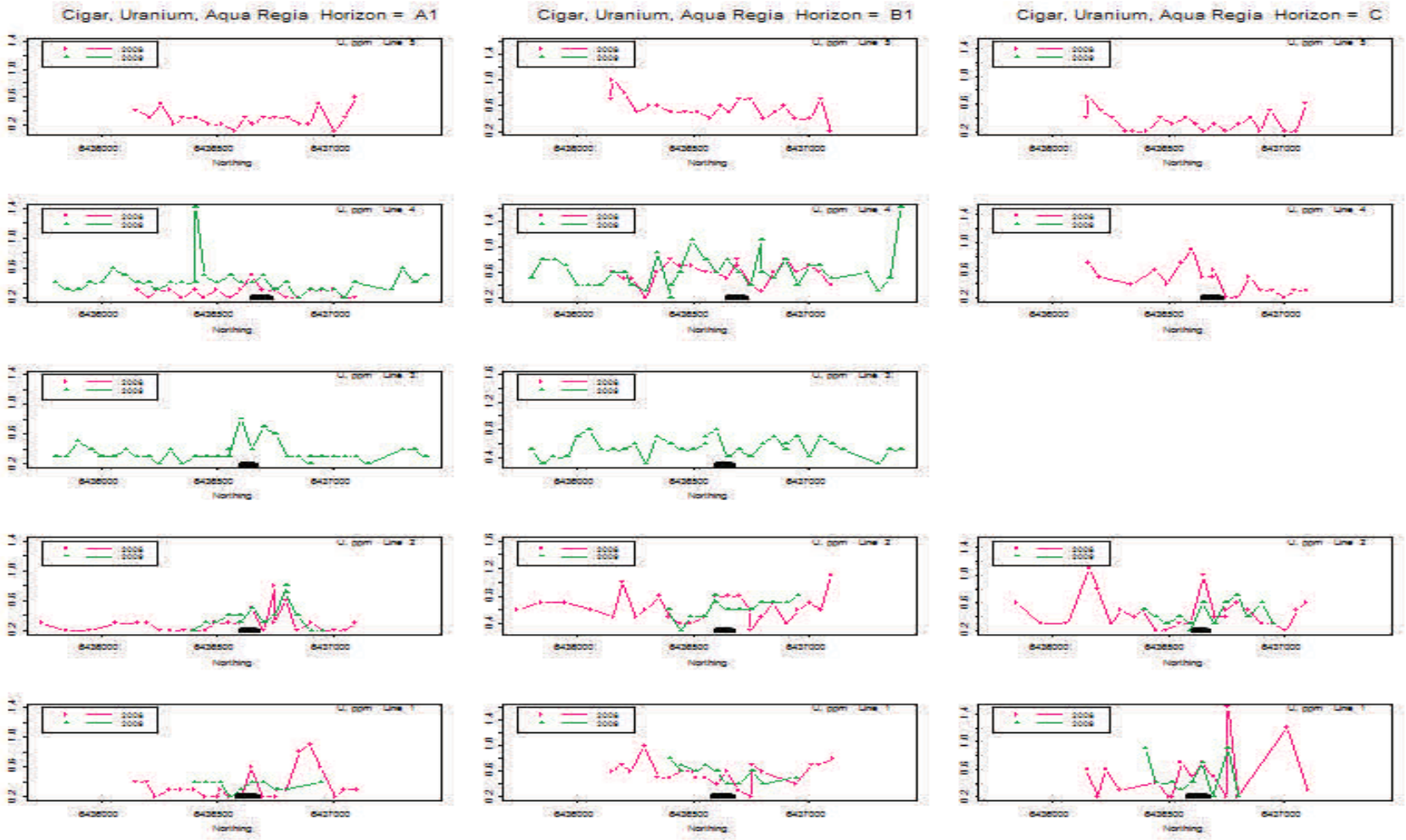

Fig. 4.8 Uranium profiles for aqua regia in A1, B1 and C horizons.

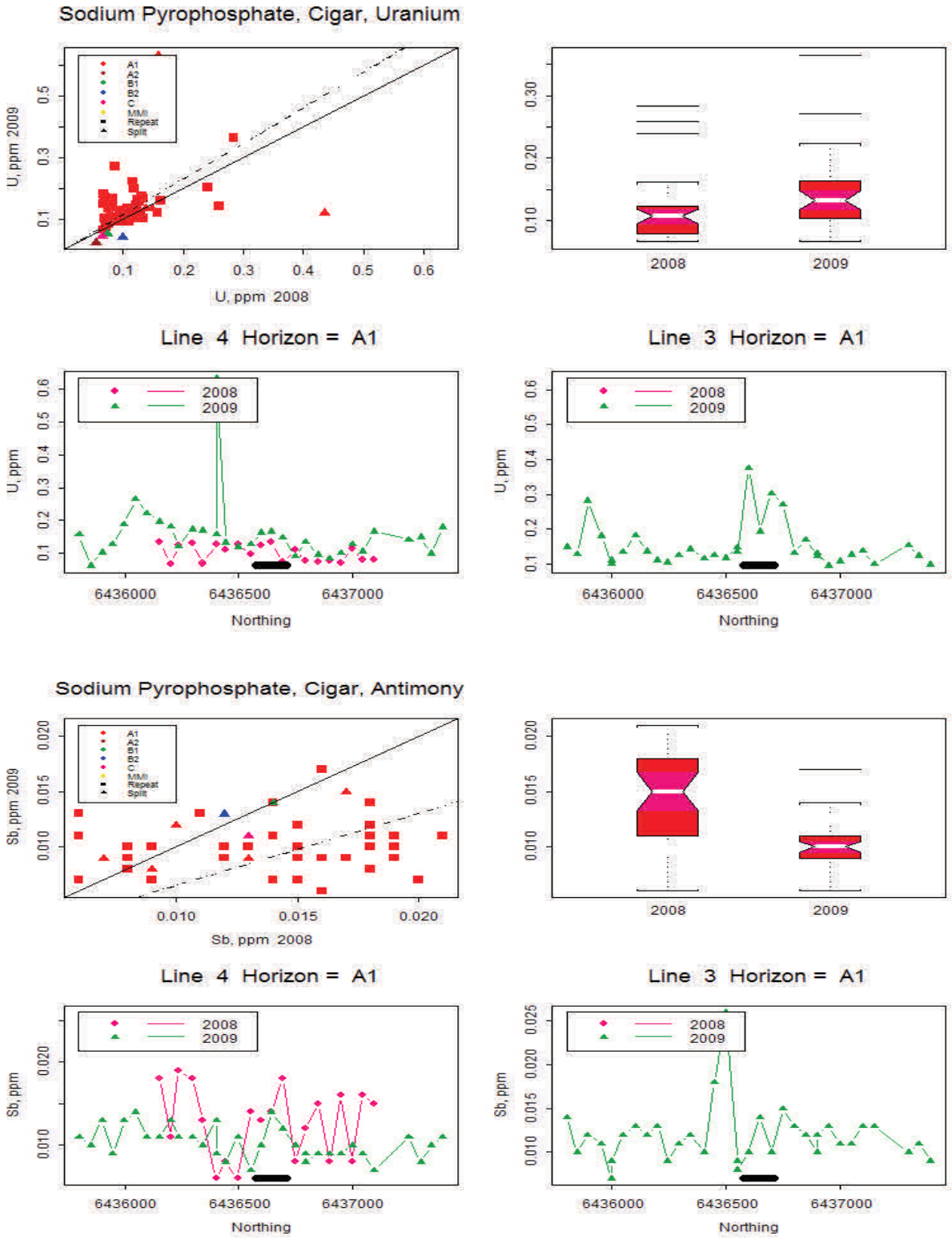

Fig 4.9 Top: Uranium by sodium pyrophosphate.
Bottom: Antimony by sodium pyrophosphate

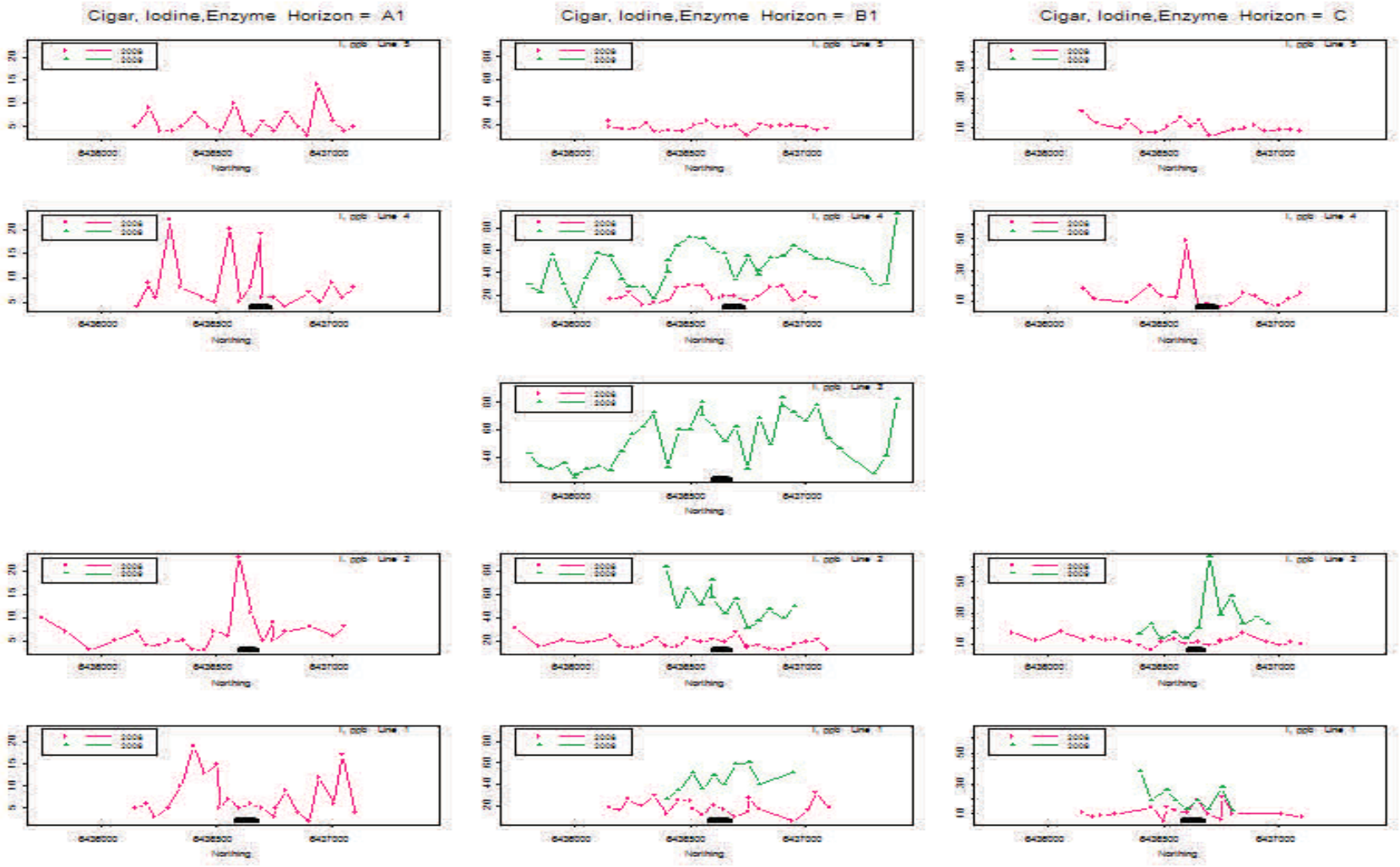

Fig 4.10 Iodine profiles at Cigar for Enzyme leach

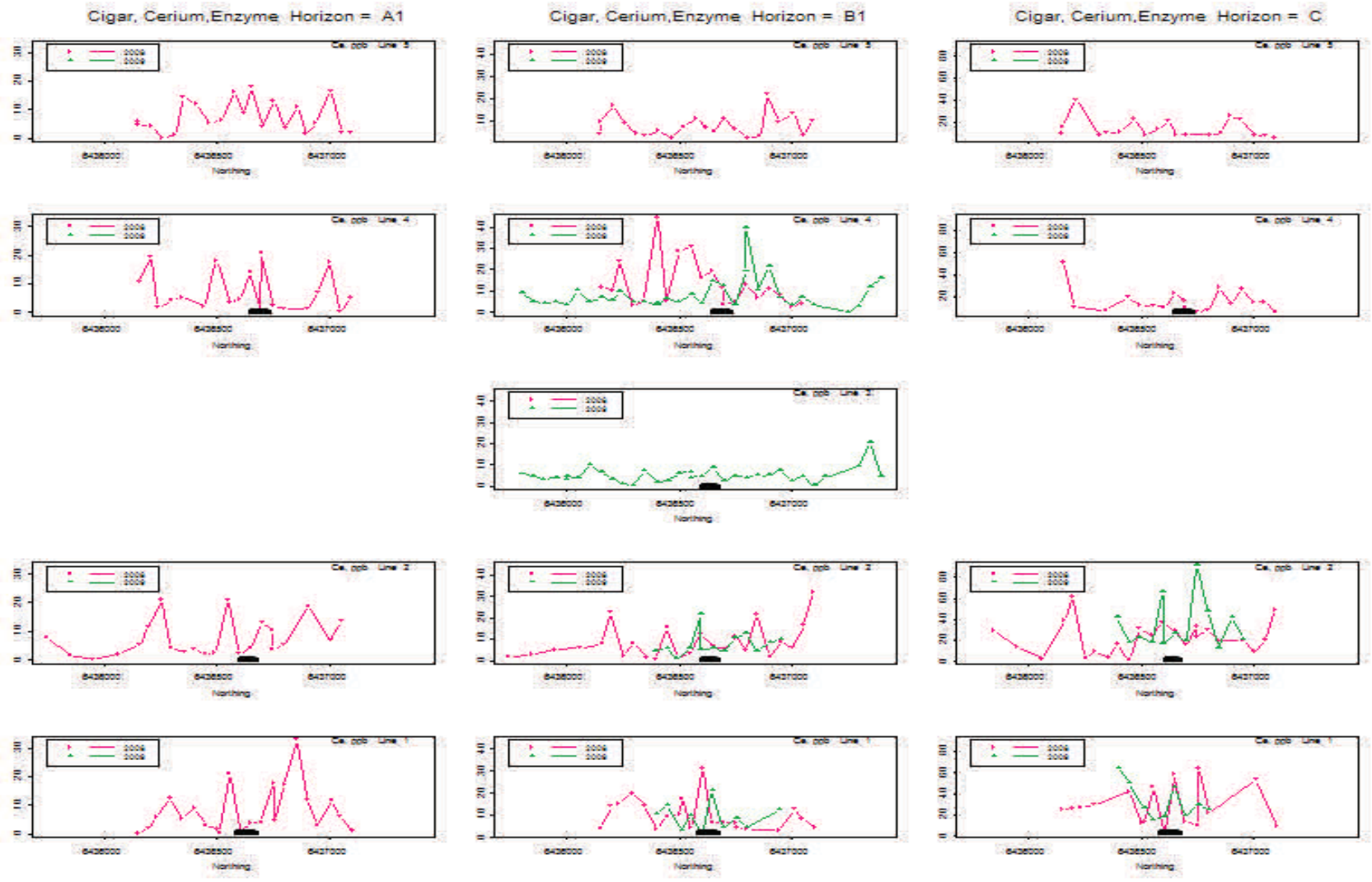

Fig 4.11 Cerium by Enzyme leach at Cigar

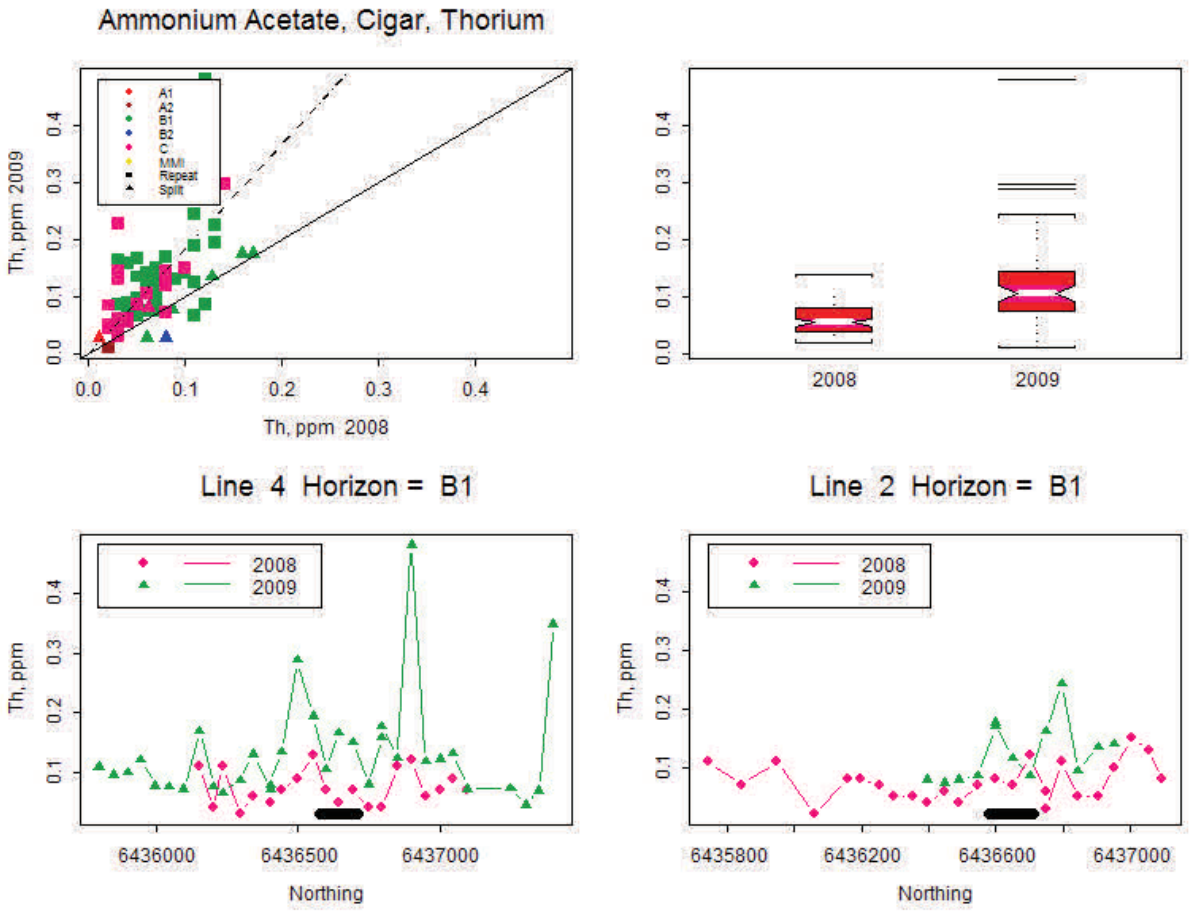

Fig 4.12 Thorium by ammonium acetate leach at Cigar.

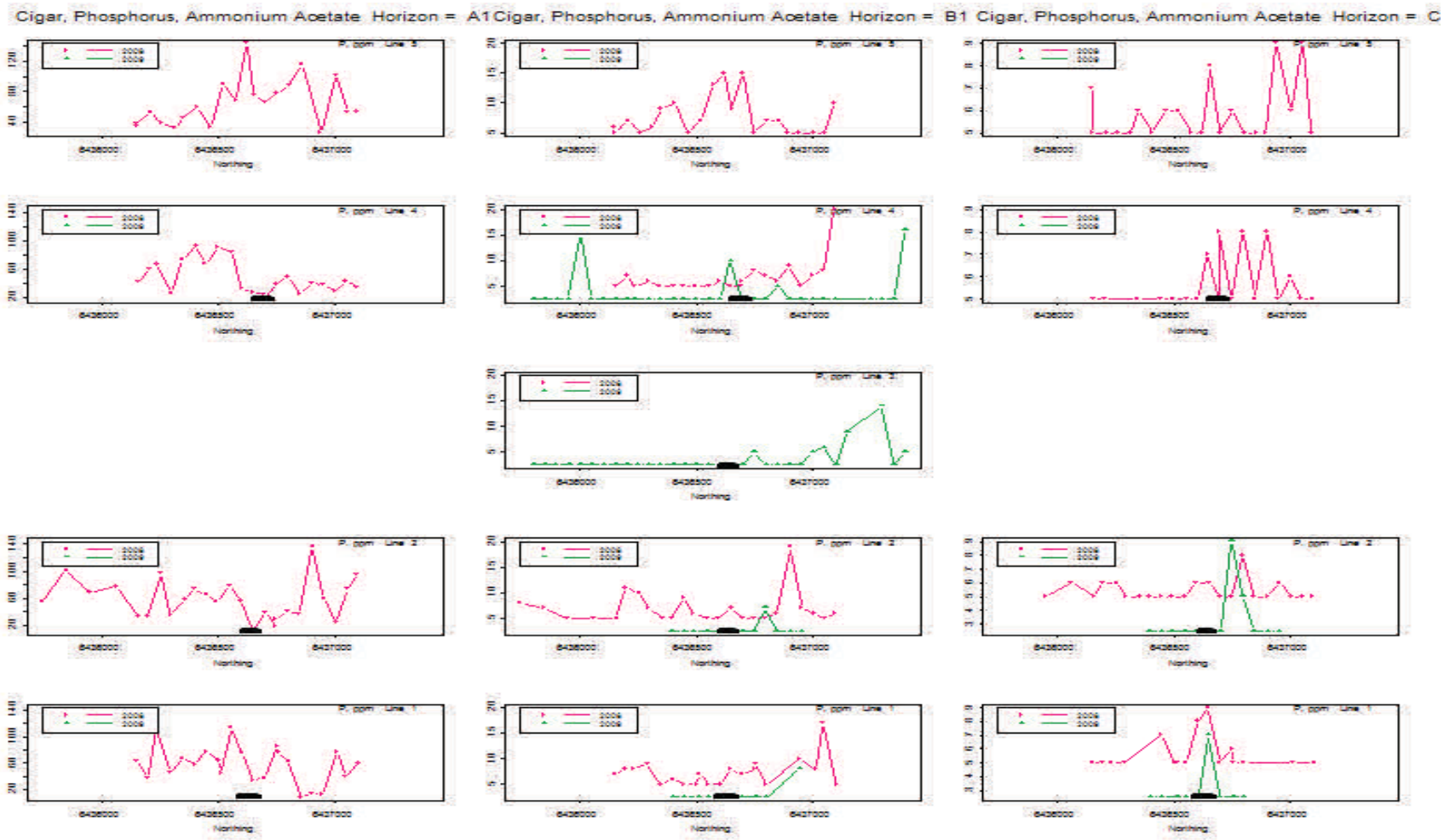

Fig 4.13 Phosphorus by ammonium acetate at Cigar.

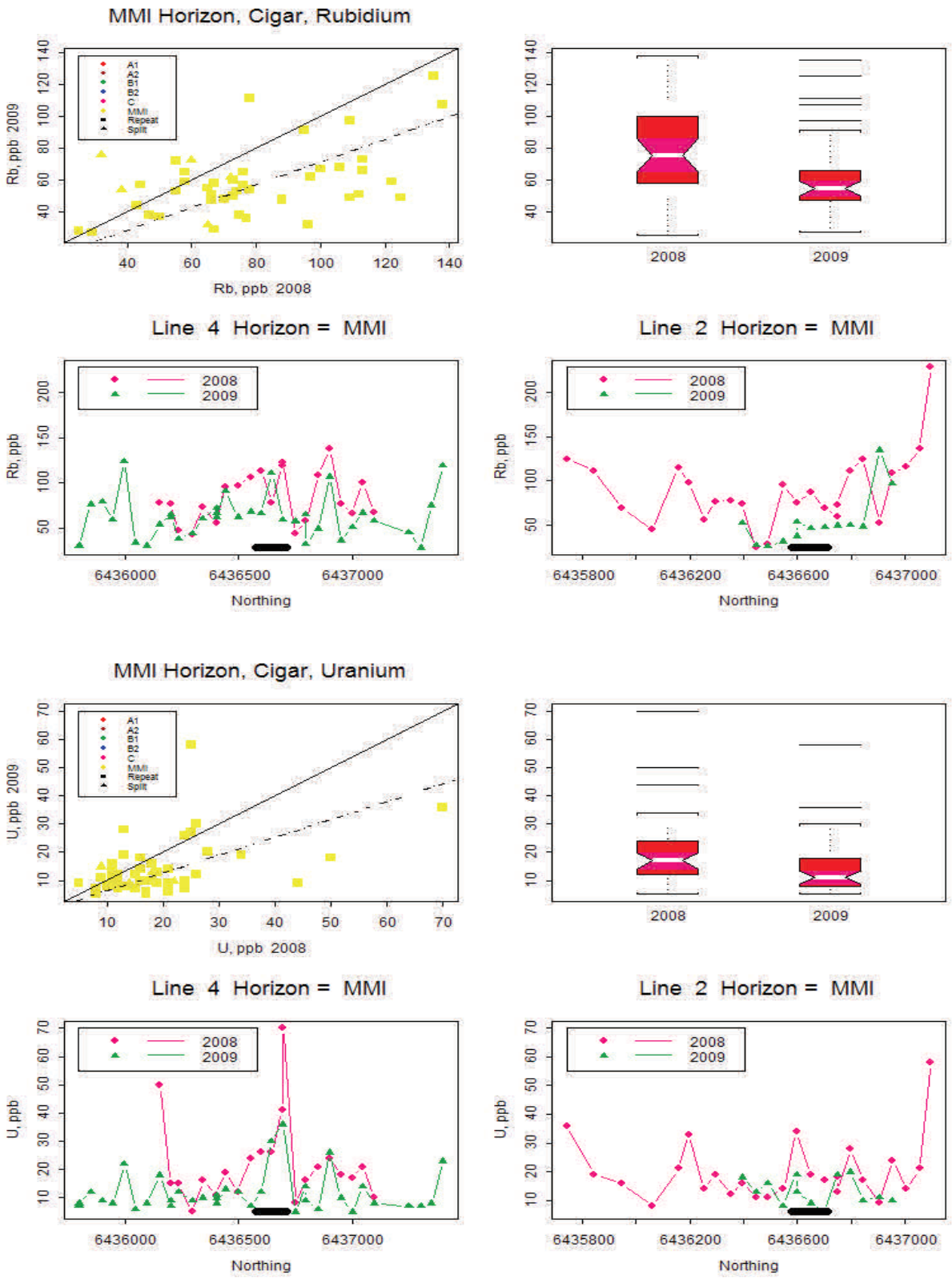

Fig 4.14 Top: Rubidium by MMI leach on MMI horizon at Cigar Bottom: Uranium by MMI leach on MMI horizon, also Cigar

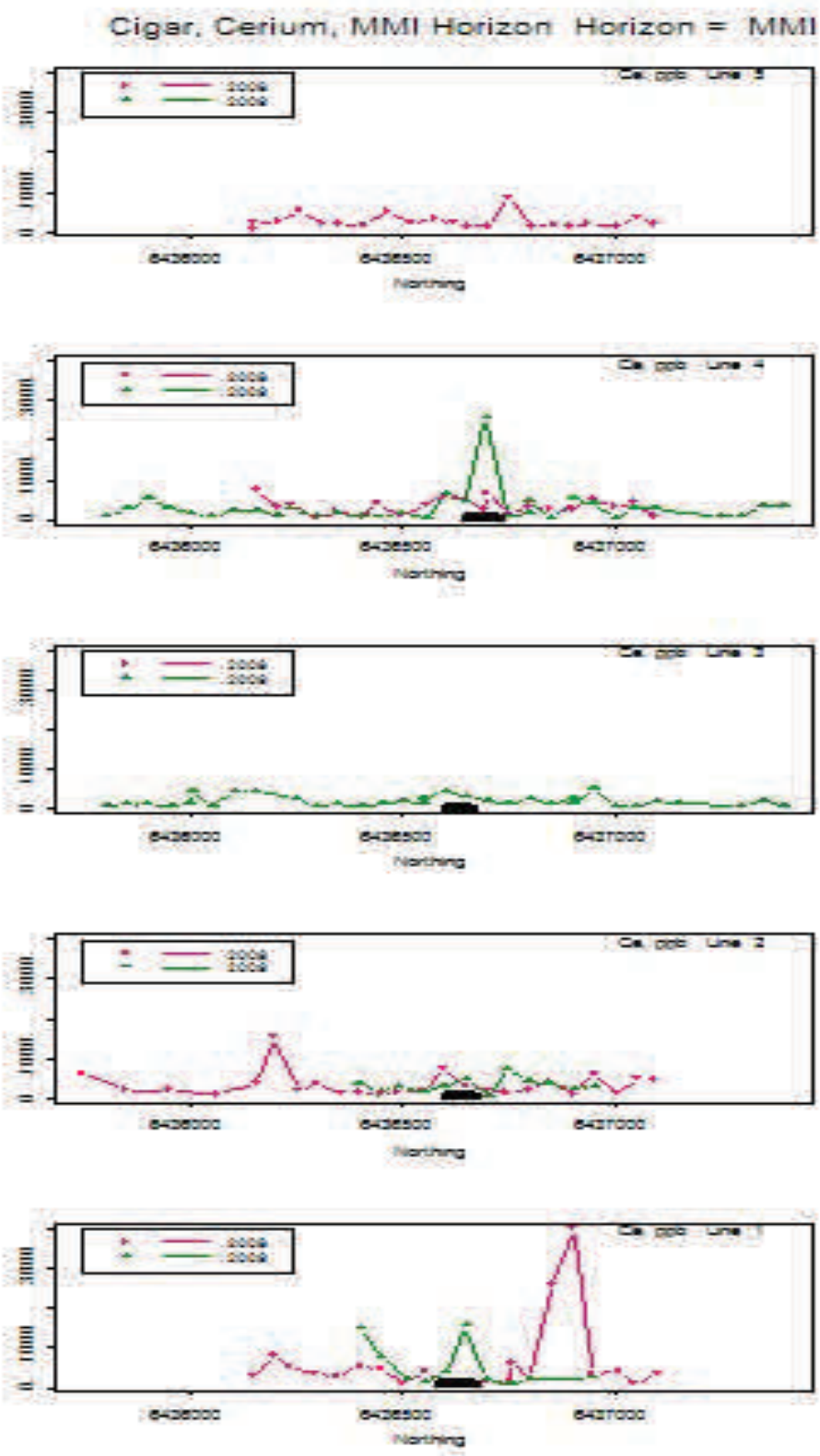

Fig 4.15 Cerium by MMI leach on MMI horizon at Cigar

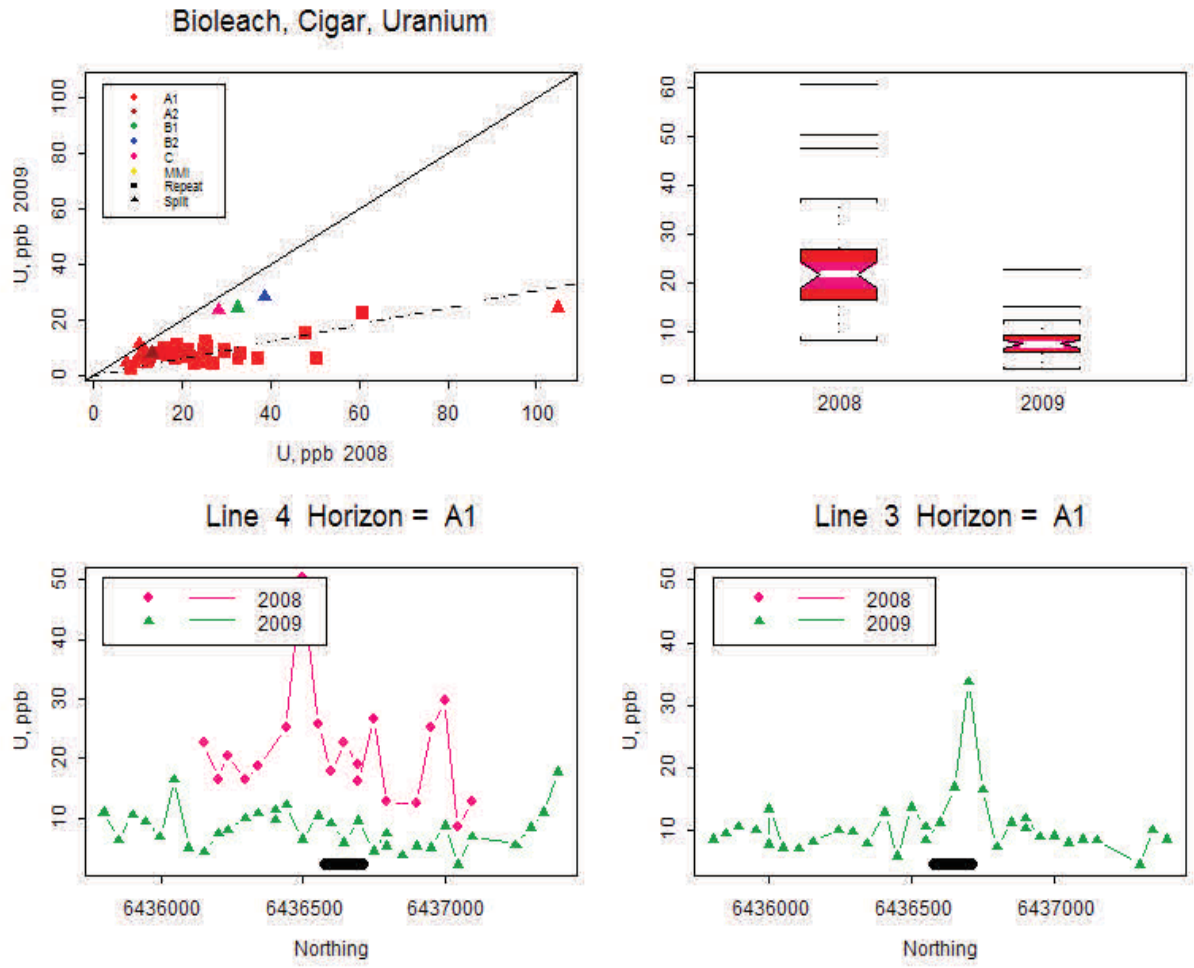

Fig 4. 16 Uranium by Bioleach at Cigar.

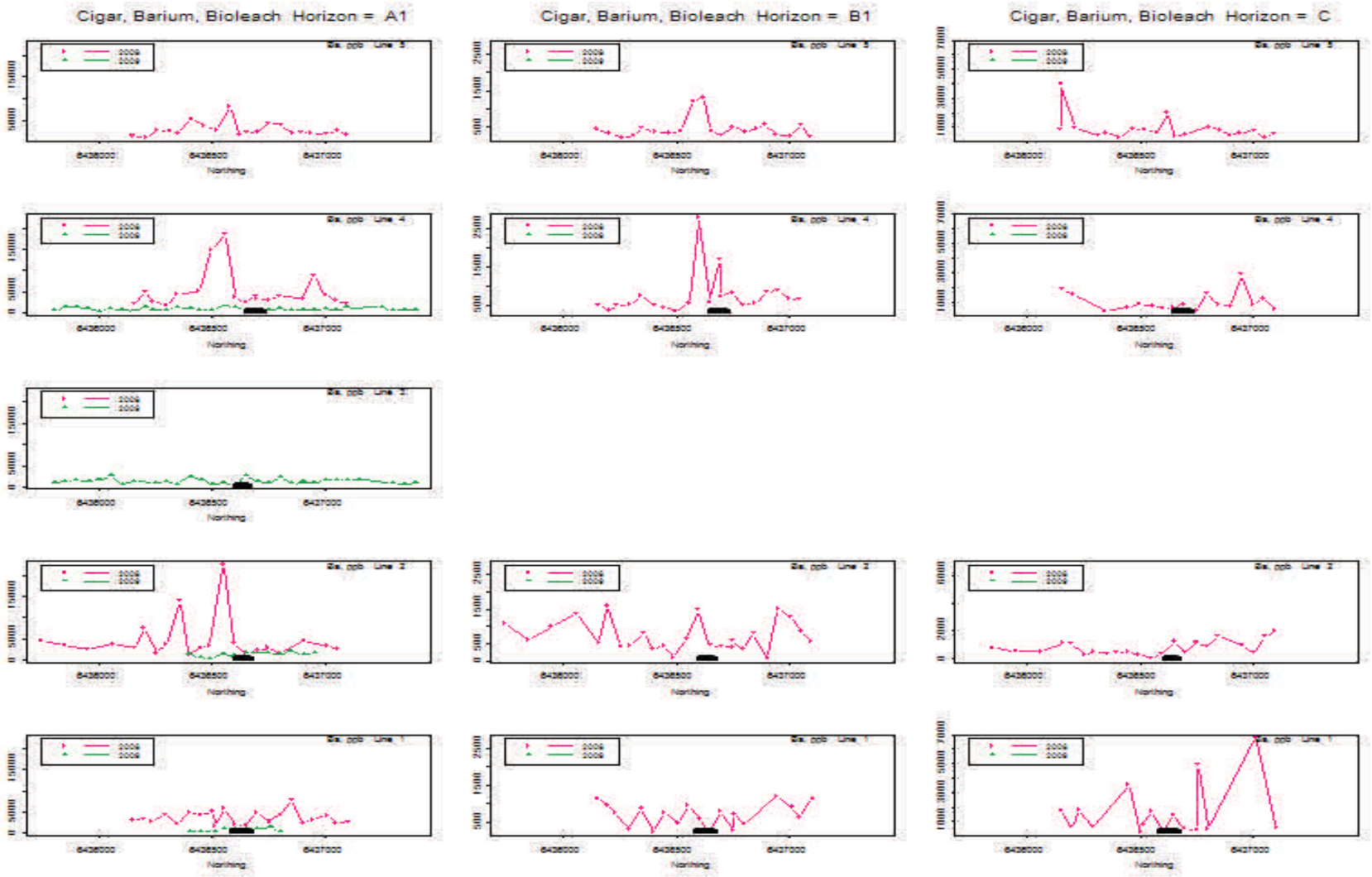

Fig 4.17 Barium by Bioleach at Cigar

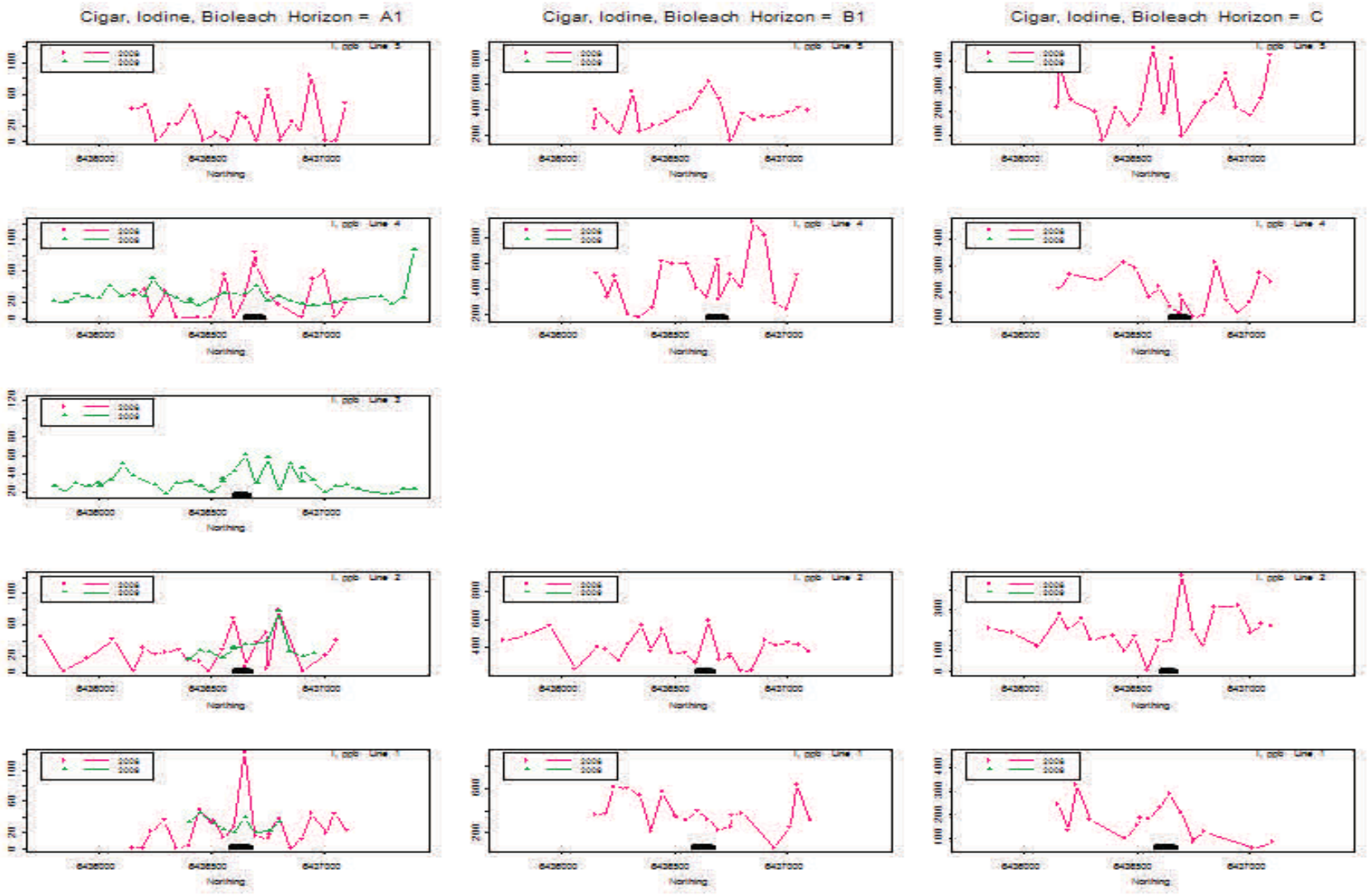

Fig 4.18 Iodine by Bioleach at Cigar

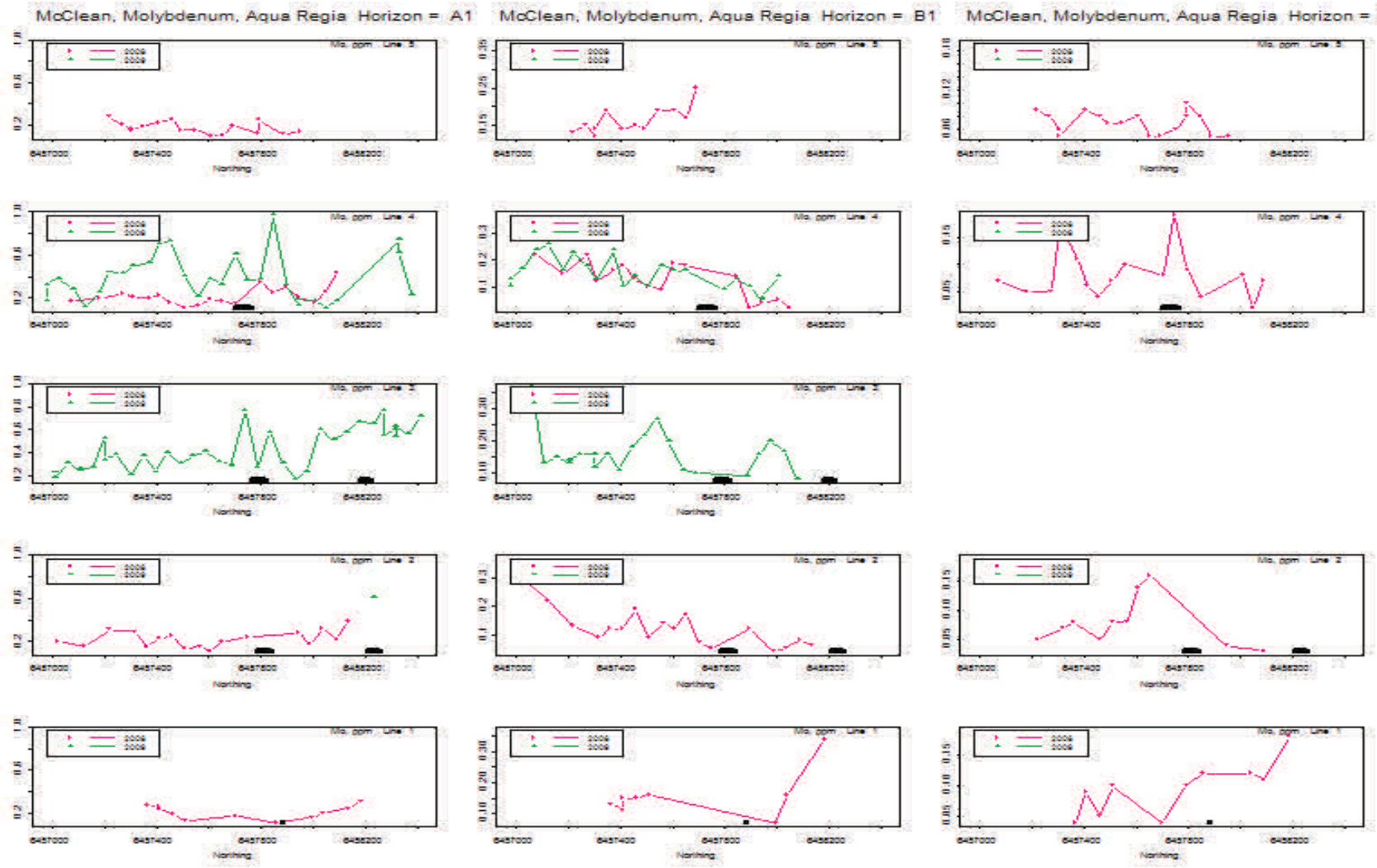

Fig 4.19 Molybdenum at McClean by aqua regia

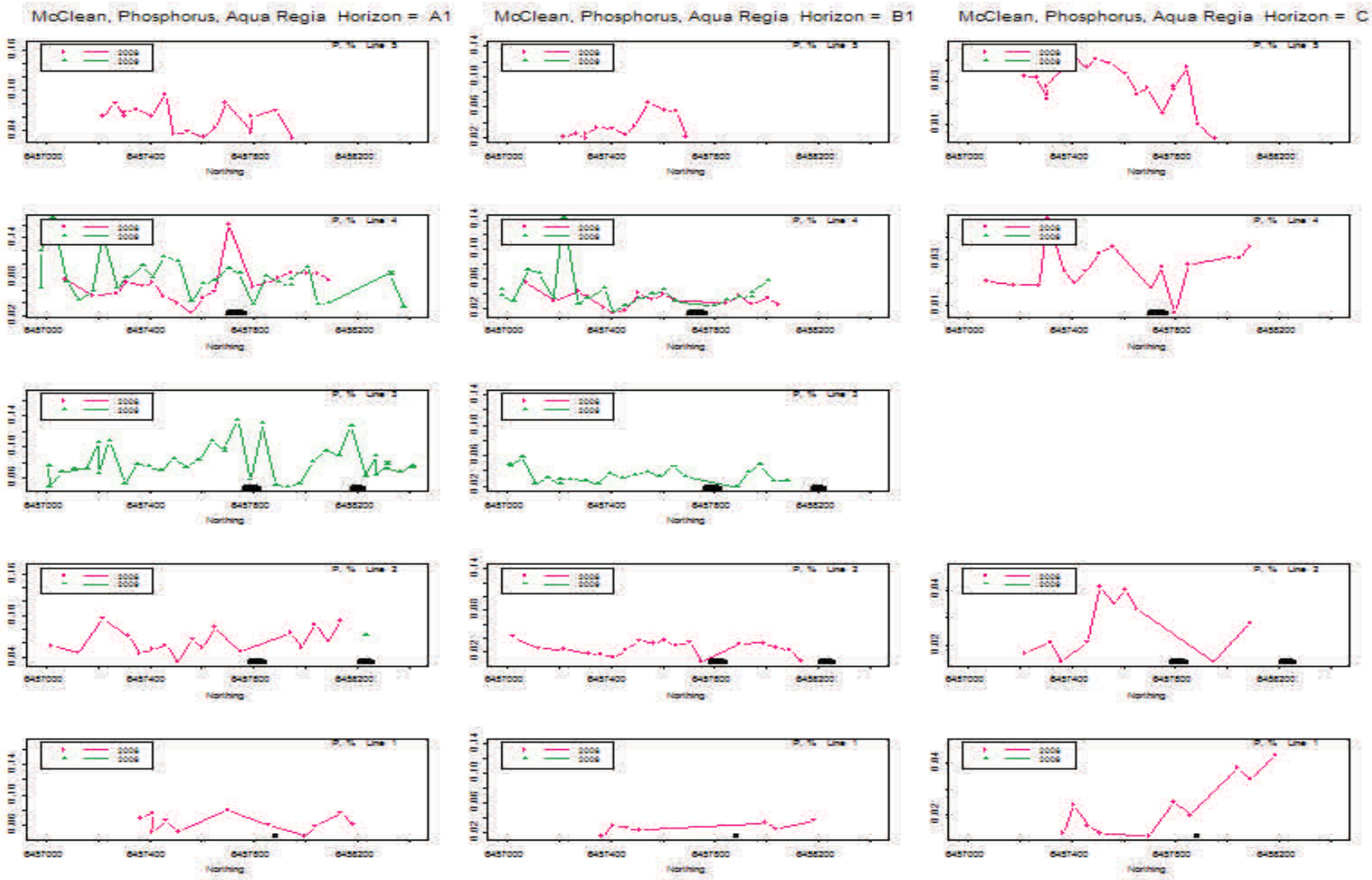

Fig 4.20 Phosphorous at McClean by aqua regia

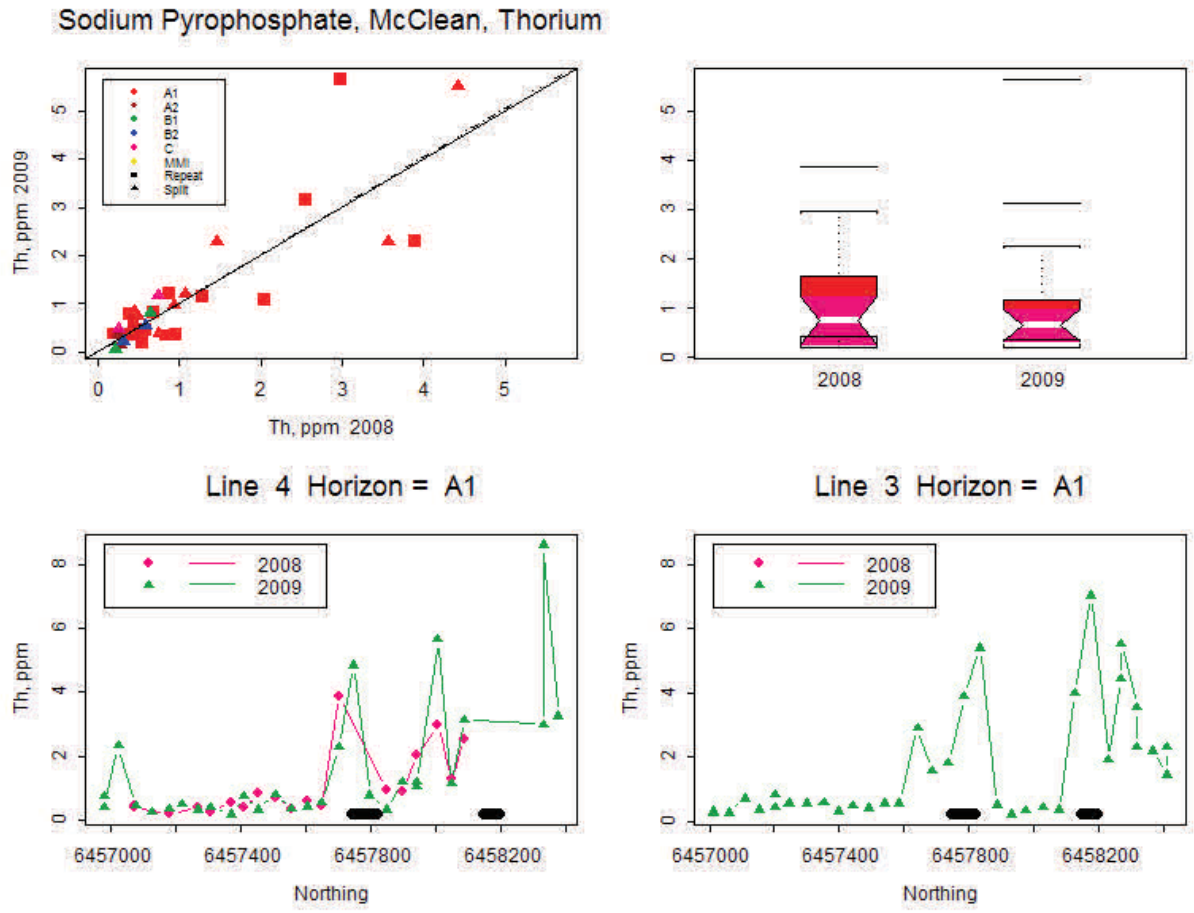

Fig 4.21 Thorium by sodium pyrophosphate at McClean

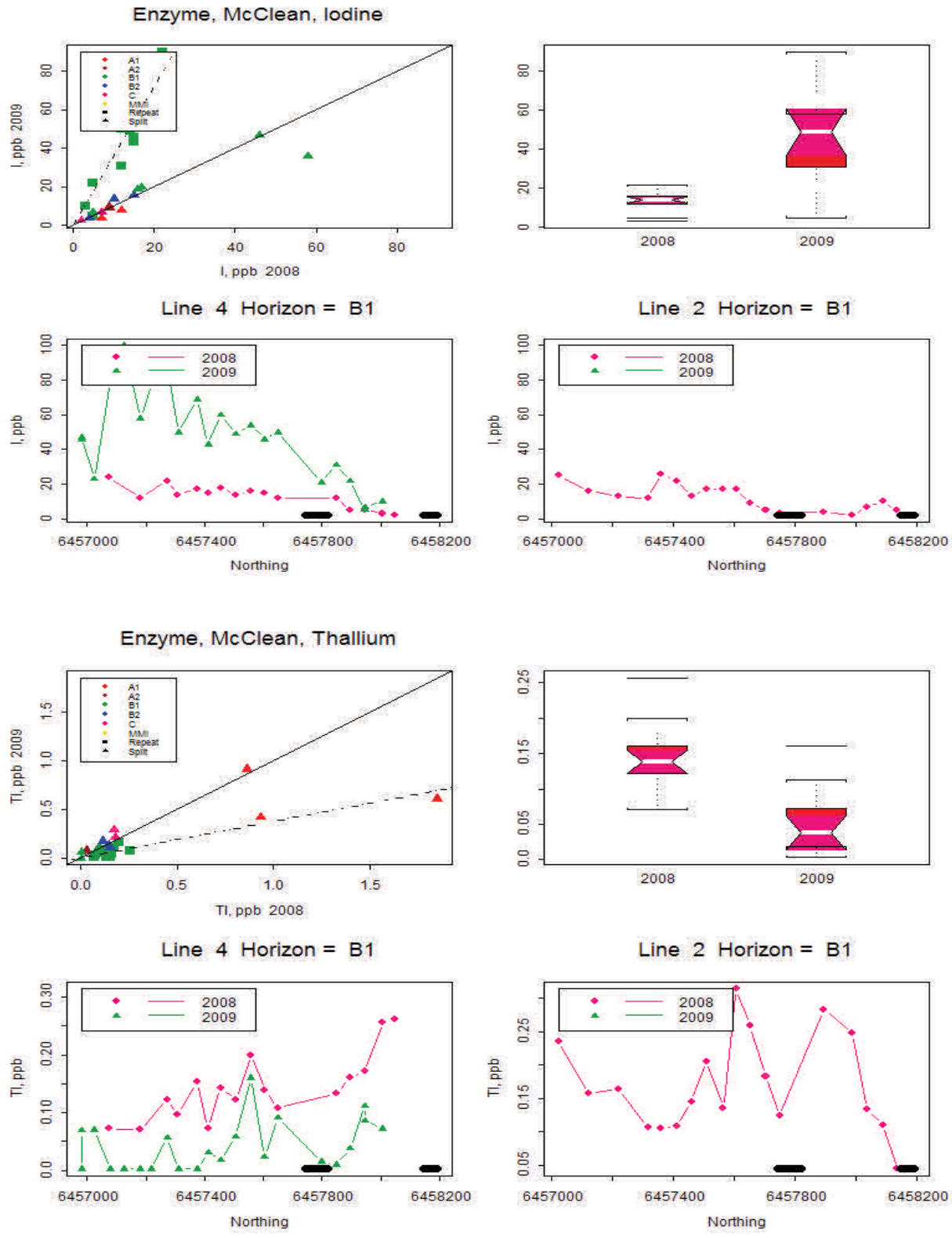

Fig 4.21 Top: Iodine by Enzyme at McClean
Bottom: Thallium by Enzyme at McClean

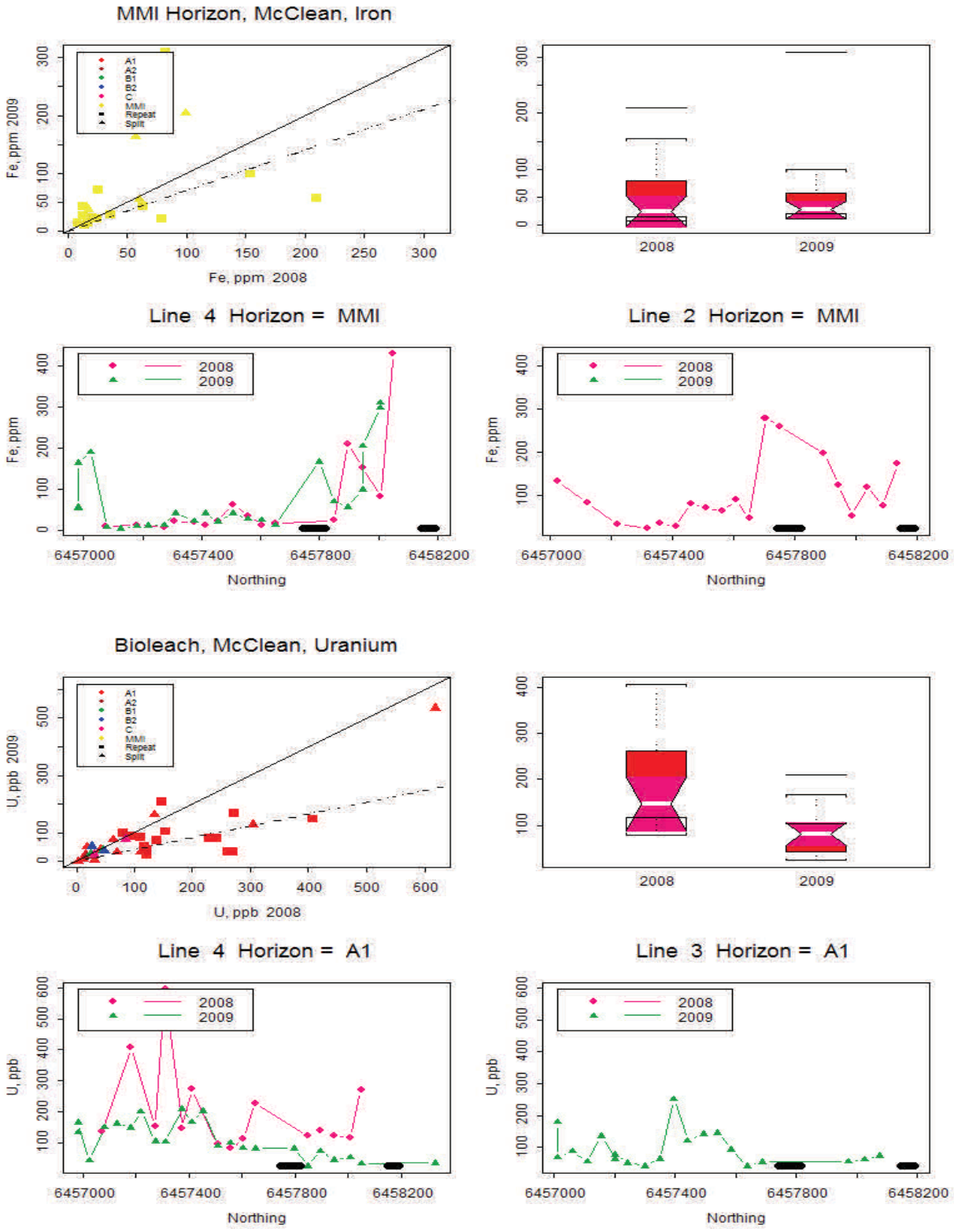

Fig 4.23 Top Iron by MMI leach on MMI horizon at McClean
Bottom: Uranium by Bioleach at McClean

REFERENCES

Cameron, E.M.C., Hamilton, S.M., Leybourne, M.I., Hall, G.E.M., McClenaghan, M.B., 2004. Finding deeply bured deposits using geochemistry. *Geochemistry: Exploration, Environment, Analysis*, 4,

Campbell, J.E., 2007, Quaternary geology of the eastern Athabasca Basin, Saskatchewan, in EXTECH IV: Geology and Uranium Exploration Technology of the Proterozoic Athabasca Basin, Sakatchewan and Alberta, Jefferson C.W., Delaney, G. (Eds.), Geological Survey of Canada Bulletin 588, p. 211-228.

Chao, T.T., 1984. Use of partial extraction techniques in geochemical exploration. *J. Geochem. Explor.,* 20, 101-135.

Clark, J.R., 1992. Enzyme-induced leaching of B-horizon soils for mineral exploration in areas of glacial overburden. *Trans. Inst. Min. Metall*., 102, B19-B29.

Hall, G.E.M., 1998. Analytical perspectives on trace element species of interest in exploration. *J. Geochem. Explo*., 61, 1-20.

Hall, G.E.M. and Bonham-Carter, G.F. (Eds.), 1998. Special Issue of Geochemical Exploration on Selective Extraction. *J. Geochem. Explor*., 61.

Jefferson, C.W., Thomas, D.J., Gandhi, S.S., Ramaekers, P., Delaney, G., Brisbin, D., Cutts, C., Portella, P., Olsen, R.A., 2007, Unconformity-associated uranium depsoits of the Athabasca Basin, Saskatchewan and Alberta, in EXTECH IV: Geology and Uranium Exploration Technology of the Proterozoic Athabasca Basin, Sakatchewan and Alberta, Jefferson C.W., Delaney, G. (Eds.), Geological Survey of Canada Bulletin 588, p. 23-67.

Wallis, R.H., Saracoglu, N., Brummer, J.J., Golightly, J.P., 1983, Geology of the McClean uranium deposits, in Cameron, E.M. (Ed.), Uranium Exploration in Athabasca Basin, Sakatchewan, Canada, Geological Survey of Canada Paper 82-11, p. 71-110.

PART II

5. Methods Used for Map-making and Data Analysis

Chapter 5 describes the methods used to display and analyze the geochemical data.

The lab datasets were cleaned up, "less thans" replaced by 1/2* detection limit, 2008 merged with 2009, a field added to indicate line (profile) number, etc. (It was some time before I realized that the 'less than values' for 2008 data had not been converted to 1/2 the detection limit by Robert Jackson. I have not changed any 2008 data, so maps of some elements with many values <DL look peculiar, but distinctive! Because the plotting has used a percentile scheme, discussed next, this usually causes no problem, but it is important to understand this in looking at the QC plots and profile plots). For each of the two areas (Cigar and McClean) data were sorted by chemical leach and soil horizon. Each leach-horizon was saved as a separate .xls file to make analysis and plotting manageable. For each area there are 5 Lines (profiles) labeled in order from east to west as 1 to 5, i.e. Line 1 is the furthest East. The data are saved as .xls file on the CD in folders organized by area\leach\horizon. Along with the .xls file is as .gas file, the proprietary format for ioGAS files.

Display of data for each geochemical element was achieved by (1) gridding in ioGAS, (2) symbol plots in ArcGIS, and (3) drawing profiles and custom QC plots with code developed in S-Plus. Where necessary, further analysis was undertaken to remove complex effects, both by a simple leveling approach and by a modified form of principal components analysis (PCA), as well as scatterplots and box plots.

5.1. Gridding.

This followed a simple routine in ioGAS, with standard settings as follows:

Cell size	12 m
Search radius	8 cells (96 m)
Smoothing radius	5 cells (60 m)
Value of cell	maximum of point values
Unequal bins	30/60/80/90/95/99/100 percentiles
Colour spectrum	dk blue-lt blue-green-yellow-red-pink (second one in the ioGAS list)
Shading	none
Background	white

Clearly, this tends to accentuate the high values (as opposed to methods that take some form of weighted average). The percentile values for the colour scheme were generated automatically in ioGAS. The grids were exported from ioGAS as geocoded images in .tif format (UTM projection, NAD83, zone 13N). See Fig 5.1 as an example. The folders containing these images on the CD (one folder for every \area\leach\horizon combination) are labeled "Grids". There are 65 Grid folders, each with an average of 40 elements, so about 2,600 gridded images altogether! Each of the 65 folders are also saved as a .jpg of thumbnails that allows a quick comparison of the elements for a particular leach-horizon. (I could not find software for this, but could print the

thumbnail index sheets from Easiprint, These sheets were then re-scanned as .jpgs—but they are not always very good quality). Because there are so many grids, maps showing symbol plots (discussed next) were generated for selected elements only.

5.2. Maps generated in ArcMap.

In ArcGIS, with shape files for streams, lakes, ore pods (all UTM projection, NAD83, zone 13N) as backdrop, each selected element was displayed with proportional circles (no colour) with radii depending on geochemical value, superimposed on the geocoded .tif colour grid imported from ioGAS. The classification was entered manually, using the same percentile cutoff values generated in ioGAS. See example in Fig 5.2. These maps have the advantage of a) showing the data with geographic features for location, b) the circles show the actual sample locations and (classified) geochemical values (usually ppm or ppb) for each point, c) the sample variability and repeatability can be evaluated by comparing differences along and across the Lines, and d) the colour grid provides general information about spatial trends. Importantly, the locations of peat and/or gleysol samples could be indicated. The output from these displays can be viewed either in ArcGIS, or as saved .jpg images. Each leach-horizon combination has an ArcGIS folder with an .mxd file (generated in ArcGIS 9.2) various shape files with associated tables in .dbf format as well as a "Map" subfolder containing the .jpg images of the selected elements.

5. 3. Profile and specialized QC plots

Each area\leach folder also contains subfolders labeled "JPEG" and "JPEG-1". The "JPEG" folder holds the QC plots and two selected Line profiles for each element. The "JPEG-1" folder holds a matrix of line profile plots: 5 rows, one for each line, and 3 columns corresponding to A1, B1 and C horizons. These plots were generated by custom-written code in S-Plus, a commercial statistics package (similar to R).

JPEG folder—QC plots.

Each .jpg file has 4 plots, as illustrated in Fig 5.3. Top left is a QC plot of element values for samples that are either repeats at the same location for the two years (i.e. 2008 vs 2009) as coloured squares, colour depending on horizon (see example figure), or sample splits (coloured triangles, colour again dependent on horizon) assigned arbitrarily to either 2008 or 2009 axes. The solid line is 45 degrees (i.e. all points would fall on the line for perfect correlation between years, and the dashed line is a line of best fit, constrained to pass through the origin. If the slope of this line differs greatly from 45 degrees, it may indicate a bias between years. Top right is a notched box plot showing a statistical summary between years (all horizons). The central coloured part of each box is bounded on the top by the 75th percentile, and on the bottom by the 25th percentile. The notch is centered on the median value, and the notch width is the 95% confidence limit on the median. If the notches from adjacent boxes do not overlap at all, then the hypothesis that the medians are the same can be rejected at the 95% level. Thus the 2009 Br levels are significantly higher than the 2008 levels. Bottom left is a profile along Line 4, B1 horizon. The heavy line along part of the x-axis shows the surface trace of the ore pod. Bottom right is similar, but for Line 2, again showing the between year bias.

JPEG-1 folder—Stacked line profiles.

These are stacked profile plots for Lines 1-5 and horizons A1, B1 and C (i.e all horizons except A2 and B2) for the indicated elements and leach. See Fig 5.4 for an example, using thorium at Cigar by ammonium acetate. Years are colour coded. In some cases, the data are on a log-y axis. The scale for the y-axis is the same for all plots on the same figure—not an ideal situation sometimes, because in the lower horizons by selective leaches concentration values are often much lower than in the upper horizons—but making inter-profile comparisons easier. Surface trace of ore pods shown as heavy black lines.

5.4 Removing artifacts from the multi-element data

Interpretation of anomalies in geochemical data often involves removing the effects of factors that produce anomalies that are either totally or partly artifacts. A well known example in stream sediment data is the effect of scavenging by Mn and Fe hydroxides, or by differences due to underlying rock type. At the McClean Lake site, the presence of peat in some areas (often over or near the surface trace of the ore pods), made this effect a concern.

A popular approach to correct for the effects of a correlated factor that is measured as a continuous variable is to use ratios. Common examples: correction for organic content by ratioing to LOI, correction for a geological factor by ratioing to perhaps an element like Al, or a rare earth like Dy. Better than ratioing is to regress the element of interest against the measured factor (preferably using a robust fitting method to downweight the effect of outliers), and substitute the residuals instead of the raw values. For element X, factor Z, the corrected values (Y) are given by:

1. Simple ratios: $Y = X / Z$ or

2. Regression: $Y = X—X'$, where $X' = a + b(Z)$, with a and b being determined by least squares.

For correction of effects using a non-continuous (categorical) variable, like rock type, year, presence/absence of peat, etc, it is common practice to 'level' the data by one of several methods. The simplest method is to replace each value by the difference from the mean value for the category. Better is to replace each value by the z-score which uses the mean and standard deviation for the category. Possibly better still is to replace the values by the corresponding percentile within the category or group. These and other leveling methods are available in ioGAS and other packages.

5.5 Principal Components Analysis (PCA), and 'residual' PCA

Geochemical survey data comprise a large number of elements measured on each sample. Multivariate statistical methods are attractive because they can provide help in examining how groups of elements behave in a similar fashion. A popular approach is to use Principal Compo-

nents Analysis (PCA) which provides information about groups of elements that are correlated. The analysis begins with the calculation of a correlation matrix between all possible pairs of elements. From this is extracted 'eigenvectors' that can be thought of as new variables that 'explain' the correlations (actually the variances) amongst the original variables. The first eigenvector will account for the most variance, and will consist of 'loadings' of each of the original variables. Elements (i.e. the original variables) with the highest loadings for that eigenvector (or principal component, PC) will be those most strongly correlated with the that PC.

Often, the first PC of geochemical data will reflect the dominant lithology affecting the sample composition. And even the first few PCs will be due to major lithological or other factors. The effects of mineralization will ofen appear later in the list of PCs. For example, in the McClean data in A1 by aqua regia, we found that PC8 is strongly related to uranium, although some of the uranium is accounted for my PCs that account for more variance (in this case PCs 1-7).

In practice, the data analyst inspects the element loadings on the first few eigenvectors to see how interpretable they are. And usually the analyst plots the new PC variables (these are linear combinations of the original variables), and are plots them as maps or graphs. Also, the option to start with a 'robust' correlation matrix, in which the influence of outliers is downweighted, is strongly advised with geochemical data. This is an option offered by ioGAS, and was used here.

In some situations, it is possible to identify PCs that can be interpreted as due to mineralization. In effect this allows the dominant effects of, say, lithological composition to be 'removed', and the 'mineralization factor' to be highlighted as a map. In practice, it is often difficult to interpret individual PCs, and considering the complex genetic processes involved in the transport and incorporation of elements (with varying behaviors), this comes as no surprise. In this study we used a new approach to remove the effects of the major PCs, and look at residual effects in individual elements.

We first ran a PCA, calculated new PC variables (these are the PC scores) and then took selected elements and calculated residuals by regression against a combination of the first few PCs. For example suppose we know that some uranium appears moderately in PC1, but we expect that this is due to uranium present in till, we can remove the uranium accounted for by PC1 by regression, as above.

$$Ures = Uobs—Upred$$

where the uranium values were predicted from PC1

$$Upred = a + b*PC1$$, fitted by least squares regression.

We can extend this to consider more PCs, cumulatively.

$$Upred = a + b1*PC1 + b2 * PC2$$

or

$$Upred = a + b1 *PC1 + b2 *PC2 + b3* PC3$$

etc for as many PCs as seem appropriate.

For the A1 aqua regia and sodium pyrophosphate data at both Cigar and McClean we applied this approach to about six ore-related elements in order to remove effects that could be caused by compositional controls in the underlying tills.

The code for this was written in S-Plus, with robust principal components calculated in ioGAS. The output was a residual .xls file, from which grids and maps could be displayed as described previously.

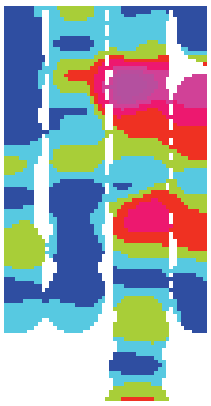

Fig 5.1 Gridded image from ioGAS. Chlorine in C horizon by Enzyme leach

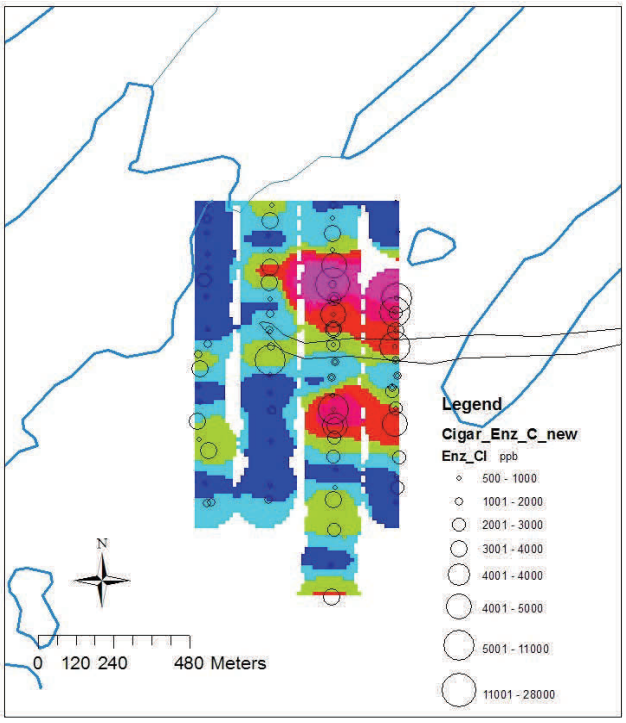

Fig 5.2 Map generated in ArcMap. Chlorine in C horizon by Enzyme leach

Notes: This is 2008 data (only 4 Lines) Colours follow percentile scheme discussed in text.

The proportional dot diameters follow the same breakpoints as used in the ioGAS grid. This has the advantage that variations at sample duplicates and variations year-year (this is 1 year only) and noisy changes along Line are immediately evident.

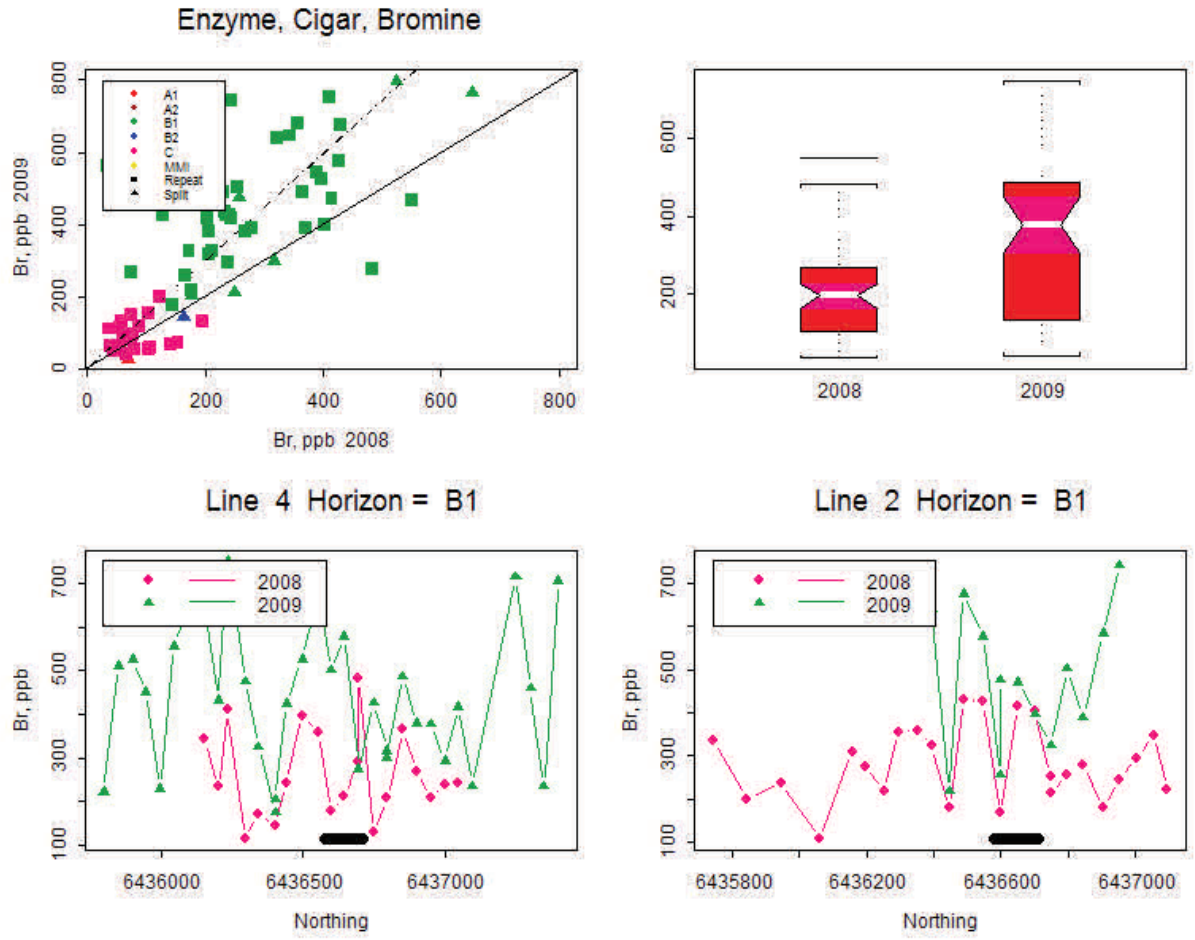

Fig 5.3 Example of QC plot saved in JPEG folder for bromine by enzyme leach at Cigar. Upper plots contain information about sample duplicates at all horizons. Top left: scatterplot of duplicates by year (i.e field duplicates, with samples taken at same locations in 2008 and 2009). Colour coded by horizon and shown as squares. Triangular symbols are sample duplicates taken in same year with arbitrary assignment to year. Solid line is 45 deg, i.e. all points would fall on line if perfectly correlated between pairs. Dashed line is best fit line, constrained to pass through (0,0) applied to year over year data only (squares, not including triangles). Top right: boxplot of year over year duplicates. The notch is centered on the median value, and its width is the 95% confidence interval on the median. This allows a quick test for significance of differences between years. Here 2009 data are significantly higher than 2008, because the notches do not overlap. And the dashed line is at a steeper angle than the solid line.

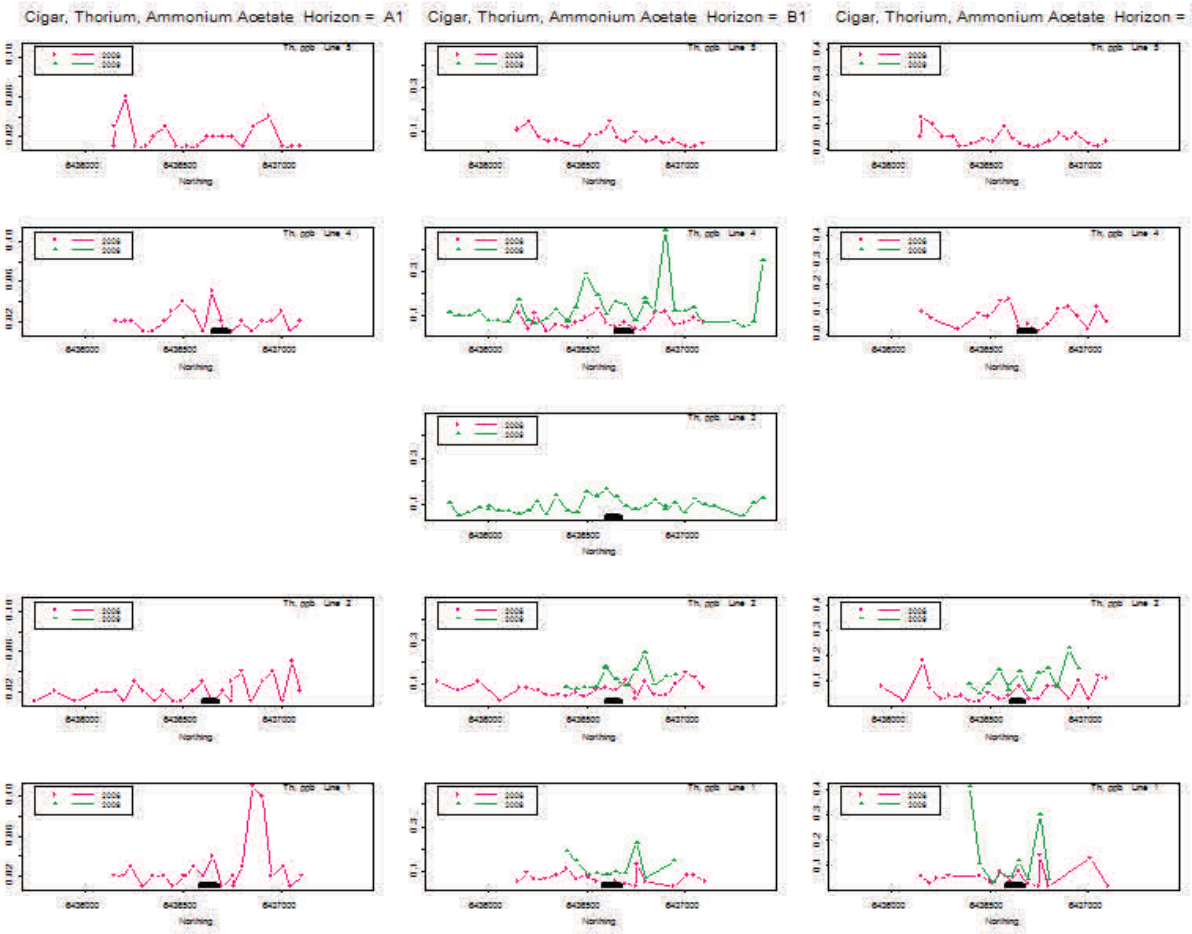

Fig 5.4 Profile plot example (saved in the 'JPEG1' folder). This is thorium by ammonium acetate at Cigar. The left column is always A1 horizon, middle column is B1 and right column is C . 2008 data are always in red, 2009 in green. This is an interesting one, because it shows that thorium data in 2009 are higher than 2008. But because the pattern of highs and lows are similar between years (for the most part) particularly in B1, it suggests that this is an analytical (lab) problem rather than a field difference.

6. DESCRIPTION OF GEOCHEMICAL GRIDS AND MAPS

6.1 Cigar Lake

6.1.1 A1 horizon, humus material

As podsols dominate at Cigar Lake, the organic medium, essentially humus (A1), is much more consistent than at McClean. There are only the two exceptions of gleysols in the northeast on Line 1, marked with crosses on the element maps, and these would give rise to false anomalies, positive or negative, for various elements. The LOI at 500 ^{o}C for these gleysols are 3 and 7%, in stark contrast to the median and 90th percentile values of 56 and 78%, respectively. Similarly, the range in pH for the humus samples is 2.7-5.3 with a median of 3.6 whereas the pH of the gleysols is 5.6 and 5.2, and the median for conductivity in humus is 54 µmhos/cm, compared to only 3 µmhos/cm for the gleysols.

Aqua regia ('AR') Grids in Fig. 6.1, Maps in Fig 6.2

There is a distinctive SW-NE anomaly which crosses the westernmost part of the pod and is evident on Lines 1-4; this feature is shown by U, REEs, Co, Cs, Fe, Ga, Sc and V (Fig. 6.2, U). The contrast is actually very small, with the minimum, median and maximum being 0.2, 0.3 and 0.9 ppm, respectively, for U (cf higher U values at McClean Lake, Fig. 6.70); however, this anomaly is maintained across the four lines. The northeastern extreme of this trend is the area of the two gleysols where anomalous behaviour (due to change in medium) might be expected but a third sample, a podsol, also shows elevated U (as is the case for Fe, Co etc). However, care needs to be exercised in drawing inferences on Line 1 in this water-saturated region.

A slightly different anomaly, also maintained across sampling lines, is shown by Ni, Cu, Cr, Se and Mo (Fig. 6.2, Ni). The anomaly is large, crosses the western edge of the pod and extends southward on Lines 3 and 4. Again, the contrast is small, with the minimum, median and maximum being only 2.9, 5.0 and 7.5 ppm for Ni; the range for Cu is greater, with the respective values being 2.1, 10.4 and 22.5 ppm.

Phosphorus appears to have a large anomaly over the western edge of the pod and perhaps a halo ~ 350 m north and south but this should be viewed with caution as the minimum and maximum concentrations are very low, at 0.02 and 0.08 ppm, respectively (Fig. 6.2, P). Elements displaying noisy patterns include As, Au, Bi, Cd, Hg, Li, Mn, Pb, Sb, Sr, Th, Ti, Tl and Zn. Most Au values are at or below the detection limit of 0.2 ppb but Site CLS1-6A, a gleysol, reports a suspiciously high concentration of 203 ppb.

Pyrophosphate leach ('PYRO') Grids in Fig. 6.3, Maps in Fig. 6.4

The SW-NE trend shown by U and the REEs in aqua regia is also evident here for the pyrophosphate leach, though the anomaly for U is slightly less coherent (Fig. 6.4, U; Fig. 6.4, La). The concentrations of U are less than half of those by aqua regia but the range is better, with the minimum, median and maximum being 0.03, 0.12 and 0.6 ppm, respectively. The anomaly to the south on Line 4 is accentuated more by the PYRO leach compared to AR (Fig. 6.2, U). It is interesting that the gleysols remain high in U concentration by PYRO, whereas they now show low concentrations in Fe and Co (Fig. 6.4, Co).

The patterns for Ni and Cu are much more fragmented by PYRO compared to AR, to the point that they simply appear to be noise (Fig. 6.4, Ni).

Bioleach ('BIO') Grids in Fig. 6.5, Maps in Fig. 6.6

Most of these element maps appear to be noise. Line 1 predominates, in sharp contrast to results for AR and PYRO, as shown by U and the REEs (Fig. 6.6, U). There is a hint of the SW-NE trend seen by AR, though there is an absence of elevated U concentrations on Line 3 (infill line). In fact, the low values in evidence on Line 3 for many elements and the lack of repeatability between years (Lines 1, 2, 4) suggest problems in calibration between years for this leach.

The most encouraging map is that for I which shows a distinctive high over the pod on Lines 1-4, regardless of the noise evident elsewhere in the survey area (Fig. 6.4, I). The range in I is extensive, from 1 to 122 ppb. The Br response is noisier.

Hydroxylamine leach ('HYD', only for 2008) Grids in Fig. 6.7, Maps in Fig. 6.8

Many elements in this A1 horizon suffer from detection limit problems by this leach. Nevertheless, the SW-NE trend is evident for the REEs, Co, Fe (Fig. 6.8, La); where U is above the DL, it was in this area.

Ammonium acetate leach ('AA5', only for 2008) Grids in Fig. 6.9, Maps in Fig. 6.10

The SW-NE trend over and north of the pod on Lines 1, 2 and 4 is the overwhelming feature of this AA5 leach and is shown by U, REEs, Co, Fe, and Ni (Fig. 27a, U; Fig, 27b, Co). The minimum, median and 90th percentile values for U are 0.005, 0.018 and 0.038 ppm, respectively, much lower concentrations than in the pyrophosphate leach.

Elements such as Ba, Bi, Br, Cd, Cu, K, Mg, Mn, Na, P, Pb, Rb, Sr, Th, Ti and Tl exhibit noisy responses.

Enzyme leach (only for 2008) Grids in Fig. 6.11, Maps in Fig. 6.12

The Enzyme leach is not intended for organic-rich samples. The SW-NE trend is rather fractured for U but is more visible for the REEs (Fig. 6.12, U). Cobalt shows this trend well and Bi outlines the pod (Fig. 6.12 , Co; Fig. 6.12 , Bi). Other patterns appear to be noise.

MMI (only for 2008). Grids in Fig. 6.13, Maps in Fig. 6.14

The MMI 'thumbnails' are included amongst the figures but this leach, like the Enzyme, is not designed for use on organic-rich samples and the dataset is incomplete.

Summary

There is a striking SW-NE feature across the pod on Lines 1-4 for many elements, including U and the REEs, shown by aqua regia and the partial leaches, pyrophosphate and ammonium acetate. Nickel, Cu, Cr, Se and Mo by aqua regia show a similar but slightly different significant anomaly, in that it crosses the western edge of the pod and extends southward on Lines 3 and 4. As was the case at McClean Lake, there is little to be gained by using a partial leach rather than aqua regia except that the halogens might prove to be useful, as suggested by the Bioleach (precision needs attention).

6.1.2 A2 horizon, eluviated zone (only 2008)

Aqua regia. Grids in Fig. 6.15, Maps in Fig. 1.16

There is little consistency in pattern from one element to another in A2 by the aqua regia digestion and there is no major trend. The U map is very different to that for A1 by AR, though values range similarly, from 0.1 to 0.9 ppm (Fig. 6.16a). The Hg pattern is the most coherent, across all four lines and over the pod, but the concentrations range from only 5 (DL) to 18 ppb (Fig. 6.16, Hg). Gold again shows some dubiously high results by aqua regia: 42 ppb at Site CLS2020A and 22 ppb at Site CLS4-7A.

Hydroxylamine leach. Grids in Fig. 6.17, Maps in Fig. 1.18

Again, many elements in this A2 horizon suffer from detection limit problems by this leach. Nevertheless, the SW-NE trend is evident for the REEs (Fig. 6.18, Ce); where U is above the DL, it is in this area.

Ammonium acetate leach. Grids in Fig. 6.19, Maps in Fig. 1.20

Many detection limits are too high for this weak leach. There is a slight SW-NE trend amongst the REEs but it is dominated by the gleysols on Line 1.

Enzyme leach. Grids in Fig. 6.21, Maps in Fig. 6.22

The most interesting pattern in A2 by this leach is that shown by Br and I, outlining the pod on Lines 1, 2 and 4 on the northern side (no influence of gleysols apparent) (Fig. 6.22, Br). The range is particularly good for Br, from 7 to 150 ppb with a median of 33 ppb. Selenium shows a similar pattern but values are close to the detection limit (range of 1-4 ppb). Tungsten appears to have a consistent anomaly north from the pod on Line 2. The SW-NE trend is evident for U and the REEs, but the response on Line 1 is dominated by the two gleysols (Fig. 6.22, U).

Bioleach. Grids in Fig. 6.23, Maps in Fig. 6.24

The SW-NE trend is present in this leach for the REEs, Co and U (Fig. 6.24, Ce). Bromine and I highlight the pod well on Lines 2 and 4 and just north of the pod on Line 1 (Fig. 31b, Br). This is encouraging, especially as the contrast in these elements is high. For example, the minimum, median and 90th percentile values for Br and I are, respectively, 5, 144 and 301 ppb, and 1, 34 and 102 ppb.

MMI . Grids in Fig. 6.25, Maps in Fig. 6.26

The MMI patterns appear very noisy but the SW-NE trend is visible for the REEs (Fig. 6.26, La). The U distribution is dominated by the gleysols which report 91 and 201 ppb U, in contrast to the median and 95th percentile values of 10 and 40 ppb, respectively (Fig. 6.26, U).

Summary

The SW-NE trend, seen in the A1 horizon, is apparent for the REEs and several other elements in A2 by the partial leaches, though not by aqua regia. Many patterns are noisy. Probably the most interesting responses in the A2 horizon are (1) that for Br and I using the Enzyme leach and Bioleach where the pod is well highlighted and the contrast is good and (2) that for Hg by aqua regia which is similar to but broader than that for Br and I by the Bioleach.

6.1.3 B1 horizon

Aqua regia. Grids in Fig. 6.27, Maps in Fig. 6.28

The U distribution in B1 by AR appears to be random and bears no resemblance to that in A1 by AR where that SW-NE trend is so prominent (Fig. 6.28, U). The range in U is similar to that in A1, from 0.2 to 1.6 ppm. The REEs behave similarly to U; other elements displaying an apparently random pattern include As, Al, Au, Bi, Ga, Hg, Na, Mo, Pb, Sb, Sc, Th and Zr.

The pattern that does dominate in B1 is that typified by Tl and shows distinctively elevated concentrations in the north (to the north of the SW-NE trend in A1) across Lines 1-4 (Fig. 33b, Tl). Other elements showing this feature include Ba, Be, Cd, Co, Cr, Cu, Cs, (Fe), Li, Mg, Mn, Ni, Nb, (P), Ti, Rb and Zn. Strontium is unusual in that there is a consistent high over the pod (Fig. 6.28, Sr).

Enzyme leach. Grids in Fig. 6.29, Maps in Fig. 6.30

Like most elements, the distribution of U in B1 by the Enzyme leach is random and concentrations are extremely low, in the range 0.2-5 ppb (Fig. 6.30, U). The only consistent pattern is that for I, showing elevated concentrations over and to the south of the pod, and to the north on Lines 3 and 4 in the western area of the anomalies shown in AR by Tl and others (Fig. 6.31, I).

Line 3 appears to be unusually low for several elements (e.g. Dy, Tl, Sm) which suggests calibration shifts between years (Fig. 34c, Dy).

Hydroxylamine leach (only for 2008). Grids in Fig. 6.31, Maps in Fig. 6.32

Although U and the REEs show an anomaly over the pod on Lines 2-4, other highs in the survey area detract from this feature (Fig. 6.32, U). The only elements displaying the northern anomaly shown by AR in B1 are Cs, K and Rb (Fig. 6.32, K). The I map does not show the anomaly over and south of the pod that the Enzyme leach does.

Ammonium acetate leach (only for 2008) Grids in Fig. 6.33, Maps in Fig. 6.34

All elements reported with adequate values above detection limit appeared to produce exclusively noisy patterns.

Bioleach (only for 2008). Grids in Fig. 6.35, Maps in Fig. 6.36

There are no consistent trends in this dataset.

MMI (only for 2008). Grids in Fig. 6.37, Maps in Fig. 6.38

The U (and REE) pattern by MMI is noisy but there is some consistency on Line 4 over and to the south of the pod (Fig. 6.38, U). Molydenum also displays this anomaly, spreading northward, though closer inspection indicates considerable variation in responses amongst samples here (Fig. 6.38, Mo).

Elevated concentrations of Zn occur in the low-lying region to the northeast (Fig. 6.38, Zn). Numerous elements suffer from detection limit problems, as is the case for the other partial leaches.

Ionic leach (only for 2009). Grids in Fig. 6.39, Maps in Fig. 6.40

The coverage of samples analysed by the Ionic leach is limited to the 2009 collection on Lines 1-4. The responses for U and Mo appear to be encouraging (Fig. 6.40, U). Concentrations of U are in the range 8.7-140 (gleysol) ppb, with a median of 18 ppb, in the approximate range of the hydroxylamine and MMI leaches and significantly higher than that of the Enzyme leach.

It is interesting that the SW-NE trend seen in the A1 horizon is somewhat in evidence here for Zn, Ge, Hf, Li, Sb, Sr and W (Fig. 6.40, Zn). The Ionic leach reports Pd in the range 1.3-18.5 ppb, with a median of 3.2 ppb: these levels are highly unlikely.

Summary

The B1 horizon does not seem to be useful, particularly for U which displays random behavior in any leach. The most coherent anomaly is that in the north across Lines 1-4 shown by Tl and many other elements in the aqua regia digestion. There appears to be a halo of I using the Enzyme leach around the western edge of the pod.

6.1.4 B2 horizon (only 2008)

Aqua regia. Grids in Fig. 6.41, Maps in Fig. 6.42

The distribution of U in B2 by AR is quite different from that in B1 (Fig. 6.42, U). Besides the subtle anomaly over the pod, there is a SW-NE anomaly across Lines 1, 2 and 4 in the south which is demonstrated by most elements including the REEs, Ca, Fe, Na and K. Elements such as Be, Co, Cu, Mg and Ni display elevated levels in the north (Fig. 6.42, Ni).

Ranges in concentration are generally small and there is an absence of a convincing response.

Hydroxylamine leach. Grids in Fig. 6.43, Maps in Fig. 6.44

The U and REE patterns are similar to those by AR and the southern SW-NE feature is evident (Fig. 6.44, Dy). The apparent halo of I around the pod is analytically sound, being too close to the detection limit of 0.1 ppm.

Ammonium acetate leach. Grids in Fig. 6.45, Maps in Fig. 6.46

The SW-NE feature in the south is evident for U and the REEs (Fig. 6.46, La).

Enzyme leach. Grids in Fig. 6.47, Maps in Fig. 6.48

The U and REE responses differ in the Enzyme leach; neither really accents the area of the pod (Fig. 6.48, U; Fig. 6.48, La). The coherent pattern in I around the pod in B1 is lost in B2 (Fig. 39c, I).

Bioleach. Grids in Fig. 6.49, Maps in Fig. 6.50

As with the AA5 leach, the most discernible pattern is the SW-NE feature in the south for U and the REEs (Fig. 6.50 , Dy). The W anomaly to the north of the pod along Line 2 is odd in that the contrast is so high, with the highs being in the order of several to 9.18 ppb over a broad back-ground of 0.01 ppb (Fig. 6.50, W). The halogen distributions appear to be random.

MMI. Grids in Fig. 6.51, Maps in Fig. 6.52

The U distribution is random in B2 and resembles that of the REEs which shows the southern SW-NE pattern displayed by AR (Fig. 52, Dy). All elements display noisy response and, as with the other partial leaches, detection limits are an issue.

Summary

The only notable coherent feature in B2 is a SW-NE anomaly across Lines 1, 2 and 4 in the south, distant from the pod, and evident for many elements by AR and, to a lesser degree, by HYD, AA5 and BIO.

6.1.5 C horizon

Aqua regia. Grids in Fig. 6.53, Maps in Fig. 6.54

The SW-NE trend across the pod that was a strong feature in A1 by AR is also present in the C horizon for U, Th, Ca, P and the REEs (Fig. 6.54, U). It could be instructive to measure Pb isotopes in the C. The elevated E-W trend in U in the south across Lines 2 and 4 is present for most elements determined, often across all four lines. This is the general area of the southern SW-NE feature noted above in B2 by AR and HYD.

Molybdenum and Ag have higher concentrations on Lines 1 and 2 just north of the pod in the low-lying region (Fig. 6.54, Mo).

Enzyme leach. Grids in Fig. 6.55, Maps in Fig. 6.56

The maps for As, Bi, Cr, Hg, In, Mo, Sb and Te are deceptive because they appear to show a wide anomaly on Lines 1 and 2: this is actually a change in handling the detection limit from 2008 to 2009, all the data being at this level. Copper also appears to show a strong anomaly over the pod but this is a shift must be a shift in calibration from one year to the other. All values for Cu in 2008 are 1 ppb, with one exception of 487 ppb (CLS1-8D, Ni also very high, flier?), whereas in 2009 they range from 2 to 6 ppb.

There is no apparent bias in U concentrations in browsing the data and it shows an anomaly over and north of the pod on Lines 1 and 2 (Fig. 6.56, U). Bromine appears to show a halo; data for Cl are too close to the detection limit for confidence and those for I have some repeatability problems (Fig. 6.56, Br).

Bioleach (only for 2008). Grids in Fig. 6.57, Maps in Fig. 6.58

Elevated concentrations of U, the REEs and several other elements are seen in the southern area, as in the aqua regia leach but of course levels are far lower. There are no other obvious patterns.

Tungsten, as in the B2 horizon, shows a remarkably high contrast with anomalies in the several ppb to 40 ppb level over an extensive background of 0.01 ppb but the highs do not correspond; these values are suspicious. Furthermore, there is a sample, that at Site CLS2-12A, which reports extremely low values for many elements such as the REES, As, V, Zn, Br and I (e.g. 7 ppb I whereas other samples report 59-466 ppb and Br at 5 ppb vs a range of 58-1100 ppb), again the analysis should be reviewed.

Hydroxylamine leach (only for 2008). Grids in Fig. 6.59, Maps in Fig. 6.60

Many elements suffer from inadequate detection limits. Uranium (and REEs) differs slightly from the response in AR in that the SW-NE trend above the pod is weak but the E-W elevated area, shown by many elements in the south, is stronger (Fig. 6.60, U). The SW-NE trend across the pod is shown by P and Ca (Fig. 6.60, P). The responses differ markedly from those by the Enzyme leach.

Ammonium acetate (only for 2008). Grids in Fig. 6.61, Maps in Fig. 6.62

The AA5 leach emulates the HYD leach: the E-W feature in the south and the SW-NE trend above the pod are evident for U and the REEs but concentrations are much lower.

MMI (only for 2008). Grids in Fig. 6.63, Maps in Fig. 6.64

Detection limits are again an issue in the MMI leach and there are some missing data. However, the E-W trend across lines in the south is still discernible, as is the SW-NE feature across the pod.

Ionic leach (only for 2009). Grids in Fig. 6.65, Maps in Fig. 6.66

There are too few samples to evaluate this leach. However, in profile, the response for Mo appears promising; that for U does not (Fig. 6.66, Mo; Fig. 6.66, U).

Summary

The noteworthy patterns in the C horizon comprise (1) the SW-NE trend across the pod shown by U, REEs, Ca and P using aqua regia, and to a lesser degree, by the partial leaches, and (2) the E-W feature in the south, distant from the pod, shown many elements such as Al, Co, U and Zn in aqua regia and, to a lesser degree, by U and the REEs in the partial leaches.

6.1.6 MMI horizon. *Grids in Fig. 6.67, Maps in Fig. 6.68*

There is a U high over the western edge of the pod but there are numerous other highs within the survey area (Fig. 6.68, U). The two gleysols on Line 1 have by far the greatest U concentrations, at 125 and 169 ppb. Many element concentrations are, for the most part, below detection limits (e.g. As, Ca, Li, Mg, Sr, Tl). The only coherent pattern is that for Pb where there could be a halo effect and it might warrant isotopic analysis (Fig. 6.68, Pb).

6.2 McClean Lake

6.2.1 A1 horizon, humus material (and P1)

Aqua regia ('AR'). Grids in Fig. 6.69, Maps in Fig. 6.70

Uranium is clearly anomalous over the N and S pods, with a low between these two groups of pods. The varied response over the peat samples suggests that these anomalies over the pods are not controlled by the changing nature of the organic medium (i.e. humus vs peat) (Fig. 6.70, U). The majority of the U values lie in a relatively narrow range of 0.6-2.6 ppm (min to 90th percentile) but the patterns are coherent. Uranium also shows a region of higher values in the southern

part of the survey area, mostly concentrated along Line 4 (Fig. 6.70, U). Molybdenum behaves similarly.

Numerous elements show the clear pattern exhibited by Ce, with anomalies over the pods and lacking any elevated response to the south (Fig. 6.70, Ce). The range in concentration is fairly broad, with a minimum of 3.1 ppm and maximum of 81 ppm. In addition to the other REEs, S, Cr, W, V, Zr and Nb show this pattern. Although the vast majority of the W values are at the detection limit of 0.1 ppm, those above it lie in the vicinity of the pods. [The dark blue N-S area in the W plot is an artifact of the different handling of <DL data in the two years, where values <DL were set to the DL in 2008 by RJ and to ½ DL in 2009 by G B-C]. Iron is elevated in the northern section of the survey area, over and between the pods (Line 4) (Fig. 6.70, Fe). Calcium, Mg, Sr, Ti and Mn are high in this NW region, though not over the S pod.

The third prominent pattern in the aqua regia data-set for A1 (and P1) is that shown by Ba (Fig. 6.70, Ba) where the southern half of the survey area, from ~ 200 m south of the S pod, is elevated in concentration compared to the northern half. Other elements showing similar behaviour, to varying degrees, include Hg, Zn, Cd, Pb, Cu, Ni, Rb, Cs, K, and Bi.

Elements which exhibit exceptionally noisy patterns include Ag, Al, As, Au, Be, Co, Mg, Mn, P, Sc, Sn, Ti, and Tl.

Pyrophosphate leach ('PYRO'). Grids in Fig. 6.71, Maps in Fig. 6.72

Most of the patterns by the $Na_2P_4O_7$ leach mimic those by aqua regia but the concentrations are simply lower, often at about one third (Fig. 6.72, U; Fig. 6.72, Cr; Fig. 6.72, W). The minimum, median and 90th values for U are 0.2, 0.8 and 1.5 ppm, respectively. This does not necessarily imply that only a fraction (e.g. 1/4, 1/3 etc) of the element is bound to organics because the $Na_2P_4O_7$ leach does not dissolve *all* humate and fulvate components in *one* leach; repeated applications would be required to complete the dissolution (Hall, 199x). Furthermore, a portion of element first bound to a more labile organic phase may have become, with time, more strongly fixed to the humin component which is not attacked by the $Na_2P_4O_7$ leach.

Molybdenum shows a more definitive pattern by this leach, with anomalies focused clearly over the pods (Fig. 6.72, Mo by PYRO; Fig. 6.70, Mo by AR). Nickel and Zn show more noise than by aqua regia and Ba, while still generally elevated in the south, also displays a high area in the NW. Iodine, not reported off an aqua regia leach, shows anomalous concentrations over and between the pods, albeit rather noisy (Fig. 6.72, I).

Bioleach ('BIO'). Grids in Fig. 6.73, Maps in Fig. 6.74

Uranium by the Bioleach is extremely noisy; there is no coherent pattern (Fig. 3a). Molybdenum, and to a lesser extent W and V, tend to outline the pods (Fig. 3b, Mo).
The halogens Br and I show identical patterns which may be highlighting the area around the pods but this tends to be only in the west (Line 4) (Fig. 3c, I); the I pattern by the PYRO leach is more definitive. The ranges in values (i.e. contrast) for Br and I by the Bioleach are exceptionally large – 5-5080 ppb for Br and 1-970 ppb for I – and thus these elements could prove to be

very useful. The highest values are between rather than on the pods, suggesting a halo effect.

The absolute values for numerous elements by the Bioleach do not compare well between the two years and this probably explains some of the noise.

Hydroxylamine leach ('HYD', only for 2008). Grids in Fig. 6.75, Maps in Fig. 6.76

Iron highlights the pods distinctly; this does not appear to be controlled by the population of peat samples (Fig. 6.76, Fe). The minimum, median and 90th percentile Fe values are 5, 260 and 540 ppm, respectively, significantly higher than the values for the AA5 leach (6, 31, 200 ppm, respectively) and lower than those for the PYRO leach (220, 1100 and 6000 ppm, respectively), as would be expected. The REEs behave similarly (Fig. 6.76, Dy).

The pattern for U is similar to that by the AA5 leach, but noisier, the concentrations being extremely low (median value of only 0.013 ppm; Fig. 6.77, U).

Ammonium acetate leach ('AA5'). Grids in Fig. 6.77, Maps in Fig. 6.78

MMI leach. Grids in Fig. 6.79, Maps in Fig. 6.80

Summary of A1 horizon

If one is searching for an expression of mineralization directly above the pods, the REE signature by aqua regia is the best. This feature is also demonstrated by uranium/aqua regia, though there is also an anomaly in the southern part of the survey area which may be linked to the high seen for Ba and numerous other elements. Although the area over and around the pods is wet and swampy, the changing nature of the medium, from dry humus to peat, does not appear to control the anomalies but this needs to be verified. The two areas of U anomalies – over the pods and to the south – require differentiation as to source.

There is little advantage in using a partial leach on the A1 except to obtain the halogen signatures which appear to show a halo around the pods (I by PYRO). The signatures, in general, by the PYRO leach, and to a lesser extent by the AA5 and HYD leaches (not designed for use of organic matter), are similar to those by aqua regia and contrast has not been improved. An exception to this is Mo which locates the pods more clearly by the PYRO leach. The Bioleach appears to be promising if the precision can be improved.

There are too few sample points by the MMI leach on this horizon (only for 2008) to evaluate the results.

6.2.2 A2 horizon, eluviated zone (only 2008)

Aqua regia. Grids in Fig. 6.81, Maps in Fig. 6.82

The vast majority of the plots, including major and trace elements, demonstrate dominance by the peat samples over the S pod and near the N pod (Fig. 6.82, U; Fig. 6.82, Ni; Fig. 6.82, Fe).

The REEs behave similarly to Fe. The highly concentrated area in the south, shown clearly by Ba in A1, is not in evidence in A2. There is a coherent E-W anomaly about 250 m south of the S pod shown by Li and, to a lesser extent, by Al, Bi, Ga, Mg, Rb and Tl (Fig. 6.82, Li).

Hydroxylamine leach. Grids in Fig. 6.83, Maps in Fig. 6.84

The results by the HYD leach are also dominated by the peat samples. However, there is more focus on the area around the pods generally, as shown by Fe and associated elements (e.g. REEs, Cd, Co, Cr, U) (Fig. 6.84, Fe; Fig. 6.84, U). Elements showing a noisy pattern, in addition to this feature, include Ag, Ba, K, Mg, Ni, Pb, Rb, V and Zn. Many detection limits are inadequate for this horizon.

Ammonium acetate ('AA5') Grids in Fig. 6.85, Maps in Fig. 6.86

Enzyme (''ENZ'). Grids in Fig. 6.87, Maps in Fig. 6.88

Bioleach ('Bio') Grids in Fig. 6.89, Maps in Fig. 6.90

Element patterns in the A2 by the Bioleach are dominated by the peat samples but there is also an E-W high across the three westerly lines about 250 m south of the S pod shown by As, Bi, Br, I, Sb and Se, and to a lesser extent by U (Fig. 6.90, U; Fig. 6.90, As; Fig. 6.90, Br).

MMI . Grids in Fig. 6.91, Maps in Fig. 6.92

The coverage around the pods for the MMI leach is almost non-existent; no peat samples were analysed. Uranium shows a suggestion of a halo south of the S and N pods (Fig. 6.92, U); the REEs and Al are similar (Fig. 6.92, Al). All other responses are noisy.

Summary

This eluviated horizon is of little use in this case study; responses are dominated by peat samples even in the aqua regia leach. However, there is an intriguing E-W anomaly about 250 m south of the S pod, shown most prominently by the halogens and metalloids in the Bioleach (and by U in the MMI leach, Li etc in AR).

6.2.3 B1 horizon

Aqua regia. Grids in Fig. 6.93, Maps in Fig. 6.94

Element patterns in the A2 by the Bioleach are dominated by the peat samples but there is also an E-W high across the three westerly lines about 250 m south of the S pod shown by As, Bi, Br, I, Sb and Se, and to a lesser extent by U (Fig. 6.94, U; Fig. 6.94, As; Fig. 6.94, Br).

There is no expression above the pods for any elements in this horizon by AR. There are two major features: (1) the E-W anomaly south of the S pod, seen in the A2 horizon, demonstrated by U (Fig. 6.94), REEs, Cu, Ni, Bi, Be, Ag and Mn; and (2) a broad anomaly in the south as shown by many elements such as Al, As, Ba, Hg, Mg, Mo, P, Sb and Zr (Fig. 6.94, As). Calcium and Sr show contrasting behaviour, being elevated in the northern half of the survey area.

Enzyme leach. Grids in Fig. 6.95, Maps in Fig. 6.96

Uranium and the REEs are anomalous in the E-W direction ~ 250 m south of the S pod, as for the aqua regia leach (Fig. 6.96, U). The U anomaly on Line 4 north of the S pod did not repeat well and should be ignored. Nickel and V behave quite differently in this leach compared to AR: they have elevated concentrations around the pods and are low in the south (Fig. 6.96, Ni). Molybdenum, W and As appear to have similar trends but the data are mostly at detection limits. [Other elements reported at or below detection limits display the artifact created by differences in handling the data below DL, e.g. Cr, Ge, In, Hg, Sc].

Hydroxylamine leach (only for 2008). Grids in Fig. 6.97, Maps in Fig. 6.98

The response for U and the REEs is similar to that by AR with the small exception that the one-point U anomaly in the NE has disappeared (indicating it was probably organically bound) (Fig. 6.98, U). Nickel, Cr, Cs, Fe, Mg, V and P are high in the northern region between the pods, unlike the AR response (Fig. 6.98, Ni). The pattern for Pb is different to AR also (Fig. 6.98, Pb) and it might be beneficial to measure Pb isotopes in this northern area.

Ammonium acetate. Grids in Fig. 6.99, Maps in Fig. 6.100

Bioleach. Grids in Fig. 6.101, Maps in Fig. 6.102

MMI (only for 2008). Grids in Fig. 6.103, Maps in Fig. 6.104

Uranium and the REEs maintain the E-W anomaly shown by AR and the other partial leaches (Fig. 6.104, U). Furthermore, MMI results mimic those by HYD in that Fe and associated elements (e.g. As, Cu, Cr, Co, Mg, Ni, Ti, W, Zn) are elevated around and between the pods (Fig. 6.104, Ni).

Ionic leach (only for 2009). Grids in Fig. 6.105, Maps in Fig. 6.106

These results pertain to only two lines (Lines 3, 4) of samples and will be viewed in profile form later. It appears that the same two patterns are developing that we see with the other partial leaches: U and REE highs south of the S pod (Fig. 6.106, U) and clusters of highs around the S pod by As, Ca, Cr, Fe, Ni and Zn (Fig. 6.106, Cr).

Summary

The B1 horizon, an established medium in exploration geochemistry, is disappointing. However, coverage above the pods was extremely poor due to the presence of peat and water. The E-W coherent anomaly ~ 250 m south of the S pod, shown by results for U and the REEs in the A2 horizon, is also shown here by all leaches. The partial leach responses differ from those by aqua regia in that numerous elements are higher in concentration around and between the pods, including Fe, Ni, Cr and V. This may be an effect of the much wetter conditions in this region. Further work should be done on Pb isotopes using the hydroxylamine leach on B1.

6.2.4 B2 horizon (only 2008)

There were very few samples taken around the pods because of the wet conditions.

Aqua regia. Grids in Fig. 6.107, Maps in Fig. 6.108

Uranium and the REEs are anomalous south of the S pod on Lines 4 and 5, similar to the results for B1 (but closer to the pod perhaps), though Line 3 is missing here (collected in 2009) (Fig. 6.108, U). Iron behaves slightly differently in that the anomaly extends southward along Line 5 (Fig. 6.108, Fe); numerous elements are associated with this pattern including Ba, Cs, Co, Cr, Mo, Ni, Ti, V and Zr . The patterns for Ca and P are alike in displaying highs south of each set of pods (Fig. 6.108, Ca).

Hydroxylamine leach Grids in Fig. 6.109, Maps in Fig. 6.110

The E-W signature south of the S pod is evident for the REEs and Cu, but is less consistent for U (Fig. 6.110, La; Fig. 6.110, U). Elements concentrated around and between the pods comprise Fe, Cr, K, Mn, P, Sr and Ti (Fig. 6.110, Fe). Lead is not associated with this Fe and has various single point anomalies in the south.

Ammonium acetate. Grids in Fig. 6.111, Maps in Fig. 6.112

Enzyme leach. Grids in Fig. 6.113, Maps in Fig. 6.114

Bioleach. Grids in Fig. 6.115, Maps in Fig. 6.116

MMI. Grids in Fig. 6.117, Maps in Fig. 6.118

The MMI response for U and the REEs in B2 shows a SW-NE trending anomaly ~ 250 m south of the S pod and parallel to it (Fig. 6.118, U; Fig. 6.118, Sm). This pattern is in sharp contrast to that showing highs clustered near the pods, as exemplified by Ca, Cd, Co, Cr, Fe, Mg, Nb, Ni, Sr, Ti, V, W and Zr (Fig. 18c, Cr).

Summary

These results bear a resemblance to those for B1 in that: (1) the E-W trend south of the S pod is still seen for U and the REEs in the aqua regia, hydroxylamine and MMI leaches, though less strong by AR; and (2) the latter two partial leaches, in contrast to aqua regia, show numerous elements, including Fe, Mg and Ni, concentrated near the pods.

6.2.5 C horizon (only 2008)

Aqua regia. Grids in Fig. 6.119, Maps in Fig. 6.120

The vast majority of elements show a remarkably consistent pattern of elevated concentration ('tuning fork' shape) in the SW of the survey area, stretching over three lines (Fig. 6.120, U). This applies not only to U and the REEs but to elements such as Fe, Na, K, Mg, Mn, Ni and Zr. Elements displaying contrasting behaviour include Mo, Se (noisy), Hg and Nb (Fig. 6.120, Mo).

Enzyme leach. Grids in Fig. 6.121, Maps in Fig. 6.122

The 'tuning fork' pattern is evident for far fewer elements, namely I, Ba, Ge and the REEs but the latter also have high concentrations around the pods (Fig. 6.122, La). The U pattern is simply noisy (Fig. 6.122, U) but that for Mo, Ni and Co highlights the areas of the pods (Fig. 6.122, Mo; Fig. 6.122, Ni). The behaviours of Ni and Co are in sharp contrast between the AR and Enzyme leaches; Mn is also concentrated around the pods in the Enzyme leach, and not in the SW as in the aqua regia leach.

Hydroxylamine leach. Grids in Fig. 6.123, Maps in Fig. 6.124

U and the REEs exhibit the 'tuning fork' pattern of the aqua regia digestion (Fig. 21a, U) but other element patterns differ from those by AR (as in the B1 and B2 horizons); these include Ca, Cr, Cu, Fe, Mg, Ni, P and Zn (Fig. 21b, Ni). The Ni responses by HYD and Enzyme leaches are almost identical but the concentrations in the latter are ~ 10 times lower.

Ammonium acetate. Grids in Fig. 6.125, Maps in Fig. 6.126

MMI. Grids in Fig. 6.127, Maps in Fig. 6.128

The results of this leach agree well with those by the Enzyme leach: the U map is very noisy (Fig. 22a, U), the tuning fork pattern shown by so many elements by AR is subdued and many elements such as Al, Fe, Bi, Cu, Co, Mo, Ni, Ti and V show high concentrations near the pods (Fig. 22b, Ni). *Check [Fe]. If fairly low, will show that it's not a scavenger and will support argument that these highs are not a function of major element phases.*

Bioleach. Grids in Fig. 6.129, Maps in Fig. 6.130

Summary

The remarkable consistency of pattern ('tuning fork' in SW of survey) shown by the majority of elements in the aqua regia digestion breaks down for the partial leaches which amongst themselves show consistency in that numerous elements cluster in concentraton near the pods (e.g. Fe, Ni, Mo, Co). The Enzyme and MMI responses are alike; U by these leaches is particularly noisy but others elements such as Ni and Mo highlight the pods (Ni is also 'good' by the HYD leach).

6.2.6 MMIh, the MMI-horizon. *Grids in Fig. 6.131, Maps in Fig. 6.132*

The MMIh pattern for U is very strong, showing that E-W anomaly south of the S pod across four lines; there is a further anomaly south of this on Lines 4 and 5 which is in the region of the 'tuning fork' pattern shown by aqua regia on the C horizon (Fig. 6.132, U). The REEs are similar in the E-W anomaly. As evidenced by partial leaches carried out on the other inorganic horizons, elements such as Co, Cr, Fe, Mg, Nb, Ni, Ti, W, Zn and Zr are elevated in the region of the pods (Fig. 6.132, Ni). Molybdenum and Pb are noisy. Copper shows a SW-NE trend around the S pod (Fig. 6.132, Cu). The patterns shown by this MMI horizon (10-25 cm below the humus) are comparable to those by MMI on the B1 horizon.

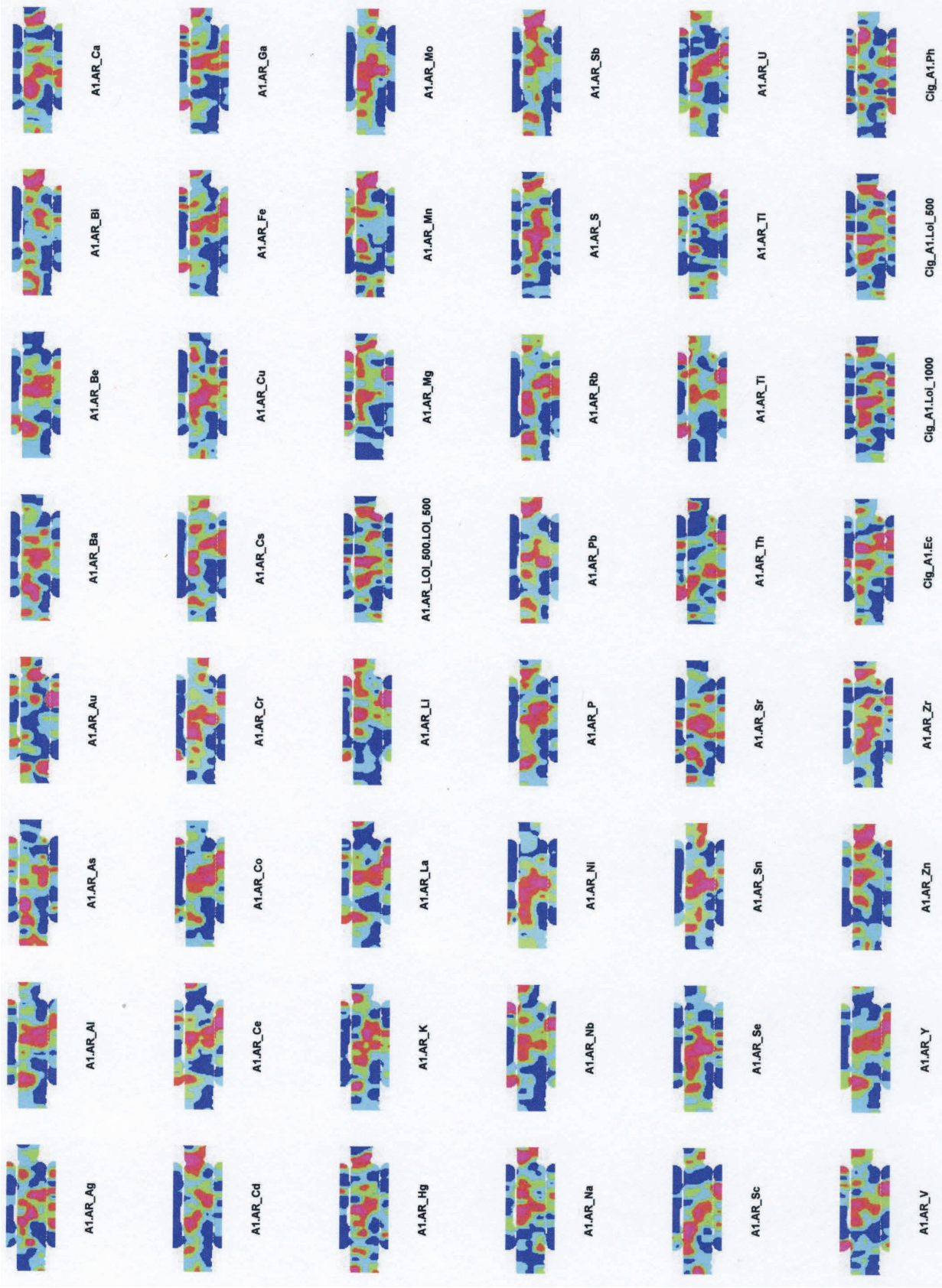

Fig 6.1 Cigar Lake Grids. A1 horizon. Aqua regia leach

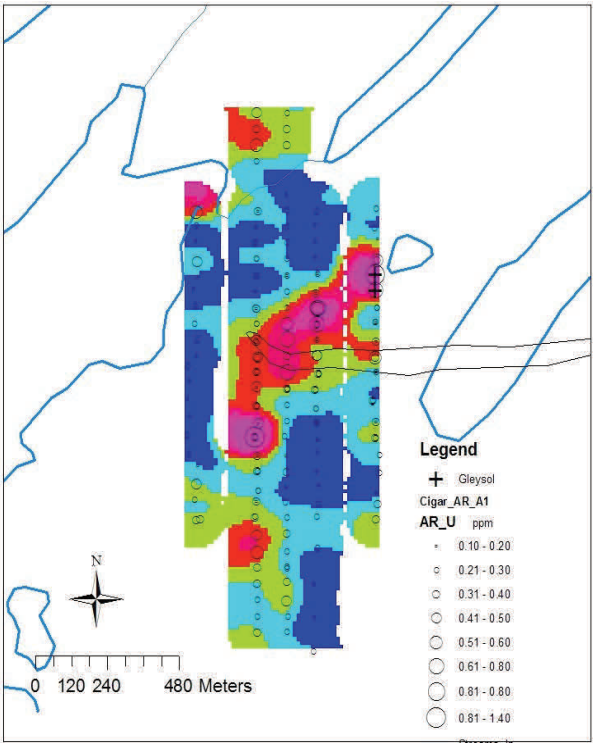

Uranium. A1 horizon. Aqua regia.

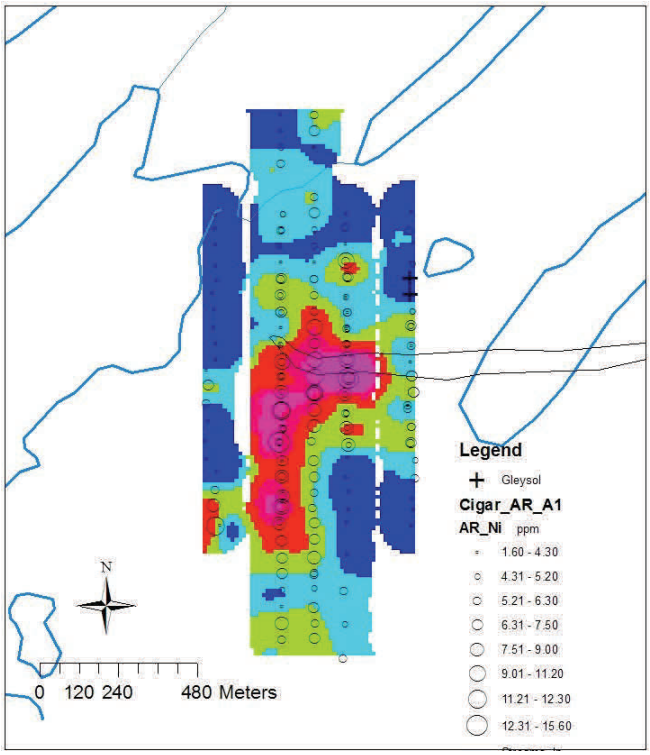

Nickel. A1 horizon. Aqua regia.

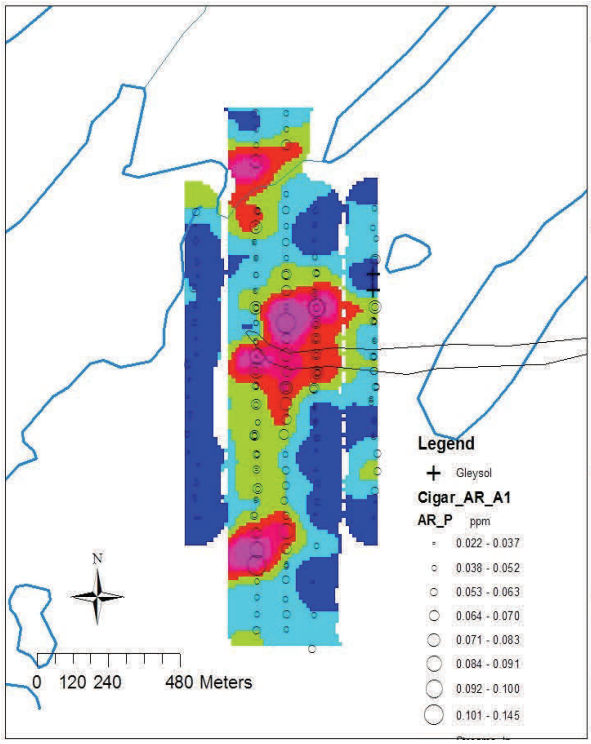

Phosphorus. A1 horizon. Aqua regia.

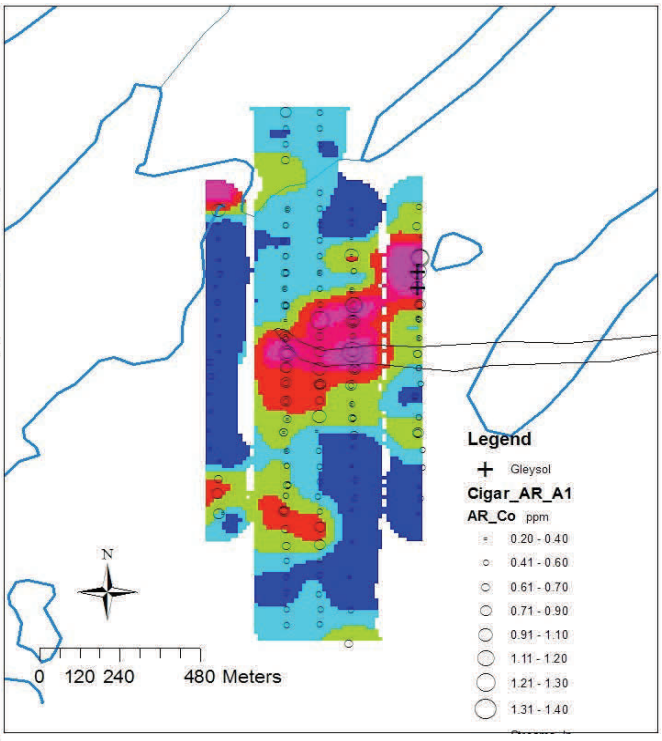

Cobalt. A1 horizon. Aqua regia.

Fig 6.2 Cigar Maps A1 horizon. Aqua regia

Fig 6.3 Cigar Lake Grids . A1 horizon. Sodium pyrophosphate leach.

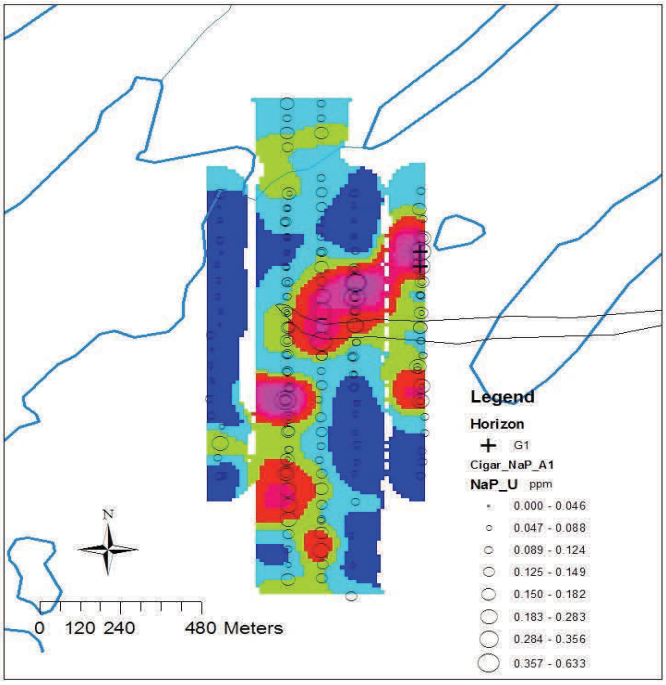

Uranium. A1 horizon. Sodium pyro leach.

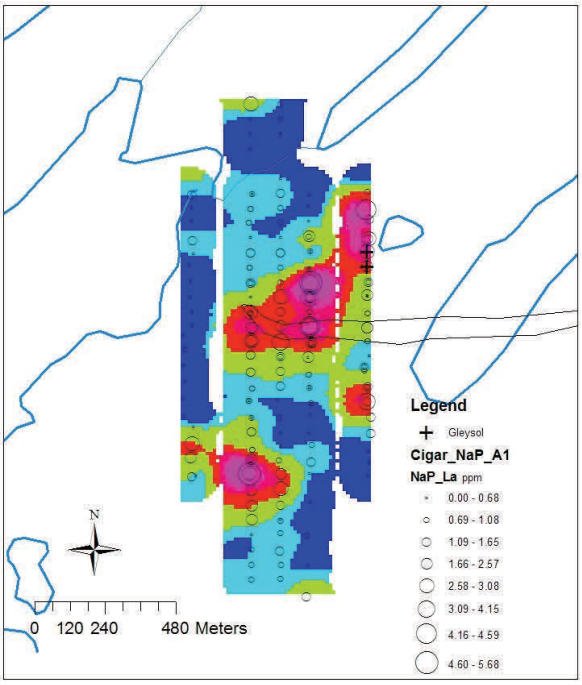

Lanthanum. A1 horizon. Sodium pyro leach.

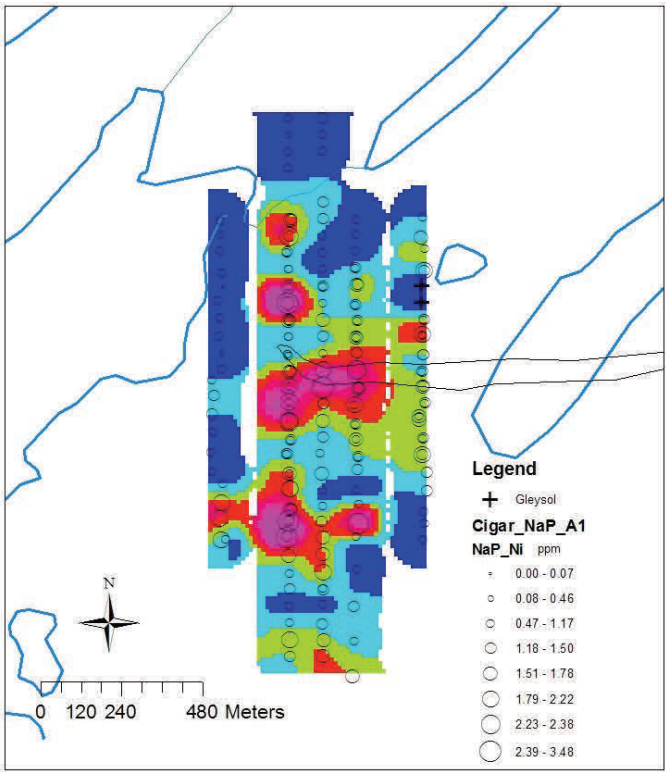

Nickel. A1 horizon. Sodium pyro leach.

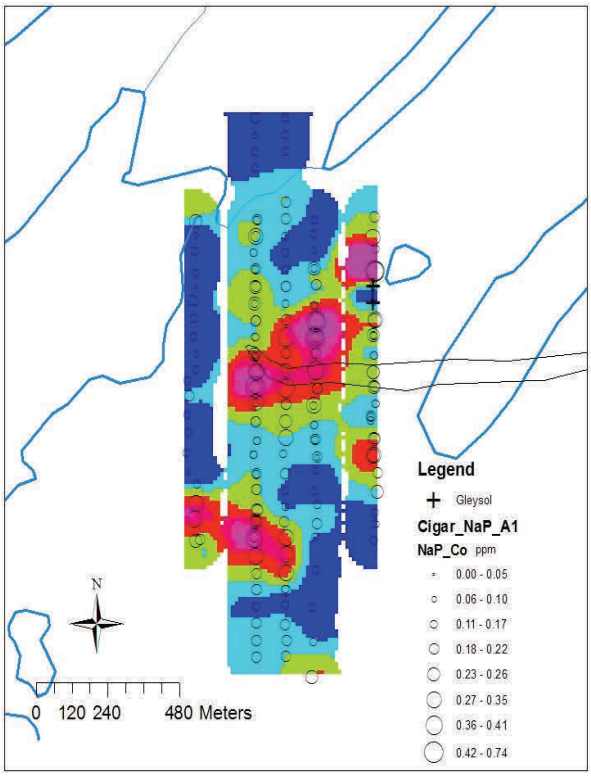

Cobalt. A1 horizon. Sodium pyro leach.

Fig 6.4 Cigar Maps. A1 Sodium pyrophosphate

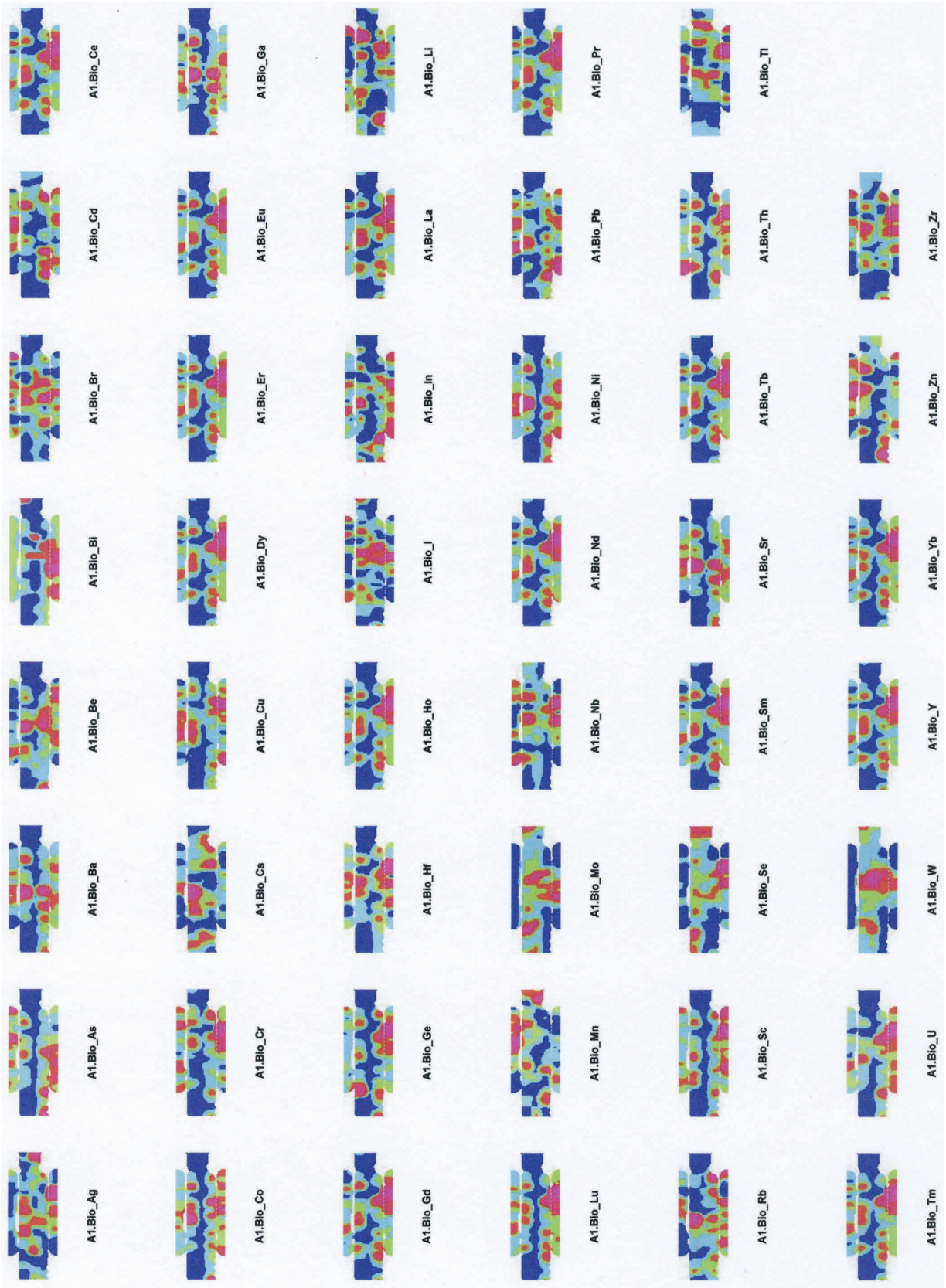

Fig 6.5 Cigar Lake Grids. A1 horizon. Bioleach.

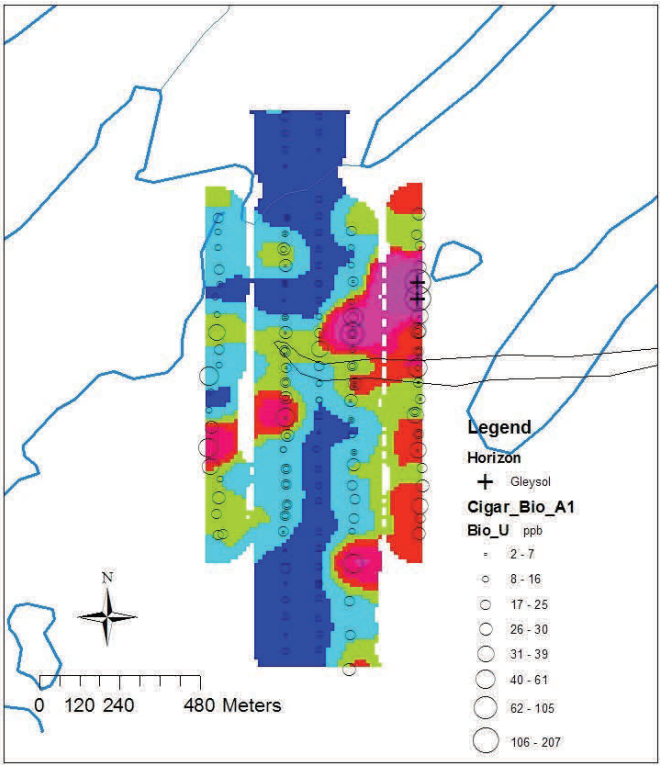

Uranium. A1 horizon. Bioleach.

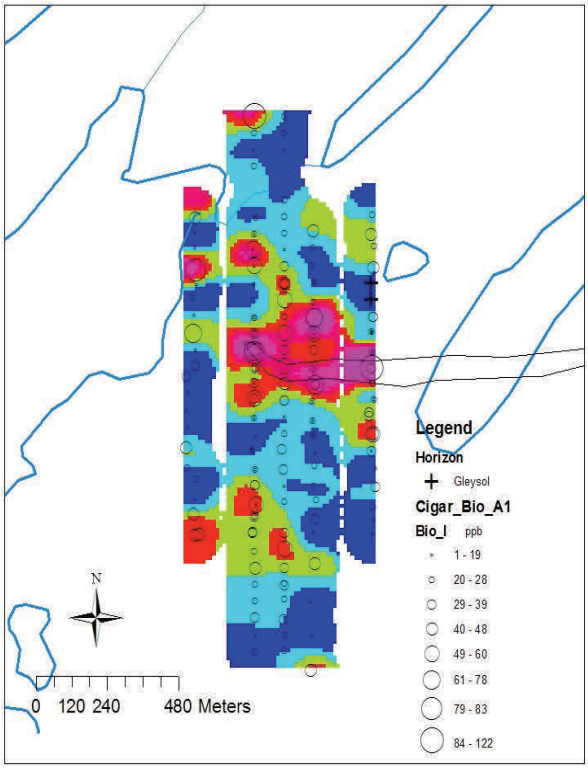

Iodine. A1 horizon. Bioleach.

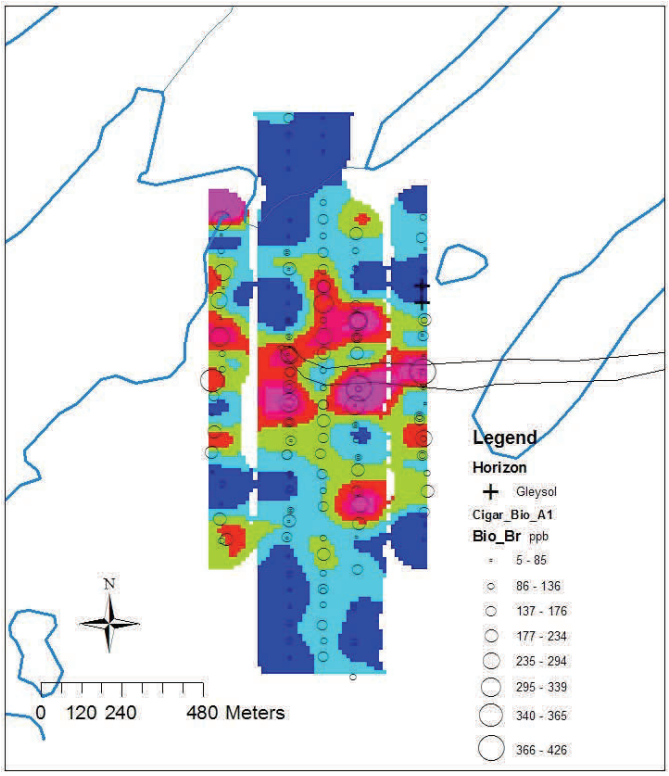

Bromine. A1 horizon. Bioleach.

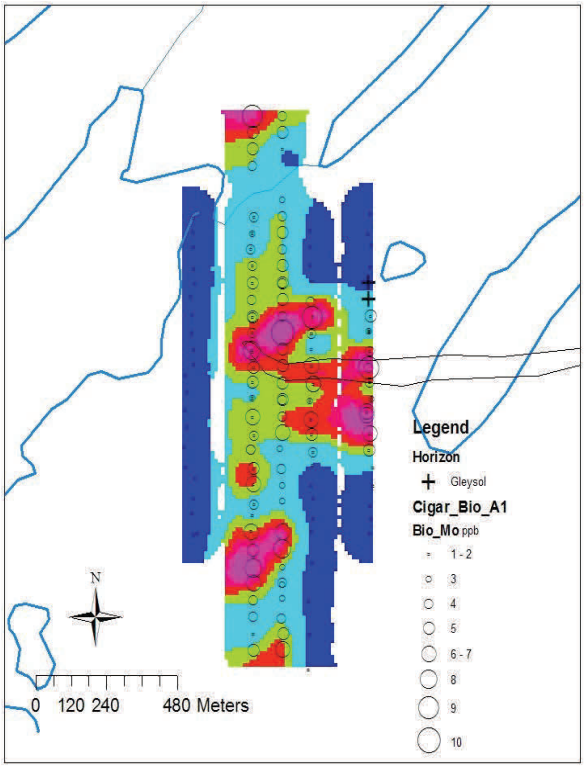

Molybdenum. A1 horizon. Bioleach.

Fig 6.6 Cigar Maps A1 Bioleach

Fig 6.7 Cigar Lake Grids. A1 horizon. Hydroxylamine leach.

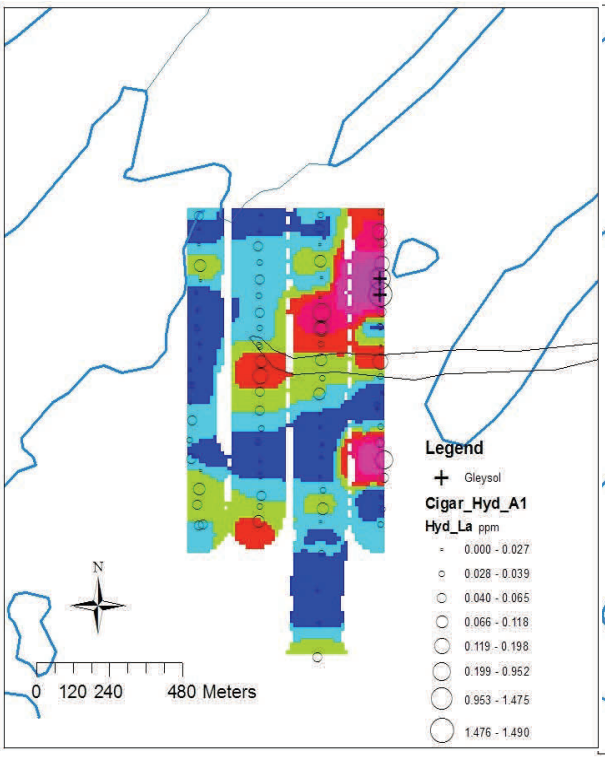

Lanthanum. A1 horizon. Hydroxylamine leach.

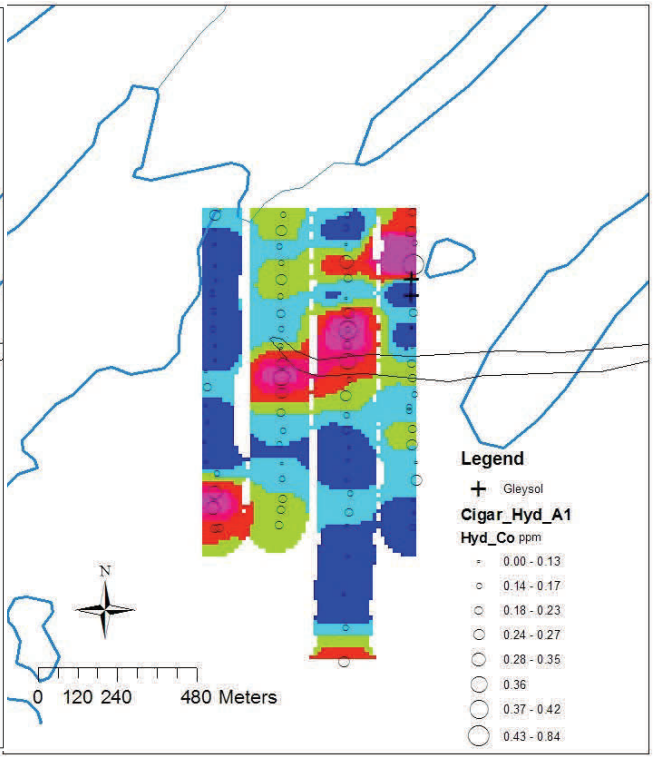

Cobalt. A1 horizon. Hydroxylamine leach.

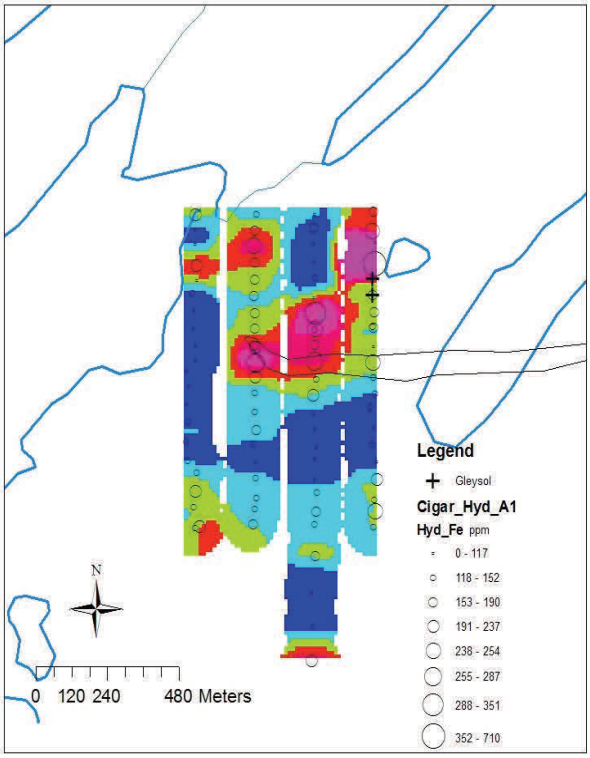

Iron. A1 horizon. Hydroxylamine leach.

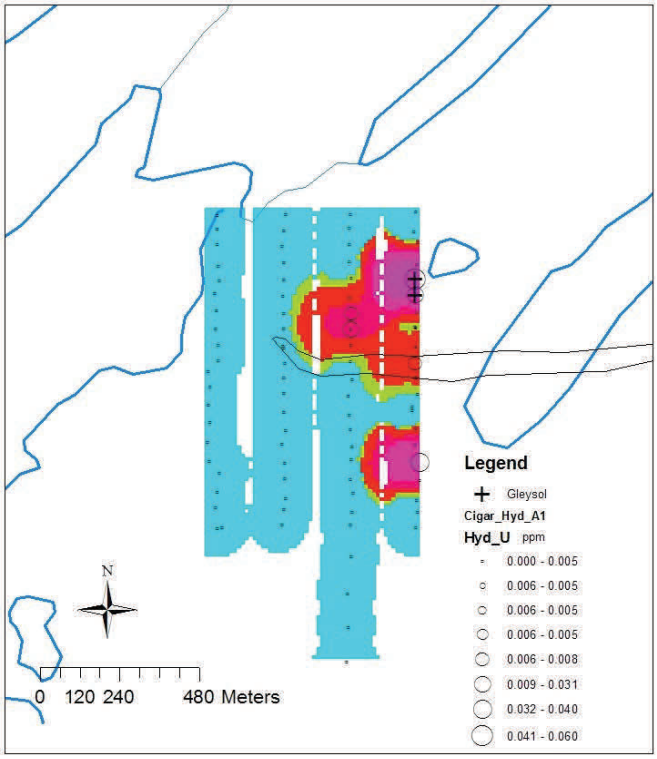

Uranium. A1 horizon. Hydroxylamine leach.

Fig 6.8 Cigar Maps. A1. Hydroxylamine

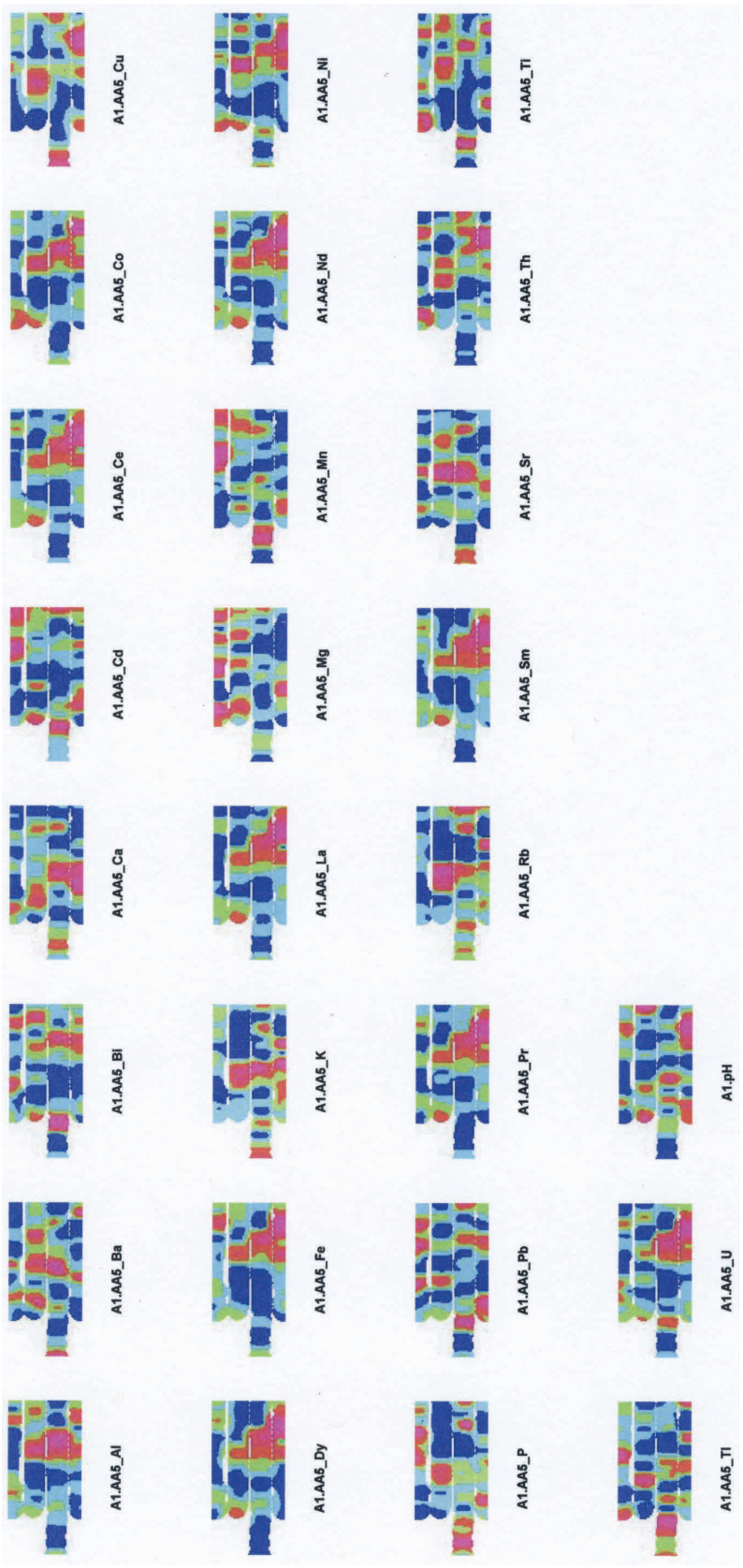

Fig 6.9 Cigar Lake Grids. A1 horizon. Ammonium acetate leach.

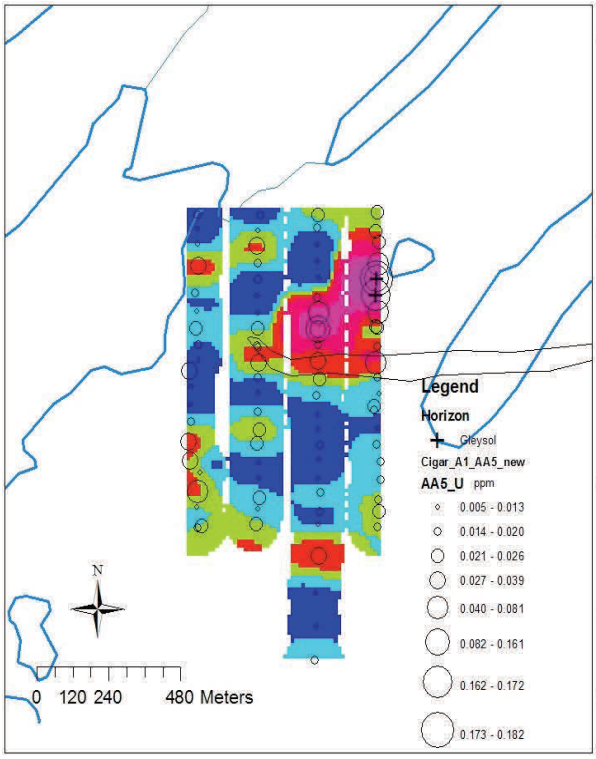

Uranium. A1 horizon. Ammonium acetate leach.

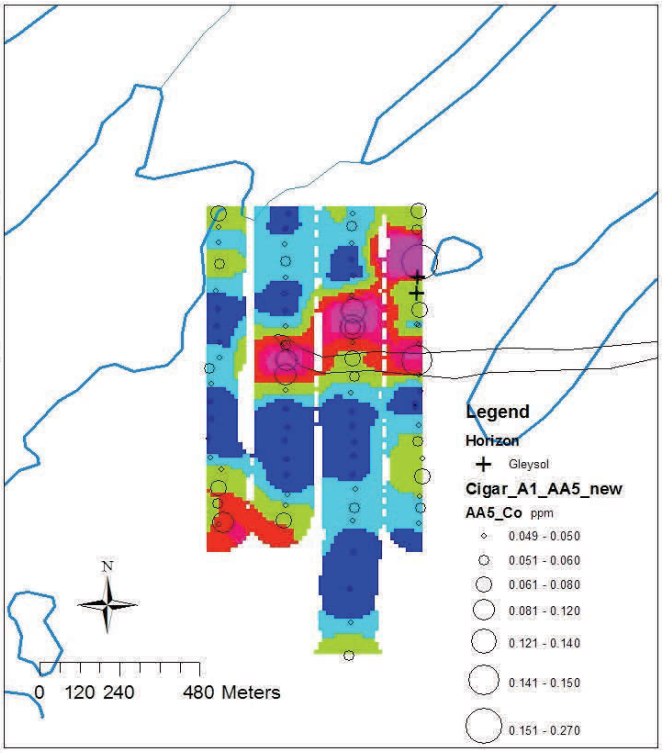

Cobalt. A1 horizon. Ammonium acetate leach.

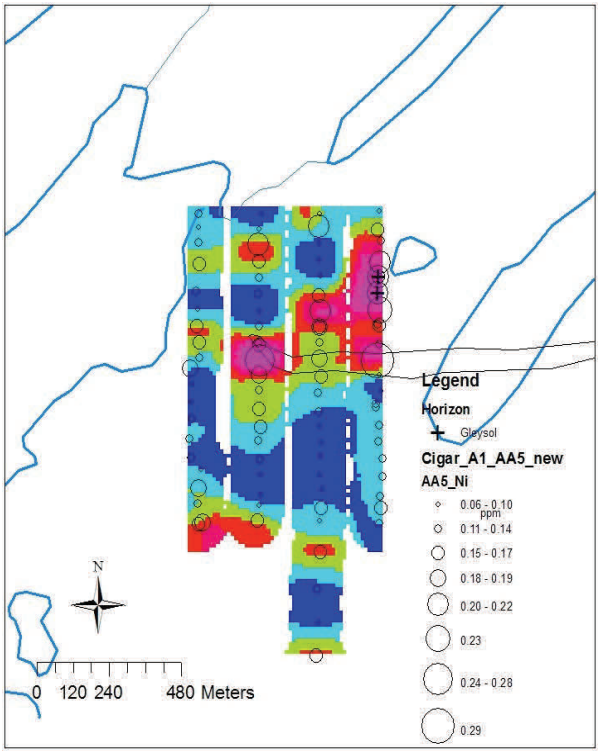

Nickel. A1 horizon. Ammonium acetate leach.

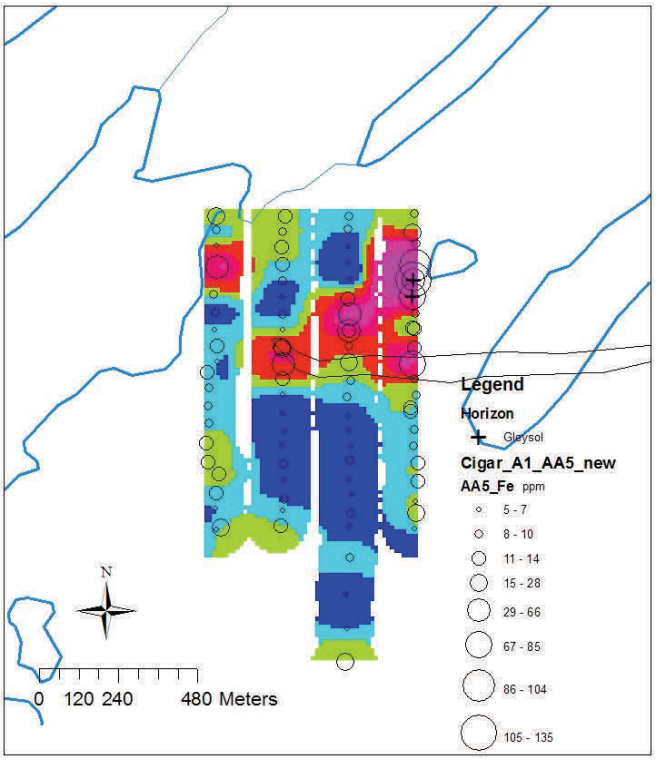

Iron. A1 horizon. Ammonium acetate leach.

Fig 6.10 Cigar Maps. A1. Ammonium acetate.

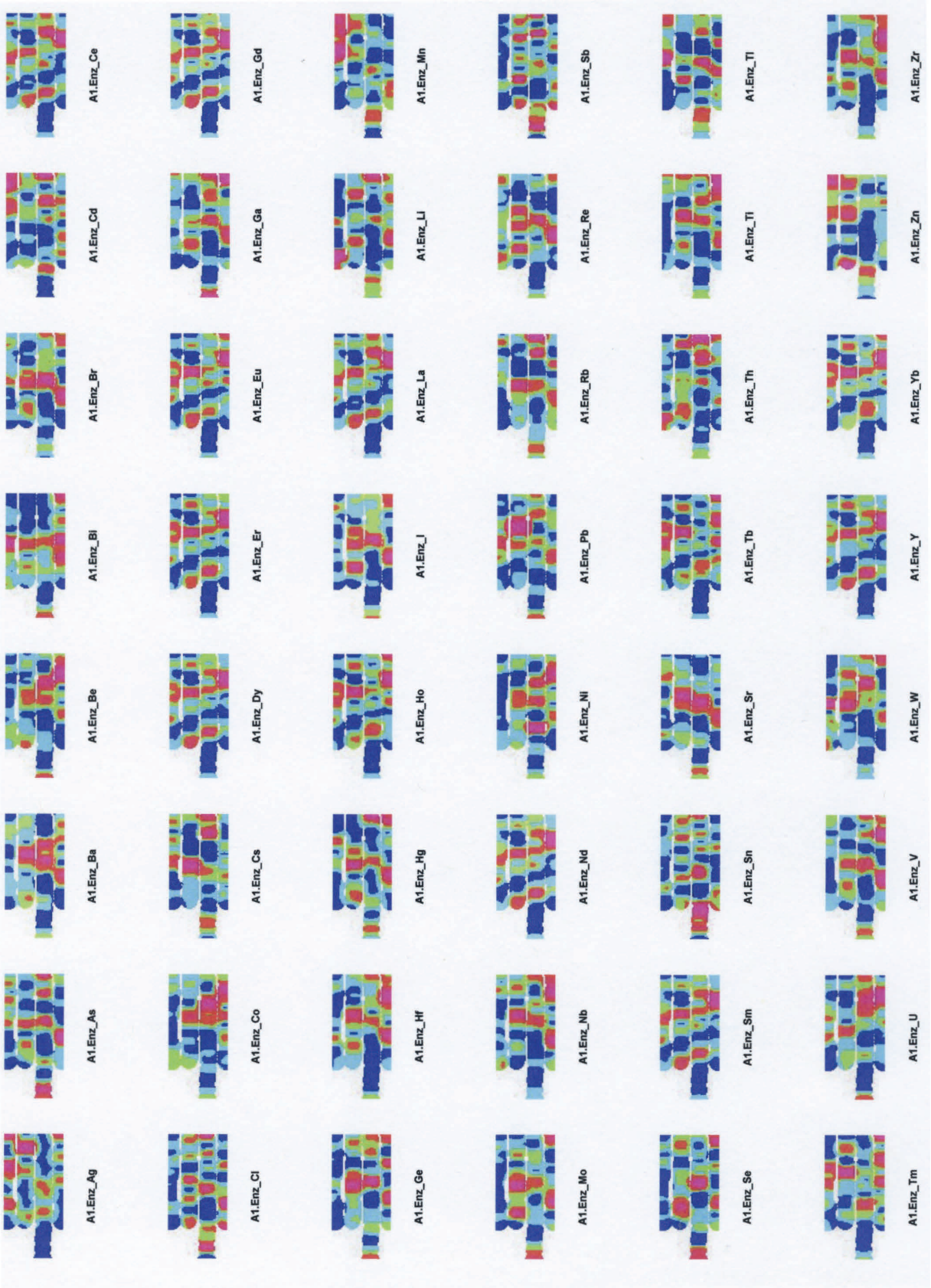

Fig 6.11 Cigar Lake Grids. A1 horizon. Enzyme leach.

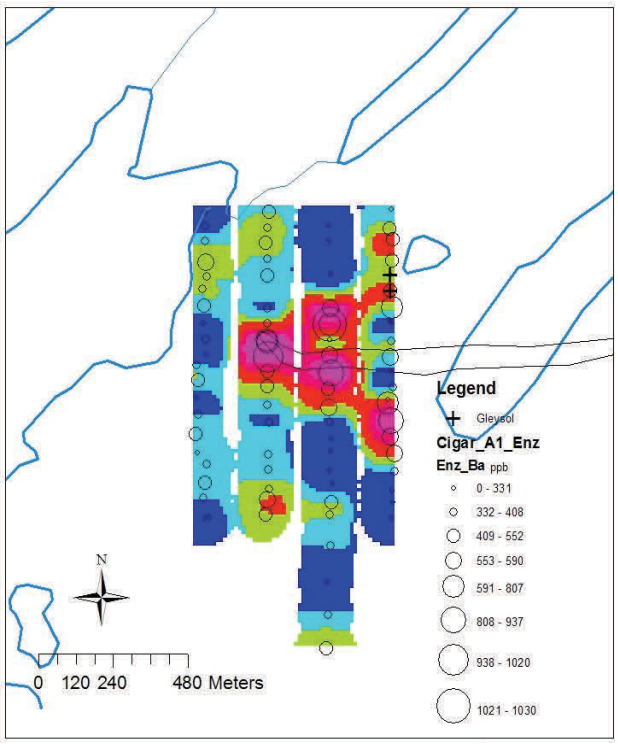

Barium A1 horizon. Enzyme leach

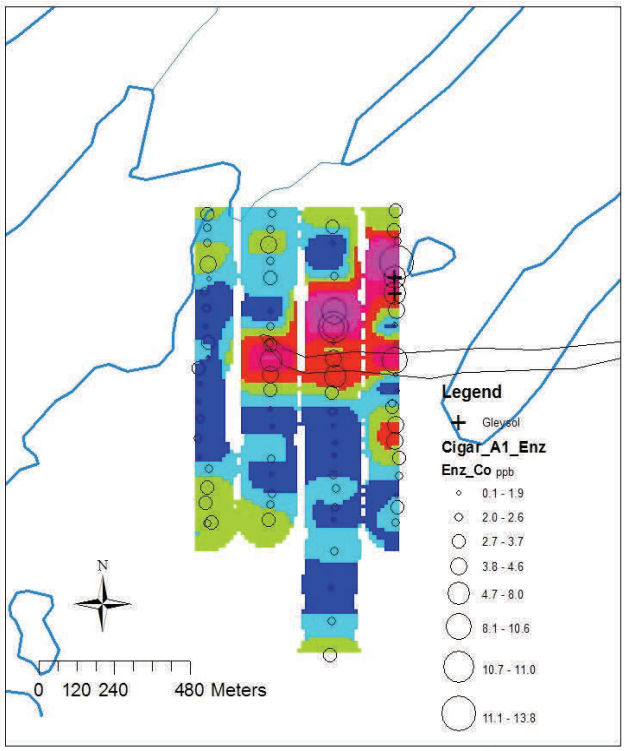

Cobalt A1 horizon. Enzyme leach

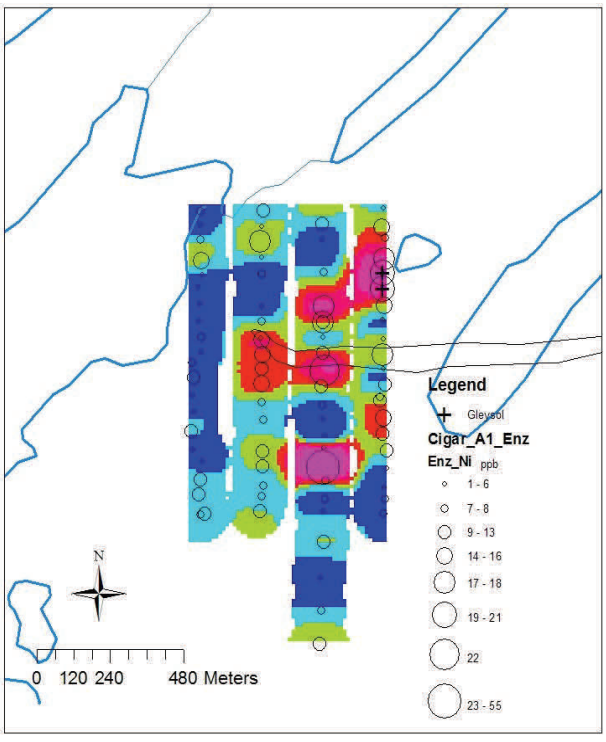

Nickel A1 horizon. Enzyme leach

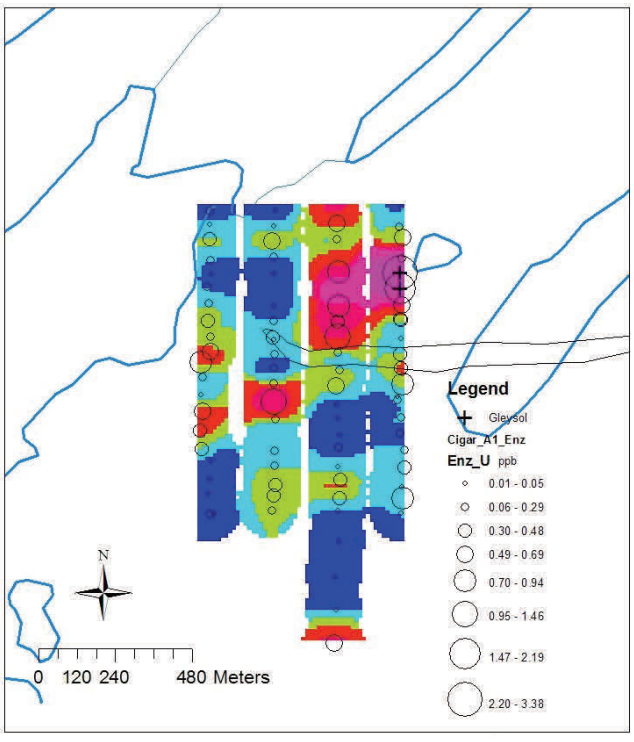

Uranium A1 horizon. Enzyme leach

Fig 6.12 Cigar Maps. A1 Enzyme

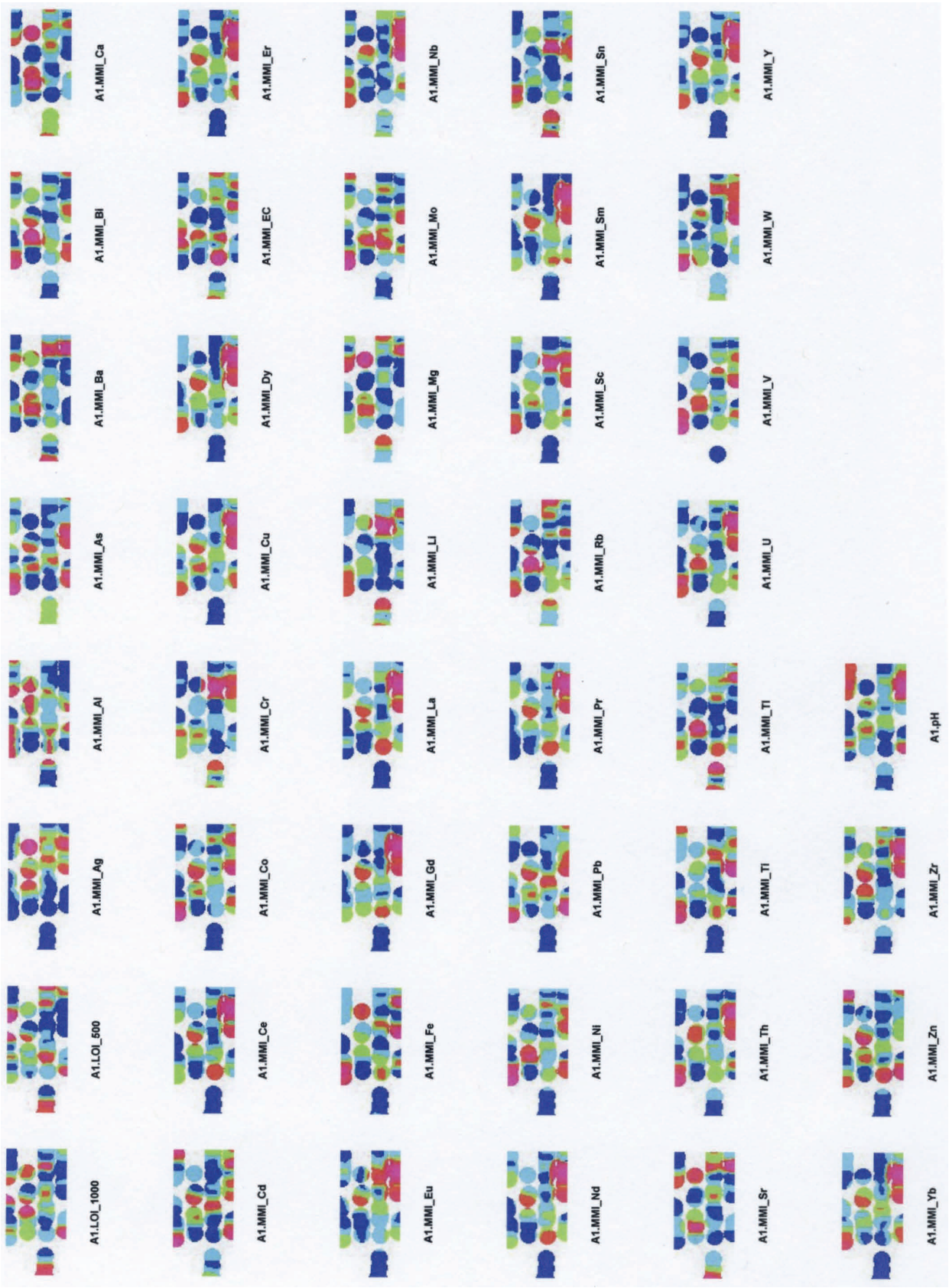

Fig 6.13 Cigar Lake Grids. A1 horizon. MMI leach.

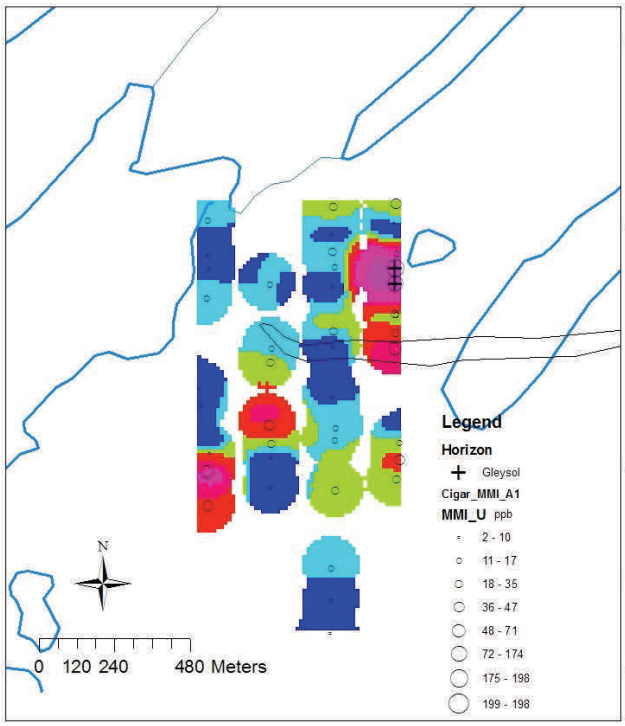

Uranium. A1 horizon. MMI leach.

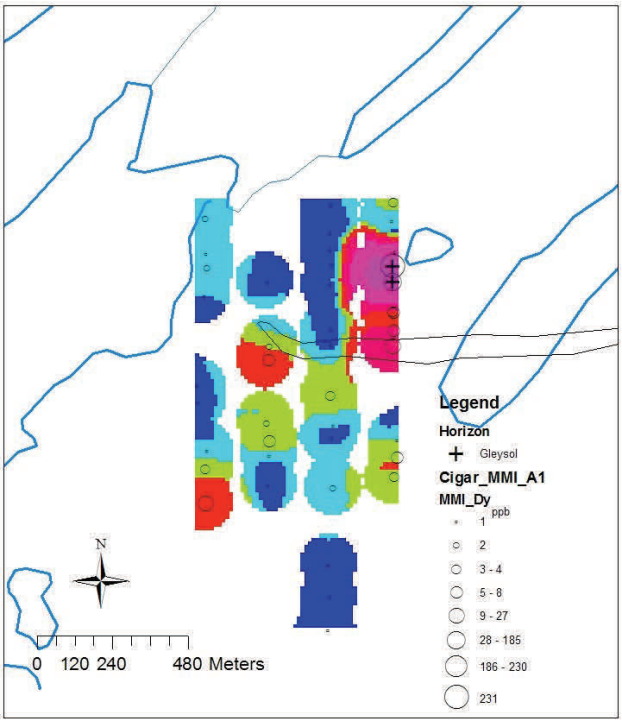

Dysprosium. A1 horizon. MMI leach.

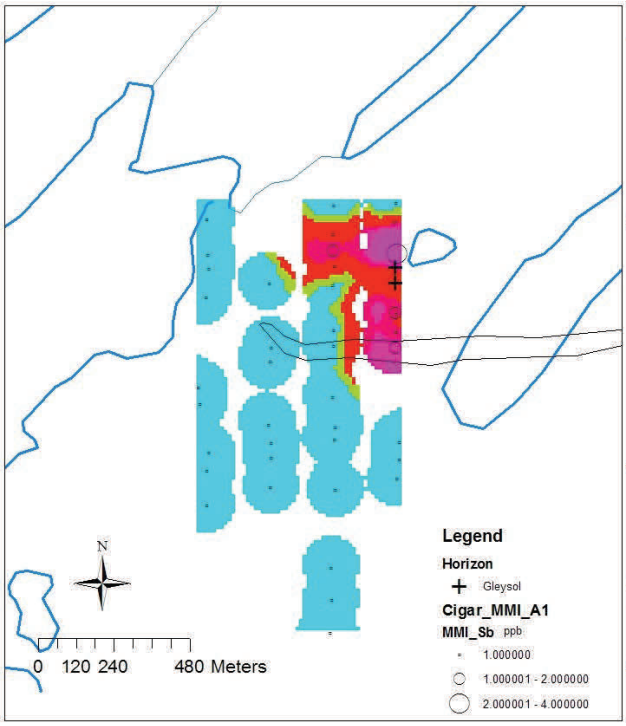

Antimony. A1 horizon. MMI leach.

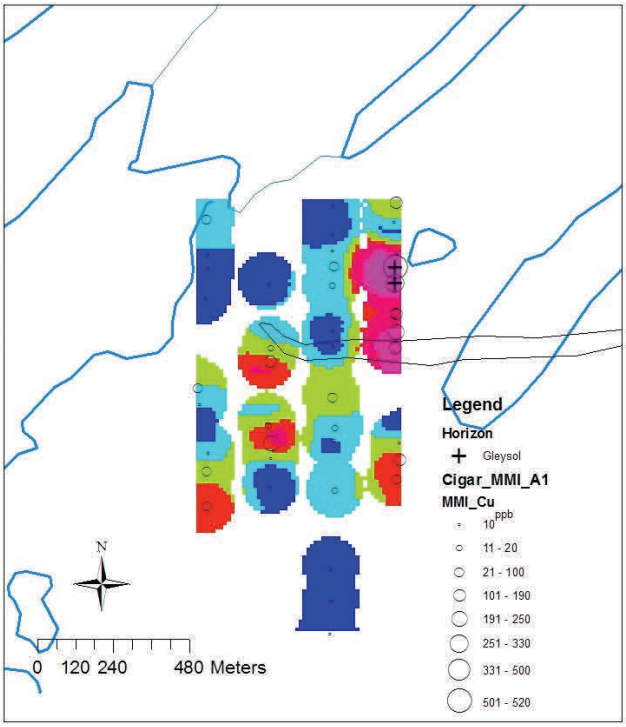

Copper. A1 horizon. MMI leach.

Fig 6.14 Cigar Maps. A1 MMI leach

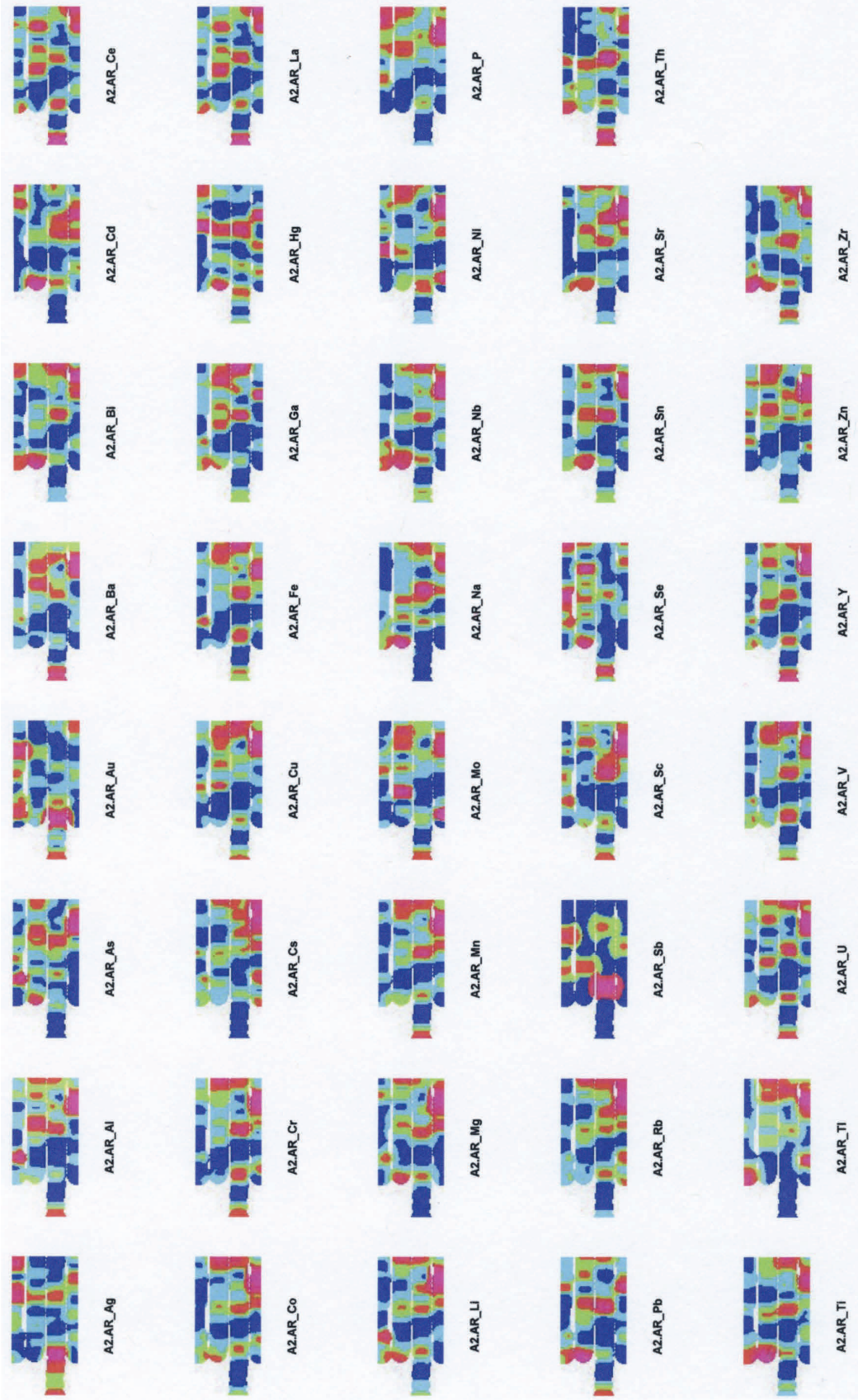

Fig 6.15 Cigar Lake Grids. A2 horizon. Aqua regia leach.

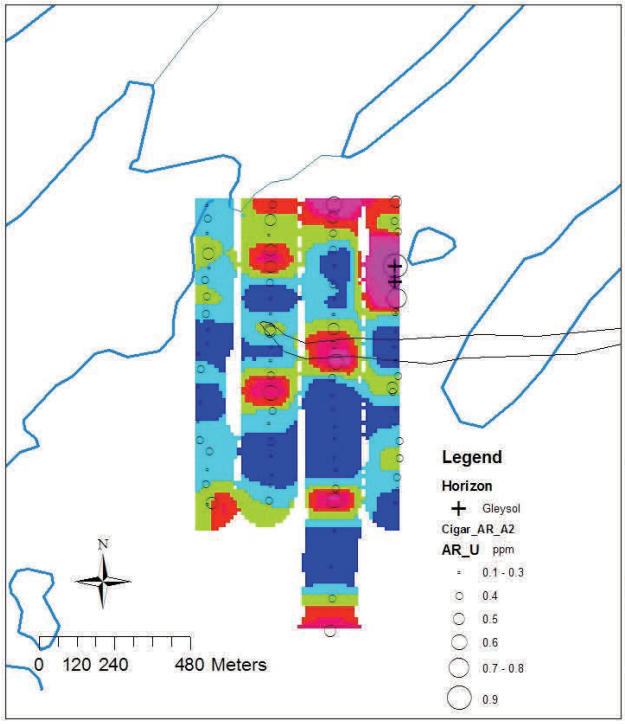

Uranium. A2 horizon. Aqua regia leach.

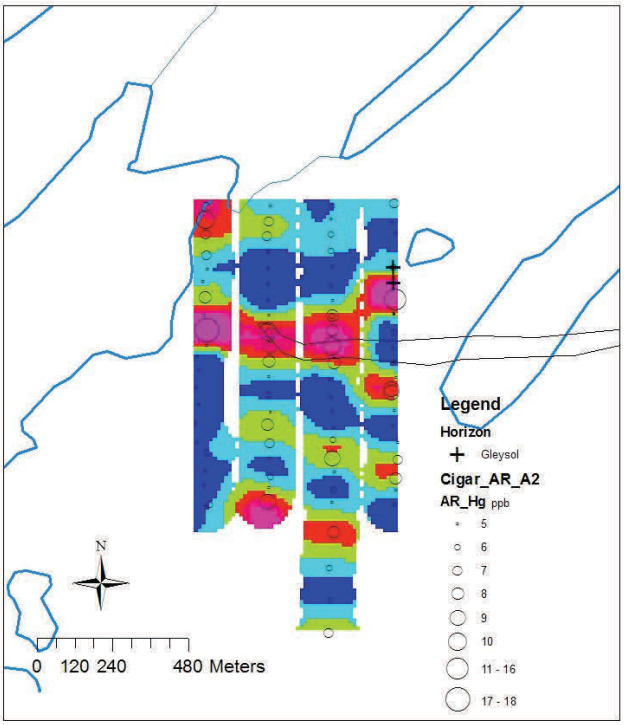

Mercury. A2 horizon. Aqua regia leach.

Fig 6.16 Cigar Maps A2. Aqua regia

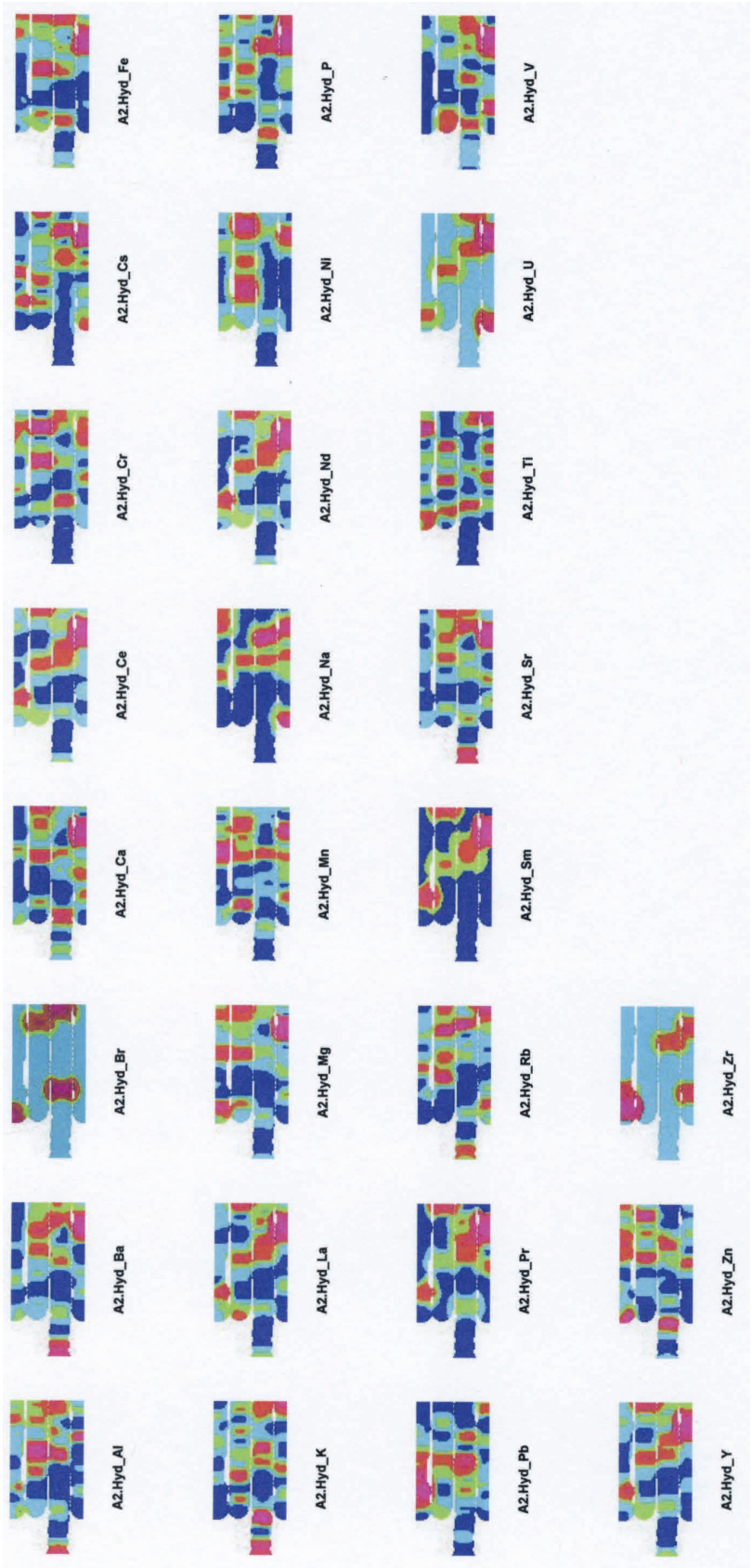

Fig 6.17 Cigar Lake Grids. A2 horizon. Hydroxylamine leach.

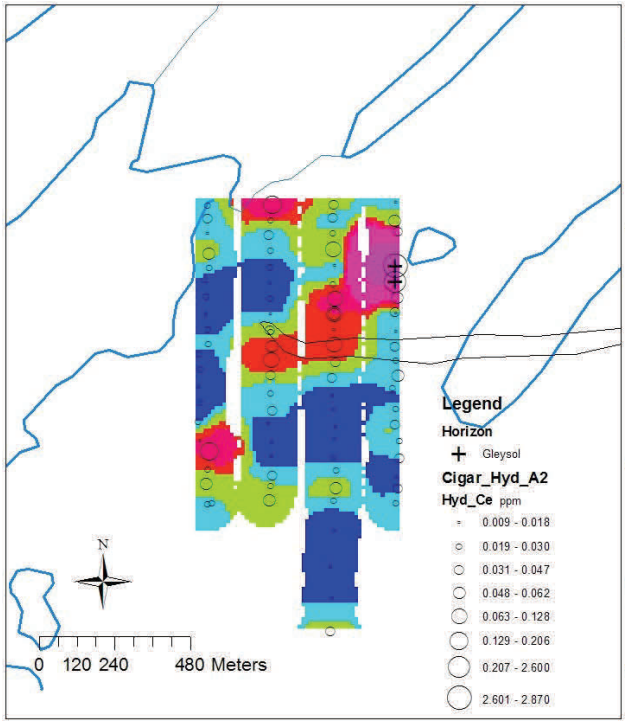

Cerium. A2 horizon. Hydroxylamine leach.

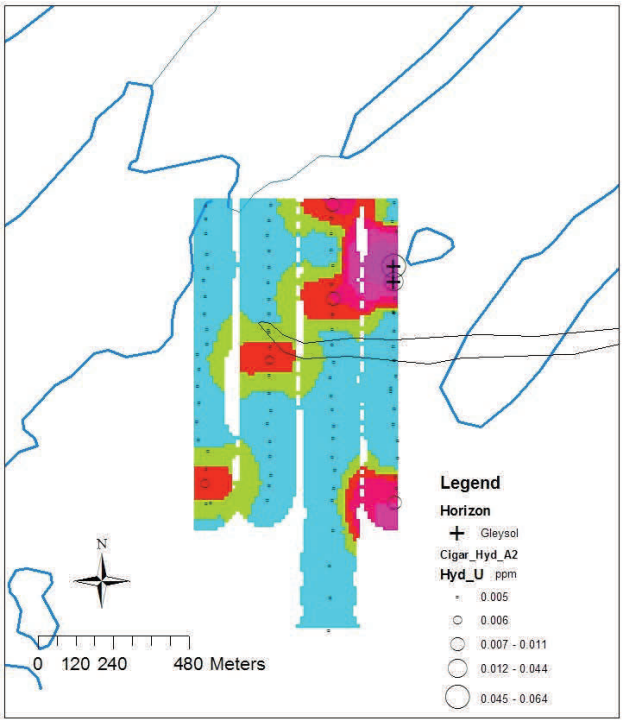

Uranium. A2 horizon. Hydroxylamine leach.

Fig 6.18. Cigar A2 Hydroxylamine

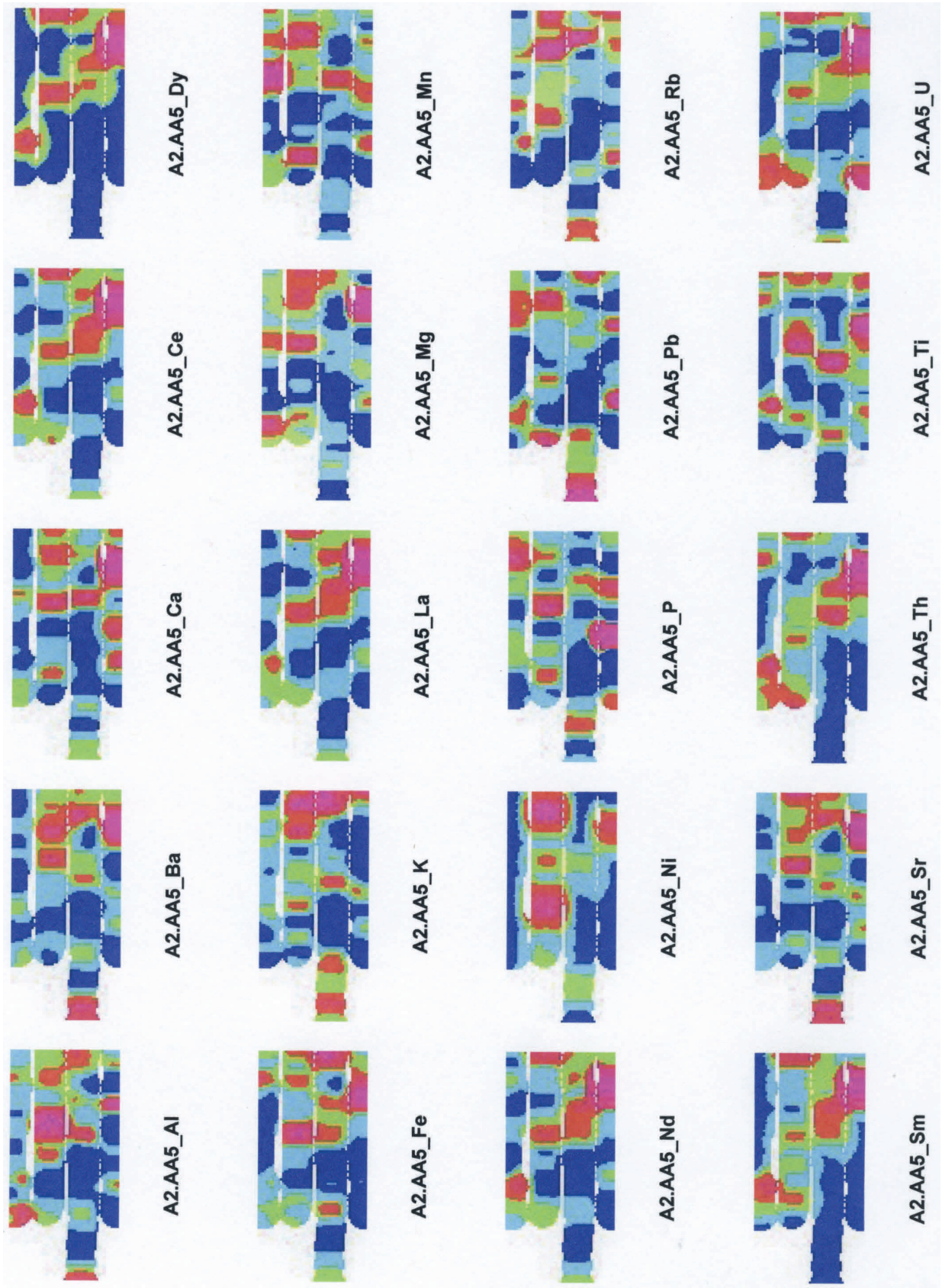

Fig 6.19 Cigar Lake Grids . A2 horizon. Ammonium acetate leach.

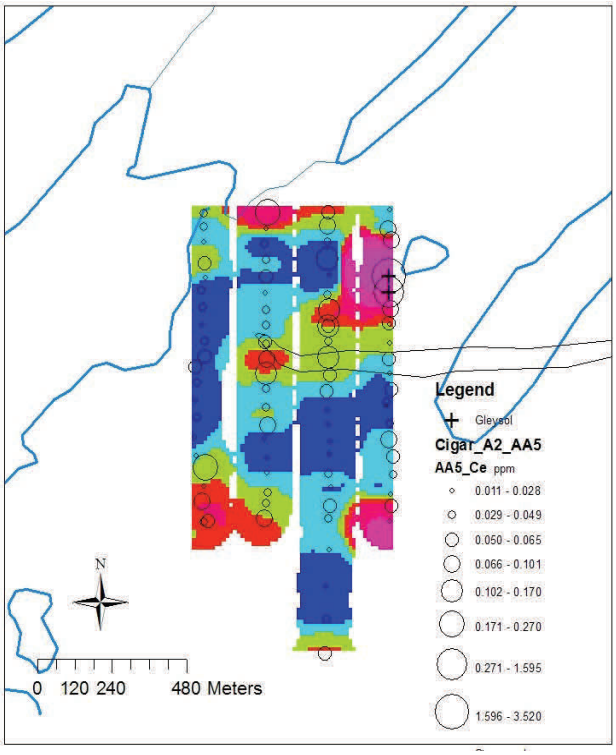

Cerium. A2 horizon. Ammonium acetate leach

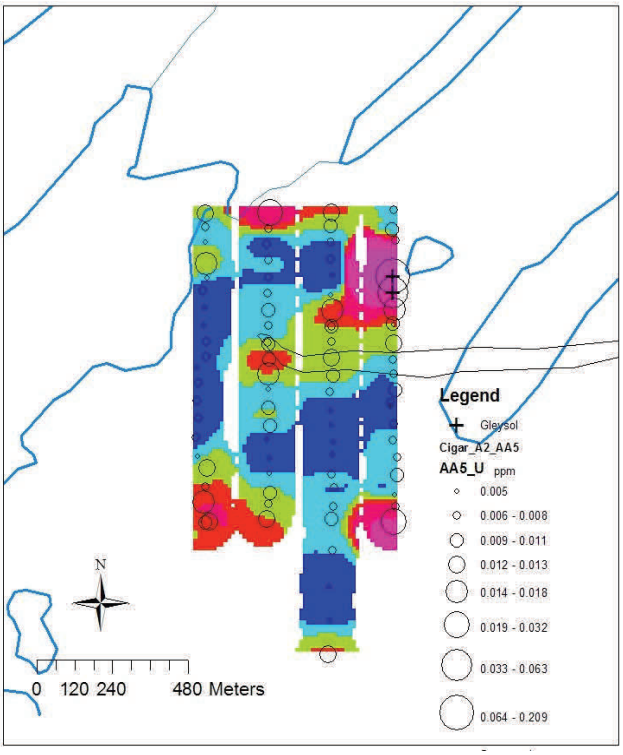

Cerium. A2 horizon. Ammonium acetate leach

Fig 6.20 Cigar A2 Ammonium acetate

Fig 6.21 Cigar Lake Grids. A2 horizon. Enzyme leach.

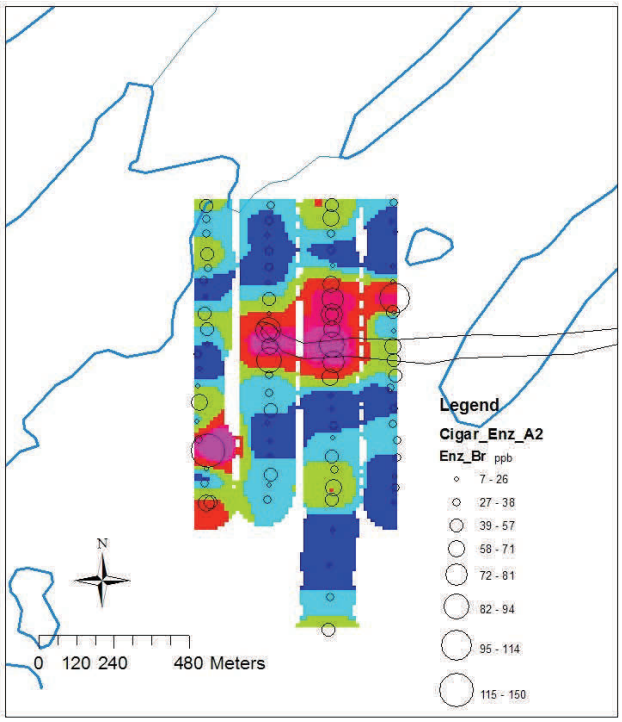

Bromine. A2 horizon. Enzyme leach.

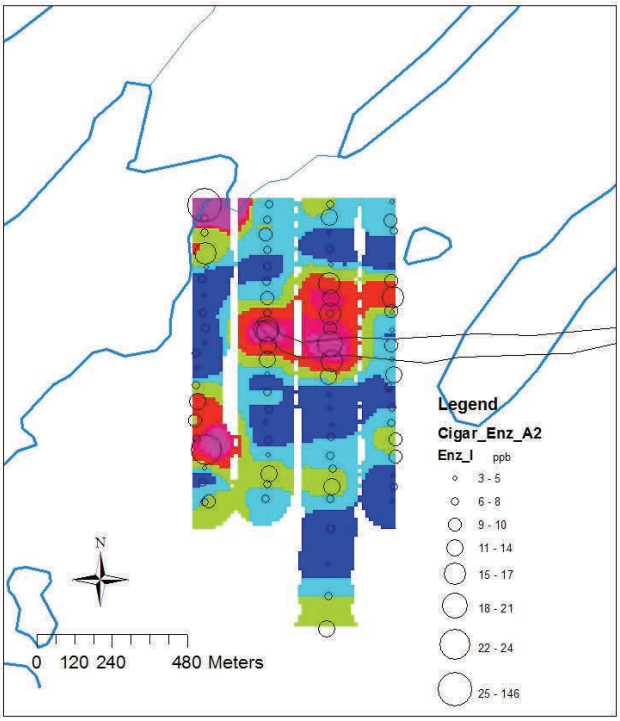

Iodine. A2 horizon. Enzyme leach.

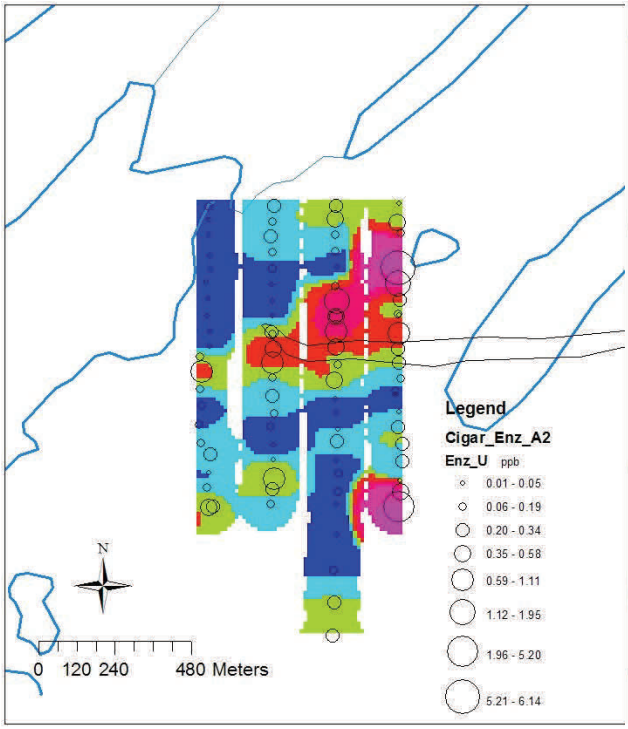

Uranium. A2 horizon. Enzyme leach.

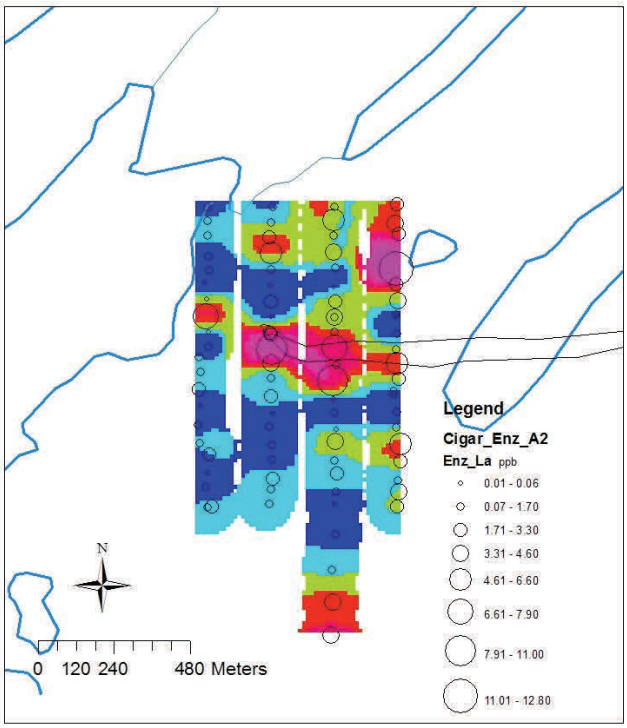

Lanthanum. A2 horizon. Enzyme leach.

Fig 6.22 Cigar Maps. A2 Enzyme

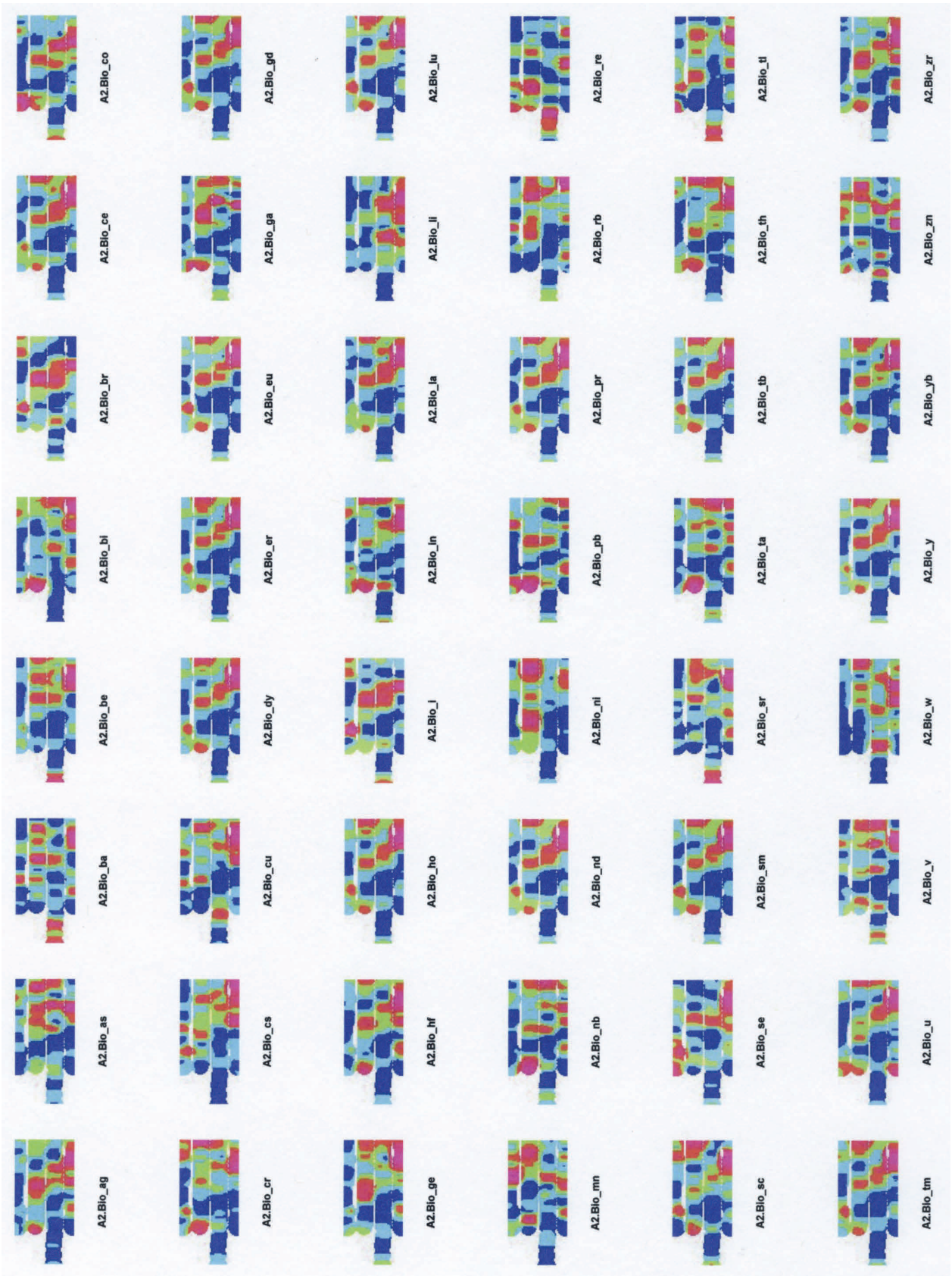

Fig 6.23 Cigar Lake Grids. A2 horizon. Bioleach.

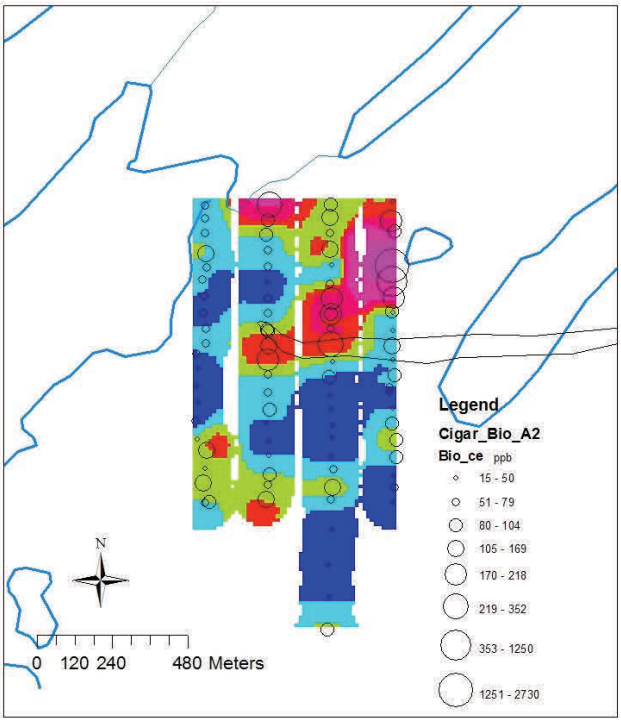

Cerium. A2 horizon. Bioleach.

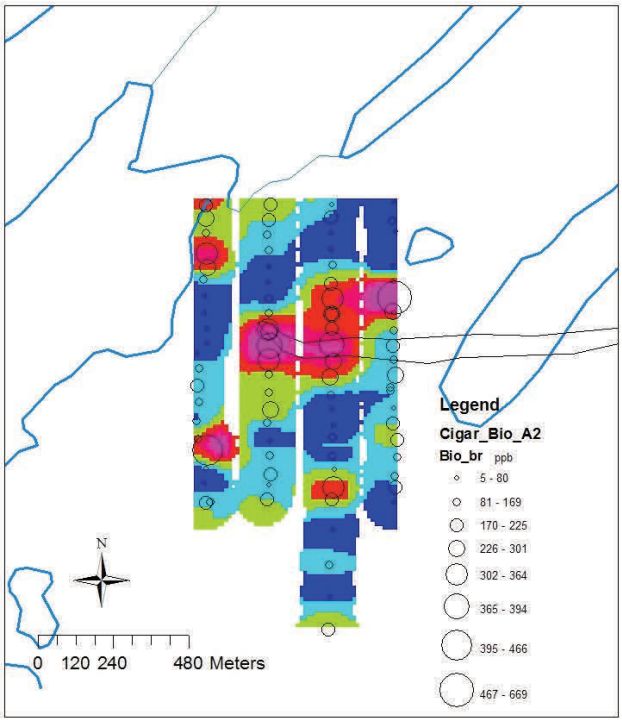

Bromine. A2 horizon. Bioleach.

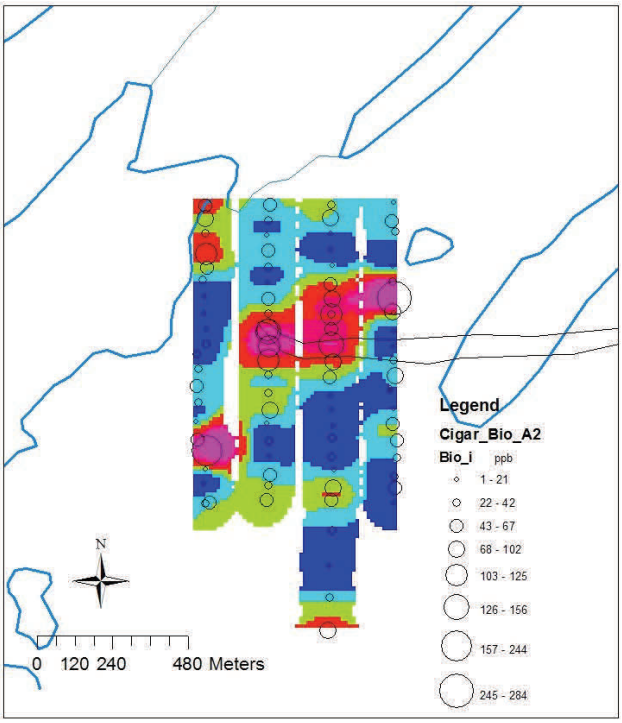

Iodine. A2 horizon. Bioleach.

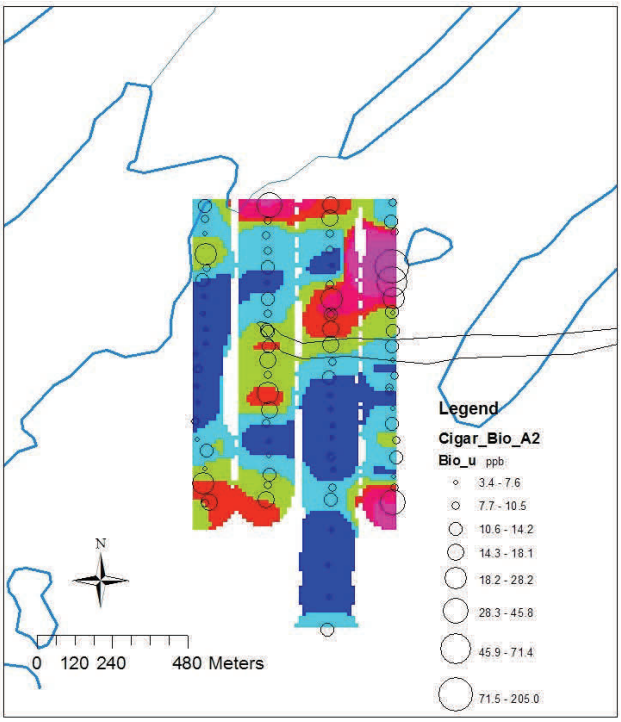

Uranium. A2 horizon. Bioleach.

Fig 6.24 Cigar Maps. A2. Bioleach

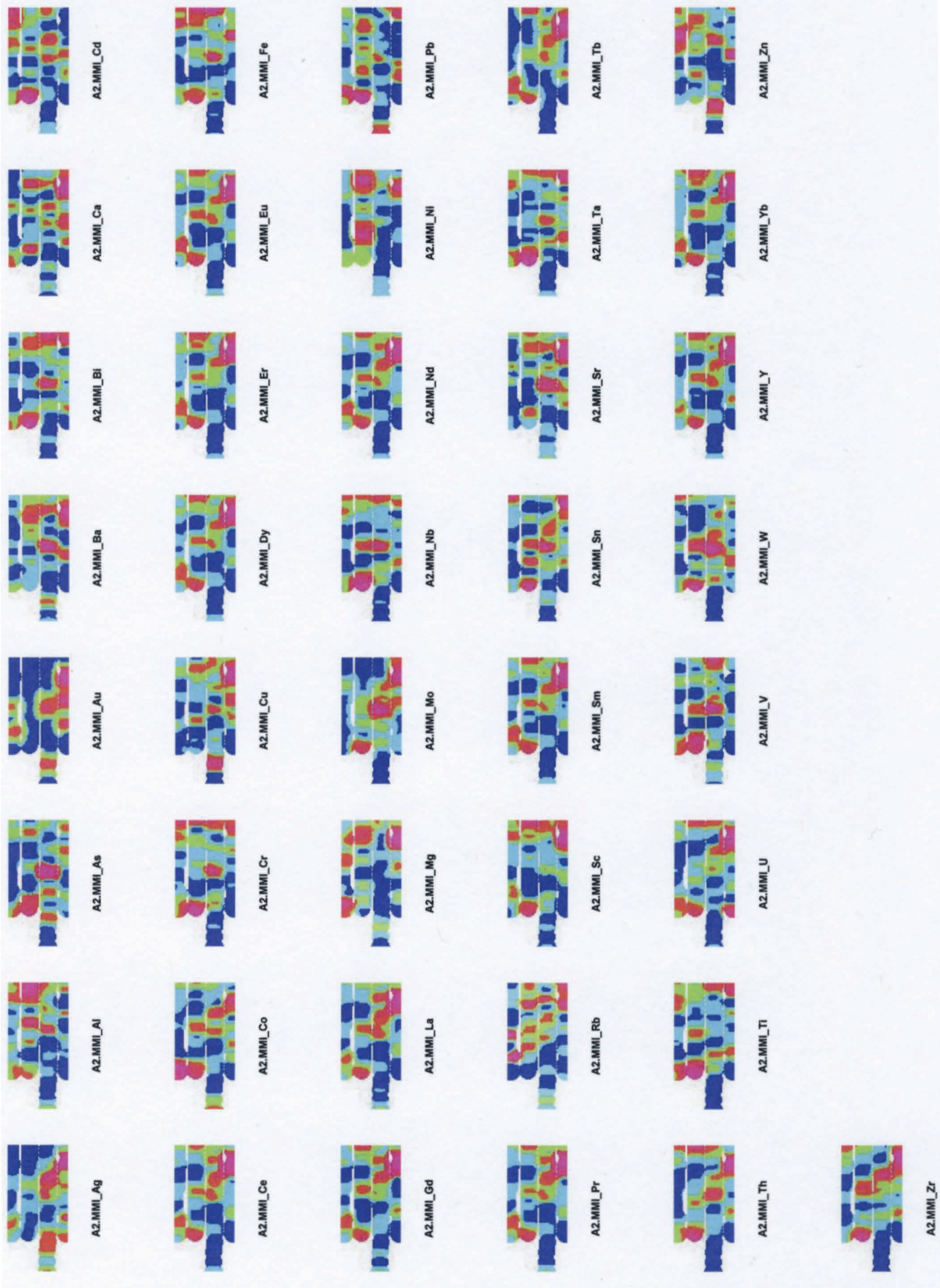

Fig 6.25 Cigar Lake Grids. A2 horizon. MMI leach.

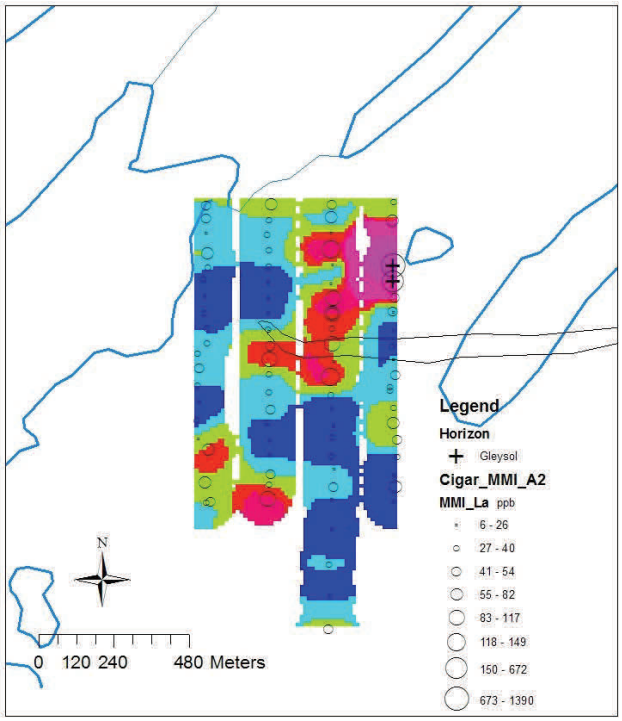

Lanthanum. A2 horizon. MMI leach.

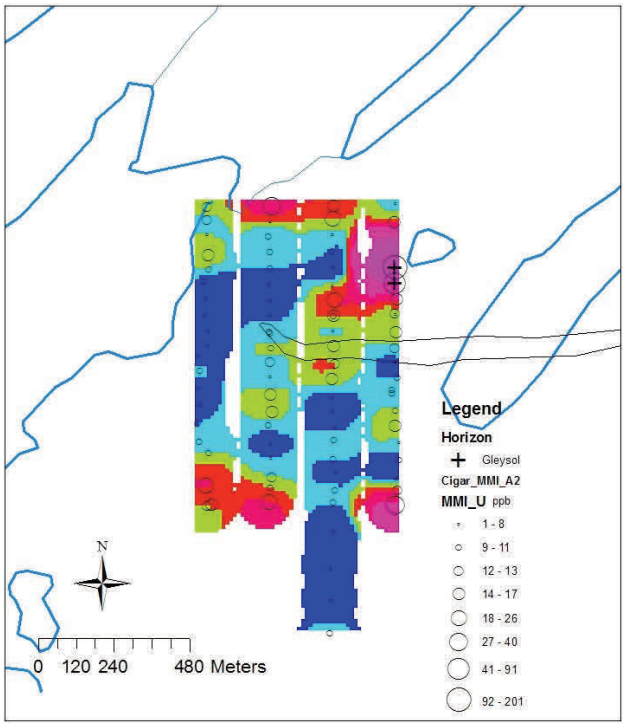

Uranium. A2 horizon. MMI leach.

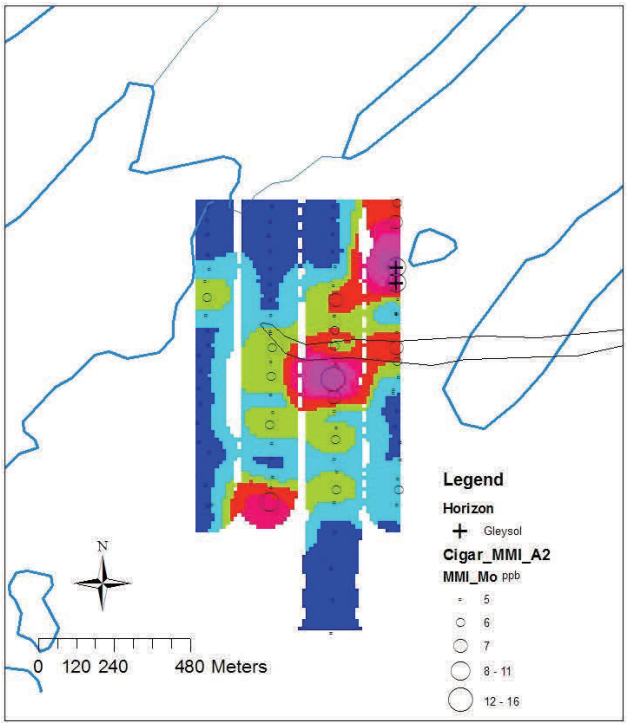

Molybdenum. A2 horizon. MMI leach.

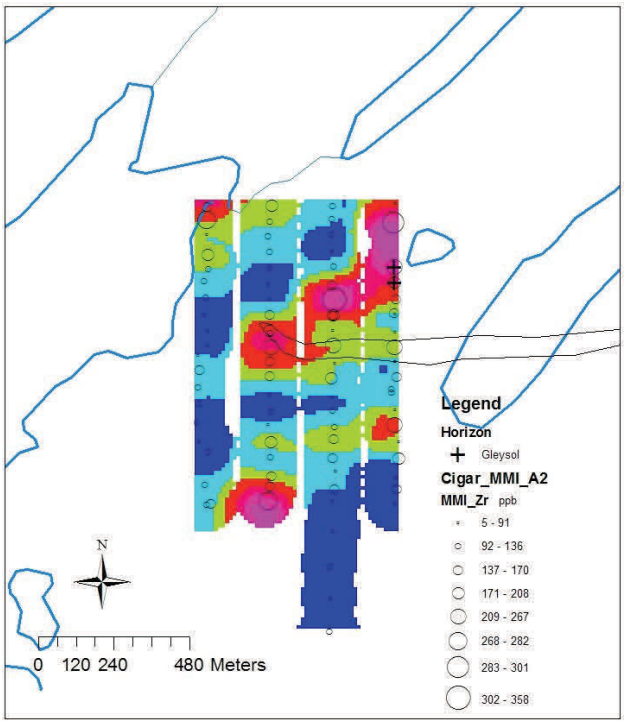

Zirconium. A2 horizon. MMI leach.

Fig 6.26 Cigar Maps. A2 MMI leach

Fig 6.27 Cigar Lake Grids. B1 horizon. Aqua regia leach

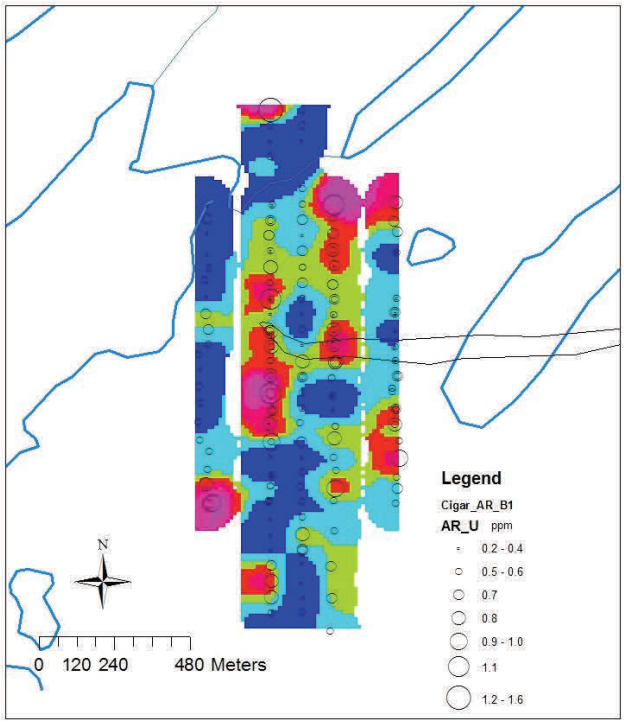

Uranium. B1 horizon. Aqua regia leach.

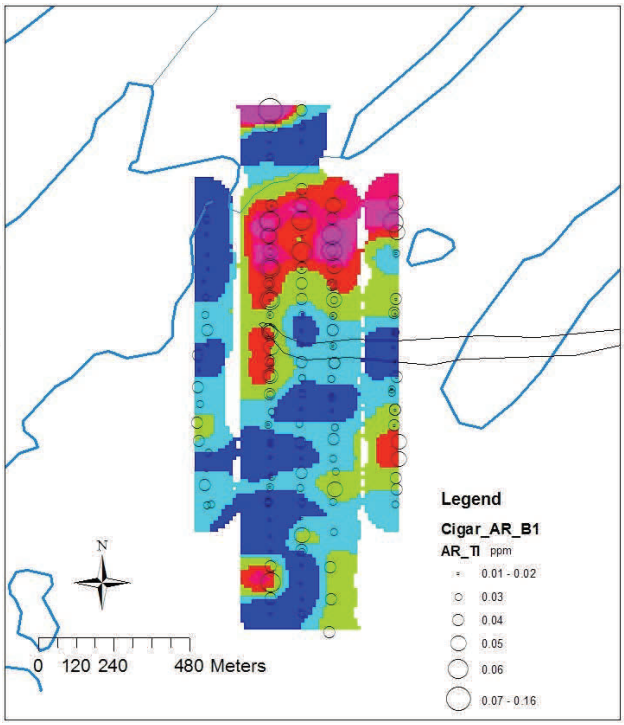

Thallium. B1 horizon. Aqua regia leach.

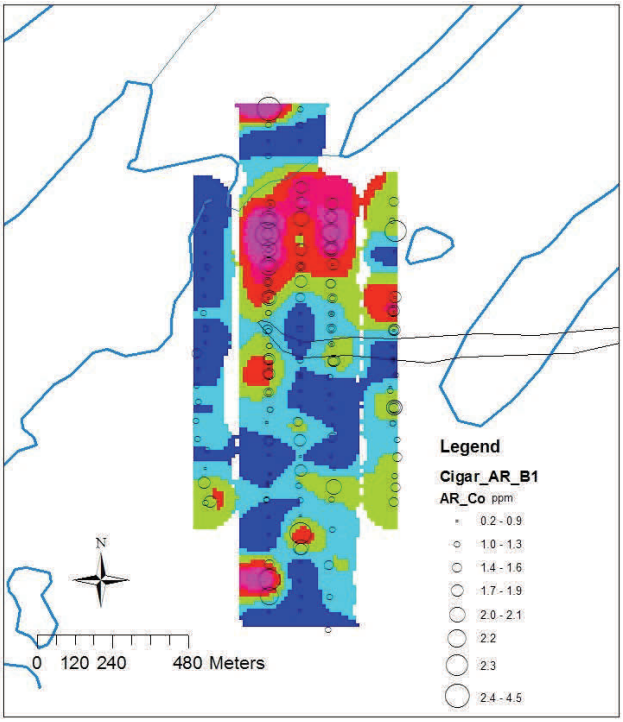

Cobalt. B1 horizon. Aqua regia leach.

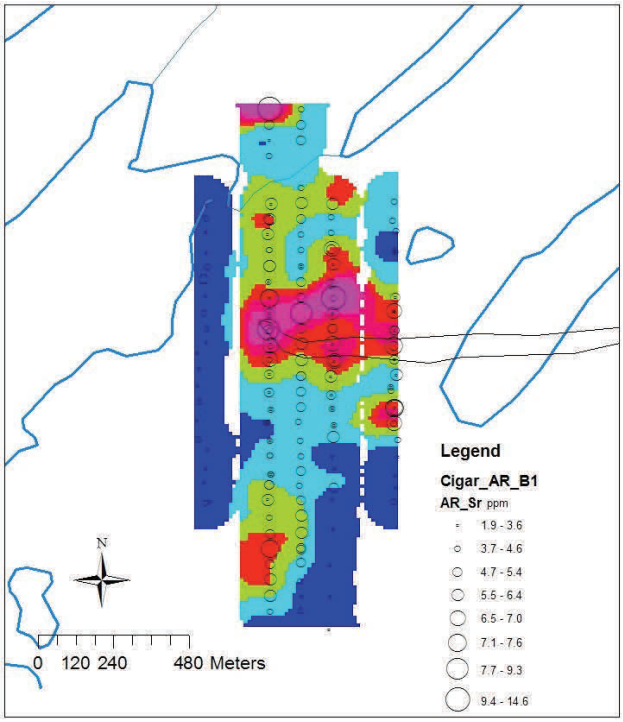

Strontium. B1 horizon. Aqua regia leach.

Fig 6.28 Cigar Maps. B1. Aqua regia.

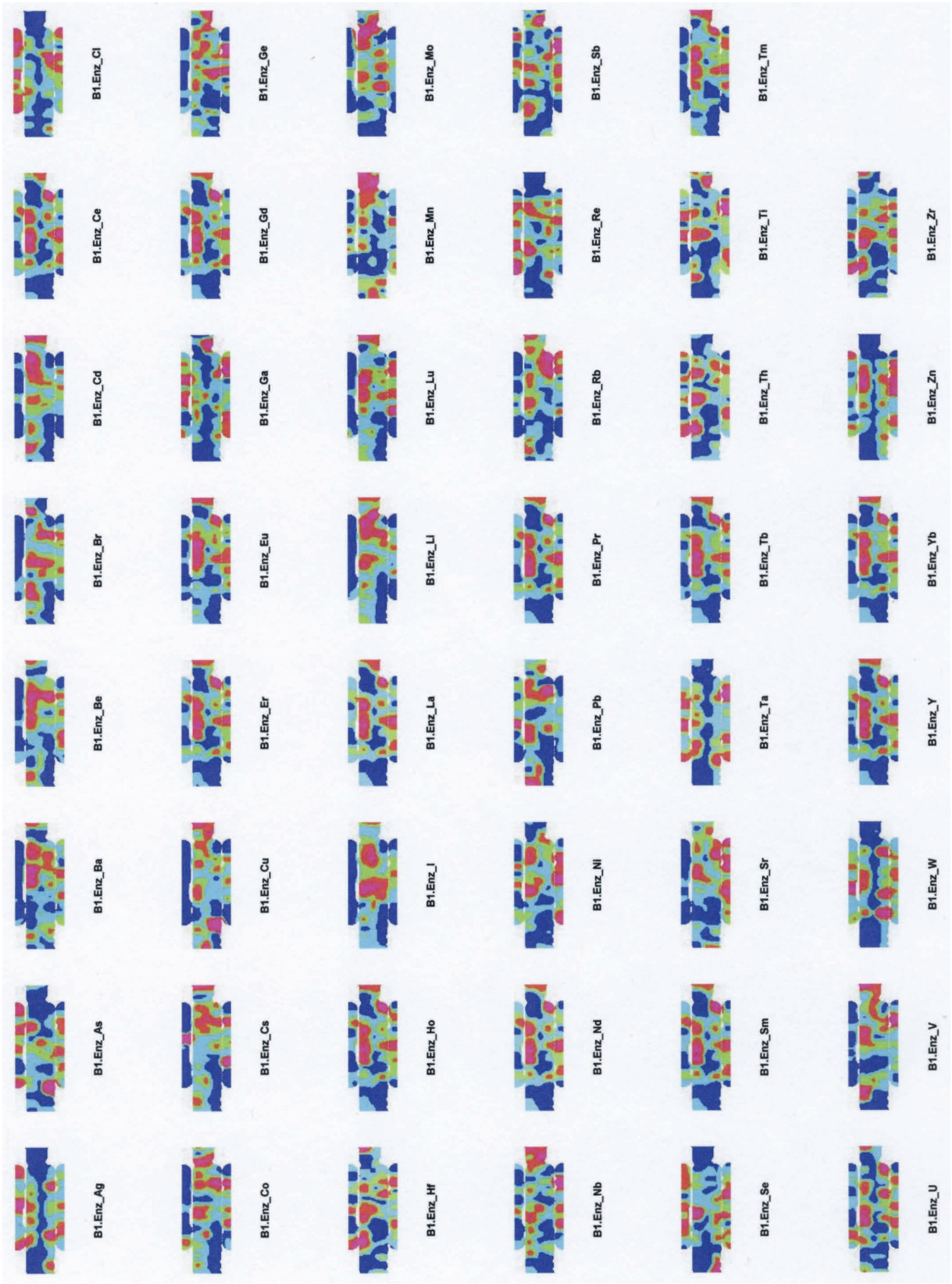

Fig 6.29 Cigar Lake Grids. B1 horizon. Enzyme leach.

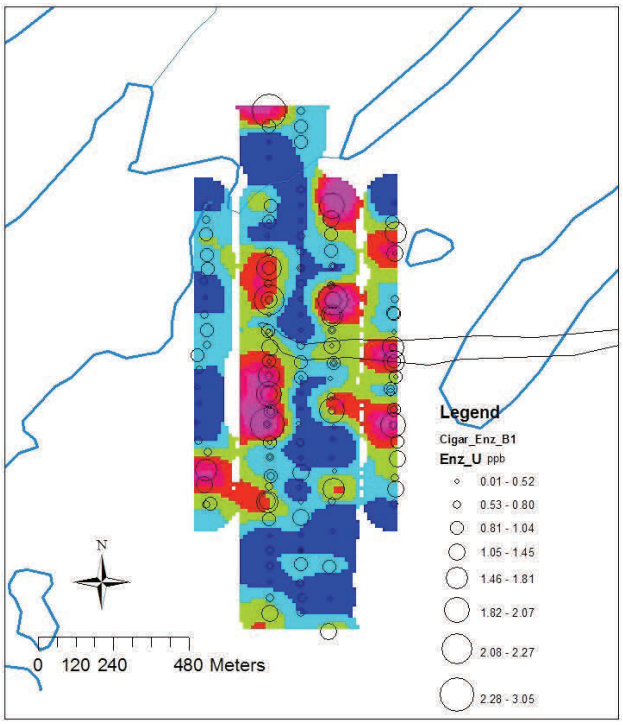

Uranium. B1 horizon. Enzyme leach.

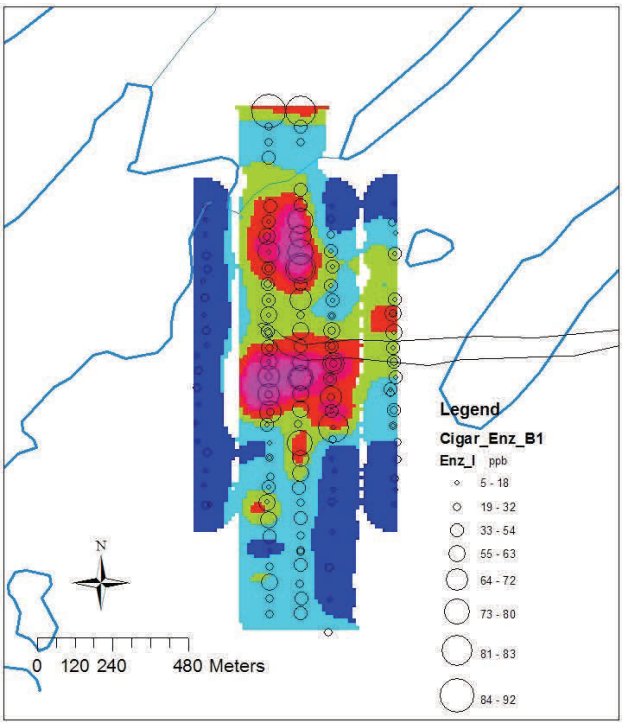

Iodine. B1 horizon. Enzyme leach.

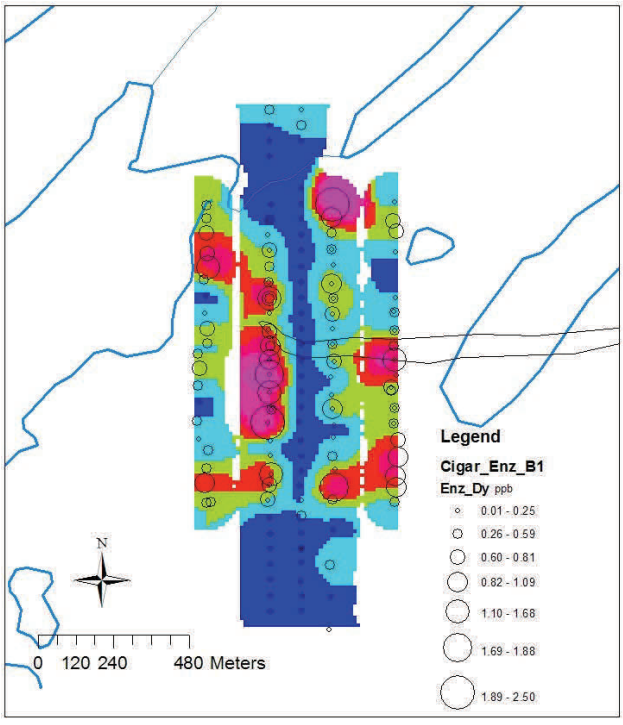

Dysprosium. B1 horizon. Enzyme leach.

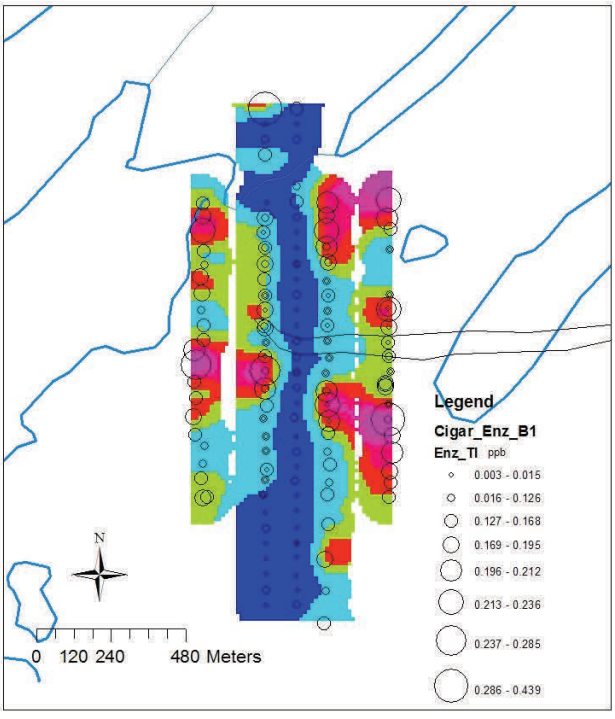

Thallium. B1 horizon. Enzyme leach.

Fig 6.30 Cigar Maps. B1 Enzyme

Fig 6.31. Cigar Lake Grids. B1 horizon. Hydroxylamine leach.

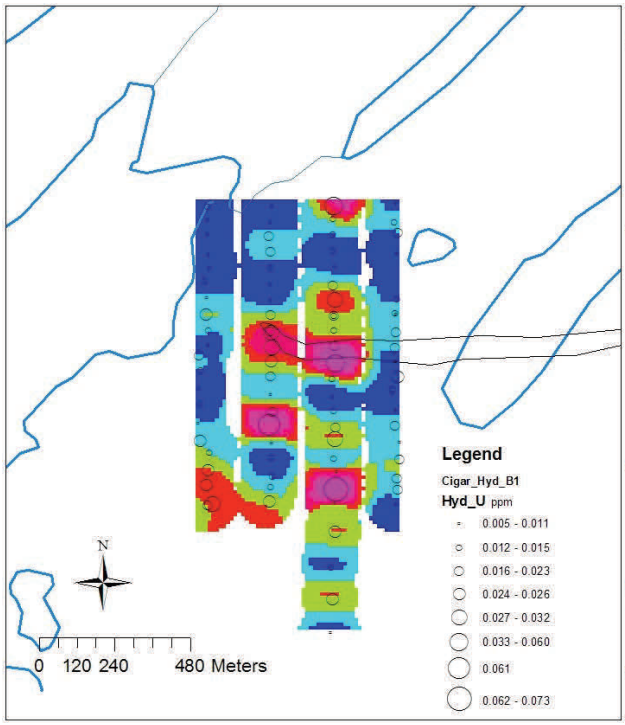

Uranium. B1 horizon. Hydroxylamine leach.

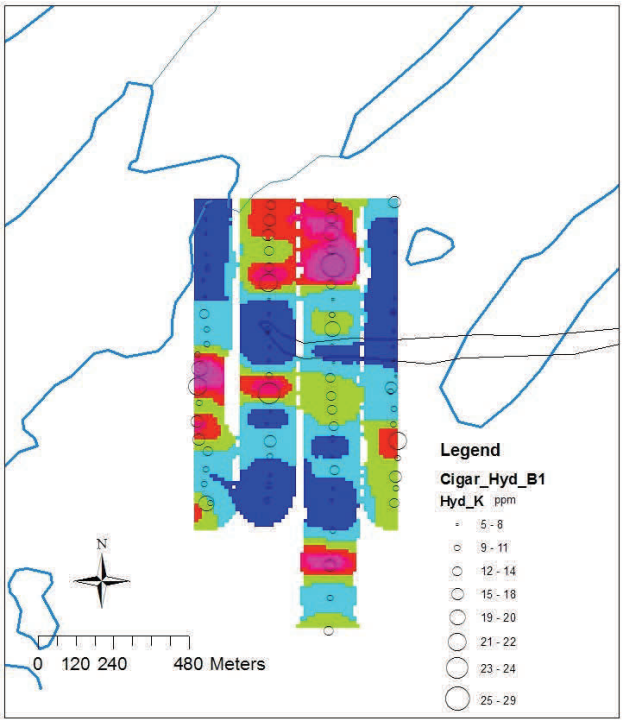

Potassium. B1 horizon. Hydroxylamine leach.

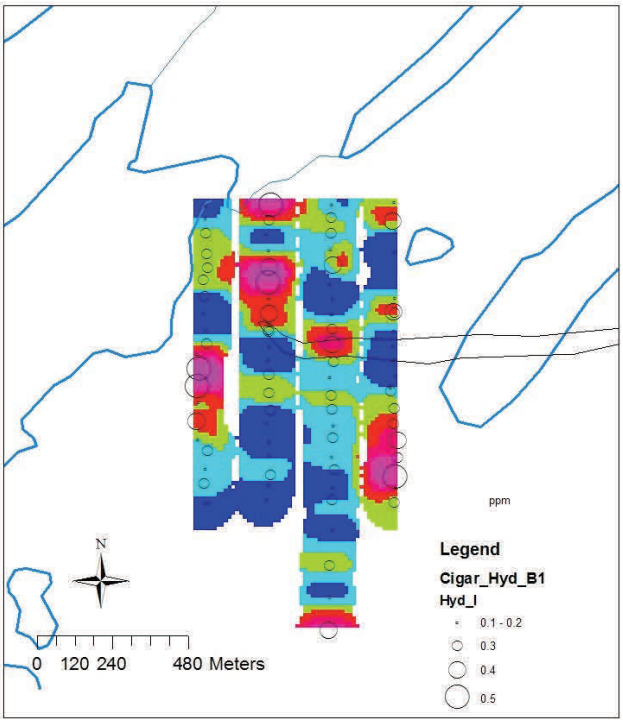

Iodine. B1 horizon. Hydroxylamine leach.

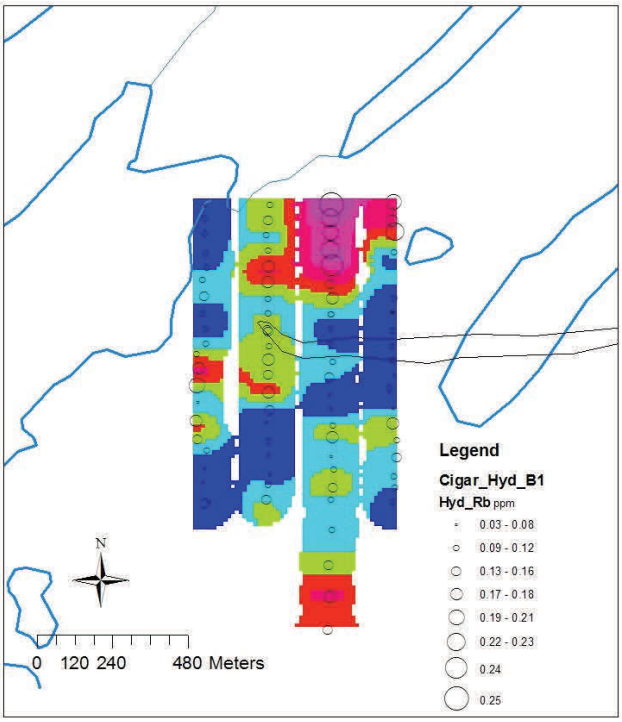

Rubidium. B1 horizon. Hydroxylamine leach.

Fig 6.32 Cigar Maps. B1. Hydroxylamine

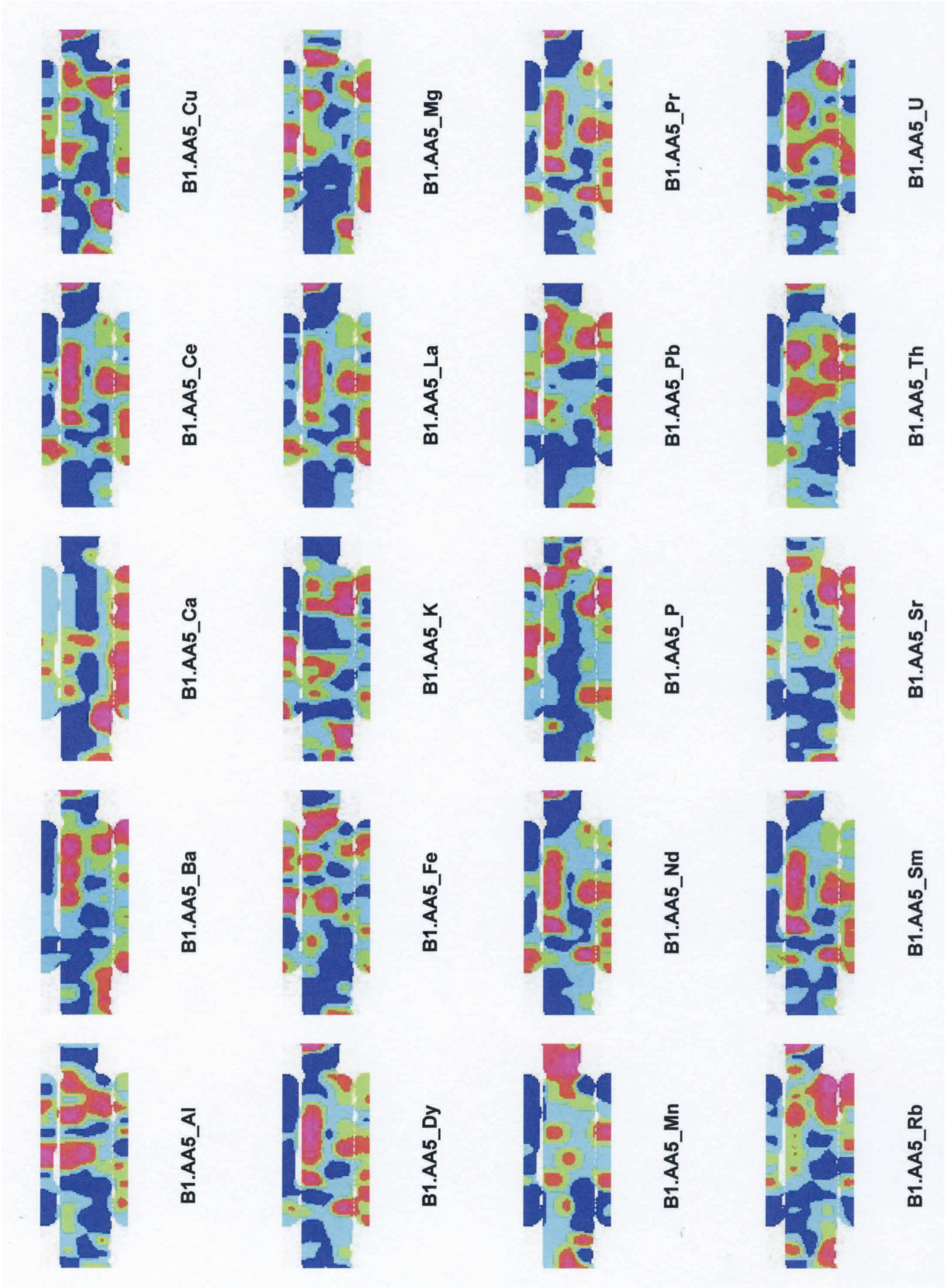

Fig 6.33. Cigar Lake Grids. B1 horizon. Ammonium acetate leach.

Fig. 6.32 Cigar Maps. B1. Ammonium acetate

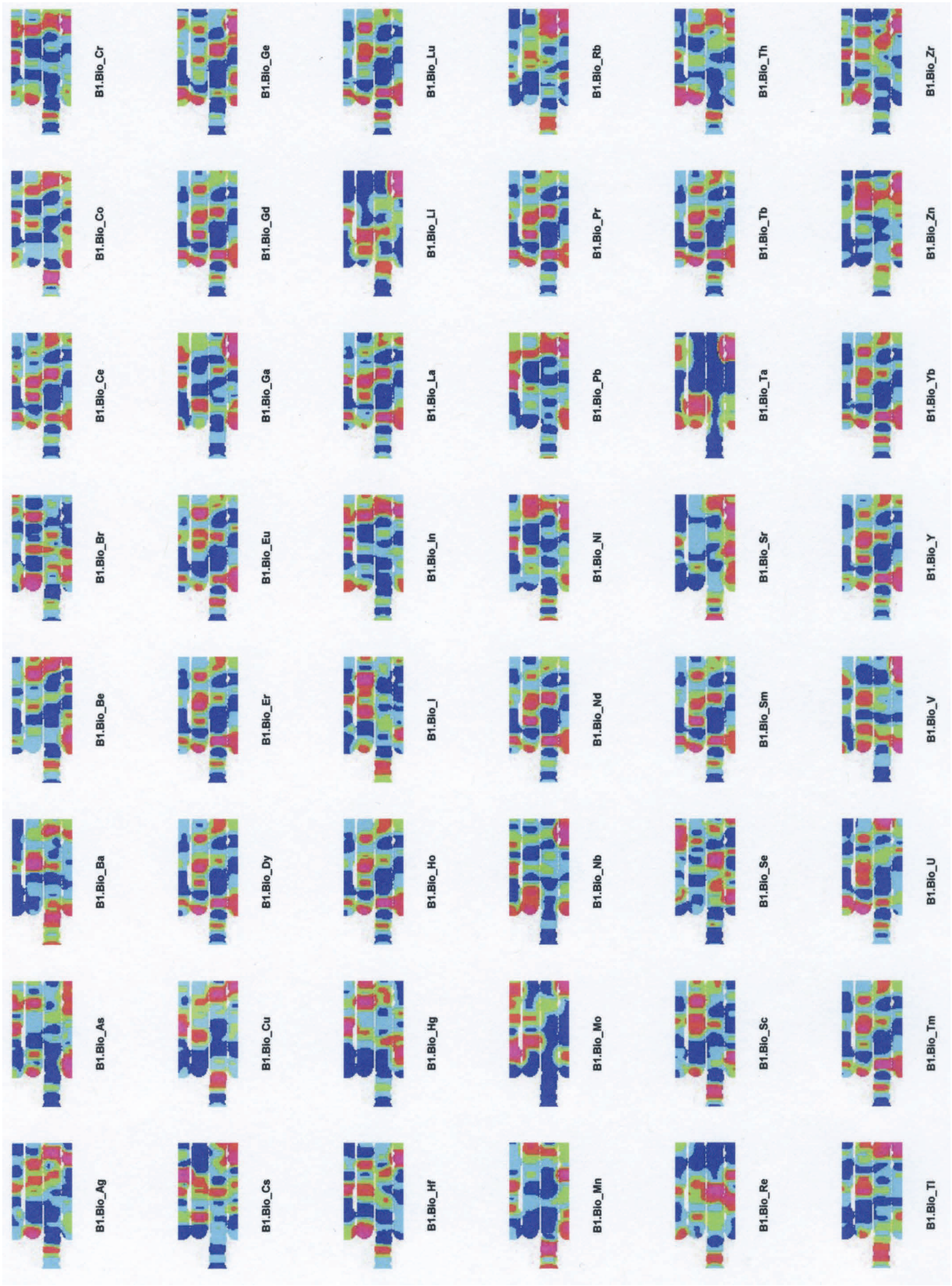

Fig 6.35. Cigar Lake Grids. B1 horizon. Bioleach.

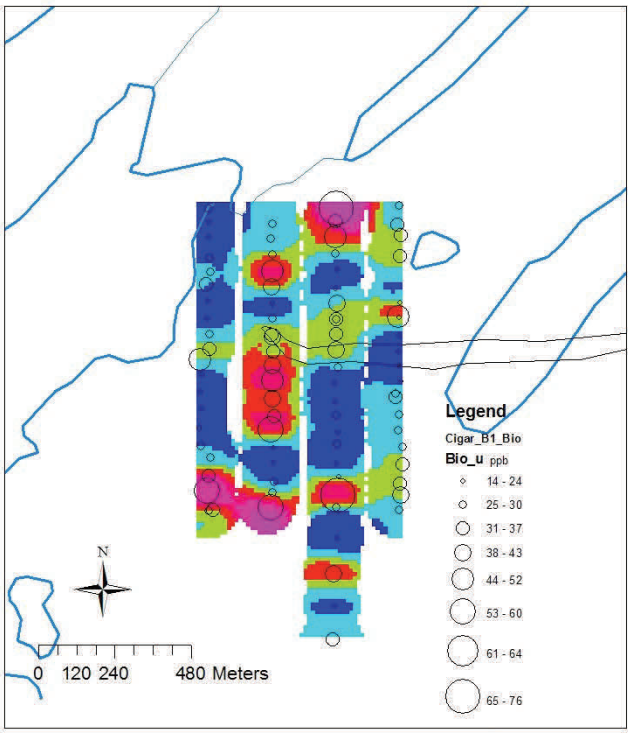

Uranium. B1 horizon. Bioleach.

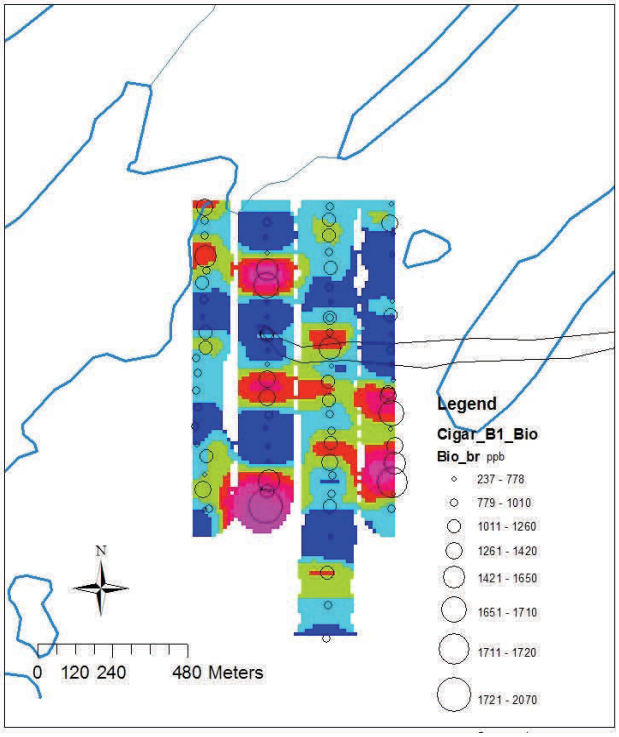

Bromine. B1 horizon. Bioleach.

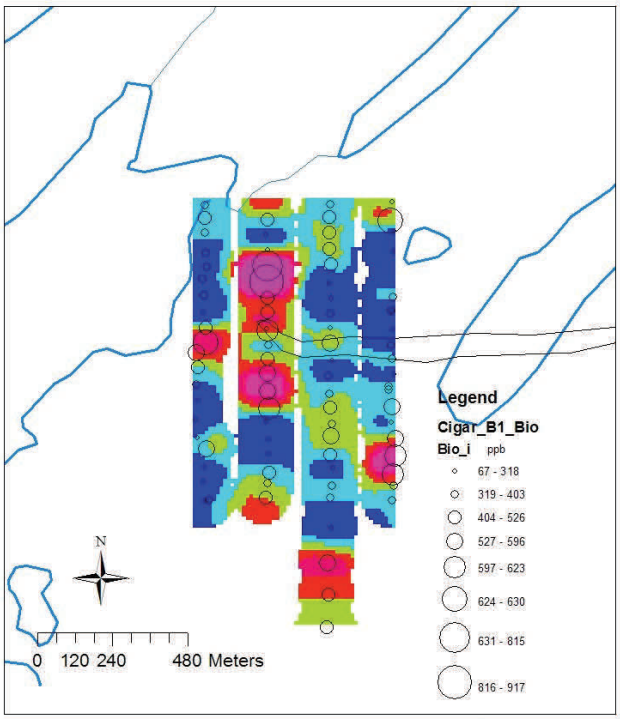

Iodine. B1 horizon. Bioleach.

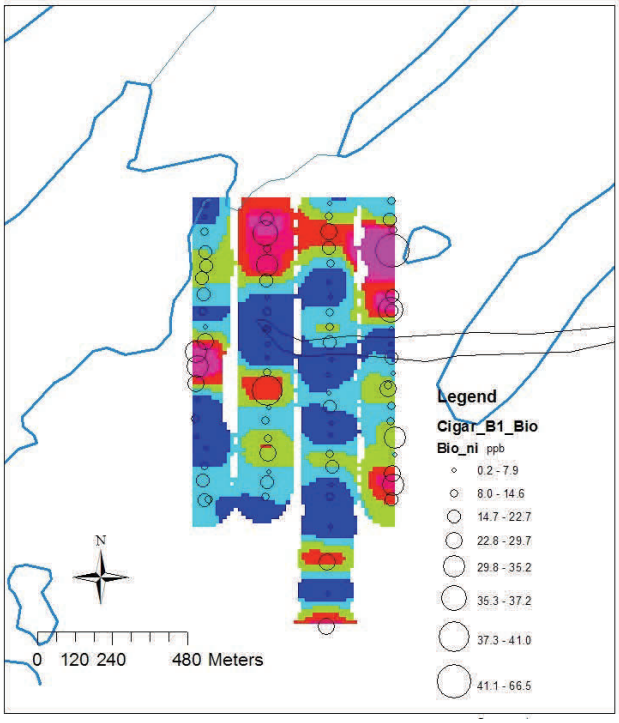

Nickel. B1 horizon. Bioleach.

Fig. 6.36. Cigar Maps. B1. Bioleach

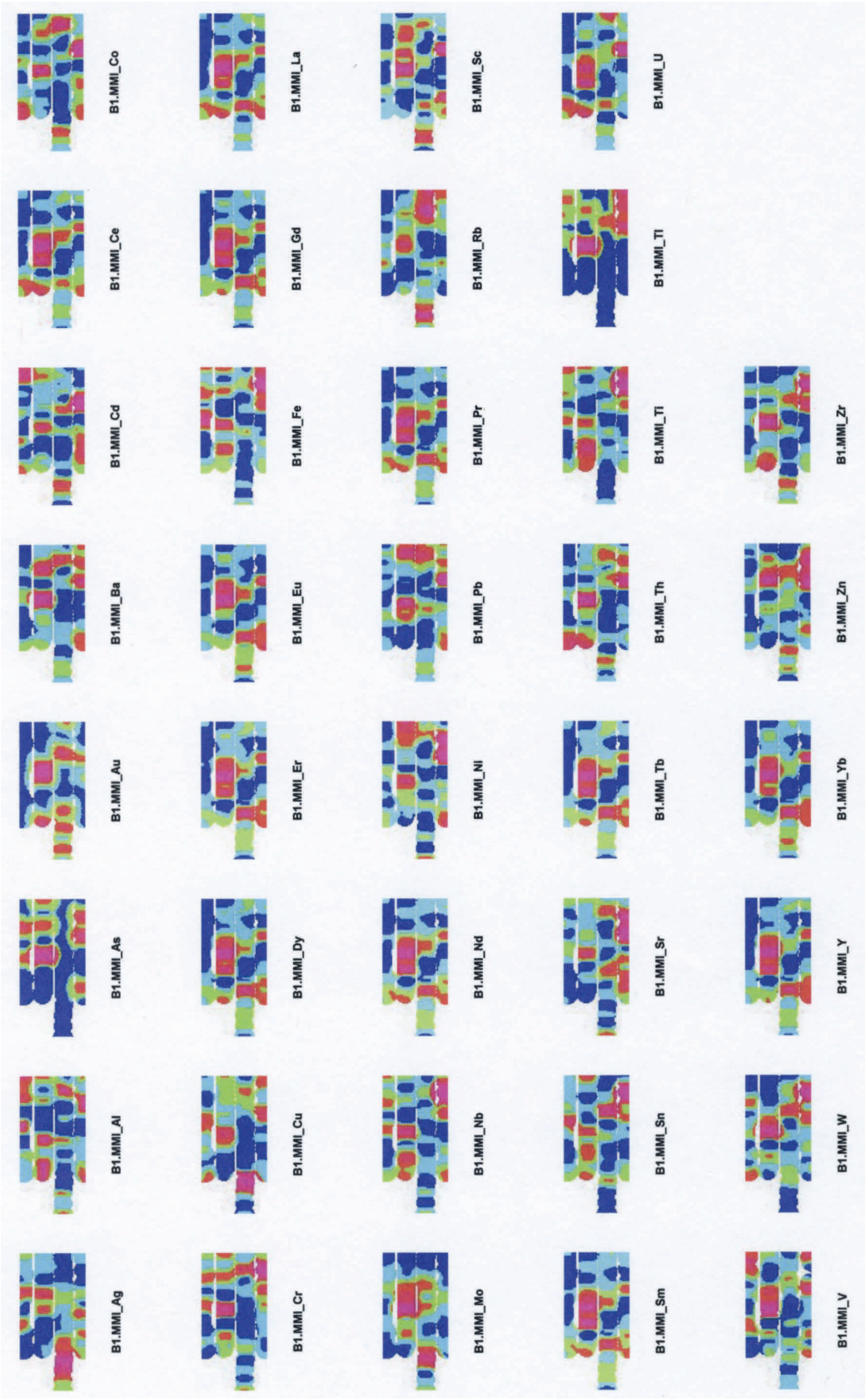

Fig 6.37. Cigar Lake Grids. B1 horizon. MMI leach.

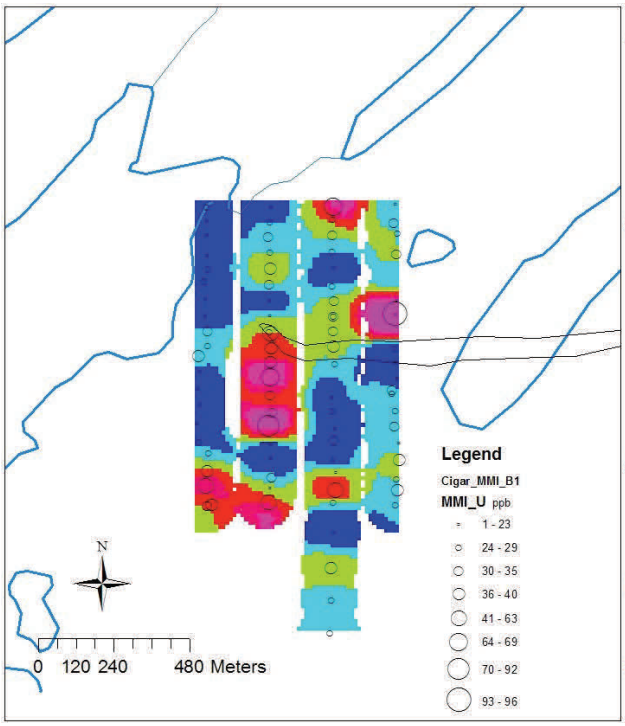

Uranium. B1 horizon. MMI leach.

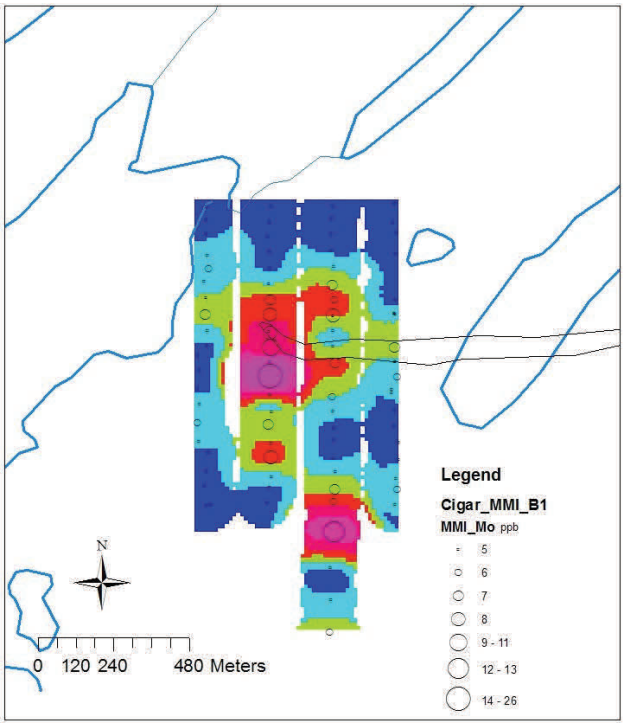

Molybdenum. B1 horizon. MMI leach.

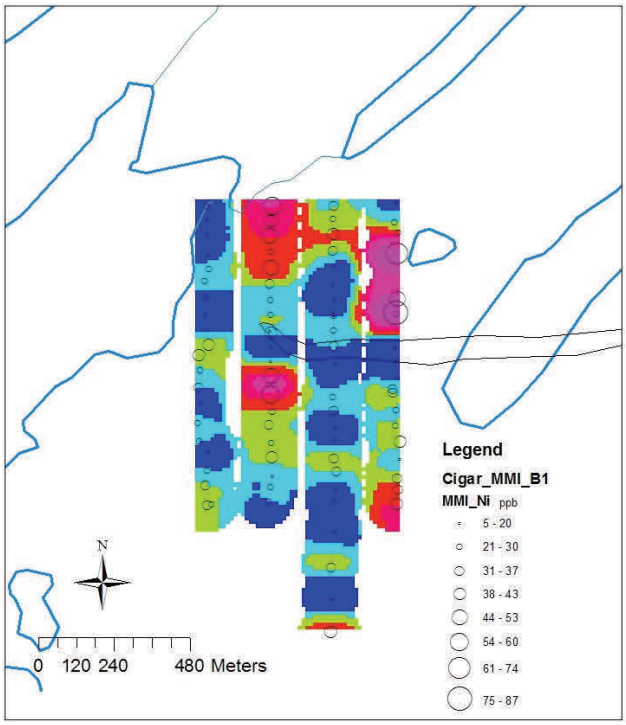

Nickel. B1 horizon. MMI leach.

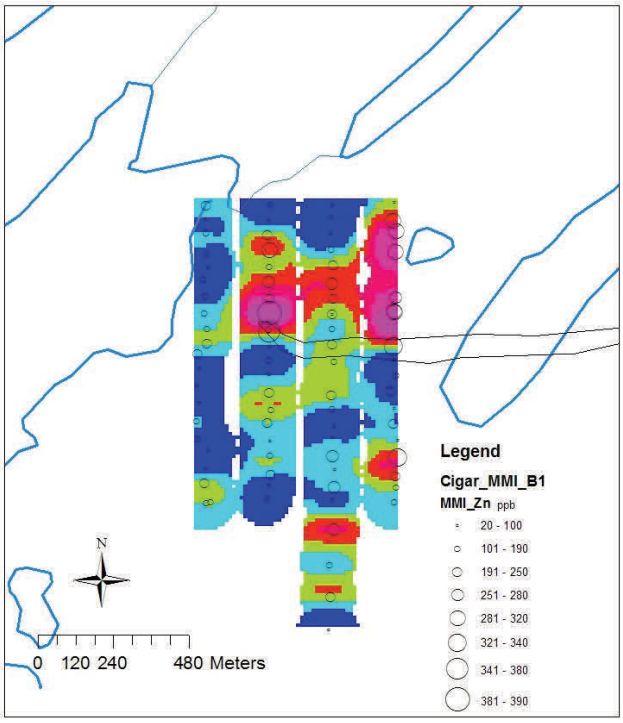

Zinc. B1 horizon. MMI leach.

Fig 6.38. Cigar Maps. B1. MMI leach.

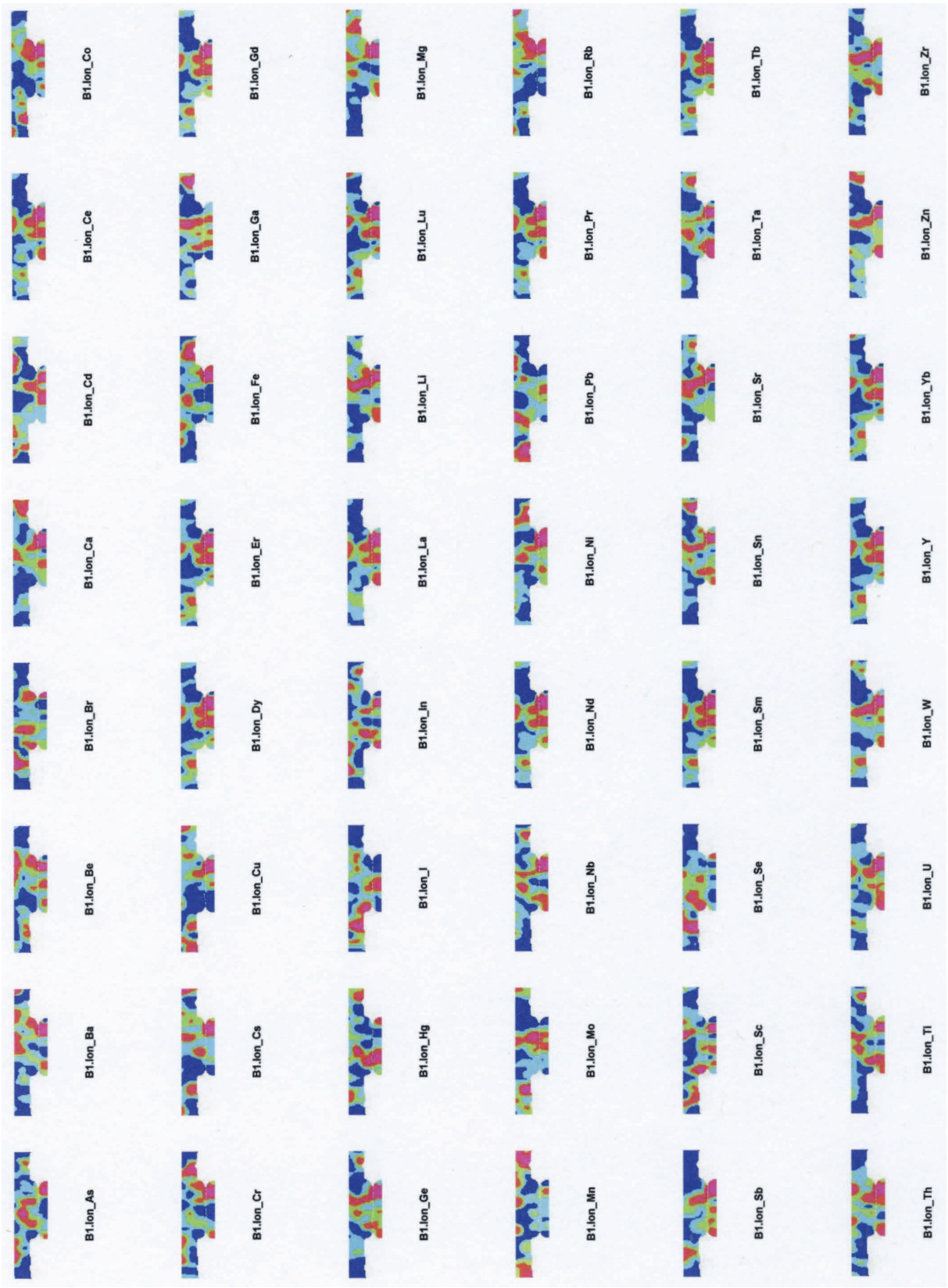

Fig 6.39. Cigar Lake Grids. B1 horizon. Ionic leach.

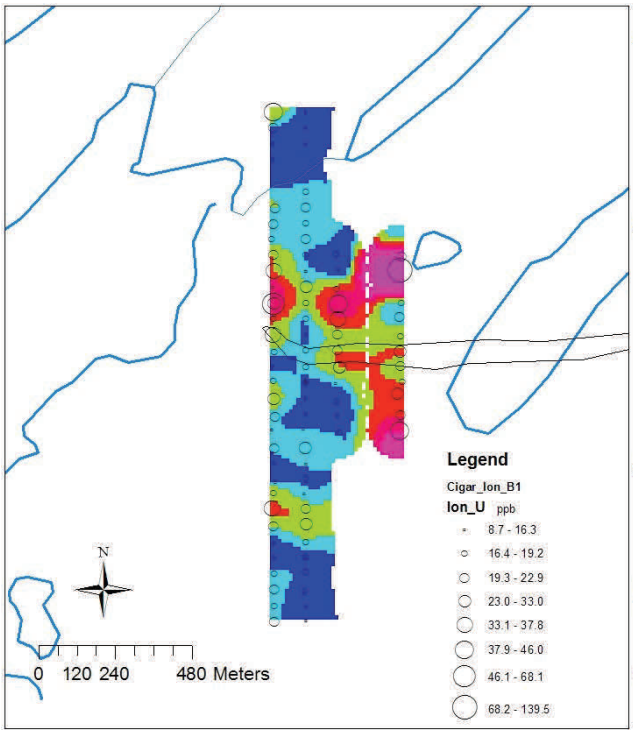

Uranium. B1 horizon. Ionic leach.

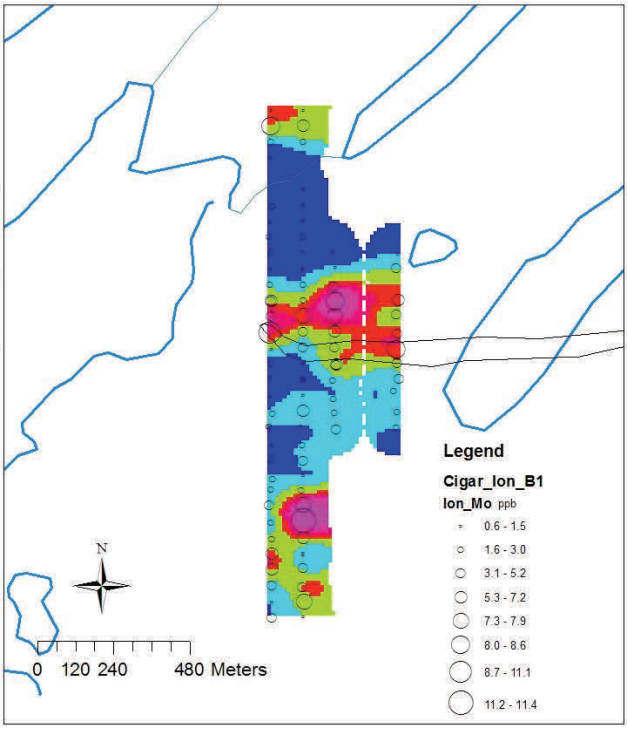

Molybdenum. B1 horizon. Ionic leach.

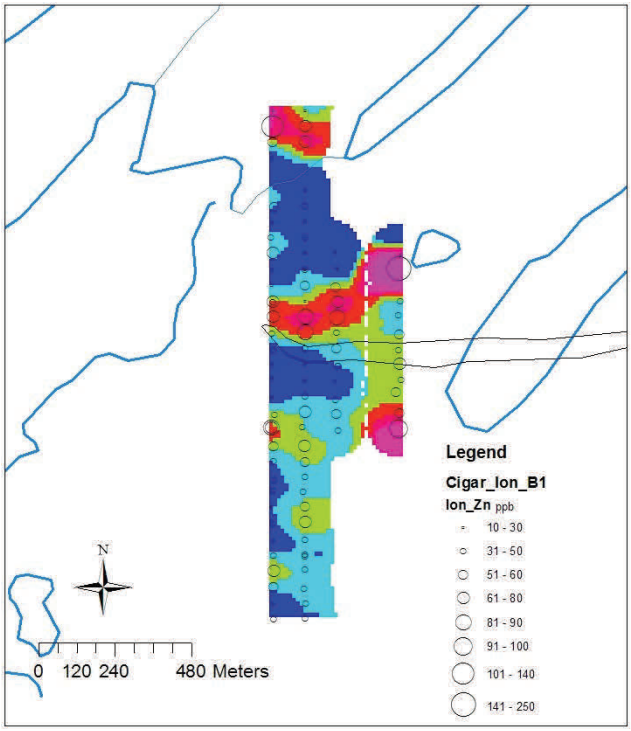

Zinc. B1 horizon. Ionic leach.

Fig 6.40. Cigar Maps. B1. Ionic.

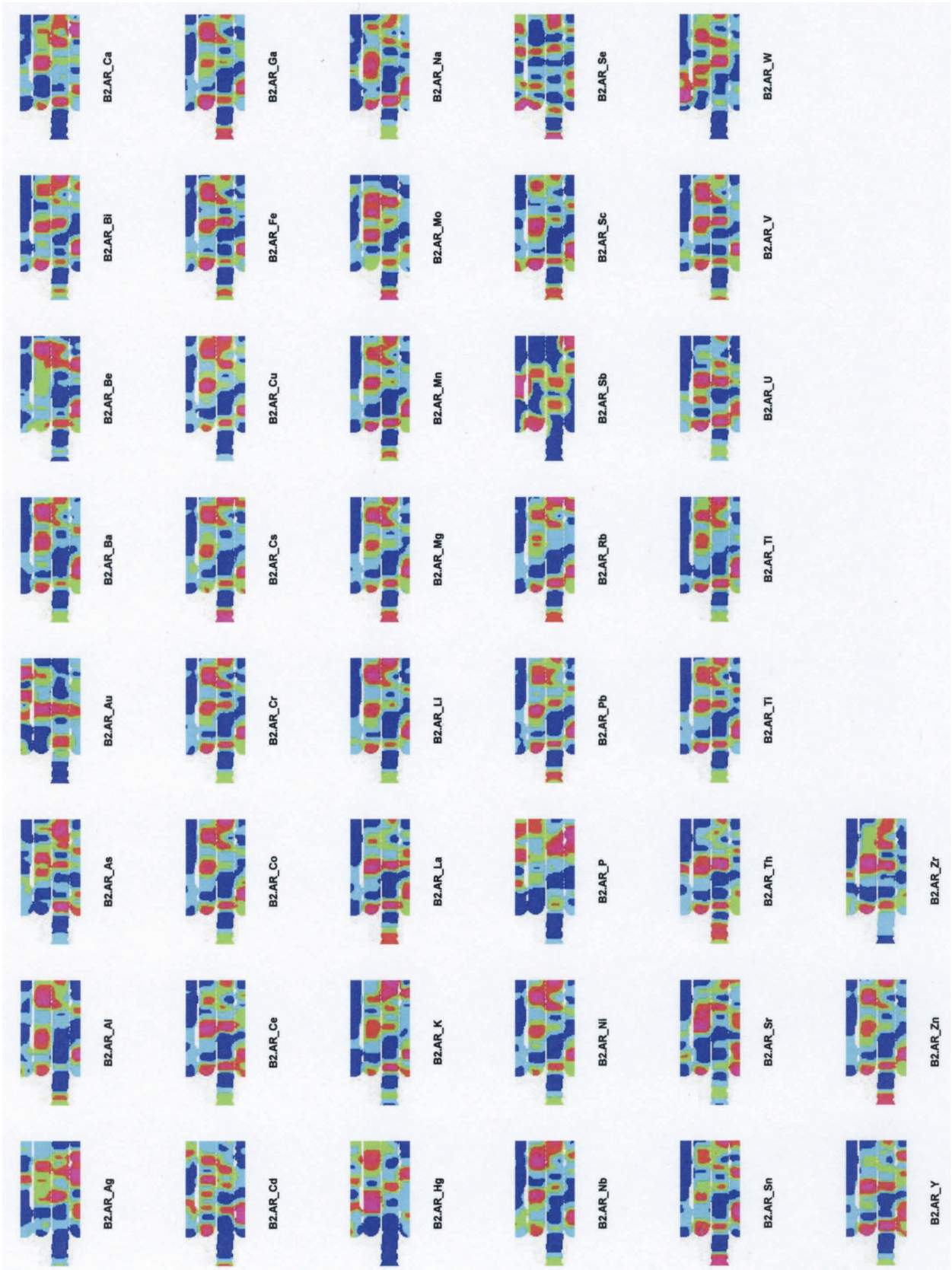

Fig 6.41. Cigar Lake Grids. B2 horizon. Aqua regia leach.

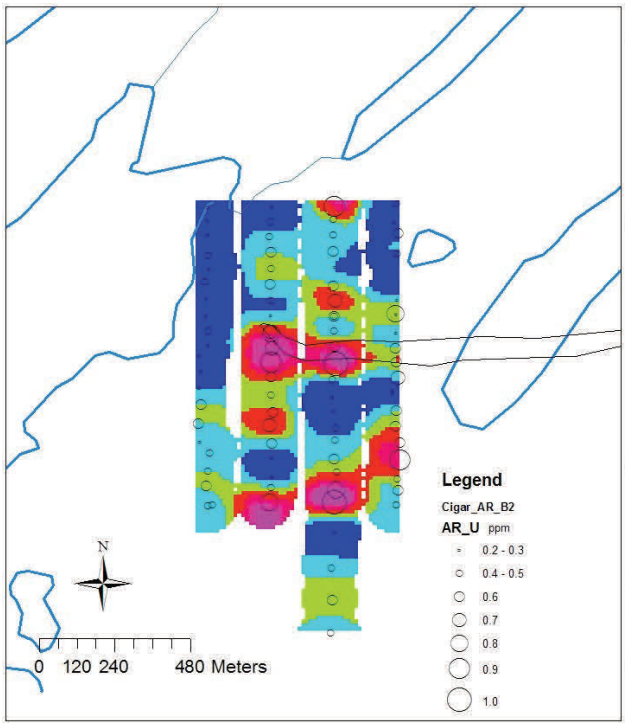

Uranium. B2 horizon. Aqua regia leach.

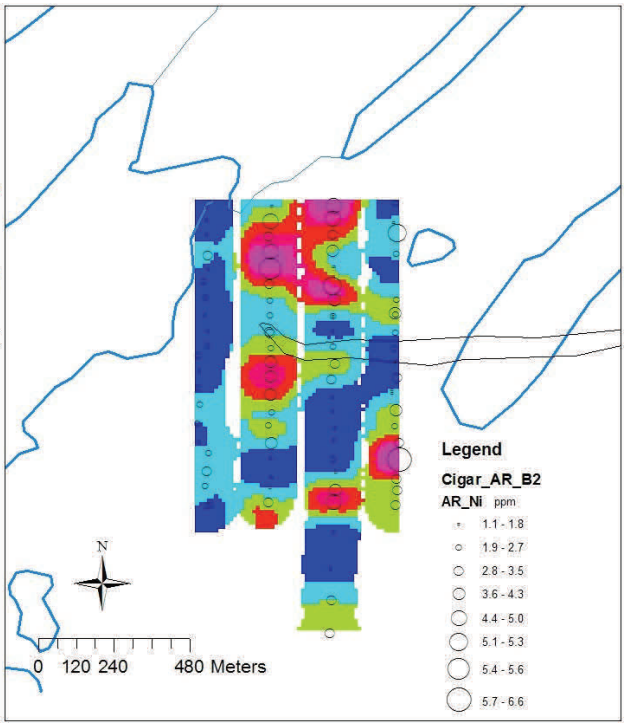

Nickel. B2 horizon. Aqua regia leach.

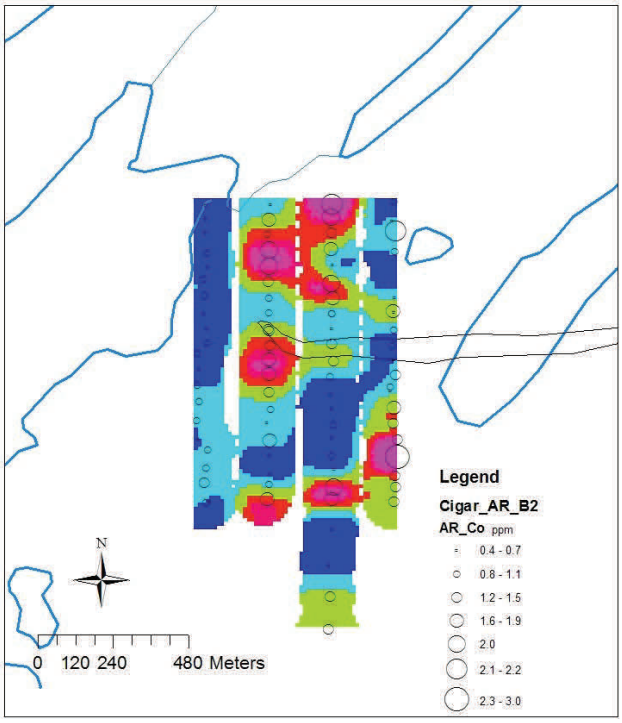

Cobalt. B2 horizon. Aqua regia leach.

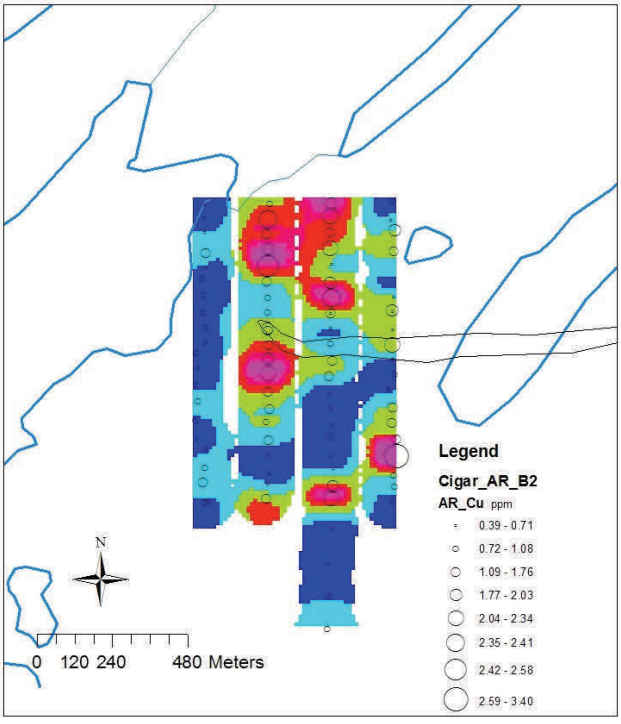

Copper. B2 horizon. Aqua regia leach.

Fig. 6.42. Cigar Maps. B2. Aqua regia

Fig 6.43. Cigar Lake Grids. B2 horizon. Hydroxylamine leach.

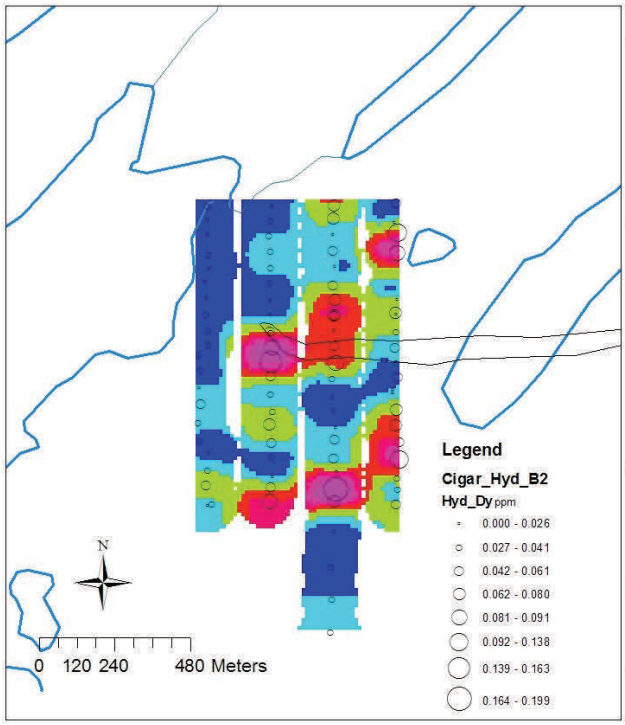

Dysprosium. B2 horizon. Hydroxylamine leach.

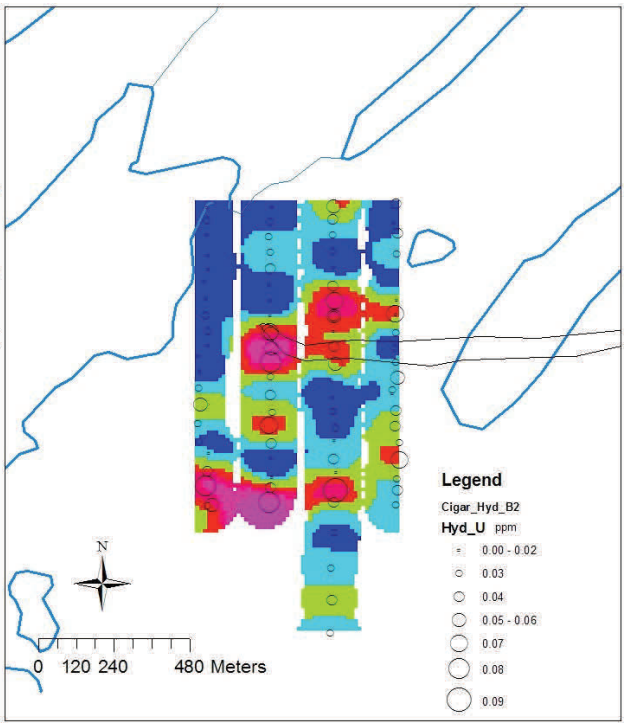

Uranium. B2 horizon. Hydroxylamine leach.

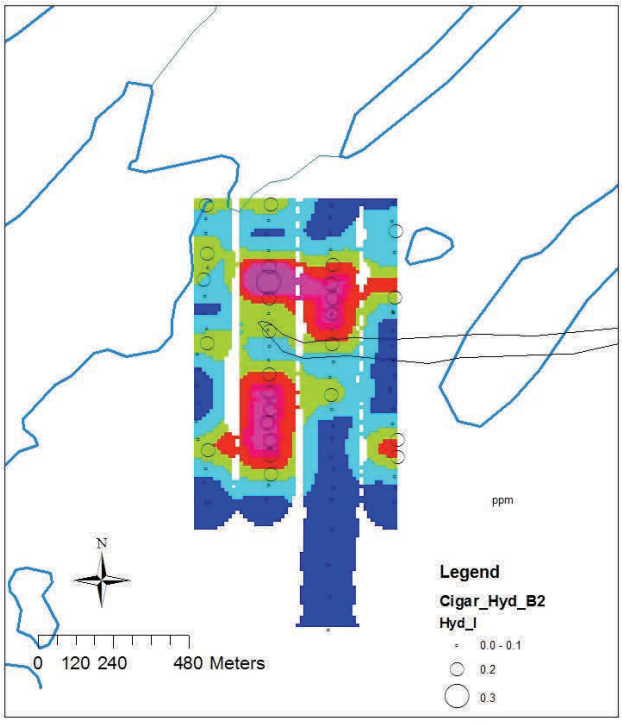

Iodine. B2 horizon. Hydroxylamine leach.

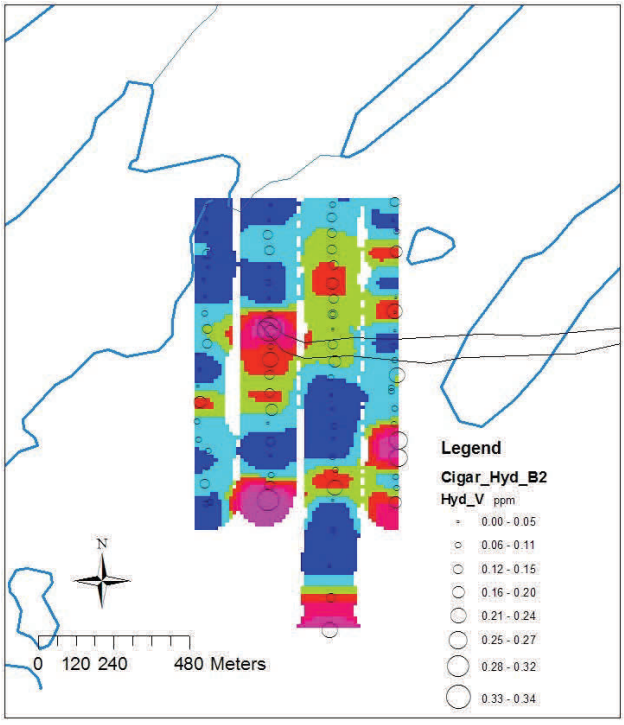

Vanadium. B2 horizon. Hydroxylamine leach.

Fig 6.44. Cigar Maps. B2. Hydroxylamine

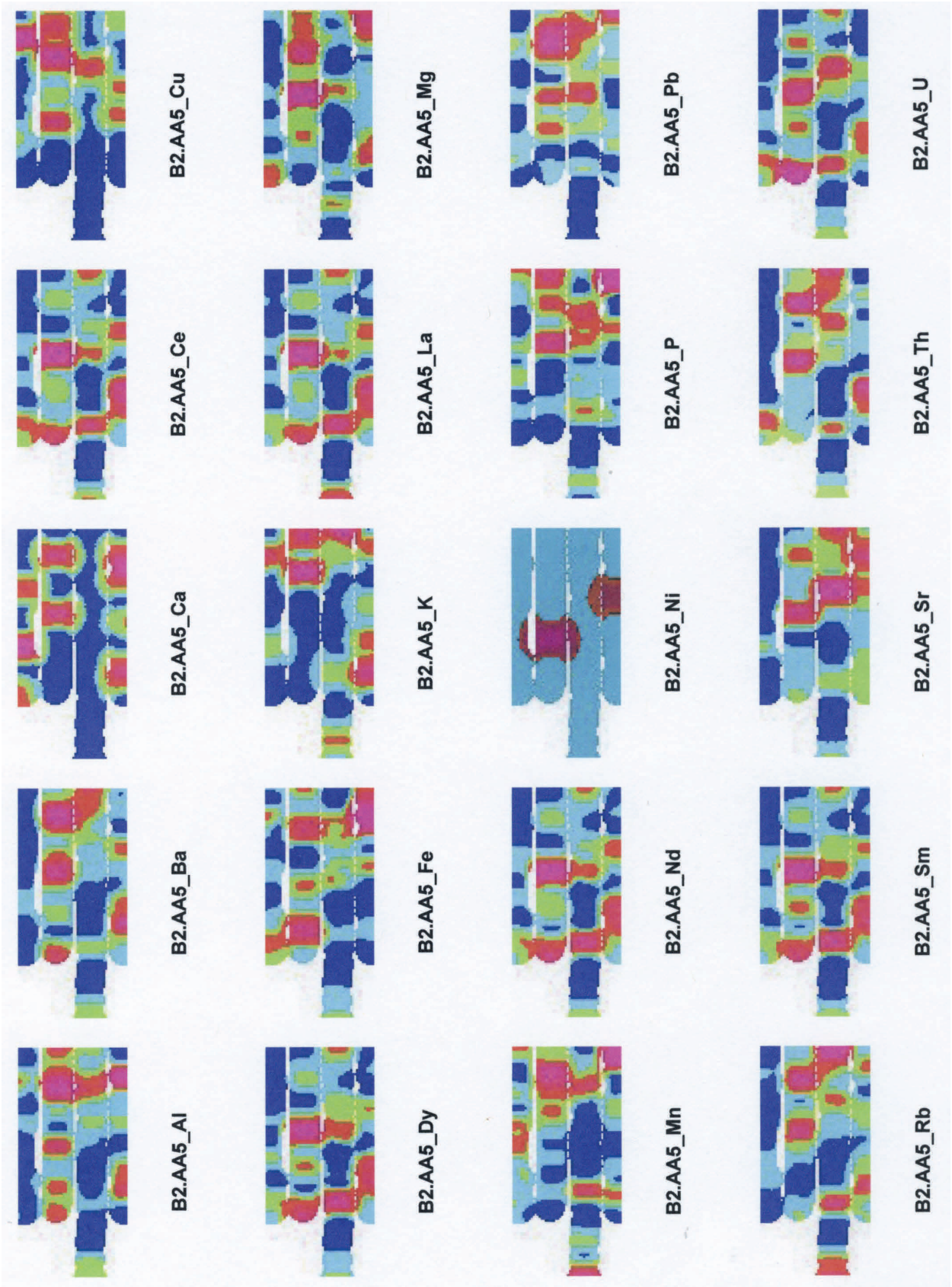

Fig 6.45. Cigar Lake Grids. B2 horizon. Ammonium acetate leach.

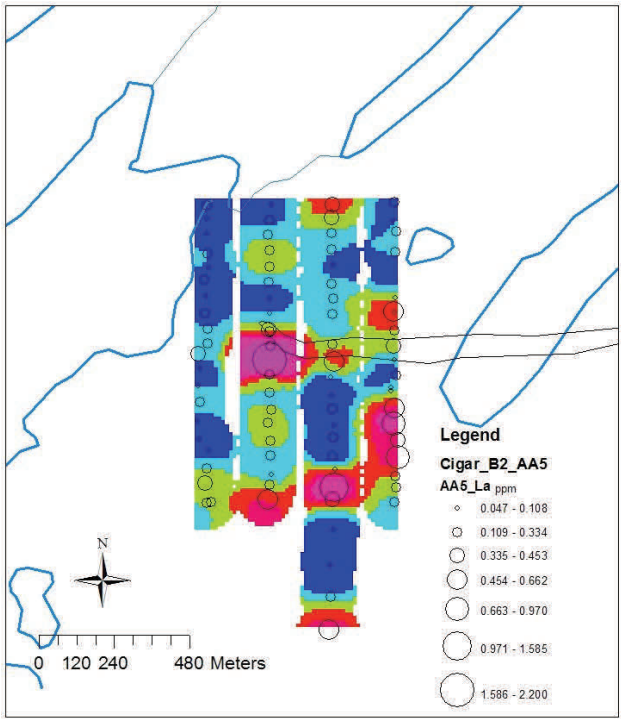

Lanthanum. B2 horizon. Ammonium acetate leach.

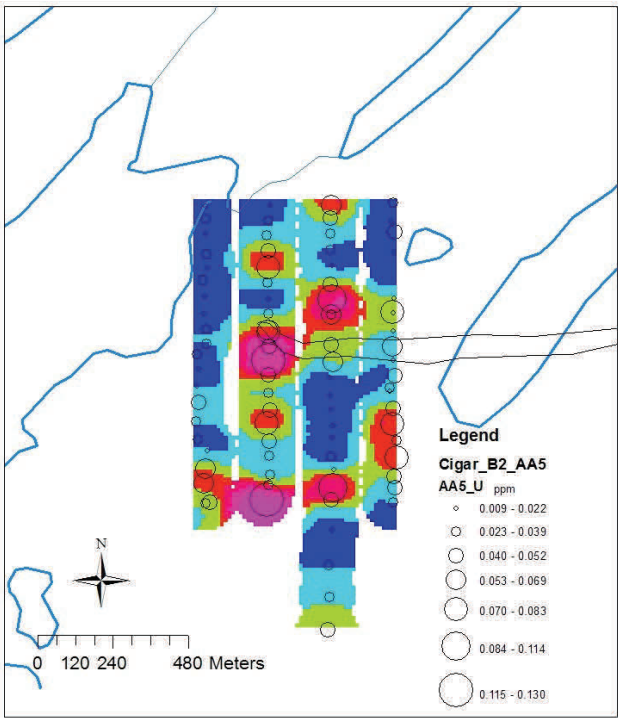

Uranium. B2 horizon. Ammonium acetate leach.

Fig 6.46. Cigar Maps. B2. Ammonium acetate.

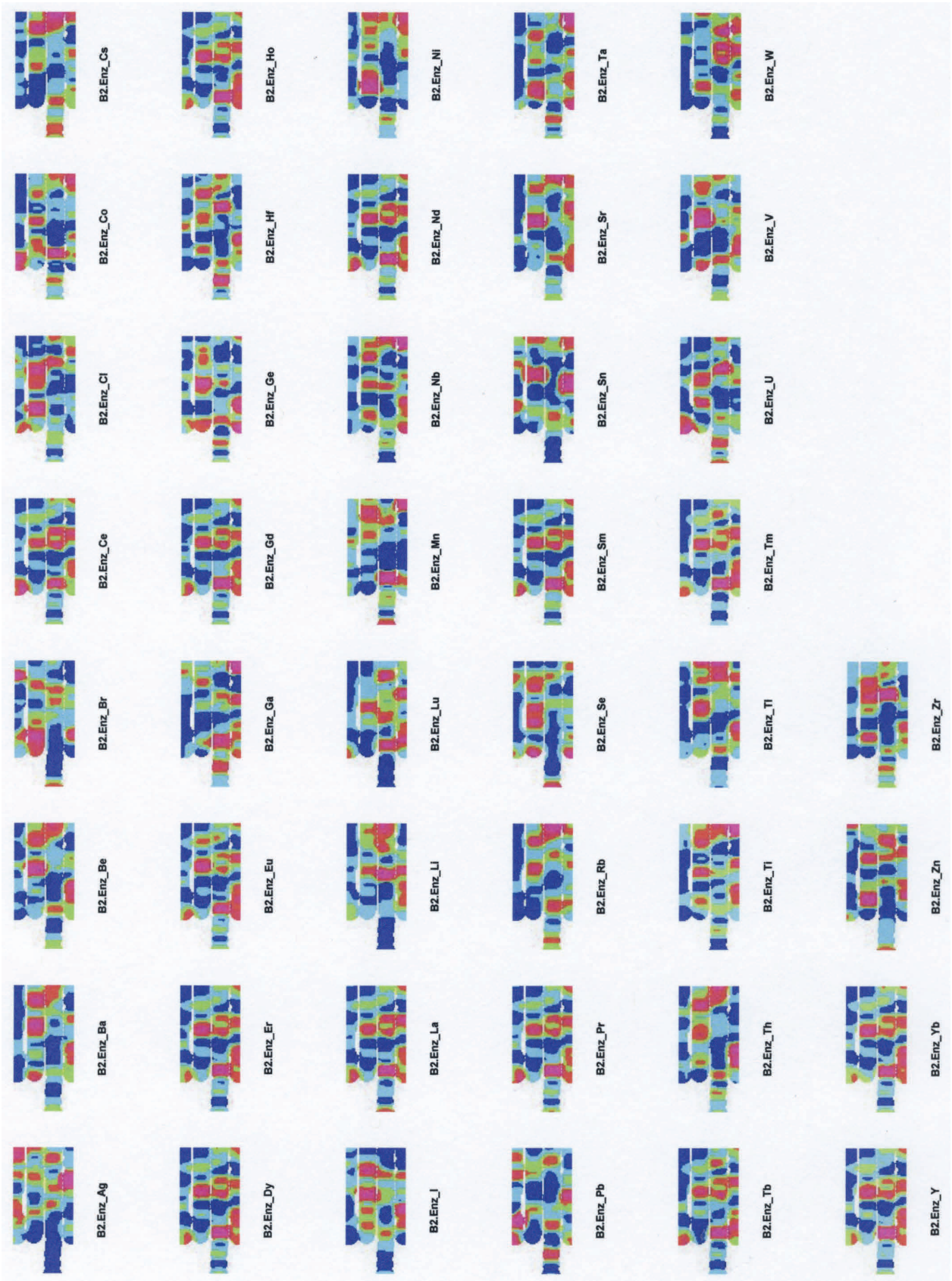

Fig 6.47. Cigar Lake Grids. B2 horizon. Enzyme leach.

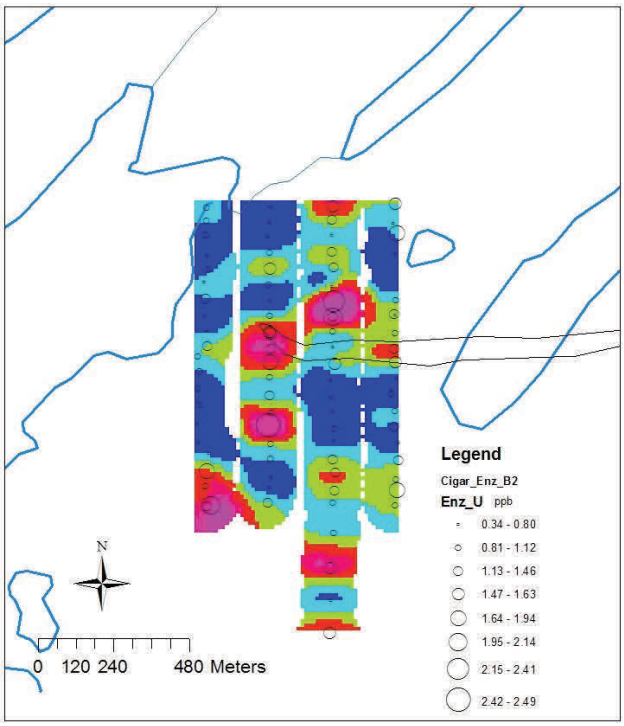

Uranium. B2 horizon. Enzyme leach

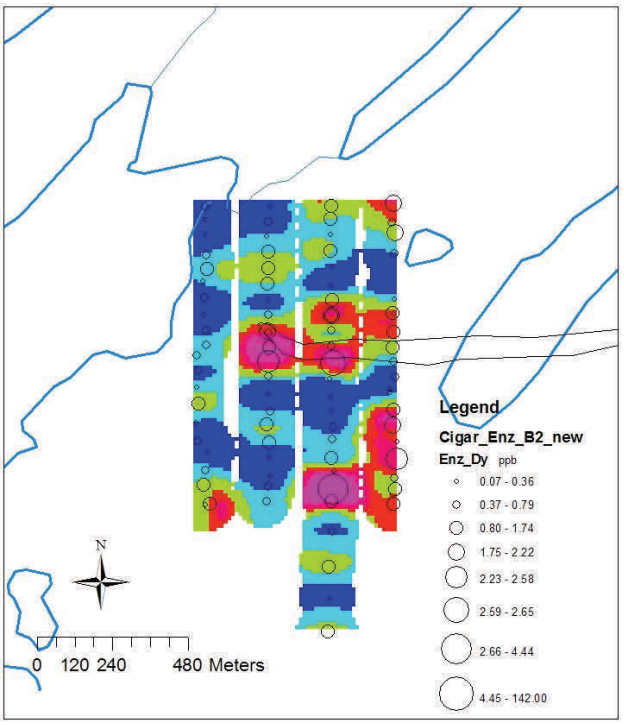

Dysprosium. B2 horizon. Enzyme leach

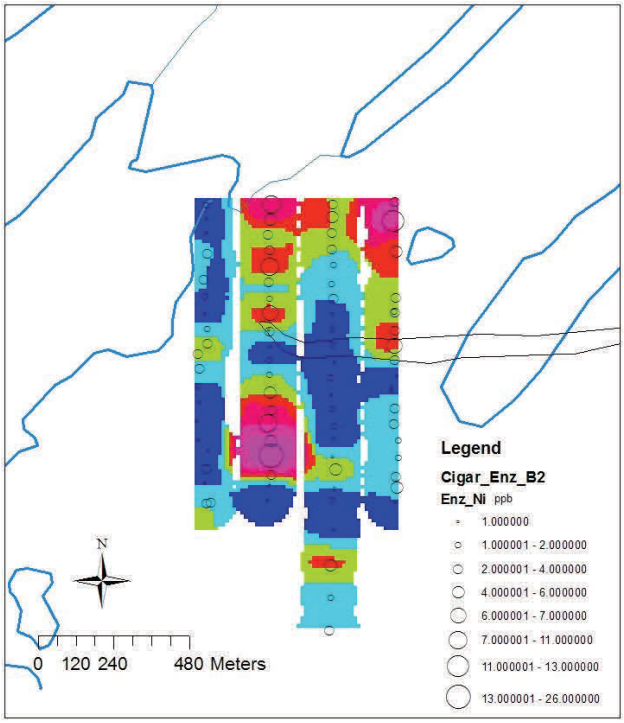

Nickel. B2 horizon. Enzyme leach

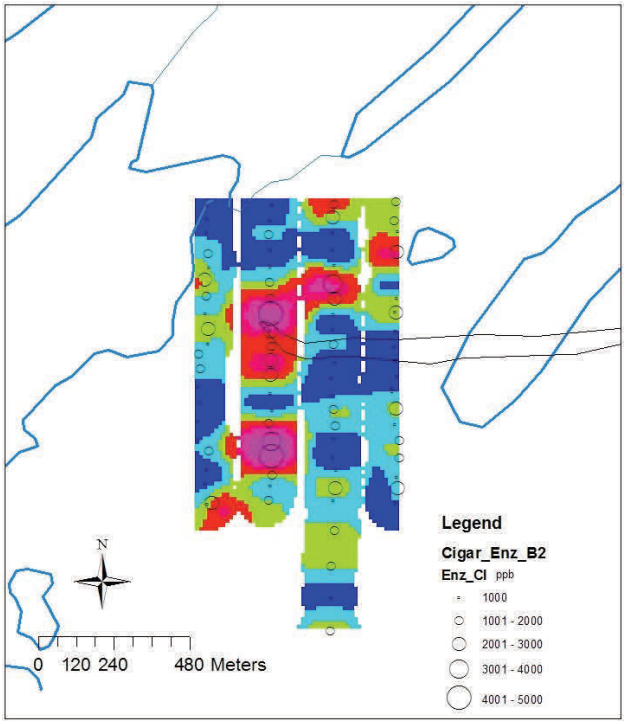

Chlorine. B2 horizon. Enzyme leach

Fig 6.48. Cigar Maps. B2. Enzyme.

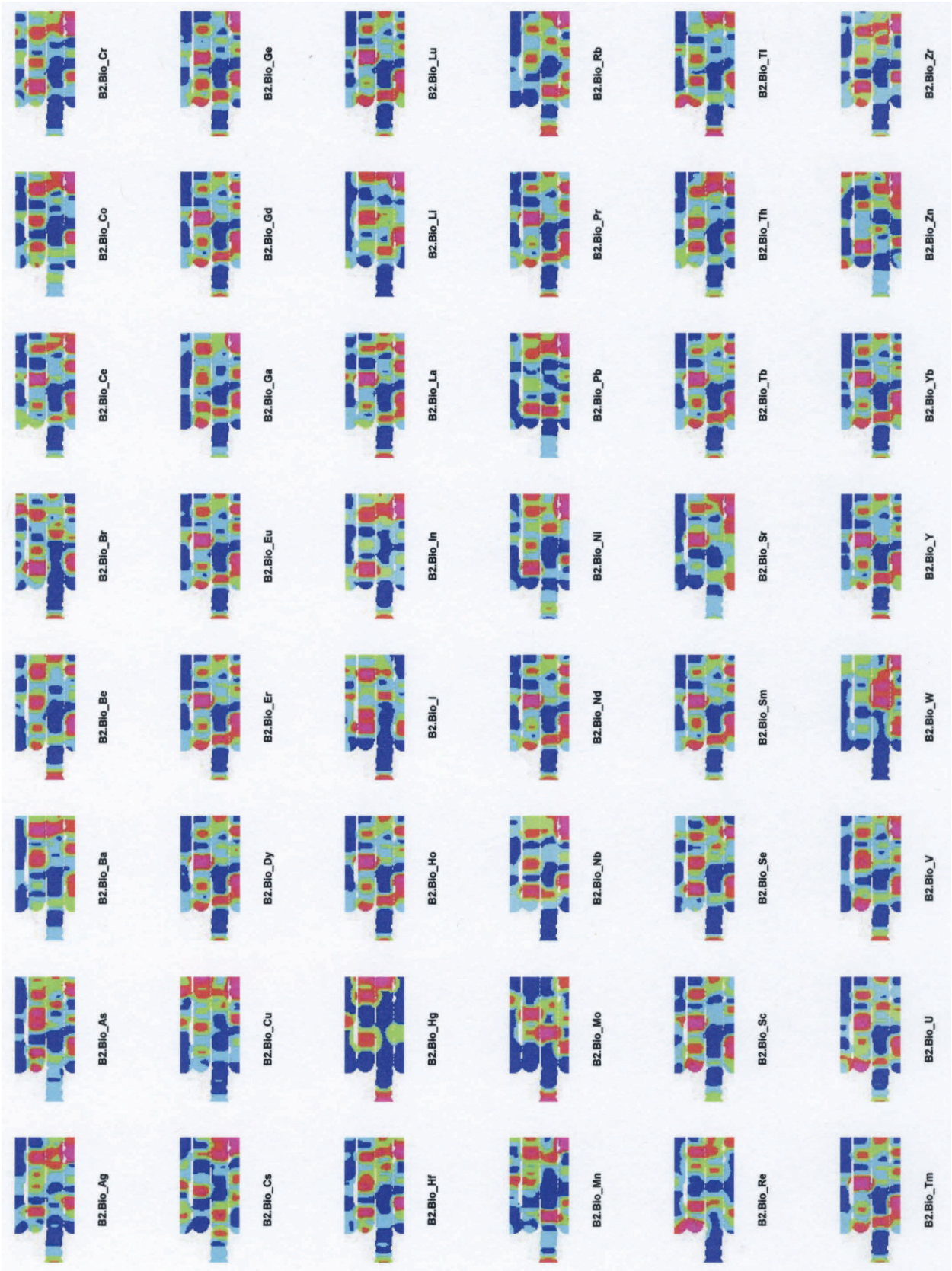

Fig. 6.49. Cigar Lake Grids. B2 horizon. Bioleach.

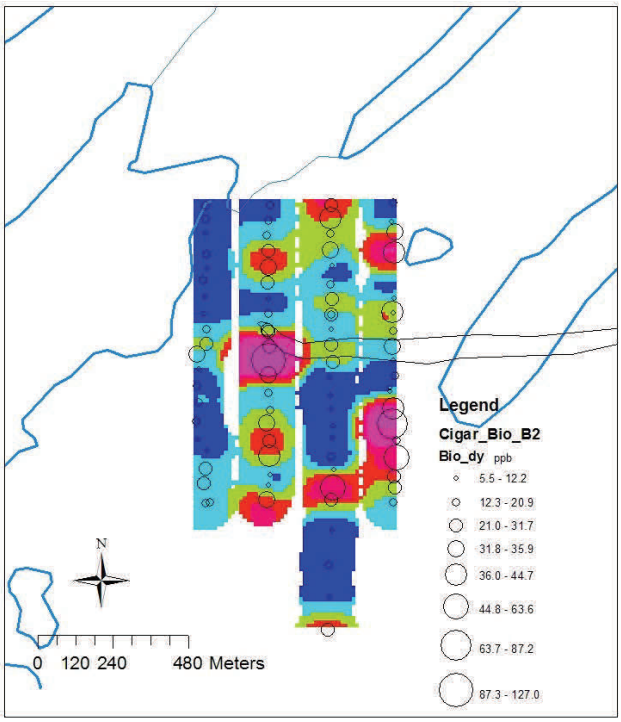

Dysprosium. B2 horizon. Bioleach.

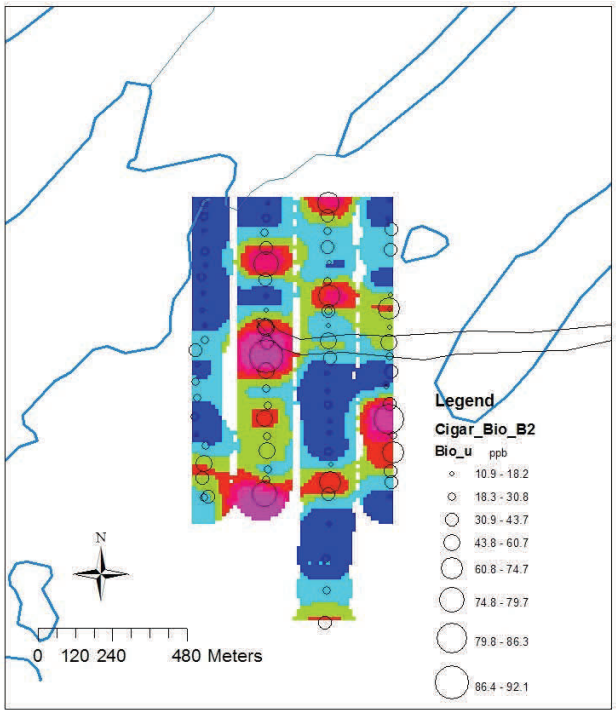

Uranium. B2 horizon. Bioleach.

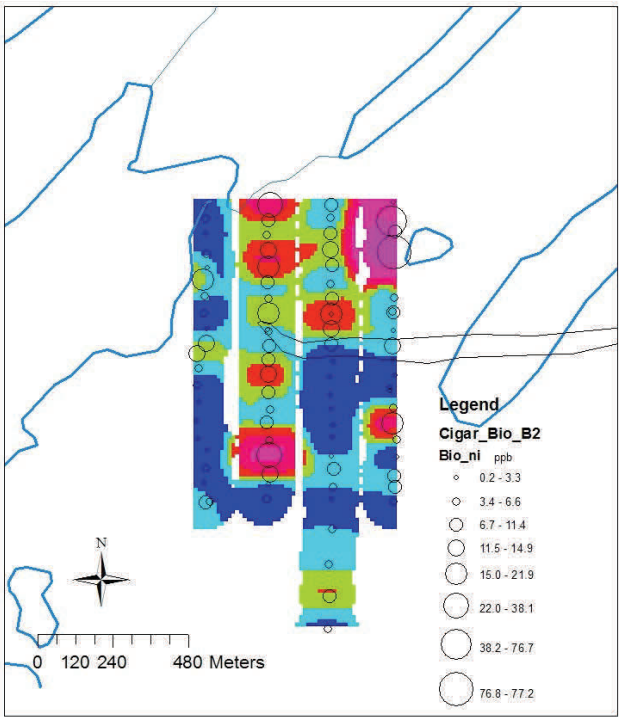

Nickel. B2 horizon. Bioleach.

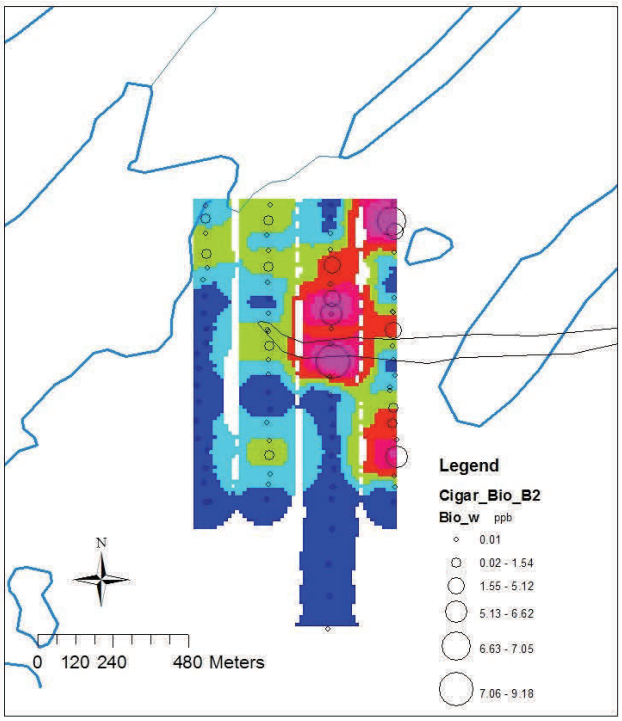

Tungsten. B2 horizon. Bioleach.

Fig. 6.50. Cigar Maps. B2. Bioleach.

Fig. 6.51. Cigar Lake Grids. B2 horizon. MMI leach.

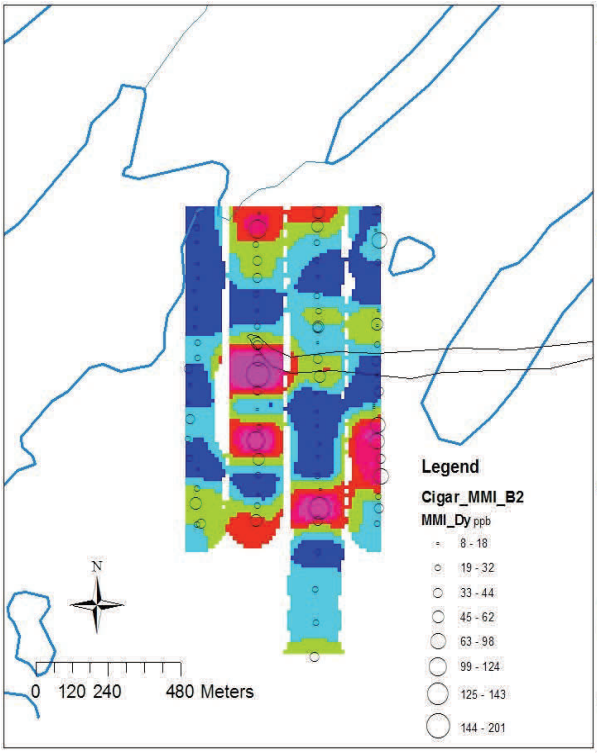

Dysprosium. B2 horizon. MMI leach.

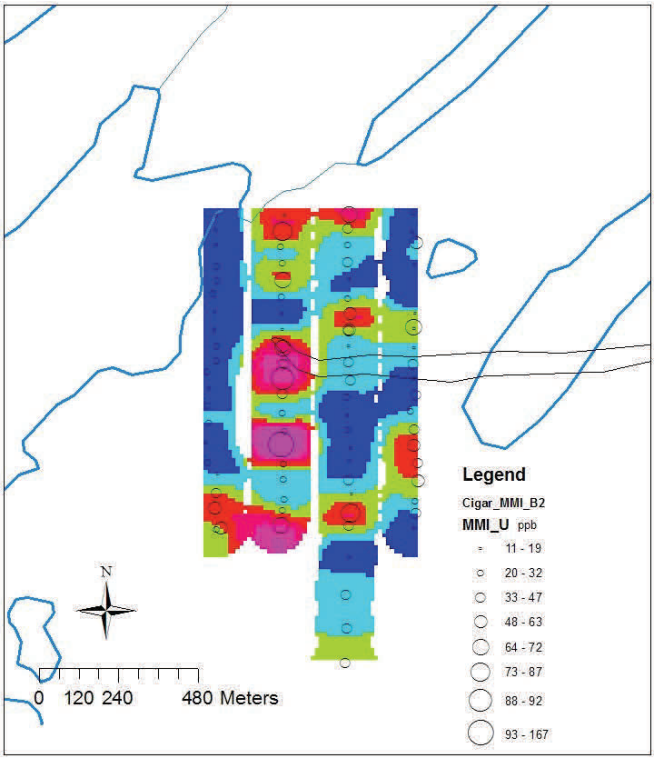

Uranium. B2 horizon. MMI leach.

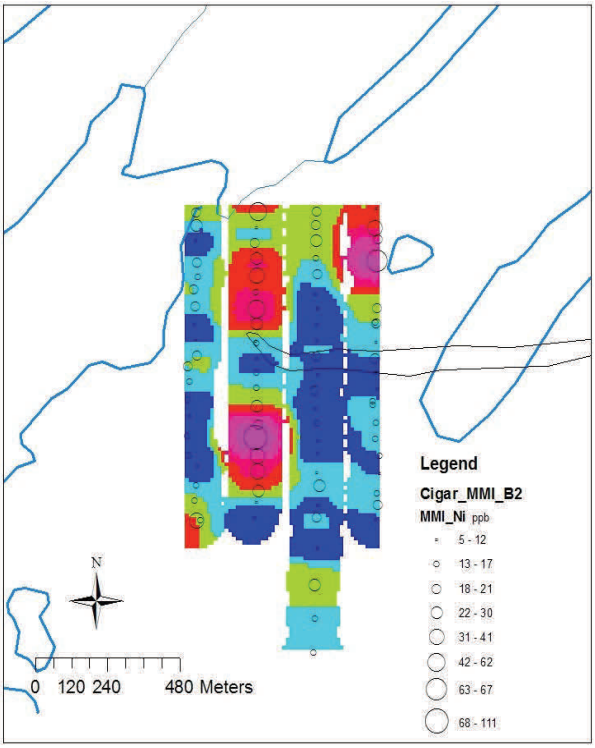

Nickel. B2 horizon. MMI leach.

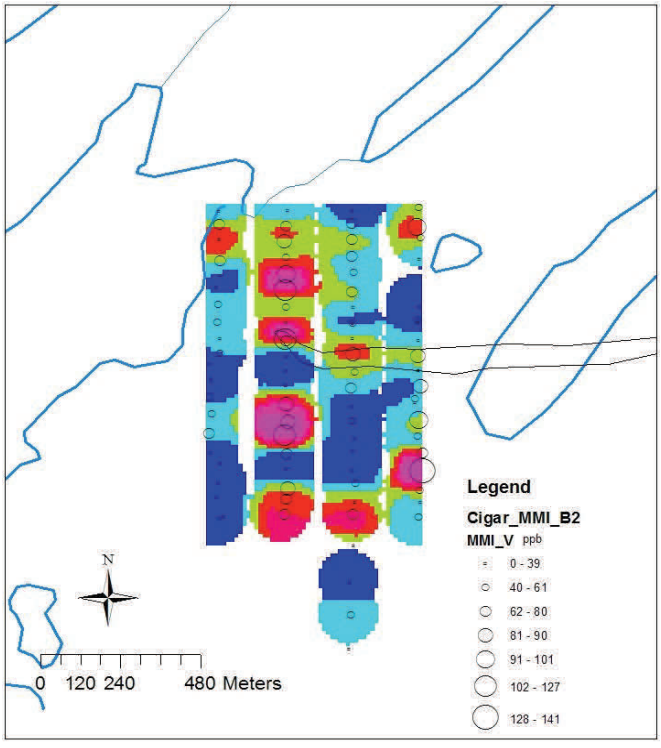

Vanadium. B2 horizon. MMI leach.

Fig 6.52. Cigar Maps. B2. MMI leach.

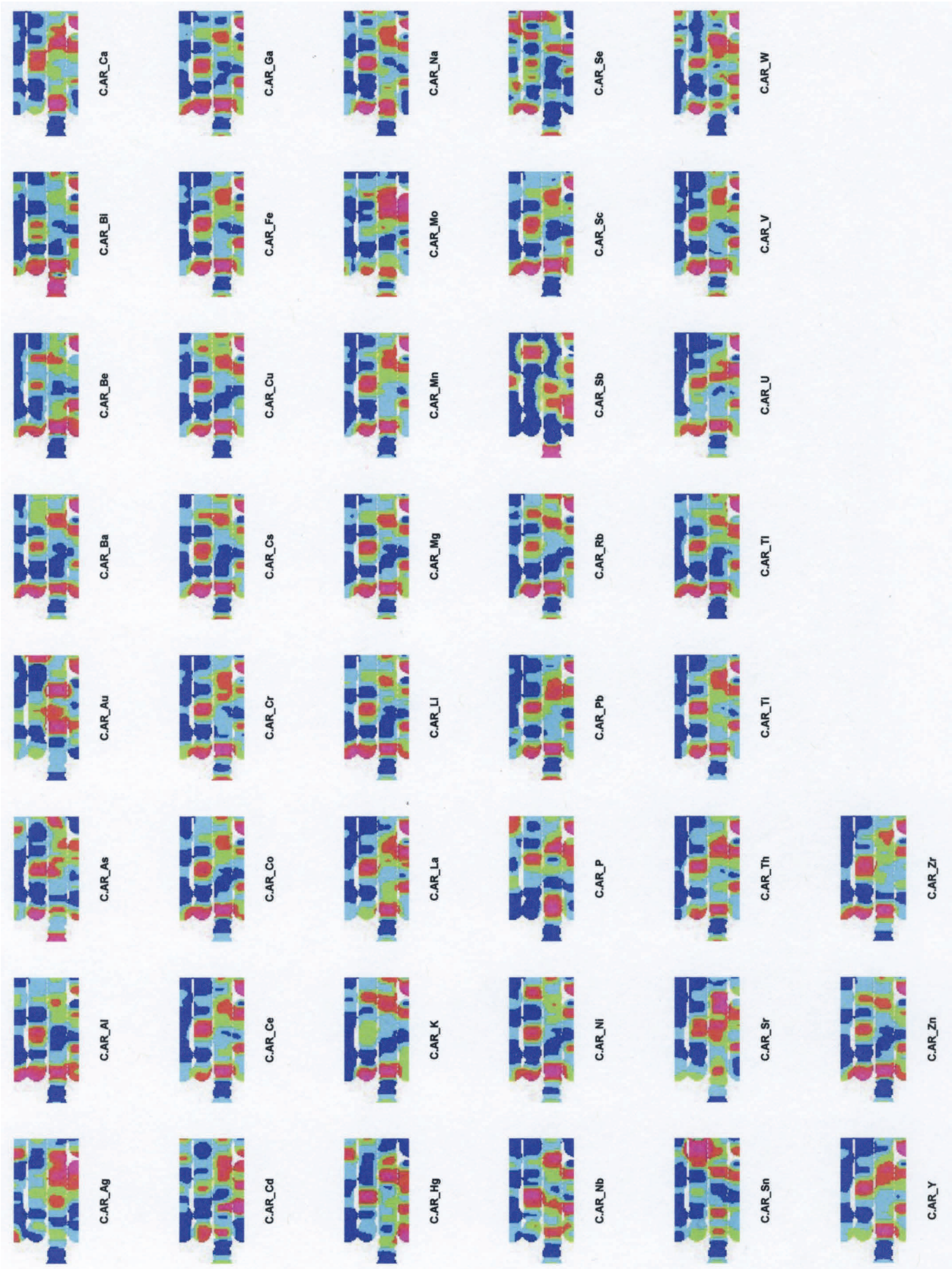

Fig. 6.53. Cigar Lake Grids. C horizon. Aqua regia leach.

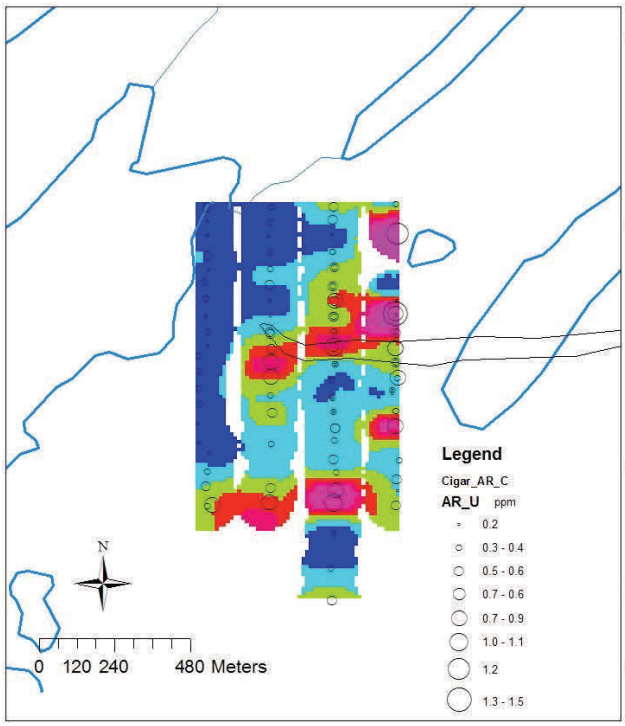

Uranium. C horizon. Aqua regia leach.

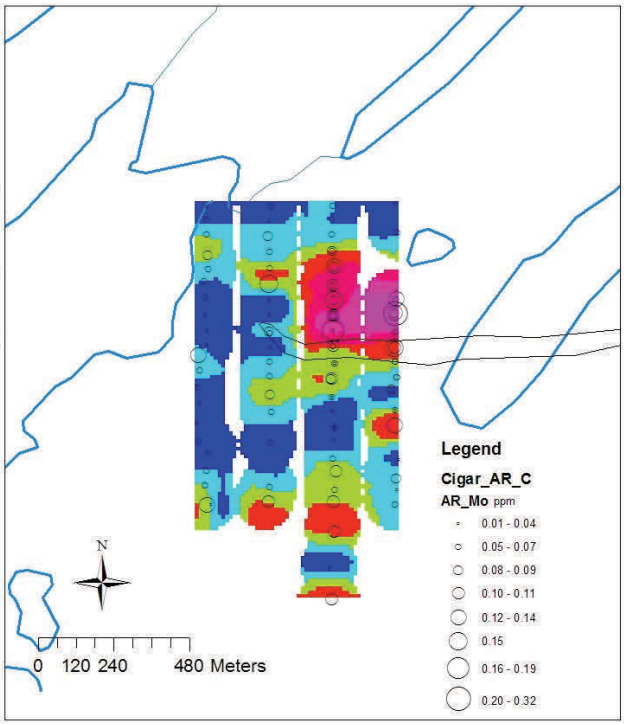

Molybdenum. C horizon. Aqua regia leach.

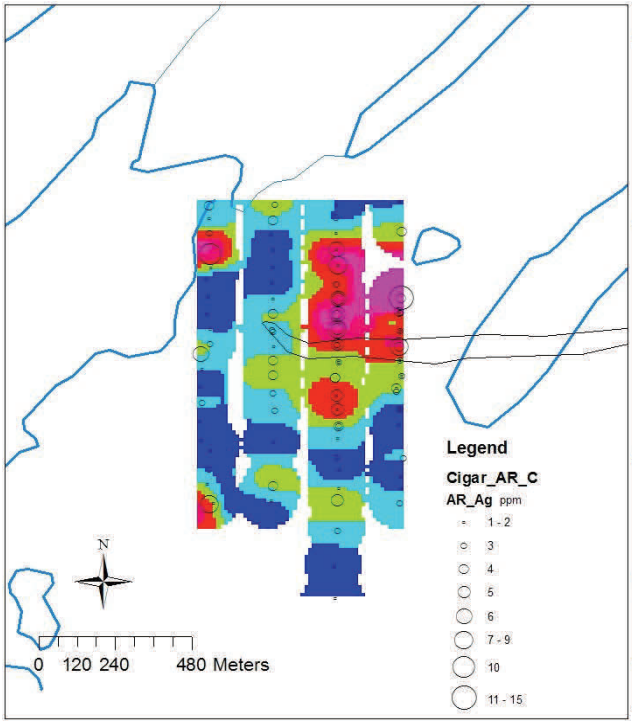

Silver. C horizon. Aqua regia leach.

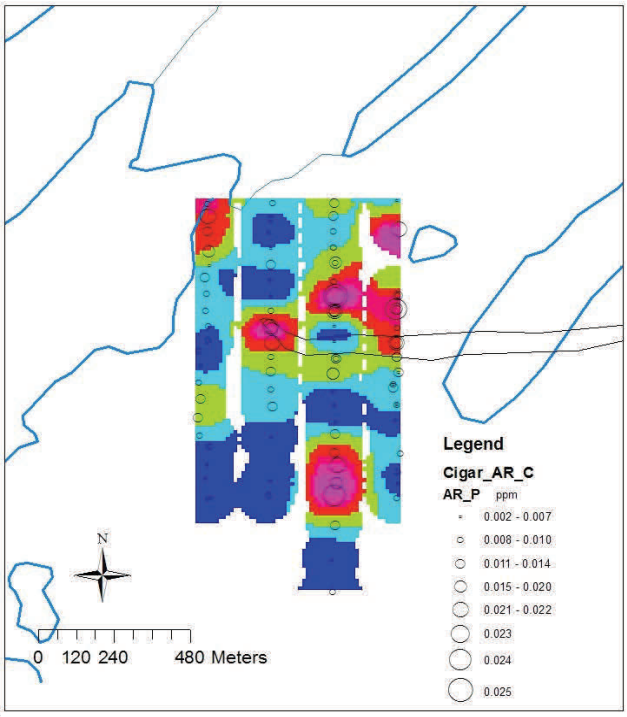

Phosphorus. C horizon. Aqua regia leach.

Fig 6.54. Cigar Maps. C. Aqua regia.

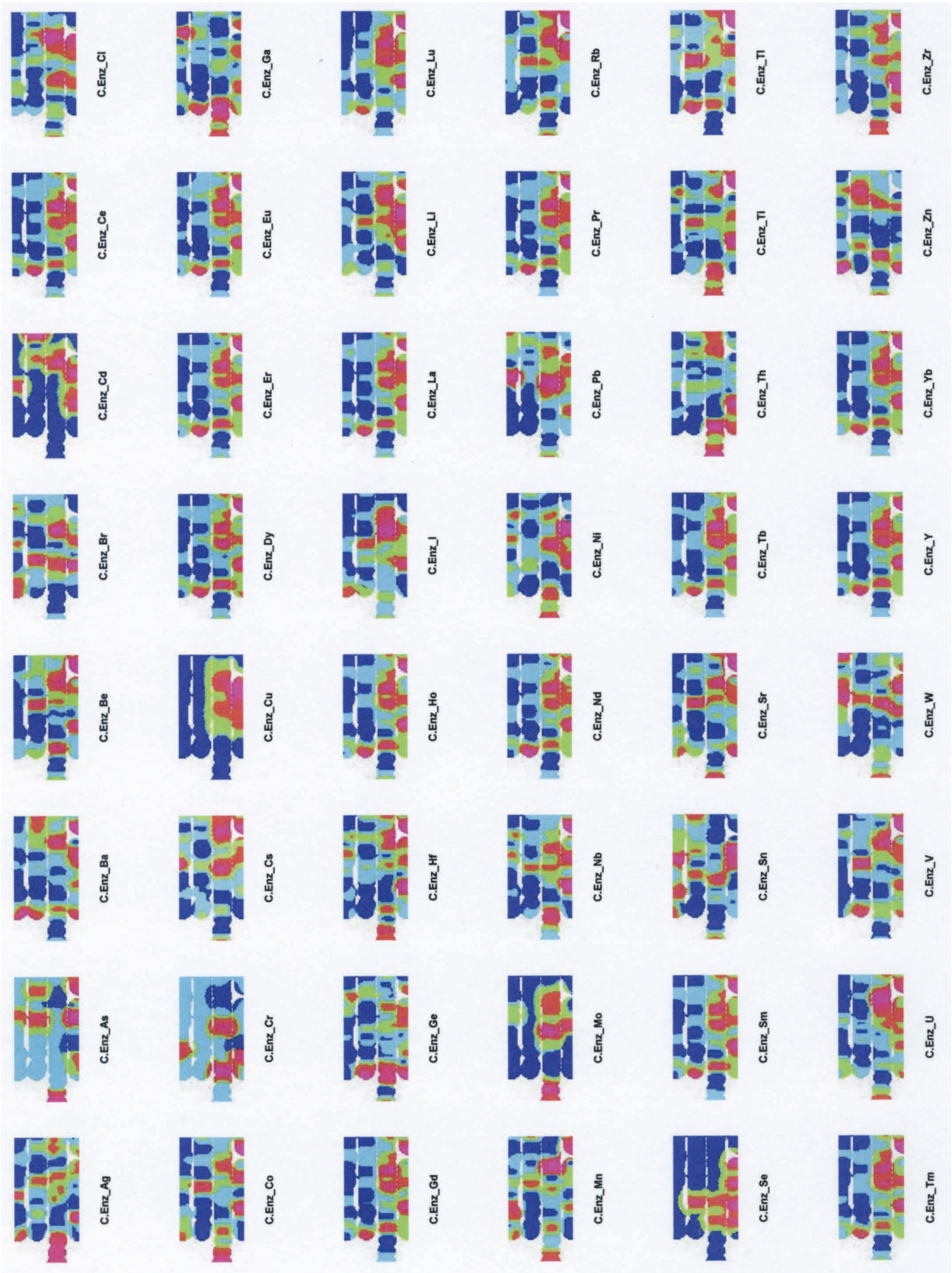

Fig. 6.55. Cigar Lake Grids. C horizon. Enzyme leach.

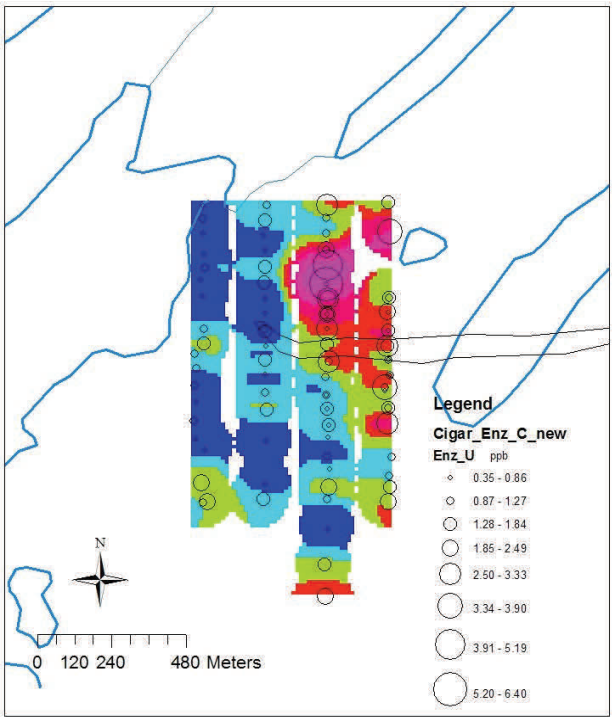

Uranium. C horizon. Enzyme leach.

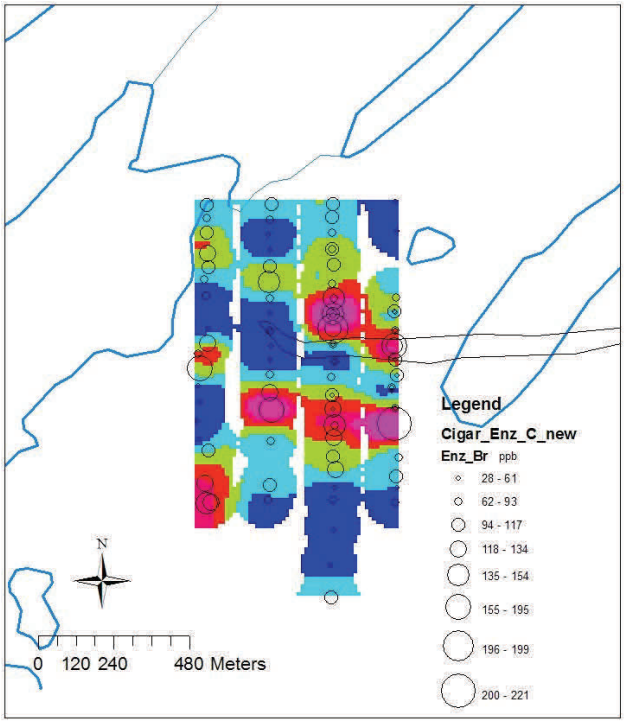

Bromine. C horizon. Enzyme leach.

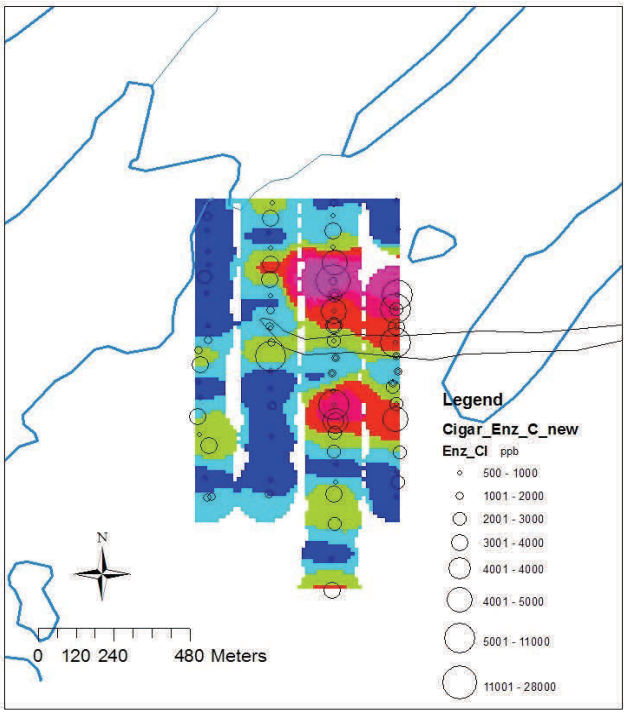

Chlorine. C horizon. Enzyme leach.

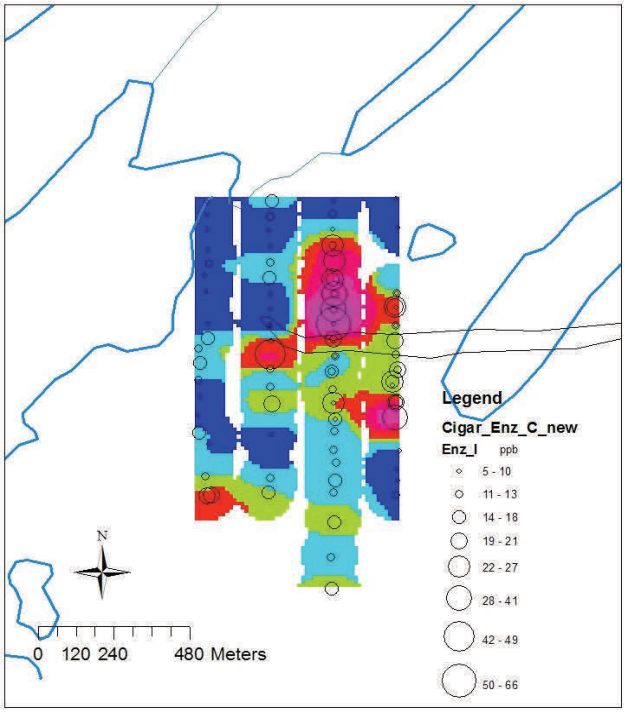

Iodine. C horizon. Enzyme leach.

Fig 6.56. Cigar Maps. C. Enzyme.

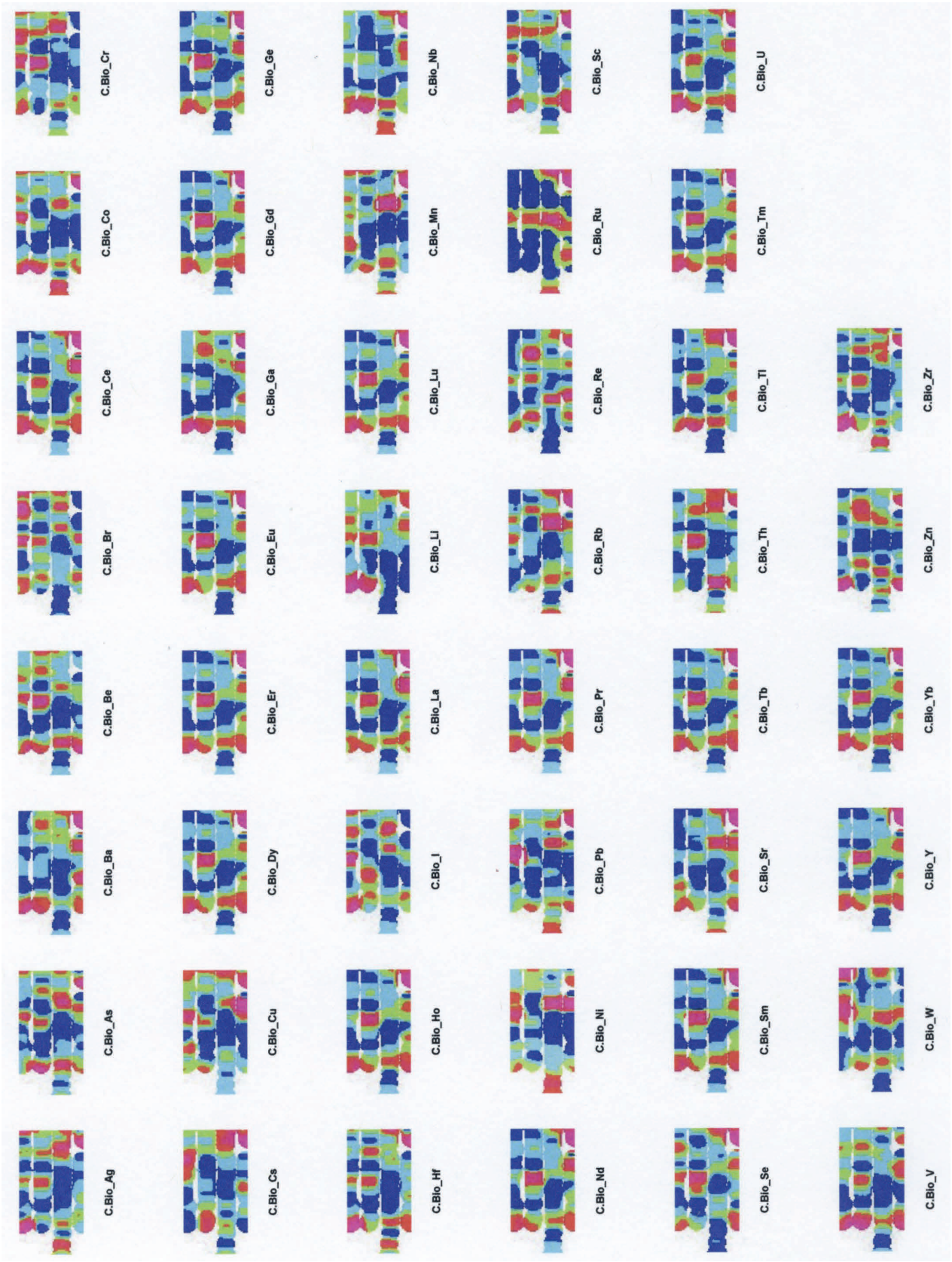

Fig. 6.57. Cigar Lake Grids. C horizon. Bioleach.

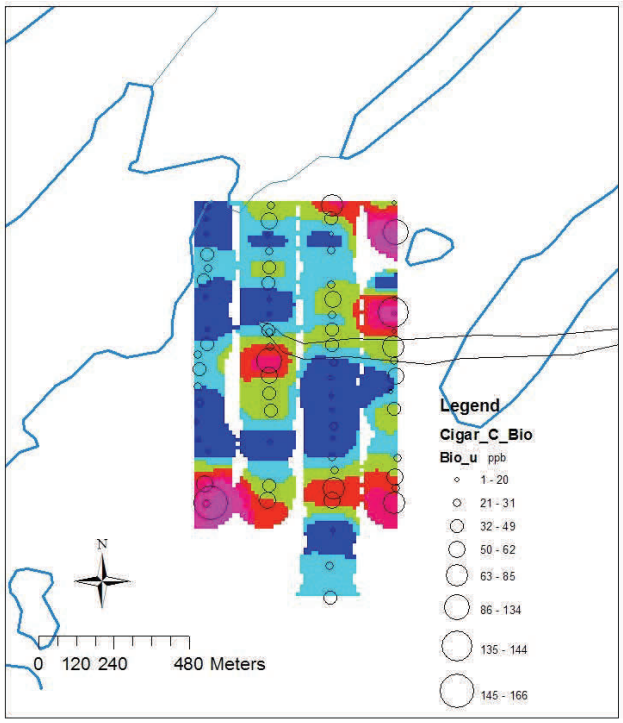

Uranium. C horizon. Bioleach.

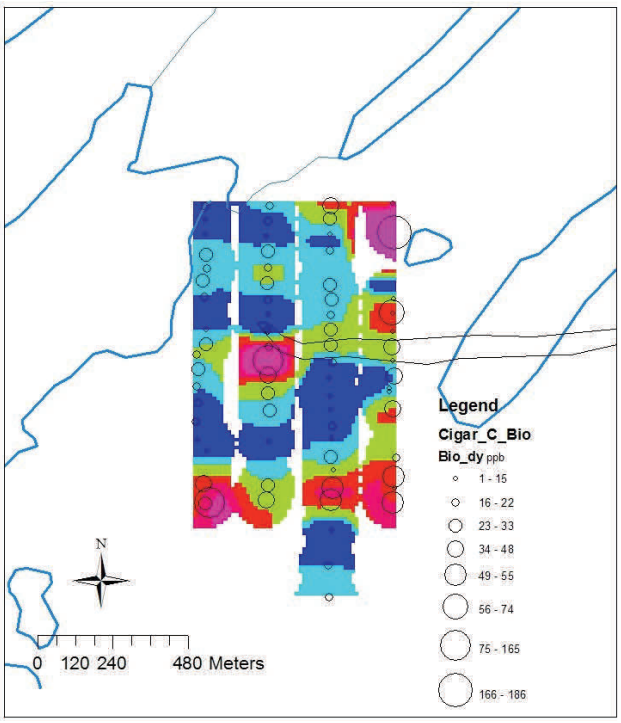

Dysprosium. C horizon. Bioleach.

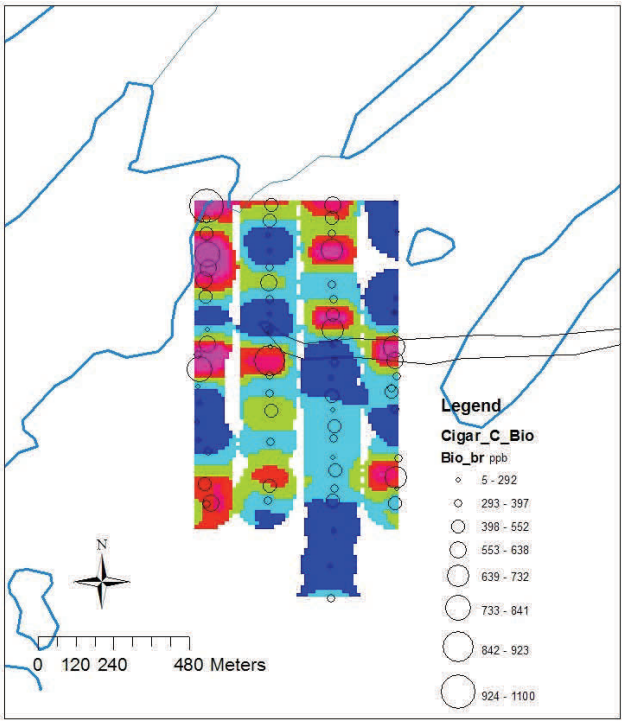

Bromine. C horizon. Bioleach.

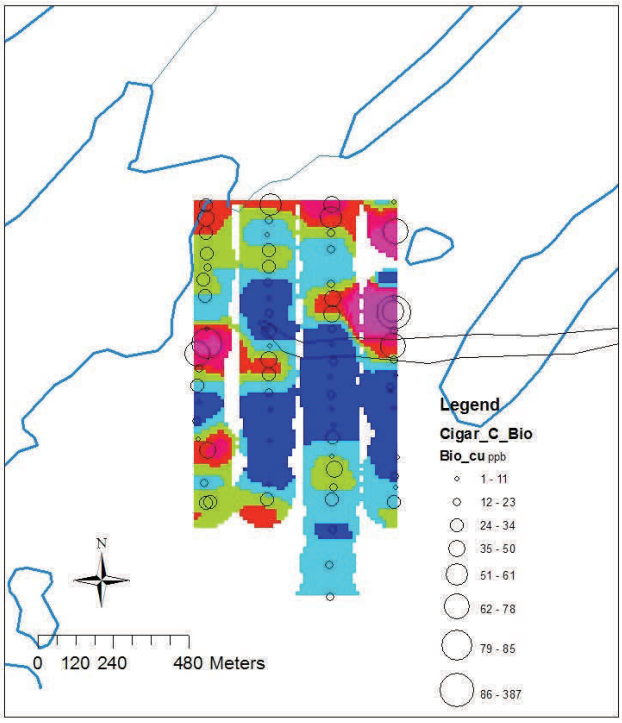

Copper. C horizon. Bioleach.

Fig. 6.58. Cigar Maps. C. Bioleach.

Fig. 6.59. Cigar Lake Grids. C horizon. Hydroxylamine leach.

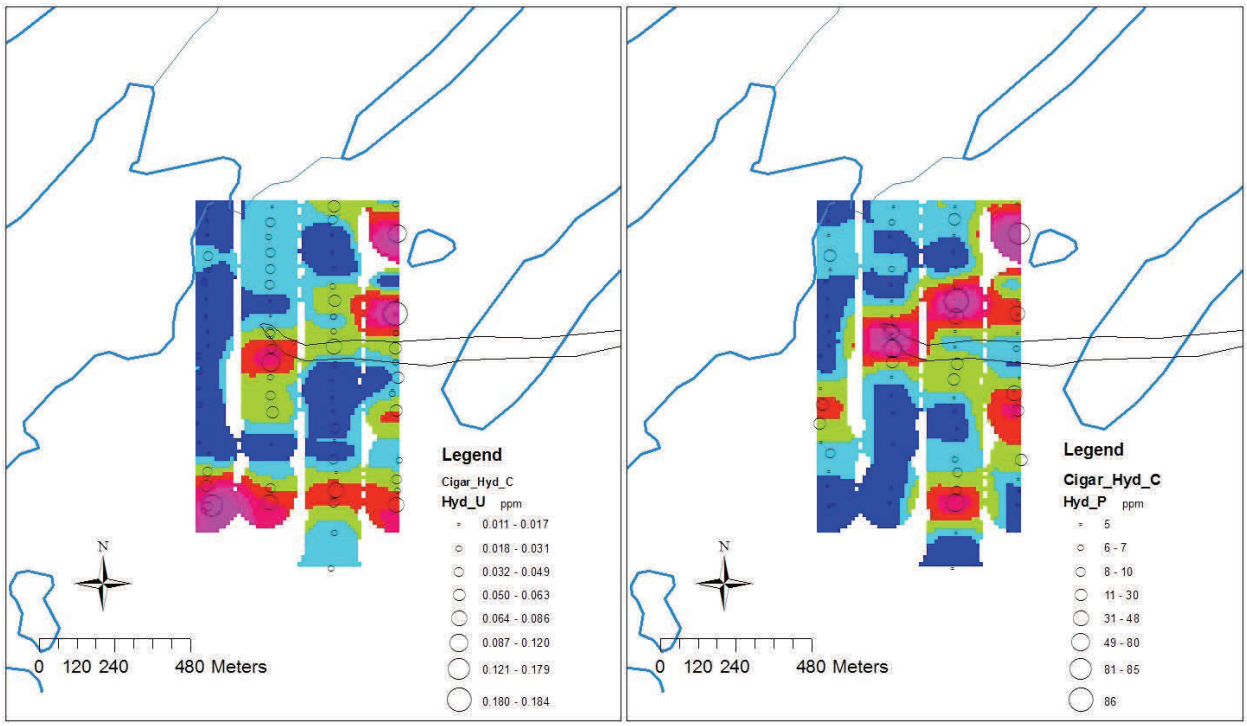

Uranium. C horizon. Hydroxylamine leach.

Phosphorus. C horizon. Hydroxylamine leach.

Fig. 6.60. Cigar Maps. C. Hydroxylamine.

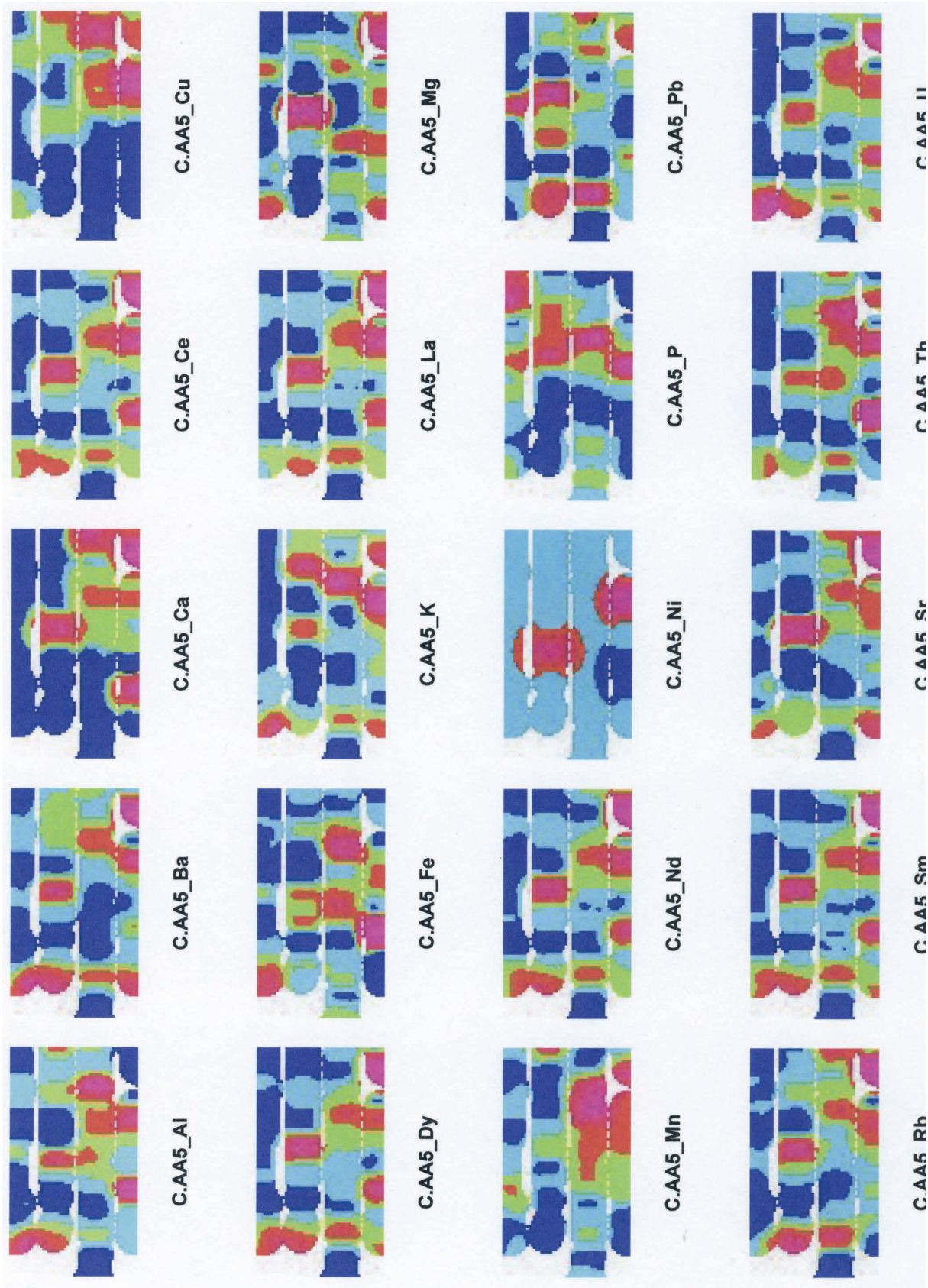

Fig. 6.61. Cigar Lake Grids. C horizon. Ammonium acetate leach.

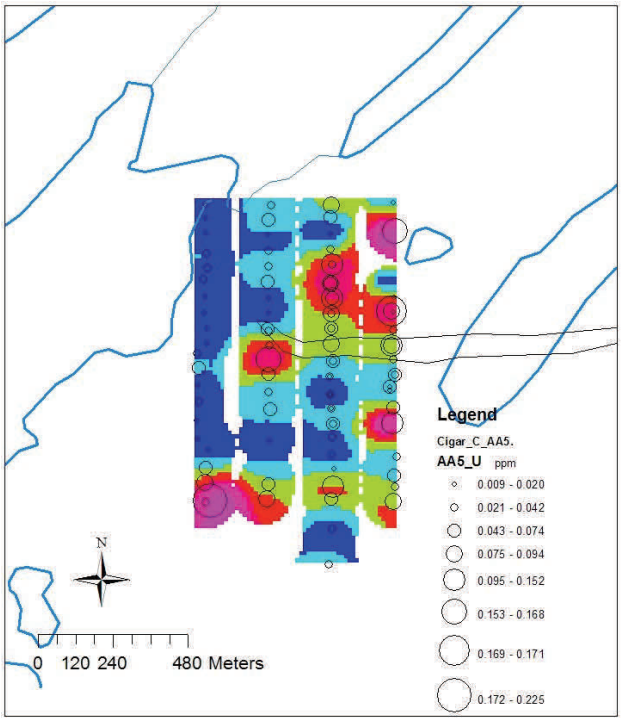

Uranium. C horizon. Ammonium acetate leach.

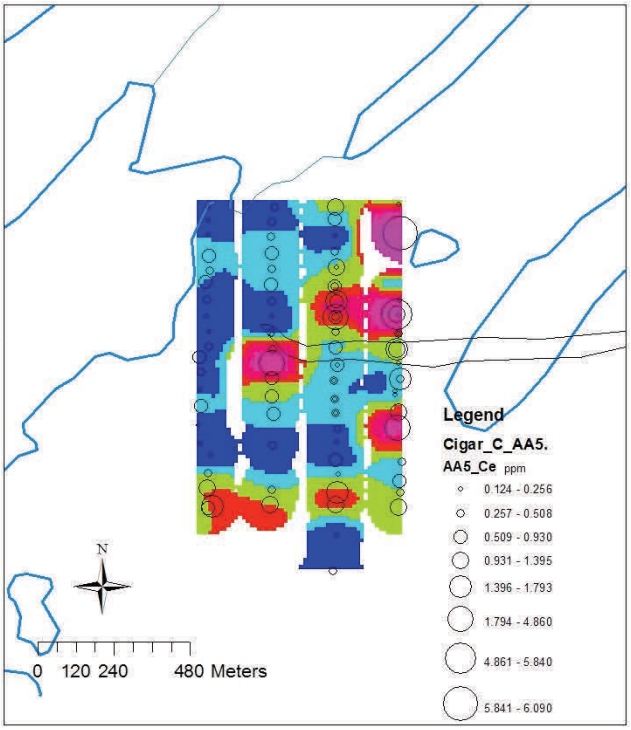

Cerium. C horizon. Ammonium acetate leach.

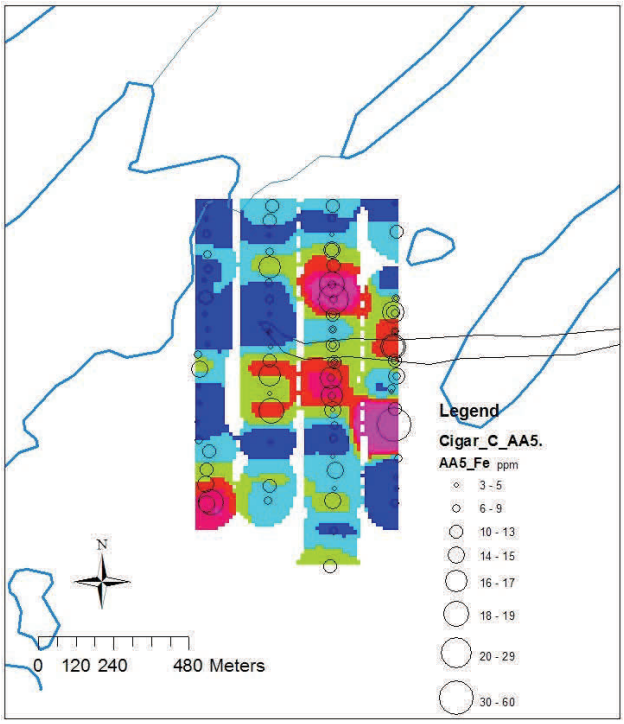

Iron. C horizon. Ammonium acetate leach.

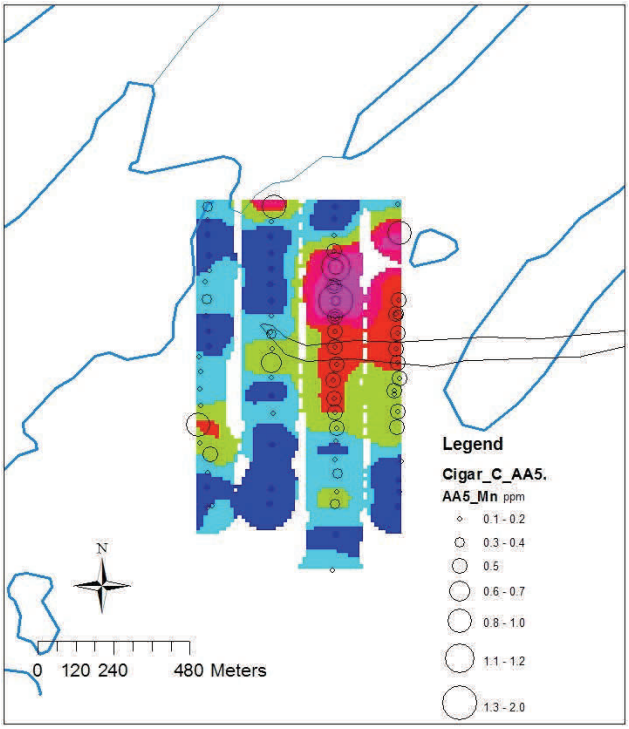

Manganese. C horizon. Ammonium acetate leach.

Fig. 6.62. Cigar Maps. C. Ammonium acetate.

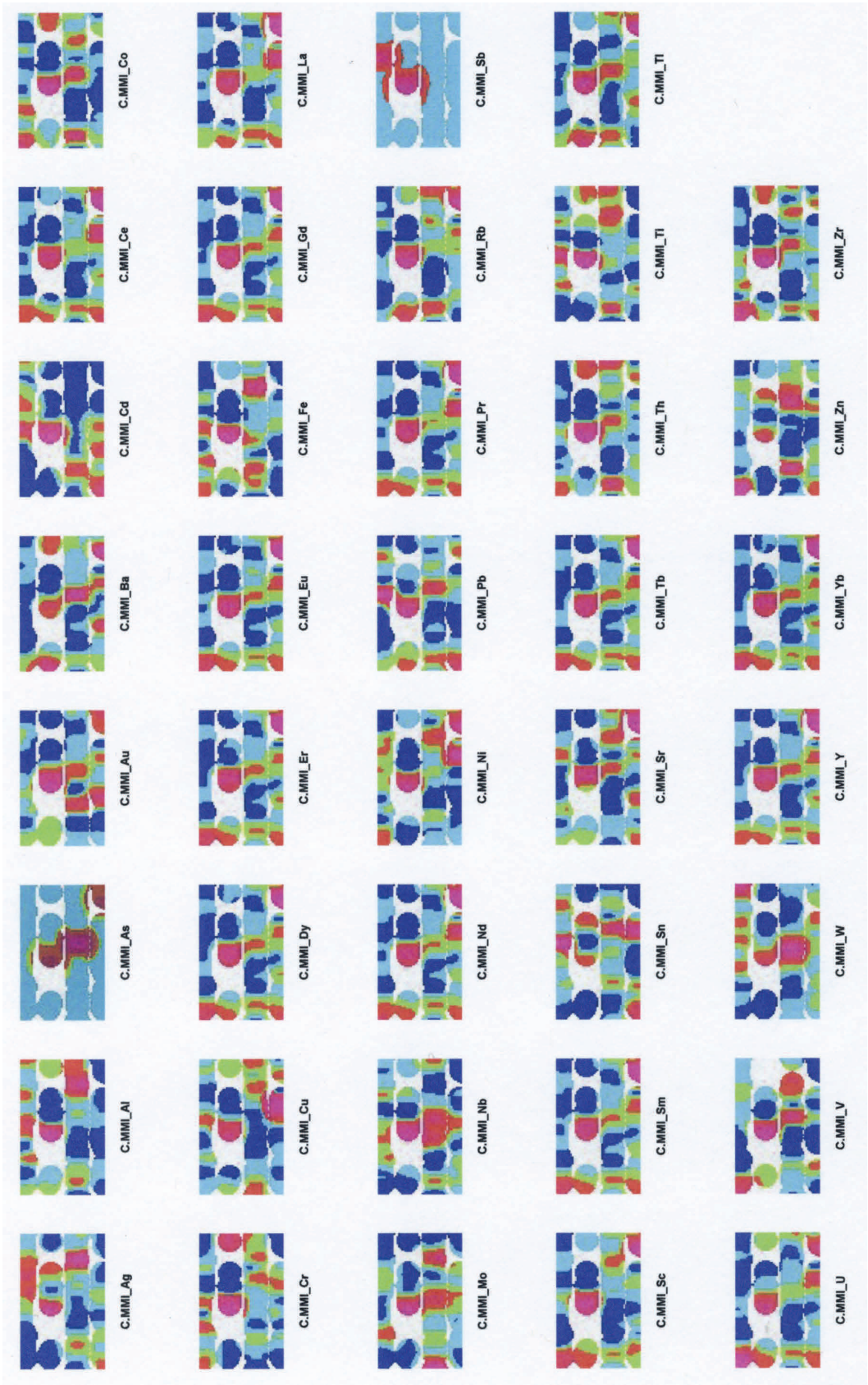

Fig. 6.63. Cigar Lake Grids. C horizon. MMI leach.

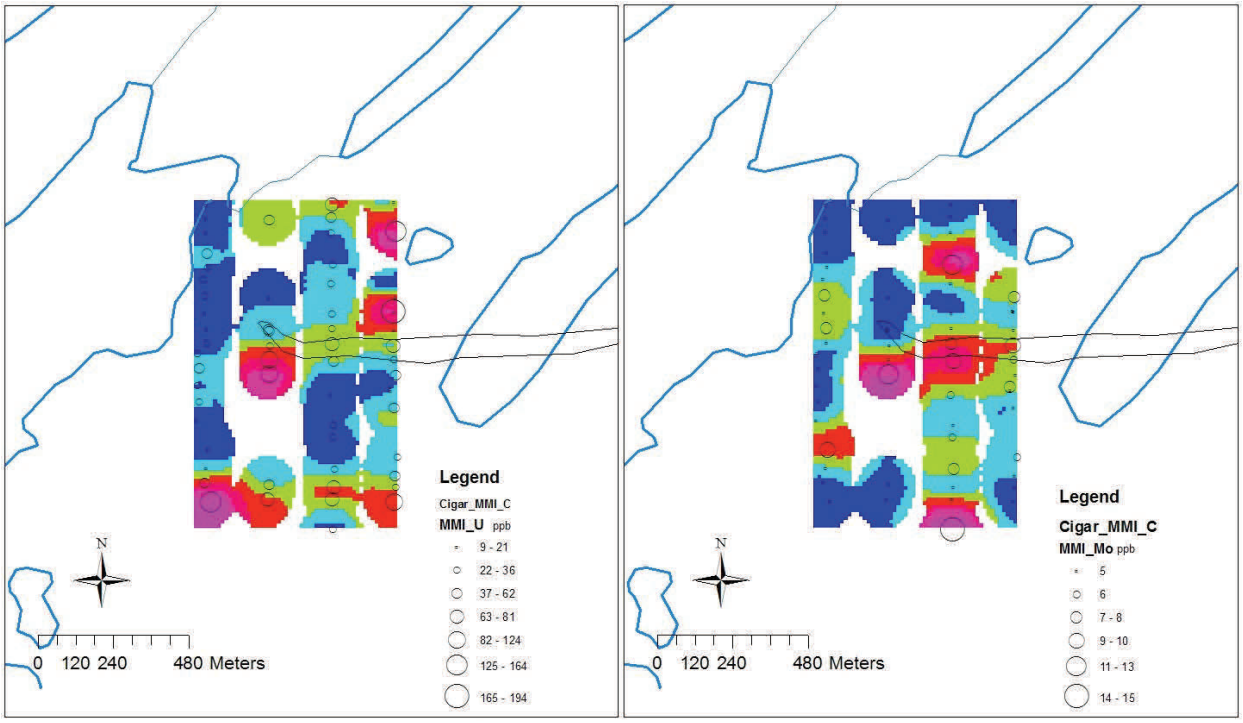

Uranium. C horizon. MMI leach.

Molybdenum. C horizon. MMI leach.

Fig. 6.64. Cigar Maps. C. MMI.

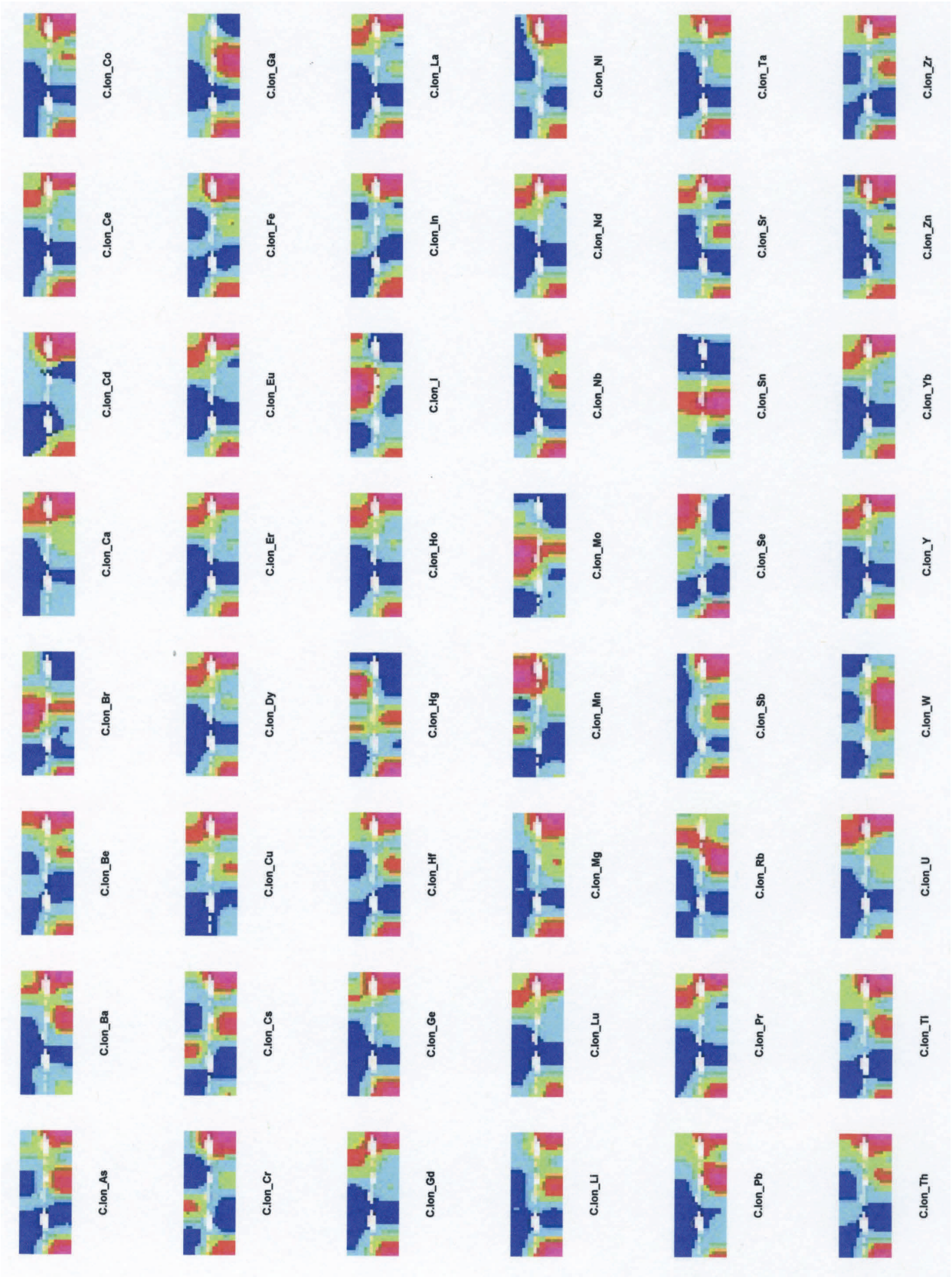

Fig. 6.65. Cigar Lake Grids. C horizon. Ionic leach.

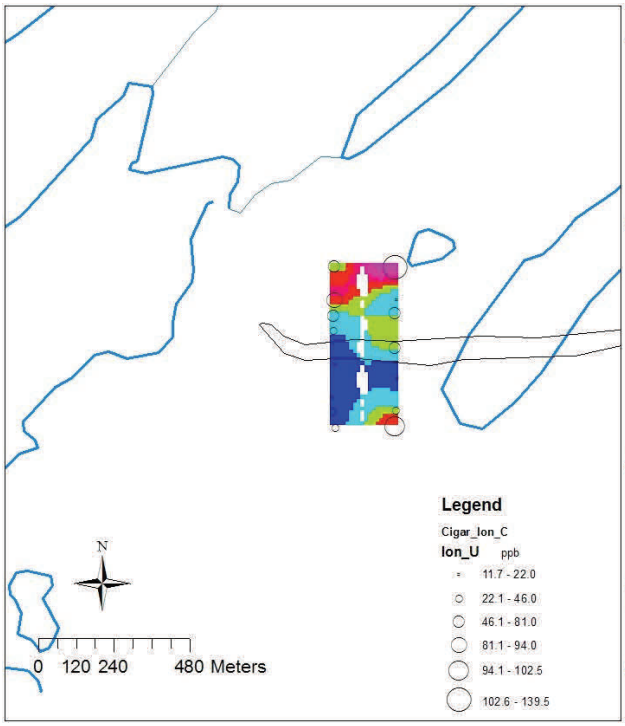

Uranium. C horizon. Ionic leach.

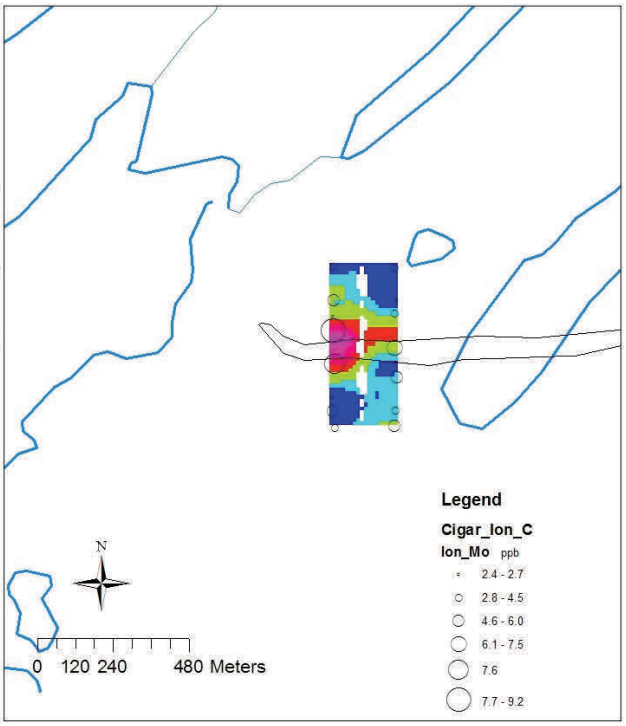

Molybdenum. C horizon. Ionic leach.

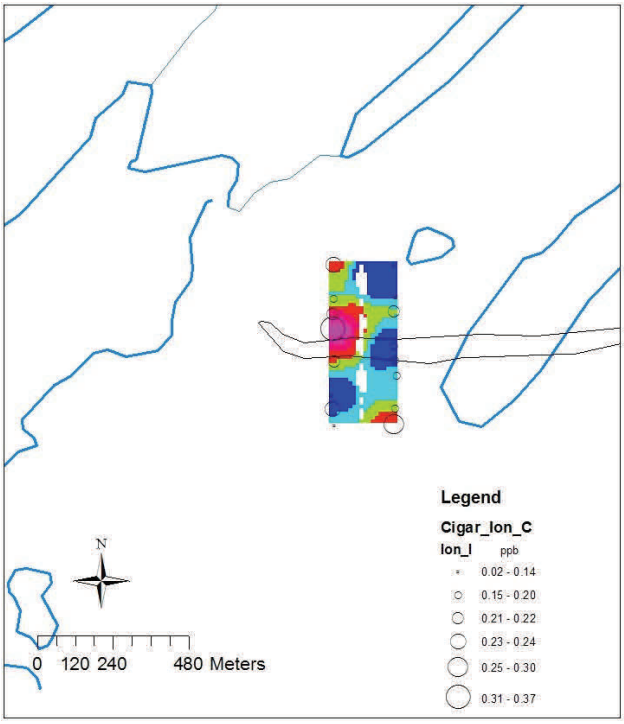

Iodine. C horizon. Ionic leach.

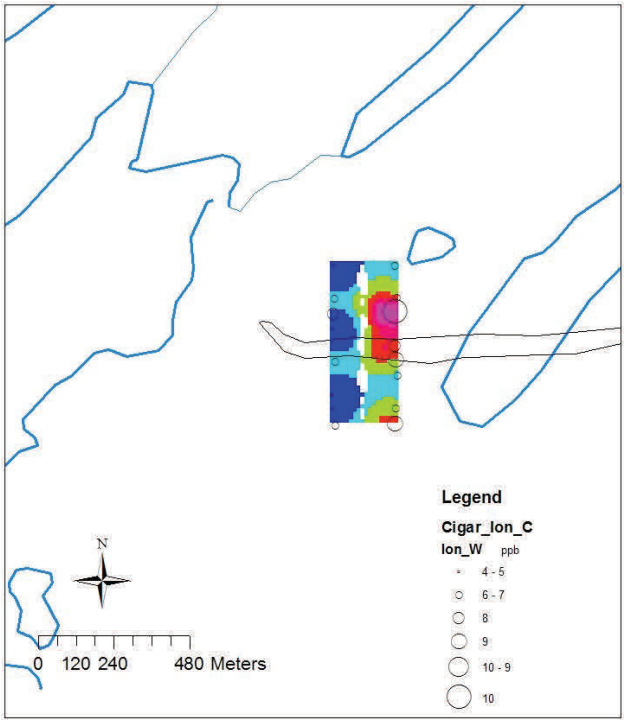

Tungsten. C horizon. Ionic leach.

Fig. 6.66. Cigar Maps. C. Ionic leach.

Fig. 6.67. Cigar Lake Grids. MMI leach on MMI horizon.

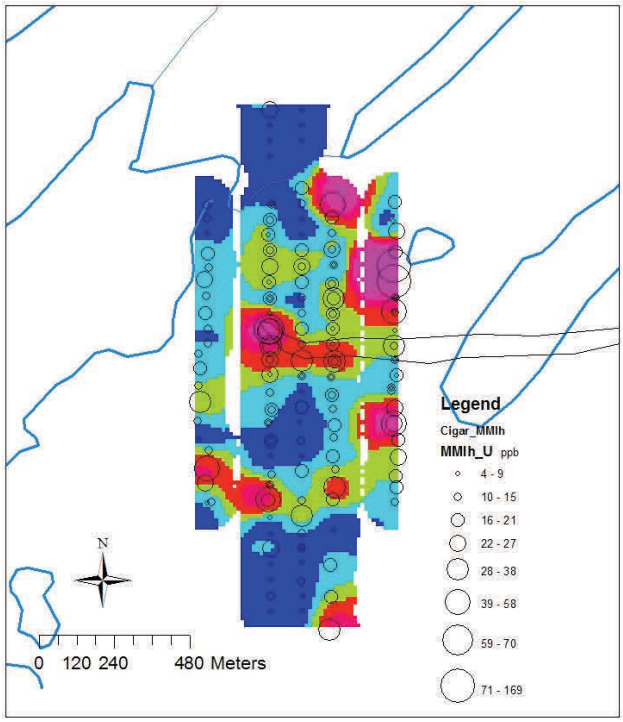

Uranium. MMI leach on MMI horizon.

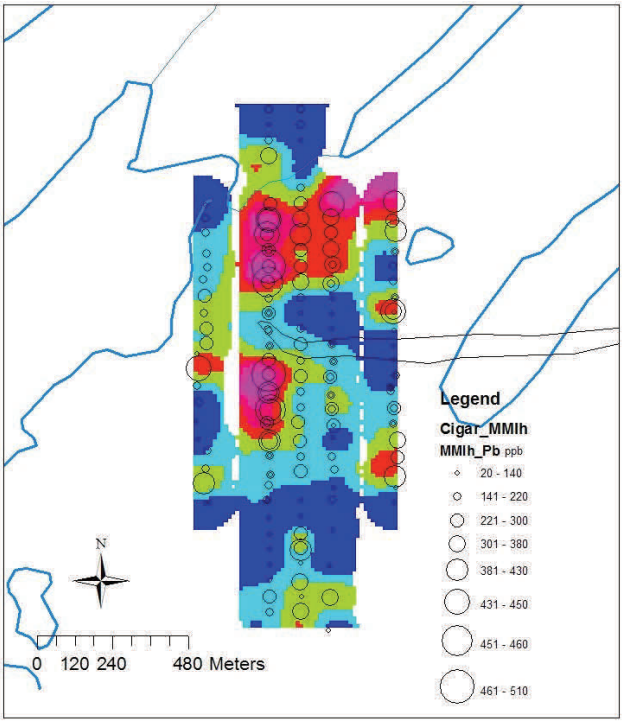

Lead. MMI leach on MMI horizon.

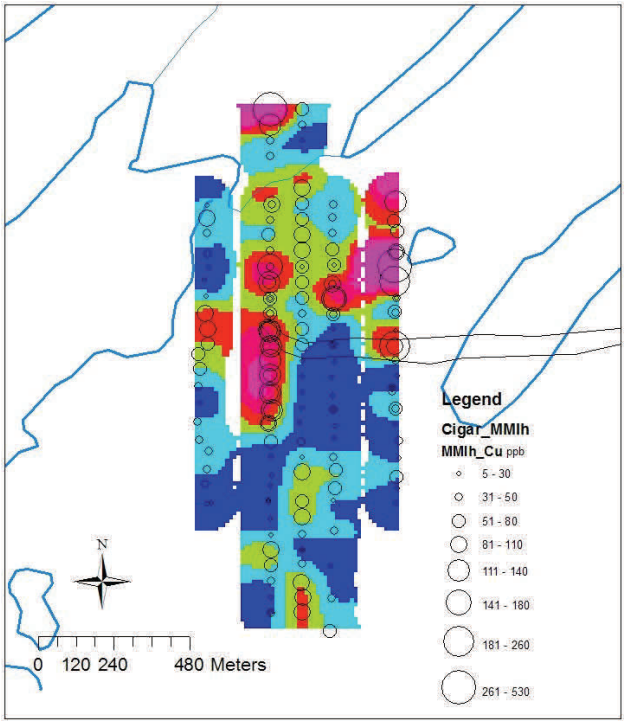

Copper. MMI leach on MMI horizon.

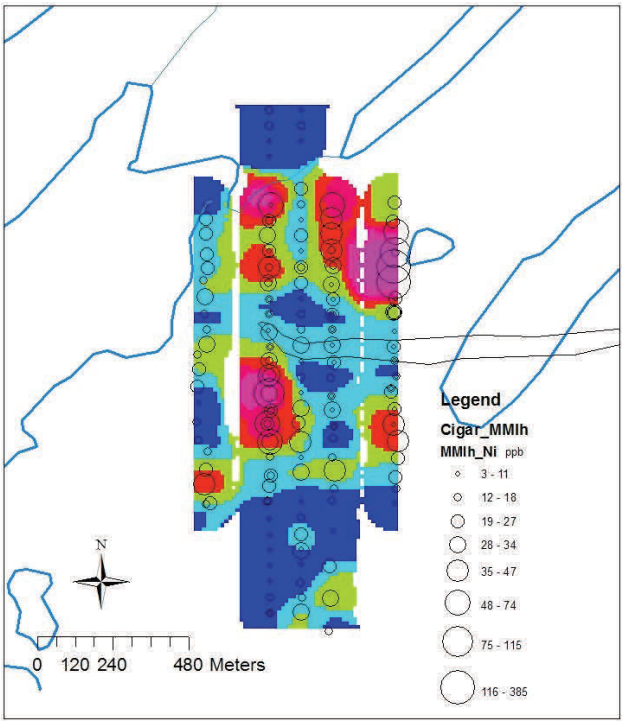

Nickel. MMI leach on MMI horizon.

Fig. 6.68. Cigar Maps. MMI horizon.

Fig. 6.69. McClean Lake Grids. A1. Aqua regia leach.

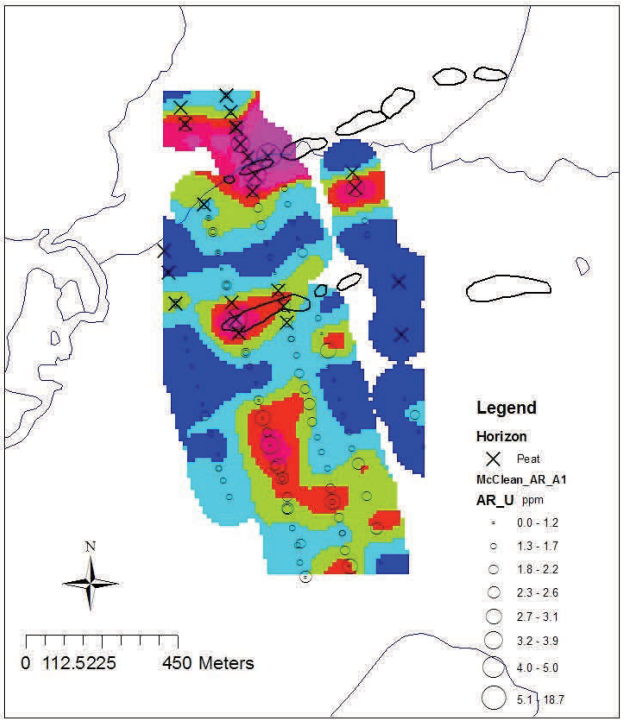

Uranium. A1 horizon. Aqua regia leach.

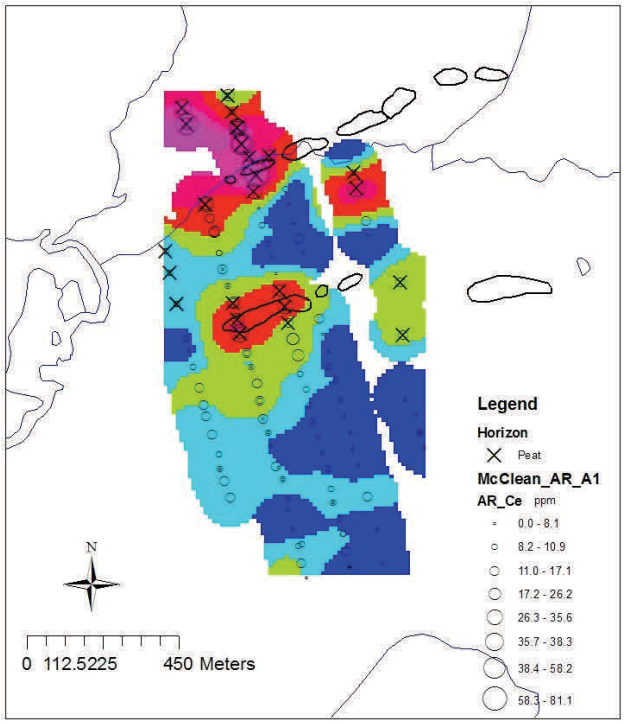

Cerium. A1 horizon. Aqua regia leach.

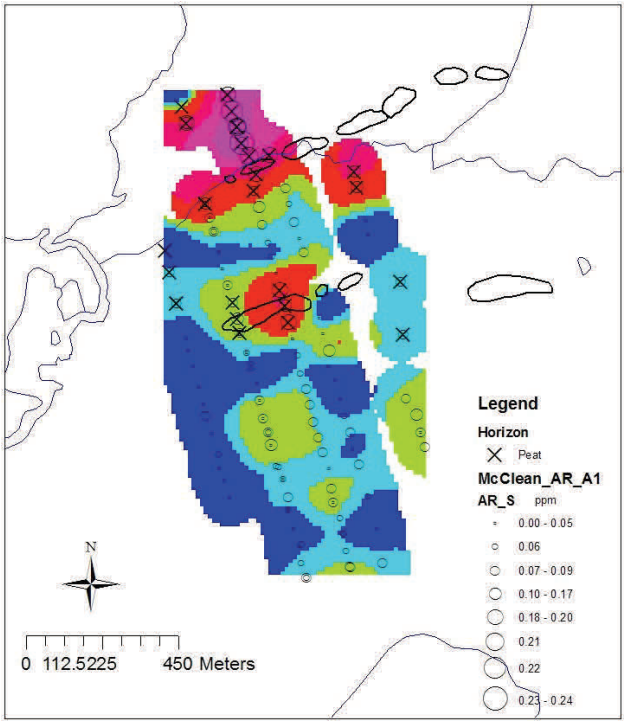

Sulphur. A1 horizon. Aqua regia leach.

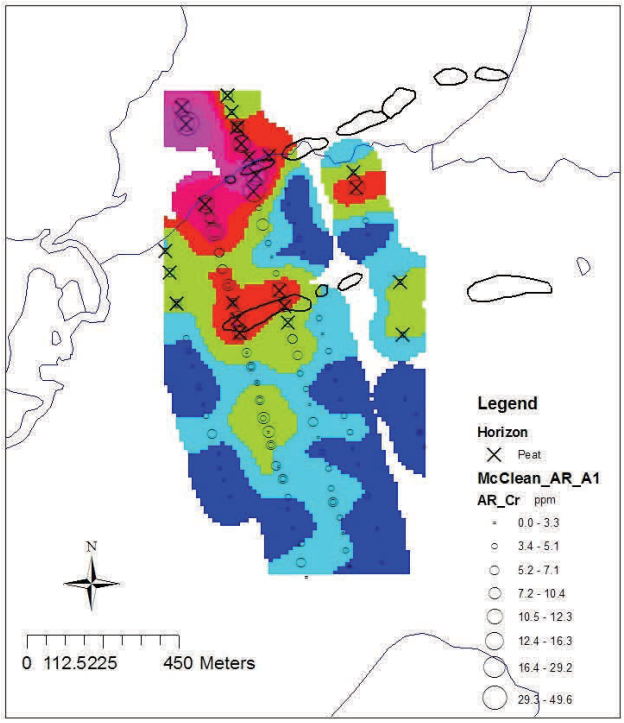

Chromium. A1 horizon. Aqua regia leach.

Fig. 6.70. McClean Maps. A1. Aqua regia.

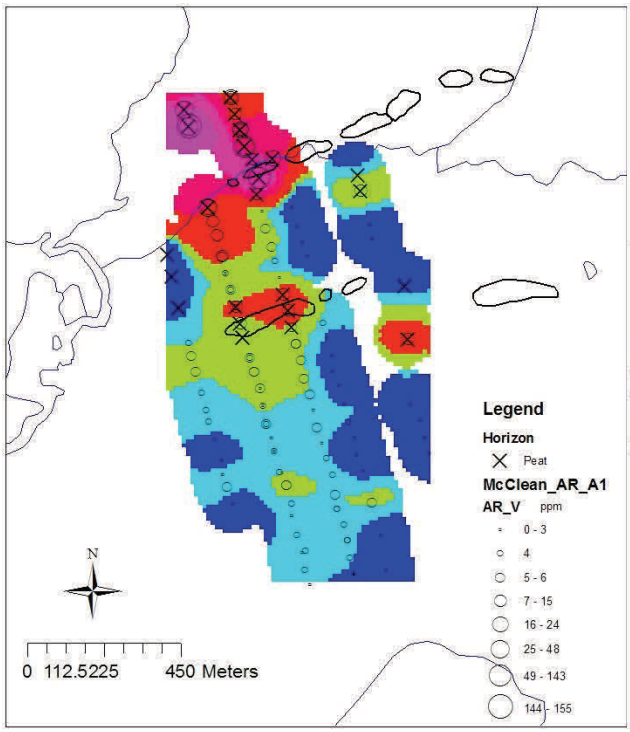

Vanadium. A1 horizon. Aqua regia leach.

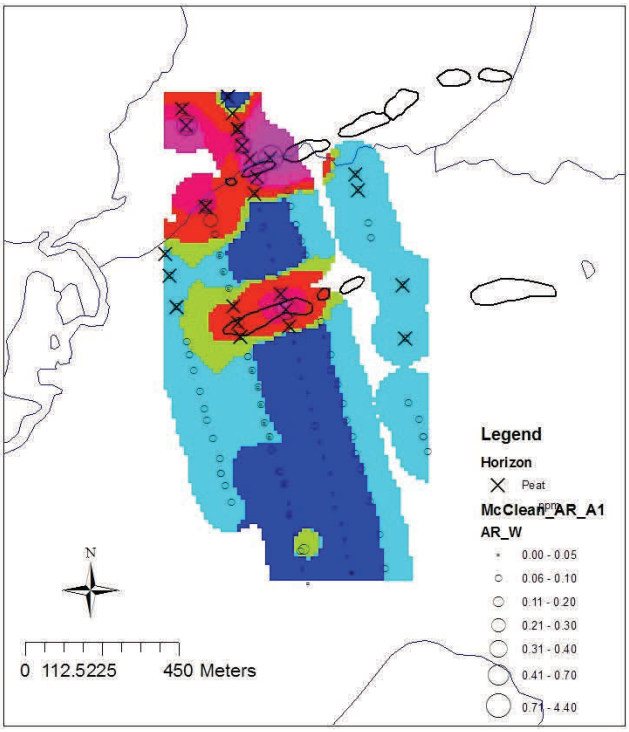

Tungsten. A1 horizon. Aqua regia leach.

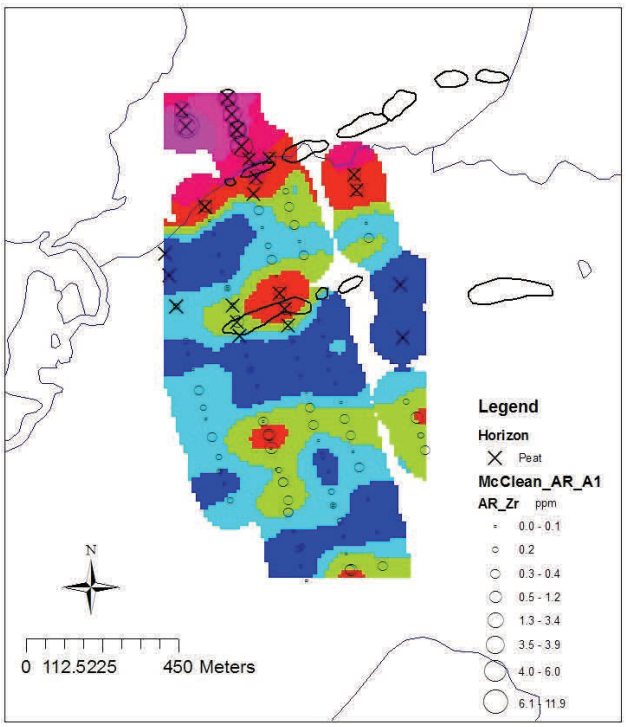

Zirconium. A1 horizon. Aqua regia leach.

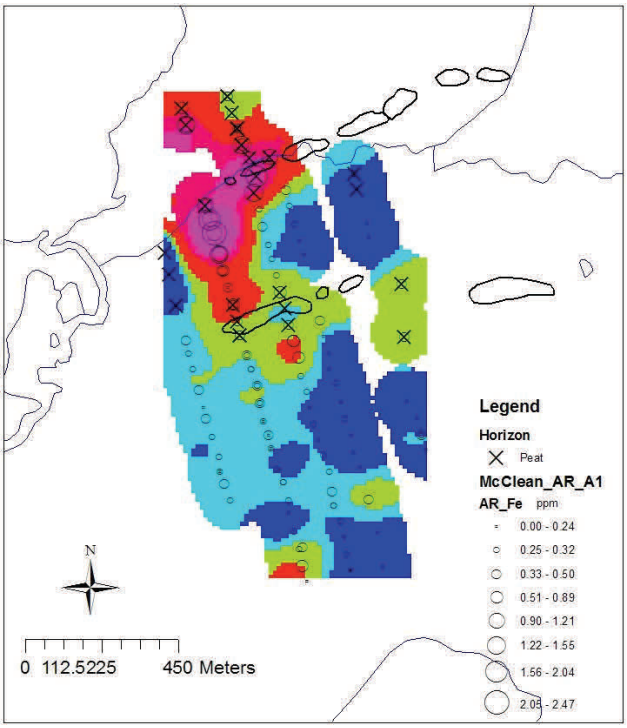

Iron. A1 horizon. Aqua regia leach.

Fig. 6.70 (continued). McClean Maps. A1. Aqua regia.

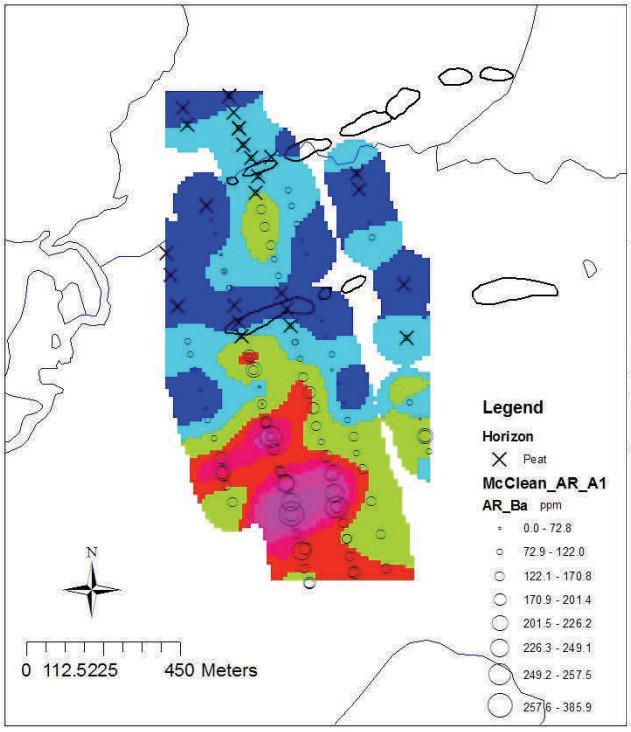

Barium. A1 horizon. Aqua regia leach.

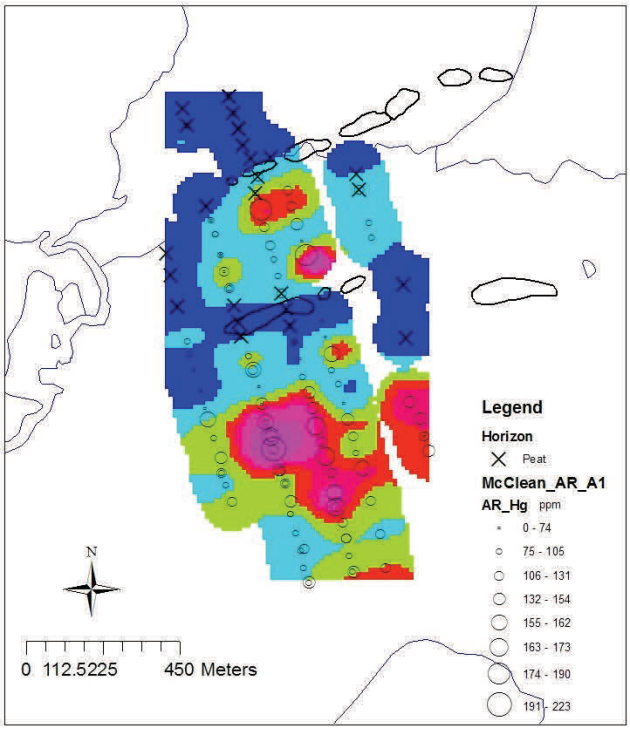

Mercury. A1 horizon. Aqua regia leach.

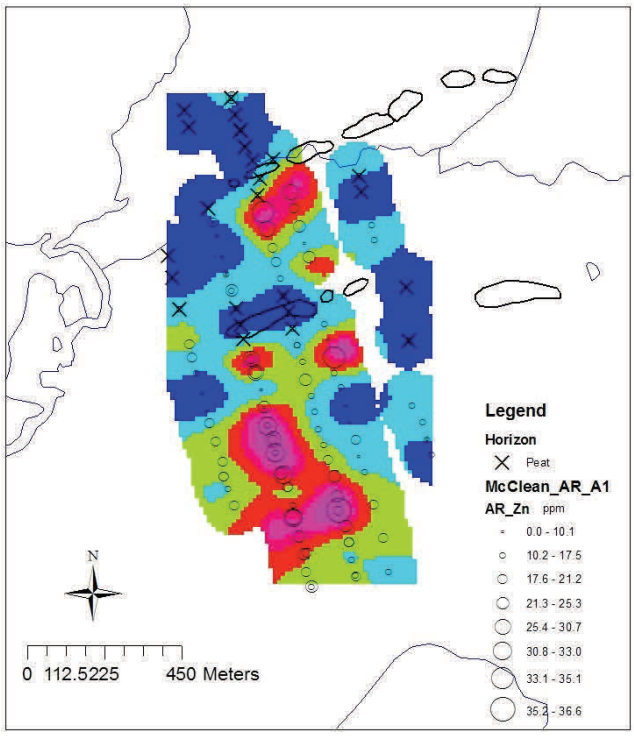

Zinc. A1 horizon. Aqua regia leach.

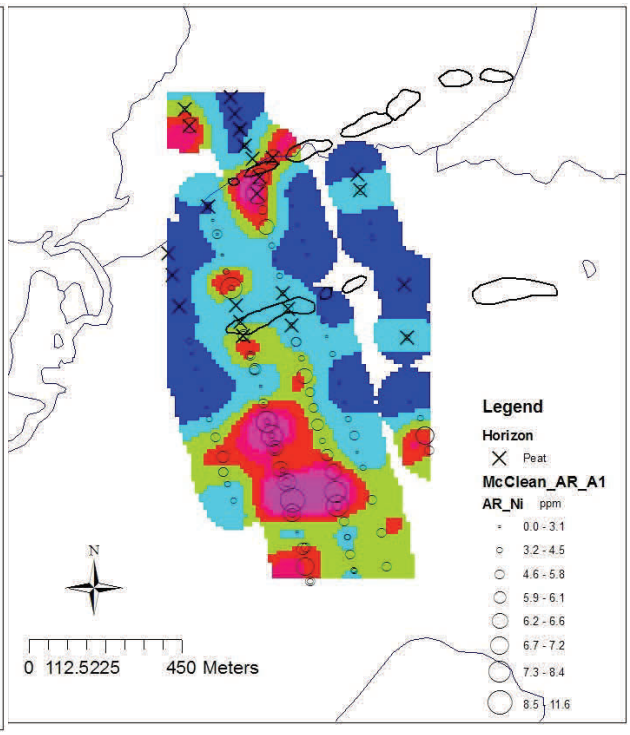

Nickel. A1 horizon. Aqua regia leach.

Fig. 6.70 (continued). McClean Maps. A1. Aqua regia.

Fig. 6.71. McClean Lake Grids. A1 horizon. Sodium pyrophosphate leach.

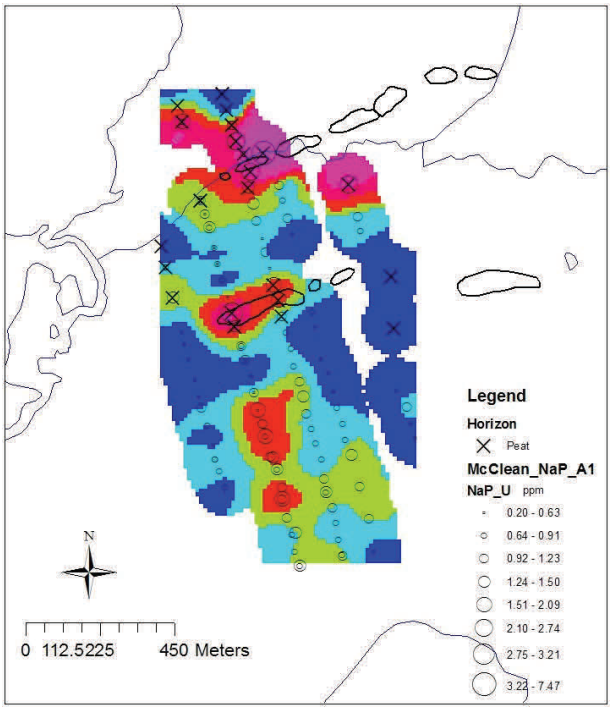

Uranium. A1 horizon. Sodium pyrophosphate leach

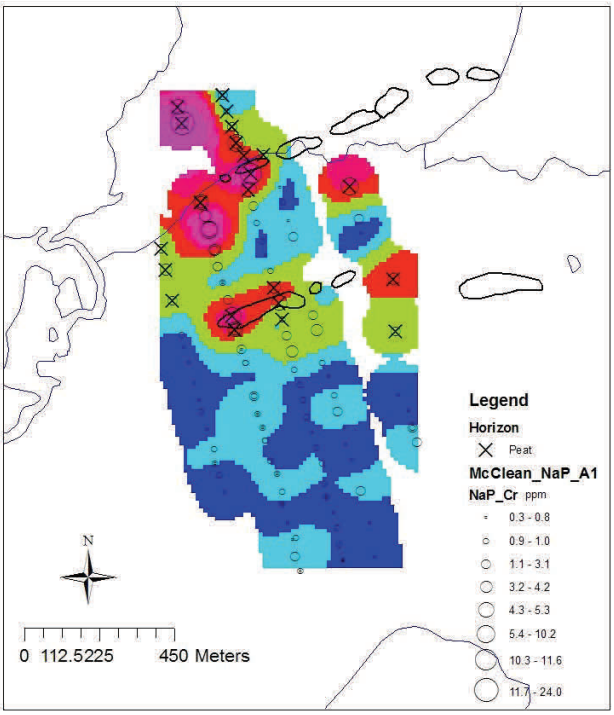

Chromium. A1 horizon. Sodium pyrophosphate leach

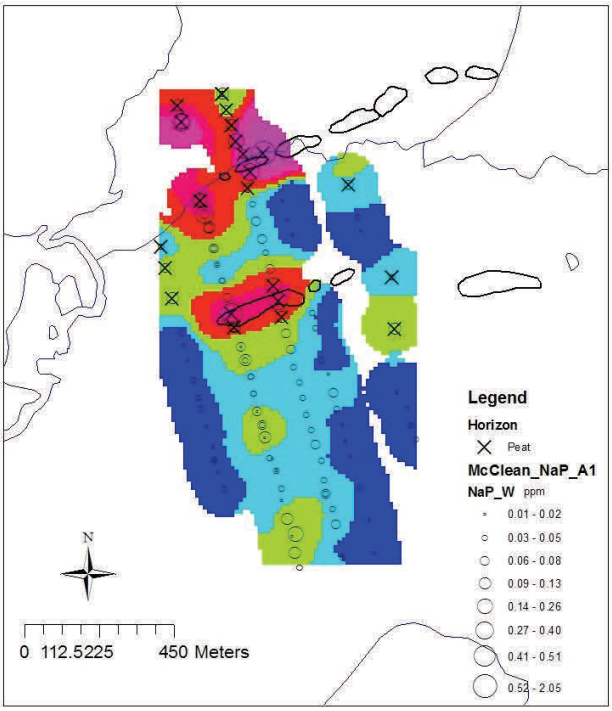

Tungsten. A1 horizon. Sodium pyrophosphate leach

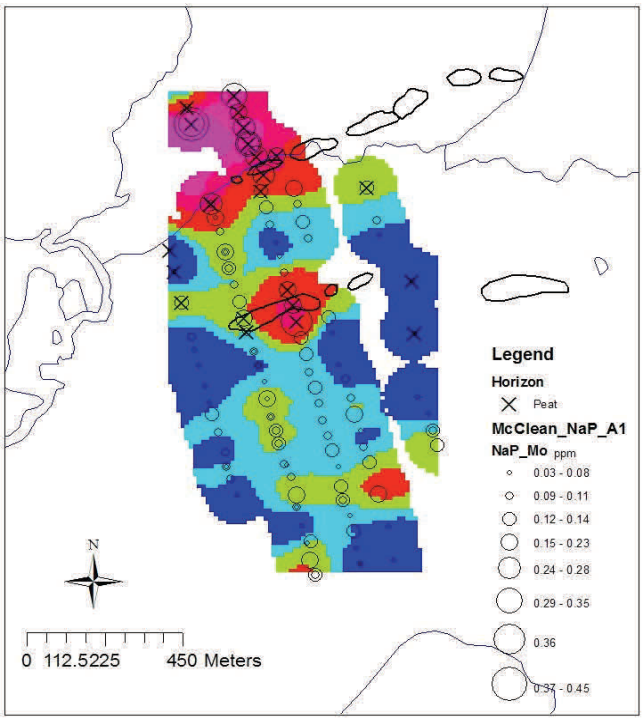

Molybdenum. A1 horizon. Sodium pyrophosphate leach

Fig. 6.72. McClean Maps. A1. Sodium pyrophosphate.

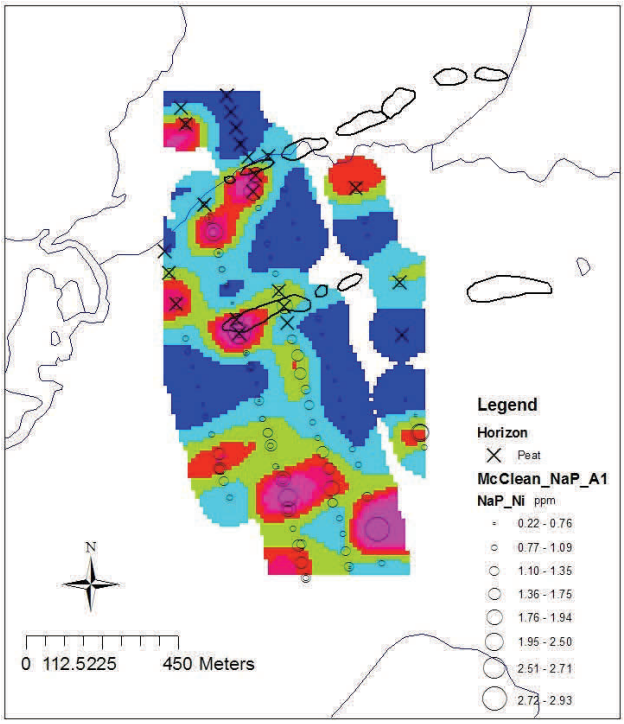

Nickel. A1 horizon. Sodium pyrophosphate leach

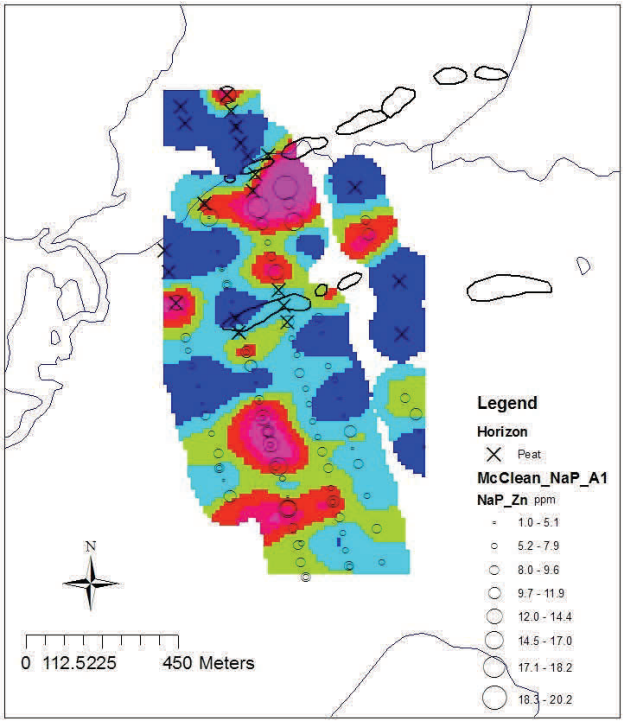

Zinc. A1 horizon. Sodium pyrophosphate leach

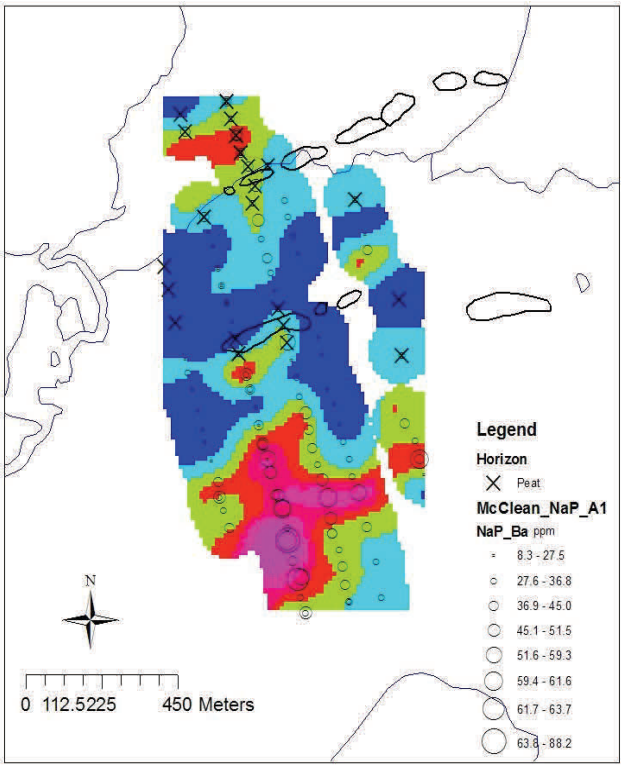

Barium. A1 horizon. Sodium pyrophosphate leach

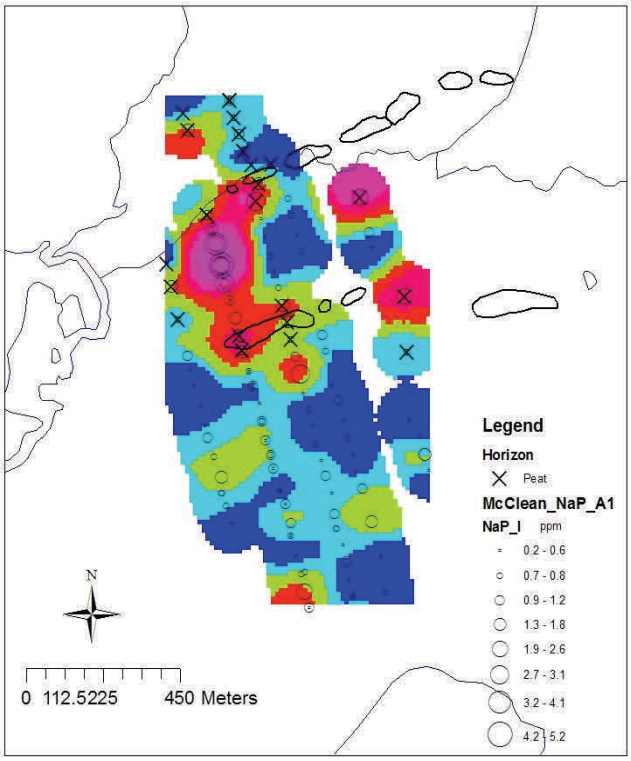

Iodine. A1 horizon. Sodium pyrophosphate leach

Fig. 6.72 (continued). McClean Maps. A1. Sodium pyrophosphate.

Fig. 6.73. McClean Lake Grids. A1 horizon. Bioleach.

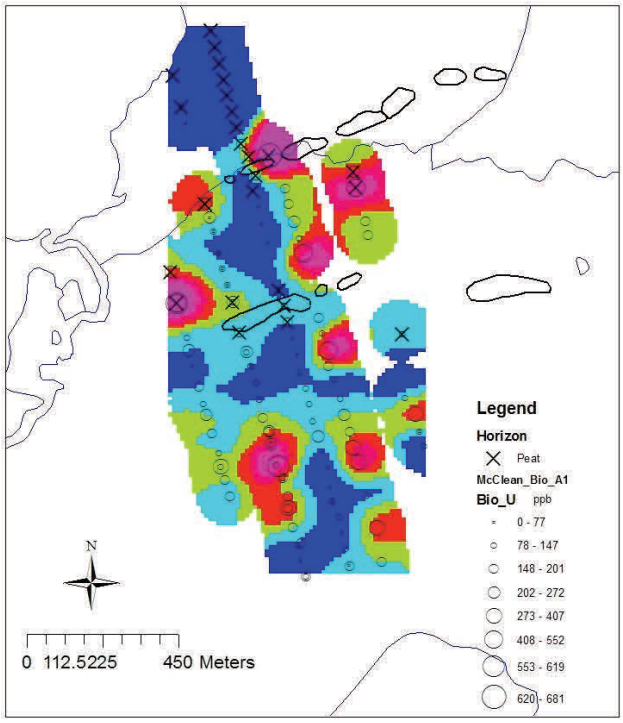

Uranium. A1. Bioleach.

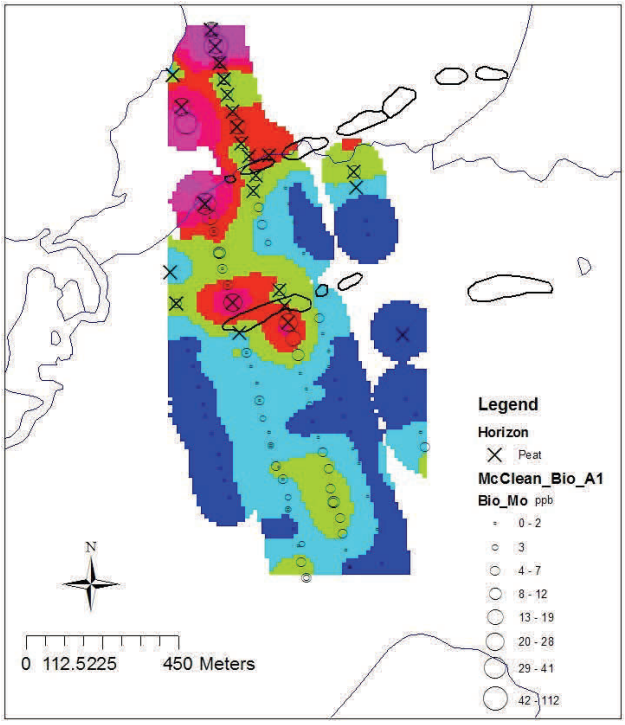

Molybdenum. A1. Bioleach.

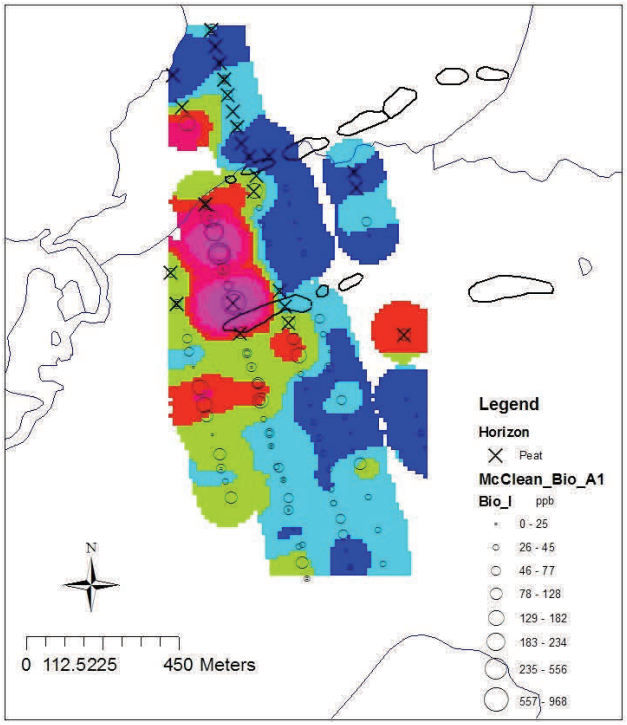

Iodine. A1. Bioleach.

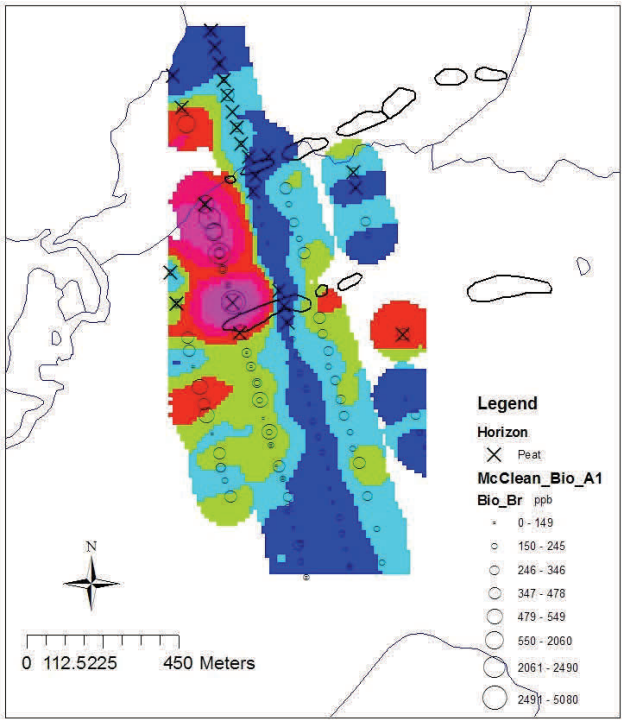

Bromine. A1. Bioleach.

Fig 6.74. McClean Maps. A1. Bioleach.

Fig. 6.75. McClean Lake Grids. A1 horizon. Hydroxylamine leach.

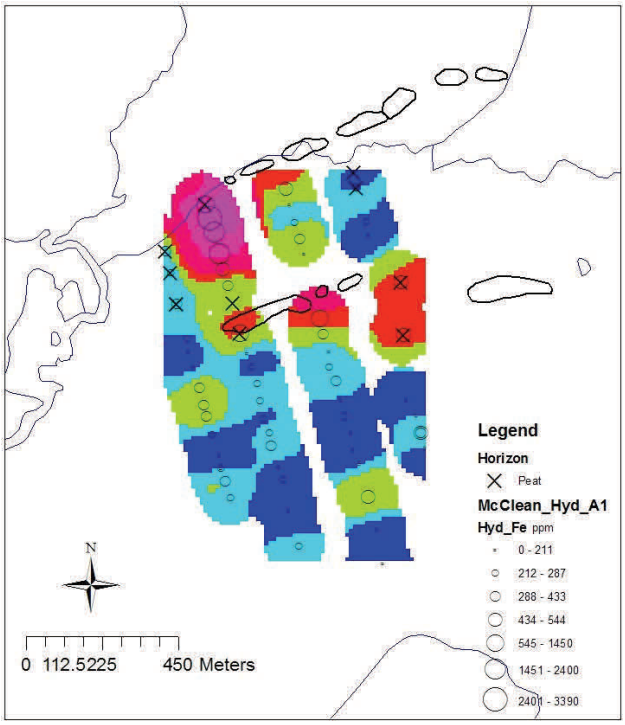

Iron. A1 horizon. Hydroxylamine leach.

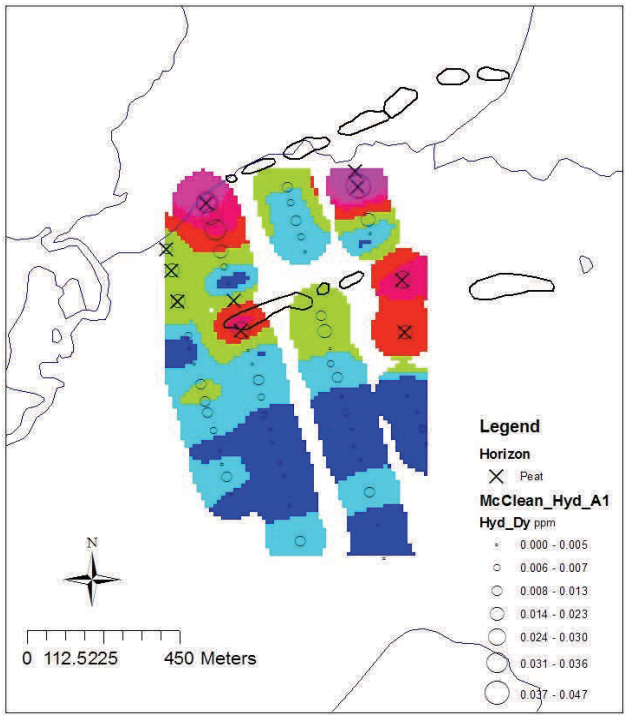

Dysprosium. A1 horizon. Hydroxylamine leach.

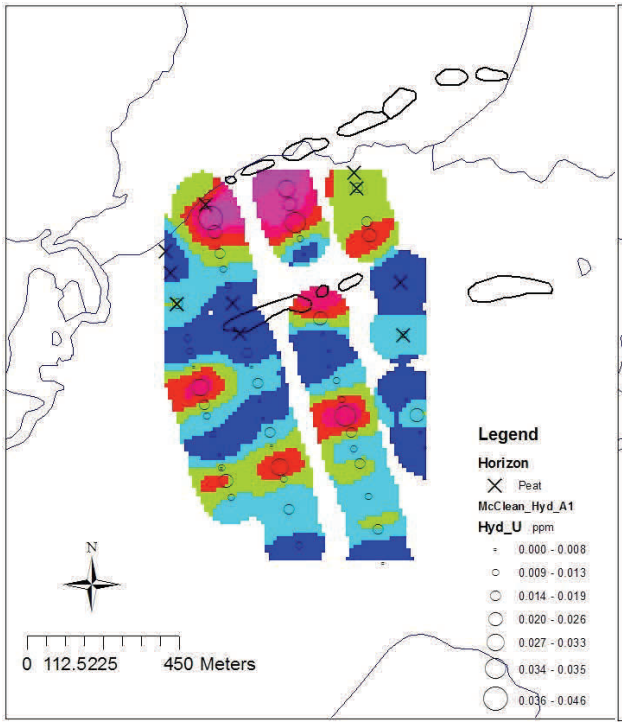

Uranium. A1 horizon. Hydroxylamine leach.

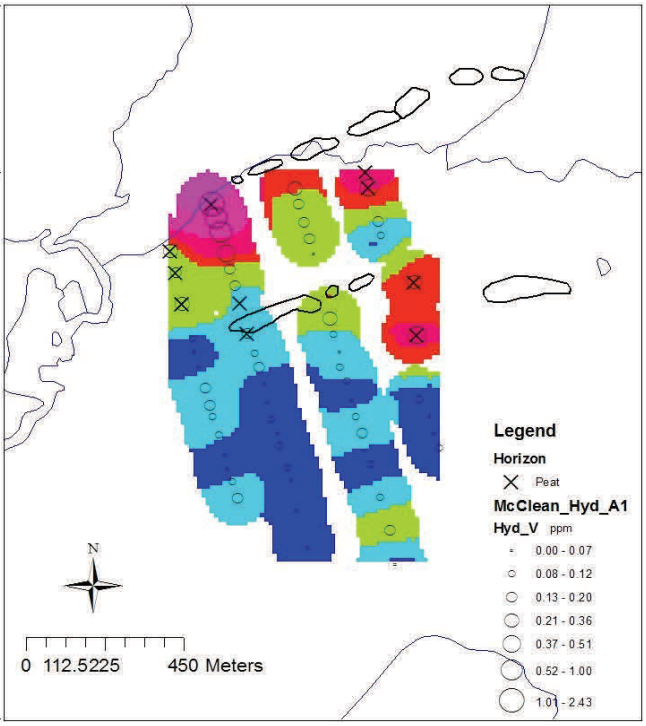

Vanadium. A1 horizon. Hydroxylamine leach.

Fig. 6.76. McClean Maps. A1. Hydroxylamine.

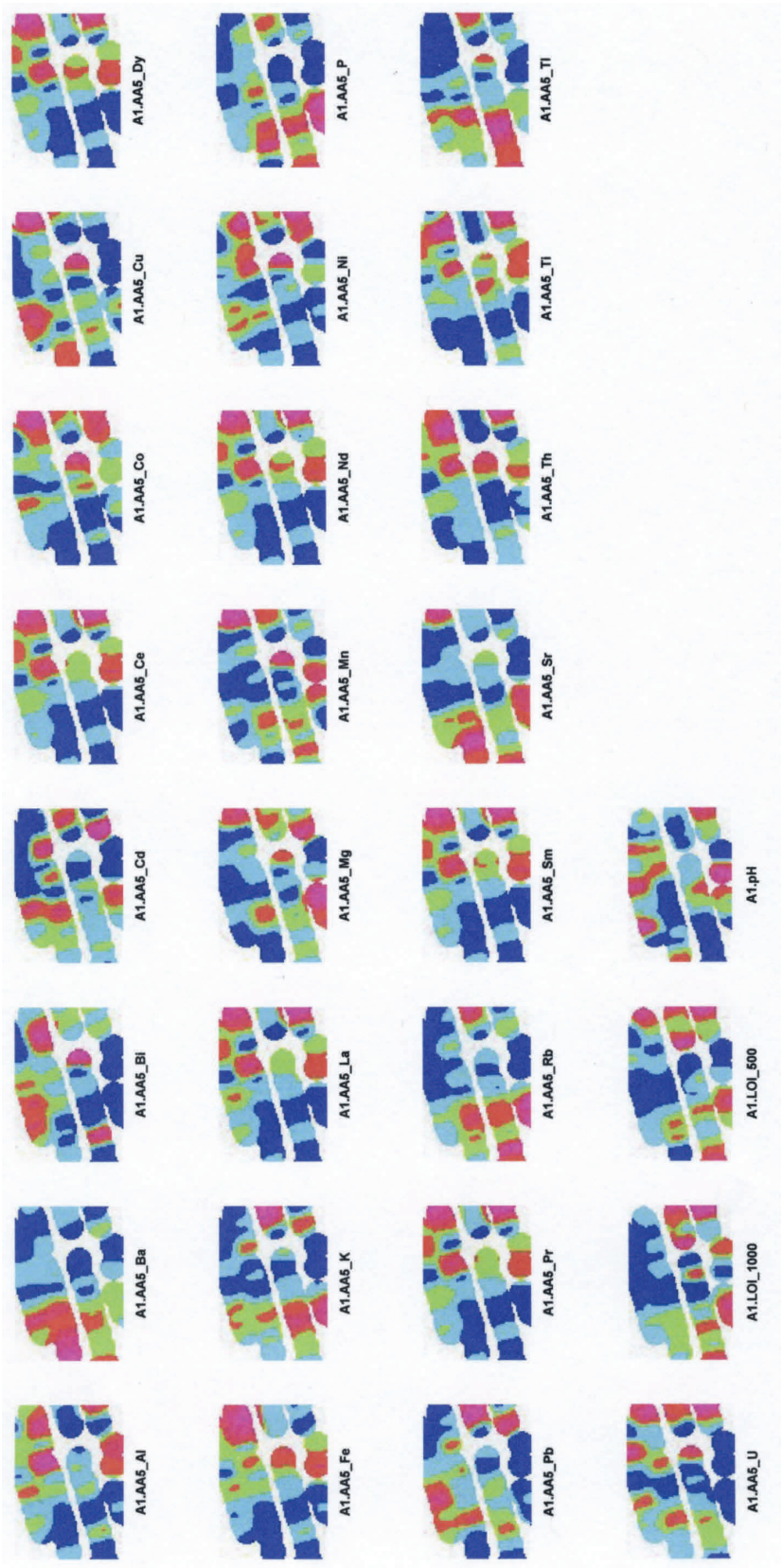

Fig. 6.77. McClean Lake Grids.. A1 horizon. Ammonium acetate leach.

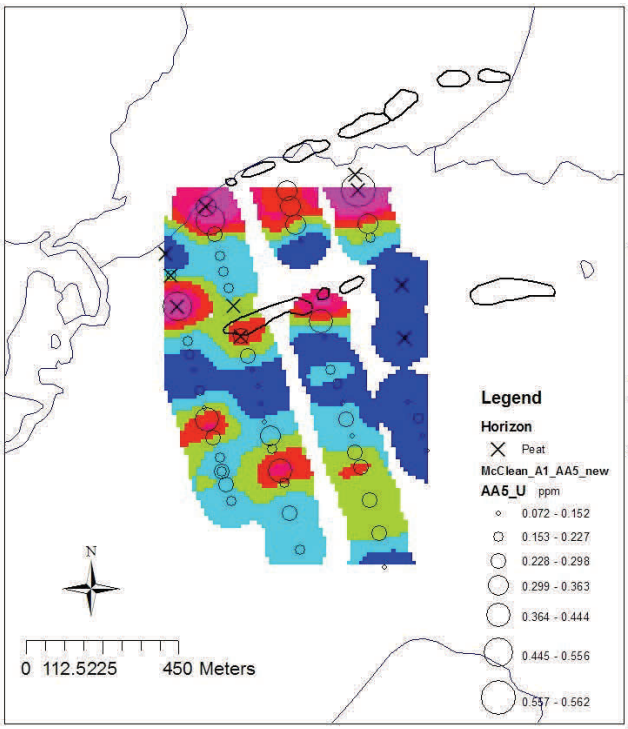

Uranium. A1 horizon. Ammonium acetate leach.

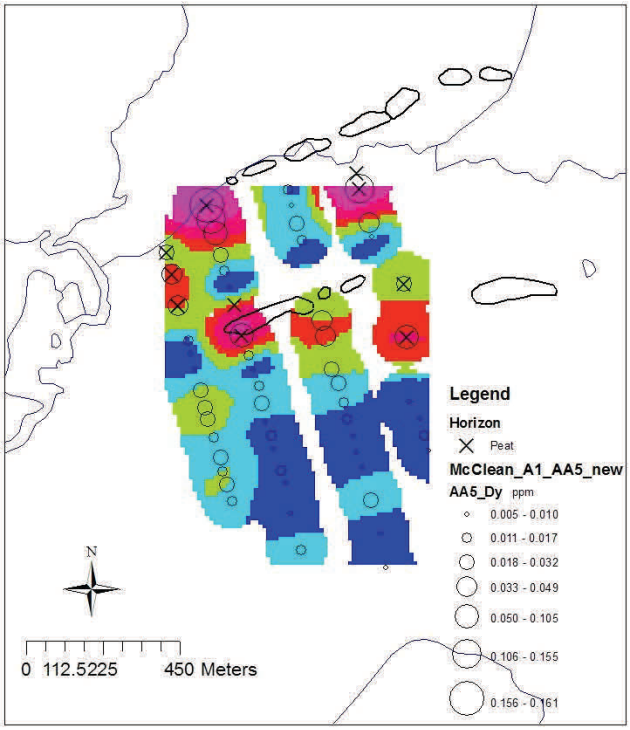

Dysprosium. A1 horizon. Ammonium acetate leach.

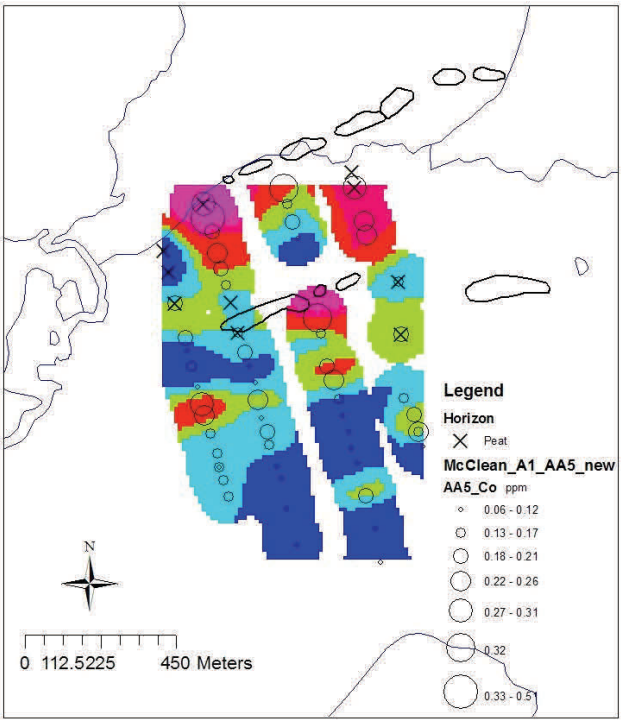

Cobalt. A1 horizon. Ammonium acetate leach.

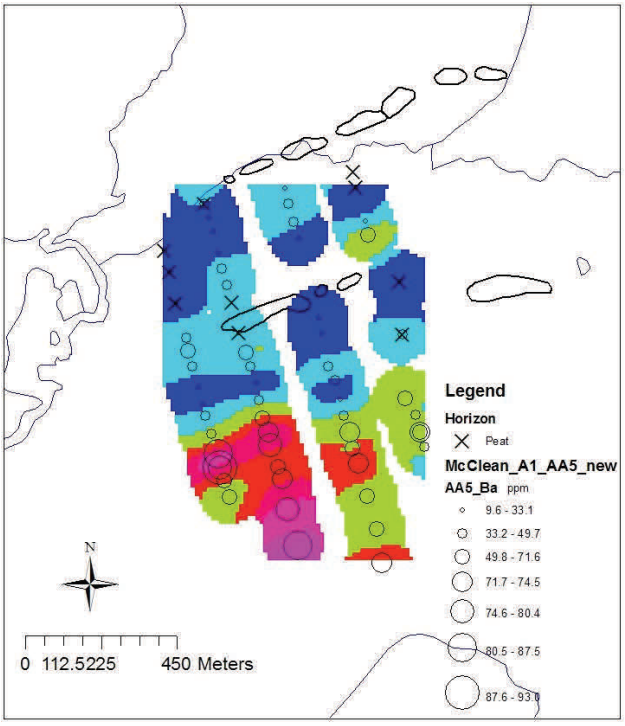

Barium. A1 horizon. Ammonium acetate leach.

Fig. 6..78. McClean Maps. A1. Hydroxylamine

Fig. 6.79. McClean Lake Grids. A1 horizon. MMI leach.

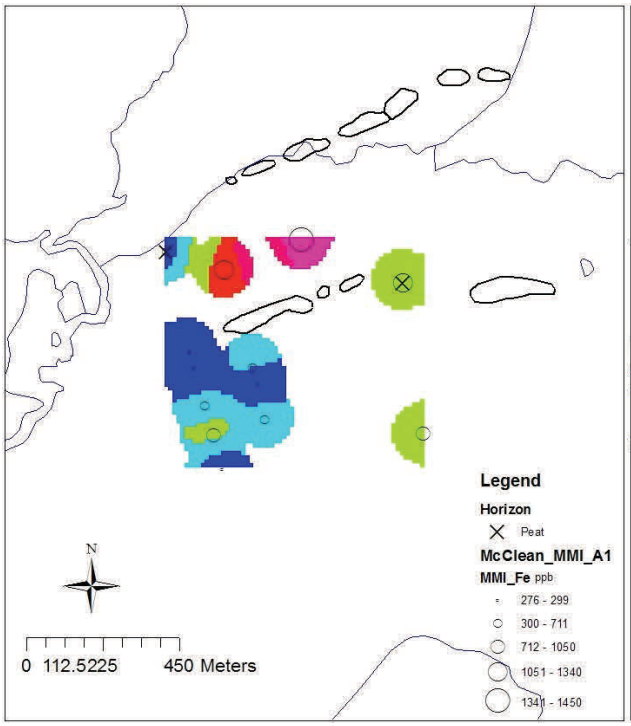

Iron. A1 horizon. MMI leach.

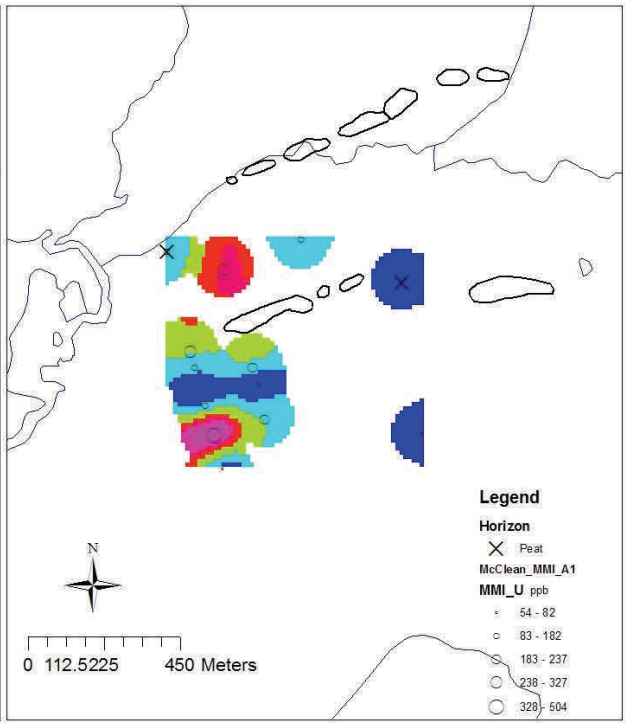

Uranium. A1 horizon. MMI leach.

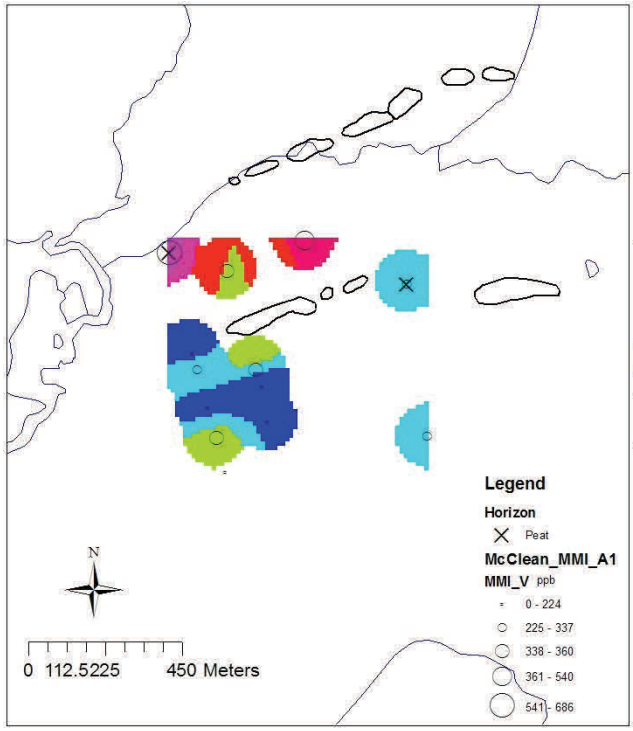

Vanadium. A1 horizon. MMI leach.

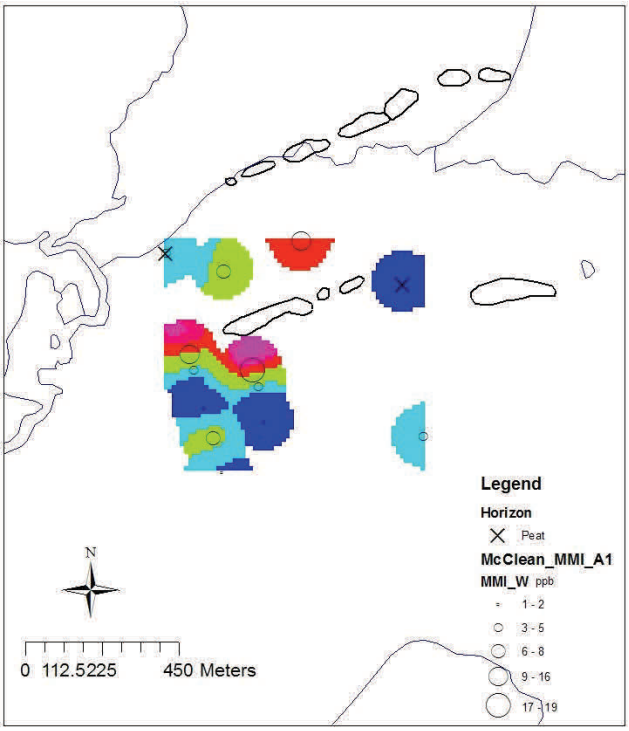

Tungsten. A1 horizon. MMI leach.

Fig. 6.80. McClean Maps. A1. MMI.

Fig. ^.81. McClean Lake Grids. A2 horizon. Aqua regia leach.

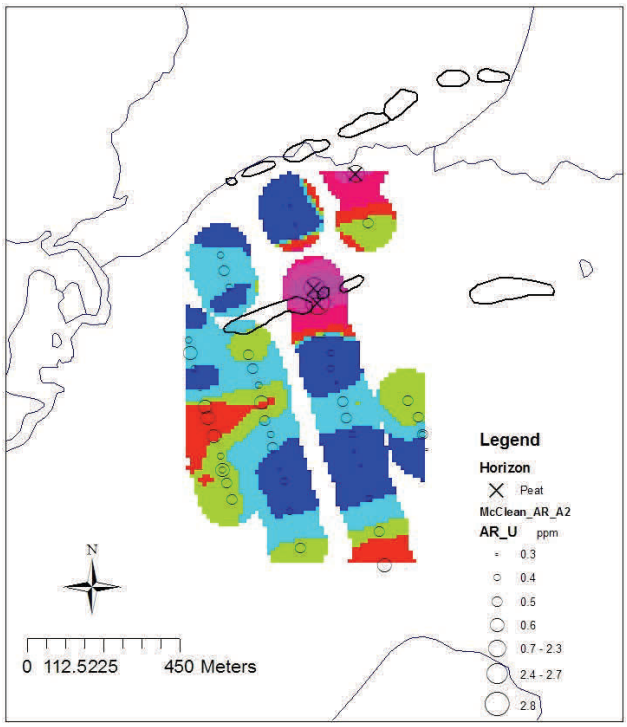

Uranium. A2 horizon. Aqua regia leach.

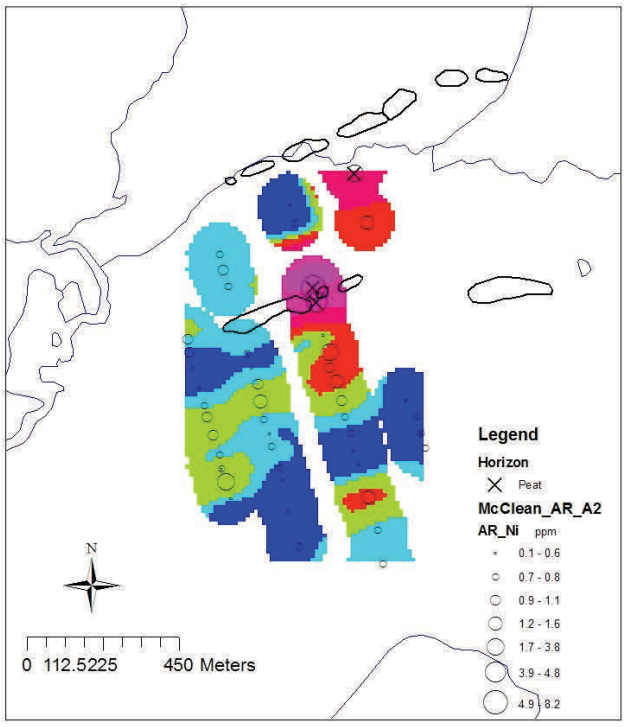

Nickel. A2 horizon. Aqua regia leach.

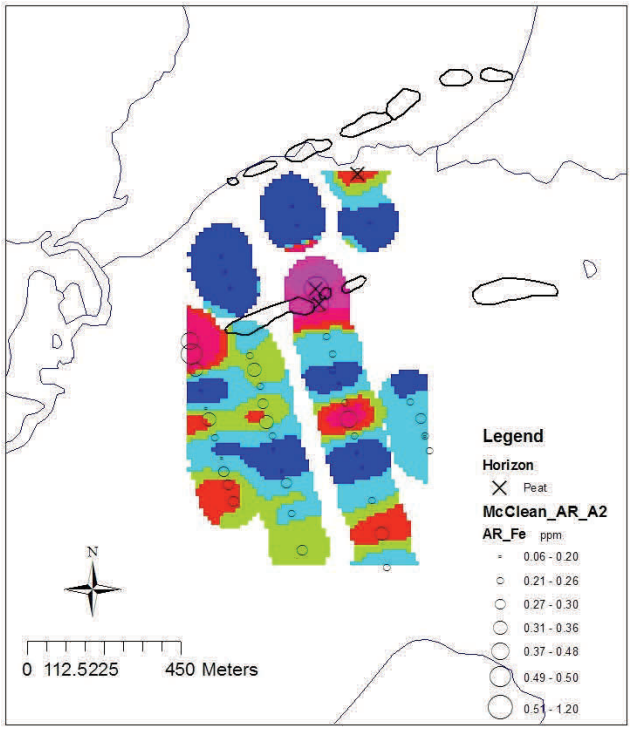

Iron. A2 horizon. Aqua regia leach.

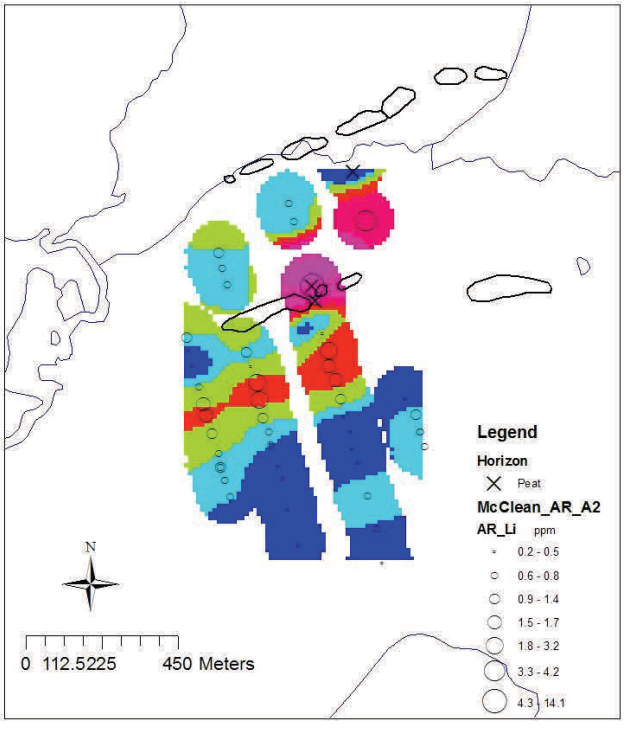

Lithium. A2 horizon. Aqua regia leach.

Fig. 6.82. McClean Maps. A2. Aqua regia.

Fig. 6.83. McClean Lake Grids. A2 horizon. Hydroxylamine leach.

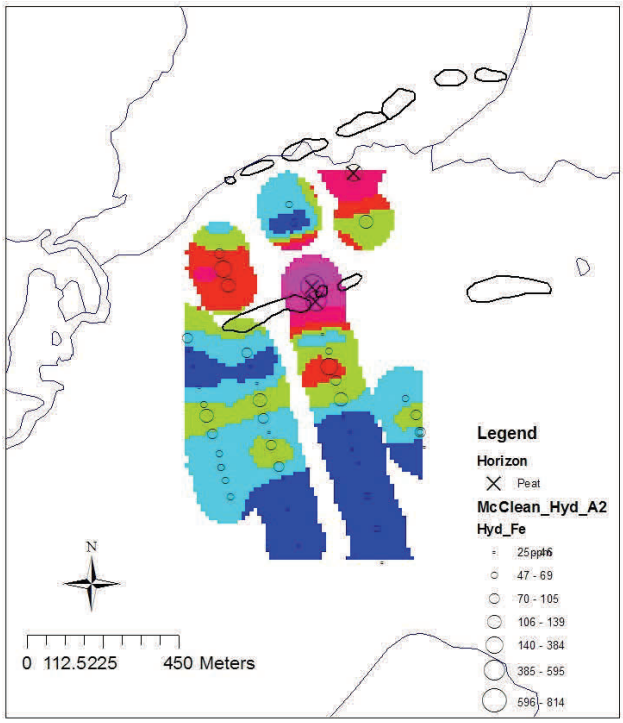

Iron. A2 horizon. Hydroxylamine leach.

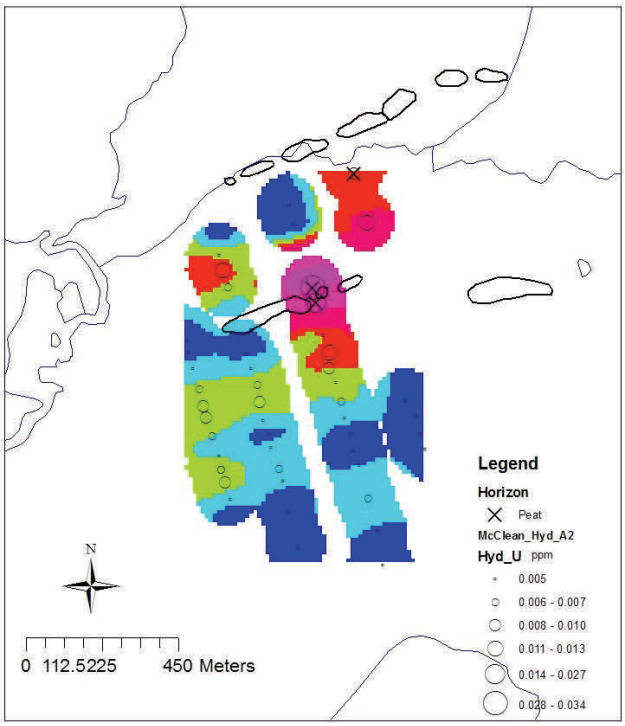

Uranium. A2 horizon. Hydroxylamine leach.

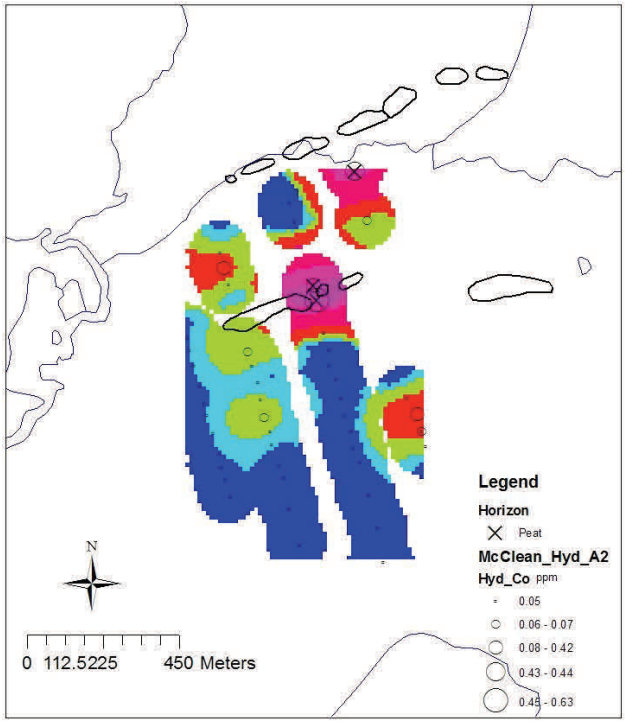

Cobalt. A2 horizon. Hydroxylamine leach.

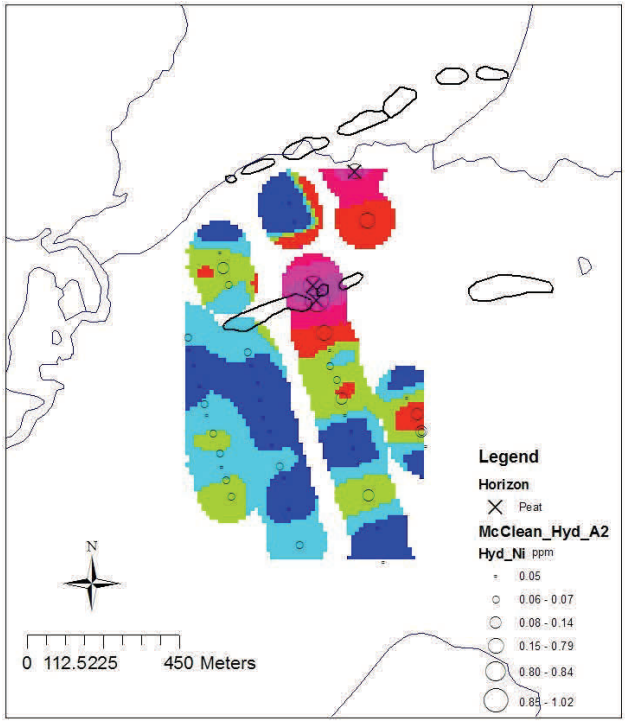

Nickel. A2 horizon. Hydroxylamine leach.

Fig. 6.84. McClean Maps. A2. Hydroxylamine.

Fig. 6.85. McClean Lake Grids. A2 horizon. Ammonium acetate

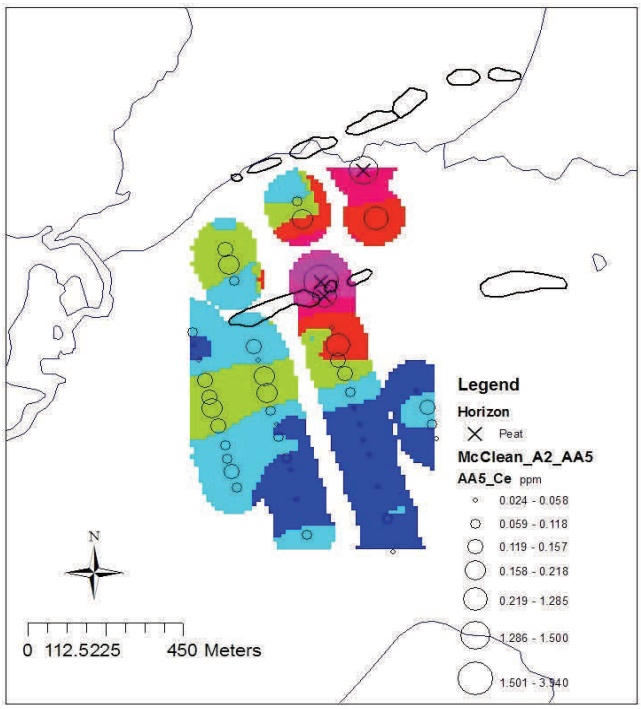

Cerium. A2 horizon. Ammonium acetate

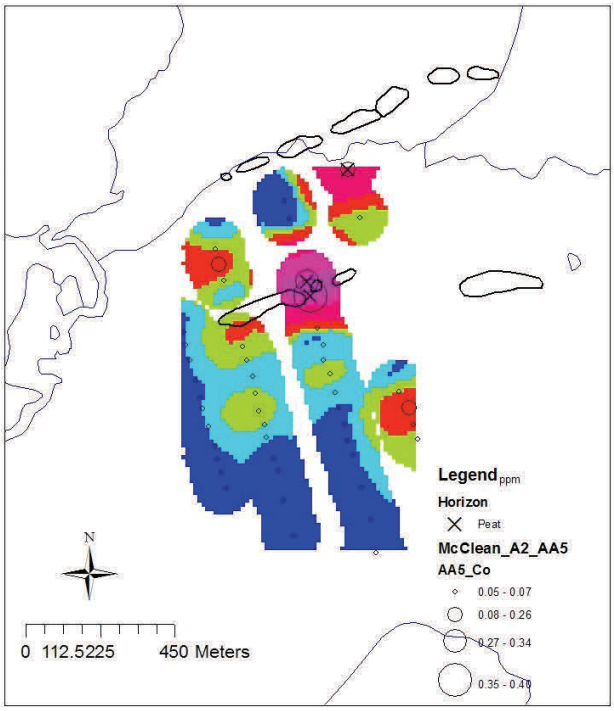

Cobalt. A2 horizon. Ammonium acetate

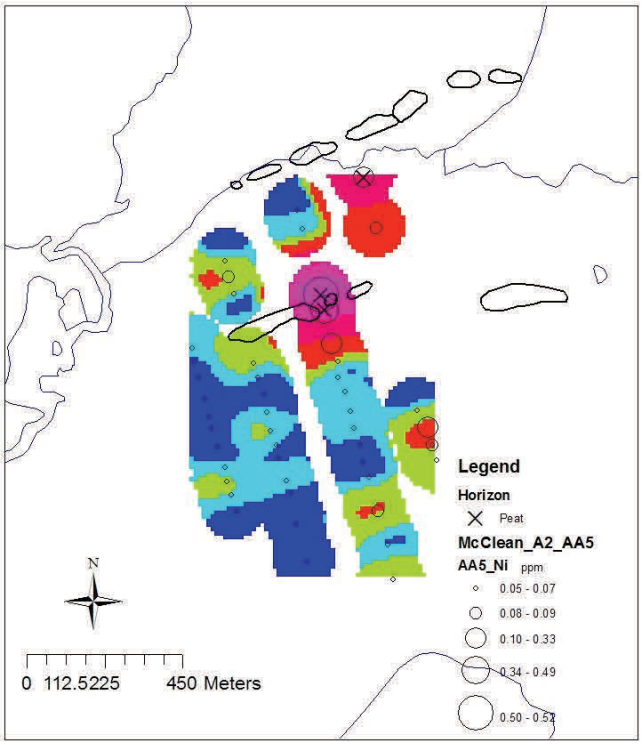

Nickel. A2 horizon. Ammonium acetate

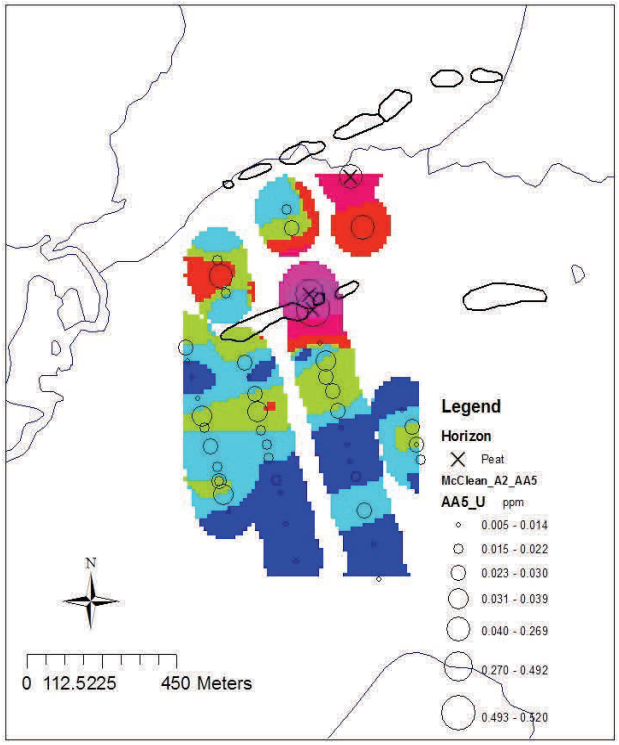

Uranium. A2 horizon. Ammonium acetate

Fig. 6.86. McClean Maps. A2. Ammonium acetate

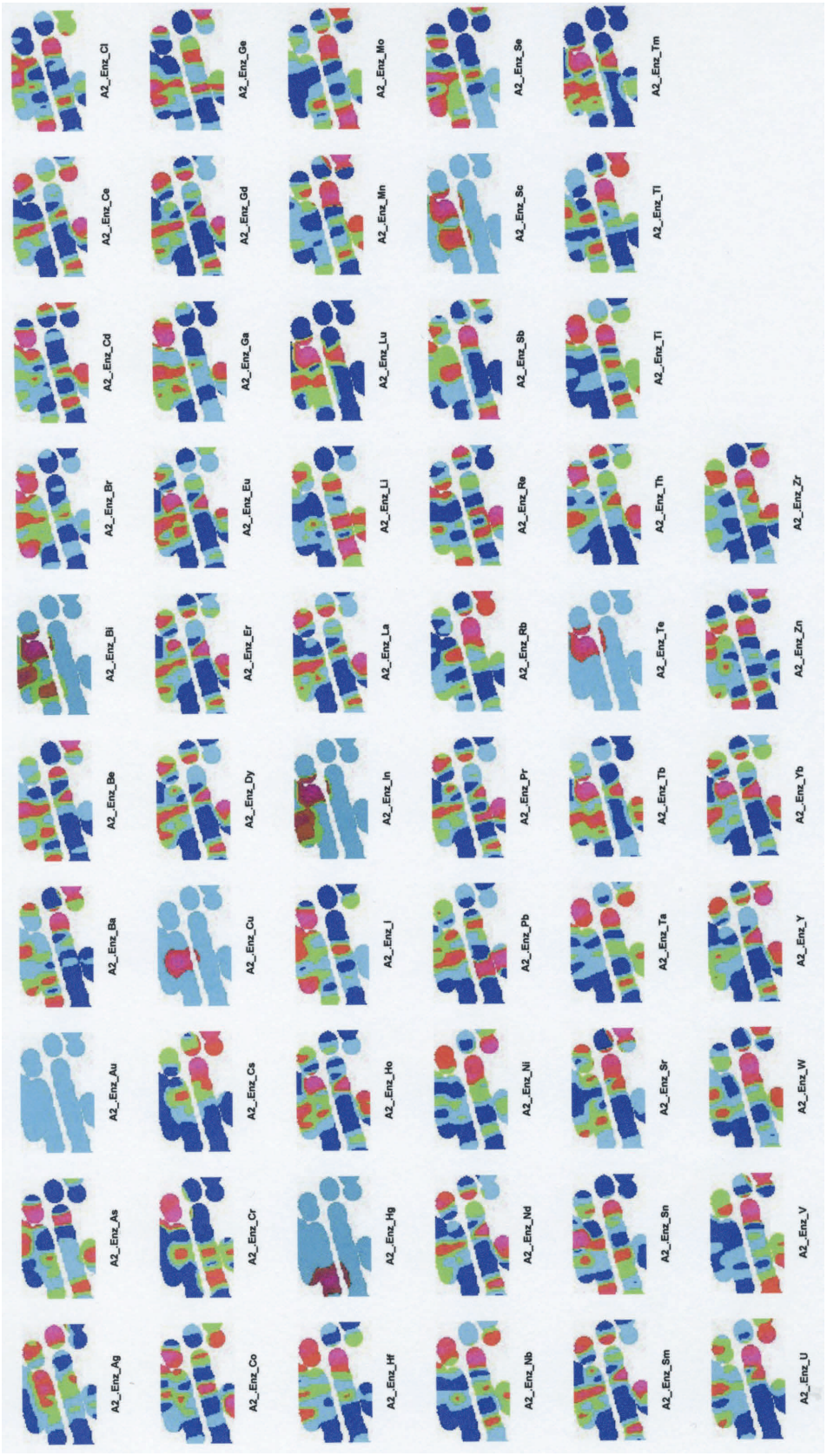

Fig. 6.87. McClean Lake Grids. A2 horizon. Enzyme leach.

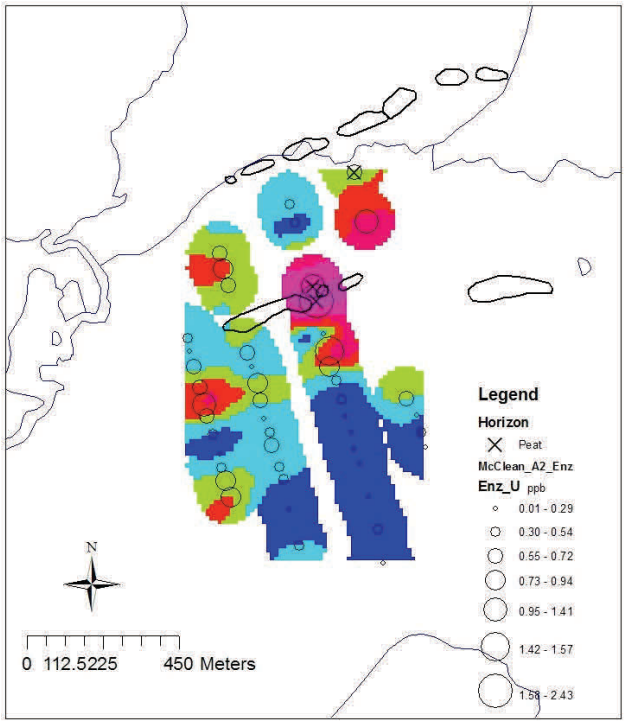

Uranium. A2 horizon. Enzyme leach.

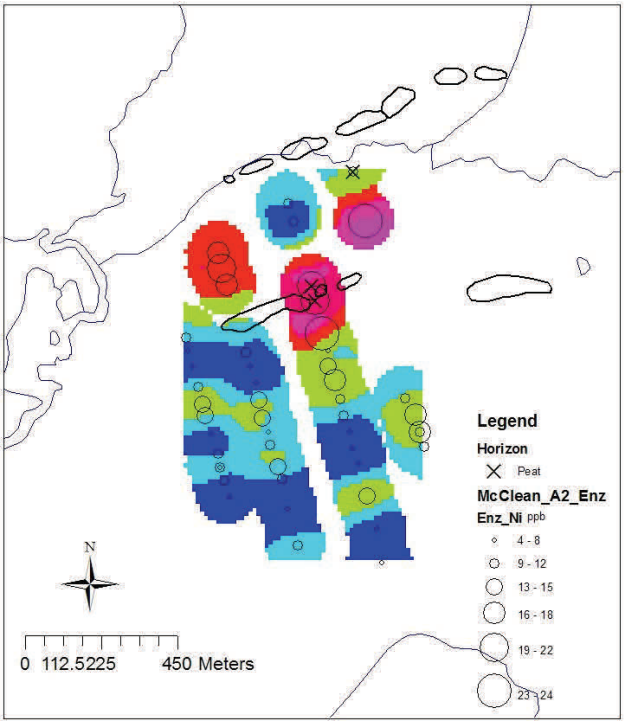

Nickel. A2 horizon. Enzyme leach.

Fig. 6.88. McClean Lake Maps. A2. Enzyme.

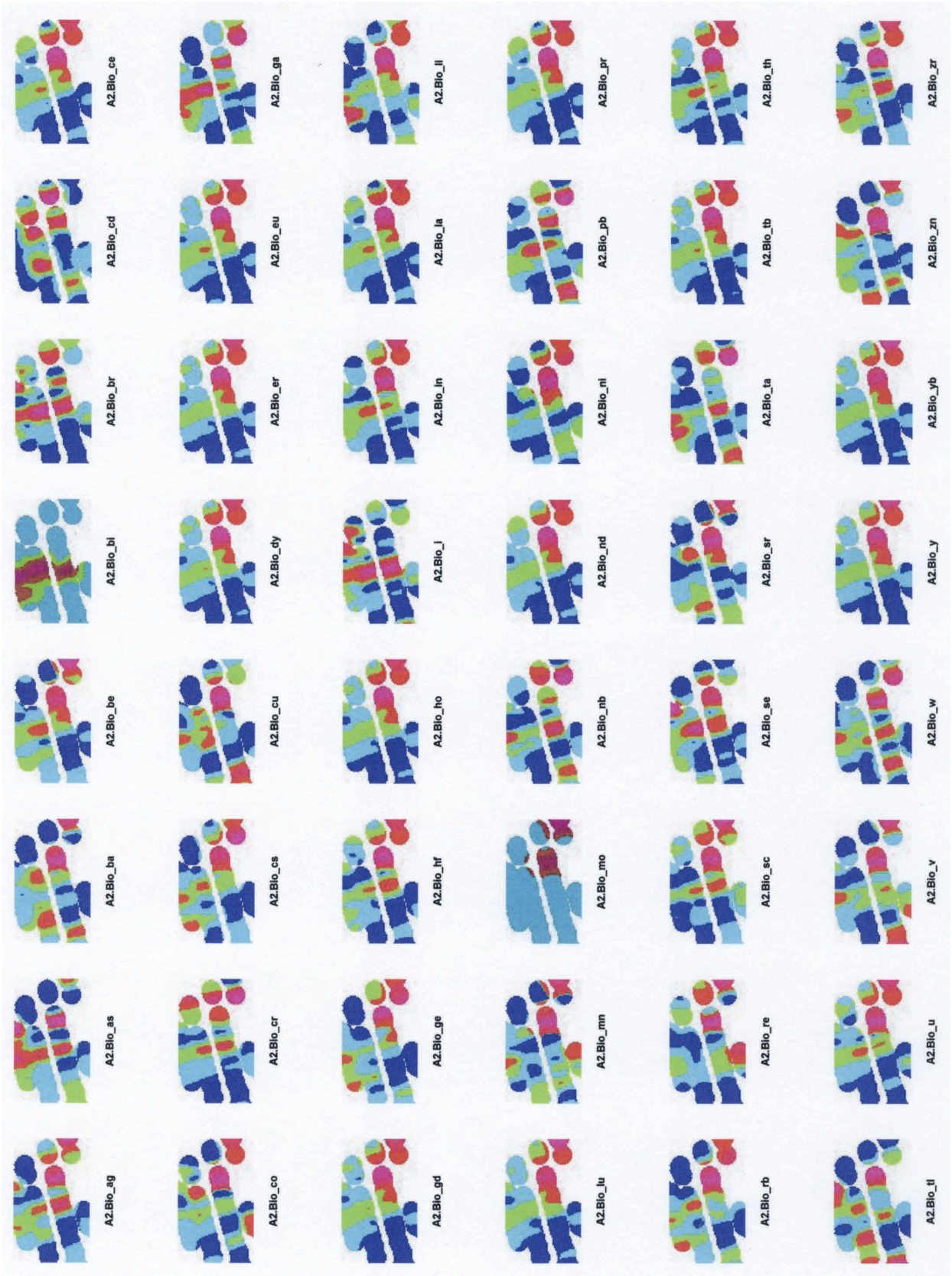

Fig. 8.89. McClean Lake Grids. A2 horizon. Bioleach.

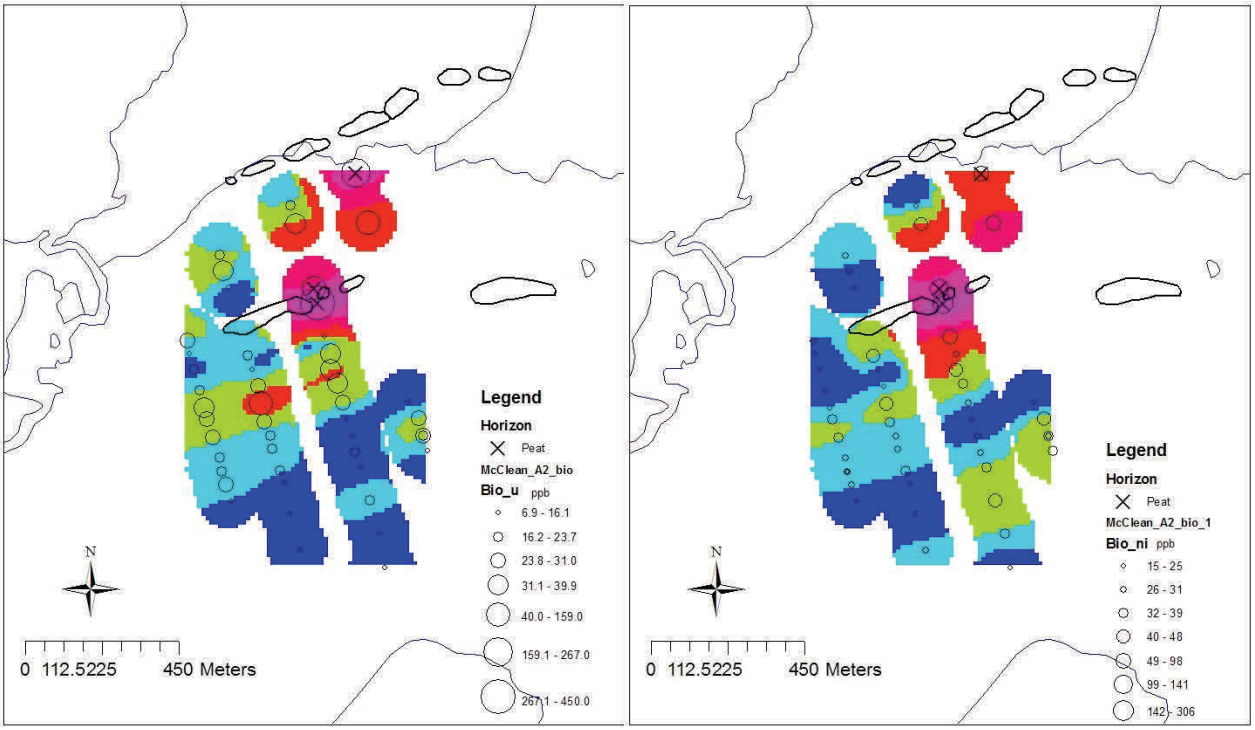

Uranium. A2 horizon. Bioleach.

Nickel. A2 horizon. Bioleach.

Fig. 6.90. McClean Maps. A2. Bioleach.

Fig. 6.91. McClean Lake Grids. A2 horizon. MMI leach.

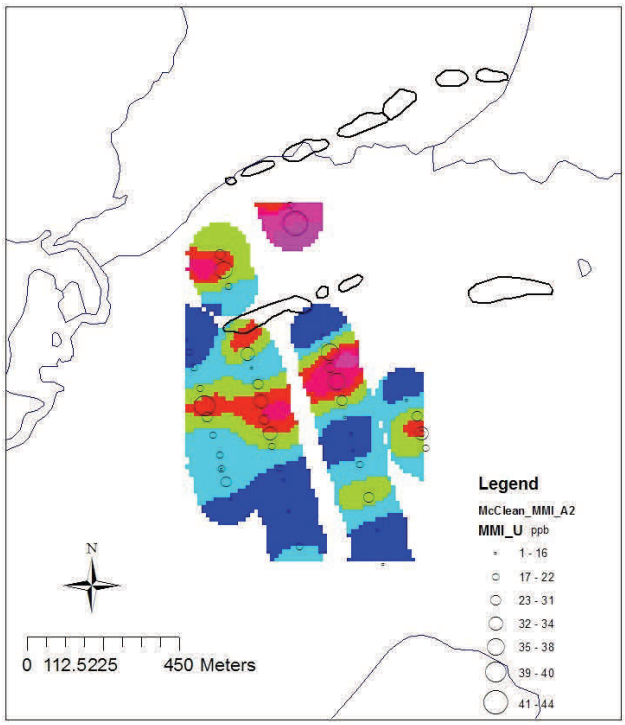

Uranium. A2 horizon. MMI leach.

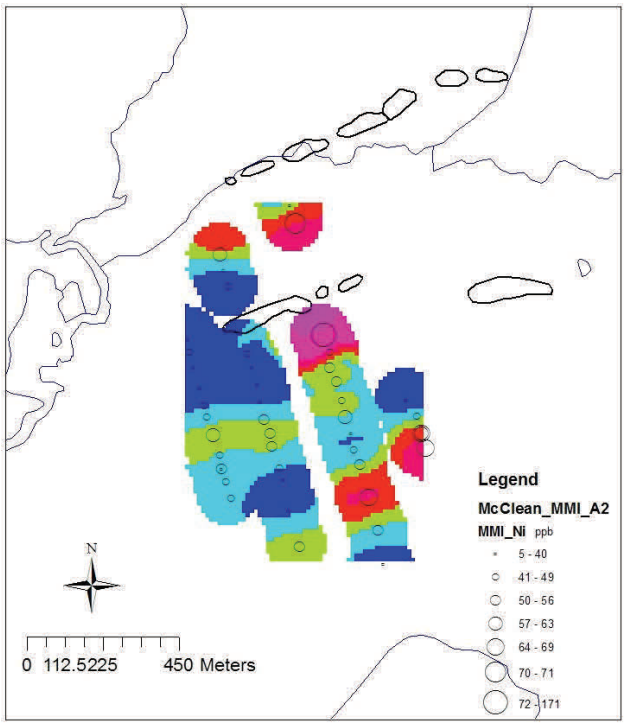

Nickel. A2 horizon. MMI leach.

Fig. 6.92. McClean Maps. A2. MMI.

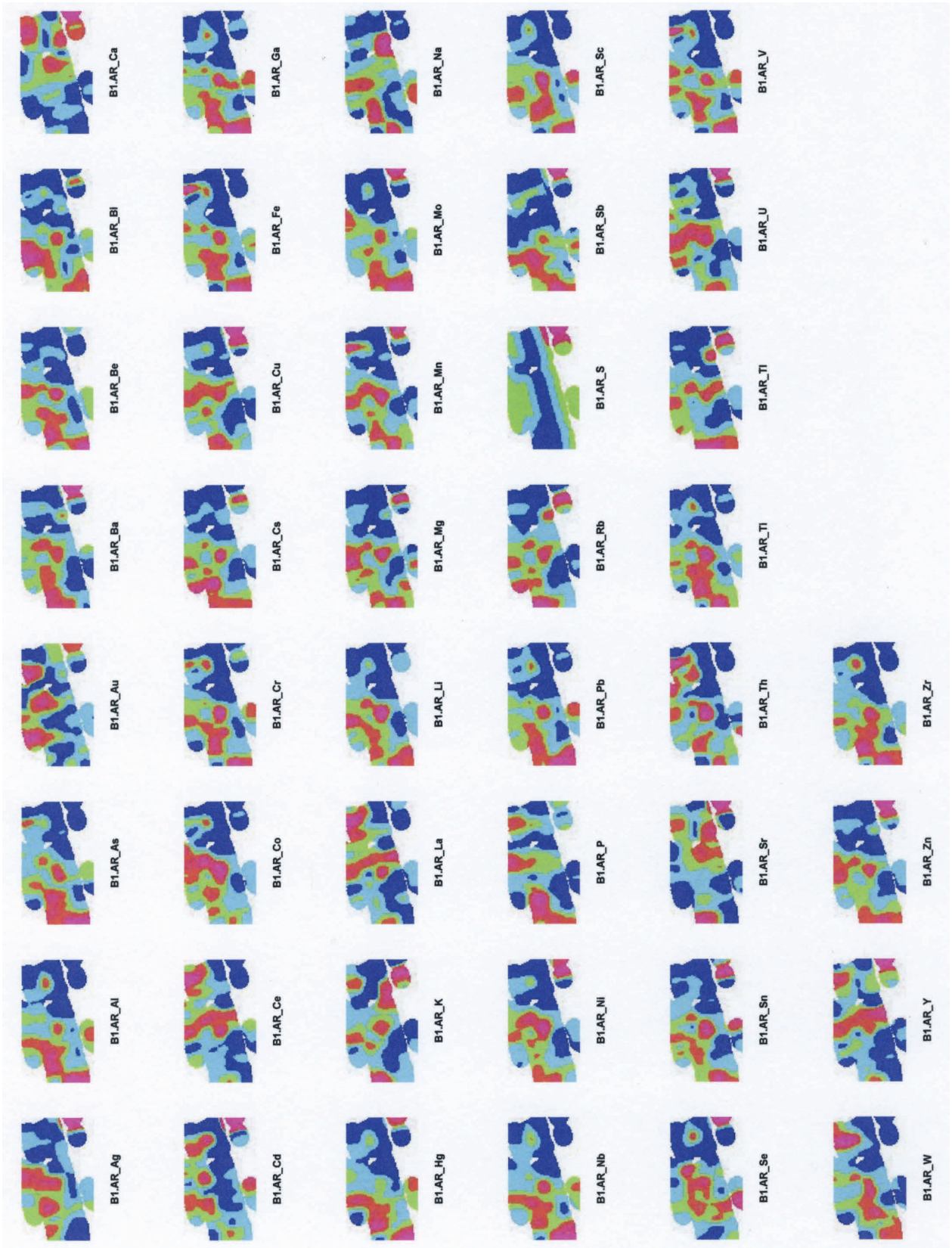

Fig. 6.93. McClean Lake Grids. B1 horizon. Aqua regia leach.

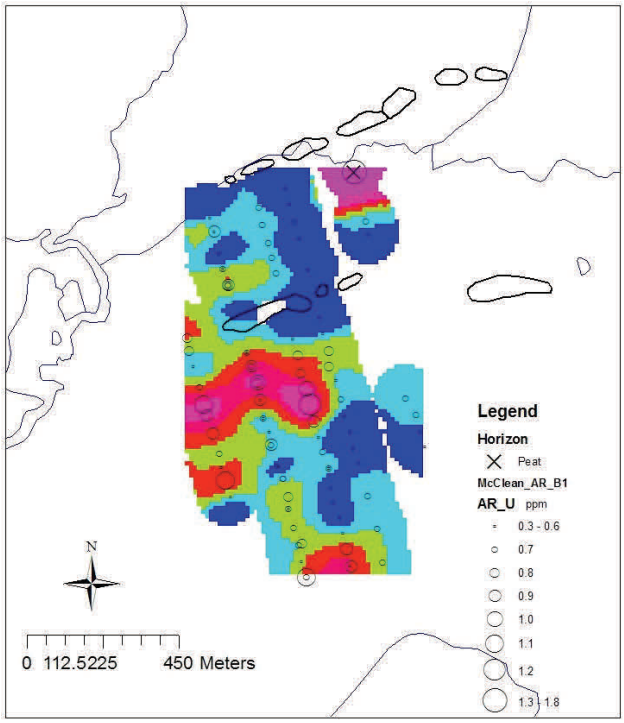

Uranium. B1 horizon. Aqua regia.

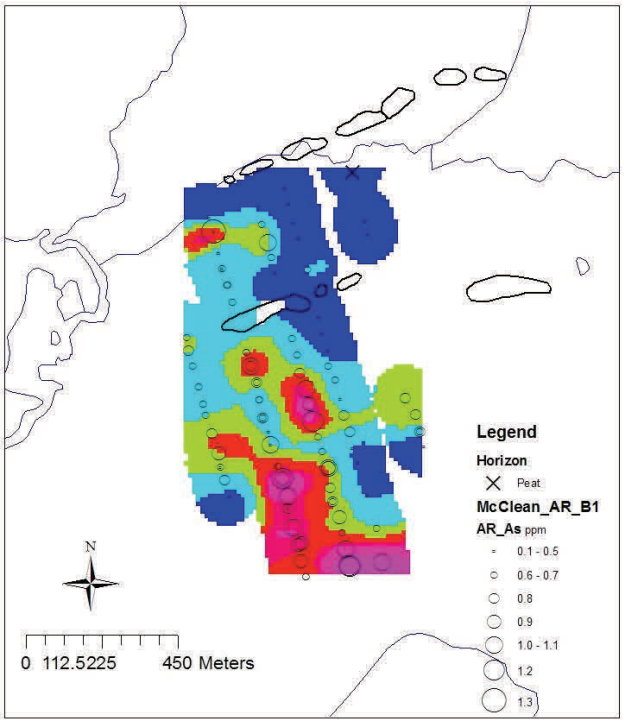

Arsenic. B1 horizon. Aqua regia.

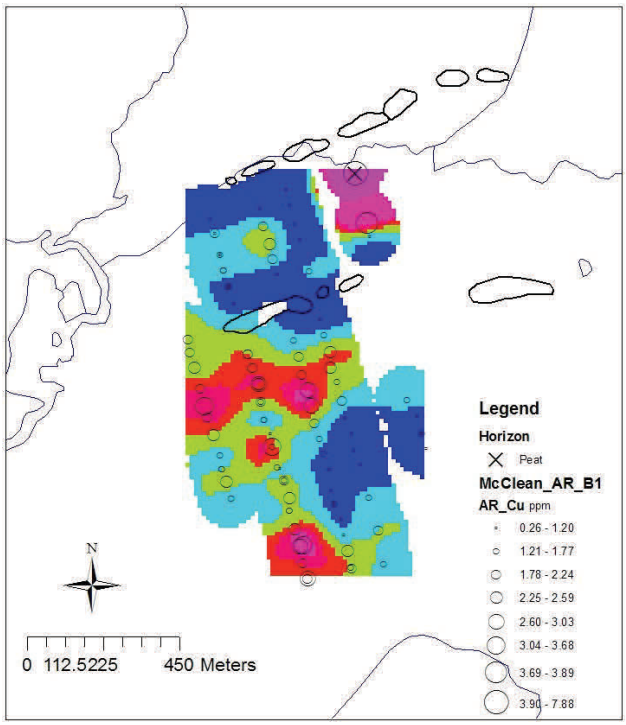

Copper. B1 horizon. Aqua regia.

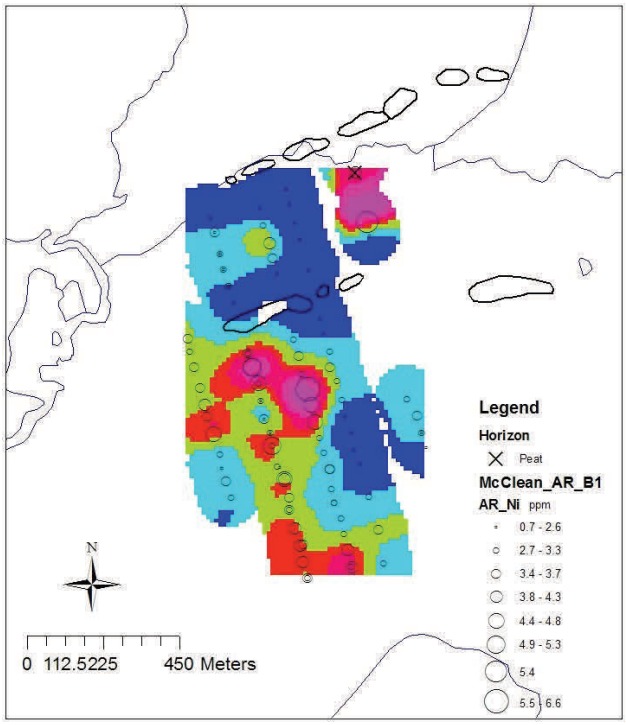

Nickel. B1 horizon. Aqua regia.

Fig. 6.94. McClean Maps. B1. Aqua regia

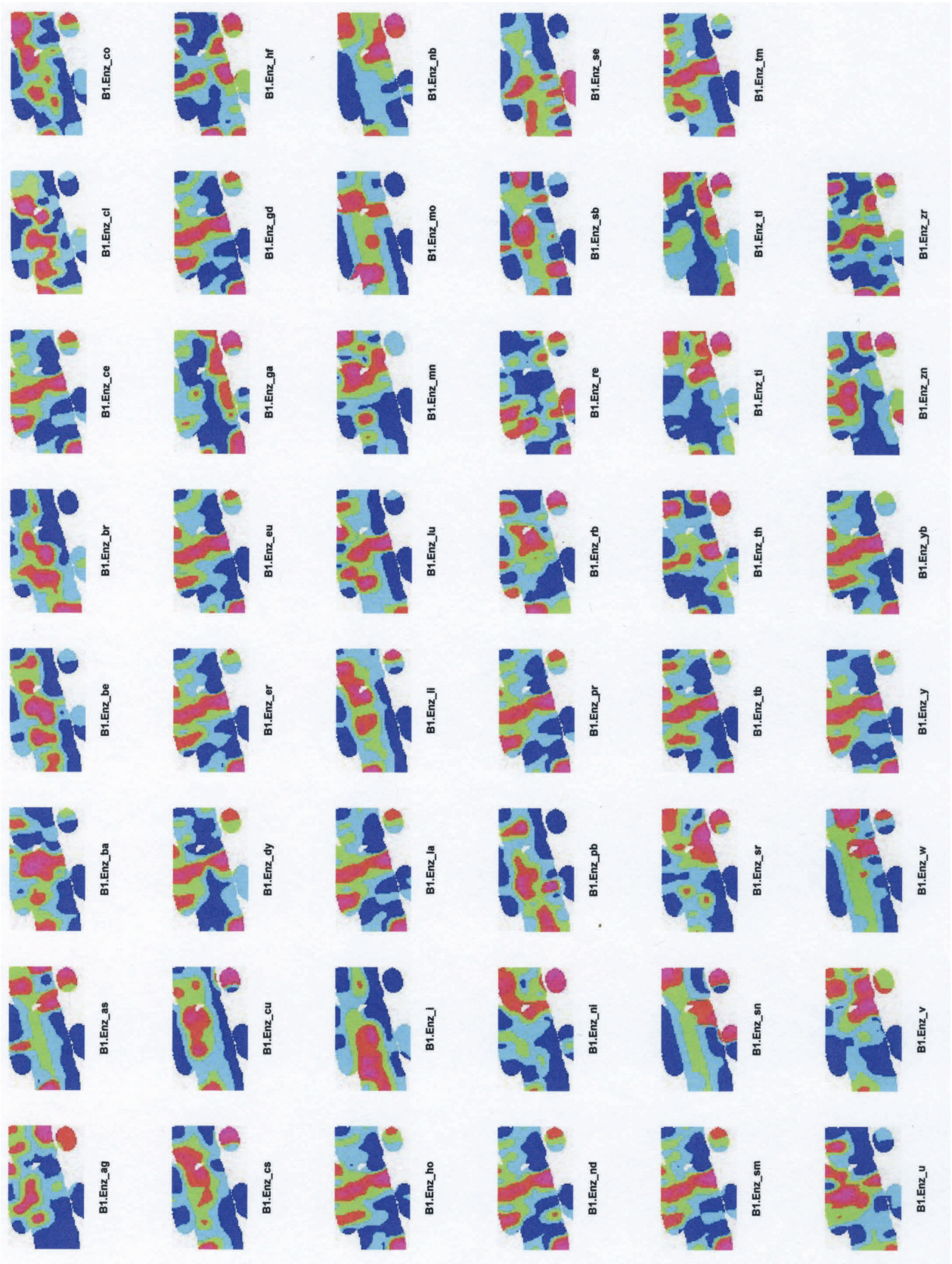

Fig. 6.95. McClean Lake Grids. B1 horizon. Enzyme leach.

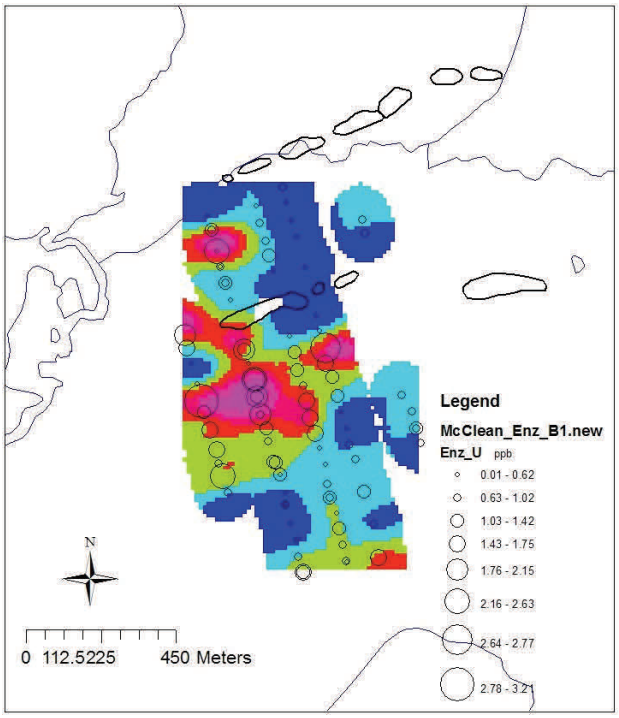

Uranium. B1 horizon. Enzyme leach.

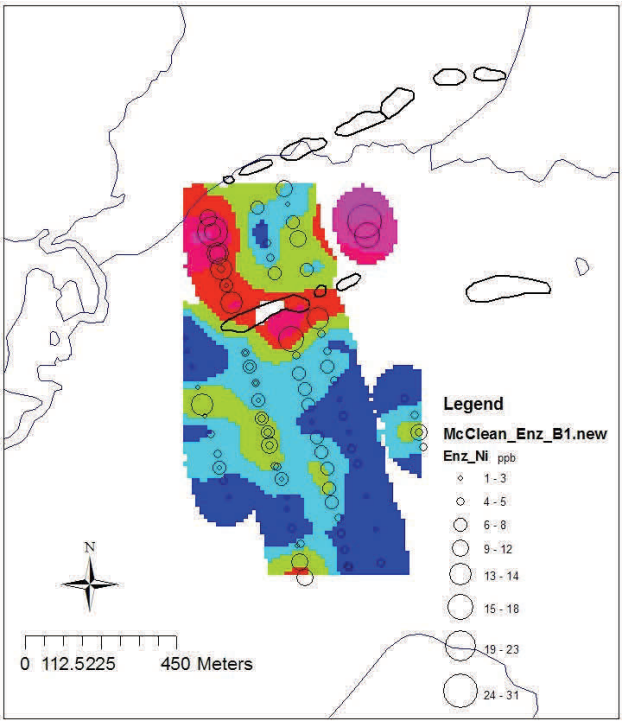

Nickel. B1 horizon. Enzyme leach.

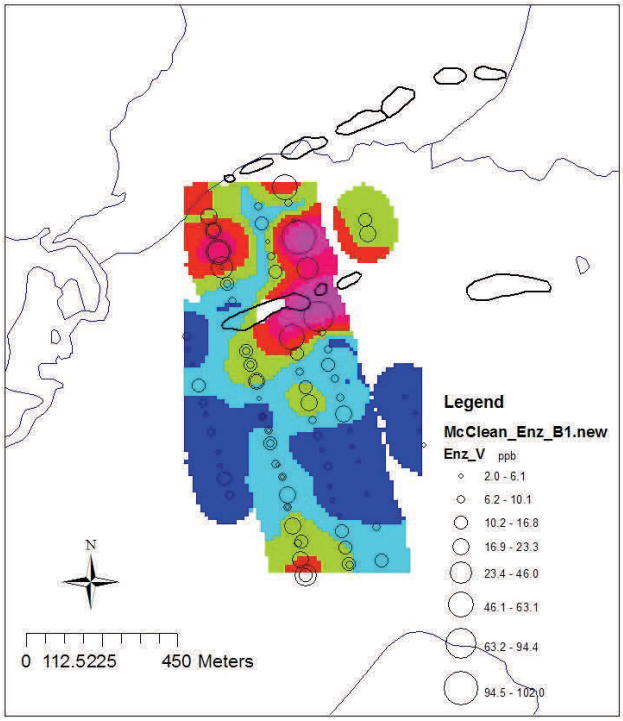

Vanadium. B1 horizon. Enzyme leach.

Fig. 6.96. McClean Maps. B1. Enzyme.

Fig. 6.97. McClean Lake Grids. B1 horizon. Hydroxylamine leach.

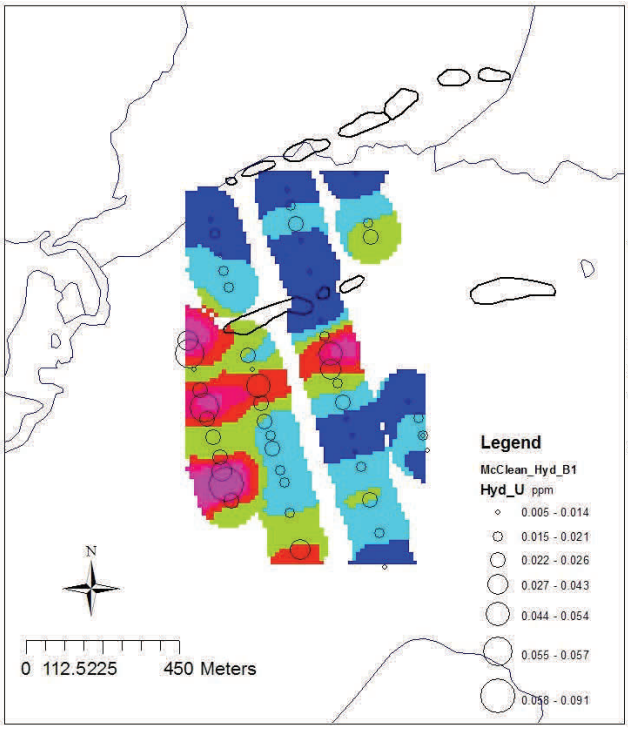

Uranium. B1 horizon. Hydroxylamine leach.

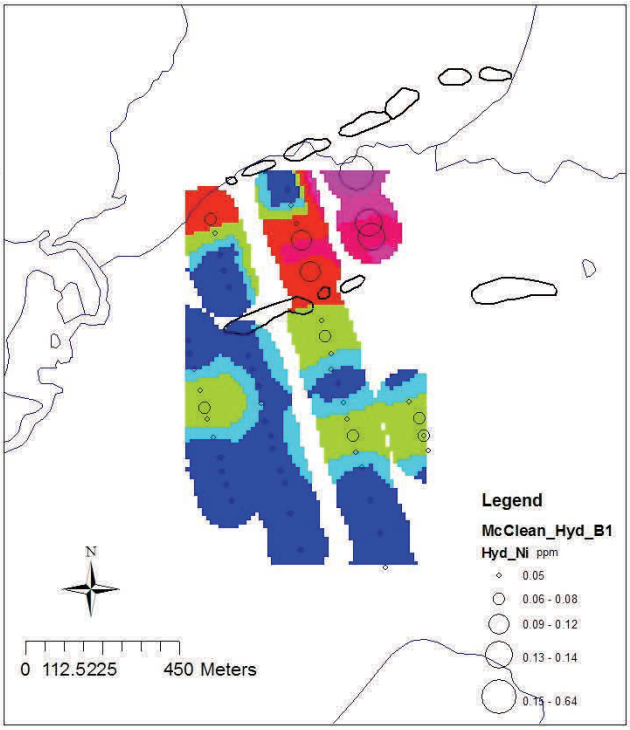

Nickel. B1 horizon. Hydroxylamine leach.

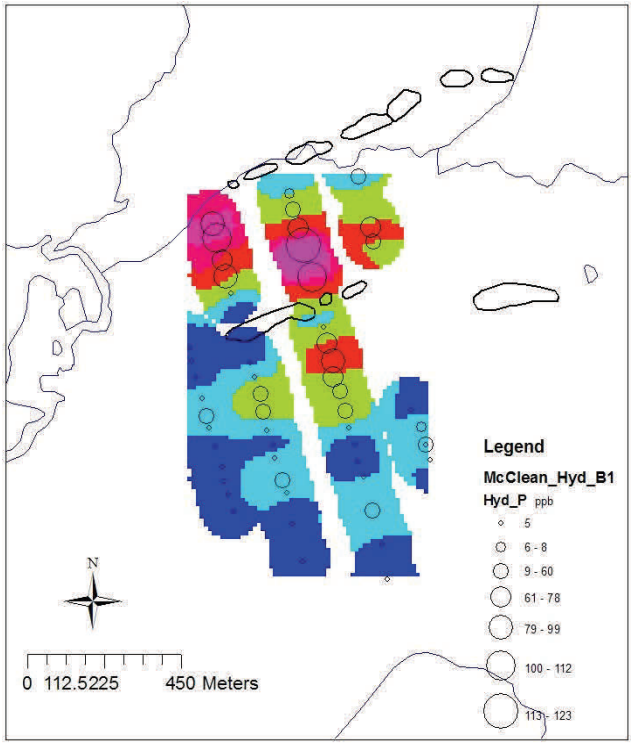

Phosphorus. B1 horizon. Hydroxylamine leach.

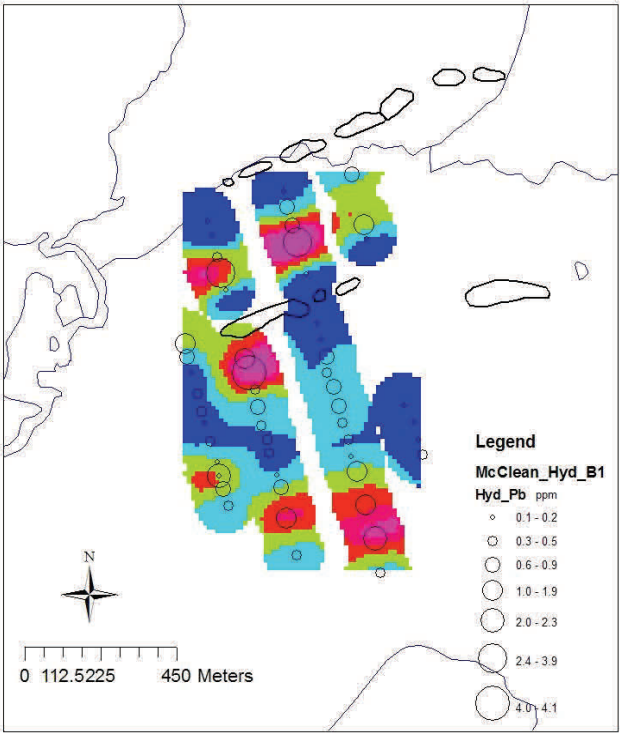

Lead. B1 horizon. Hydroxylamine leach.

Fig. 6.98. McClean Maps. B1. Hydroxylamine.

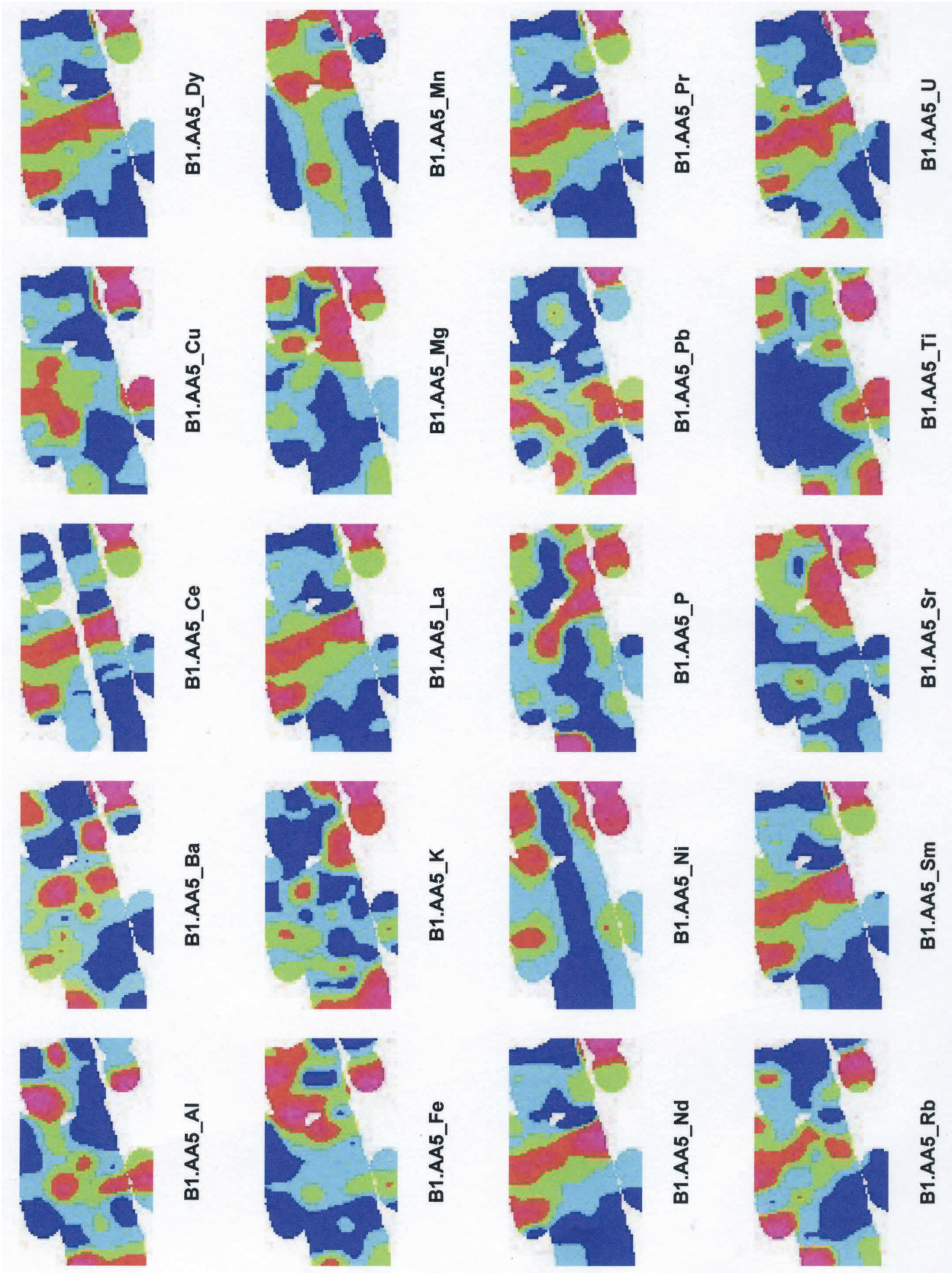

Fig. 6.99. McClean Lake Grids. B1 horizon. Ammonium acetate leach.

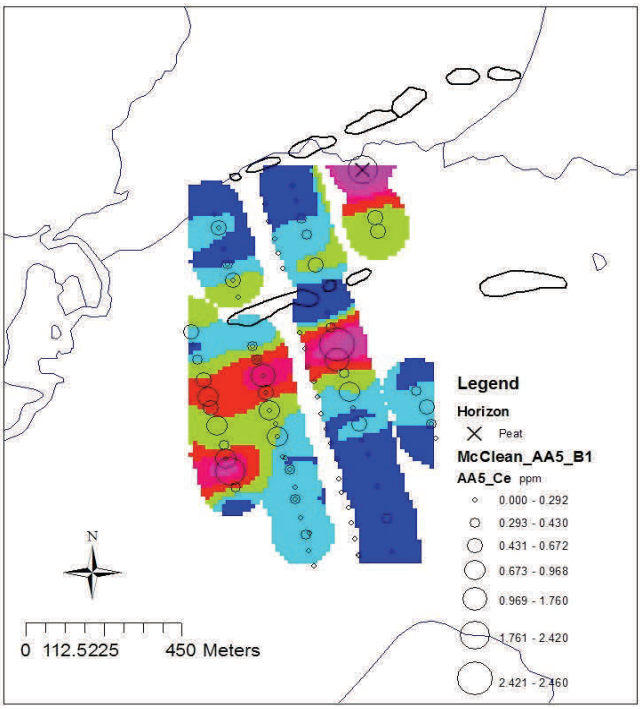

Cerium. B1 horizon. Ammonium acetate

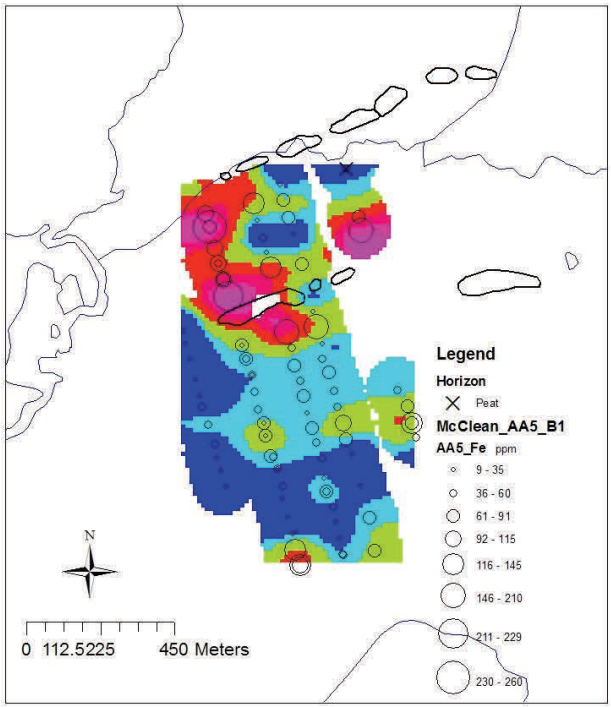

Iron. B1 horizon. Ammonium acetate

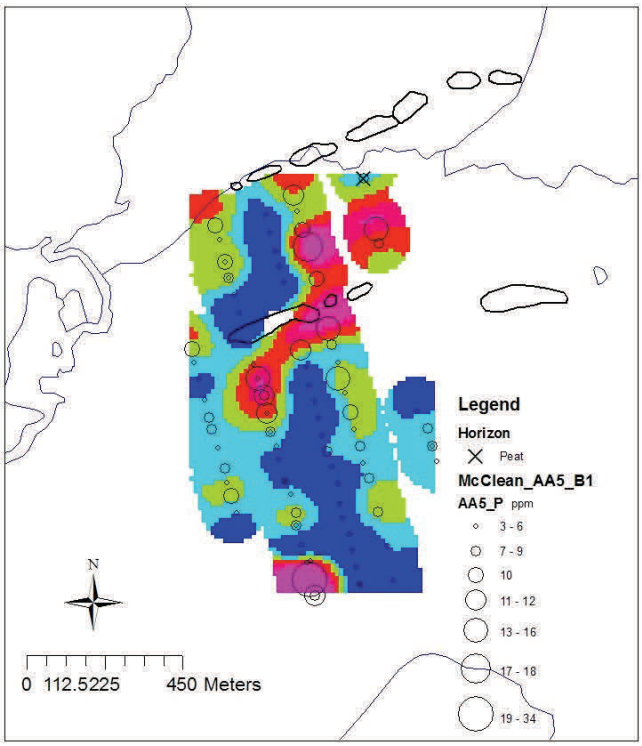

Phosphorus. B1 horizon. Ammonium acetate

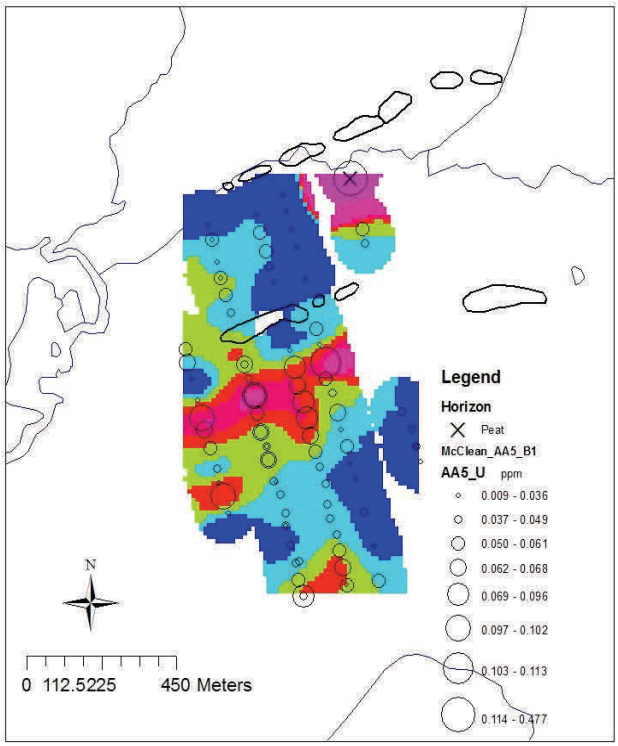

Uranium. B1 horizon. Ammonium acetate

Fig. 6.100. McClean Maps. B1. Ammonium acetate.

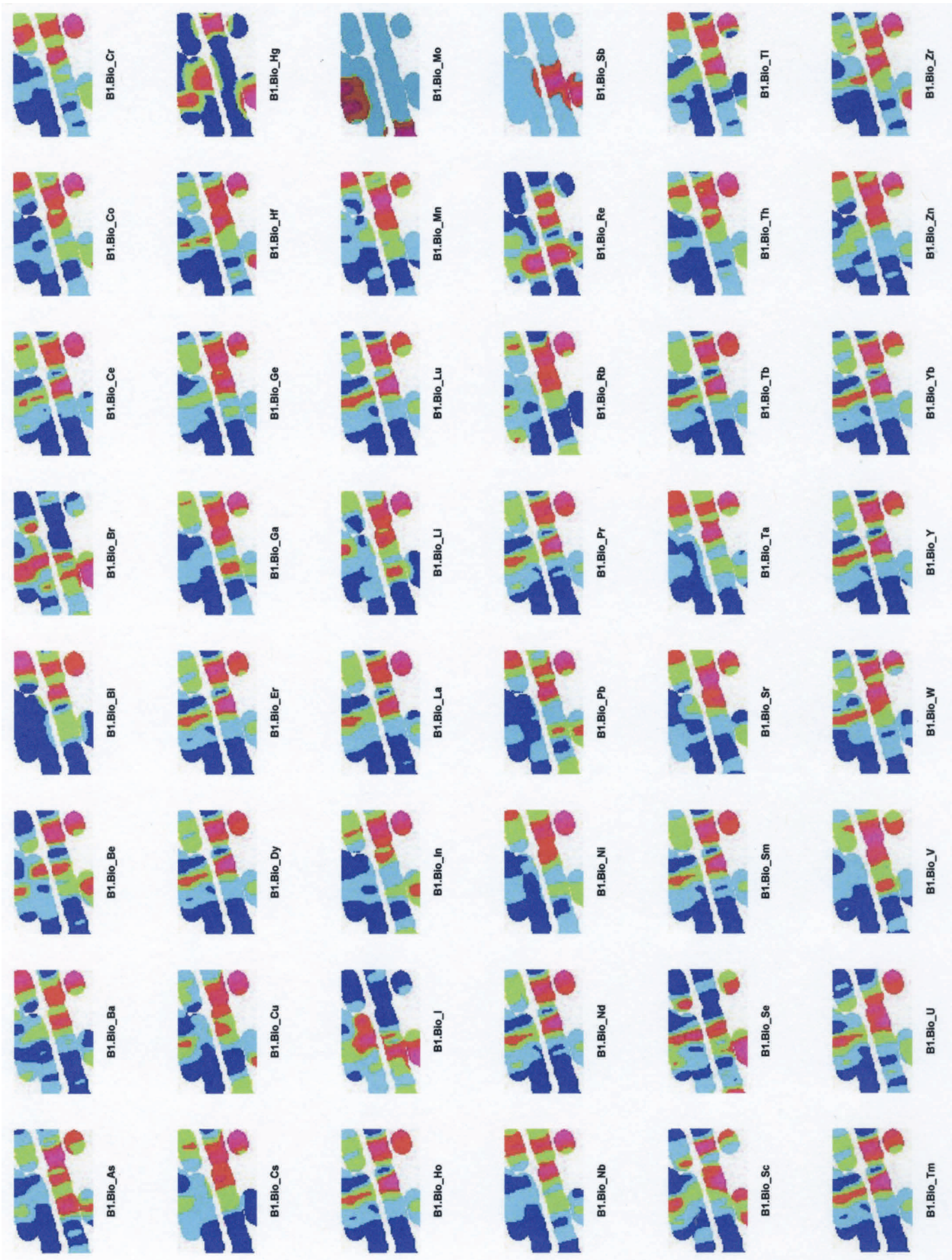

Fig. 6.101. McClean Lake Grids. B1 horizon. Bioleach.

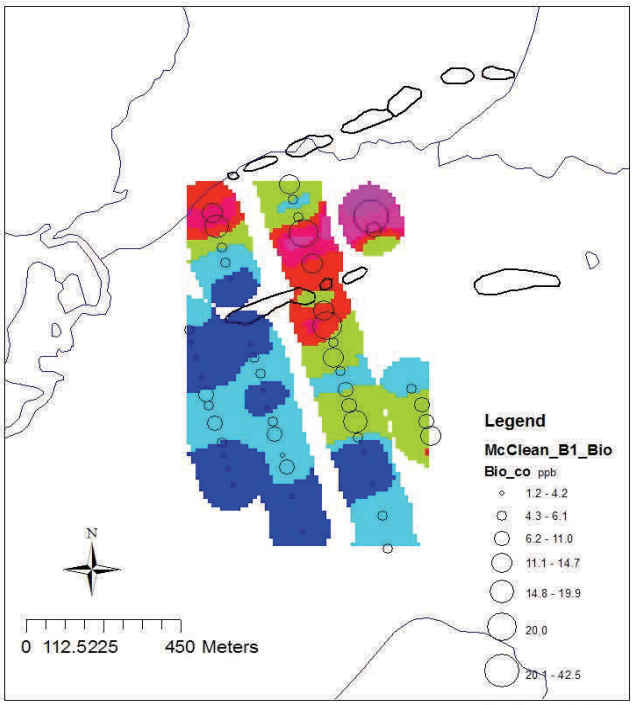

Cobalt. B1 horizon..Bioleach.

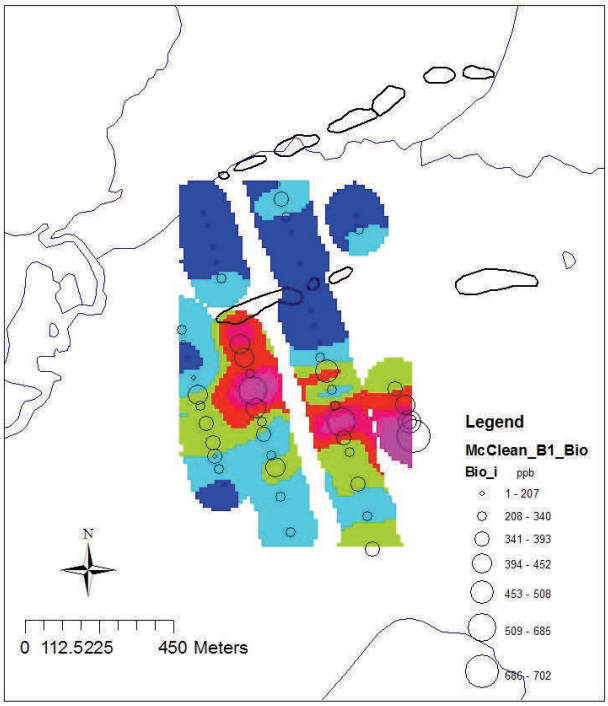

Iodine. B1 horizon..Bioleach.

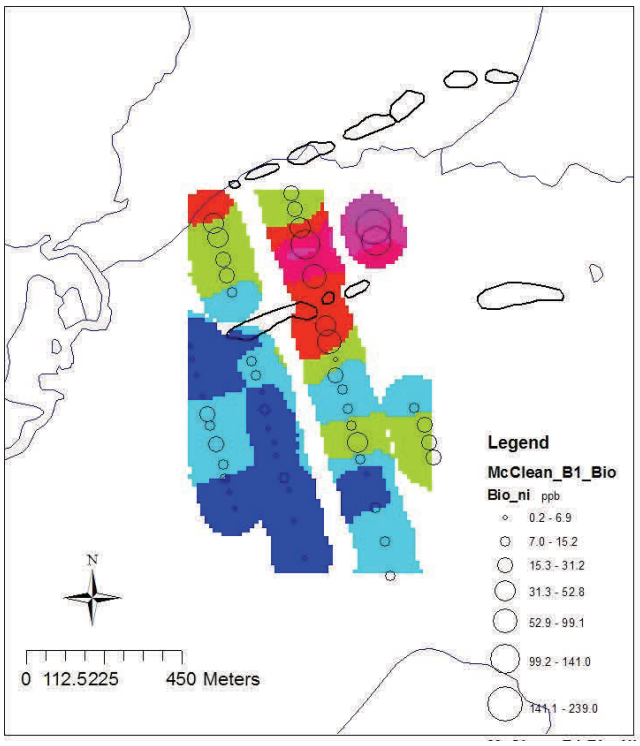

Nickel. B1 horizon..Bioleach.

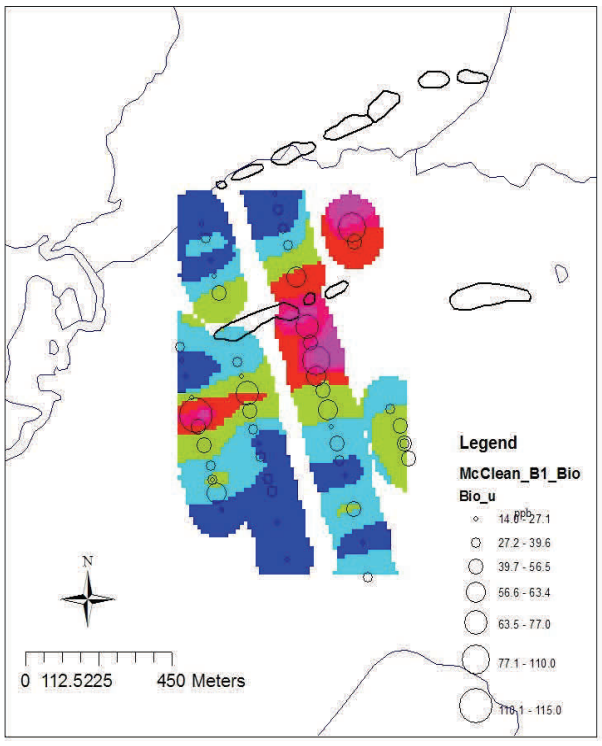

Uranium. B1 horizon..Bioleach.

Fig. 6.102. McClean Maps. B1. Bioleach.

Fig 6.103. McClean Lake Grids. B1 horizon. MMI leach.

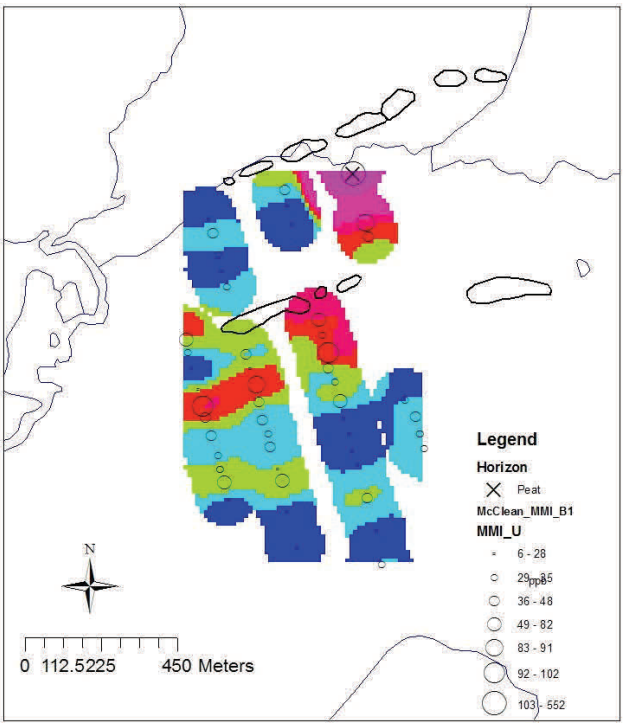

Uranium. B1 horizon. MMI leach.

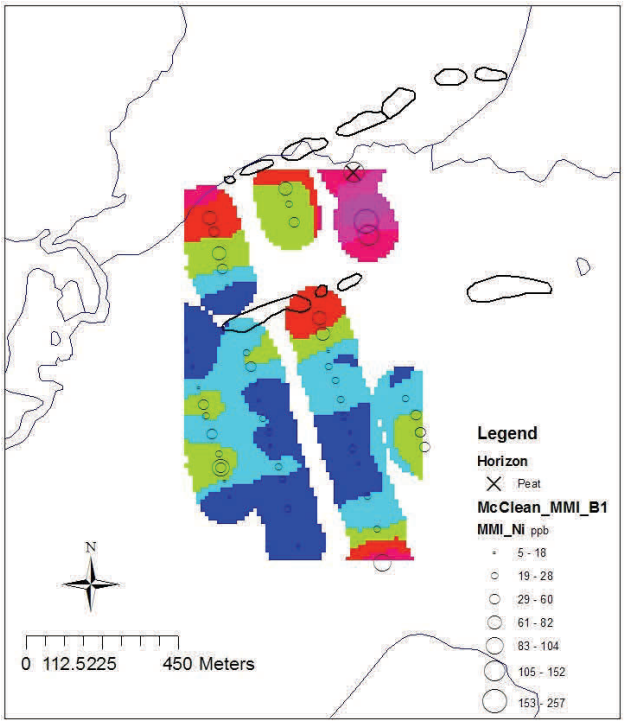

Nickel. B1 horizon. MMI leach.

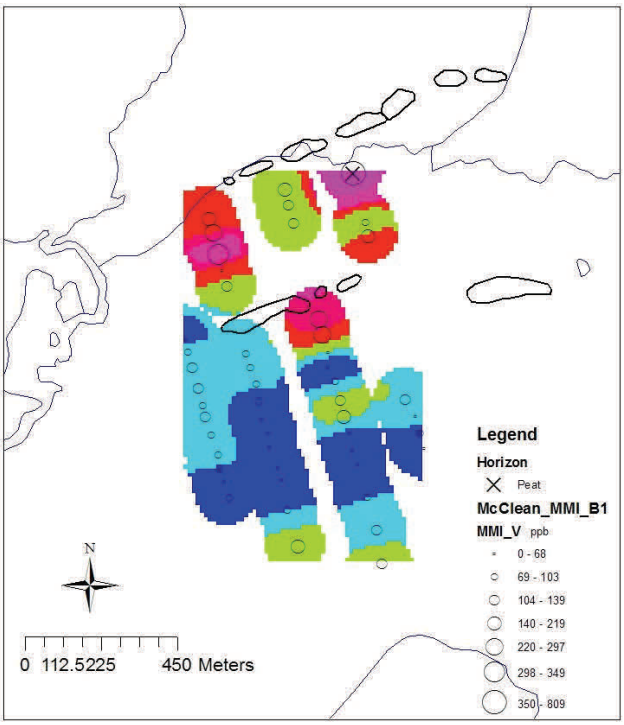

Vanadium. B1 horizon. MMI leach.

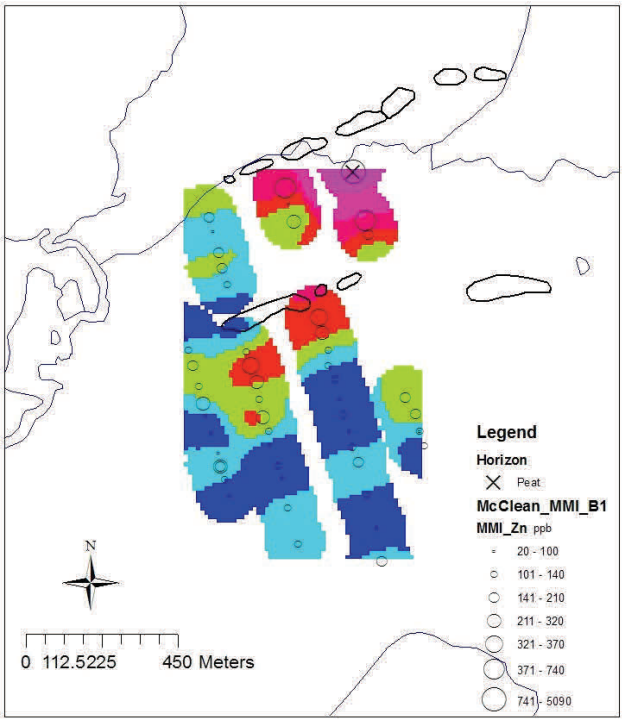

Zinc. B1 horizon. MMI leach.

Fig. 6.104. McClean Maps. B1. MMI.

Fig. 6.105. McClean Lake Grids. B1 horizon. Ionic leach.

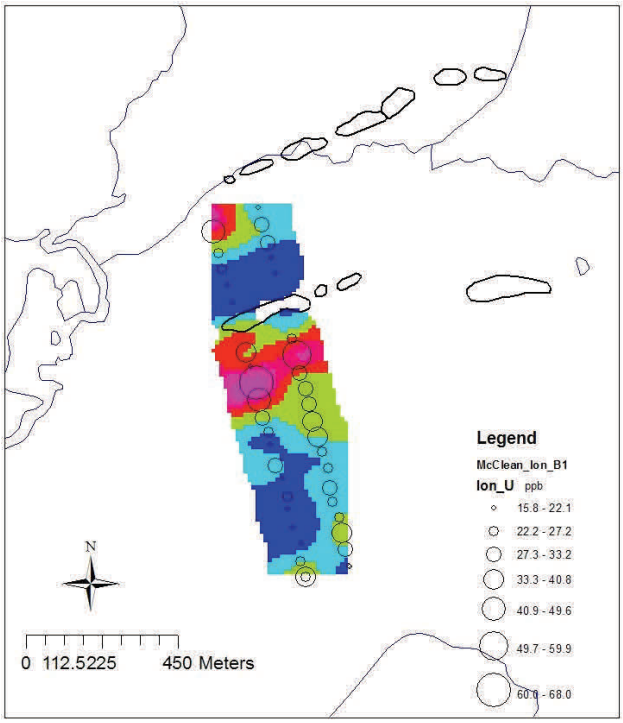

Uranium. B1 horizon. Ionic leach.

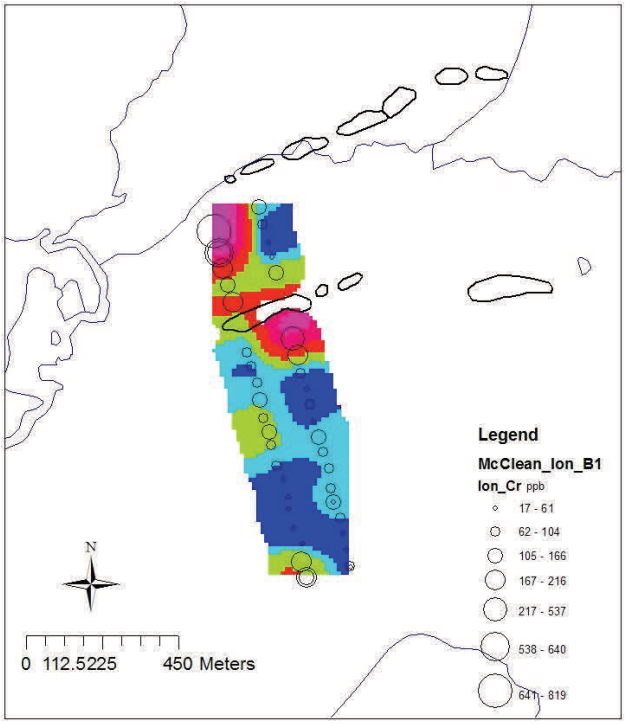

Chromium. B1 horizon. Ionic leach.

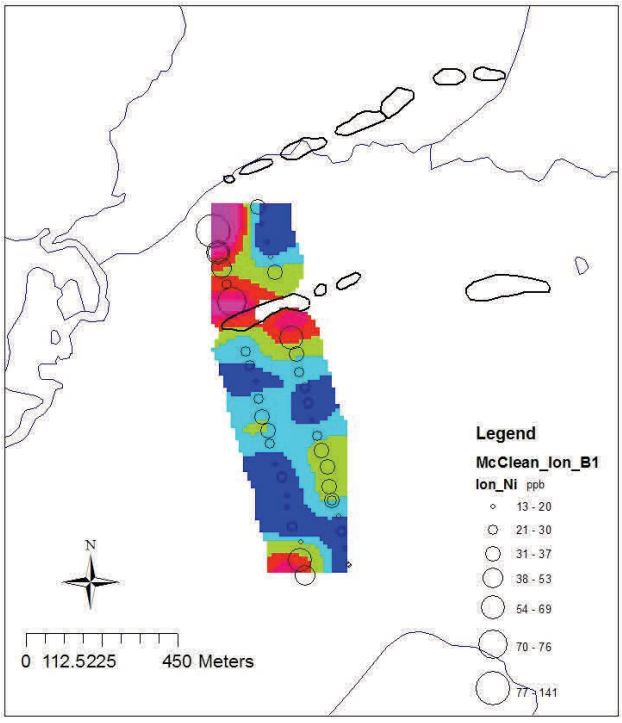

Nickel. B1 horizon. Ionic leach.

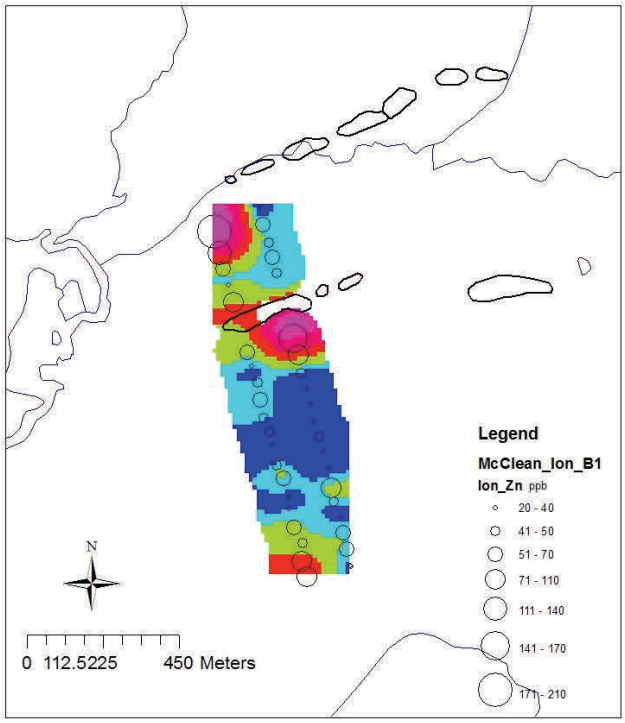

Zinc. B1 horizon. Ionic leach.

Fig. 6.106. McClean Maps. B1. Ionic.

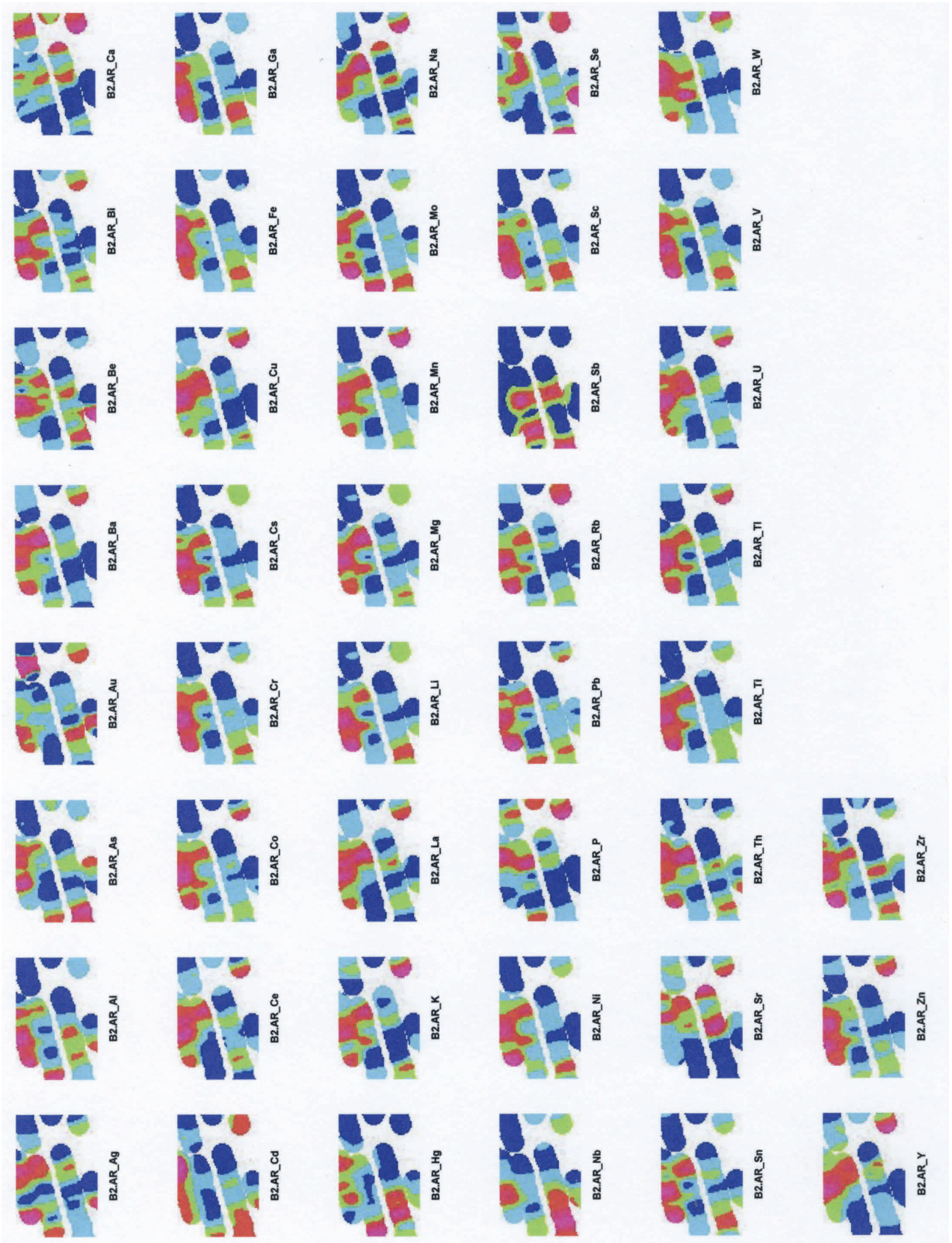

Fig, 6.107. McClean Lake Grids. B2 horizon. Aqua regia leach.

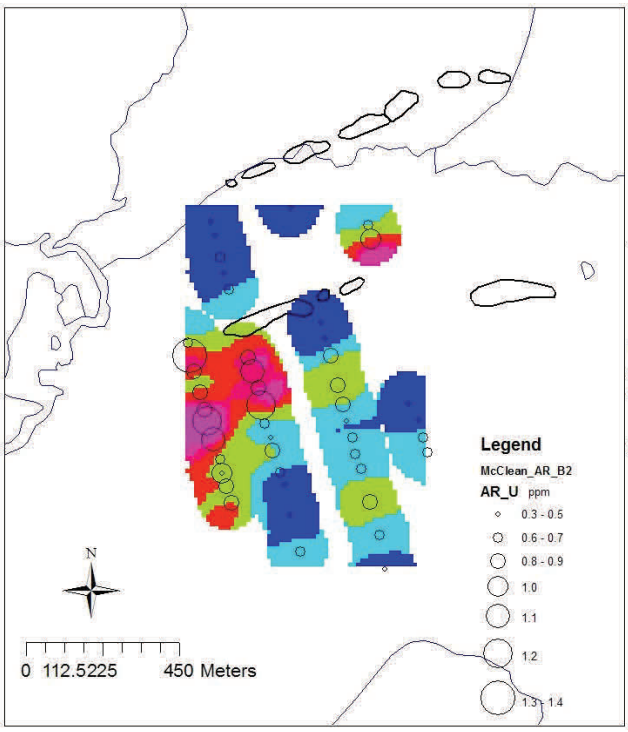

Uranium. B2 horizon. Aqua regia leach.

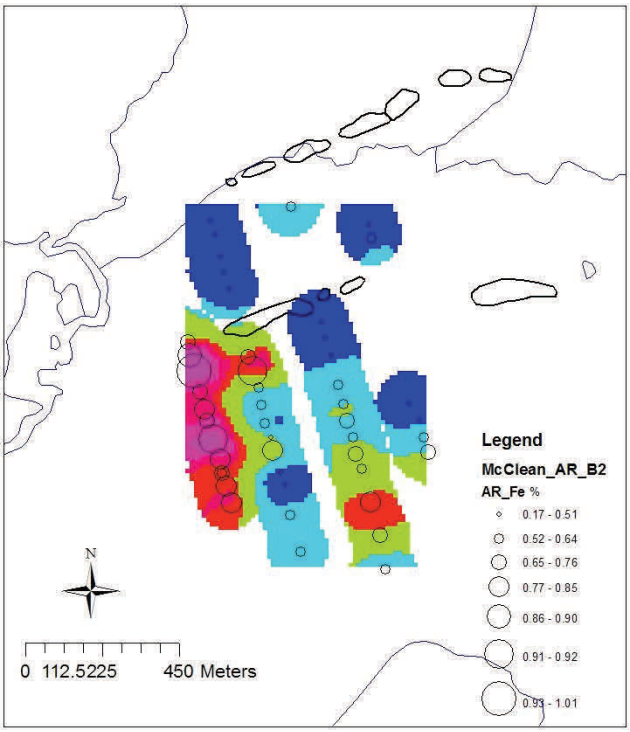

Iron. B2 horizon. Aqua regia leach.

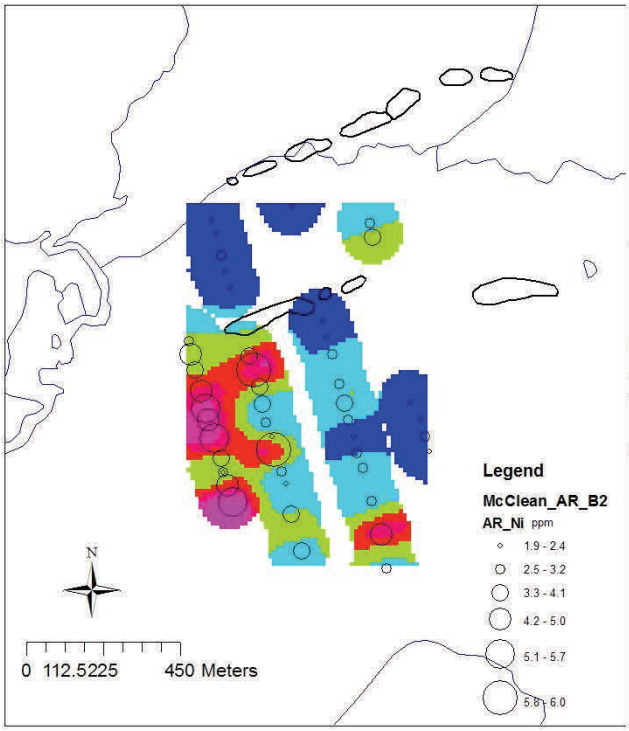

Nickel. B2 horizon. Aqua regia leach.

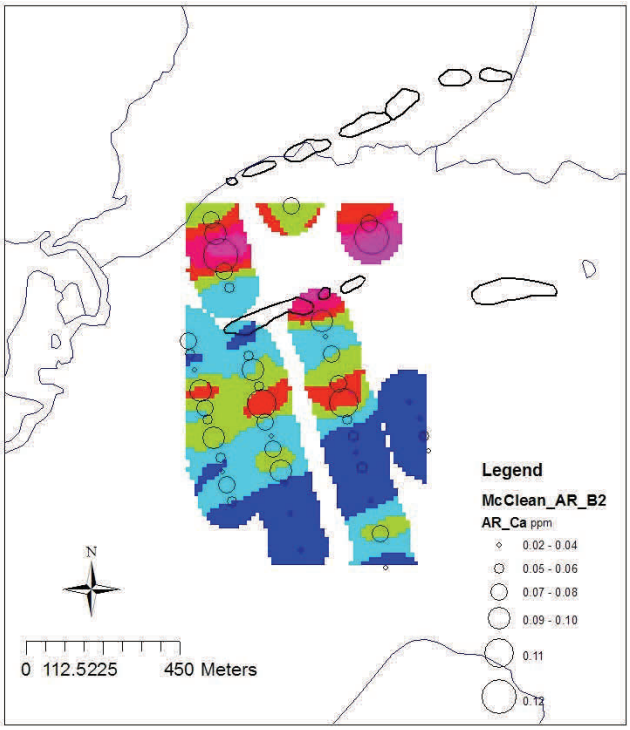

Calcium. B2 horizon. Aqua regia leach.

Fig. 6.108. McClean Maps. B2. Aqua regia.

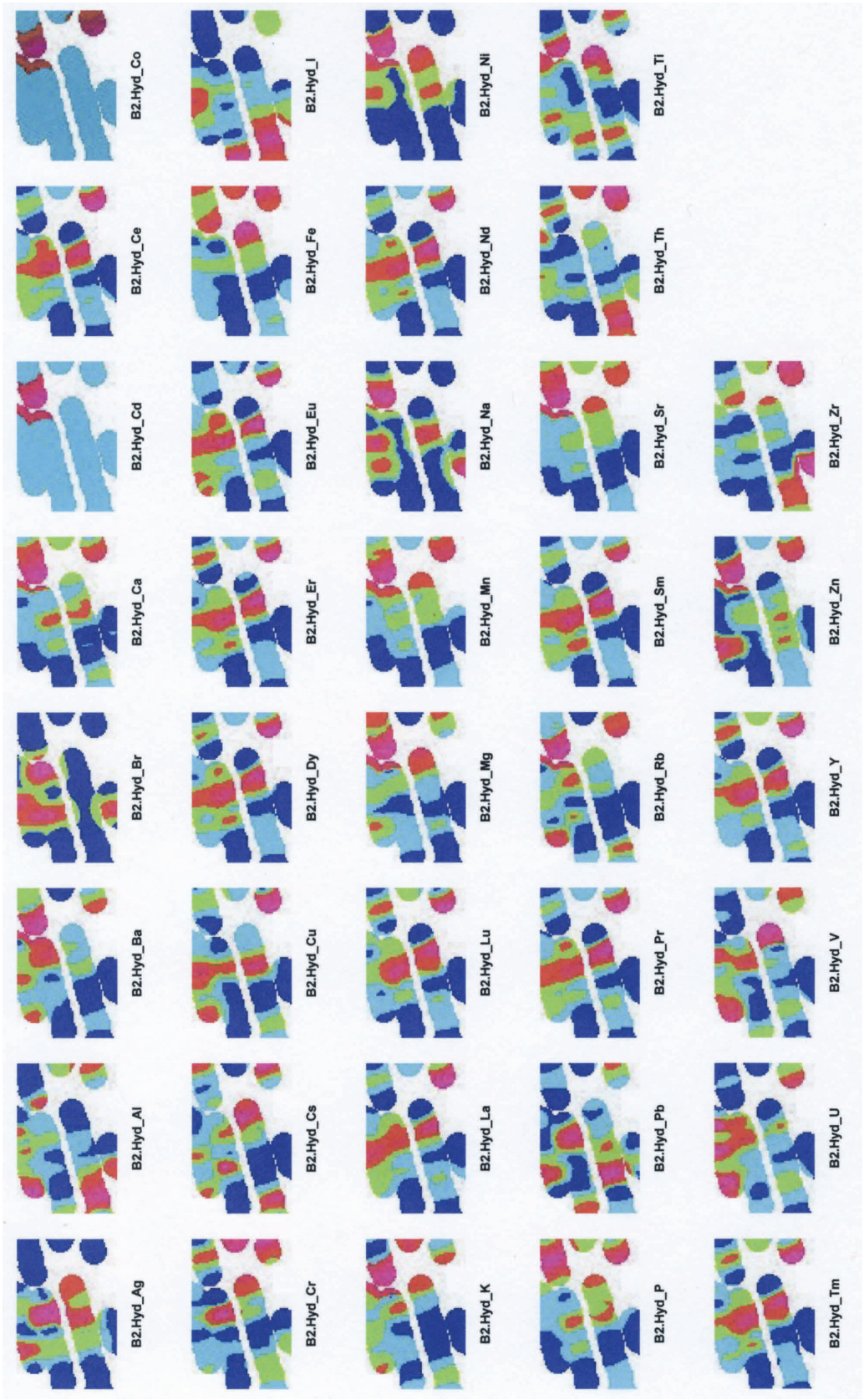

Fig. 6. 109 McClean Lake Grids. B2 horizon. Hydroxylamine leach.

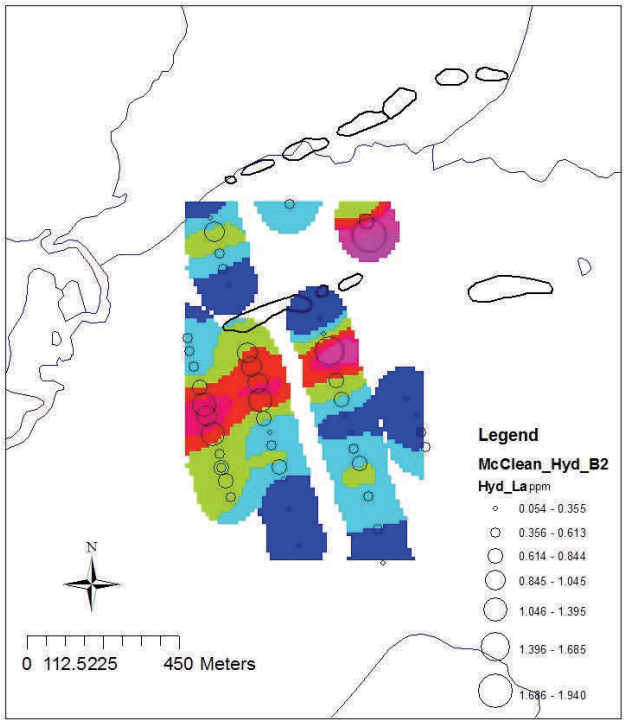

Lanthanum. B2 horizon. Hydroxylamine leach.

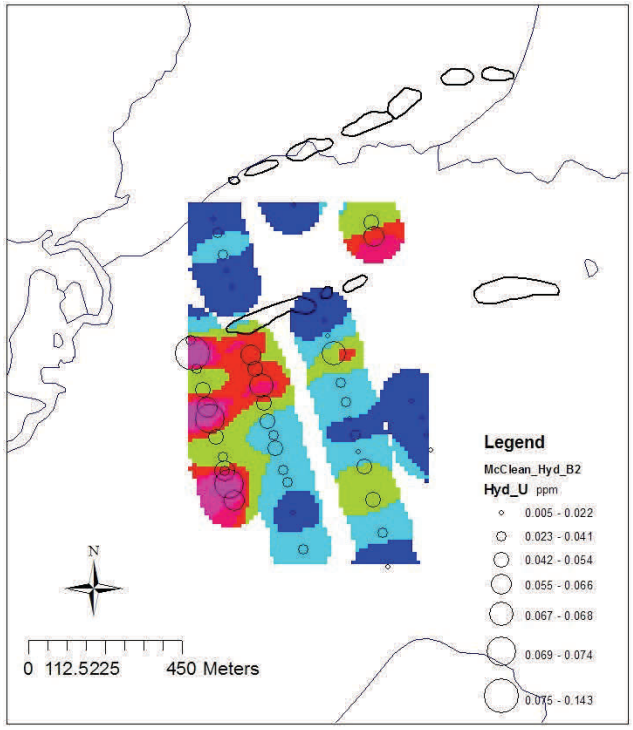

Uranium. B2 horizon. Hydroxylamine leach.

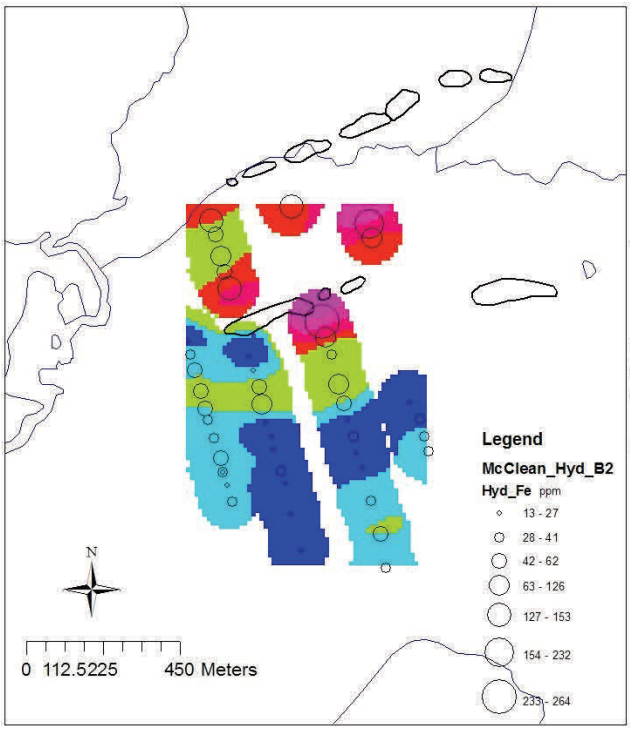

Iron. B2 horizon. Hydroxylamine leach.

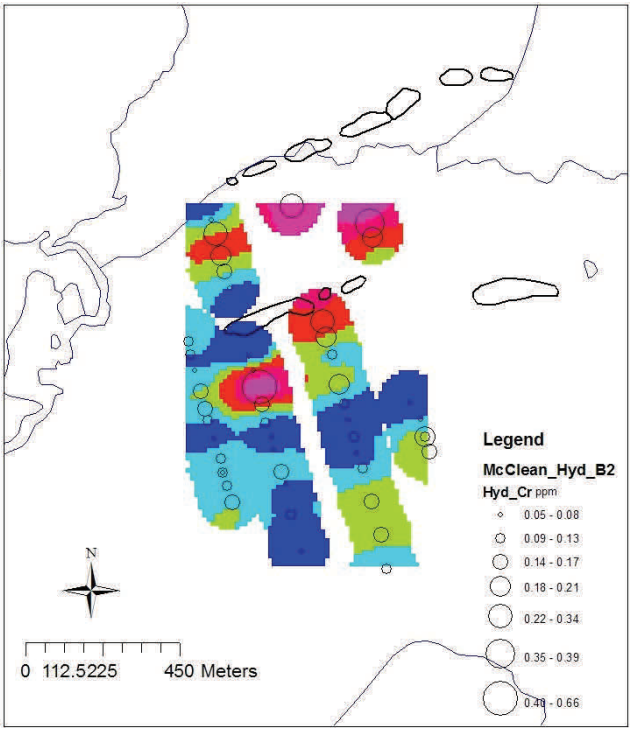

Chromium. B2 horizon. Hydroxylamine leach.

Fig. 6. 110. McClean Maps. B2. Hydroxylamine.

Fig. 6.111. McClean Lake Grids. B2 horizon. Ammonium acetate leach.

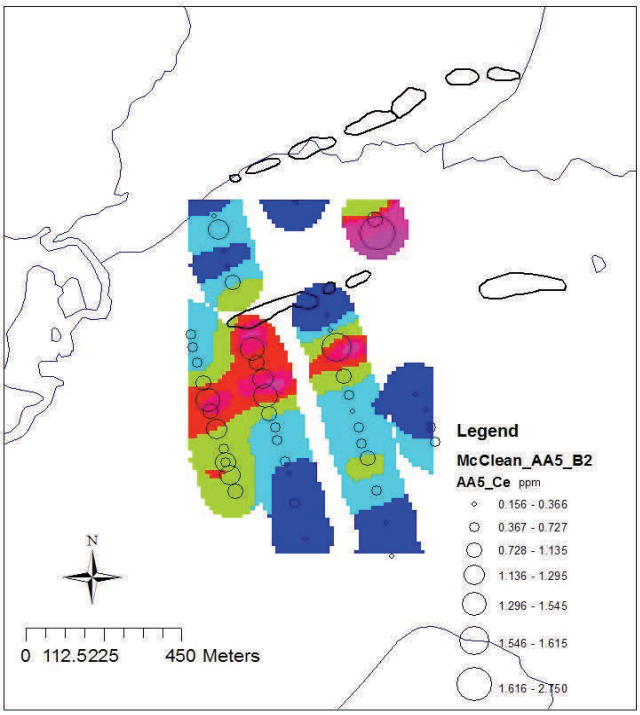

Cerium. B2 horizon. Ammonium acetate.

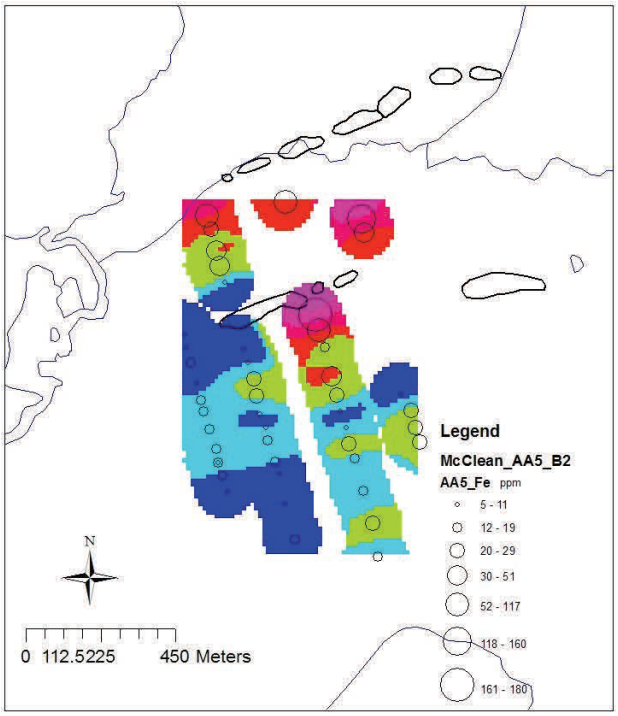

Iron. B2 horizon. Ammonium acetate.

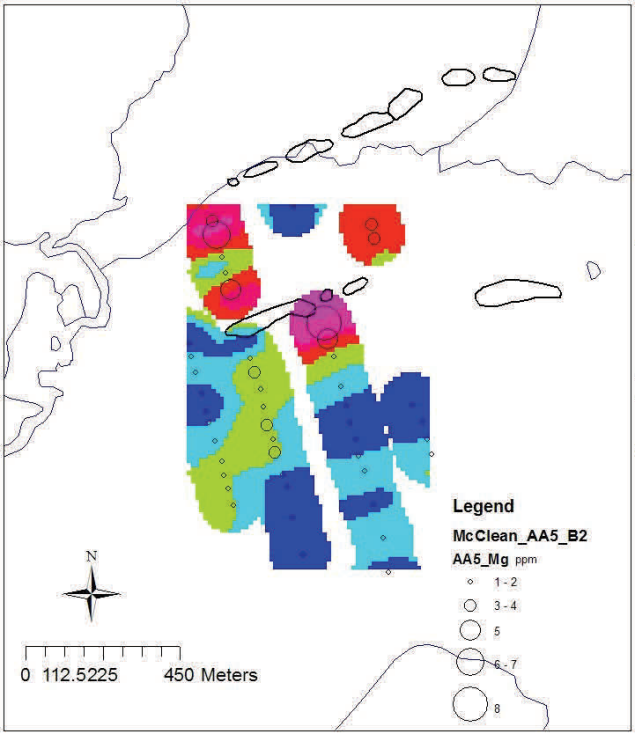

Magnesium. B2 horizon. Ammonium acetate.

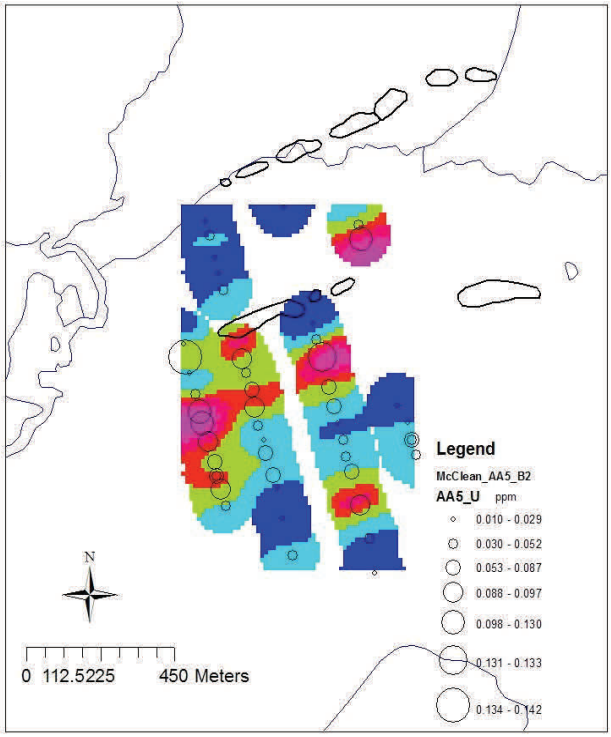

Uranium. B2 horizon. Ammonium acetate.

Fig. 6.112. McClean Maps. B2. Ammonium acetate.

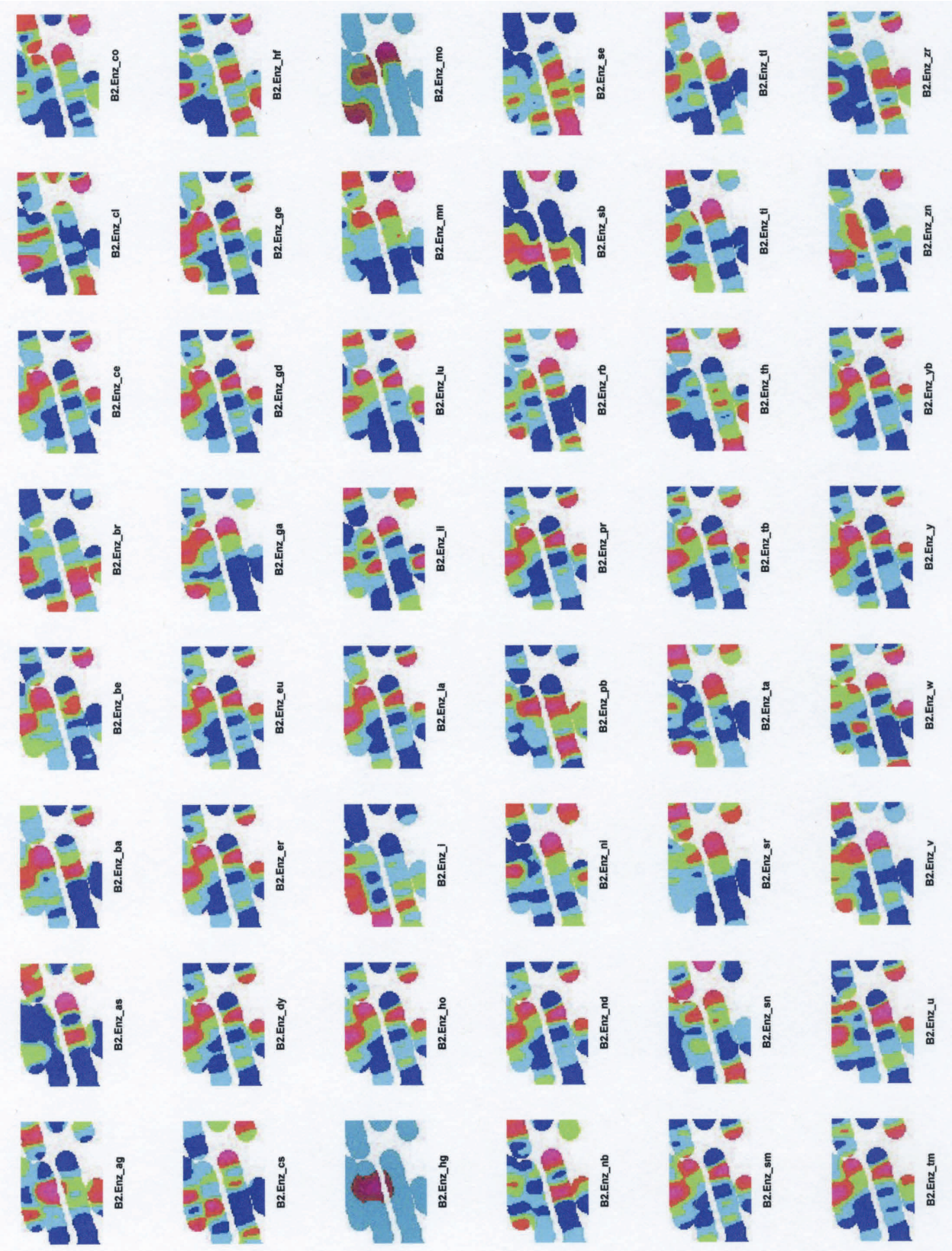

Fig. 6.113. McClean Lake Grids. B2 horizon. Enzyme leach.

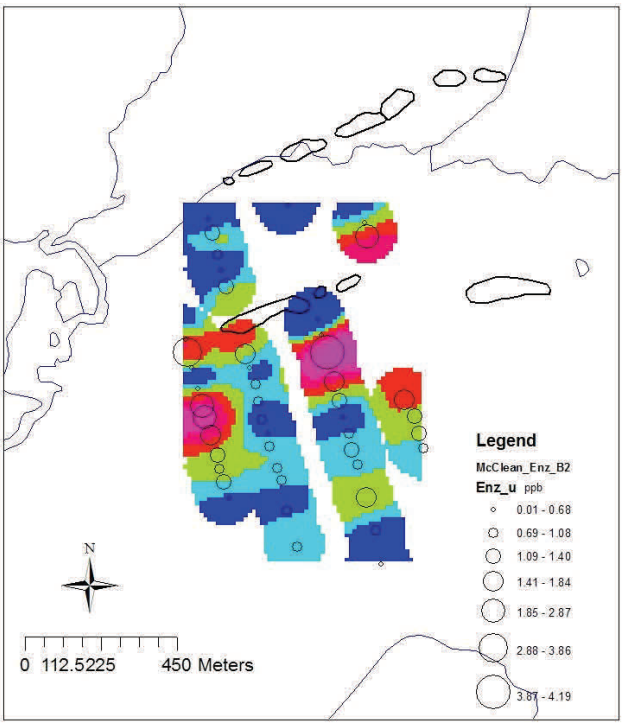

Uranium. B2 horizon. Enzyme leach.

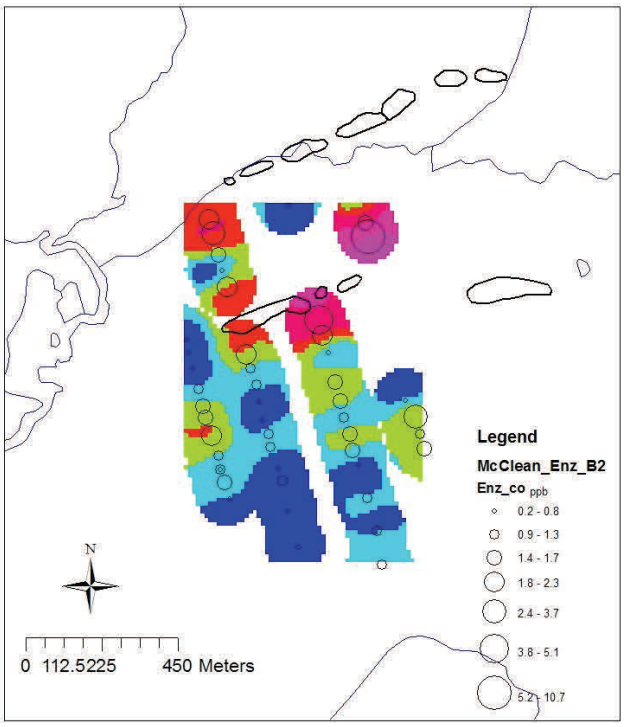

Cobalt. B2 horizon. Enzyme leach.

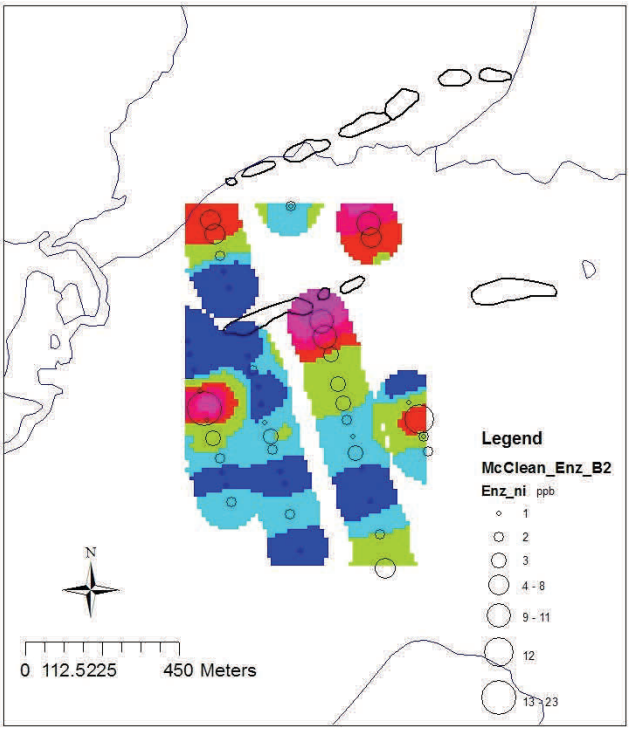

Nickel. B2 horizon. Enzyme leach.

Fig. 6.114. McClean Maps. B2. Enzyme.

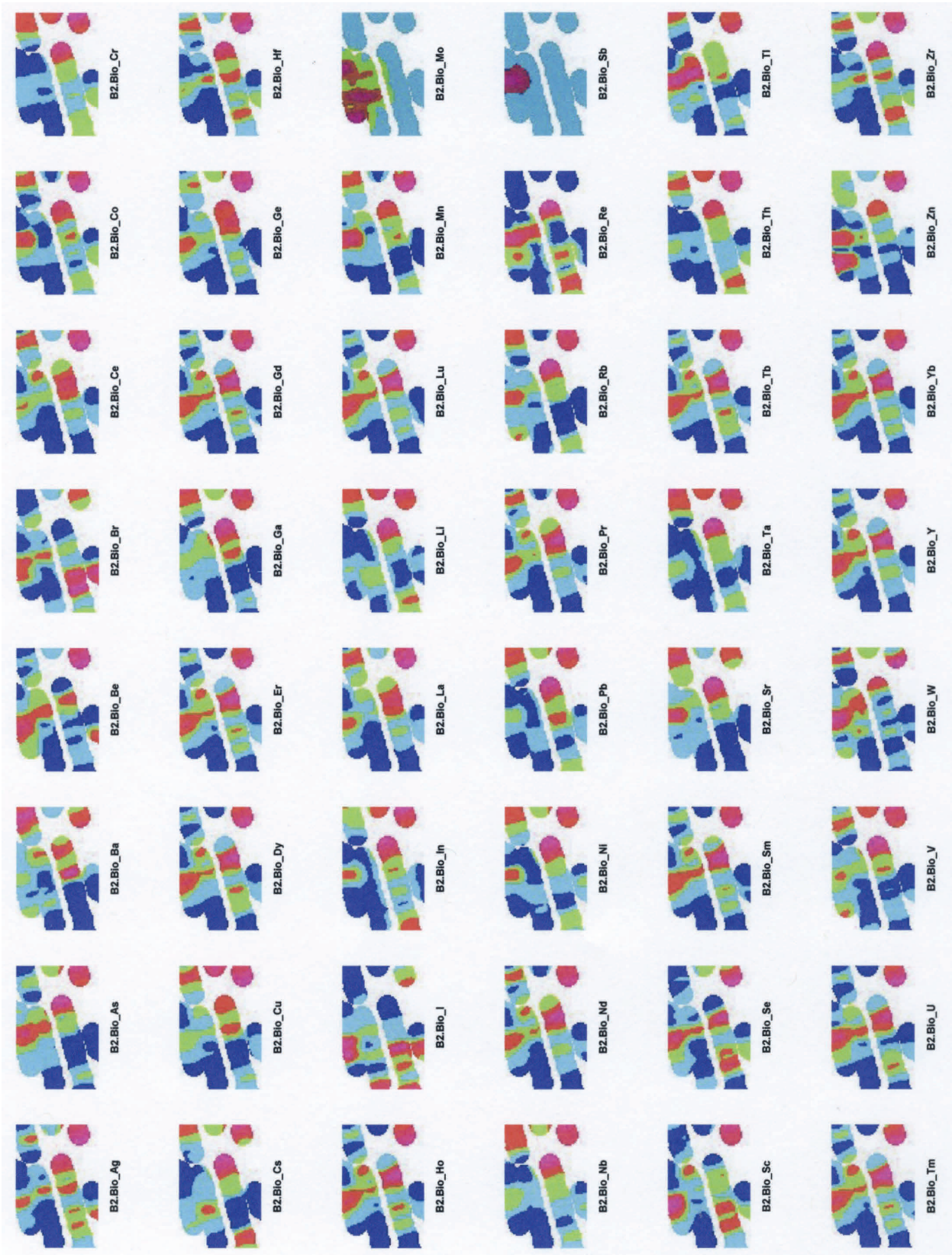

Fig. 6.115. McClean Lake Grids. B2 horizon. Bioleach.

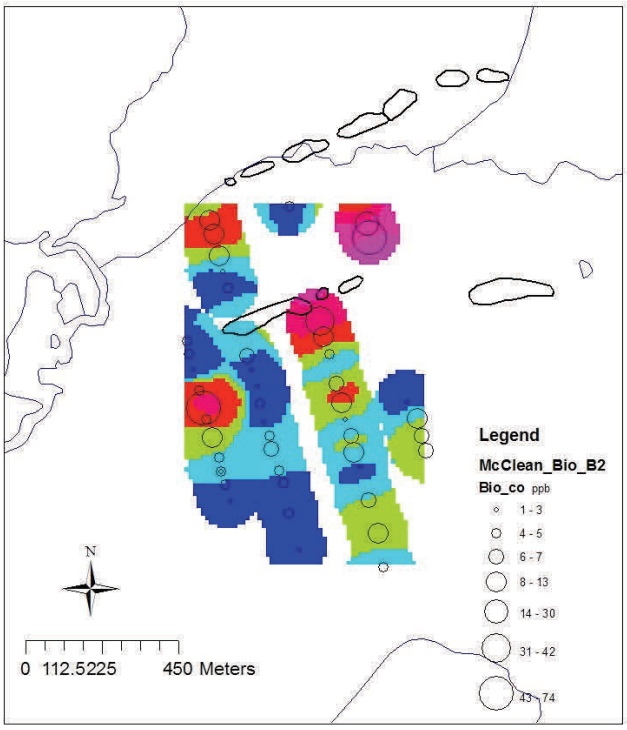

Cobalt. B2 horizon. Bioleach.

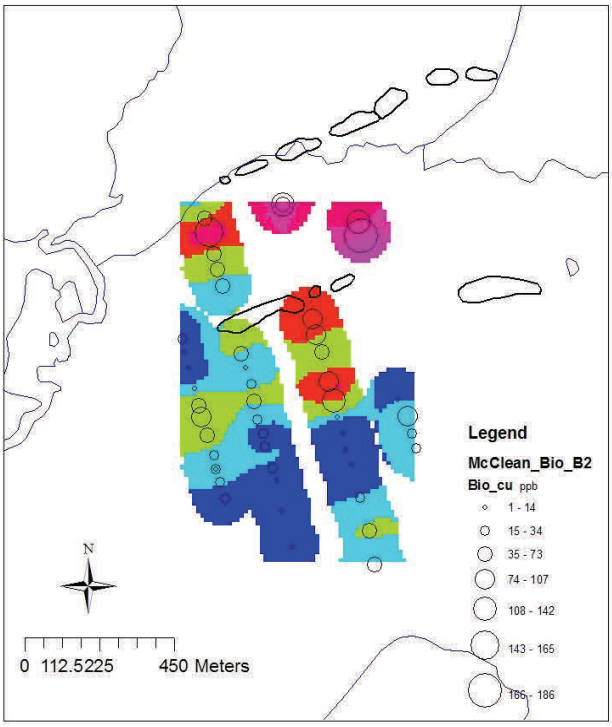

Copper. B2 horizon. Bioleach.

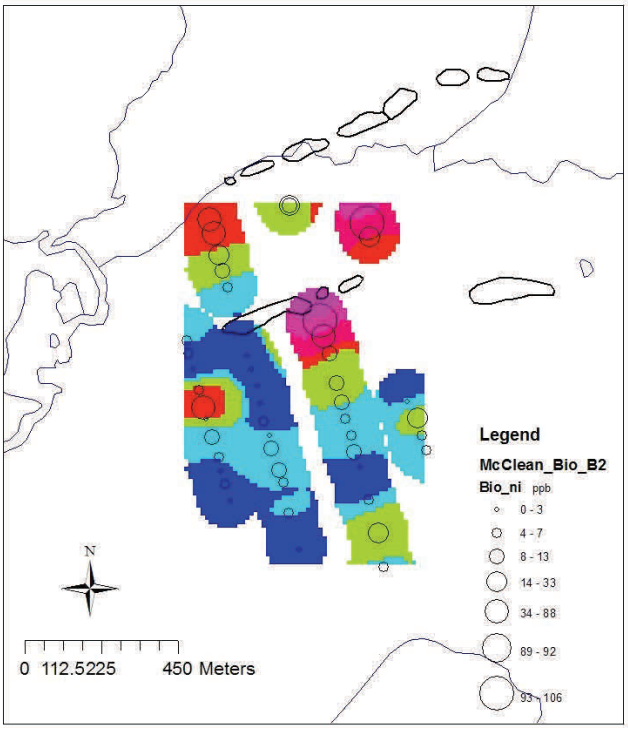

Nickel. B2 horizon. Bioleach.

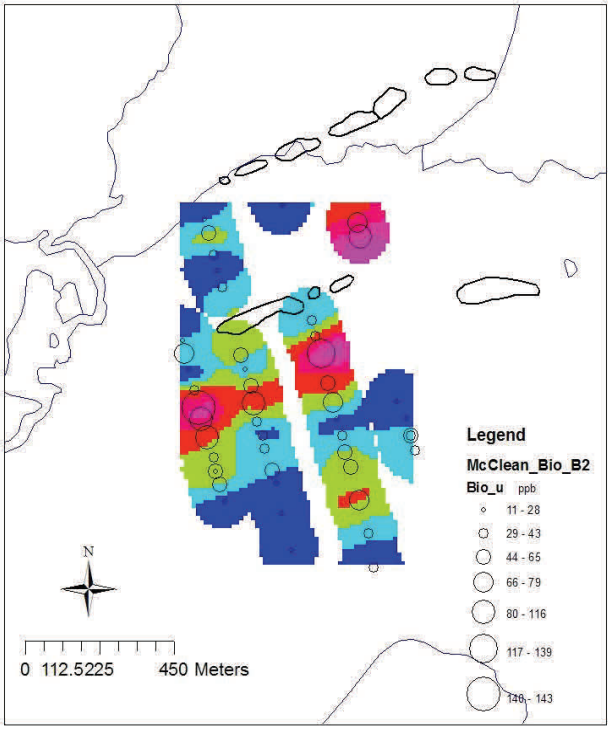

Uranium. B2 horizon. Bioleach.

Fig. 6.116. McClean Maps. B2. Bioleach.

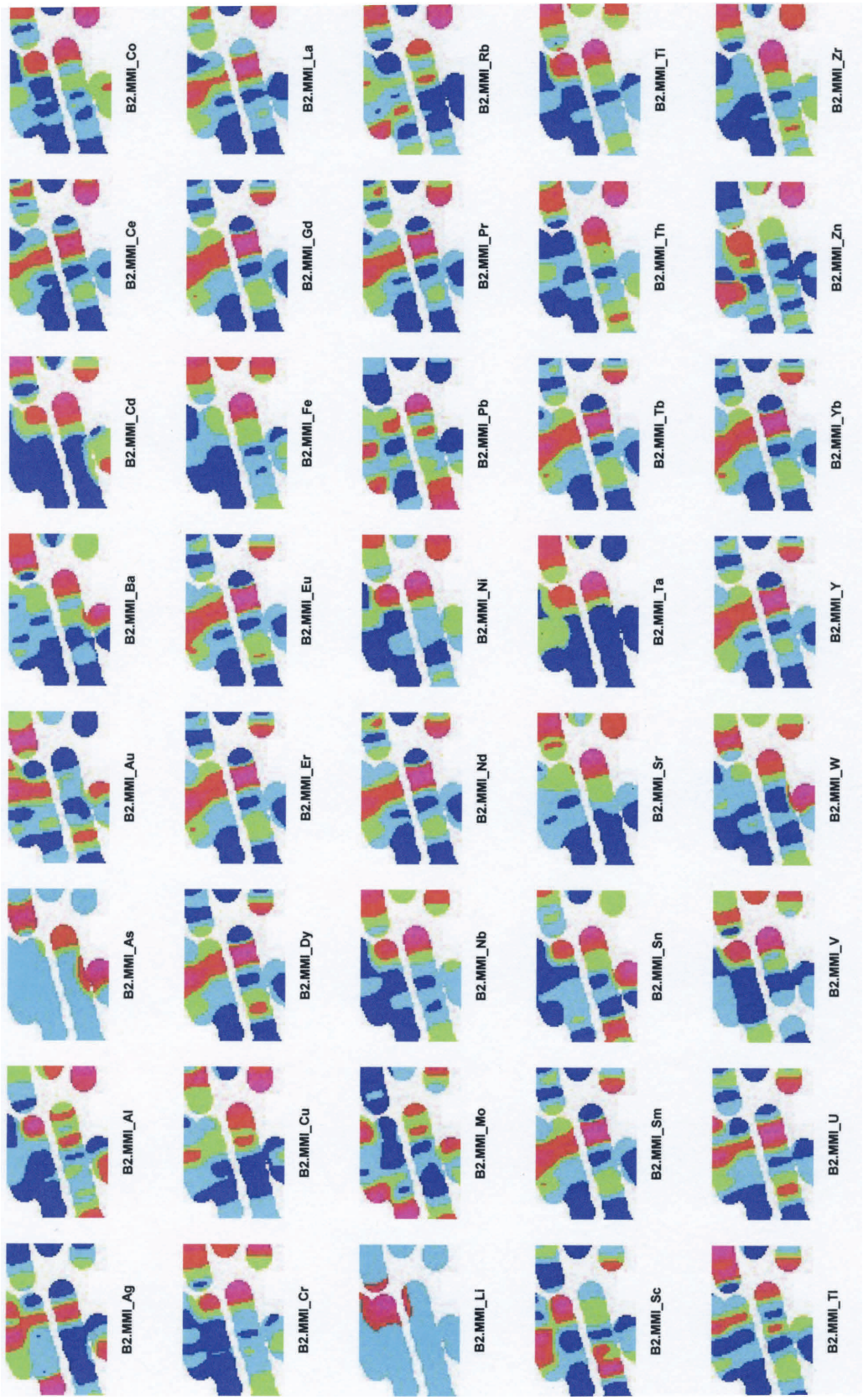

Fig. 6.117. McClean Lake Grids. B2 horizon. MMI leach.

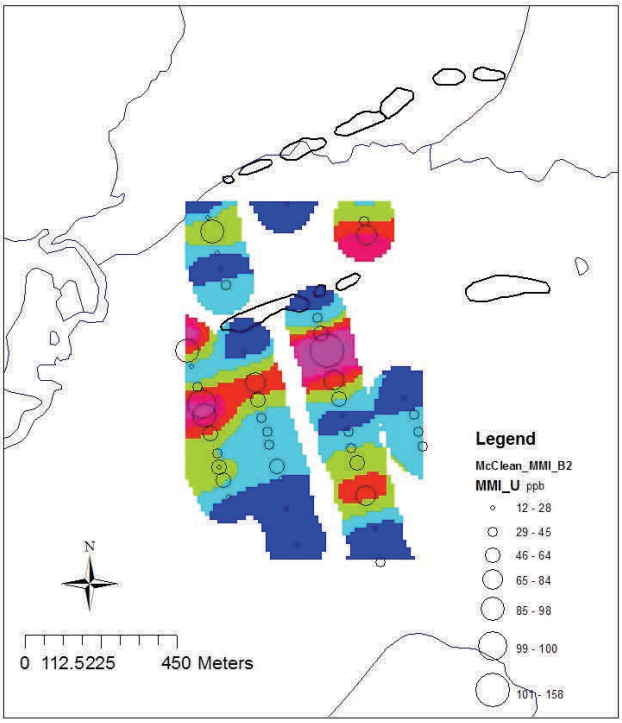

Uranium. B2 horizon. MMI leach.

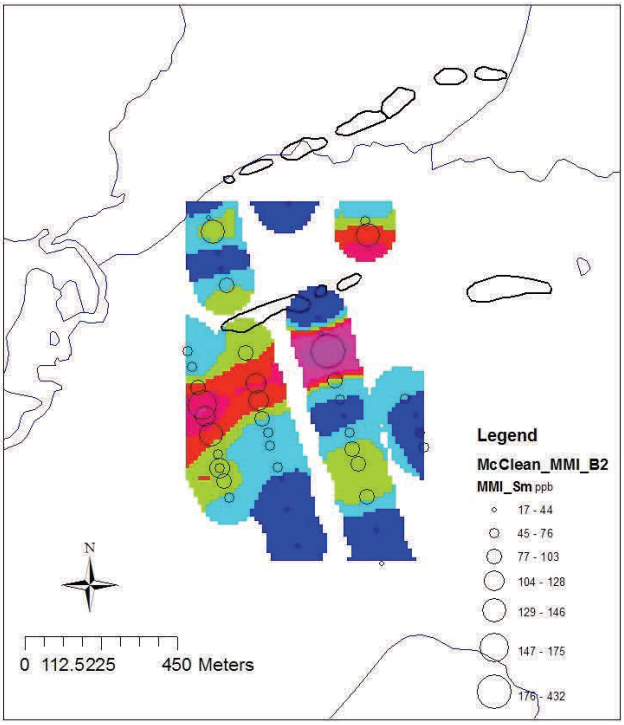

Sumerium. B2 horizon. MMI leach.

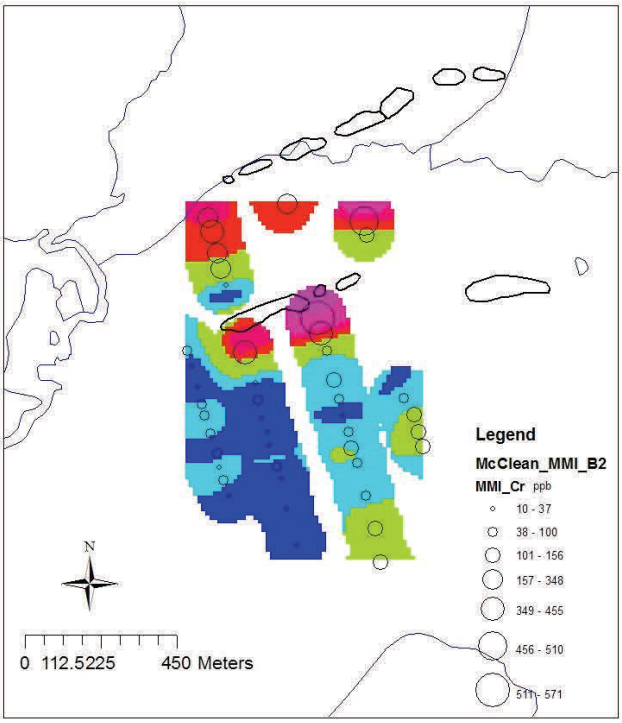

Chromium. B2 horizon. MMI leach.

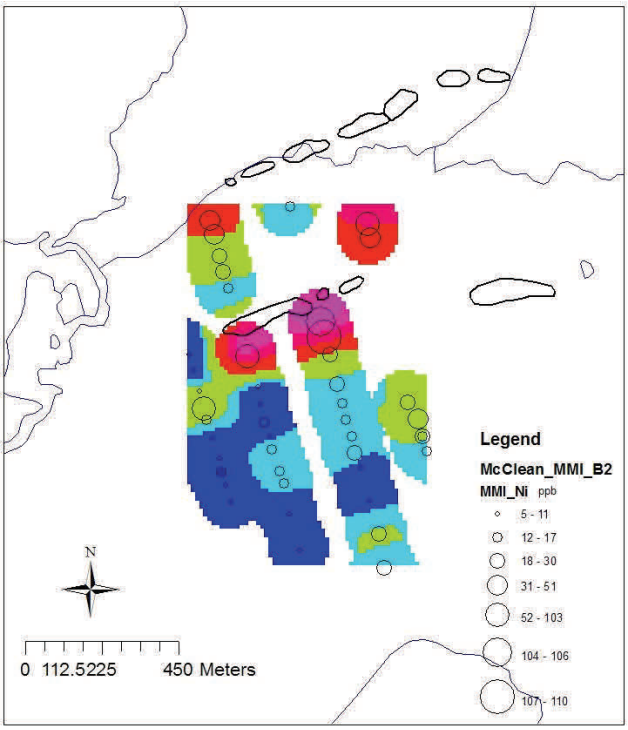

Nickel. B2 horizon. MMI leach.

Fig. 6.118. McClean Maps. B2. MMI leach.

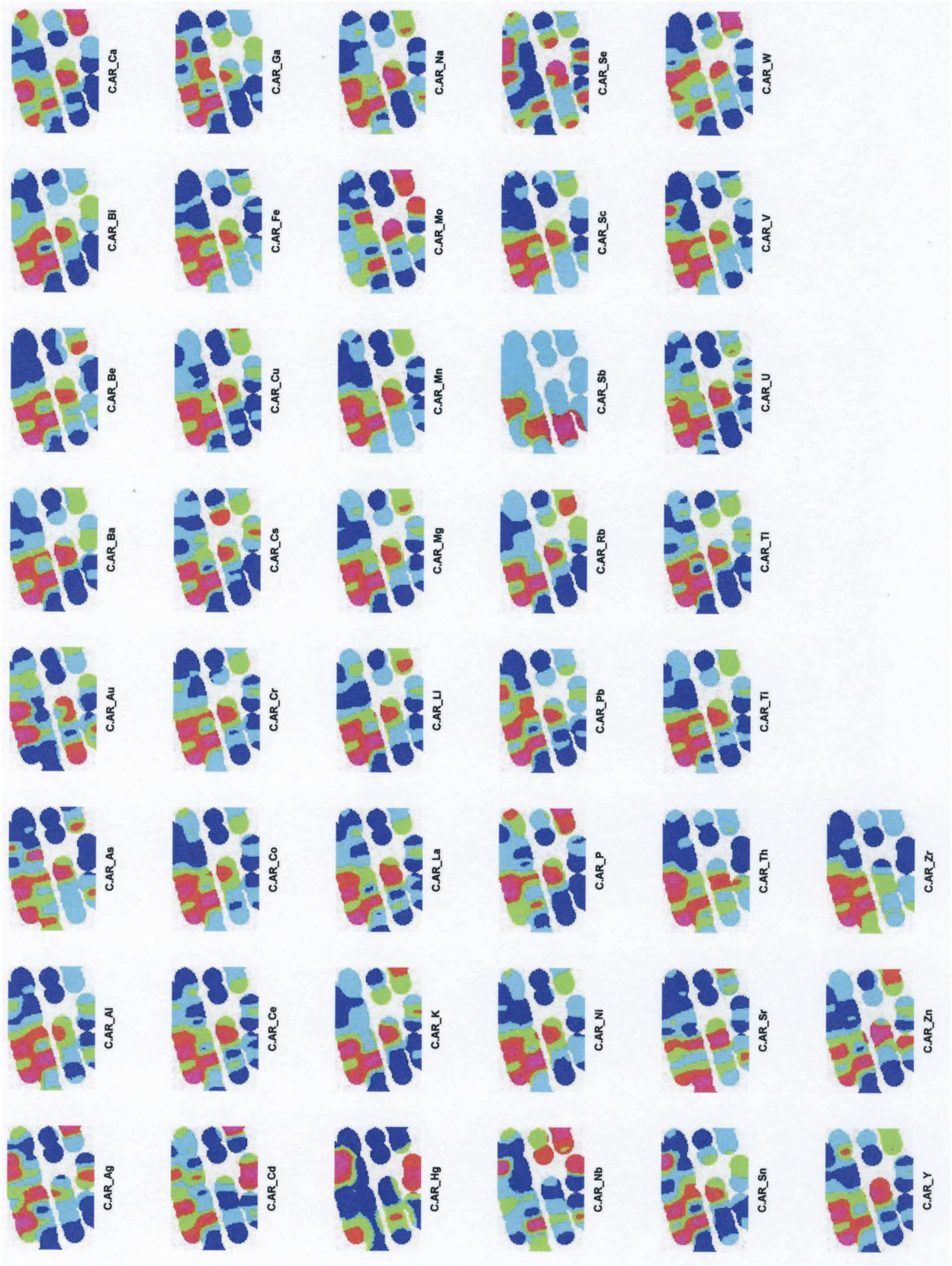

Fig. 6.119. McClean Lake Grids. C horizon. Aqua regia leach.

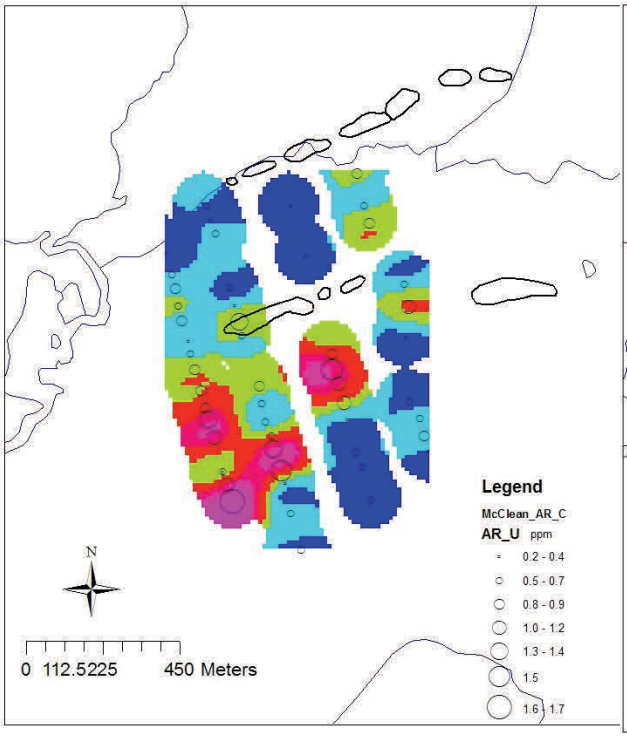

Uranium. C horizon. Aqua regia leach

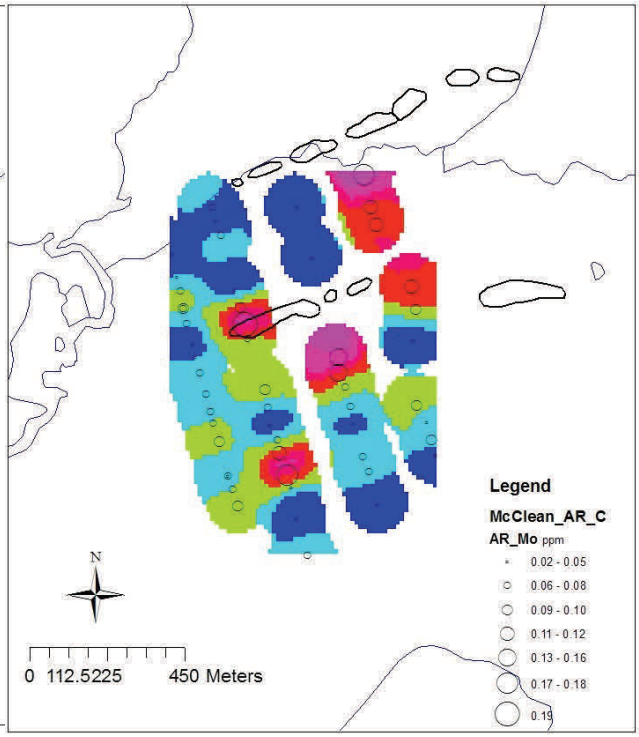

Molybdenum. C horizon. Aqua regia leach

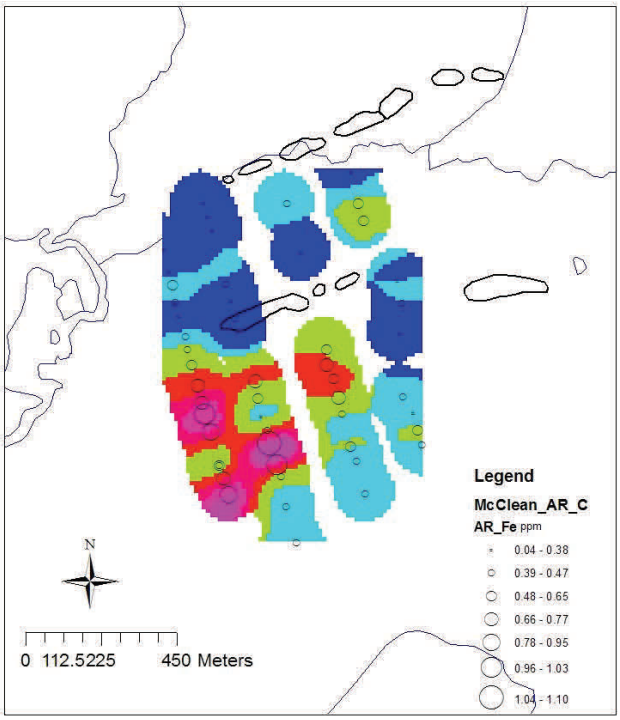

Iron. C horizon. Aqua regia leach

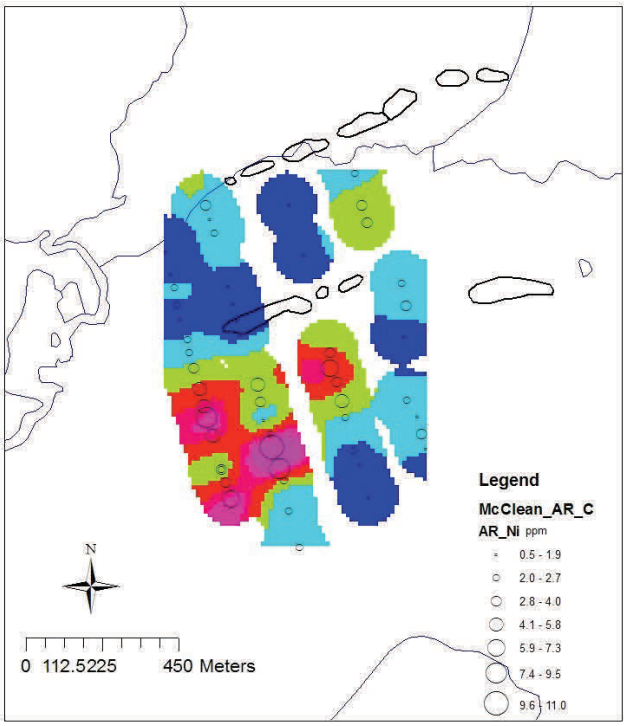

Nickel. C horizon. Aqua regia leach

Fig. 6.120. McClean Maps. C. Aqua regia.

Fig. 6.121. McClean Lake Grids. C horizon. Enzyme leach.

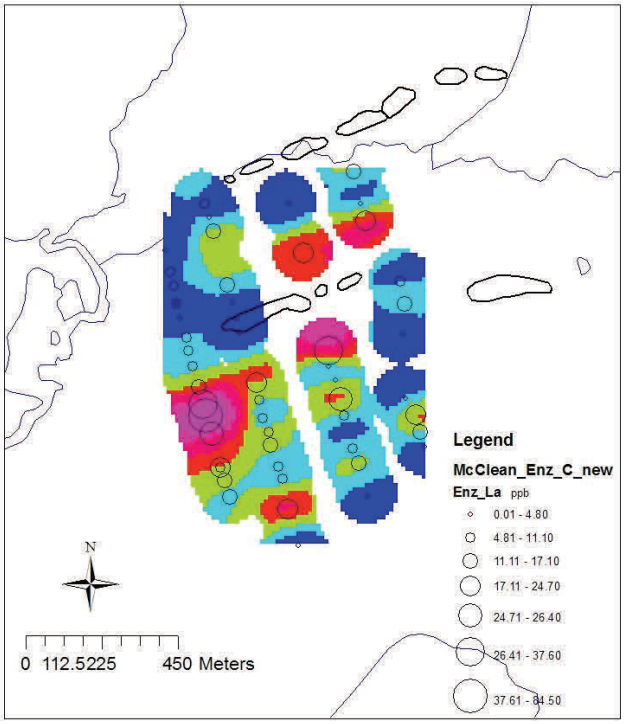

Lanthanum. C horizon. Enzyme leach.

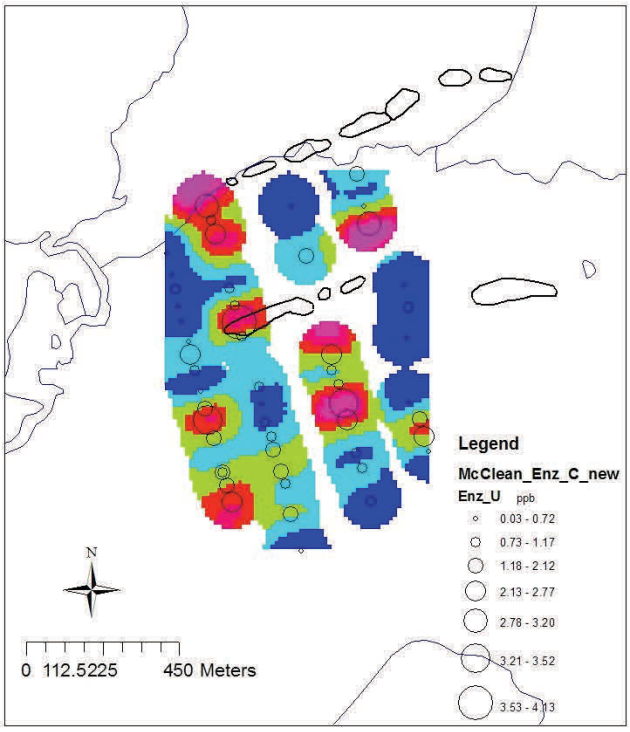

Uranium. C horizon. Enzyme leach.

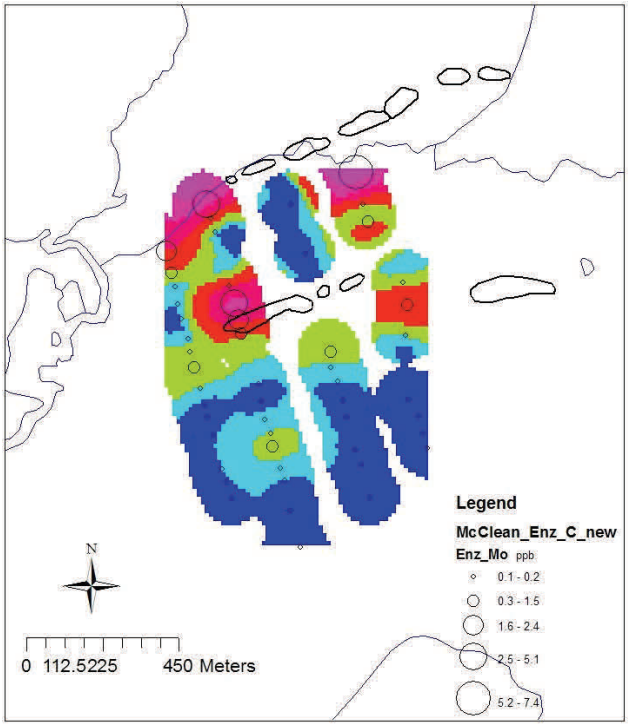

Molybdenum. C horizon. Enzyme leach.

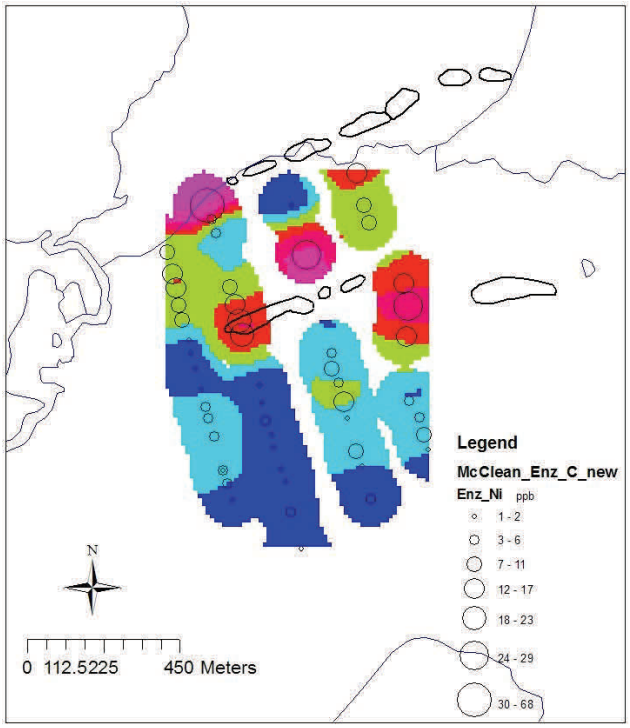

Nickel. C horizon. Enzyme leach.

Fig. 6..122. McClean Maps. C. Enzyme.

Fig. 6.123. McClean Lake Grids. C horizon. Hydroxylamine leach.

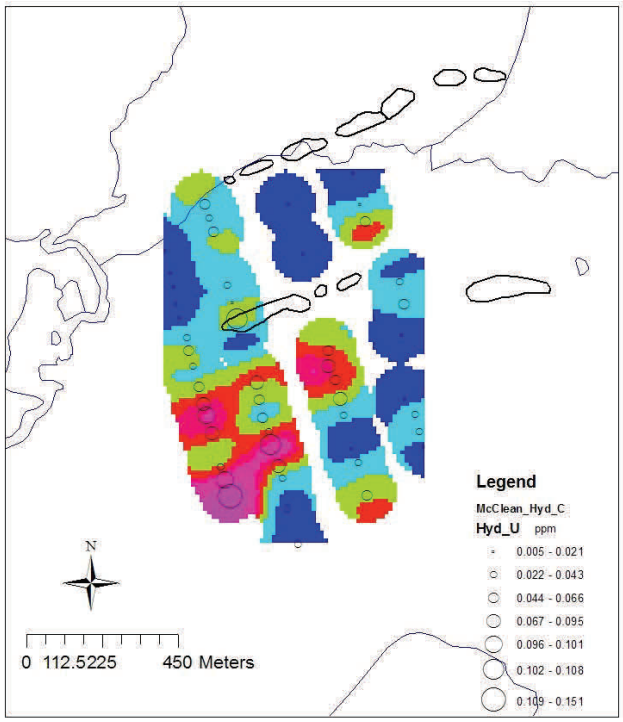

Uranium. C horizon. Hydroxylamine leach.

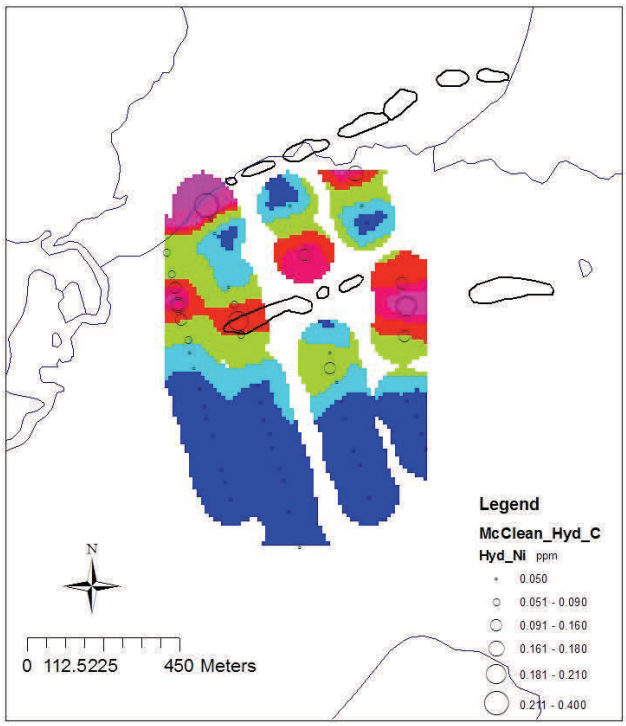

Nickel. C horizon. Hydroxylamine leach.

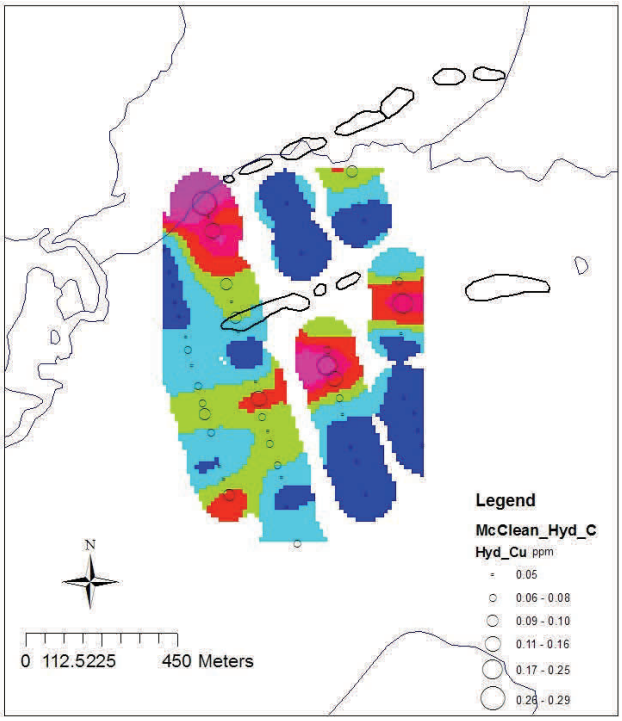

Copper. C horizon. Hydroxylamine leach.

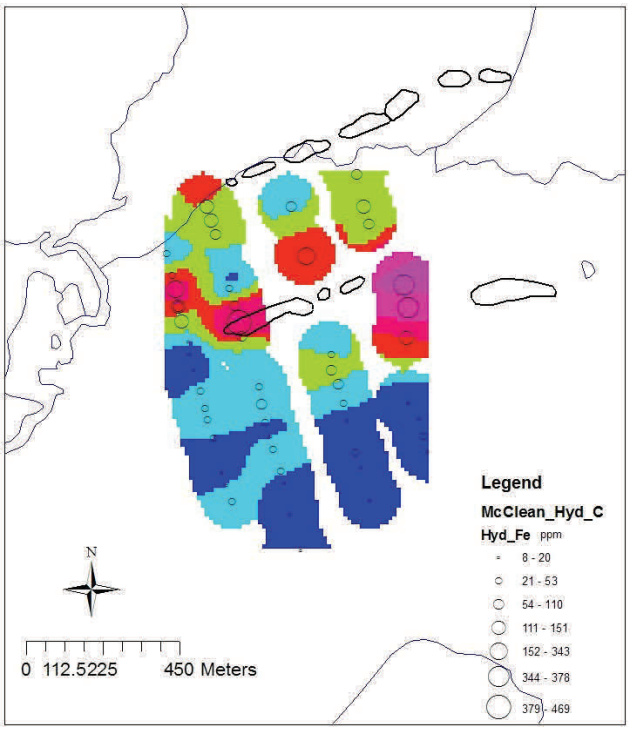

Iron. C horizon. Hydroxylamine leach.

Fig. 6.124. McClean Maps. C. Hydroxylamine.

Fig. 6.125. McClean Lake Grids. C horizon. Ammonium acetate leach.

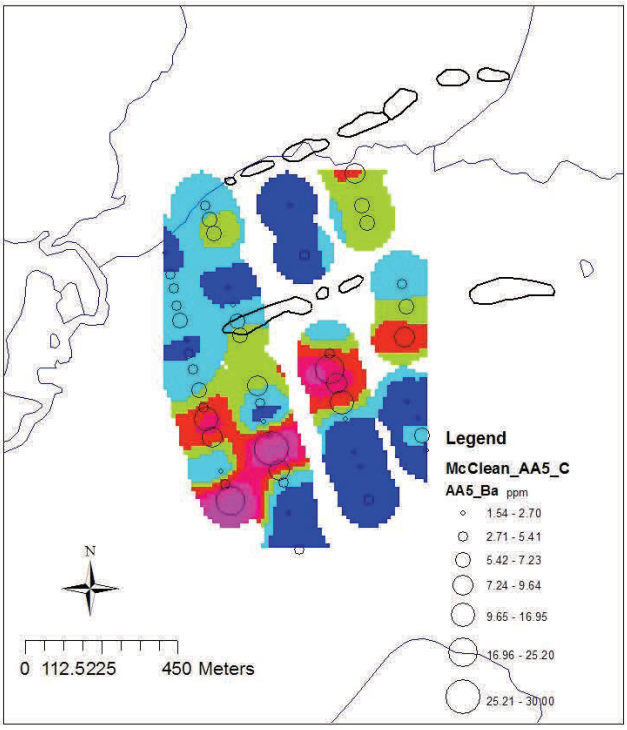

Barium. C horizon. Ammonium acetate

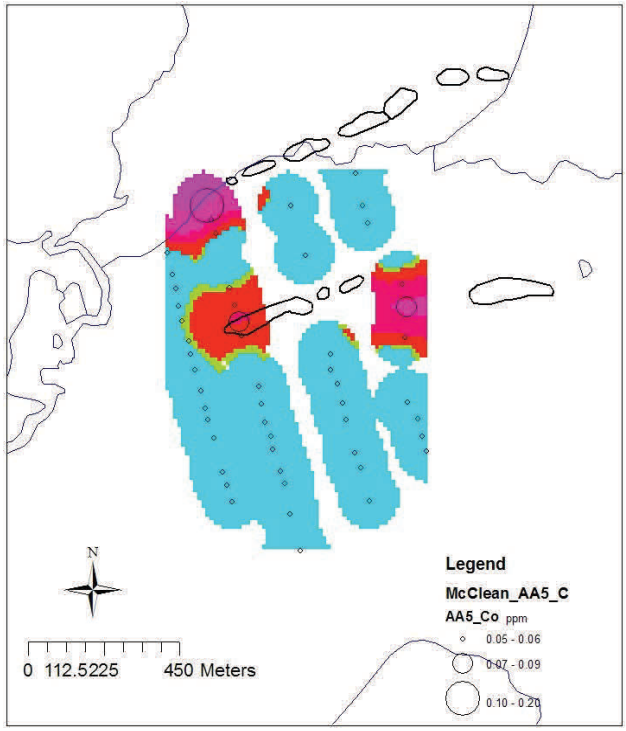

Cobalt. C horizon. Ammonium acetate

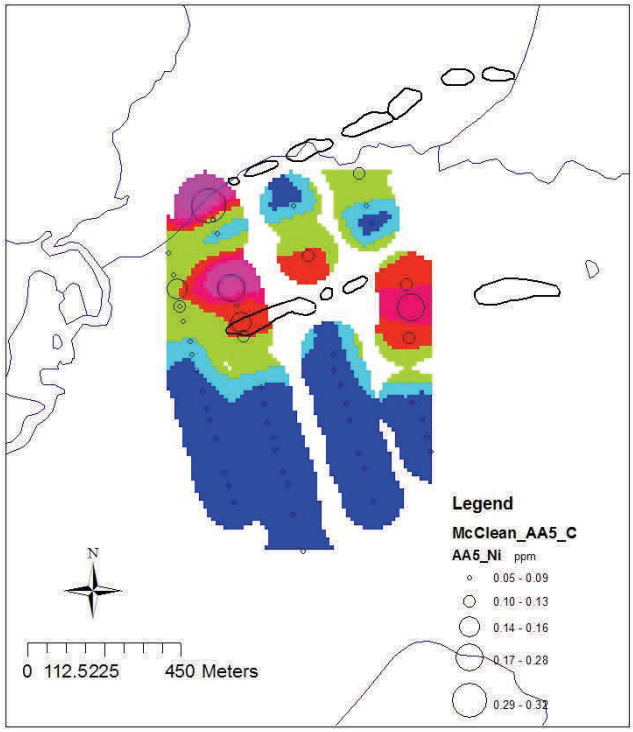

Nickel. C horizon. Ammonium acetate

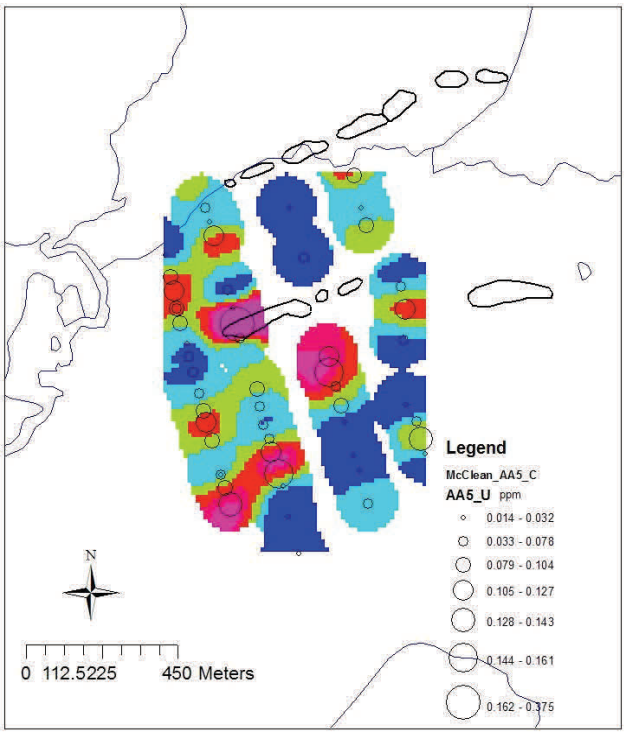

Uranium. C horizon. Ammonium acetate

Fig. 6. 126. McClean Maps. C. Ammonium acetate.

Fig. 6.127. McClean Lake Grids. C horizon. MMI leach.

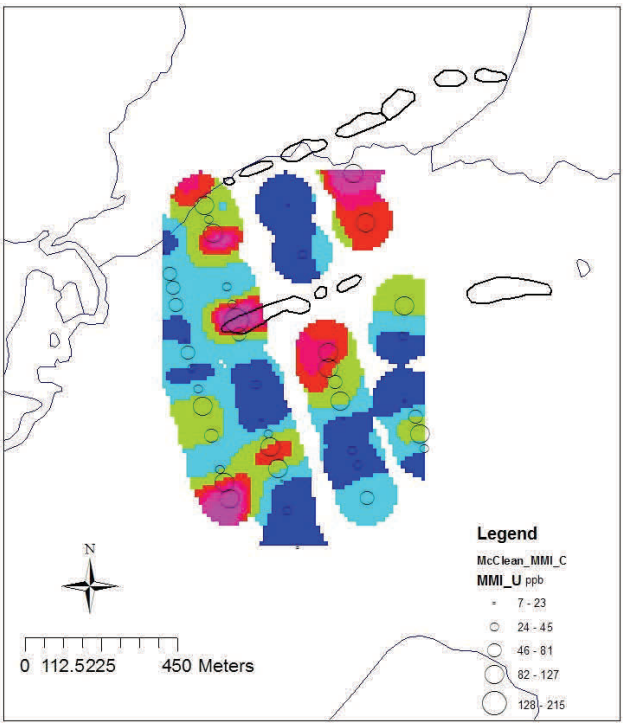

Uranium. C horizon. MMI leach.

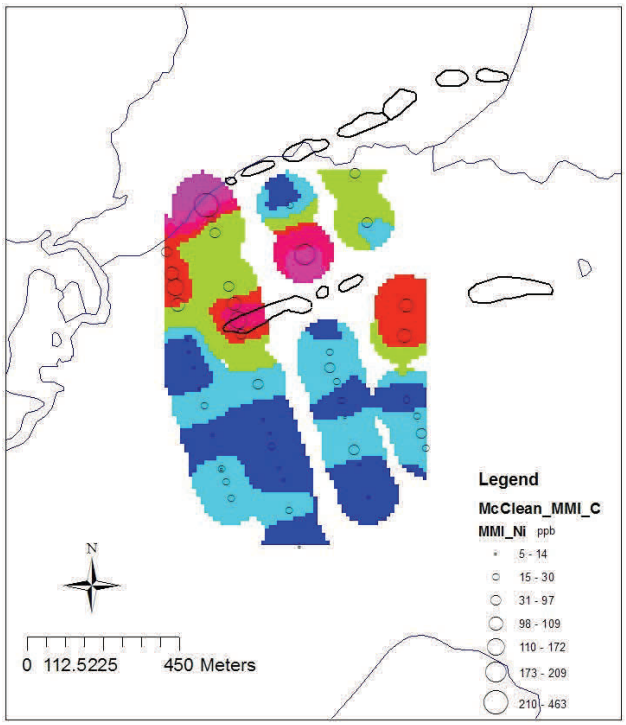

Nickel. C horizon. MMI leach.

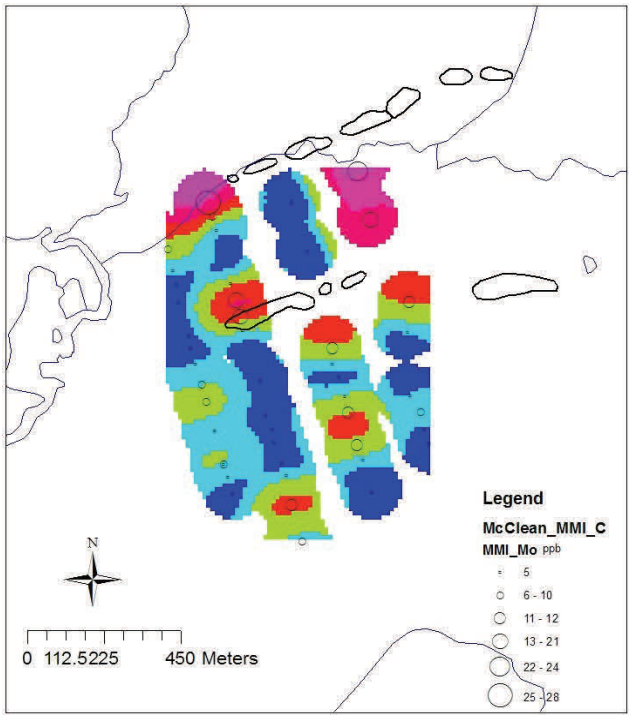

Molybdenum. C horizon. MMI leach.

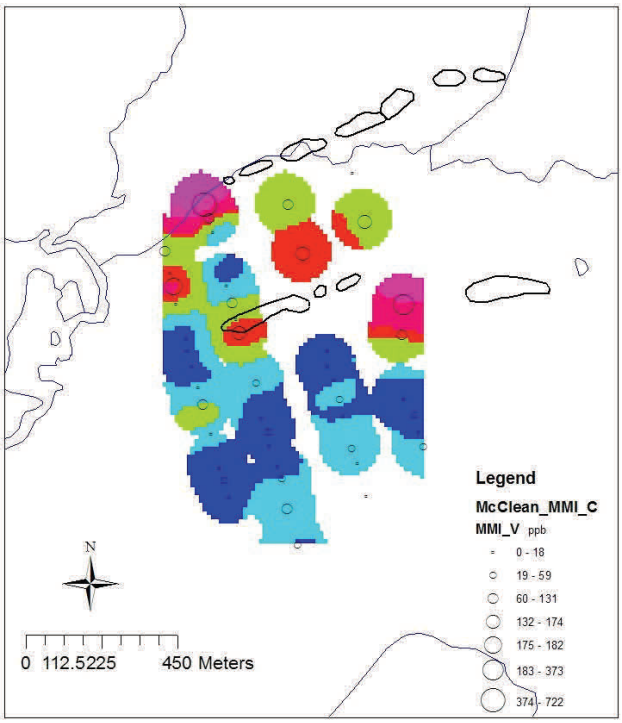

Vanadium. C horizon. MMI leach.

Fig. 6.128. McClean Maps. C. MMI.

Fig. 6.129. McClean Lake Grids. C horizon. Bioleach.

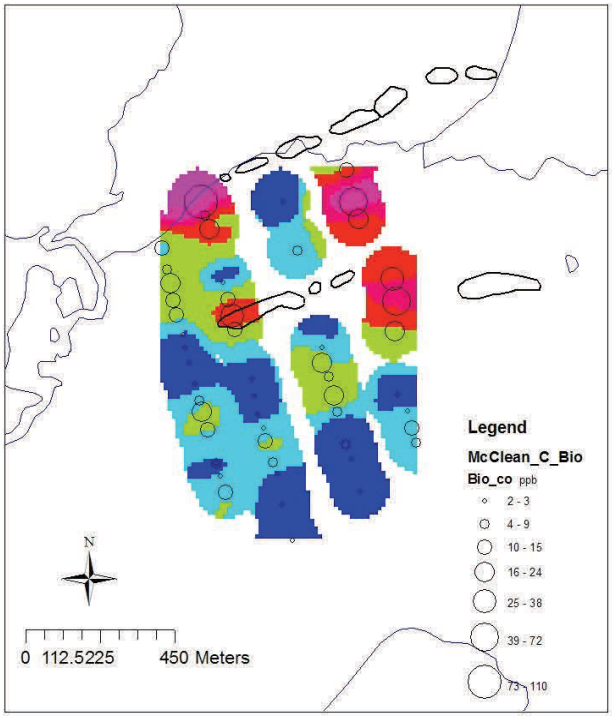

Cobalt. C horizon. Bioleach.

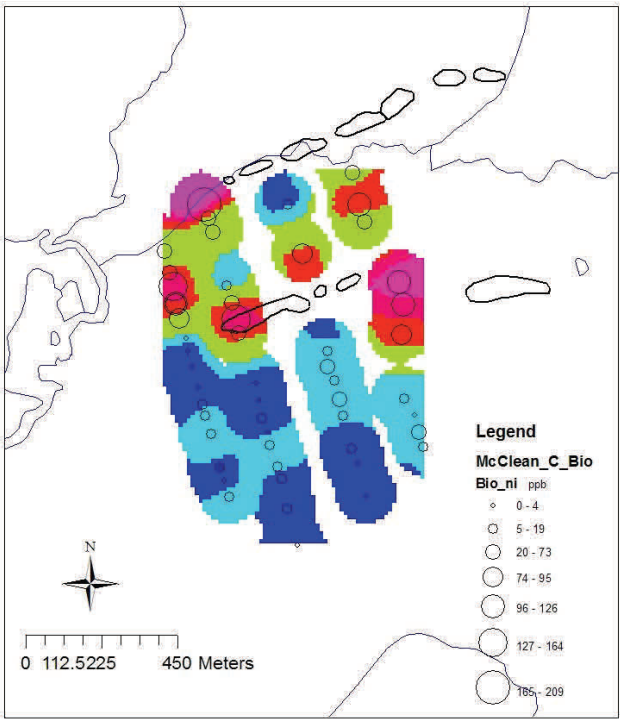

Nickel. C horizon. Bioleach.

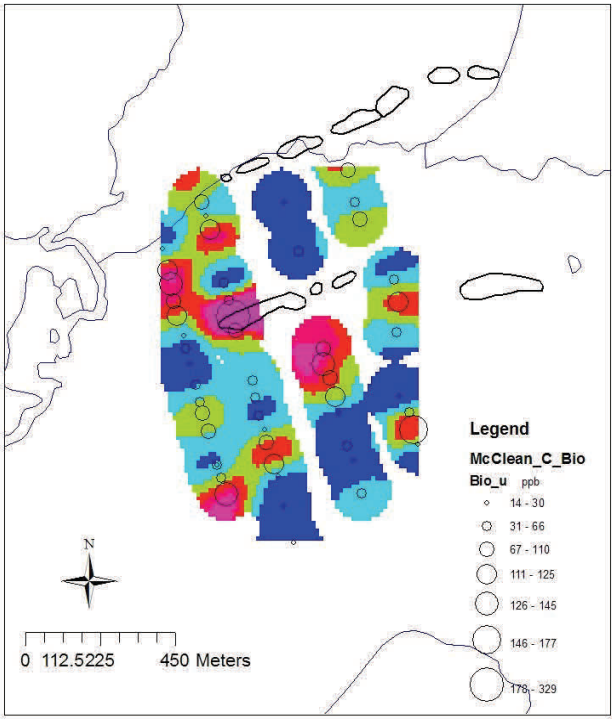

Uranium. C horizon. Bioleach.

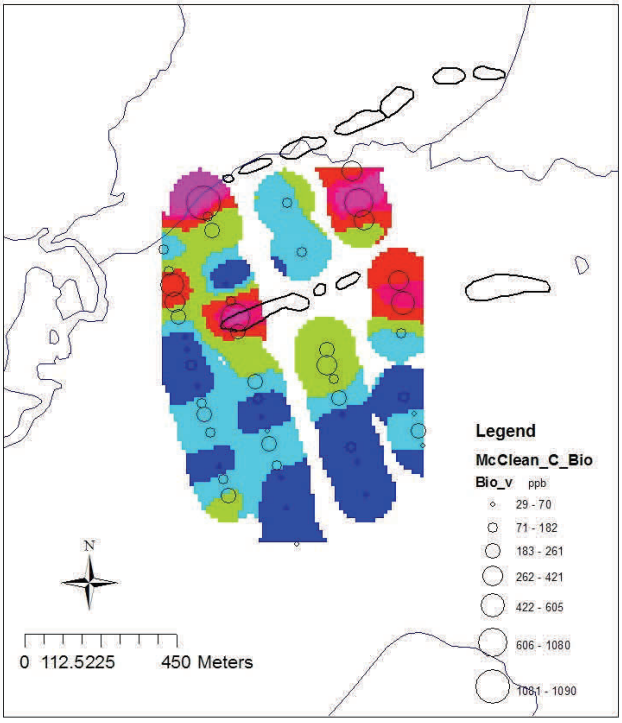

Vanadium. C horizon. Bioleach.

Fig. 6.130. McClean Maps. C. Bioleach.

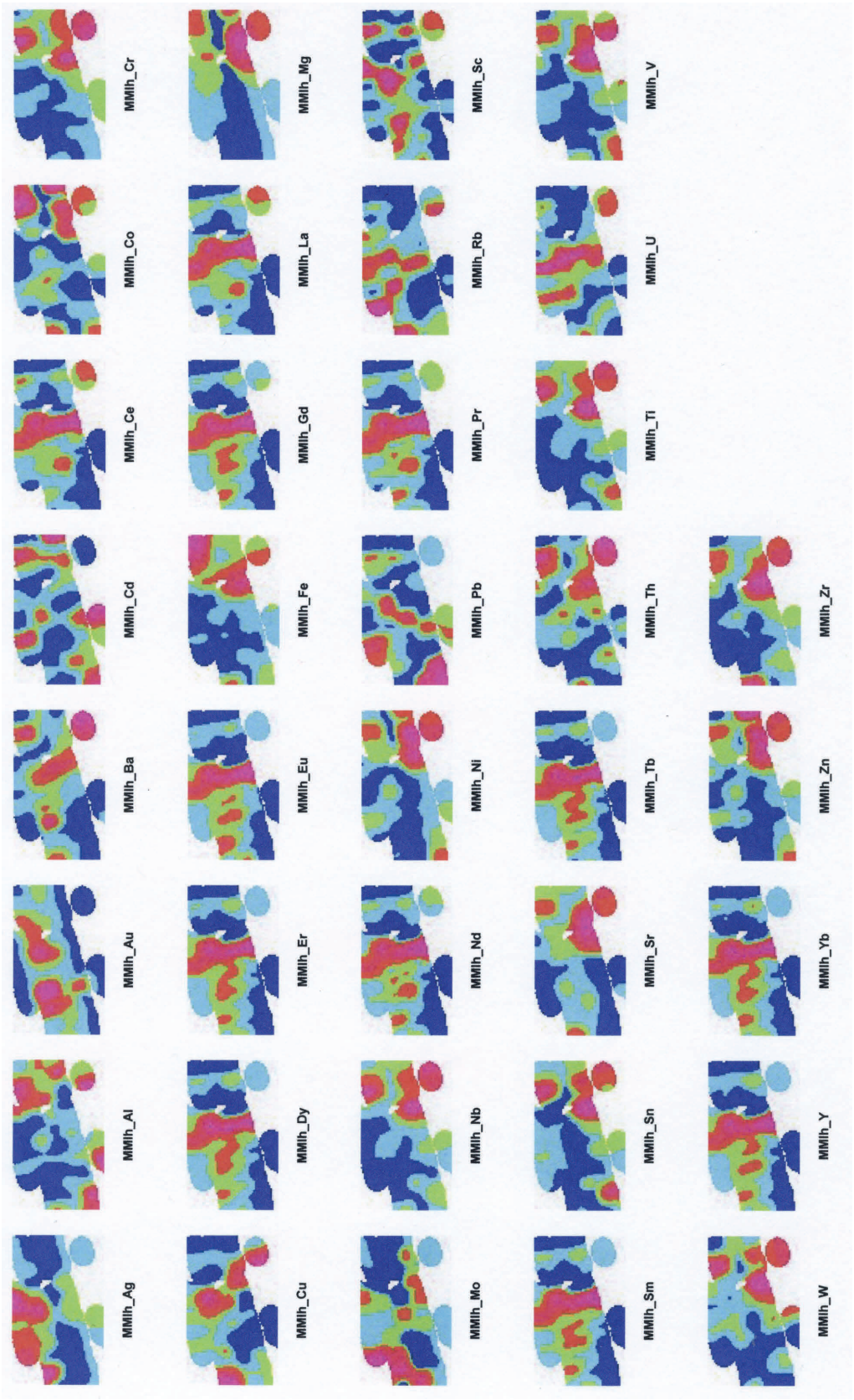

Fig. 6.131. McClean Lake Grids. MMI leach on MMI horizon.

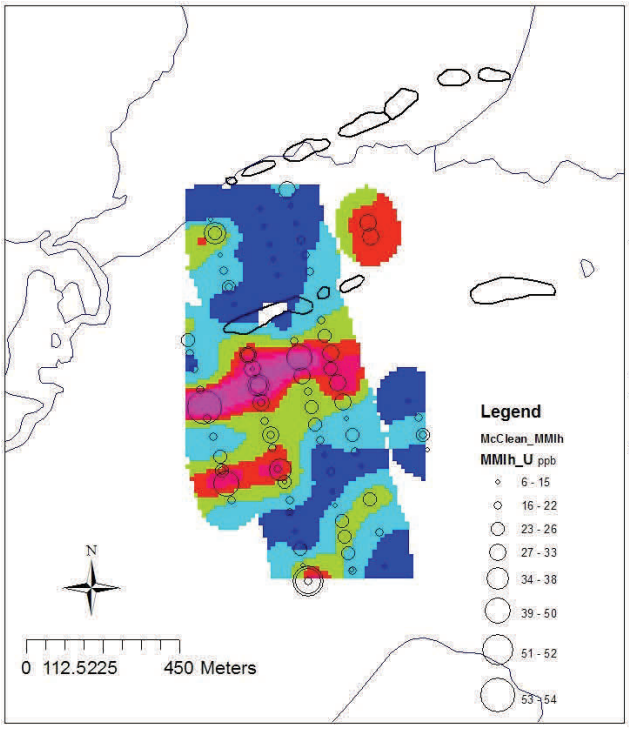

Uranium. MMI leach on MMI horizon.

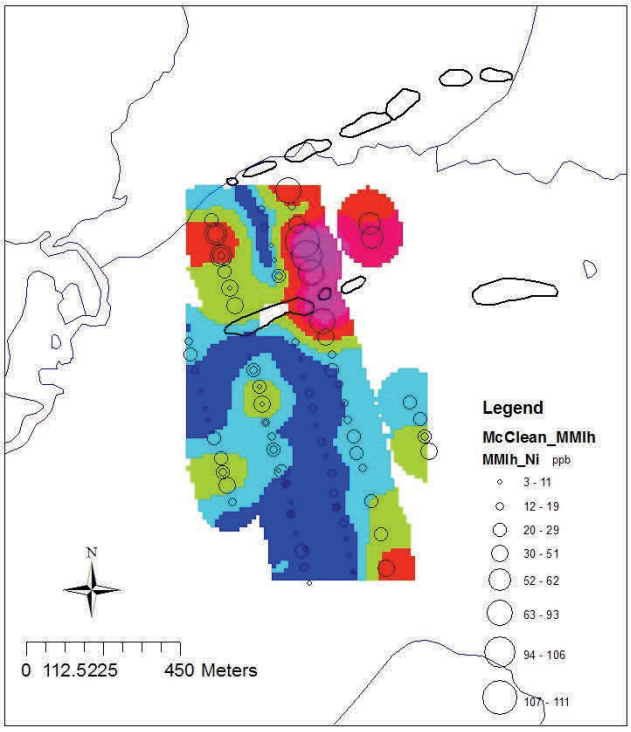

Nickel. MMI leach on MMI horizon.

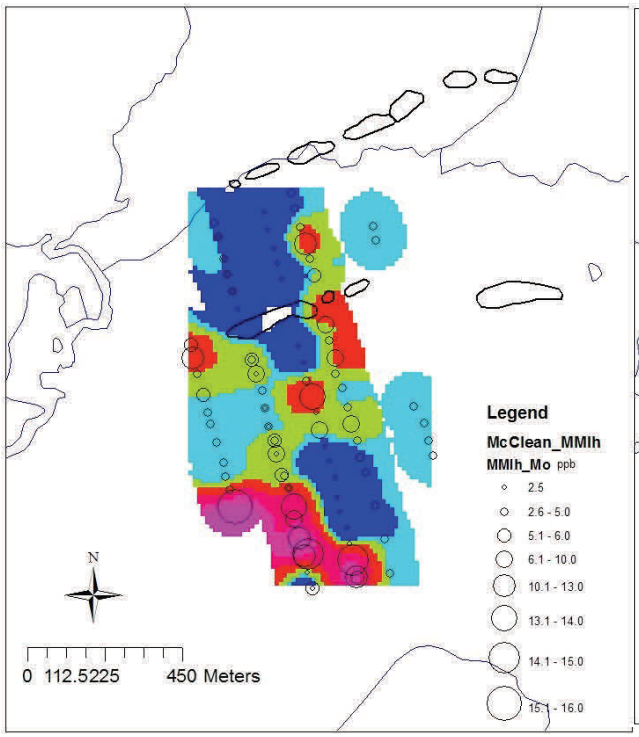

Molybdenum. MMI leach on MMI horizon.

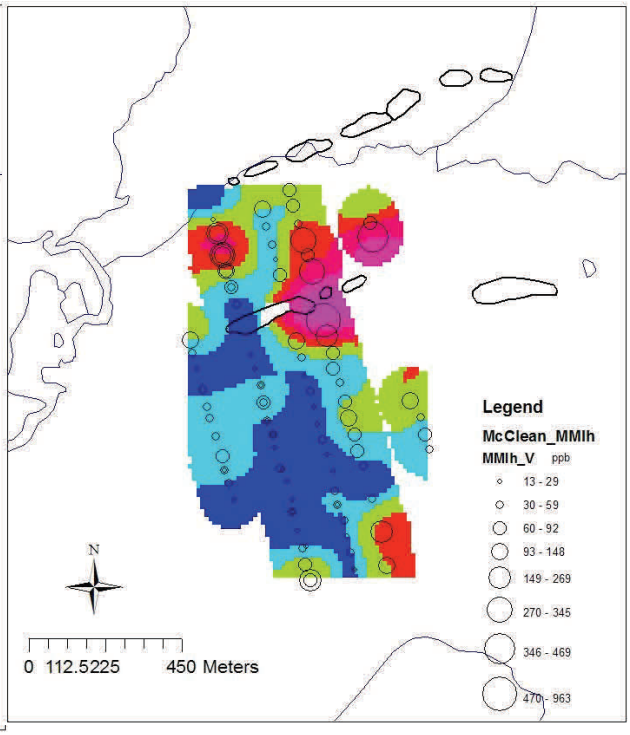

Vanadium. MMI leach on MMI horizon.

Fig. 6.132. McClean Maps. MMI leach on MMI horizon.

7. QC Plots and Profile Plots

This chapter repeats some of the material from Part I, Chapter 4, but is more thorough and complete.

7.1. Quality Assurance

Relative Standard Deviations of Duplicates

Field duplicate samples were taken in both years; crews were asked to take field duplicates at a rate of 1 in 20 but this rule was adhered to more in the second year of sampling. Duplicate holes were dug within a metre of the first where possible. Field duplicates were treated as separate samples and given different numbers. The various lines that were resampled in 2009 provided year-to-year field duplicates; the proximity of these samples to each other is generally less than that of the field duplicates sampled in the same year but the crews attempted to sample within ~ 2 m.

No standards were inserted in the first year but in the second a bulk sample of A1 humus and one of B1 horizon were obtained and these were prepared along with the samples at SRC. Each laboratory was asked to intersperse the standards equally amongst the samples (i.e. they were identifiable to the lab). Laboratory duplicates are splits of samples that the lab has taken through the leach and analytical procedures separately.

There are several contributions to the variance of the data for each sample site; these comprise the sampling variance and the analytical variance. These are additive and therefore the variance obtained for field duplicates is the sum of both the sampling and the analytical variances, the latter usually being much lower (smaller) than the former. In this survey, we have two sets of field duplicates: those representing differences in sample sites spaced ~ 1 m apart, and those representing differences in time (almost 14 months) and space (within ~ 2 m of the original sample). No splits were taken after sample preparation so we cannot estimate the variance of the sample processing step itself but this should be small as only sieving was employed (Au, a typically heterogeneous element, is not a critical one in this work).

Analytical reproducibility depends mostly on (1) the reproducibility of the leaching process and (2) the variation of the instrumental response (ICP-MS; less frequently ICP-ES) during the run. Reproducibility of a strong digestion such as aqua regia should not be an issue because the concentrations of elements determined will, by and large, be well above analytical detection limits. However, very weak partial leaches will inherently be associated with greater analytical variance as this increases as the element concentration decreases. The analytical variance here is based on laboratory repeats where a separate sample was leached and analysed (confirmed with lab).

The mean and RSD (relative standard deviation) of each dataset were calculated; the RSD was obtained using the formula:

$s^2 = (\sum(x_i - x_j)^2)/2N$

where the squares of the differences between duplicate pairs are summed, then divided by 2N, N being the number of pairs, to produce the variance s^2. The RSD in %, or Coefficient of Variation, is calculated from

$RSD = 100s/X$

where X is the mean of all duplicates.

Histograms of these RSD data were then created; elements where > 90% of the data was below detection limit were omitted. Values below detection limit were set to DL/2 for the 2009 data (Jackson set them to the actual DL in 2008). Examples of these histograms are shown in Figures 7.1-7.3 for aqua regia digestion of the A1 and P1 (organic) soils. We see a typical steady progression to more variability as we go from lab duplicates, to the A1 STD, to field duplicates and finally to year-to-year duplicates.

Table 7.1 provides the RSD data (minimum, median and maximum) for field and year-to-year duplicates whereas Table 7.2 provides the RSD data for the standard, A1 for an organic suite and B1 for an inorganic suite, where analysed and for lab duplicates, where provided by the lab.

Table 7.1. Relative standard deviation for field duplicates and year-to-year duplicates for various leaches. 'n' refers to the number of duplicates, for example there are 15 field duplicate pairs for aqua regia on organic samples and 58 pairs of year-to-year field duplicates. Organics include A1 and P1 (peat) horizons. Inorganics are all other samples.

	Field dup RSD, %			Yr-to-Yr field, RSD, %		
Leach	**Min**	**Median**	**Max**	**Min**	**Median**	**Max**
Aqua regia, organics, n=15, 58	13, Cu	28, Sb	105, Sn	22, Ga	36, K	118, Au
Aqua regia, inorganics, n=21, 75	14, Ti	25, Li	241, Au	20, Pb	28, La	66, Ag
Enzyme leach, inorganics, n=10, 60	11, Ta	52, Re	142, Mo	33, Rb	72, La	174, Sb
Pyrophosphate, organics, n=12, 58	12, Pb	32, Bi	107, Mn	25, Ba	51, I	257, Ta
Ammonium acetate, inorganics, n=22, 73	9.6, Tl	38, La	75, Sr	28, Rb	56, Mg	105, La
MMI, n=10, 56	17, Ta	53, La	132, Sn	29, Sc	68, Ag	173, Sn
Hydroxylamine, inorganics, n=12	8.0, Co	30, U	217, Zn			
Hydroxylamine, organics, n=3	7.4, V	28, La	108, Pb			
Bioleach, organics, n=19, 51	33, Sc	62, Tl	384, Cd	61, Be	109, Sc	319, W
Bioleach, inorganics, n=12	20, Mo	32, Lu	315, Li			

Table 7.2. Relative standard deviation for the standard ('STD', A1 for organics and B1 for inorganics, 2009 only) and laboratory duplicates. 'n' refers to the number of STD samples analysed and to the number of laboratory duplicates, for example there are 7 subsamples of the STD analysed and 4 lab duplicate pairs for aqua regia on organic samples.

	STD RSD, %			Lab dup RSD, %		
Leach	**Min**	**Median**	**Max**	**Min**	**Median**	**Max**
Aqua regia, organics, n=7, 4	6.2, S	11, Li	70, Au	1.1, Pb	4.4, Rb	37, Au
Aqua regia, inorganics, n=5, 5	4.3, Zn	10, Sr	103, W	1.8, Mn	6.1, Sc	51, Cd
Enzyme leach, inorganics, n=6, 11	6.3, Mn	24, Tb	140, Dy	2.6, I	16, Pr	53, Pb
Pyrophosphate, organics, n=6	4.6, Gd	9.5, La	59, Li			
Ammonium acetate, inorganics, n=6, 6	5.2, Rb	9.2, Ce	160, V	1.0, Zn	4.5, Gd	175, V
MMI, n=11				4.2, Dy	9.4, Fe	33, Cd
Bioleach, organics, n=11				4.9, U	20, La	293, Li
Ionic leach, n=3	1.3, Au	6.2, Ag	Eu, 21			

Aqua regia, organic soils

Not surprisingly, the RSDs for the field duplicates are generally significantly better than those for the year-to-year duplicates, the median RSD for the former being 28% cf to 36 % for the latter (Table 7.1, Fig. 7.1). These RSDs are quite acceptable; those elements reporting most concentrations within a decade of the DL generally have the highest RSD (e.g. Au, Li, Sn). Molybdenum has fairly high RSDs of 66 and 79%, respectively, for field and year-to-year duplicates and yet most concentrations are well above the 0.01 ppm DL; the respective RSDs for U are 35 and 51% but most values are within a decade of the 0.1 ppm DL.

RSDs for the lab duplicates and the A1 STD are indeed excellent, with the medians at 4 and 11%, respectively (Table 7.2, Fig. 7.2). Molybdenum is much less noisy than for the field duplicates, the RSDs being 4.7% for A1 and 8.5% for lab duplicates and yet the concentrations are similar, perhaps suggesting that Mo is rather heterogeneously distributed in the field. RSDs for U are low, at 7.1 and 13% for the lab duplicates and the A1 STD. X-Y plots (not shown) of U for any of the three duplicate datasets exhibit no bias whatsoever.

Aqua regia, inorganic soils

The overwhelming majority of the RSDs for the year-to-year and field duplicates fall in the ranges 20 (Pb) – 35% (Ba) and 14 (Ti) – 45% (Zn), respectively, most acceptable values (Fig. 3, Table 7.1). Uranium has RSDs of 30 and 28% for field and year-to-year duplicates, respectively, and shows no bias between years (none of the elements do). Median values of RSD for the B1 STD and lab duplicates are excellent, at 10 (Sr) and 6.1%, respectively, and RSDs for U are 16 and 13%, respectively, also good (Fig. 7.4, Table 7.2). The elements appearing at the right end of the histograms are those with concentrations close to the DL, as would be expected. Although the precision of the aqua regia results is good, it would be helpful to obtain better DLs for the following elements: B (currently 20 ppm), W (0.1 ppm), Tl (0.02 ppm) and S (0.02%), and additionally for inorganic media, Cd (currently 0.01 ppm), Sb (0.02 ppm), Bi (0.02 ppm) and Se (0.1 ppm).

Enzyme leach (inorganic soils)

A quick comparison of Figures 7.3 (aqua regia) and 7.5 (Enzyme) and Figures 7.4 (aqua regia) and 7.6 (Enzyme) indicates that the RSDs for the equivalent datasets are significantly inferior to those by aqua regia: this is true for any of the partial leaches as concentrations of elements are so much lower. The median RSDs for field duplicates and year-to-year duplicates for the Enzyme leach are 52 and 72%, respectively (cf. 25 and 28% for aqua regia), and those for B1 and lab duplicates are 24 and 16%, respectively (cf 10 and 6% for aqua regia (Tables 7.1, 7.2). The RSDs for U for the field and year-to-year duplicates are 45 and 72%, respectively, much higher than that for lab duplicates of only 8.5%. There does seem to be a bias in the U year-to-year data (Fig. 7.7), with higher values on 2009.

Perusal of the year-to-year datasets shows that Br and I are displaying a significant bias, with much higher concentrations reported in the second year of sampling and analysis (Figs. 7.8, 7.9). The associated RSDs of this dataset for Br and I are 52 and 73%, much higher than the RSDs for the field and lab duplicates of 27 and 14% and 5.2 and 2.6%, respectively. This bias could easily distort the patterns of these two elements in both surveys where the data are combined. It is a pity we do not have a control sample analysed both years to determine whether this is a calibration shift in the analysis or a real feature of time of sampling.

Pyrophosphate leach (organic soils)

The majority of the RSDs for the field and year-to-year duplicates, where most data are not very close to the DL, are in the range 12 (Pb) – 60 % (La) and 25 (Ba) – 74% (Mn), respectively (Fig. 7.10); the RSDs for U are 47 and 67%, respectively. Most of the RSDs for the A1 STD lie in the range 4.5 (Gd) to 19% (Pb), with U at 7.9% (Fig. 7.11). There does not appear to be any bias in values between years, including iodine (Fig. 7.12), suggesting perhaps that the bias seen with the Enzyme leach is an analytical one, though the media are different (organic vs inorganic horizons). Unfortunately there were no lab duplicates for this leach.

Ammonium acetate leach (inorganic soils)

It is clear by glancing at Figures 7.13 and 7.14, presenting the RSDs for this leach, that there are far fewer elements reported with adequate detection limits for concentrations in the B1 and other inorganic horizons (unlike the situation with the pyrophosphate leach where concentrations in the organic medium tend to be elevated compared to the inorganics). The RSDs for U for B1 and lab duplicates is 9.5 and 4.0%, respectively, and these increase to 43 and 41% for field and year-to-year duplicates. The median RSDs for this leach are better than those for the Enzyme leach (9.2, 4.5, 38 and 55% cf to 24, 16, 52 and 72% for Enzyme; Tables 7.1, 7.2) but the element suite is too limited. There is no apparent bias between years.

MMI (MMI horizon)

The RSDs obtained for the various duplicate sets for the MMI leach are similar to those for the Enzyme leach (Tables 7.1, 7.2; Figs. 7.15, 7.16). The RSDs for U in the laboratory, field and year-to-year duplicates are 7.2, 49 and 47%, respectively. The high RSDs of some elements such as Cr, Ti, Fe and Zn, plotting at the right-hand end of Figure 7.15, are not due to concentrations near to DL, rather these elements appear to be heterogeneously distributed with respect to this method. Uranium tends to show a bias in the year-to-year duplicates, reporting higher in 2008, as does Zn (Figs. 7.17, 7.18).

Hydroxylamine leach (inorganic soils)

This leach was not employed in the 2009 survey and hence there are no year-to-year duplicates or B1 STD data. There were too few lab duplicates to use.

Figure 7.19 presents the RSDs for field duplicates; the range in RSD is acceptable at 8-30%, with that for U at 30%. Although most of the concentrations of Zn and Pb are within a decade of the DL, the reason for the high RSDs of 217 and 161%, respectively, lies more with several poorly reproducible ‘highs’ such as 6.2 and 0.3 ppm for Zn and 1.1 and 6.1 ppm for Pb.

Bioleach (organic soils)

The Bioleach has the poorest performance of all the leaches in terms of RSD (range and median), with median RSDs of 20, 62 and 109 % for lab, field and year-to-year duplicates (Tables 7.1, 7.2); the corresponding RSDs for U are 4.9, 50 and 102%, respectively.

The most important concern is the extremely poor year-to-year reproducibility: most of the elements report significantly lower concentrations in 2009, as shown by Figures 7.22 and 7.23a for U and Br, respectively. Tunsgten, however, has far higher concentrations in 2009 (Fig. 7.23b). This poor performance is a pity there is a large suite of elements at good detection limits reported with this leach and especially interesting are the halogens.

Ionic leach (inorganic soils)

There are data only for 2009 and there are no lab duplicates or field duplicates (probably owing to large sample size required). Like the Bioleach, the suite of elements reported, including the halogens, with adequate detection limits is large. The RSDs shown for the B1 STD (Fig. 7.24), though only three subsamples were analysed, are encouraging, with a tight range and a median of 6.2% (RSD for U is 8.0%). Palladium is reported at 4.5±0.6 ppb (<0.5 ppb by Enzyme, <10 ppb by aqua regia) which is highly unlikely; the lab should revisit its interference corrections.

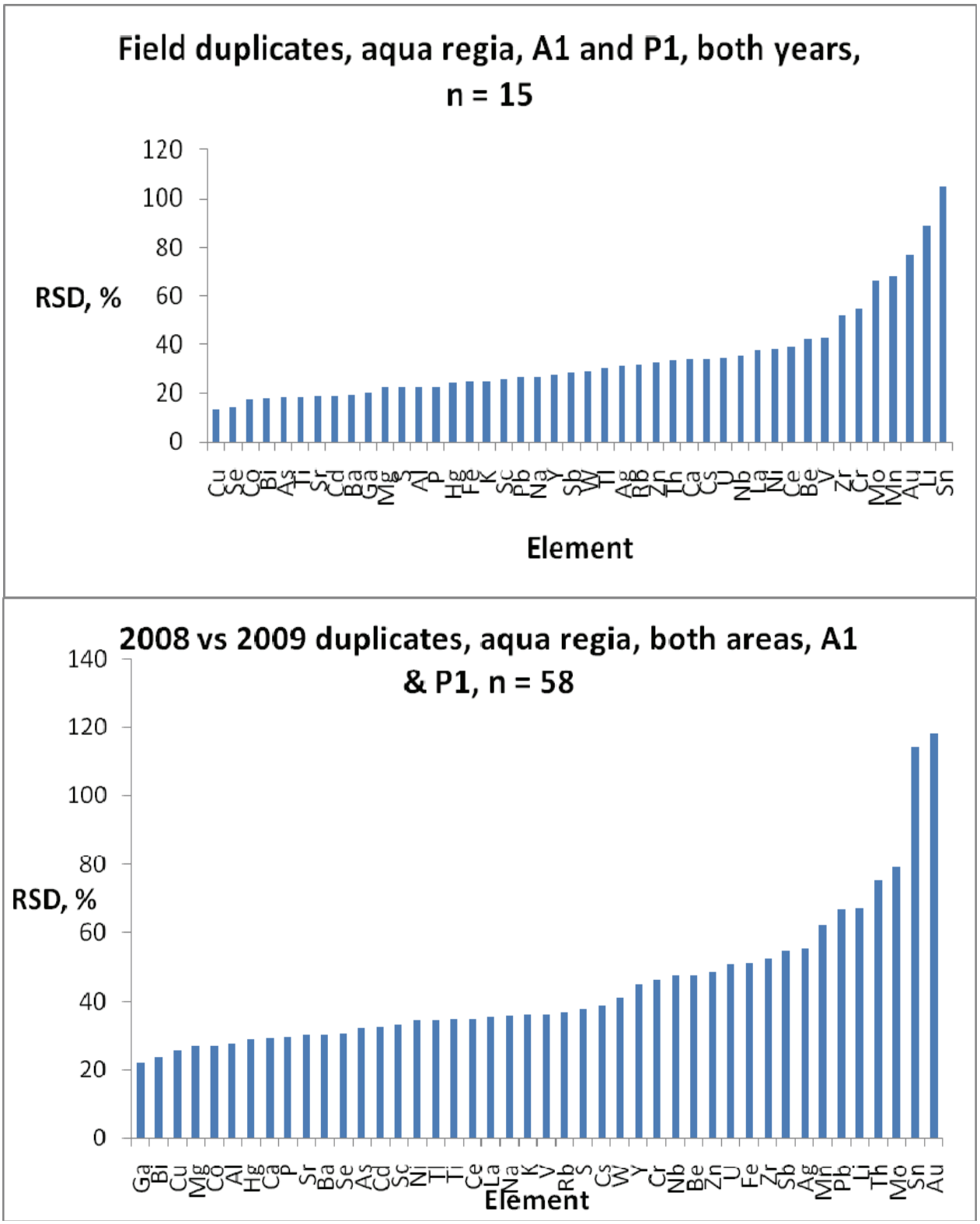

Fig 7.1 RSDs for aqua regia on organic soils (a) for field duplicates and (b) year-to-year duplicates.

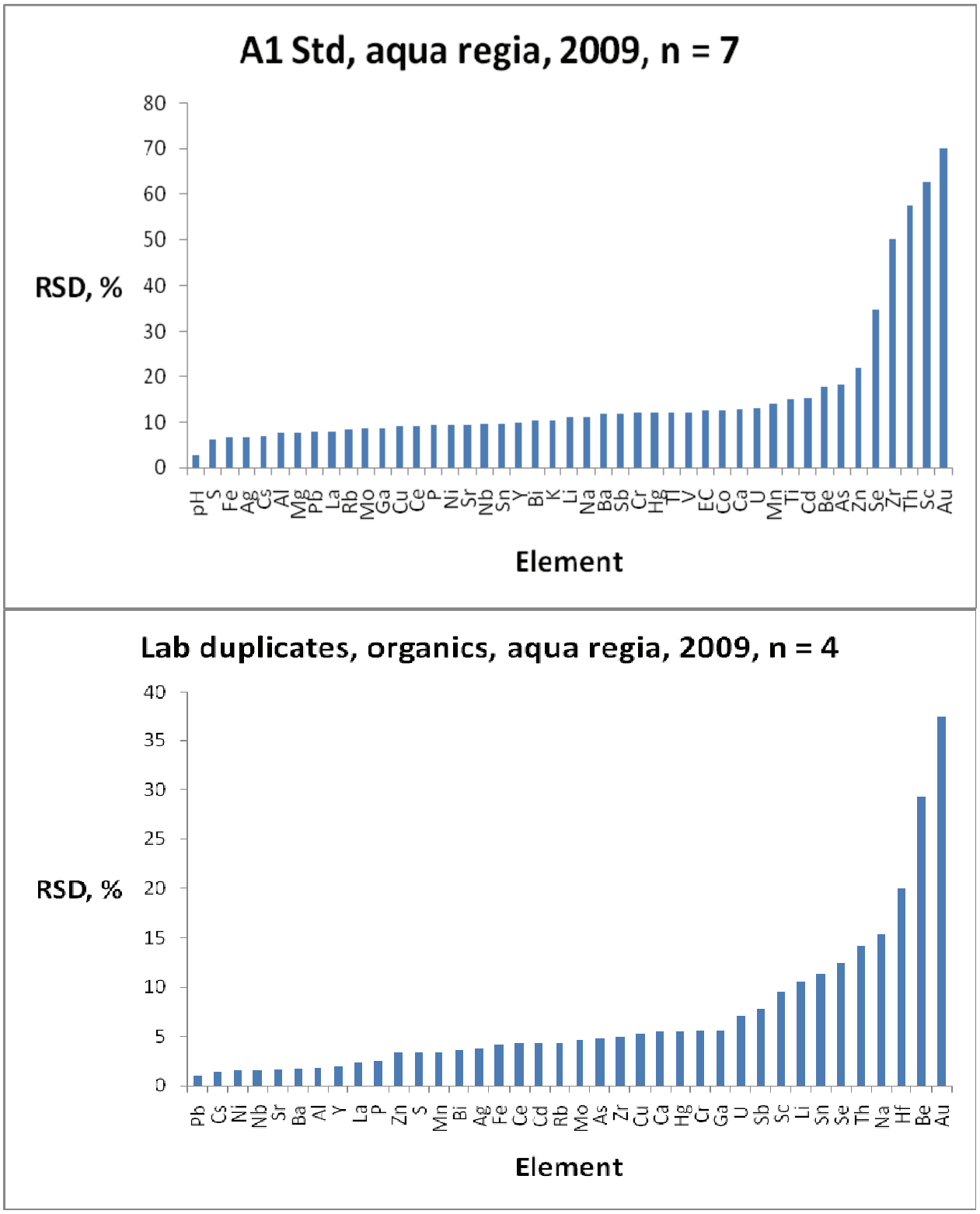

Fig. 7. 2. RSDs for aqua regia on organic soils (a) for A1 STD and (b) lab duplicates.

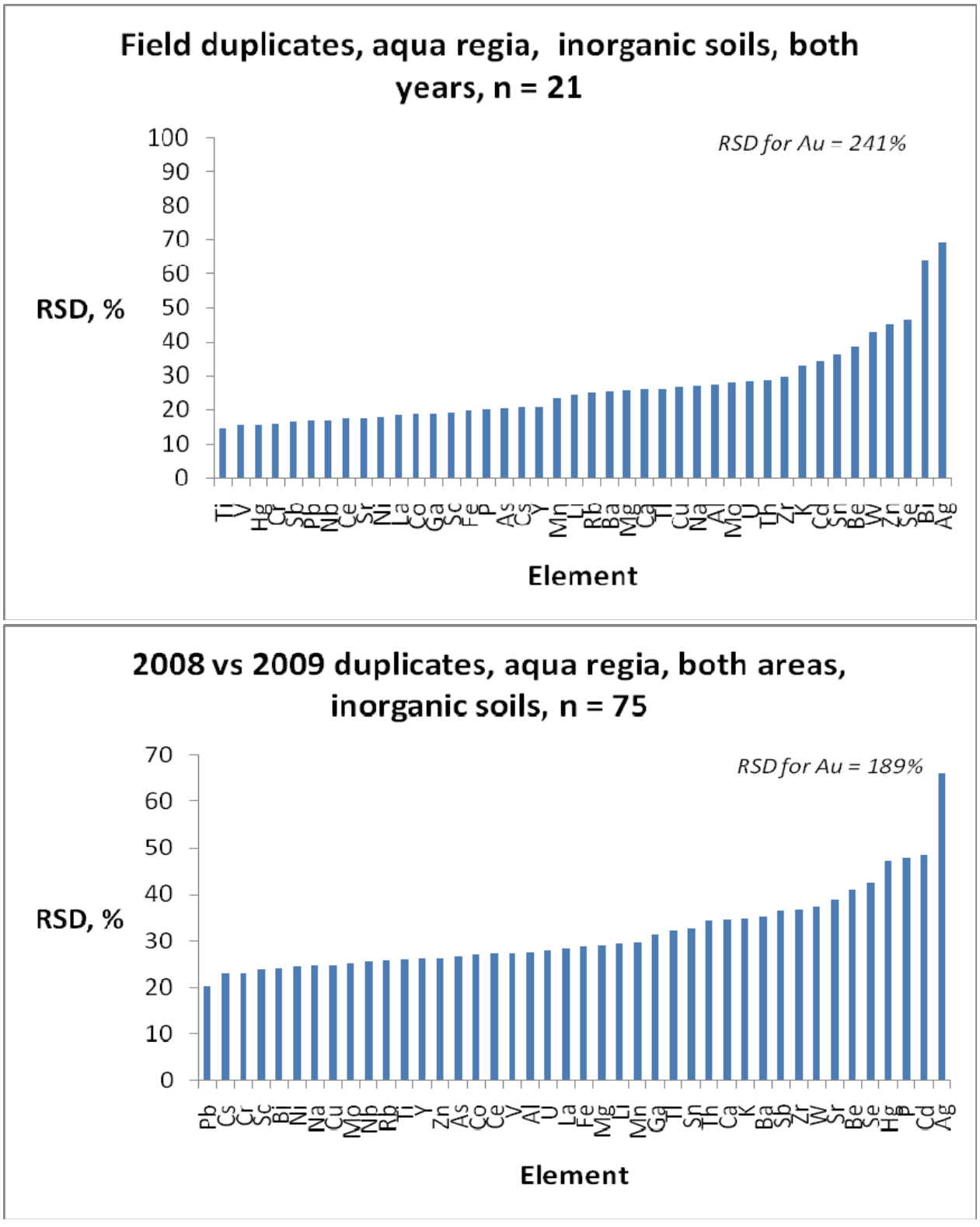

Fig. 7.3. RSDs for aqua regia on inorganic soils (a) for field duplicates and (b) year-to-year duplicates.

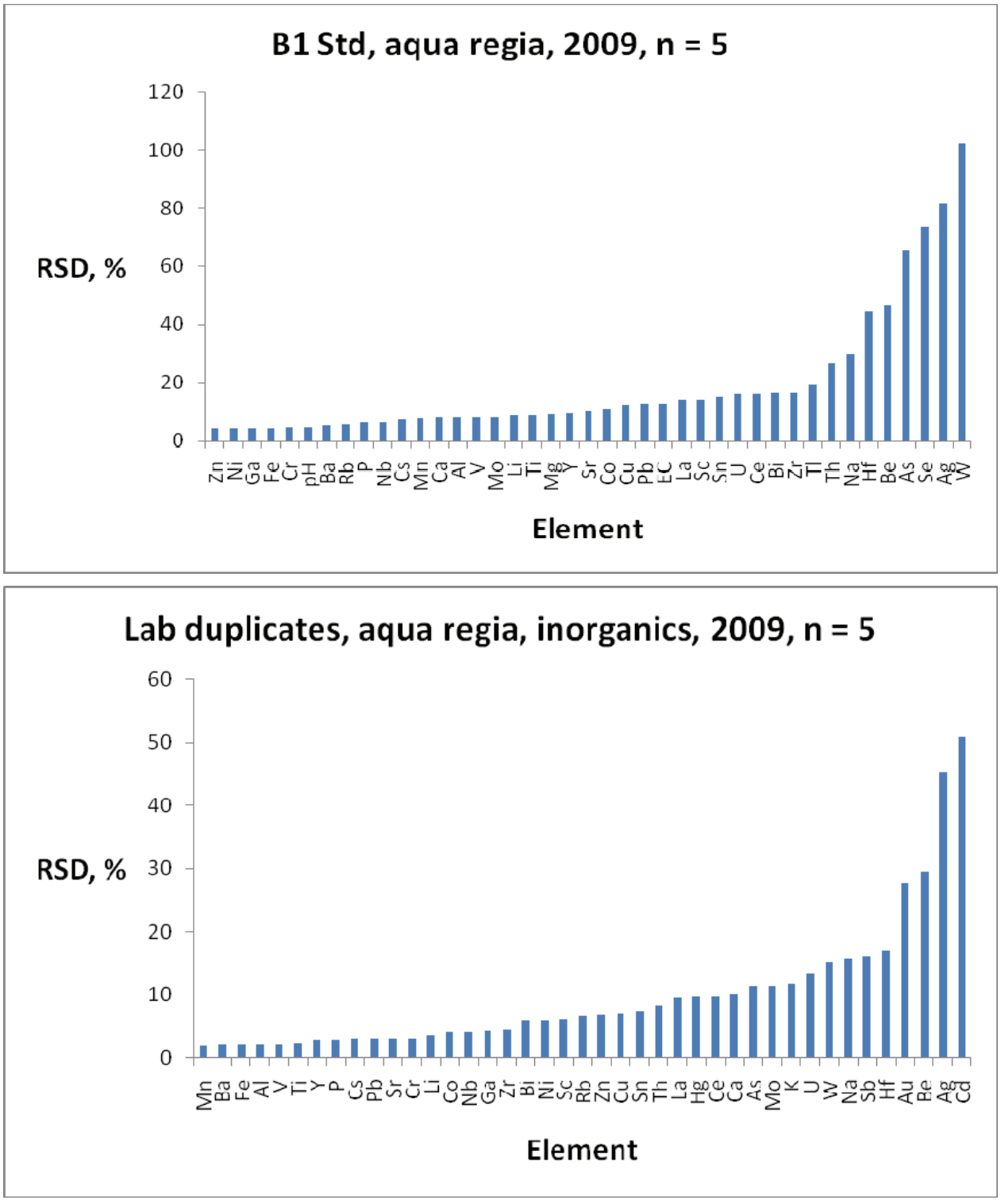

Fig. 7.4. RSDs for aqua regia on inorganic soils (a) for A1 STD and

(b) lab duplicates.

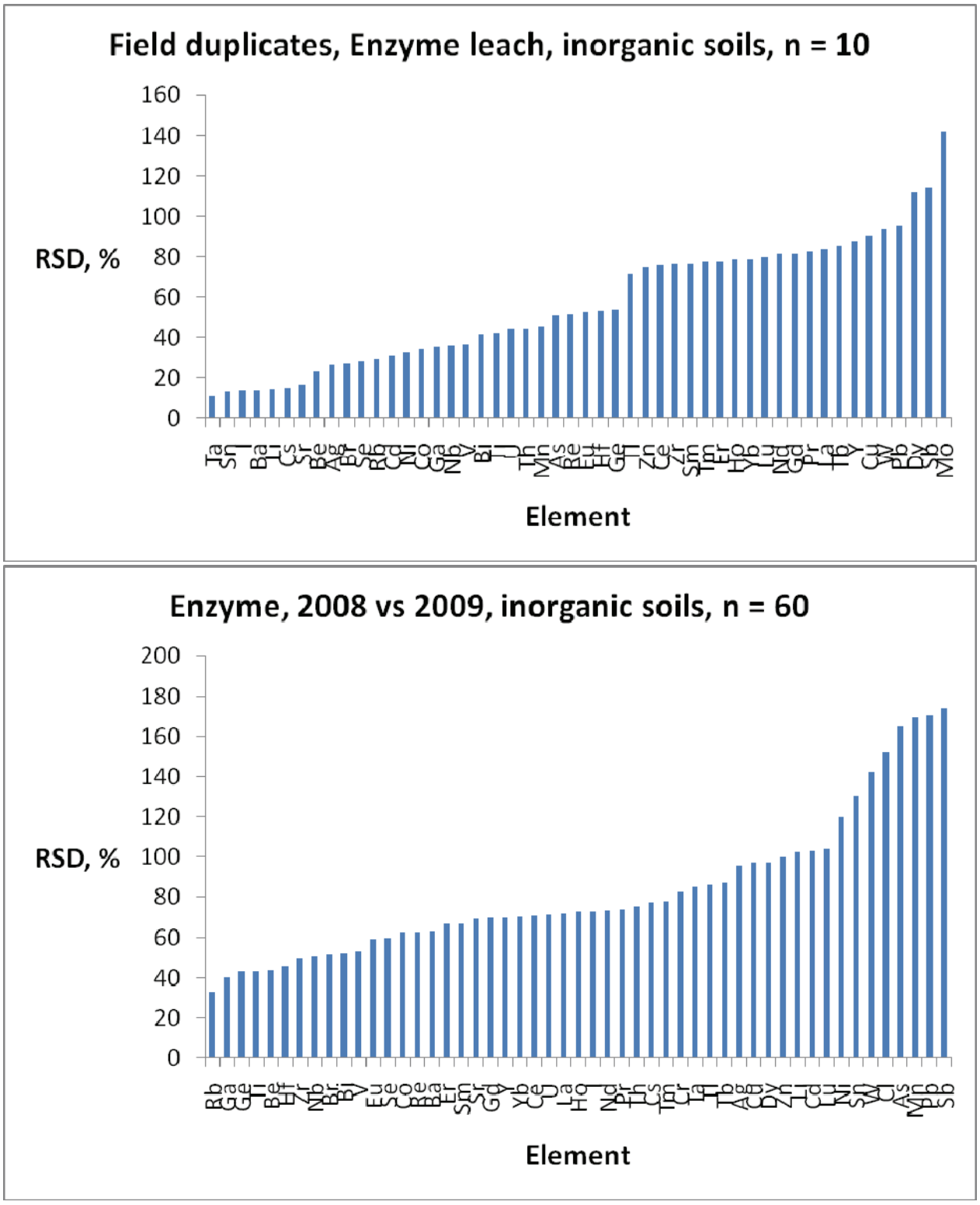

Fig. 7.5. RSDs for Enzyme leach on inorganic soils (a) for field duplicates and (b) year-to-year duplicates.

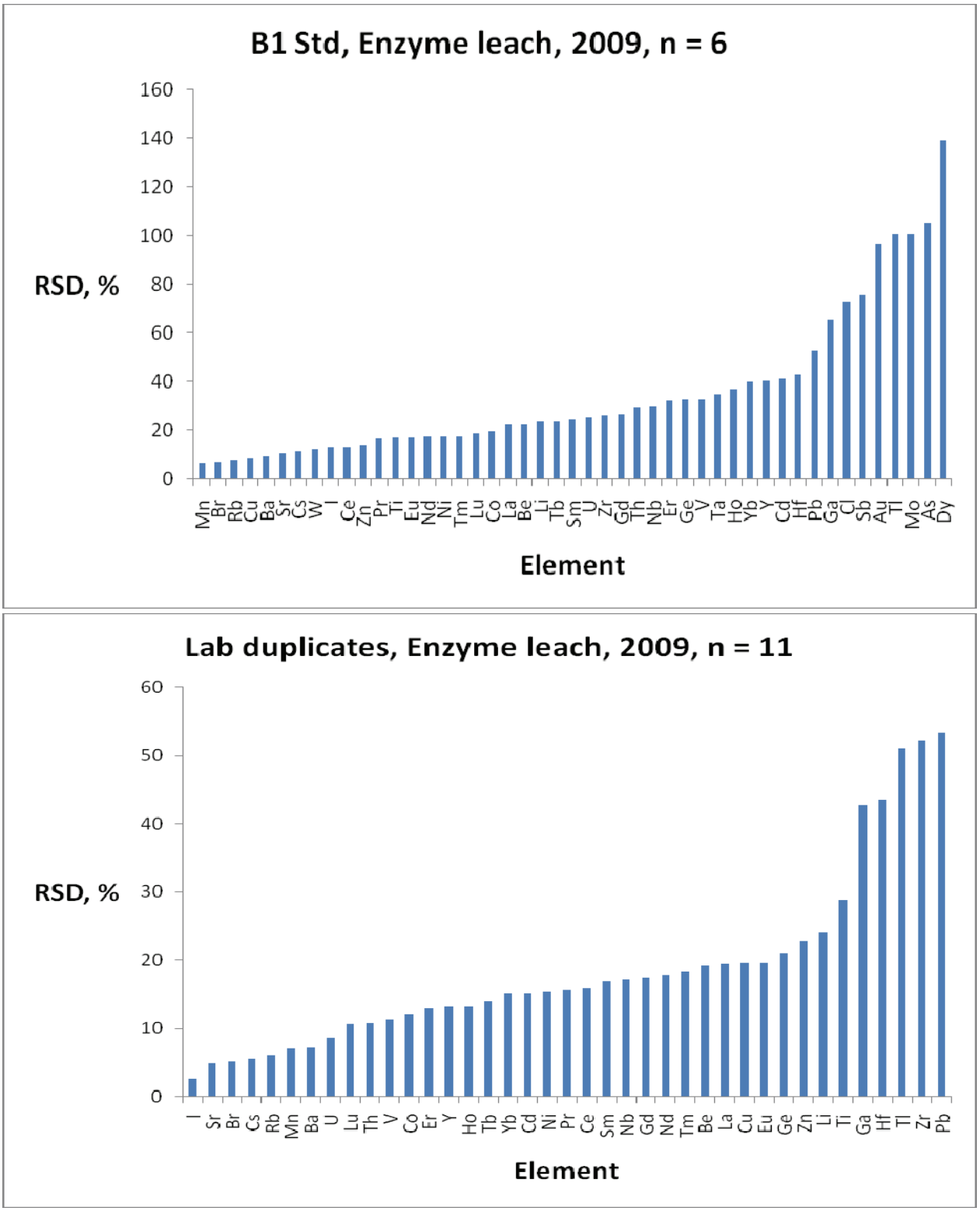

Fig. 7.6. RSDs for Enzyme leach on inorganic soils (a) for B1 STD and (b) lab duplicates.

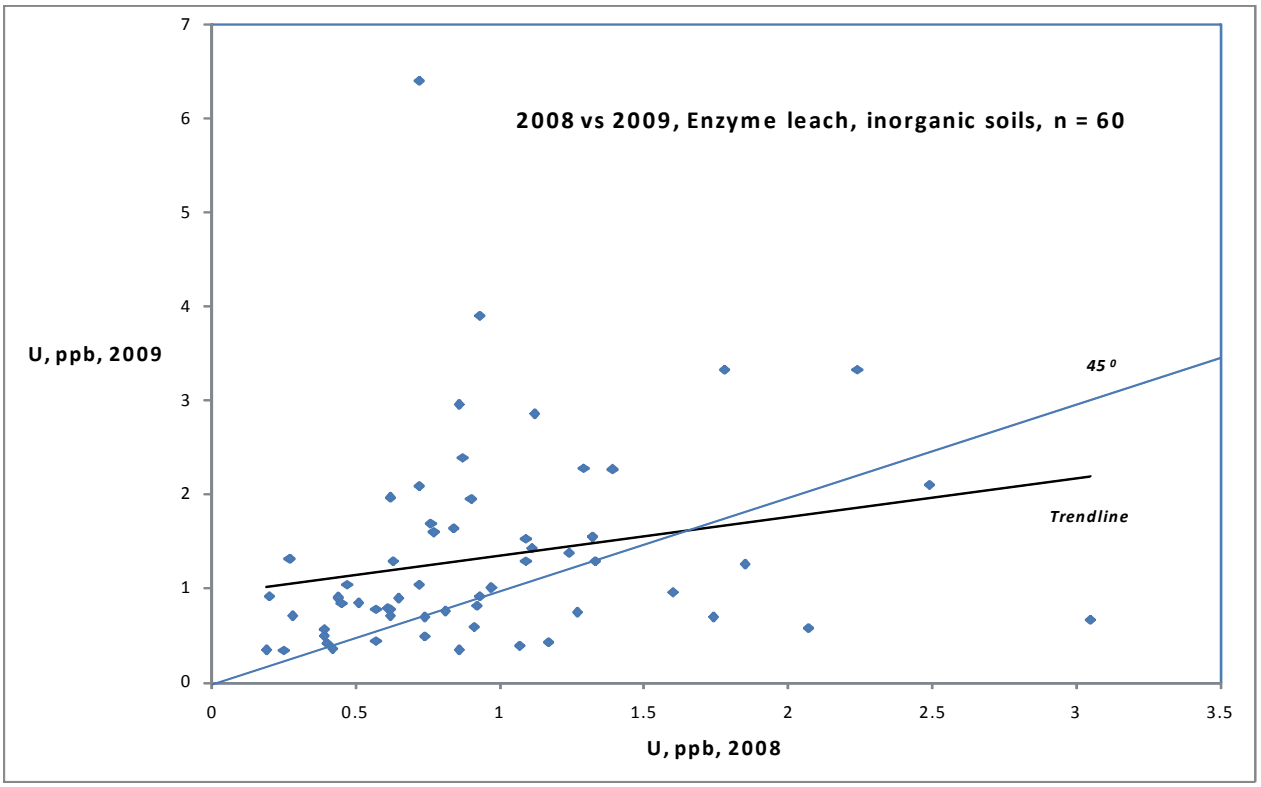

Fig. 7.7. Uranium in 2009 vs U in 2008, year-to-year duplicates for the Enzyme leach.

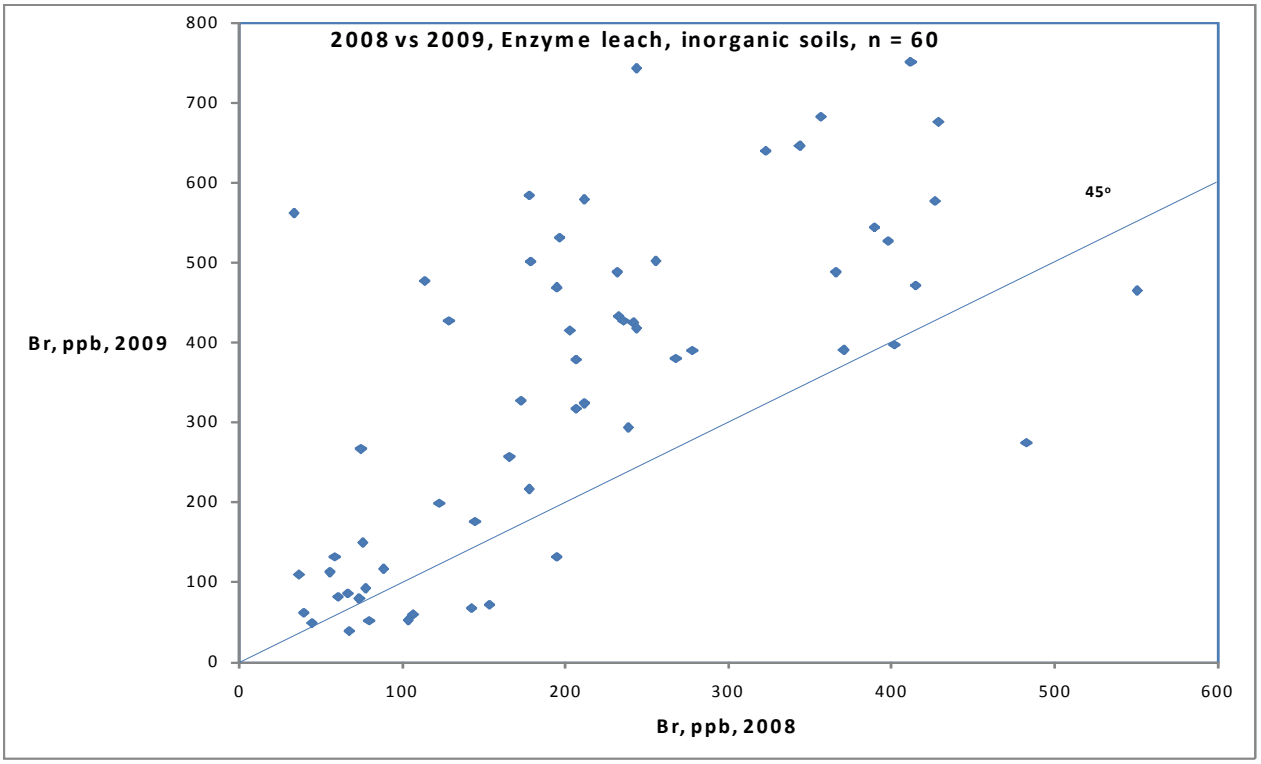

Fig. 7.8. Bromine in 2009 vs Br in 2008, year-to-year duplicates for the Enzyme leach.

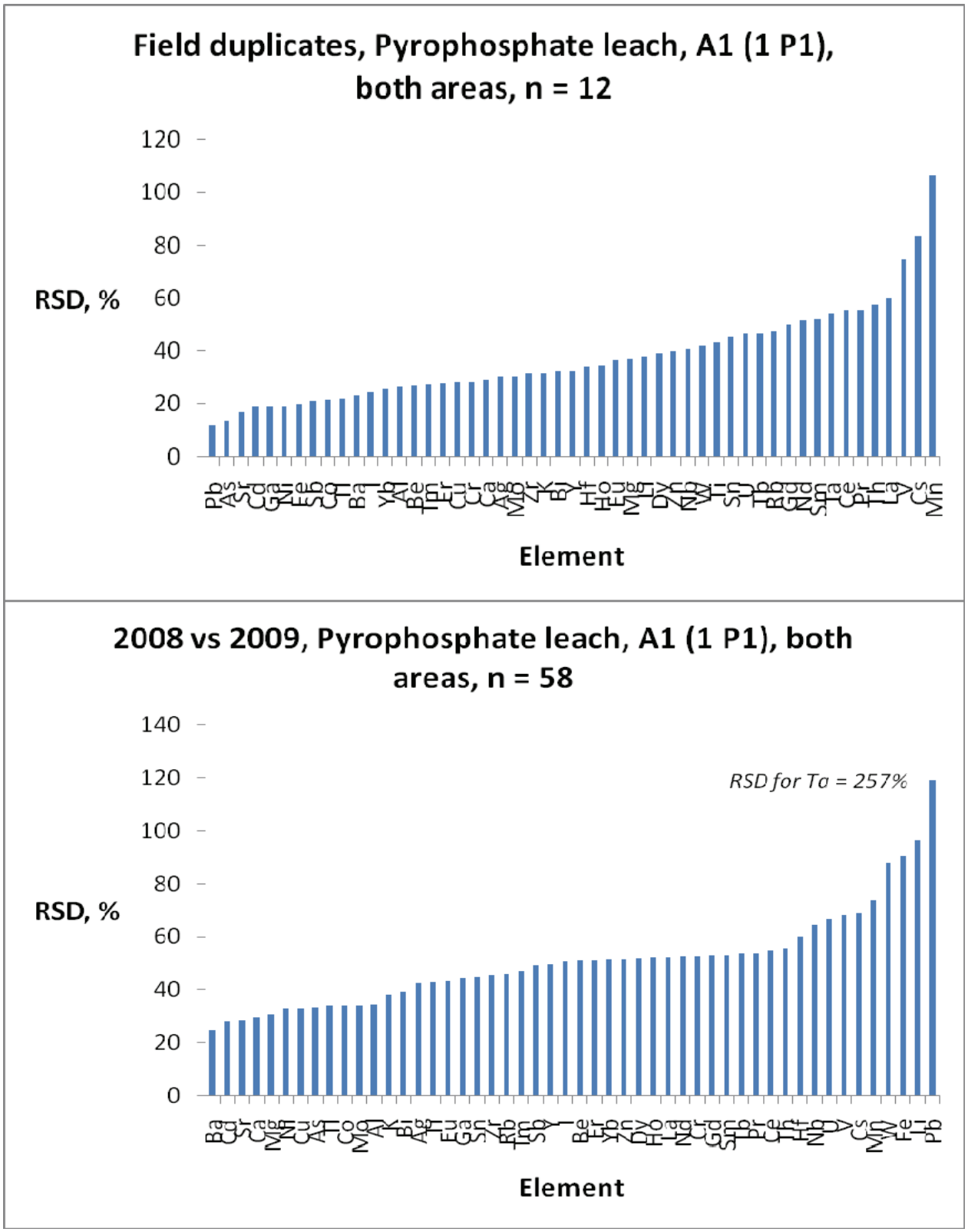

Fig. 7.10. RSDs for pyrophosphate leach on organic soils (a) for field duplicates and (b) year-to-year duplicates.

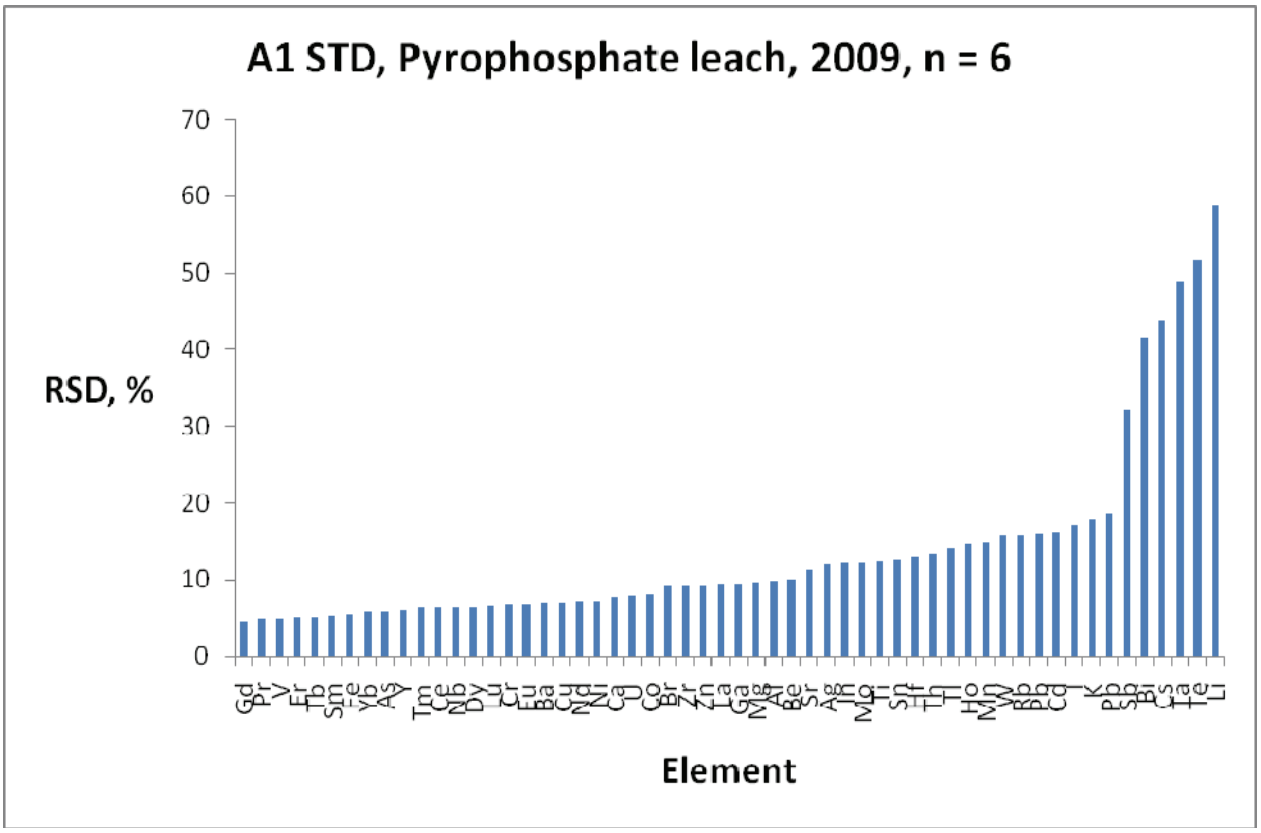

Fig. 7.11. RSDs for pyrophosphate leach on organic soils for A1 STD.

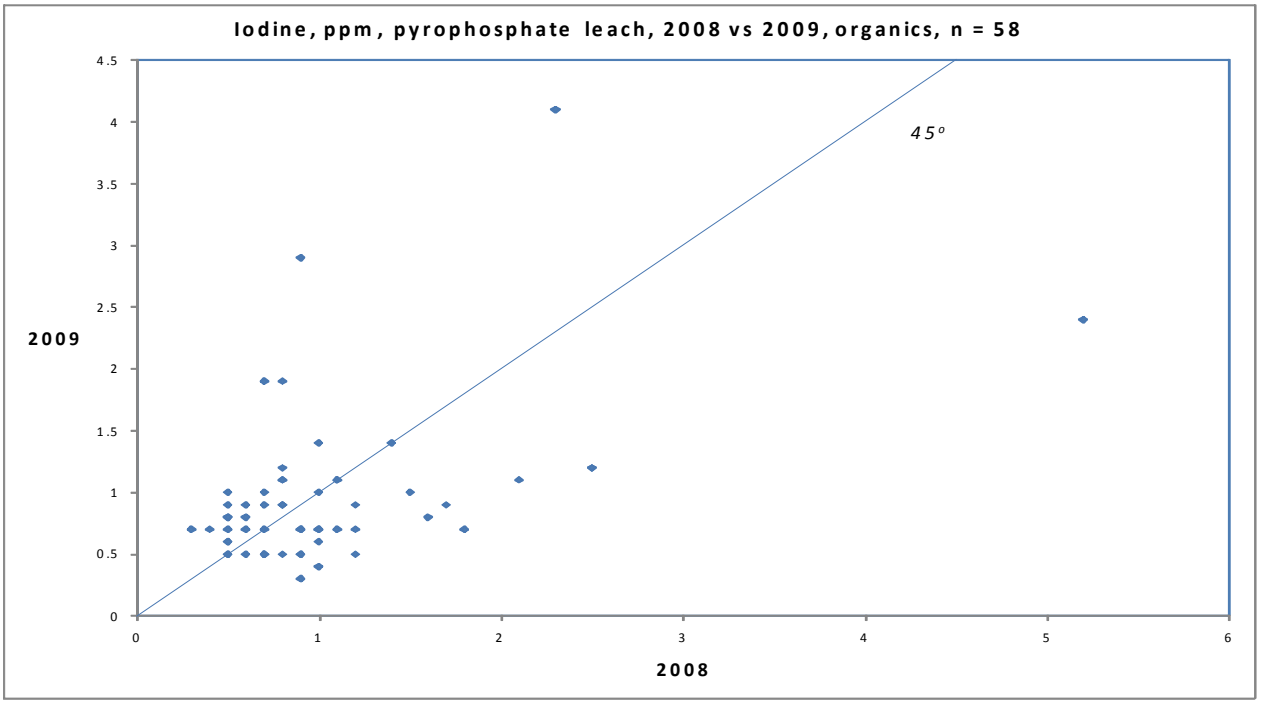

Fig. 7.12. Iodine 2009 vs I 2008, year-to-year duplicates for the pyrophosphate leach.

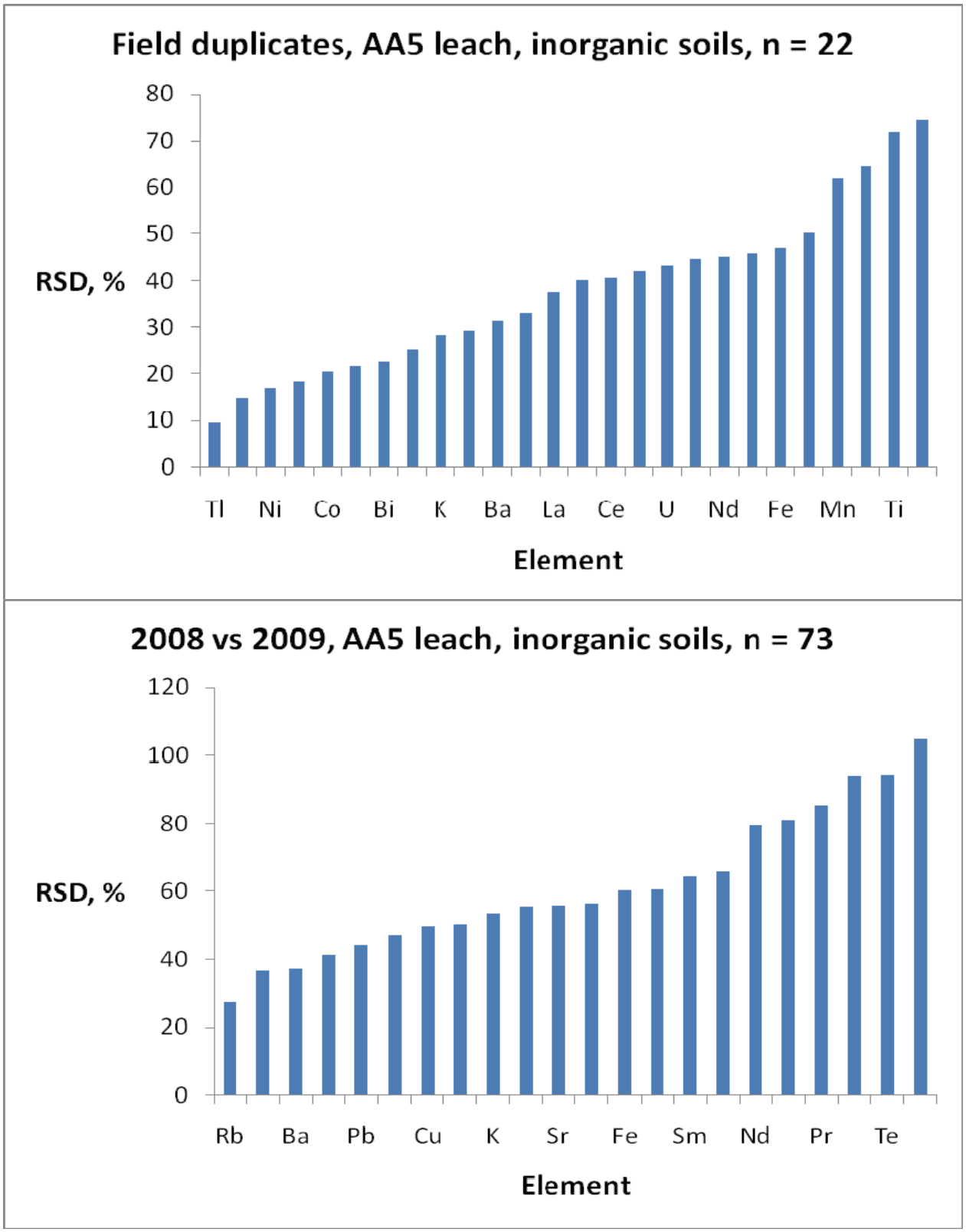

Fig. 7.13. RSDs for ammonium acetate leach on inorganic soils (a) for field duplicates and (b) year-to-year duplicates.

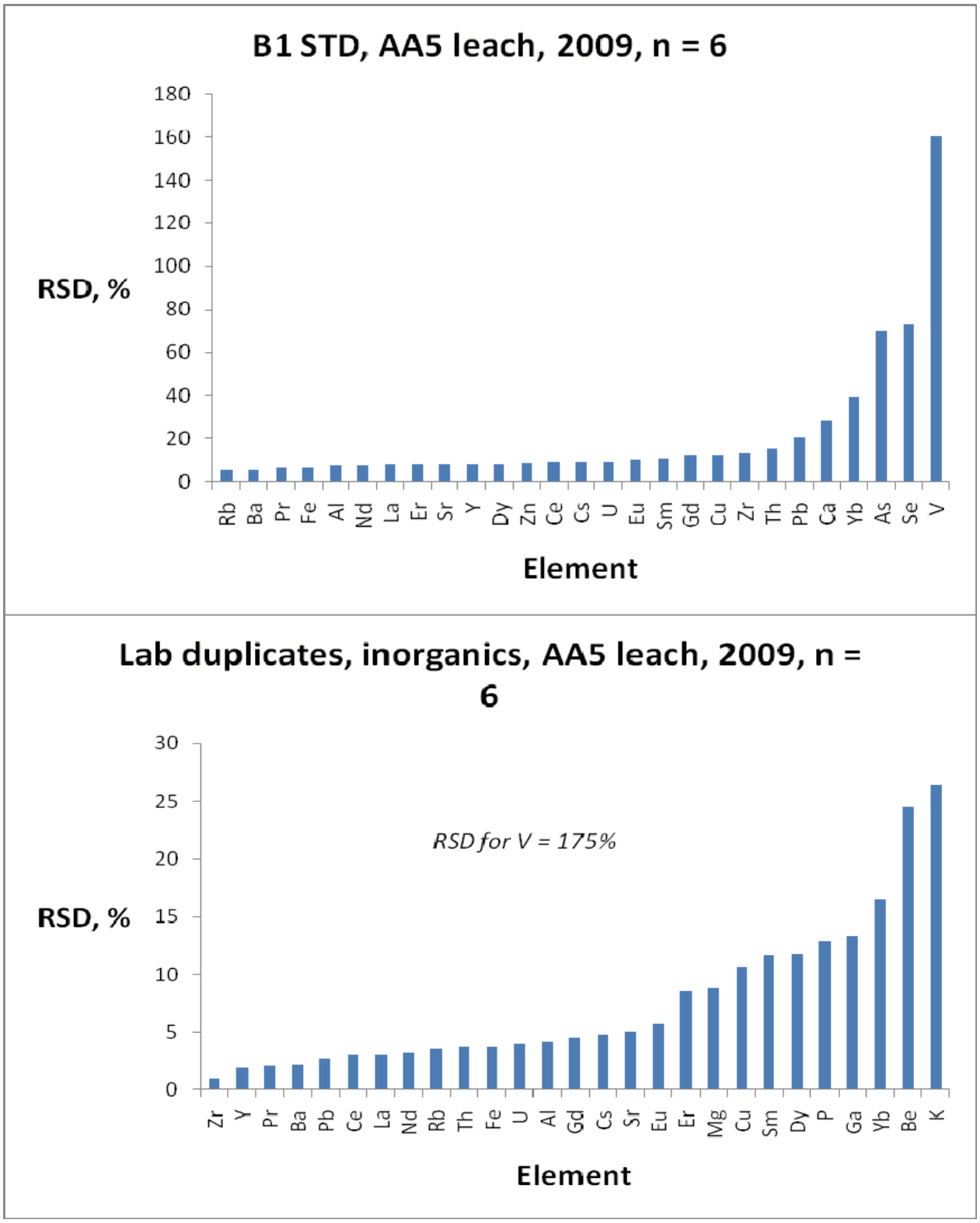

Fig. 7.14. RSDs for ammonium acetate leach on inorganic soils (a) for B1 STD and (b) lab duplicates.

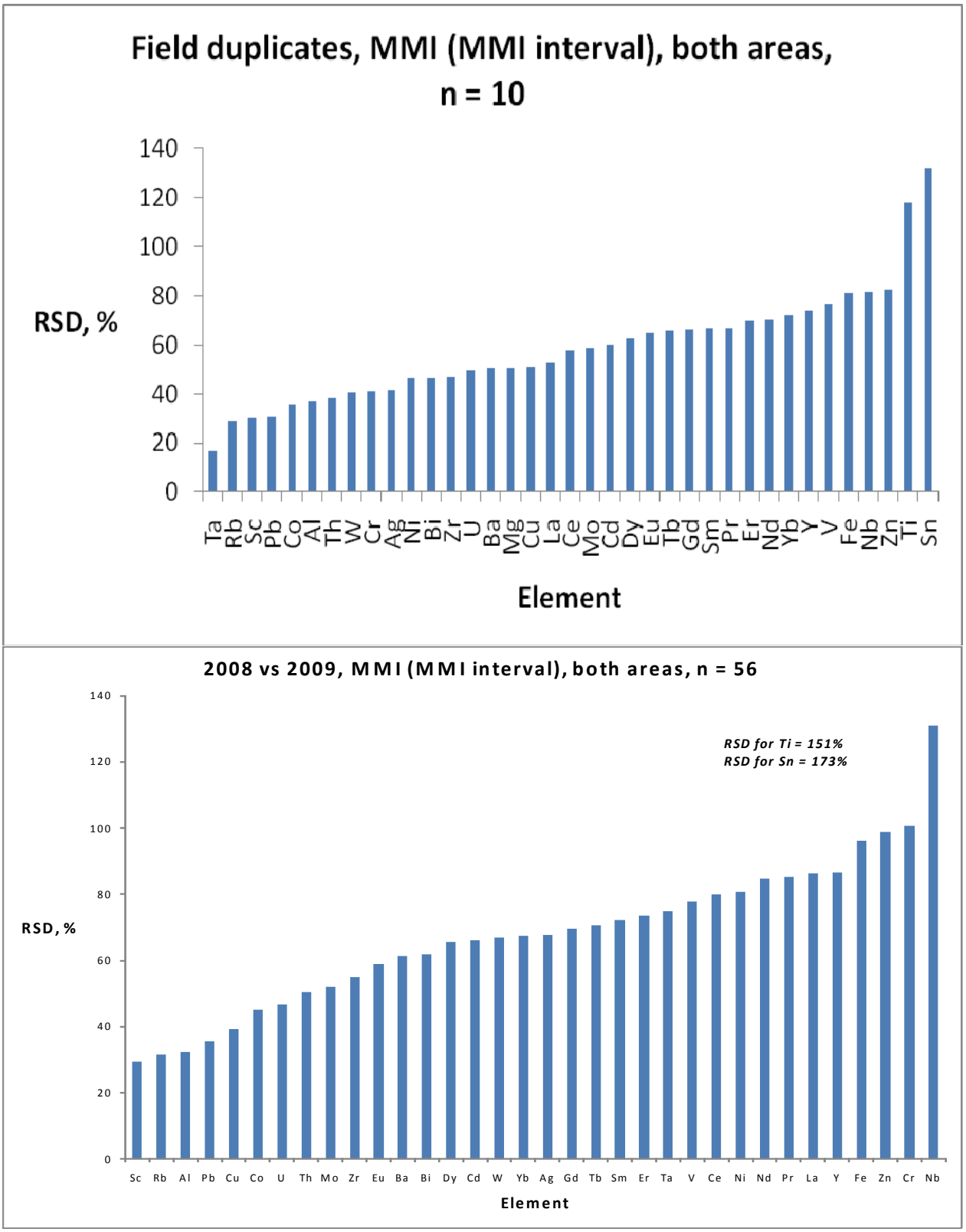

Fig. 7.15. RSDs for MMI leach on inorganic soils (a) for field duplicates and (b) year-to-year duplicates.

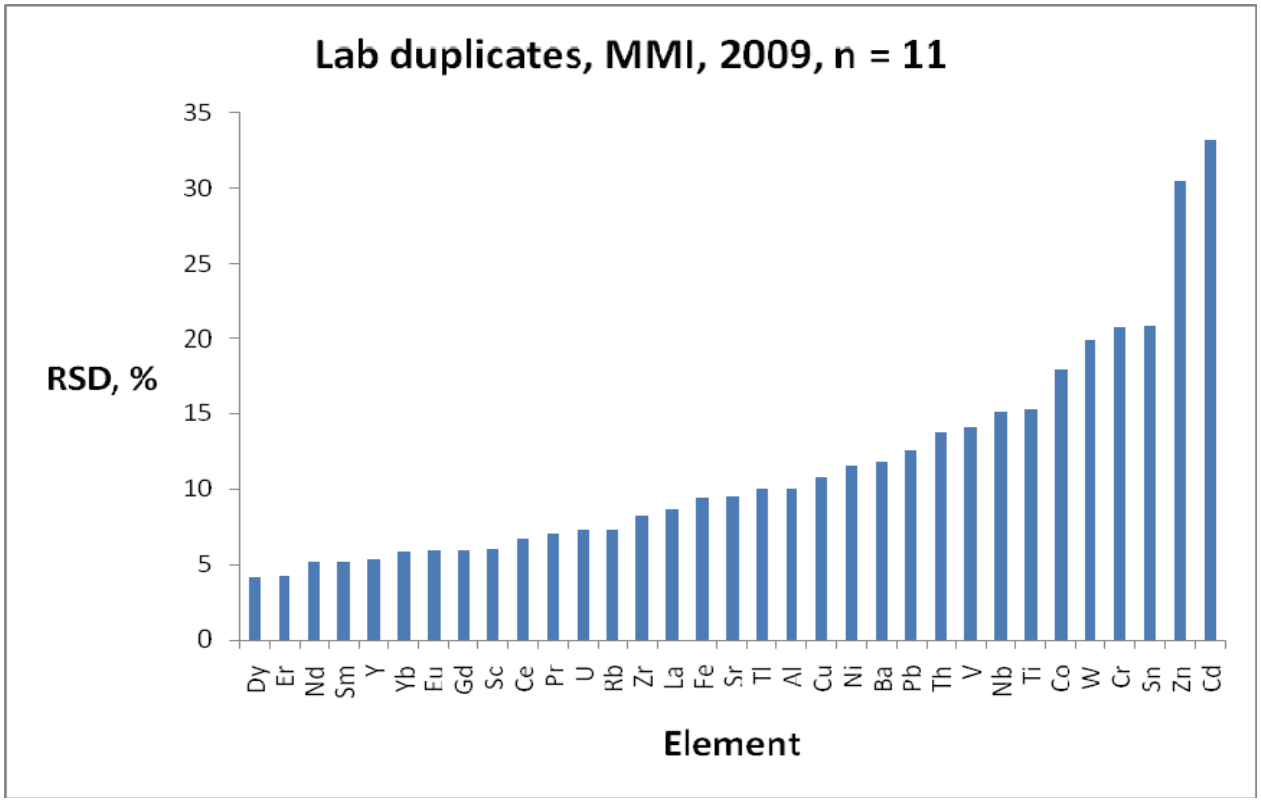

Fig. 7.16. RSDs for MMI leach on inorganic soils lab duplicates.

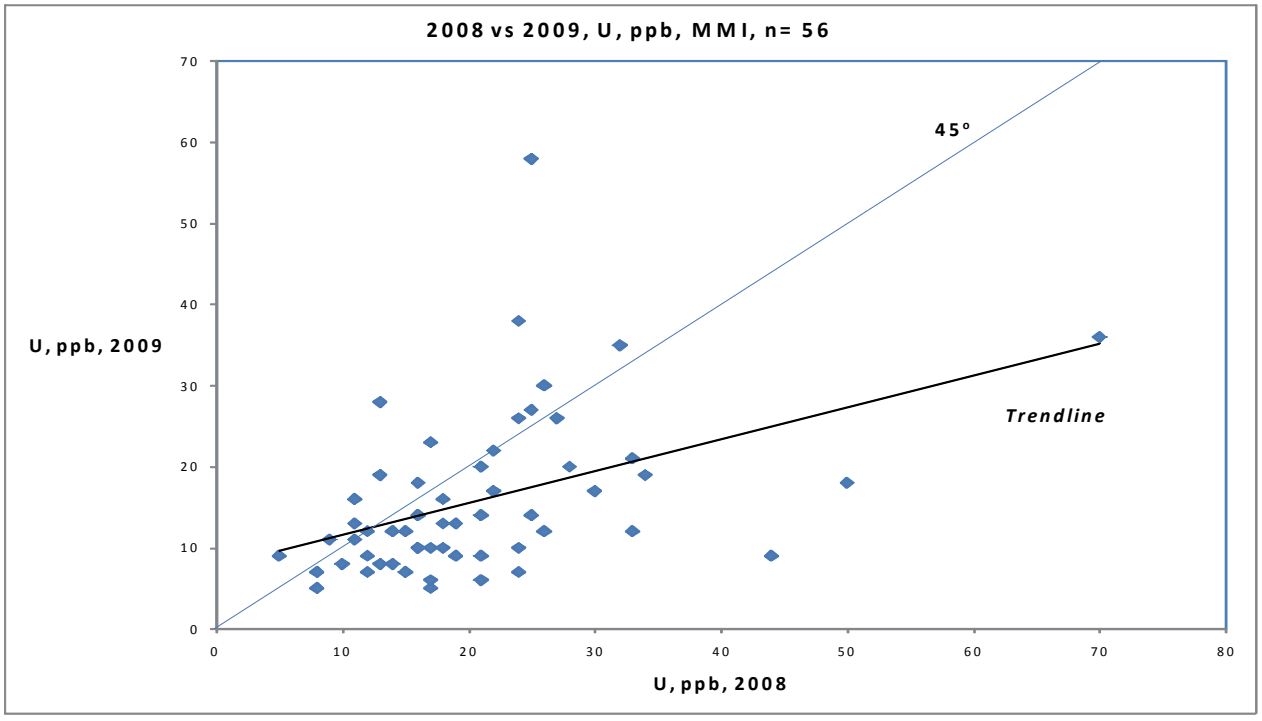

Fig. 7.17. Uranium 2009 vs U 2008, year-to-year duplicates for the MMI leach.

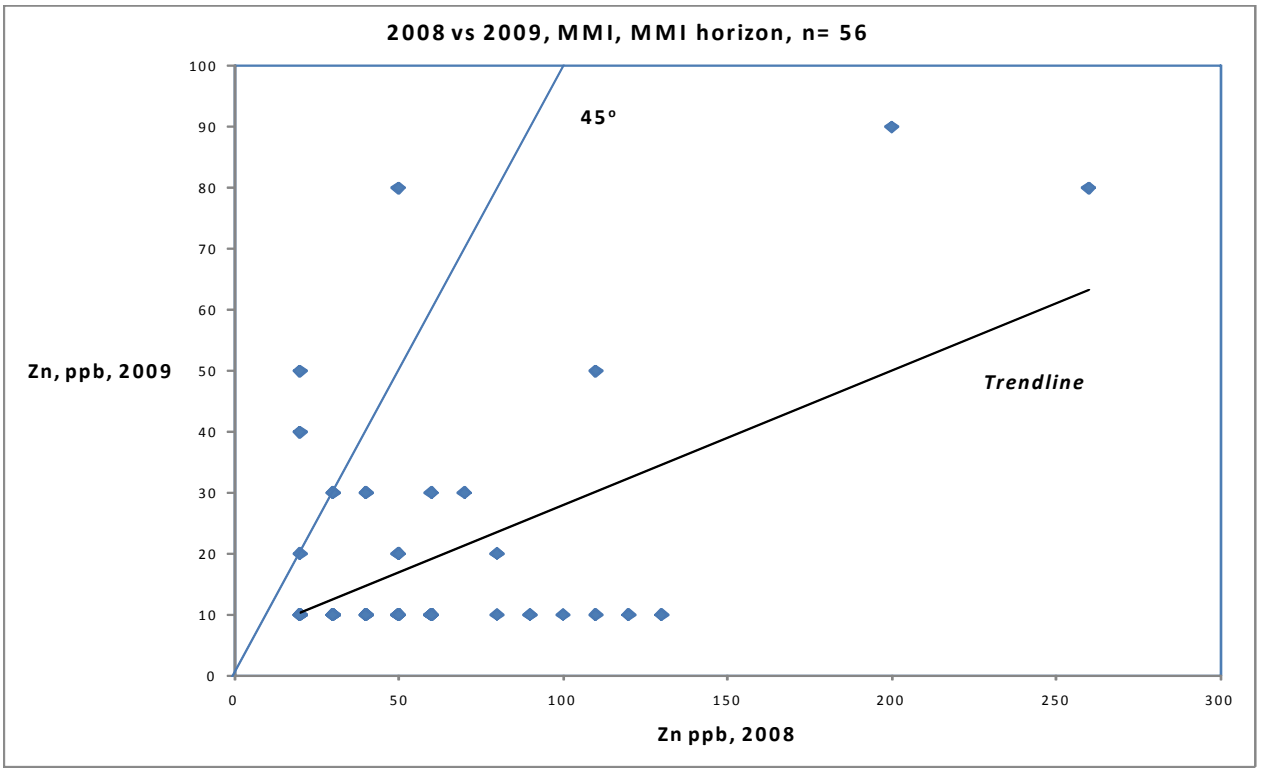

Fig. 7.18. Zinc 2009 vs Zn 2008, year-to-year duplicates for the MMI leach.

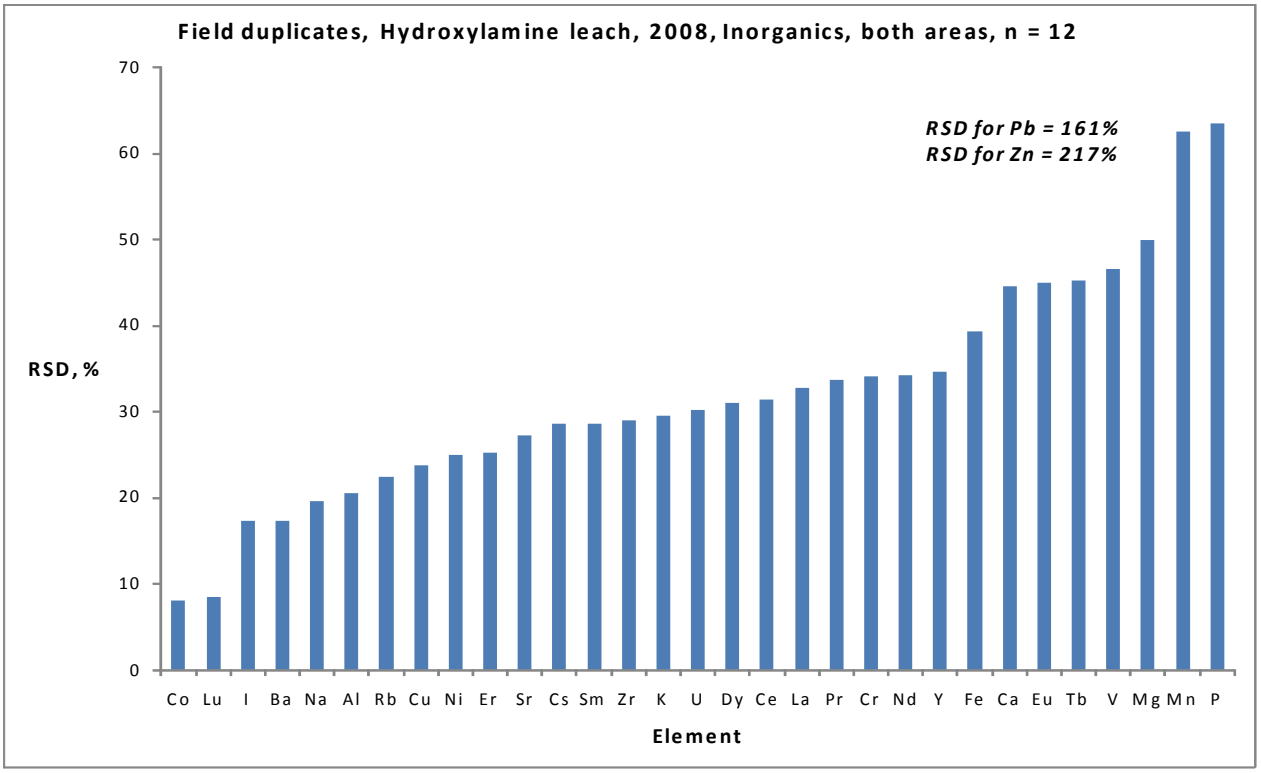

Fig. 7.19. RSDs for hydroxylamine leach on inorganic soils for field duplicates

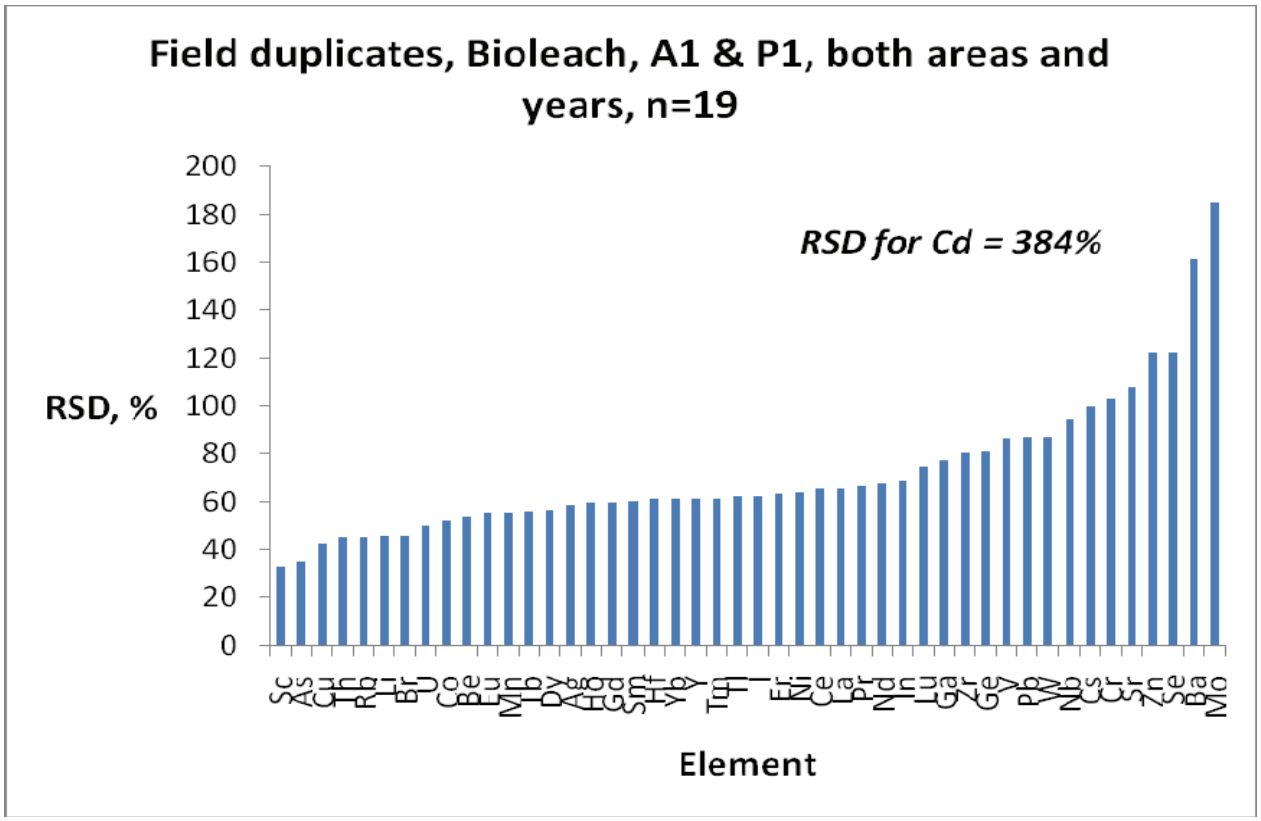

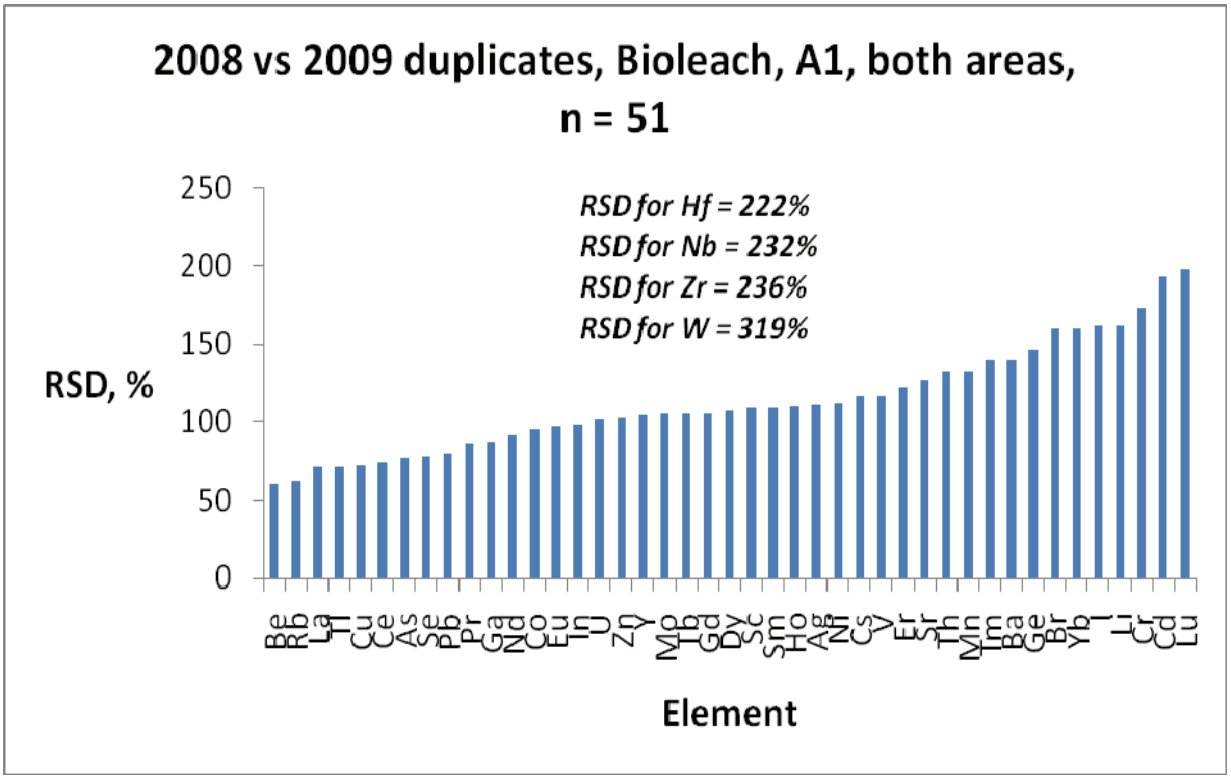

Fig. 7.20. RSDs for the Bioleach on organic soils (a) for field duplicates and (b) year-to-year duplicates.

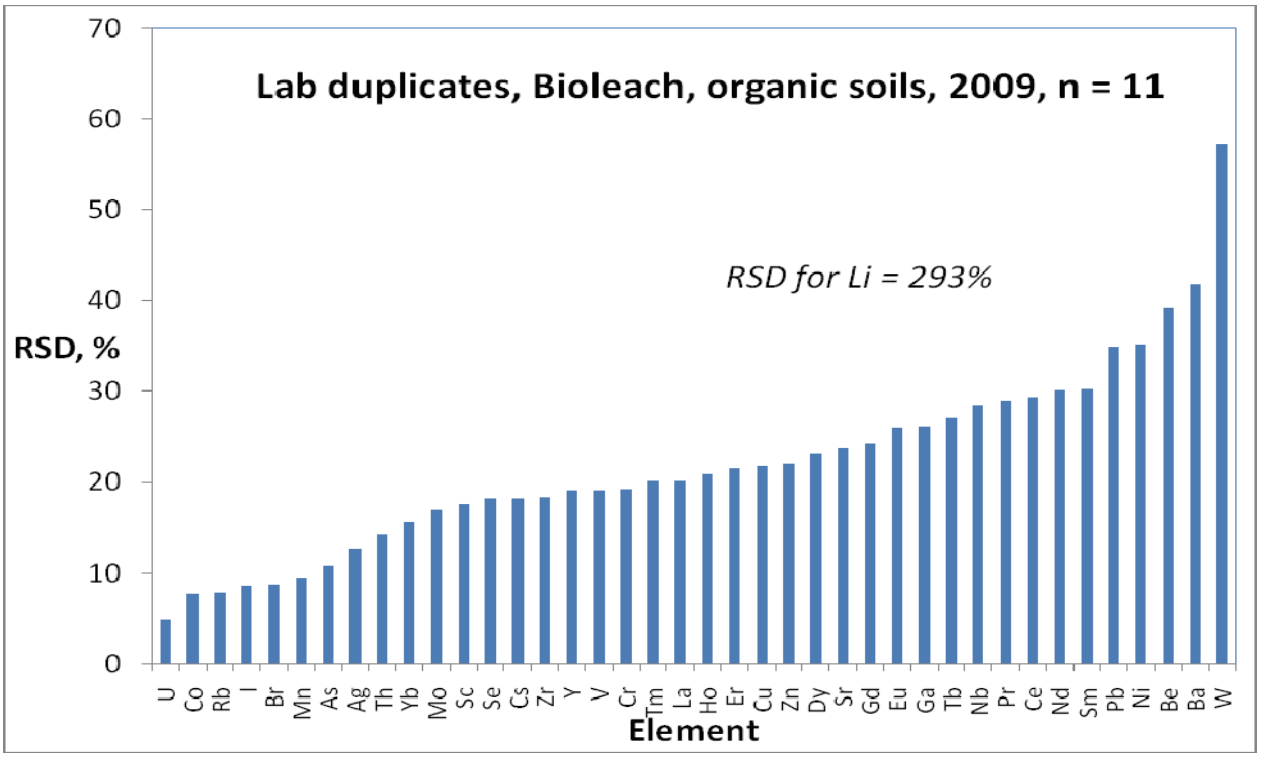

Fig. 7.21. RSDs for the Bioleach on organic soils for lab duplicates

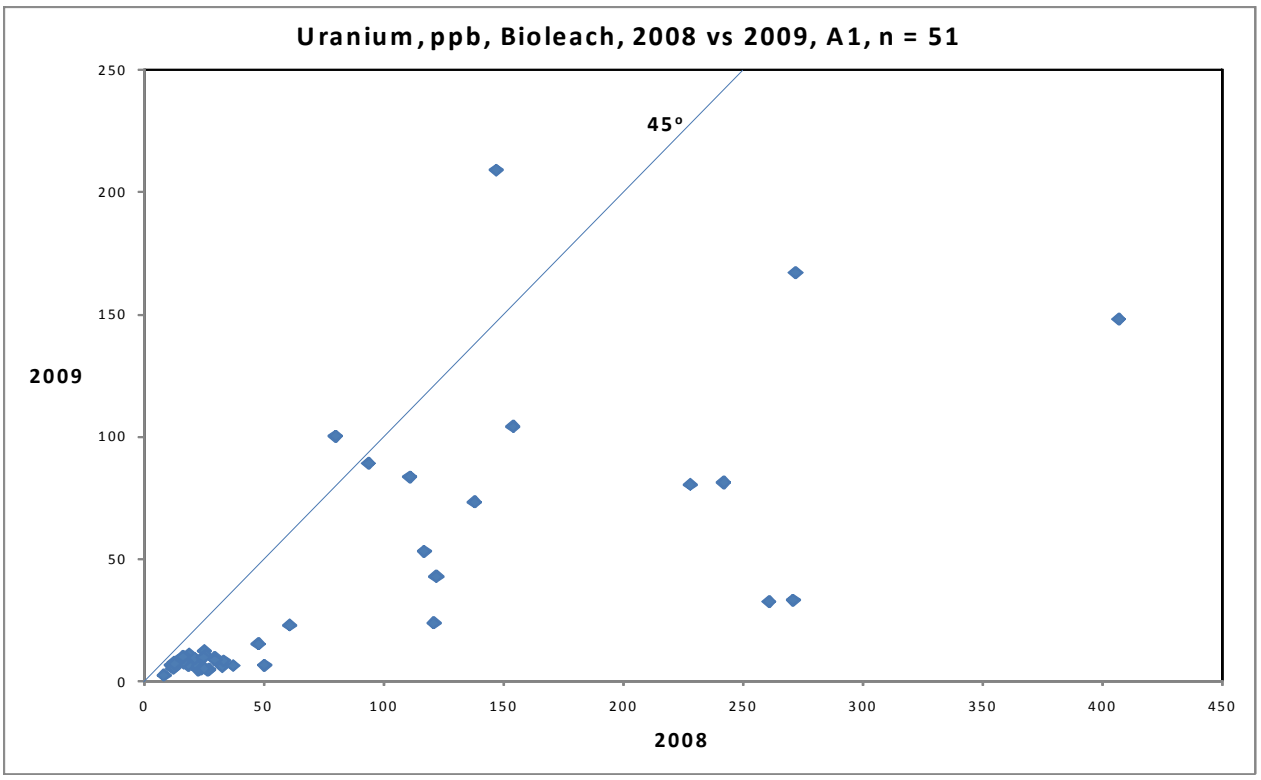

Fig. 7.22. Uranium 2009 vs U 2008, year-to-year duplicates for the Bioleach.

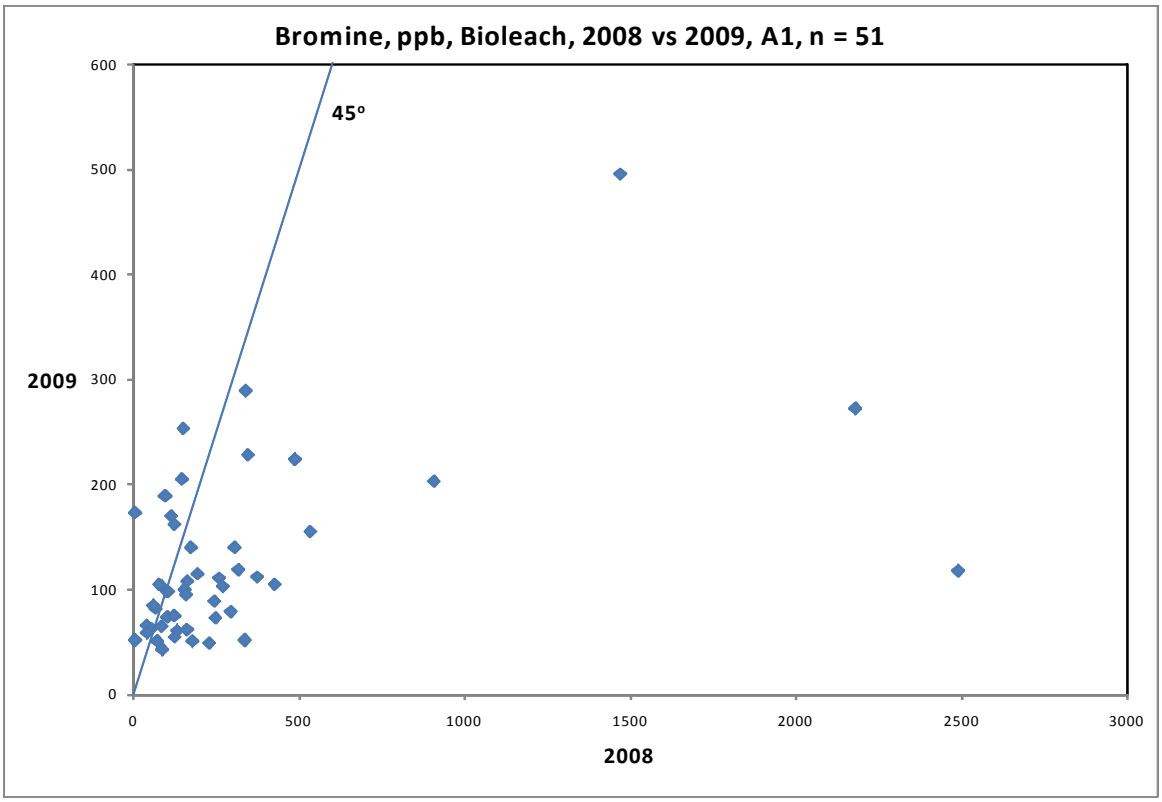

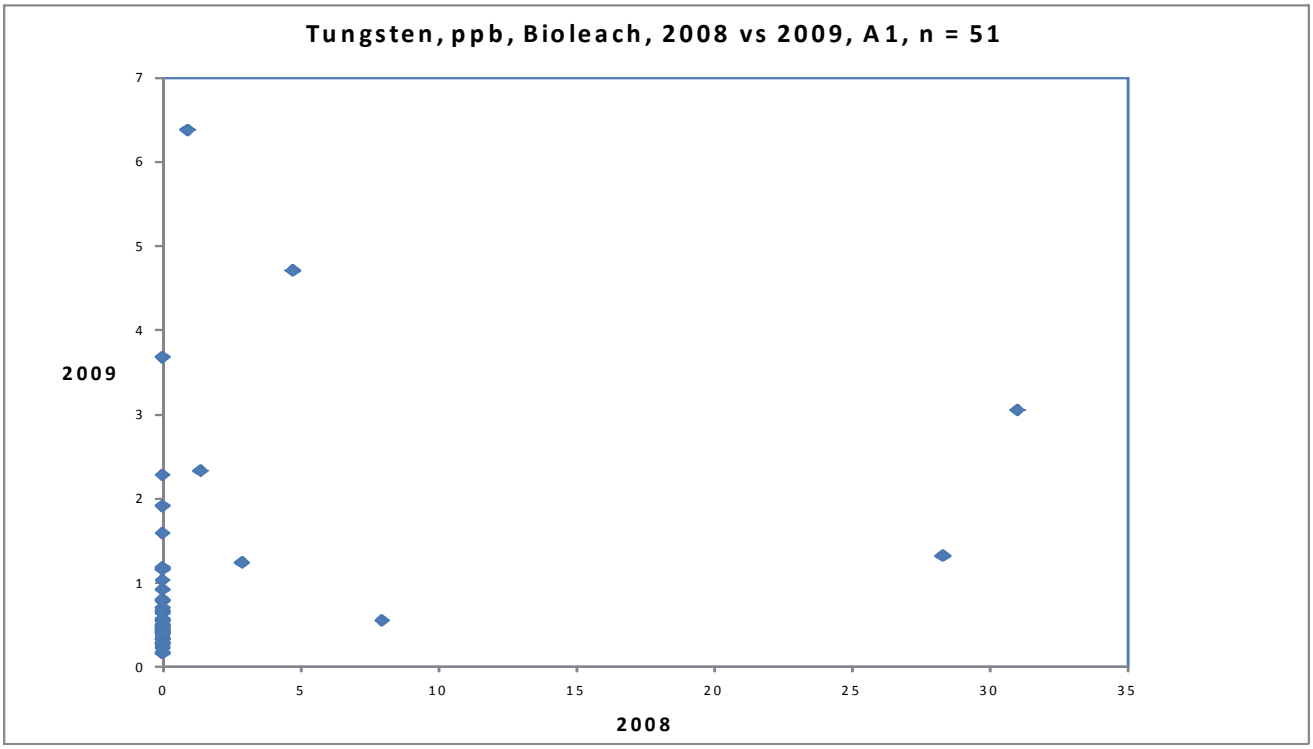

Fig. 7.23. Year-to-year duplicates for the Bioleach for (a) Br and (b) W.

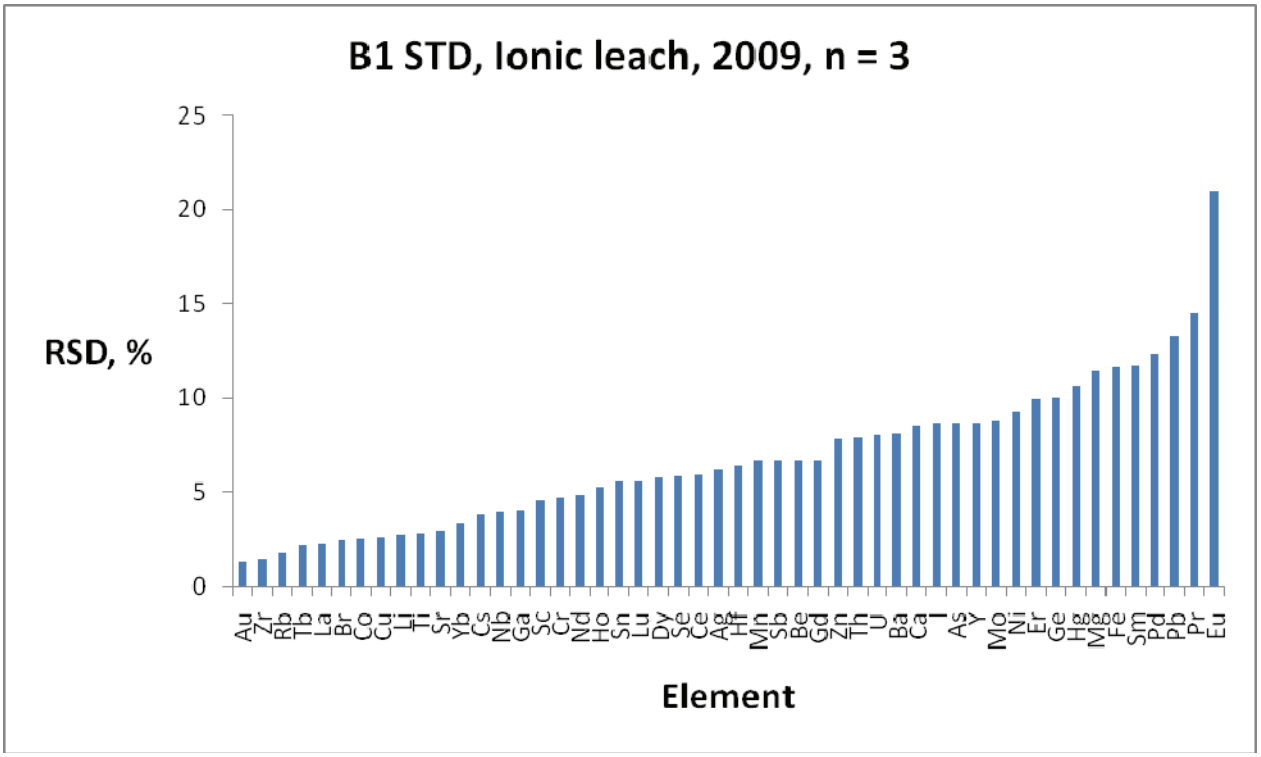

Fig. 7.24. RSDs for the Ionic leach on inorganic soils for the B1 STD.

7.2 Quality Assurance: Variability using Element Profiles

See Part II Chapter 5 for an explanation of these plots.

The folders of plots under review are those labelled 'jpeg' on the CD (showing Box and Whisker and X-Y plots of year-to-year duplicates, to evaluate any bias between years of sampling) and 'jpeg 1' (showing responses of A1, B1 and C horizons for all five lines, to evaluate consistency of anomalies). Only those element profiles where there is a problem are commented upon here and therefore, by inference, those not mentioned show no significant bias. Furthermore, those elements where most of the values are close to the detection limit are omitted from discussion (i.e. there may be sporadic one-point highs along some lines but these are ignored). There are year-to-year duplicates for: aqua regia (A1, P1, B1, C); pyrophosphate leach (A1); Enzyme (B1, C); MMI (MMI horizon); and Bioleach (A1).

7.2.1 Cigar Lake

In 2009 parts of Lines 1 and 2 were resampled for A1, B1 and C horizons while Line 4 was completely resampled (and extended) for A1 and B1 horizons.

Aqua regia (year-to-year duplicates: A1, B1 and C horizons)

The year-to-year variability by this digestion in the three horizons is very low indeed, except at concentrations near detection limit. Sulphur is at detection limit for most of the inorganic soil samples but is measurable, albeit at very low levels, in the A1 horizon (Fig. 7.25, S in A1). While the Box and Whisker (B&W) plots indicate a significant different in medians and therefore a bias, this is probably the influence of setting values < DL to DL/2 in the second year and not in the first. However, there is clearly a bias towards higher values in 2009. The response of S in the A1 horizon on Line 3 over the deposit is interesting, a consistently elevated signal over ~ 500 m of the line. Antimony also shows a bias - higher levels in 2009 - and this is noticeable in the A1 horizon (Fig. 7.26, Sb in A1). These are the only elements of 'concern' and even here it is a detection limit issue.

Care should exercised in viewing the multiple profile figures (where A1, B1 and C horizon are profiled across the five lines) as some of the ranges on the y-axis are small and hence anomalies may appear more significant than they actually are. Anomalies that do not repeat from one year to the other, and most are only one-point, include: Mo in A1, Lines 2 and 4; Pb in A1, Line 2; U in A1, Line 4; and, notably, in A1 on Line 1, Ce, Fe, La, Nb, Th, Ti, U, V, Y and Zr (e.g. Fig. 7.27, Mo; Fig. 7.28, U). The multi-element anomalies in A1 on Line 1 that are present in 2008 are in the gleysol area. The U and Co profiles (Fig. 7.28 and Fig. 7.29, Co) are typical in that the same trends are evident in each year but there may be variation in response at individual sites.

Pyrophosphate leach (year-to-year duplicates: A1 horizon)

There is a small bias evident between years for Bi, Cd, Mo, Pb, Tl, U and V, all showing higher concentrations in 2009 and for Nb, Sb and Ti showing higher concentrations in 2008 (Fig 7.30, U; Fig. 7.31, Sb).

The elements that show an anomaly in A1 on Line 1 by aqua regia that did not repeat in 2009 - the lithophile elements, Fe, REEs, Nb, Th, Ti, U, V, Zr – also display this phenomenon in the pyrophosphate leach, clearly caused by sampling/temporal variance in this area of the gleysols (Fig. 7.32, U). The U and Pb one-point anomalies in A1 on Lines 4 and 2, respectively, and shown in 2009 but not in 2008, are also present by the pyrophosphate leach, and hence this rules out analytical error (Fig 7.33, Pb). Though there is the bias between years mentioned above for elements such as Mo, the trends are generally still maintained, except for an element at very low concentrations such as Sb where the responses along the lines are noisy (Fig 7.34. Sb).

Enzyme leach (year-to-year duplicates: B1 and C horizons)

There is a bias, high for 2009 compared to 2008, for Br by the Enzyme leach, demonstrated by the B&W plots and by Lines 2 and 4 in Figure 7.35 (Br with B1). The signals for Br are very noisy. In the C horizon, this bias high for 2009 is not nearly as evident (Br in C). Note the low in Br over the pod in the C in 2008 on both Lines 2 and 4 and that this low is repeated on Line 2 in 2009 (Fig. 7.36, Br in C). There is a huge shift in concentrations of iodine between years, with much higher values in 2009, as seen in the B&W plots and the responses along Lines 2 and 4 in the B1 and 1 and 2 in C (Fig. 7.37, I- B1). There are far more B-horizon soils (and C horizon) reporting Cd above the DL of 0.1 ppb in 2009 than there were in 2008 (Fig. 7.38, Cd-B1). Like Cd, Co is significantly higher in 2009, in both B and C horizons (Fig. 7.39, Co-B1). Dysprosium, however, displays significantly higher concentrations in 2008, with many above the DL of 0.01 ppb (Fig. 7.40, Dy-B1). Like Dy, thallium's concentrations in 2008 are well above those in 2009 and most data are far removed from the DL of 0.005 ppb.

The anomaly for Ce on Line 4 in B1 just south of the pod in 2008 has shifted to just north of the pod in 2009; this is evident for others REEs such as La (Fig. 7.41, Ce). Figure 7.42 for Mo demonstrates the noise for this element in terms of sporadic highs in both years, most data being below the DL of 0.1 ppb. The one-point Ni anomaly in B1 and C horizons over the pod on Line 1 in 2008 is not repeated the following year (Fig. 7.43, Ni). The substantial change to higher concentrations in 2009 for Br and I is particularly evident for I (Fig. 7.44, Br; Fig 7.45, I). Uranium shows the same shift mentioned above for Ce and the REEs and the patterns for the two years are quite different for C horizon on Line 2 (Fig. 7.46, U). The noise seen in responses for W, close to the DL of 0.1 ppb, suggests caution when interpreting these data (Fig. 7.47, W). The lack of agreement in patterns between years for Zn and Cu is not surprising given these elements' lack of coherency in their maps (Fig. 7.48, Zn).

Ammonium acetate leach (year-to-year duplicates: B1 and C horizons)

There *appears* to be a bias for elements reporting at or close to the detection limit but this is due to the difference in handling <DL data between years. Bias is not evident for most elements at measurable levels (e.g. Al, Ba, Ce, Fe, K, Mg, Pb, Rb, U). Thorium, however, has significantly higher concentrations in 2009 (Fig., 7.49, Th).

Although, like many element responses compromised by detection limit problems, there are some values above the DL in Ca in one year that do not agree in the other year (Fig. 7.50, Ca). In general, there does not appear to be a bias between years in this leach but there are numerous

one-point anomalies close to the DL that do not repeat, as demonstrated for P (Fig. 7.51, P).

MMI (MMI horizon)

As with other partial leaches, much of the data are at or close to the detection limit for elements such as As, Bi, Ca, Mg, Mo and Tl. Concentrations of Rb, U, V, Zn and Zr are significantly higher in 2008 (Fig. 7.52, Rb; Fig.7.53, U). Note the high in U over the pod on Line 4 repeats in the 2009 data, though of less magnitude, but that to the south does not. There is a small bias between years for Co and Pb with higher values in 2008, but the trends are maintained (Fig. 7.54, Co). Agreement between years in not good for Cd or Cr; however, the responses in either year are noisy so this is not unexpected (Fig. 7.55, Cr).

In the multiple line plots, there is an anomaly on Line 4 for Ba in 2009 that was barely evident in 2008 (Fig. 7.56, Ba). Lines 1 and 4 show two one-point anomalies for Ce (and other REEs) over the pod in 2009 that were not in evidence in 2008 (Fig. 7.57, Ce). The Fe patterns on Line 1 are quite different between years. The Ti and V responses do not match well between years; the odd high at the north end of Line 4 in 2008 is also seen for Fe, Nb and W (Fig. 7.58, Ti).

Bioleach (year-to-year: A1 horizon)

There is a large difference in As concentrations between years with those in 2008 being much higher (Fig. 7.59, As). Barium is also much higher in 2008 and on Line 4 shows several anomalies whereas the response in 2009 is very muted (Fig. 7.60, Ba). Bromine also appears to be higher in 2008 (Fig. 7.61, Br); the signals are noisy in both years, as seen in the Enzyme leach. The responses over and around the pod on Line 4 for Ce in 2008 are not in evidence in the lower and more muted signals of 2009 (Fig. 7.62, Ce). There is no similarity in the intensities for Co in the two years of sampling, those in 2008 being much higher, unlike the situation for the Enzyme leach (Fig. 7.63, Co). In fact, the REEs, Cr, Nb, Pb, Rb, Th, U, V, Zn and Zr are all behaving like Co and Br (Fig. 7.64, U).

The multiple line plots support the distinctly higher values in 2008 for many elements, including Cu, Ni and Sr in addition to those mentioned above (Fig 7.65, Co). Molybdenum is different in that in 2009 there are many more values above the detection limit than in 2008 (Fig. 7.66, Mo). The rather noisy response of I in 2008 is not seen in the muted signals of 2009 (Fig. 7.67, I).

7.2.2 McClean Lake

Only part of Line 4 was repeated in 2009.

Aqua regia (year-to-year duplicates: A1 and B1 horizons)

There is very little bias shown between the two years in the aqua regia digestion (e.g. Fig.7.67, U-B1). Results for Mo in the A1 horizon are higher generally in 2009 compared to 2008, but not in the inorganic media (Fig. 7.68, Mo).

The repeatability in the line profiles from year-to-year is also excellent, as typified by Ba and Y, where for the former element, for example, the gradual increase in concentration on Line 4 to the south is clearly evident in both years (Figs. 7.69, Ba, 7.70, Y). [It is interesting to see how well Lines 2—5 show this increase]. The only elements showing inconsistency between years along Line 4 are Mo in the A1 horizon and P (Fig. 7.71, P)

Pyrophosphate leach (year-to-year duplicates: A1 horizon)

As with aqua regia, the year-to-year repeatability of the pyrophosphate leach is excellent. Cerium is an example, with a 'quiet' baseline in both years on Line 4, rising to a subtle high over the southern pod and again over the north (Fig. 7.72, Ce). Note the clear multi-point anomalies over the pods on Line 3 which are evident for numerous elements. This excellent repeatability is also demonstrated by U and Th; note that the anomalies over the pods on Line 3 are much more pronounced for Th by pyrophosphate compared to aqua regia (Figs. 7.73, U; 7.74, Th). Molybdenum agreement is also excellent and that trend to higher concentrations in 2009 by aqua regia is not in evidence here (Fig. 7.75, Mo). Tungsten tends to show slightly higher values in 2009 but the B&W plots indicate this is not significant and concentrations are within a decade of the detection limit (Fig. 7.76, W).

The multi-line plots also indicate the excellent year-to-year precision and repeatability of anomalies, as shown by Nb (Fig. 7.77, Nb). Elements such as Ba (Zn, Cu) continue to show the increase in concentrations to the south (Fig. 7.78, Ba). The poorest performance is probably shown by Ni and Sb (Figs. 7.79, Ni; 7.80, Sb). The noisy response along the line in any one year suggests high field variability for Ni in any case, the analytical RSD at these levels being low and insignificant (e.g. 7% for the A1 STD). For Sb, the A1 STD has a high RSD of 32%, suggesting analytical noise, in addition to field variability, is a significant factor.

Enzyme leach (year-to-year duplicates: B1 horizon)

Elements that do not show any significant difference in concentrations between years include Ce, Nb, Rb, Se, Th, U, V, Yb and Zr. Elements that have significantly higher concentrations in 2009 include Br, Cd, Co, Cu, Mn, Ni, I, Pb and Sr (Fig. 7.81, I). Note that the trend towards higher levels of I in the south is still there but is much more dramatic in 2009. Significantly greater values in 2008 are evident for Dy, Tl, W and Zn (Figs. 7.82, Dy; 7.83, Tl). It is interesting that there is a difference between years for Dy whereas the other REEs do not show this.

Zinc shows what could be interpreted as a halo around the south pod on Line 4 in 2008 but the response is flat in 2009 (Fig. 7.84, Zn). Nickel, Cu, and Sr show more variability along Line 4 in 2009 (Fig. 7.85, Ni). The REEs are quite similar in response between years, as is U (Fig. 7.86, La; 7.87, U).

Ammonium acetate leach (year-to-year duplicates: B1 horizon)

Only thorium has significantly higher concentrations in 2009 (Fig. 7.88, Th). As this was seen for Th at Cigar Lake and as it is the only element behaving this way, the cause is probably a calibration change in the analysis.

Numerous elements, such as Ni, Co and Tl, are at or close to their DLs and hence one-point anomalies are not uncommon and these do not repeat well from one year to the next. Elements such as Ba, La, P, Sr and U show good agreement year-to-year (Figs. 7.89, Ba; 7.90, U). The trends along Line 4 are similar between years for Fe but a few sites do not replicate well (Fig. 7.91, Fe).

MMI (MMI horizon)

The Box and Whisker plots indicate that there are no instances of significant bias between years for this small dataset on Line 4. Uranium and Pb tend to be higher in 2008; year-to-year responses are noisy, the peaks and valleys not necessarily co-located (Fig.7.92, U).

Most of the trends (subtle) on Line 4 match well year-to-year, as shown by Co and Th (Figs. 7.93, Co; 7.94, Th). Nickel shows elevated concentrations between the pods but at different intensities (Fig. 7.95, Ni). Both years show the increase in Fe from the south pod towards the north but it is erratic (Fig. 7.96, Fe). Niobium (+ V, Cr) behaves similarly to Fe and Ti shows poor agreement at this end of the line (Fig. 7.97, Ti).

Bioleach (year-to-year: A1 horizon)

Arsenic, Cd, Co, Pb, Th, U and the REEs all show significant differences in concentrations between years, with higher values in 2008 (Figs. 7.98, As; 7.99, Co). The 2008 survey shows elevated As and Co concentrations extended north of the pod on Line 4, unlike the 2009 set. Caesium concentrations are significantly higher in 2009 (Fig. 7.100, Cs).

Niobium and Cr show elevated concentrations just south of the pod in 2008, not in 2009, and anomalies over and north of the pod differ significantly in intensity (Fig. 7.101, Nb). Uranium, Ni and Cu responses along Line 4 differ markedly year-to year (Fig. 7.102, U) and Se shows a shift in locations of peak intensities (Fig. 7.103, Se). Bromine and I have anomalies over and to the north of the pod in both years but they differ slightly in contrast and location, being broader in 2008 but more intense in 2009 (Fig. 7.104, Br).